Localization and function of anionic lipids in cell organization and plant development

Matthieu Platre

Numéro National de Thèse : 2017LYSEN098

THESE de DOCTORAT DE L'UNIVERSITE DE LYON
opérée par
l'Ecole Normale Supérieure de Lyon

Ecole Doctorale N° 340
Biologie Moléculaire, Intégrative et Cellulaire

Spécialité de doctorat : Sciences de la Vie
Discipline : Biologie cellulaire des plantes

Soutenue publiquement le 01/12/2017, par :

Matthieu PLATRE

Localisation et fonction des lipides anioniques dans l'organisation cellulaire et le développement des plantes

---

Devant le jury composé de :

Robert, Stéphanie	Professeure	Université d'Umea	Rapporteure
Faure, Jean-Denis	Professeur	INRA-AgroParis Tech	Rapporteur
Boutté, Yohann	CR CNRS	Université de Bordeaux	Examinateur
Antonny, Bruno	DR CNRS	IMPC UMR7275	Examinateur
Ingram, Gwyneth	DR CNRS	ENS de Lyon	Examinatrice
Jaillais, Yvon	DR CNRS	ENS de Lyon	Directeur de thèse

REMERCIEMENTS

Sans nul doute cette partie de ma thèse sera lu par le plus grand nombre et pour cause les remerciements c'est important ! Mais aussi moins long et compréhensible d'entre tous comparé aux parties suivantes. C'est aussi selon moi, là, qu'en quelques paragraphes on peut sentir par le choix des mots ce qu'a signifié l'expérience d'une thèse. Dans ce but, j'ai pris le temps de m'adonner à ce délicat exercice quelques semaines après la rédaction de mon manuscrit.

Il est vrai que derrière plusieurs années de travail que représente une thèse se cache de nombreuses personnes qui ont été indispensable et qui méritent d'être remerciés. Très certainement, chacun(e) d'entre vous qui lirons ce passage chercherons assidûment par la suite leur prénom dans la liste des personnes énumérées pour voir s'ils y figurent « ou pas » ! Je tiens donc à m'excuser si par mégarde j'ai pu égarer certains prénoms car chacun(e) d'entre vous que j'ai pu croisé durant ces 5 années au RDP mérite réellement d'être remercié. Alors toi qui a pris le temps de lire cette phrase, MERCI !

Mes premiers remerciements s'adressent à celui sans qui cette thèse n'aurait pas été possible et sans qui je n'en serai pas là aujourd'hui. Comme mentionné, il y a cinq ans de cela je suis arrivé au RDP pour mon stage de fin d'étude d'ingénieur. Par mon cursus, je n'étais pas vraiment préparé à travailler en laboratoire, c'est avec patience, pédagogie et courage qu'Yvon a su me transmettre les connaissances et sa passion pour la recherche. Je mentionne le courage car je me demande encore comment as-t-il pu faire pour ne pas perdre espoir face à certaines questions de néophyte que j'ai pu lui poser ! Ainsi, je tiens à le remercier pour ces choses-là mais aussi pour la confiance et la liberté qu'il a su m'accorder. J'ai encore du mal à imaginer comment je vais pouvoir m'en sortir par la suite car il est devenu bien plus qu'un directeur de thèse. J'ai beaucoup aimé apprendre à ses côtés et espère, si la chance m'en est donné, transmettre à mon tour ce qu'il m'a appris (tout en restant bien bien souple !). Je finirai ce paragraphe en perpétuant la tradition en citant le dicton favori de Thierry qu'on apprécie dire en équipe le vendredi après-midi autour d'un bon verre de rhum, « On ne fait pas un métier facile tous les jours » (Gaudosome et al., 1873).

En parlant d'équipe, je remercie toute l'équipe SiCE qui est tellement « So SiCE », les discussions scientifiques à la fraiche (« ou pas ») du lundi matin, les repas chez TG, les BBQ chez Zorg, les apéros chez Yvon, j'en passe et des meilleures… J'espère que perdurera l'entraide au sein de l'équipe et remercie à cette occasion, Laia, Mathilde, Mar, Lise et Mehdi pour leur aide précieuse. J'aimerais remercier plus précisément la « ROP » loveuse de l'équipe Christine (aka kikouette) pour les longues discussions et réflexion. Mais aussi Vince pour m'avoir transmis ses talents de microscopiste et pour finir Laia pour avoir pris le soin de relire l'ensemble ma thèse.

Il est maintenant temps de parler du cadre exceptionnel dans lequel j'ai eu la chance d'évoluer, la grande famille RDPienne ! Le RDP a été pour moi ma première expérience en laboratoire et ne peux donc pas avoir d'élément de comparaison. Cela étant, il ne m'a pas fallu beaucoup de temps pour comprendre dans quel endroit j'étais tombé. Le RDP, c'est bien plus qu'un laboratoire, c'est bien plus que du développement, c'est bien plus que de la reproduction. C'est aussi des instants foyers, des repas de noël, d'innombrables pots, de multiples skiminars mais surtout des gens d'exceptions. Cette cohésion durant ces années a été une réelle chance et a participé à entretenir ma motivation chaque jour ! A travers tous ces moments j'ai vécu de beaux instants et rencontrer des amis, Léo, Steven et Jo.

Une thèse ça ne se fait pas sans avoir de quoi penser à autre chose pour se changer l'esprit. A ce compte-là, je remercie tous les membres du groupe des « The Broken Teeth », Nico, Ruby et Vicky ! Nos répétitions assidues nous ont mené au top du top de la scène pop Lyonnaise :-P. Single bientôt dispo « Chez martine » la disquaire d'Oullins et chez Gilbert Joseph ! Et bien sûr dans ce paragraphe musical, je ne peux inévitablement pas oublier Ringo, qui est un bassiste de talent et avec qui j'ai eu l'immense privilège de jouer durant maintenant 10 ans (it's been a long time bro !). Je tiens aussi à adresser mes remerciements à des objets car ils ont fait partie de l'équilibre qui m'a permis de mener cette thèse jusqu'à la fin. Mais aussi ils m'ont permis (« de force ») de faire des pauses plus ou moins prolongées durant ma thèse. Dans l'ordre chronologique, je pense à mon skate longboard, deux semaines d'arrêt pour un coude cassé, mon snowboard, un mois et demi d'arrêt pour une

clavicule cassée et pour finir mon vélo, quelques jours d'arrêt pour une omoplate/scapula cassée.

Bien entendu, je ne peux pas faire de remerciements sans m'adresser à ma famille. Rétrospectivement, au début, j'ai eu l'impression qu'ils ne comprenaient pas vraiment les raisons pour lesquelles je m'engageais dans cette aventure mais cela sans même faire oscillé leur soutien. Au fur et à mesure que le temps avançait et voyant que cela m'épanouissait, ils ont bien entendu trouvé raisons malgré l'obscurité que peut leur évoquer le but de mes recherches. Je voudrais plus particulièrement, remercier mes parents, Isabelle et François, qui ont toujours cru en moi, soutenu dans les moments difficiles et toujours su agir, selon moi, en parent exemplaire. Je pense aussi à ma sœur, Emmanuelle, mon frère, Hugo, mes grands parents, Louis et Marcelle ainsi qu'à mon oncle, Hervé. Dans ce paragraphe, je voudrais aussi m'adresser à mes amis de longue date. Plus spécialement, je voudrais remercier Thomas, Jean et Jean-Baptiste qui ont été des personnes sur lesquelles j'ai pu compter durant cette expérience et je leur signifie ici ma reconnaissance. Ringo, Simon, Damien, Lucie, Bertrand, Pierre, Paul, Thomas, François, Samy qui ont toujours étaient là pour me changer les idées. Je voudrais remercier des gens qui m'ont accompagné au jour le jour durant la rédaction de ma thèse. Leur tâche n'a pas dû être évidente à certain moment, s'échinant à rendre la mienne plus paisible. Je pense à mes super colocs, Mary, Mehdi, Thibault et Karim ainsi qu'à ma Jeannette la plus chouette.

Pour conclure, je garderai un très bon souvenir de ma thèse pour de multiples raisons. Les plus évidentes sont : l'aboutissement de nombreuses années de travail et le « début de la fin » de la formation scientifique :-P. Mais celles-ci ne sont pas des plus essentielles. La thèse c'est avant tout une vraie expérience de vie. A travers elle, on apprend à acquérir une certaine rigueur, à se tromper, persévérer mais aussi confronter ses idées ou ses convictions et à les étayer. On apprend aussi à interagir avec autrui, les écouter, réfléchir et bâtir des choses ensemble. Selon moi, cette interaction et cette construction constituent l'essence même de la science. De manière antagoniste, on comprend aussi que nous sommes le seul acteur de notre propre sujet. Bien que les discussions et les échanges soient centraux ce qui compte *in fine* c'est l'expérience. Et seul l'expérimentation fait avancer notre sujet, « Parce que c'est notre SUJET » (Macron et al., 10 décembre 2017). Comme vous l'aurez compris

précédemment une thèse ce n'est pas que la science, j'en garderai un très bon souvenir par l'ensemble des moments vécus et des personnes qui m'ont entouré au RDP mais pas seulement. Affectueusement, merci à tous !

Je dédicace ma thèse à tous les gens que j'aime.

L'imagination est plus importante que le savoir. Le savoir est limité alors que l'imagination englobe le monde entier, stimule le progrès, suscite l'évolution.

« What Life Means to Einstein », George Sylvester Viereck, *The Saturday Evening Post*, 26 October 1929, p. 17 »

Préambule

Ma thèse se compose en trois parties :

A. Introduction

B. Résultats

C. Discussion et perspectives

L'introduction fait l'état de l'art du maintien et du rôle du champ électrostatique membranaire dans l'organisation de la cellule eucaryote. Cette propriété membranaire a été le support de mes travaux de thèse liant les trois chapitres de la partie résultats. Les deux premiers chapitres décrivent l'organisation du champ électrostatique dans la cellule végétale et son maintien par les lipides anioniques. Le troisième chapitre fait l'objet d'une introduction portant sur la voie de signalisation « non génome » de l'auxine. En effet, cette propriété membranaire s'est révélée être centrale dans la transduction du signal auxinique. Le premier chapitre ayant donné lieu à une publication, par soucis d'homogénéité ma thèse est ainsi rédigée en anglais.

A. INTRODUCTION

ABA	Abscisic acid
AFB	AUXIN SIGNALING F-BOX
AKT	PROTEIN KINASE B
ALA	AMINOPHOSPHOLIPID TRANSLOCASE
ALPS	Amphipathic lipid packing sensor
AP	ADAPTATOR
Arf	ADP-ribosylation factor
Arl	ADP-ribosylation factor-like
ASM	ACID SPHINGOMYELINASE
ATP	Adenosine triphosphate
BFA	Brefeldin A
C2LACT	C2 Lactadherine
CDC	CELL DIVISION CONTROL
CDP-DG	CYTIDINE DIPHOSPHATE DIAGLYCEROL
CDS	PHOSPHATIDATE CYTIDYLTRANSFERASE
CLC2	CLATHRIN LIGHT CHAIN 2
DGK	DIACYLGLYCEROL KINASE
DNF	DRS2 NEO FAMILY
DRM	Detergent resistant membrane
DRP1	DYNAMYN RELATED PROTEIN 1
DRS2	DEFICIENCY OF RIBOSOMAL SUBUNITS
ED	Electrostatic domain
EE	Early endosomes
ER	Endoplasmic reticulum
EVCT2	EVECTIN 2
FAPP1	FOUR PHOSPHATE ADAPTOR PROTEIN 1
GEF	Guanine nucleotide exchange factors
FKBP	FK506 binding protein
FM4-64	N-(3-Triethylammoniumpropyl)-4-(6-(4-(Diethylamino)Phenyl)Hexatrienyl)pridinium dibromide
FRB	FKBP-rapamycin binding
FRET	Förster resonance energy transfer
GAP	GTPase-activating proteins
GCS1	GROWTH COLD SENSITIVE 1
GDI	Guanosine nucleotide dissociation inhibitor
GDP	Guanosine diphosphate
GIPC	Glycosyl Inositol Phospho Ceramides
GPI	Glycosylphosphatidylinositol
GTP	Guanosine triphosphate
HRV	Hyper variable region
INPP5E	INOSITOL 5 POLYPHOSPHATASE PHOSPHATASE
K-Ras	V-KI-RAS2 KIRSTEN RAT SARCOMA VIRAL ONCOGENE HOMOLOG
KA1	KINASE ASSOCIATED DOMAIN 1

KAT	KATANIN
LE	Late endosome
MARCKS	MYRISTOYLATED ALANINE-RICH C-KINASE SUBSTRATE
MD	Molecular dynamics
MSC	Membrane surface charge
MT	Microtubule
MVB	Multi-vesicular body
Myr	Myristoylation
NAA	Naphthaleneacetic acid
NADPH	Nicotinamide adénine dinucléotide phosphate
Nir2	PYK2 N-TERMINAL DOMAIN-INTERACTING RECEPTOR
ORP	OSBP-RELATED PROTEIN
OSBP	OXYSTEROL BINDING PROTEIN
OSH	OXYSTEROL BINDING PROTEIN HOMOLOGUE
P4MSidM	PI4P binding of SidM
PA	Phosphatidic acid
PAH	PHOSPHATIDIC ACID HYDROLASE
Palm	Palmytoylation
PAT	PROTEIN S-ACYL TRANSFERASE 4
PBR	Polybasic region
PC	Phosphatidylcholine
PCs	Pavement cells
PDE	RETINAL ROD RHODOPSIN cGMP 3',5'-CYCLIC PHOSPHODIESTERASE SUBUNIT DELTA
PE	Phosphatidylethanolamine
PH	Pleckstrin homology
PIN	AUXIN EFFLUX CARRIER
PIP	Phosphatidylinositol phosphate
PIP2	Phosphatidylinositol biphosphate
PIP3	Phosphatidylinositol triphosphate
PIS	PHOSPHATIDYLINOSITOL SYNTHASE
PKC	PROTEIN KINASE C
PLC	PHOSPHOLIPASE C
PLD	PHOSPHOLIPASE D
PM	Plasma membrane
Pre	Prenylation
PS	Phosphatidylserine
PSD	PHOSPHATIDYLSERINE DECARBOXYLASE
PSS	PHOSPHATIDYLSERINE SYNTHASE
PVC	Prevacuolar compartment
RE	Recycling endosomes
RHD4	ROOT HAIR DEFECTIVE MUTANT 4
RIC	ROP INTERACTIVE CRIB MOTIF-CONTAINING PROTEIN4

Rin	RIC-LIKE IN NEURONS
Rit	RIC-LIKE EXPRESSED THROUGHOUT THE ORGANISM
RLK	RECPETOR-LIKE KINASE
ROP	RHO OF PLANT
Sac	SUPPRESSOR OF ACTIN
Scr	SARCOMA
Sec14	SECRETORY PROTEIN 14
SM	Soluble membrane
SPK	SPIKE
SptPALM	Single particule tracking photo activated localization microscopy
TAG	Triacylglycerol
TAGL	TRIACYLGLYCEROL LIPASE
TGN	*trans*-Golgi network
TIRF	Total internal reflexion microscopy
TIR	TRANSPORT INHIBITOR RECEPTOR 1
TMK	TRANSMEMBRANE KINASE
TOR	TARGET OF RAPAMYCIN

A. INTRODUCTION

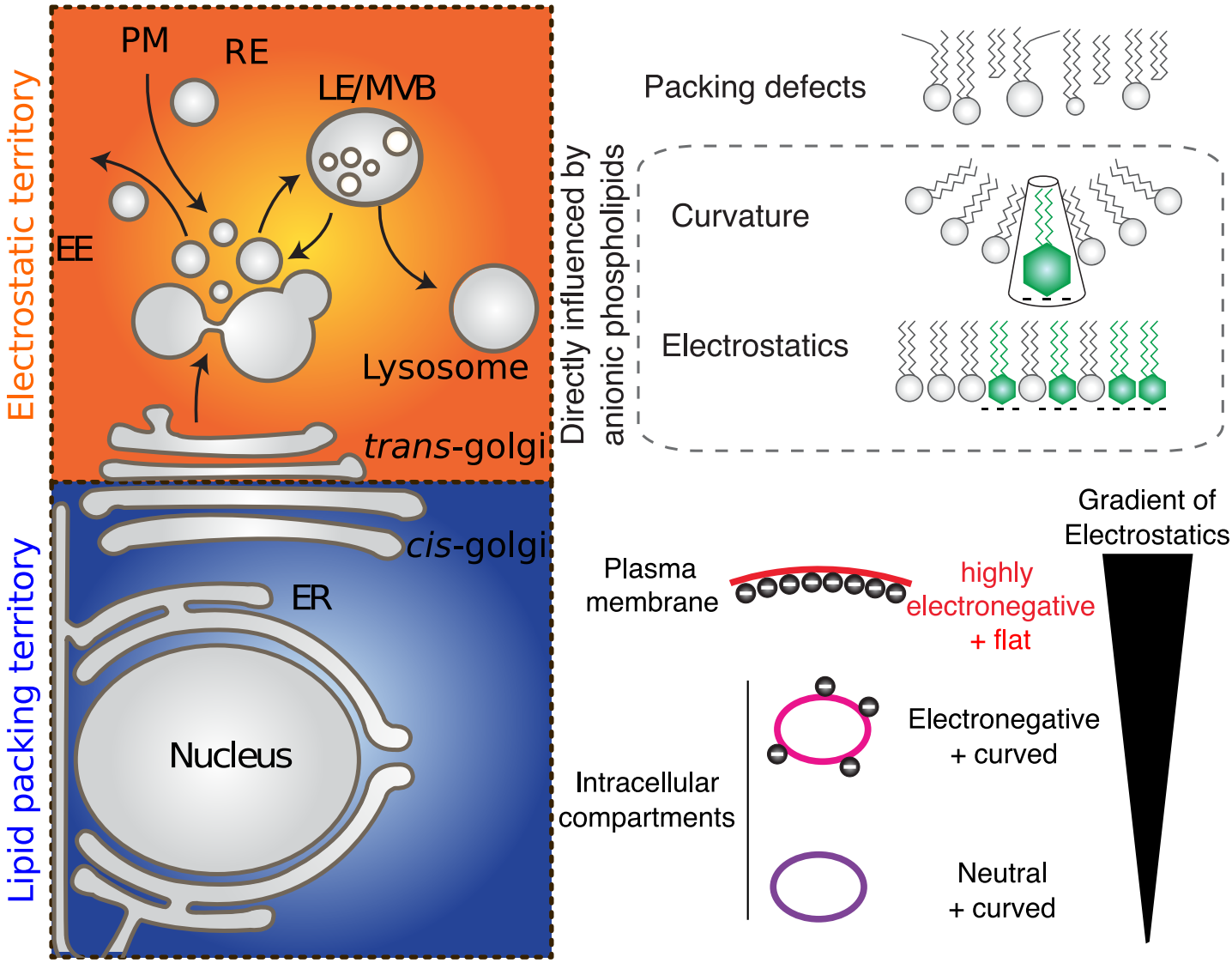

Figure 1. Cellular organization dictated by lipid biophysical properties. **A.** Schematic representation of an eukaryotic cell divided in two main lipid territories. PM: plasma membrane, EE: early endosomes, RE: recycling endosomes, LE/MVB: late endosomes/multi vesicular bodies, ER: endoplasmic reticulum. **B.** Membrane physicochemical properties may be conceptualized in three main categories including lipid packing defects, curvature and electrostatics. The latter two are directly influenced by anionic phospholipids. **C.** Schematic representation of the electrostatic territory, which includes membranes with varying degree of negative surface charges, the highest being at the PM. The triangle indicates the concentration gradient of the electrostatic field.

I. General introduction on the electrostatic field

A wide range of processes, including endocytosis, exocytosis and signaling occur at the cell surface through the reversible association of proteins from the cytosol. Some rare lipids are enriched in specific compartments and thereby contribute to the identity of cell organelles by acting as biochemical landmarks. Lipids also influence membrane biophysical properties, which emerge as an important feature in specifying cellular territory. Such parameters are crucial for signal transduction. In broad terms, eukaryotic cellular membranes can be categorized in two main territories: a territory of loose lipid packing that corresponds to ER-derived organelles and an electrostatic territory that specifies post-Golgi membranes (Bigay and Antonny, 2012) (Figure 1A). The cytosolic leaflet of ER derived membranes is characterized by its low electrostatic property (as the vast majority of anionic phospholipids in the ER are orientated toward the lumen) and by its high occurrence of lipid packing defects, which are promoted by unsaturated lipids and the presence of small lipid head groupe (Bigay and Antonny, 2012) (Figure 1B). By contrast, PM-derived organelles have few packing defects but are electrostatic, as they accumulate anionic phospholipids. In this electrostatic territory, anionic membranes recruit proteins with polybasic regions to the membrane surface and as such participate in the localization of a large number of cellular factors at the cell surface and along the endocytic pathway (Jackson et al., 2016) (Figure 1C).

During my PhD thesis, I studied the characteristics, properties and functions of the electrostatic territory in plants. In this introductory chapter, I will define membrane electrostatics, review how this property was studied in vivo (using the known examples in yeast and mammalian cell lines) and discuss some physiological implications of membrane electrostatics on cellular organization and cell signaling.

C-terminal modification/irreversible:

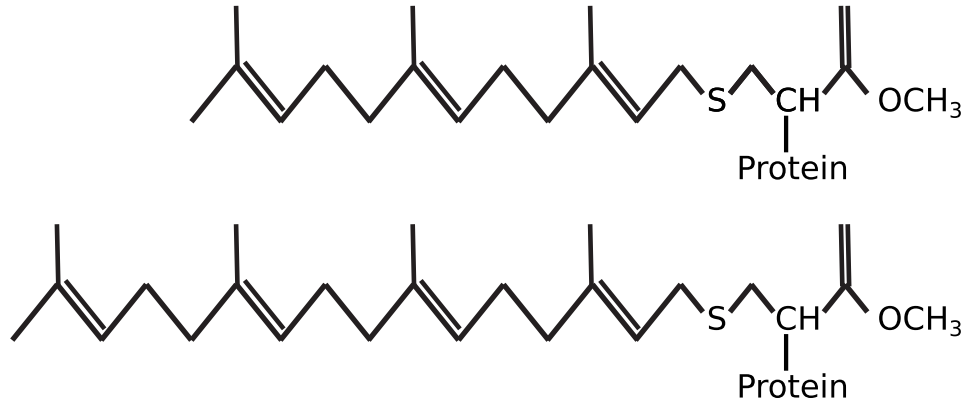

Farnesylation
e.g. K-ras4B

Geranylgeranylation
e.g. Rab GTPase

N-terminal modification/irreversible:

Myristoylation
e.g. MARCKS

Terminal or internal modification/reversible:

Palmitoylation
e.g. H-ras

Figure 2. Lipid anchors adjacent to stretch of cationic residues.

a. Definition of the electrostatic field

Association and dissociation of peripheral proteins from membranes fine-tune cellular signaling. Parameters such as hydrophobic and electrostatic interactions controlled protein-membrane association. Hydrophobic interactions are provided by the insertion of aromatic amino acids into the hydrophobic core of the lipid bilayer and by protein post translational modifications such as lipid modifications (eg. palmitoylation, myristoylation and farnesylation; Figure 2). Electrostatic protein-membrane interactions are often highly reversible compare to hydrophobic interaction. An electric potential at the inner leaflet of the plasma membrane is generated by negatively-charged phospholipids and attracts cations and proteins-containing polybasic motifs.

To be entirely clear, membrane surface charge (MSC) (also refered to as surface/electric potential or electrostatic field) and membrane potential are two different concepts. The first one refers to charge distributed within the same surface (cytosolic leaflet). Membrane potential (also refered to as transmembrane potential or membrane voltage) corresponds to the difference in electric potential across the membrane (e.g. between the inner and outer leaflet of the plasma membrane) and is mostly driven by cation pumps. I will discussed how these two concepts are linked (see section V.c) but for the rest of the introduction, I will focus on membrane surface charge of the inner, cytosol-facing, leaflet of membranes.

At the inner membrane leaflet, anionic lipids concentration determine the surface charge of the membrane. However, the effective electric potential (refered as electrostatic field) depends not only on the surface charge density but also on the concentration of counter ions in the solution. Cations (eg. K+ and Na+) are attracted to the charge surface to form a layer of positively charged ions. The consequent recruitment of cations creates the so called ion shielding effect which substantially reduces the apparent membrane surface charge. The zeta potential reflects the apparent electrostatic field (net negative membrane charge minus ion shielding; Figure 3A). The zeta potential has been investigated by physicists and is described by the Gouy-Chapman-Stern theory of the electrical double bilayer. In addition, the net electrostatic effect of a charged surface onto molecules in solution can be quantified by the Debye length, which is inversely proportional to the square root of the ionic strength of the solution. When a protein senses the

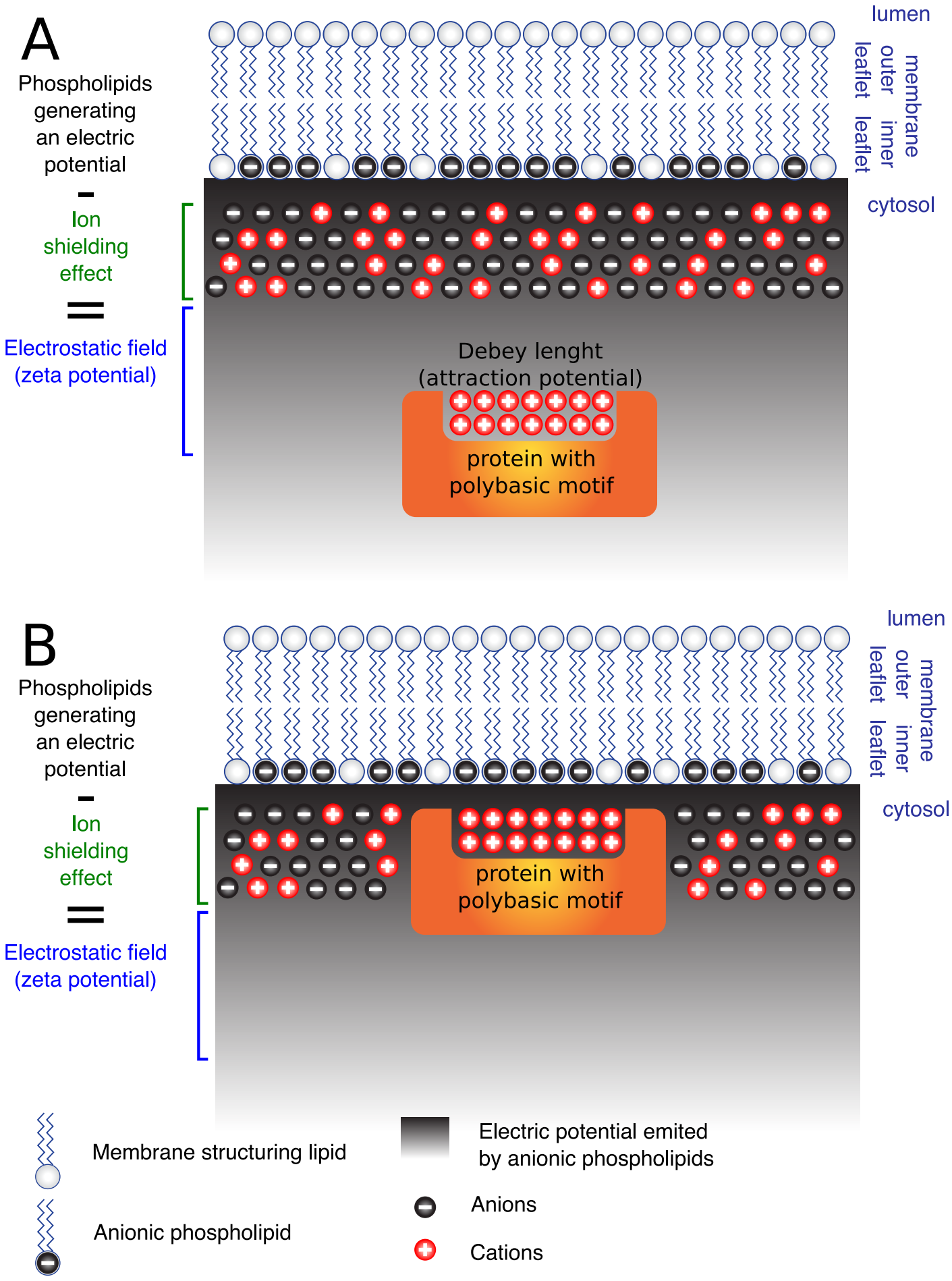

Figure 3. Schematic representation of the electrostatic field. A. Case where the cationic protein is localized in the cytosol prior to its interaction with the anionic membrane. **B.** Case where the cationic protein interacts with the anionic membrane. The electric potential emited by anionic phospholipids is represented by black-gray-white gradient. The relative strength of the ion shielding effect and of the electrostatic field is represented by the lenght of the square bracket.

zeta potential depending on its own Debey length, the protein will be attracted by the negatively charged membrane and remove the ion shield to interact directly with the membrane (Figure 3B). This theoritical framework is well understood from a physics point of view since the eighties (McLaughlin, 1989), however tools to study these properties in vivo have been developped in the past decade. Bellow, I review how membrane electrostatic properties were dissected in vivo and how these methodological developments led to the discovery of the electrostatic territory and helped to describe how this territory is established and maintained and what are its functions.

b. The membrane surface charge (MSC)

i. Principle

While the concept of MSC for protein localization was postulated long ago, tools to sense this predicted feature were only developed during the last decade via the generation of genetically encoded biosensors (sensors/probes; Figure 4A). These biosensors are based on peptides or protein domains that binds to anionic phospholipids (based on their negative charge and irrespective of their head group) and fused to a fluorescent protein. At least ten independent probes have been described to act as sensors of anionic membranes. Each one contains cationic amino acids required to interact with anionic lipids. However, purely electrostatic interactions are not sufficient for membrane binding, which often requires additional hydrophobic interactions. Hydrophobicity can be provided either by a lipid anchor or hydrophobic/aromatic residues. In the following paragraphs, I will discuss the design of some of these “electrostatic” sensors and how they were validated in vitro and in vivo.

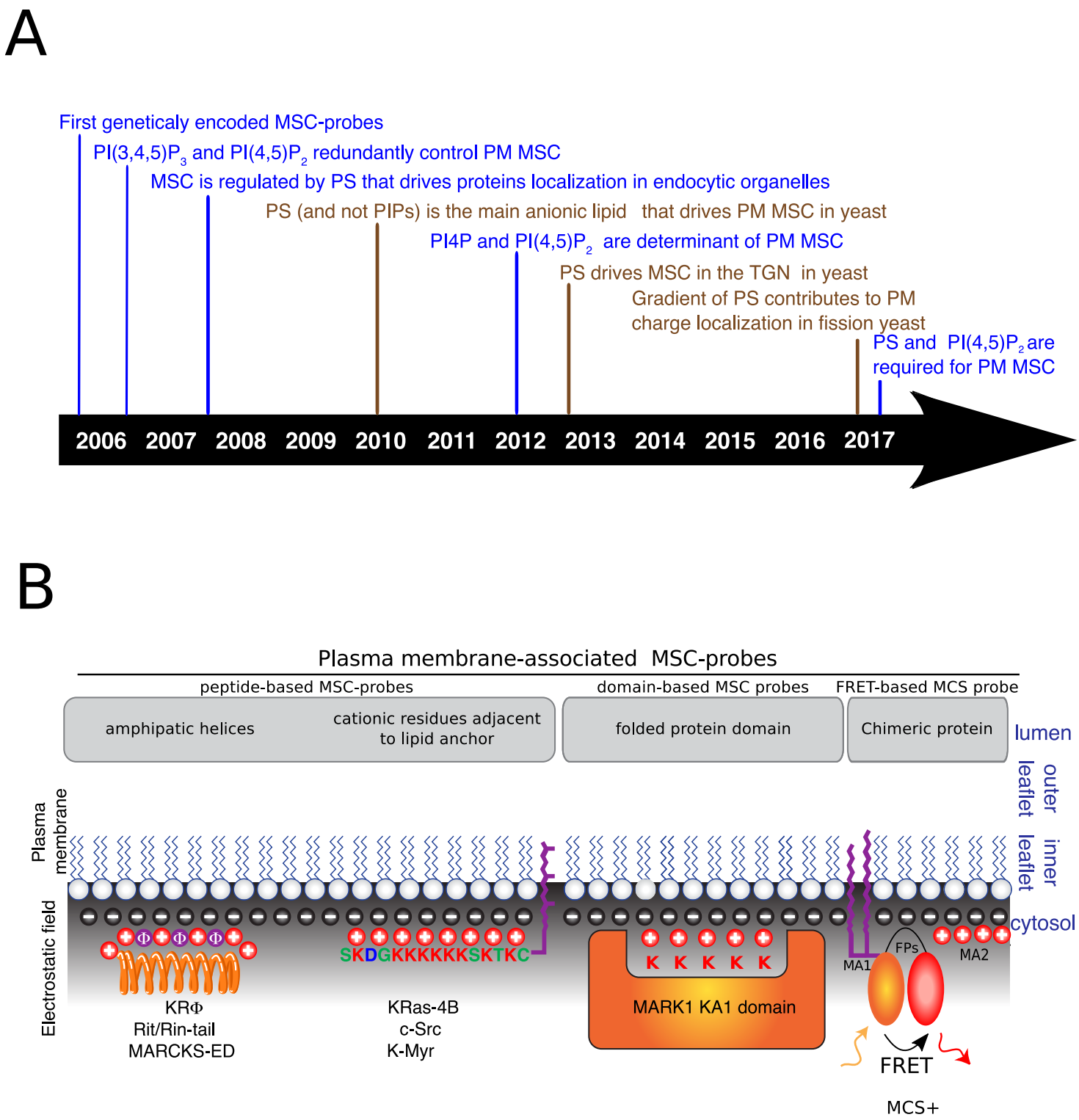

Figure 4. Tools to investigate membrane surface charge in vivo. A. Timeline showing landmark papers for the in vivo study of membrane surface charges (MSC) in various organisms. Color indicates the model system used in the study: blue, human cell lines; brown, *Saccharomyces cerevisiae*. **B.** Schematic representation of, from the left to the right, peptide-based MSC-probes, domain-based MSC-probes, FRET-based sensor. Black circles indicate negative membrane surface charges, red circles show cationic residues in MSC-probes that interact with MSC through electrostatic interactions, and purple circles indicate aromatic residues that provide hydrophobic interaction for membrane anchoring. The lipid anchor is represented in purple (for clarity only farnesylation is given as an example, but other lipid modifications have been used, such as the N-terminal myristoylation in c-Src or K-myr reporters). K-Ras4B MSC-probe corresponds to the C-terminal tail of K-Ras4B, c-Src probe corresponds to the N-terminal tail of c-Src, K-myr is a synthetic construct that has a N-terminal myristoylation adjacent to the K-Ras4B charged peptide. MSC, membrane surface charges, KA1 domain, Kinase Associated1 domain; MARK1, Microtubule Associated Regulated Kinase1; MARCKS-ED, Myristoylated Alanine-Rich C Kinase Substrate-Effector Domain; FRET, Förster resonance energy transfer; MCS+, Membrane Charge sensor +; MA, Membrane Attachment. Adapted from Platre and Jaillais, 2017.

ii. Tools to investigate PM surface charge

Peptide-based MSC sensors: The first type of peptide-based MSC sensor was described by Yeung et al., and is composed of a polybasic peptide containing a signal for lipid anchoring. It includes, the N-terminal tail of c-Src (Nt-Src), the C-terminal tail of *V-Ki-ras2 Kirsten rat sarcoma viral oncogene homolog* (K-Ras tail), the polybasic region of K-Ras containing a signal for myristoylation (myr-K), a mutated version of K-Ras tail to prevent serine phosphorylation (K-pre) and a K-pre version where every lysine is replaced by arginine (R-pre)). These probes are based on the N- or C-terminal tails of small GTPases or kinases. The lipid anchor can be either in N-terminal (e.g. Nt-Src, myr-K-) or C-terminal (e.g. K-Ras tail, K-pre, R-pre) and the polybasic region (PBR) contains from 6 to 8 cationic residues (i.e. either lysines (K) or arginines (R); Figure 4B).

The second peptide-based MSC sensor is composed of a PBR in conjugation with hydrophobic amino acids (W, Y, L, F). This includes, the synthetic sequence (KRϕ), the C-terminal tail of the small GTPases ric-like in neurons (Rin) and ric-like expressed throughout the organism (Rit) and the myristoylated alanine-rich C-kinase substrate electrostatic-domain (MARCKS-ED)). These peptides form an amphiphathic helix required for membrane interaction (Figure 4B).

Domain-based MSC sensors: The KA1 membrane-associated domain binds acidic phospholipids without discrimination. This is the first domain known to bind unselectively anionic phospholipids. Structure of beta and alpha helix is crucial for binding as well as cationic residues associated with the helices (Figure 4B).

FRET MCS sensor: This sensor was named, MCS+ for membrane charge sensor +, and is based on Förster resonance energy transfer (FRET). This sensor is composed of three main region: a first part (MA1) is a membrane attachment unit (myristoylation and palmitoyltion lipid anchors) that allows the anchoring of the sensor to the plasma membrane (PM) independently of its electrostatic field. A second part (FPs) is made of two fluorescent proteins, mVENUS (a yellow FP variant) and mCHERRY (a red FP variant) to quantify the energy transfer. A third part (MA2) corresponds to the entity which sense the electrostatics field and that is a synthetic PBR region,

which is loosely inspired by the C-terminal tail of K-Ras. The principle is the following: in the case of a low electrostatic field at the PM, the MA2 part will be less associated with the PM and consequently the FRET signal will be decreased due to a higher average distance between the two fluorescent proteins in the FPs part. Inversely, in case of high electrostatic field, the MA2 will be more associated with the PM resulting in the emission of higher FRET signal due to a close proximity of the two fluorescent proteins. This MCS+ sensor has the advantage to be quantitative and more sensitive than the previously described probes (as it can report changes of 10 to 20% of the PM electrostatic field). However, the design of such probe first requires to know which membrane is electronegative (as it required the membrane targeting MA1 anchor). In this case, the PM was first determined to by highly electronegative (thanks to the reporters described above), which then allowed the rational design of the FRET-based reporter. Therefore, these tools are complementary, with the direct reporter binding (peptide and domain based reporters) being important to map membrane electrostatic properties within the cell and quantitative reporters (here FRET-based reporter) to explore more physiological changes within a membrane (note that this remark is valid for the study of the electrosatic field, but also to study other membrane parameter such as local lipid enrichment; Figure 4B).

Membrane integrity sensors: A way to investigate anionic phospholipids participation in MSC is to modulate lipid pools. However, lipids are crucial for membrane organization. Studying membrane surface charge therefore requires a number of controls to verify that lipid modification does not have unwanted side effects on membrane integrity and other non-targeted lipids. Such controls include monitoring the localization of PM proteins that are not targeted to membrane based on electrostatic interactions. These controls will thereafter be referred to as “membrane integrity sensors” and include both integral transmembrane and lipid anchored proteins, that resides in both the raft and non-raft fraction of the PM. For example, the C-terminal tail of N-ras is used as a marker of non-lipid raft portion of the membrane, while glycosylphosphatidylinositol (GPI) and H-ras are used as raft resident proteins and the transmembrane of GT46 protein as a non-diffusive PM protein.

c. The plasma membrane is the most ionic compartment in eukaryotes

Even though the above-mentioned probes have different mechanistic anchoring and present some variation in their net positive charges (from 5 to 13 positive charges), each individual probe interacts in vitro with anionic phospholipids.

When fused to a fluorescent protein, these probes label strictly the plasma membrane in all eukaryotic cell types analyzed including yeast, and animals (Hammond et al., 2012; Heo et al., 2006; Moravcevic et al., 2010; Yeung et al., 2006, 2008) (Figure 5). This common feature highlights a unique signature of the plasmalemma as the most anionic compartment in the cell versus intracellular membranes. However what are the lipids that powers this high PM electrostatic field in different organisms?

d. Anionic phospholipids present in the inner leaflet of cellular membrane

i. Phosphatidylinositol phosphates, phosphatidic acid and phosphatidylserine are anionic lipids presenting different charges and concentration in cellular membrane

Most phospholipids are zwitterionic, meaning that they form a dipole with both positive and negative charges and that their overall charge at physiological cytosolic pH is neutral. These lipids, are often referred to as structural lipids, and they form the bulk of plasma membrane phospholipids (which themselves corresponds to about 30% of total PM lipids), with phosphatidylcholine (PC) and phosphatidylethanolamine (PE) representing up to 50% and 35% of plasma membrane phospholipids, respectively. However, as aforementioned, negative charges at the membrane are carried by anionic phospholipids. By contrast to zwitterionic phopholipids, anionic phospholipids contain a negatively charged head group, the negative charges being notably carried by phosphate groups. From the least to the most anionic phospholipids, we find phosphatidylserine (PS) and phosphatidylinositol (PI) (1 negative charge), phosphatidic acid (PA,

A

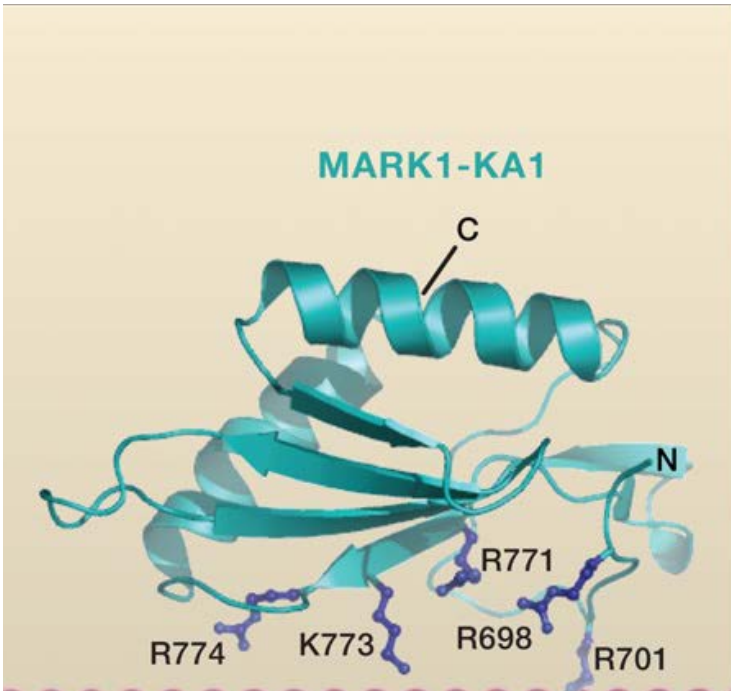

B

Mammalian Cell
(Human)

Yeast Cell
(*Saccharomyces cerevisiae*)

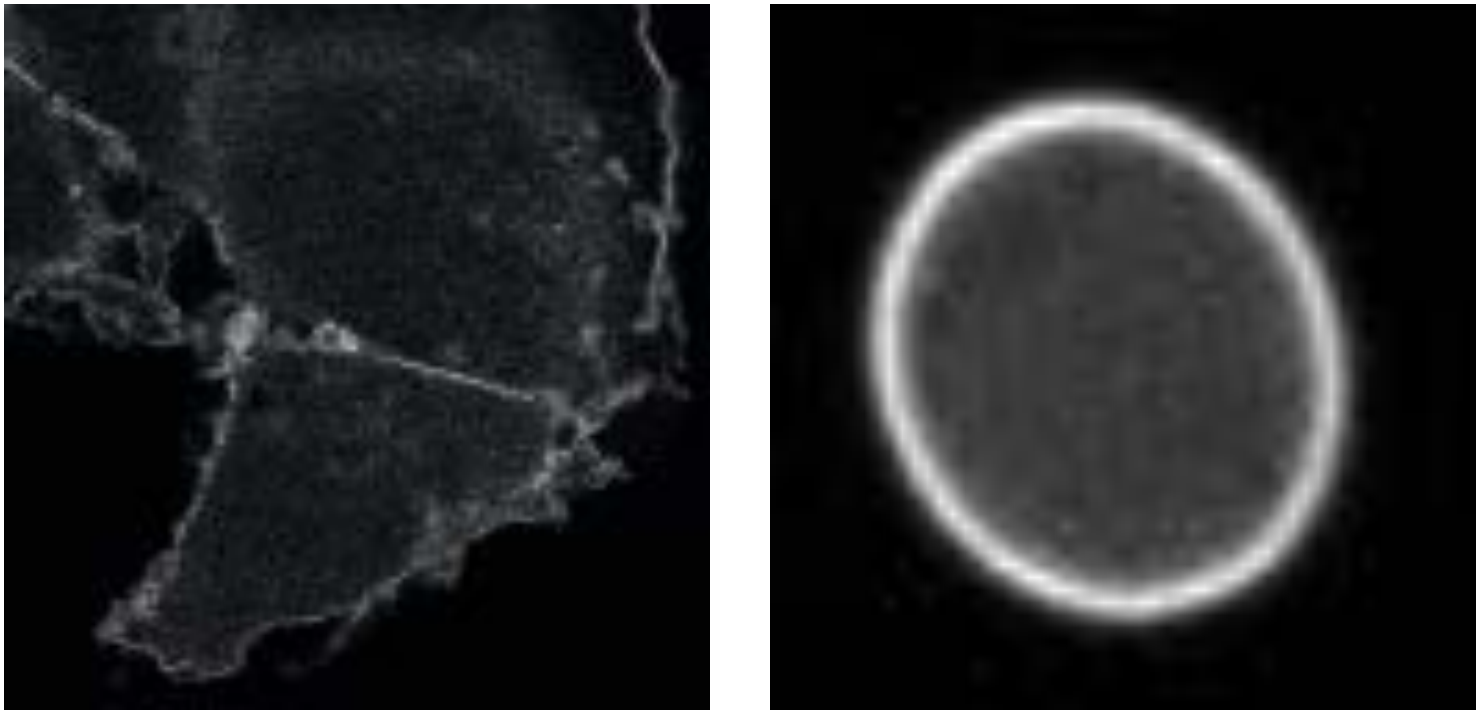

KA1^{MARK1}

Figure 5. The plasma membrane is the most anionic compartment regarding membrane surface charge sensors. A. Structure of Kinase associated-1 domain (KA1) from MAP/microtubule affinity-regulating kinase 1 (MARK1). Residues involved in membrane binding are labeled and depicted as ball and stick. **B.**Confocal pictures showing the localization of the KA1 domain of MARK1 in human fibroblast cells (left), S. cerevisiae (right). KA1 is a domain that interacts with all negatively charged lipids and therefore acts as a sensor of membrane electrostatics (so called MSC -probe). Pictures of fibroblasts are from Hammond et al. 2012 and yeast from Simon, Platre et al., 2016.

2 negative charges), and phosphoinositides (phosphatidylinositol phosphates or PIPs from 3 to 7 negative charges; Figure 6B). Concerning PIPs, the more the inositol ring is phosphorylated, the more negatively charged the lipid is. Consequently, a phosphatidylinositol 3,4,5,-trisphosphate ($PI(3,4,5)P_3$, overall charge -7) is more charged than a phosphatidylinositol 4,5,-bisphosphate ($PI(4,5)P_2$, overall charge -5), which is itself more anionic than phosphatidylinositol 4-phosphate (PI4P, overall charge -3). Anionic lipids contain different negative charges, but their concentration in cell also differ. In human erythrocyte, PIPs represent about 0.1% of total lipids (0.05% of $P(4,5)P_2$, 0.05% of PI4P and less than 0.005% of other PIPs), PI about 1%, PA about 1.5% and PS about 8.5% (Figure 6B). In budding yeast, PA is the most abundant phospholipid representing about 12%. PI is about 3%. PI4P and PI(4,5)P2 are the two most abundant PIPs close to 5% of total PIs (which are approximately 10–20% of total glycerophospholipids) (Payrastre et al., 2001). PS accounts for 1.5% of total lipids. However, PS concentration have a high propensity to fluctuate depending on growth phase and environmental conditions, reaching about 7% in media supplemented with different source of carbon such as glucose (Klose et al., 2012).

Because anionic phospholipids have different net negative charges, but also accumulate at different levels, it is difficult to predict a priori, which lipids will contribute significantly to the membrane electrostatic field. For example, PS is the most abundant anionic lipid in animal cells, but its charge is only -1, while $PI(3,4,5)P_3$ is present at far lower concentration (0.0001% of total lipids) but is highly electronegative (-7). Which one is more likely to contribute to membrane electrostatics? Given the set of numbers I introduced in the previous paragraph (Figure 6B), one would assume that PS should be a major contributor as compared to $PI(3,4,5)P_3$, since it is present almost four order of magnitude higher than PIP_3. However, these set of numbers may be deceiving because I presented bulk lipid measurements, which does not take into account the local lipid enrichment and their position in the inner (cytosolic) or outer (luminal/extracellular) membrane leaflets. Indeed, only PS present at the PM inner leaflets is relevant for PM electrostatics, while bulk measurements also include PS molecules that are present in luminal/outer membrane leaflet and organelle membranes (e.g., mitochondria). In addition, while PIP_3 molecules are rare, they may be clustered and thereby form patches of highly electrostatic

A

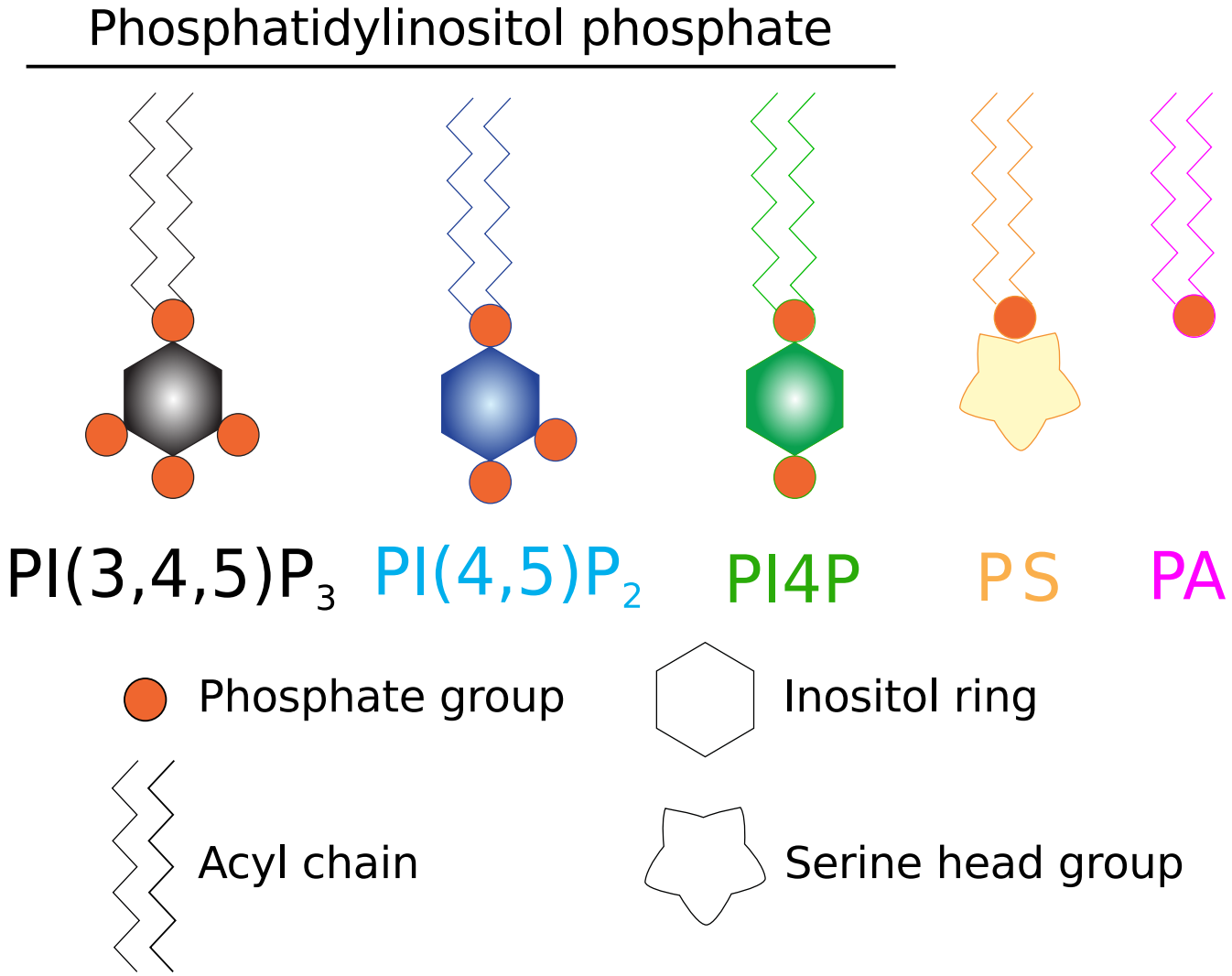

B

Lipid species	PS	PA	PI	PIPs	
				PI(4)P	PI(4,5P$_2$
Total lipid (%) Erythrocytes	8.5%	1.5%	1%	0.05%	0.05%
Total lipid (%) Yeast	1.5-7%	12%	3%	0.5%	0.5%
Negative charge(s)	1	2	1	3	4

Figure 6. Structural organisation of anionic lipids and their concentration in cellular membranes.

membranes. To conclude, while the number presented in Figure 6B are informative, they do not bypass the requirement to experimentally analyze the subcellular localization of each individual lipid species and their respective role in membrane electrostatics.

ii. Regulation, turnover and localization of anionic phospholipids in yeast and mammals

1. Phosphatidylinositol (PI) and phosphatidylinositol phosphates (PIPs)

Phosphatidylinositol phosphates (PIPs) possess an inositol ring facing the cytosol that can be phosphorylated and dephosphorylated in position 3, 4 and 5 by appropriate kinases or phosphatases. This property can give rise up to seven PIP species including phosphatidylinositol monophosphate (PI(3)P, PI(4)P, PI(5)P), phosphatidylinositol biphosphate ($PI(3,4)P_2$, $PI(3,5)P_2$, $PI(4,5)P_2$) and phosphatidylinositol triphosphate $PI(3,4,5)P_3$. PIPs derive from phosphatidylinositol (PI) that is generated facing the cytosol in the endoplasmic reticulum (ER) for de novo synthesis by phosphatidylinositol synthase (PIS) from CDP-diacylglycerol and L-myo-inositol or by sac1 phosphatase from PI(4)P, in yeast and mammals (A) (Figure 7A) (Bochud and Conzelmann, 2015). The PIS enzyme localizes in the ER and in an ER-derived highly mobile “organelle” that may serve as a dynamic PI distribution device to several organelles (Kim et al., 2011). PI is then distributed throughout the cell presumably by several PI transfer proteins (PITPs) and possibly via vesicular trafficking (Figure 7B). In particular, PI is extracted from the ER at membrane contact sites by PI transfer protein such as secretory protein 14 (sec14) or Pyk2 N-terminal domain-interacting receptor 2 (Nir2) to reach *trans*-golgi network (TGN) or the plasma membrane, respectively (Bankaitis et al., 2010; Kim et al., 2015). Sec14 exchanges PI from the ER to *trans*-golgi network and in counterpart exchanges PC located at the TGN to the ER, while Nir2 exchange PI from the ER to the plasma membrane and phosphatidic acid (PA) in the way back (PM -> ER)[12,13] (Figure 7C; Bankaitis et al., 2010; Kim et al., 2015). PIPs can be transported through the cellular membrane by regular trafficking such as endocytosis or exocytosis (Balla, 2013). Depending on the location and enzymatic specificity for a given PIP

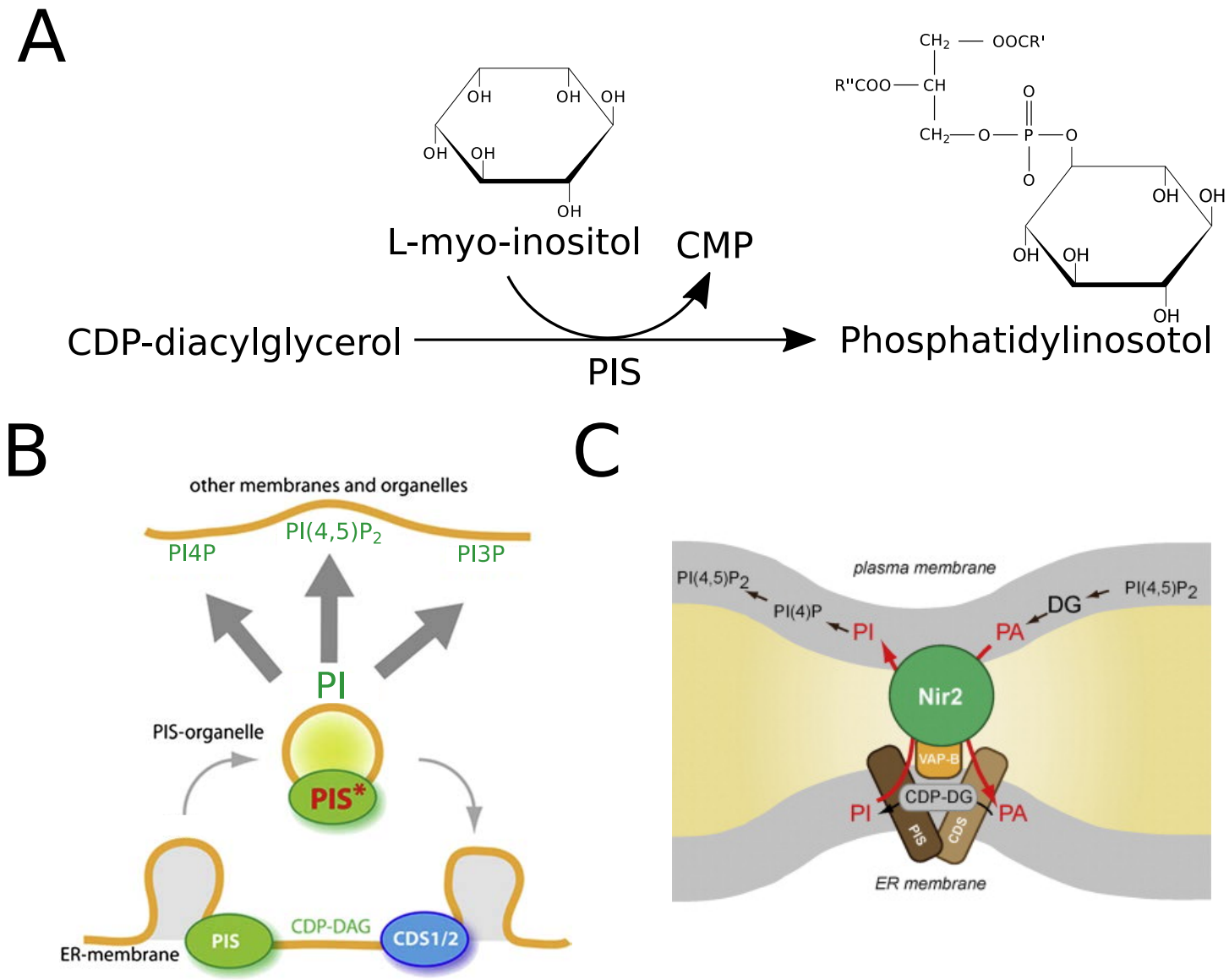

Figure 7. Phosphatidylinositol, synthesis and regulation. A, Biosynthesis pathway for phosphatidylinositol generation. **B,** Representative scheme showing the subcellular trafficking of phopshatidylinositol in order to produce phosphatidylinositol phosphate at different subcellular compartments, adapted from Kim et al., 2011. **C,** Representative scheme of the PI/PA countertransport between the endoplasmic reticulum (ER) and the plasma membrane (PM), adapted from Kim et al., 2015. PIS, phosphatidylinositol synthase; CDP, cytidine diphosphodiacylglycerol; CMP, cytidine monophosphate diacylglycerol; DG or DAG, diacylglycerol; CDS, CDP-diacylglycerol synthase; Nir2, Pyk2 N-terminal domain-interacting receptor 2; VAP-B, Vesicle-associated membrane protein-associated protein B; PI, Phosphatidylinositol; PA, phosphatidic acid; PI4P, phosphatidylinositol 4 phosphate; $PI(4,5)P_2$, phosphatidylinositol 4,5 biphosphate; PI3P, phosphatidylinositol 3 phosphate.

species, kinases and phosphatases (Mayinger, 2012) generate the large range of PIPs in different subcellular compartments (e.g. plasma membrane, early endosomes, trans-golgi network, Golgi, late endosomes and lysosomes/tonoplast). The enrichment of a PIP in a given subcellular compartment is used as a landmark for protein targeting and signaling (Platre and Jaillais, 2017) (Figure 8). The spatiotemporal PIPs dynamics is highly regulated by phosphatases and kinases and their constant interconversion confers a high potential for phosphoinositides to be involved in the regulation of membrane surface charge.

2. Phosphatidylserine

In mammals, PS is produced by two enzymes: PS synthase1 (PSS1) and PSS2. These two genes encode exchange type enzymes that generate PS by exchanging the choline or ethanolamine head group from PC or PE with a serine. PSS1 uses preferentialy PC as a substrate, while PSS2 uses preferentialy PE. While PSS1 carries the major PS enzymatic activity in cells, accounting for 60 to 70% of PS production, both enzymes are redundant and the corresponding double mutant is embryonic lethal (Sousa et al., 2013) (Figure 9B). PSS enzymes are integral transmembrane protein that localize in the ER and produce PS in the luminal leaflet (Figure 9B). Based on immunogold labelling in mammals, PS distribution differs not only among organelles but frequently also between the two leaflets of the membrane suggesting regulations by “flip-flop” mechanisms (Hankins et al., 2015). Flippases are aminophospholipid translocases that are able to transport PS, from the extracellular or the luminal leaflet of an organelle to the cytosolic side and are localized at the TGN, early endosomes and plasma membrane. Unlike flippases, which transport lipids unidirectionally, plasma membrane localized-scramblases are bidirectional and function to randomize or at least reduce the asymmetry of phospholipids in membranes and are particularly active during apoptosis and blood clotting (Hankins et al., 2015) (Figure 9C). Historically, PS was thought to follow a secretion route from the ER to the Golgi/TGN and then the PM (Figure 8). In this scenario, specific lipid flippase would flip PS either at the trans-face of the Golgi or at the PM from the outer to the inner membrane leaflet (Hankins et al., 2015). While such pathway might account in part for the cellular distribution of PS, recent work revealed that

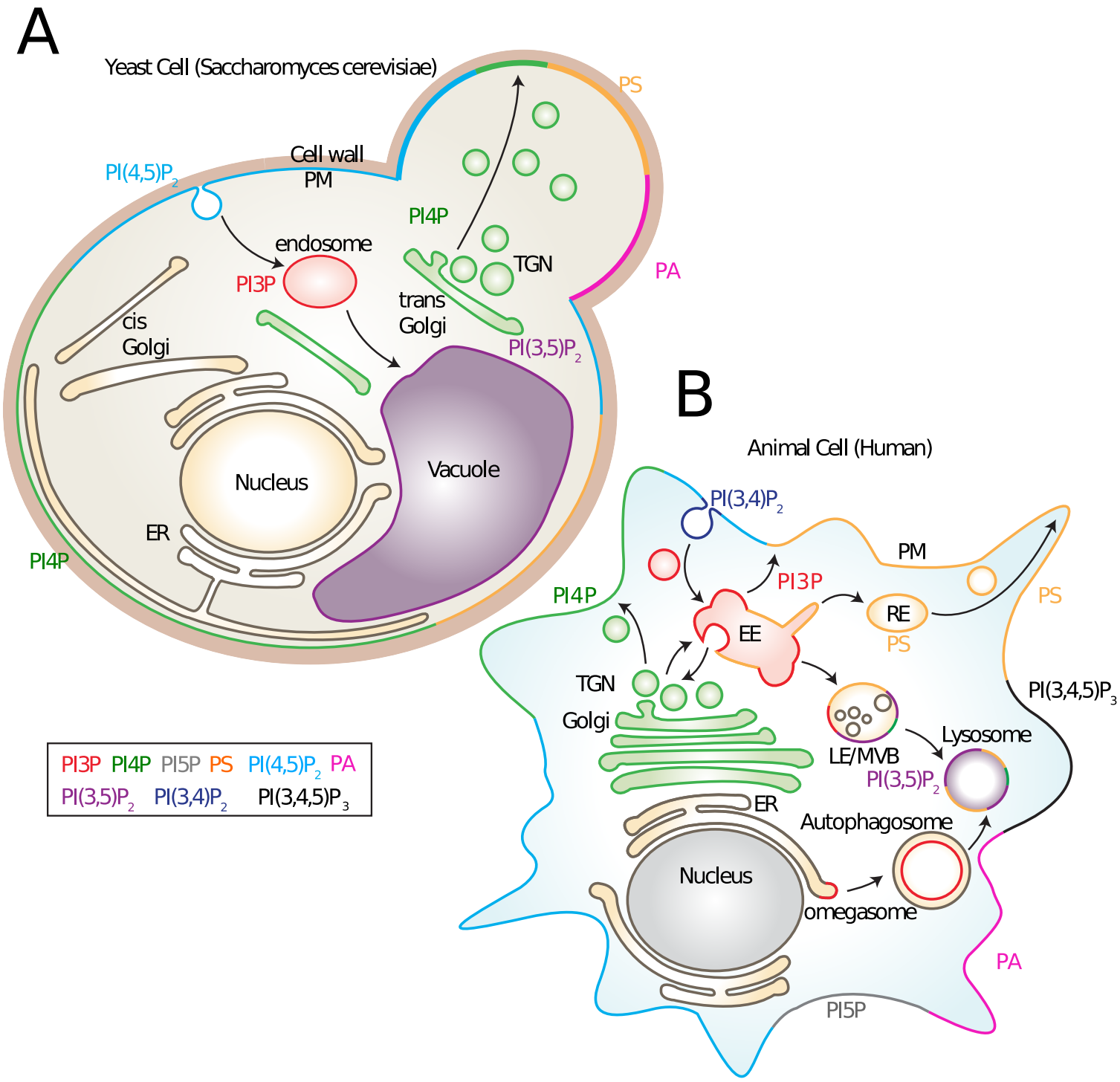

Figure 8. Summary of the subcellular localization of anionic phospholipids in yeast (A) and animal (B) cells. Note that the reported localization are not exhaustive and might vary depending on cell types or signaling activities. The cartoon representing the cell in panel B is adapted from Jean and Kiger 2012. Adapted from Platre and Jaillais, 2016.

the major pathway to bring PS at the PM is through lipid transfer at ER/PM contact sites (Chung et al., 2015; Filseck et al., 2015; Maeda et al., 2013; Sohn et al., 2016). In this later model, it is probable that PS is flipped directly at the ER before being transferred to the PM. In counterpart, PI4P is transported back to the ER from the cell surface to be degraded into PI by a phosphatidylinositol 4-phosphatase (sac1). This process links PI4P and PS metabolism in regulating its concentration to the cell surface (Figure 9D). However, the exact nature of the flippase involved is still unkown. PS production is finely tuned since PSS proteins are inhibited by their own product. This negative feedback regulation is critical for PSS1 activity and normal development. A rare genetic disease named Lenz Majewski Syndrome (LMS) is caused by gain of function mutations in PSS1 that alleviates PS-feedback inhibition of PSS1 activity. LMS syndrome is characterized by osteosclerosis, intellectual disability, characteristic facies and distinct craniofacial, dental, cutaneous and distal-limb anomalies (Sousa et al., 2013). In addition, removal of PSS1 autoinhibition alters PI4P spatial organization. In yeast, PS degradation is required to yield phosphatidylethanolamine. This reaction is catalyzed by two PS decarboxylases (PSD1 and PSD2), which are localized in the mitochondria and Golgi complex/vacuole membranes, respectively. A single gene, PSD1 has been reported in mammals and localized to the mitochondrial membrane. But, PS can also be hydrolyzed by two phospholipases (phospholipase A1 and A2) located in the plasmalemma (Leventis and Grinstein, 2010). PS high abundance and its concentration regulation between inner and outer leaflet by flippases argue for au plausible role of PS in the maintenance of the intracellular electrostatic field.

3. Phosphatidic acid

Phosphatidic acid (PA) is a backbone lipid since it is an essential substrate for enzymes participating in the synthesis of phospholipids and triacylglycerol (TAG; Figure 10A). Phospholipids generation from PA involves CDP-diacylglycerol synthase (CDS) while TAG involves PA phosphatases (PAP) enzymes (Athenstaedt and Daum, 1999). The *de novo* synthesis of PA is catalyzed by two different pathways corresponding to the Gro3P (glycerol 3-phosphate) pathway, and the GrnP (dihydroxyacetone phosphate) pathway. Two other pathways are involved

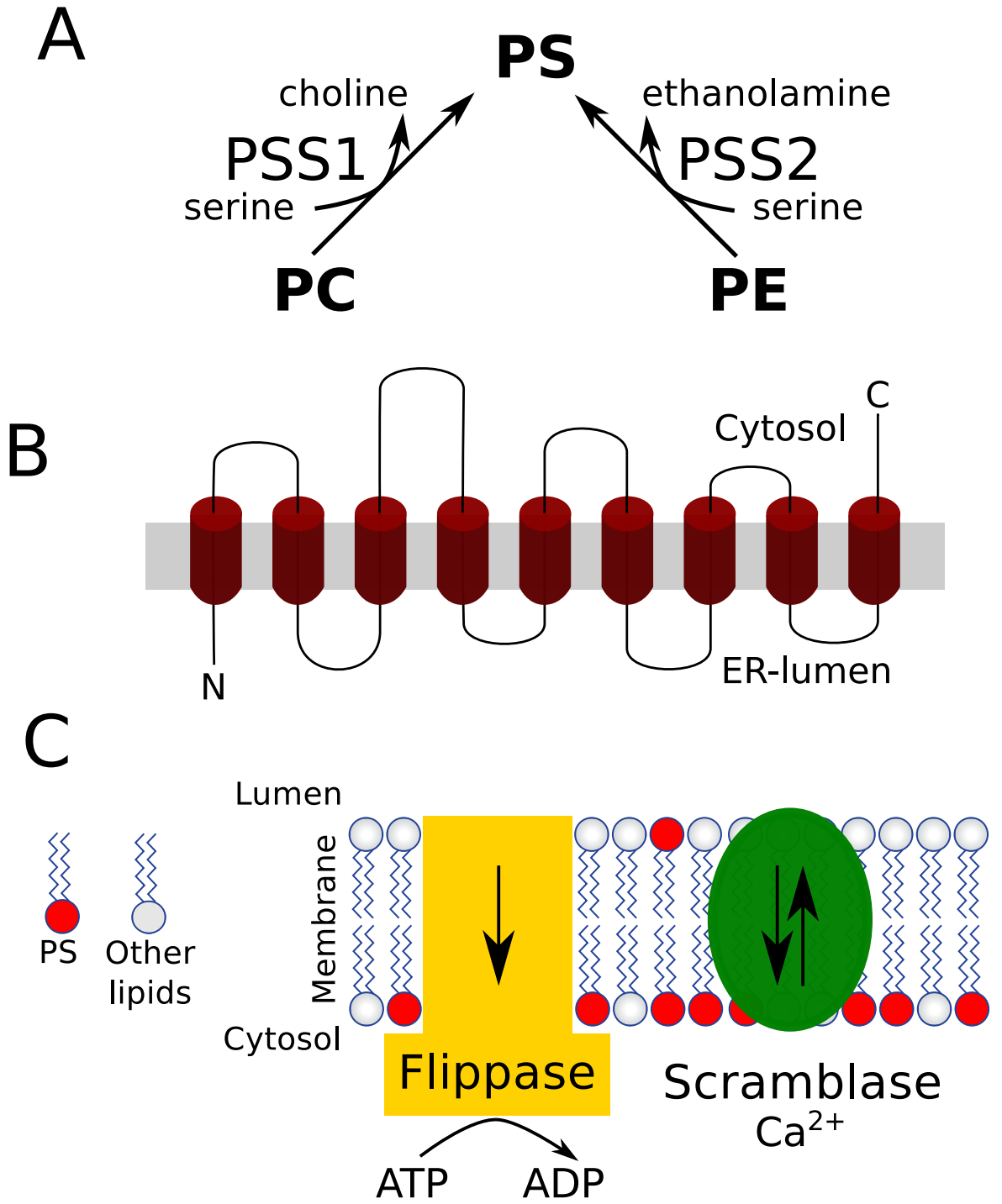

Figure 9. Phosphatidylserine synthesis and regulation. A, Biosynthesis pathway of phosphatidylserine in mammals. **B,** PSS1 protein topology. Cylinders represent transmembrane, N and C indicate the terminal tail. **C**, Schematic representation of proteins involved in phosphatidylserine asymetry between inner and outer leaflet. Arrows indicate the direction of flipping. **D,** Schematic representation of ER-PM contact site allowing to countertransport PI4P and PS. PSS1 and 2, phosphatidylserine synthase 1 and 2; PI4Ka, phosphatidylinositol 4 kinase A; Sac1, supressor of actin 1; PS, phosphatidylserine; PI4P, phosphatidylinositol 4 phosphate. PI; phosphatidylinositol; PC; phosphatidylcholine; PE; phosphatidylethanolamine; PM, plasma membrane; ER, endoplasmic reticulum; ATP, adenosine triphosphate; ADP, adenosine diphosphate. Adapted from Sohn et al., 2016.

in PA production. The first one, uses phospholipids as substrat through the action of phospholipase D (PLD) and the second one diacylglycerol through the activity of diacyglycerol kinases (DGKs) that is generated from phospholipids by Phospholipase C (PLC) or triacylglycerol by triacyglycerol lipase (TAGL) (Figure 10B). Based on the subcellular localization of enzymes involved in PA biosynthesis, PA is thought to be present in mitochondria, ER and PM but also in lipid droplet in yeast and peroxisomes in mammals (Hermansson et al., 2011). Genetically-encoded biosensor sensing PA reveals that most cells do not accumulate significant level of free PA in the cytosolic leaflet of the plasma membrane (Bohdanowicz et al., 2013) (Figure 8). However, PA is acutely produced by PLD in response to receptor kinase activation (Zhang et al., 2014). In addition, it is constitutively produced at significant level (i.e. sufficient to trigger the constitutive PM association of PA sensors) in phagocytic cells (e.g. Macrophages and dentritic cells) by PM localized DGK enzymes (Bohdanowicz et al., 2013). As mentioned previously, PA is exchanged at membrane contact sites by Nir2, which extracts PI from the ER to the PM and transports back to ER PM-associated PA. PA is generated from diacylglycerol (DAG), itself generated by PLC activity, which hydrolyzes PI(4,5)P_2 at the plasma membrane. In this case, PA synthesis depends on PI(4,5)P_2 and PLC activity at the PM. However, PI(4,5)P_2 production requires PI(4)P that itself required PI synthesis. The production of PI occurs in the ER and depends on CDP-diacylglycerol, which is generated from PA by CDP-diacylglycerol synthase. To sum up, we have a kind of "schizophrenic" system, where PA is localized at the PM and requires ER-generated PI and conversely PI synthesis in the ER depends on PA production which is localized at the plasma membrane. Nir2 lipid transfer protein play a central role in this lipid synthesis and homeostasis as an ER-PM lipid exchanger (Figure 7C) (Kim et al., 2015). PA regulation is complex as it is a highly dynamic phospholipids, which can be produced by many different pathways in different compartments. Although I highlighted earlier the regulation of PS localization in inner and outer membrane leaflets by lipid scramblase and flippase, it worth noting that the presence (and regulation) of PA in inner vs outer leaflets in not well documented and is probably important for its activity and availability.

PA is an anionic phospholipid (net charges -2) present at the PM. However, to my knowledge, its potential role in the establishment/maintenance of the PM electrostatic field has not been explored in yeast and animals. I will therefore describe below how the role of PIPs and PS in

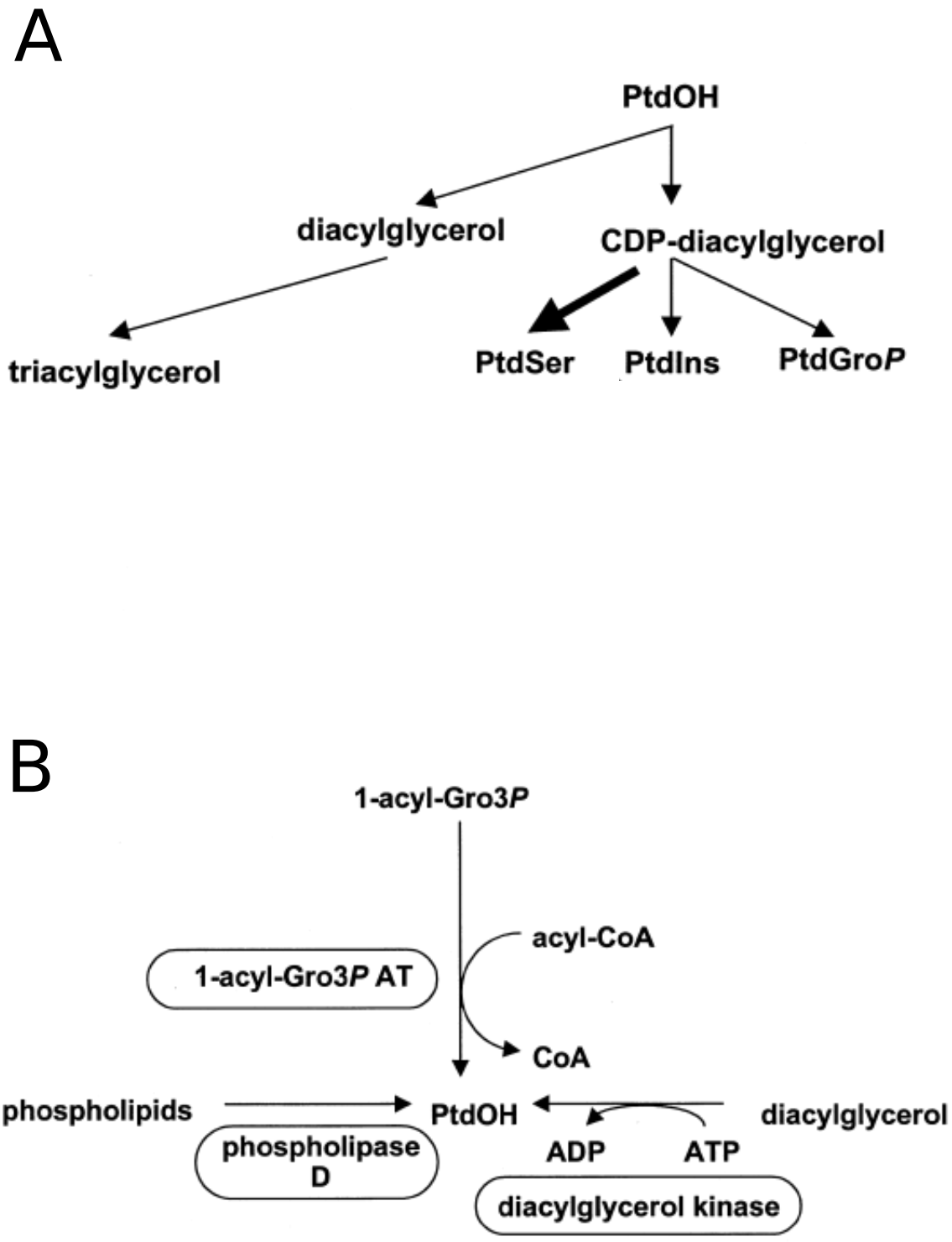

Figure 10. Degradation and synthesis of phosphatidic acid. A, Phosphatidic acid, a key intermediate in glycerophospholipid and triacylglycerol synthesis. The large arrows indicate reactions restricted to yeast. Di-PtdGro, cardiolipin. **B**, Formation of phosphatidic acid. Number indicates the four pathways that are involved in PA synthesis. Adapted from Athenstaedt et al., 1999. PtdOH, phosphatidic acid; CDP, cysteine diphosphate diacylglycerol pyrophosphate; PtdSer, phosphatidylserine; PtdIns, phosphatidylinositol; PtdGRO, phosphatidylglycerol; CoA, coenzyme A; ADP, adenosine diphosphate; ATP, adenosine triphosphate.

membrane electrostatics has been studied but will not discuss further the potential role of PA. However, I believe this could be an interesting avenue of future research, notably in yeast and mammalian cells with active phagocytic activities.

II. Anionic lipids in the maintenance of the PM electrostatic field in mammals

a. Anionic lipids are required to maintain the plasma membrane electrostatic field

The first study to analyze the role of anionic lipids in MSC-establishment was published by the group of Sergio Grinstein in 2006 (Yeung et al., 2006). In this seminal paper, Yeung et al., described and validated the first set of MSC-reporters and showed that the cytosolic leaflet of the PM is highly electrostatics. They then perturbed anionic phospholipid pools using pharmacological approaches to determine their roles for the generation of the PM electrostatic field.

Ionomycin elevates cytosolic calcium, which induces $PI(4,5)P_2$ hydrolysis through activation of phospholipase C (PLC). At the same time, the increase of cytosolic calcium activates lipid scramblase, which results in the translocation of PS from the inner (cytosolic facing) leaflet of the PM to the outer leaflet. Therefore, ionomycin induces the concomitant loss of $PI(4,5)P_2$ and PS in the inner PM leaflet. Ionomycin treatment delocalized the cationic probes (K-pre, Krphy, K-myr), while membrane integrity sensors (GPI, GT46 and Palmitoylation) were not affected (Figure 11A). A more recent study (Ma et al., 2017) using the MCS+ based-FRET sensor verified this observation. Indeed, the concomitant depletion of $PI(4,5)P_2$ and PS following ionomycin treatment induced a decrease of the FRET signal Figure 11B). Dibucaine promotes PS flipping from the inner to the outer leaflet independently of PIPs metabolism and induced a delocalization of cationic probes into the cytosol and a decrease FRET-ratio of the MSC+ probe. In addition, the drug fendiline sollubilizes PS and impacts PM MSC (Ma et al., 2017) (Figure 11A-B). Taken together, these results suggest that a decrease of $PI(4,5)P_2$ and PS concentration at the PM inner leaflet affects membrane surface charge.

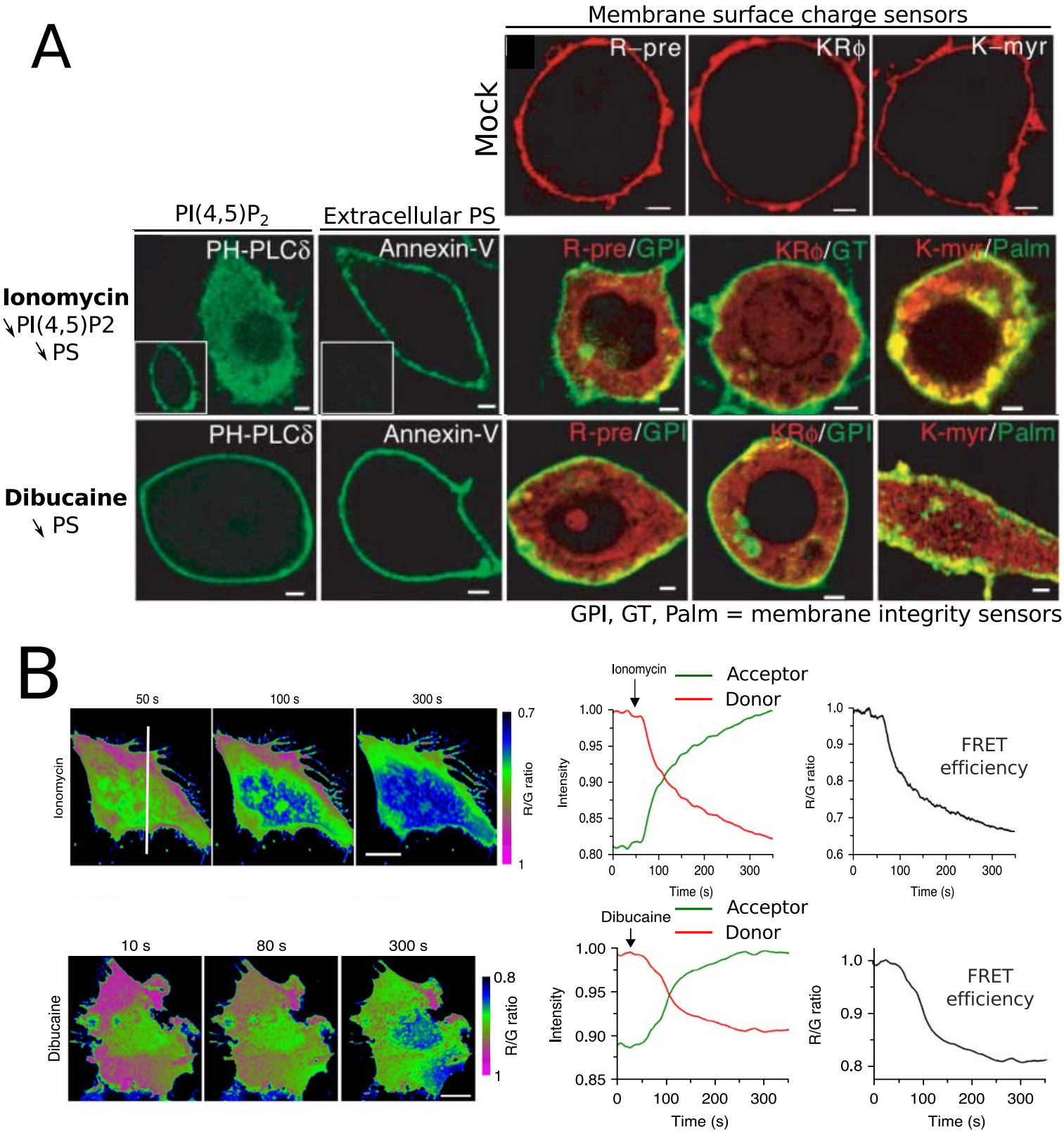

Figure 11. Anionic lipids maintain the signature of the plasma membrane as the most anionic compartment. **A,** Top panel, macrophages transfected with R-pre, KRf, or K-myr corresponding to the MSC probes labelling the plasma membrane. Middle and lower panel, distribution of probes in cells treated with ionomycin (top) or dibucaine (bottom). Insets: cells before ionomycin. Scale bars, 2 mm. **B,** Ratiometric FRET images (R/G ratio, pseud-colored as indicated by the color scale) of MCS+ in live COS-7 cells during Ca2+ influx induced by ionomycin (10 mM) or dibucaine (1mM) to promote the flipping of PS from the inner to the outer leaflet of the plasma membrane . Scale bars represent 10 µm. Change in donor (green) and acceptor (red) intensity and FRET efficiency (R/G ratio, black) for the ionomycin and dibucaine-treated cells. Arrows indicate when drugs were added. Adapted from Yeung et al., 2006 and Ma et al., 2017.

However, these results must be taken with some care given the side effects of the chemical compounds used. Indeed, ionomycin induces a massive calcium entry into the cell, which might contribute in part to the release of cationic probes from the PM by increasing ion shiedling. In addition, dibucaine is cationic, and therefore its own positive charges could participate in displacing cationic probes from the membrane. Moreover, this experiment lacks control on other PM-associated anionic phospholipids such as PI4P, PI(3,4)P_2, and PI(3,4,5)P_3. Finaly, fendiline inhibits acid sphyngomyelinase (ASM), which decreases the level of ceramide and increase those of sphyngomyelin, leading to a depletion of PM cholesterol and PS (Cho et al., 2015)·(van der Hoeven et al., 2013)· Why variations of ceramide/sphyngomyelin impact PS biosynthesis is unknown and suggest an indirect mode of action.

b. Involvement of PIPs in the plasma membrane surface charge

The drugs mentioned above are expected to have pleiotropic effects. It is therefore impossible to exclude that they might induce a large-scale remodeling of global cell physiology and membrane lipids thereby affecting the localization of MSC sensors. In parallele to pharmacological approaches, a number of genetic strategies were implemented to modify anionic lipid pools. Most of these tools are based on the targeting of lipid phosphatase activities at the PM. For example, overexpression of Inp54p, a 5-specific phosphatidylinositol 4,5-bisphosphate phosphatase (5-phosphatase) induced a significant reduction in the FRET efficiency of the MCS+ reporter. However, in this case, Inp54 is constitutively overexpressed, leading to chronic PI(4,5)P_2 depletion. Such chronic depletion may also have side effects and therefore it is difficult to pin point the change in the FRET efficiency of the MCS+ probe to the sole depletion of PI(4,5)P_2 (Ma et al., 2017).

To overcome these drawbacks, (Heo et al. 2006), designed an elegant method based on the inducible recruitment of phosphoinositide phosphatases at the PM. This inducible phosphatase recruitment is built on genetically encoded PM-localized FK506-binding protein (FKBP12)-rapamycin-binding (FRB) construct and a cytosolic inositol polyphosphate 5-phosphase (Inp54p)

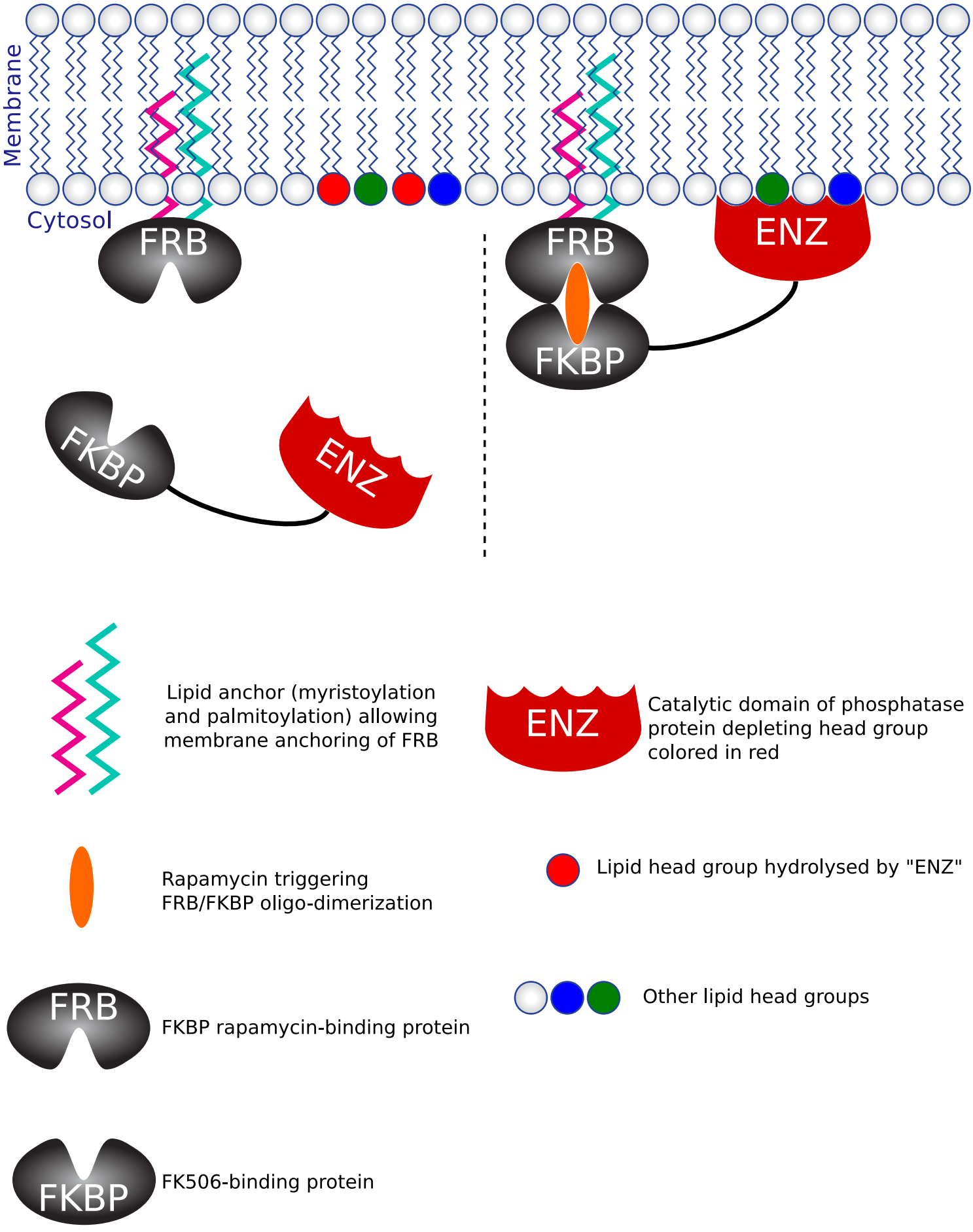

Figure 12. Schematic representation of the FRB/FKBP-based inducible system to perturb plasma membrane -associated anionic lipids. ENZ, in our case corresponds to the catalytic domain of Inp54p a 5′ specific PI(4,5)P2 phosphatase or the chimeric enzyme pseudojanine corresponding to the fusion between the catalytic domain of the PI4-phosphatase sac1p and INPP5e a 5′ specific PI(4,5)P2 phosphatase.

enzyme conjugated with FKBP12 (CF-Inp; Figure 12). Rapamycin treatment induces CF-Inp translocation from the cytosol to the PM by chemical heterodimerization that triggers Inp54p activity at the PM and thereby inducible and rapid (i.e. minutes) depletion of PI(4,5)P_2 specifically to this membrane. By contrast to chronic depletion of PI(4,5)P2, rapamycin-induced PM-Inp54p recruitment did not affect cationic probes localization (MARCKS-ED, Rin and Rit tail; Figure 13A-B). This result suggests that PI(4,5)P_2 is not required, by itself, for MSC and that another anionic phospholipid(s) might act redundantly with PI(4,5)P_2 to control PM MSC.

A limitation of the approach from Heo et al., was that dephosphorylation of PI(4,5)P_2 by Inp54p induces the production of PI4P, another PM phosphoinositide which is also anionic, albeit to a lesses extent (roughly -3 vs -5 net charges, for PI4P and PI(4,5)P_2, respectively). This could explain the absence of effect of PI(4,5)P_2 depletion on cationic probes, since only part of the charges carried by PI(4,5)P_2 are depleted with this technique. Hammond et *al.*, in 2012 found that PM PI4P is not only a precursor of PI(4,5)P_2 biosynthesis but also an important regulator of PM identity. Gerry Hammond indeed built a rapamycin–triggered system, which allows the inducible recruitment at the PM of a chimeric synthetic enzyme, composed of 4- and 5-phosphatase catalytic activities. He named this enzyme *"pseudojanine"* by analogy to the protein synaptojanin, which naturaly carries 4- and 5-phosphatase catalytic activities. The 4- and 5-phosphatases catalytic domains of pseudojanin came from the yeast Sac1p and human INPP5E proteins, respectively. Point mutations within the Sac1p or INPP5E catalytic domains shut down either the 4-phosphatase or 5-phosphatase activity or both and are used as a control. Depending on the mutations, this system allows altering either PI4P, PI(4,5)P_2, both, or none (when both phosphatase domains are mutated). Using an optimized immunolocalization protocol (Hammond et al., 2009), they validated their system and showed that the rapamycin-inducible PM-targeted 5-phosphatase had no effect on PI4P, but depleted PI(4,5)P_2 from the PM. Similarly, decreasing the PM-PI4P pool by PM-targeted 4-phosphatase had no effect on the PM PI(4,5)P_2 abundance. This unexpected observation suggested a relative independence of the PI4P and PI(4,5)P_2 pools at the PM, even though PI(4,5)P_2 is made from PI4P. Depletion of either PI4P or PI(4,5)P_2 had no effect on the PM targeting of various MSC probes (including Kras-tail, MARCKS-ED, Rit tail and the KA1 domain; Figure 13A-B). Therefore, PI4P and PI(4,5)P_2 are not required (on their own) to maintain PM surface charge. However, the concomitent depletion of both PI4P and PI(4,5)P_2 altered the PM localization of MSC reporters but did not affect membrane integrity

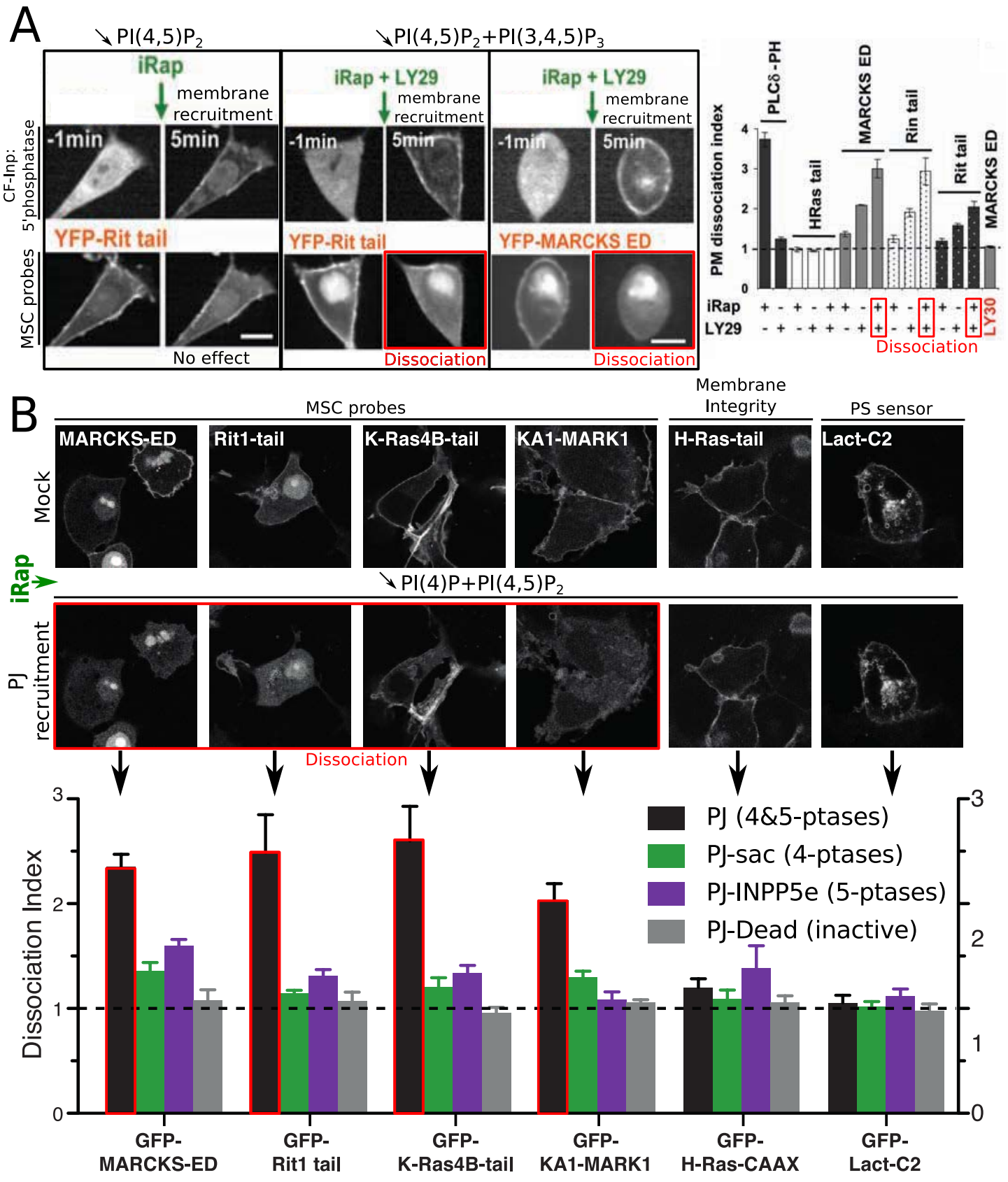

Figure 13. Depletion of PI(4,5)P2 with PI(3,4,5)P3 or PI(4,5)P2 with PI(4)P dissociates MSC probes from the PM. A, Development of a chemically inducible translocation method (FRB/FKBP) to deplete PI(4,5)P2 from the inner leaflet of the PM. Depletion of PI(4,5)P2 caused only a small reduction in the PM localization of YFP-conjugated Rit tail. Joint reduction in PI(4,5)P2 and PI(3,4,5)P3 triggered a near-complete dissociation of Rit tail and MARCKS ED from the PM. Quantitative analysis of the CF-Inp and/or LY29-triggered PM dissociation of MARCKS ED, and Rit and Rin tails. PLCd-PH (PI(4,5)P_2 and HRas (membrane integrity sensor) tails are shown as controls. The inactive LY29 analog LY30 was used as a control. Scale bars, 10 µm. **B,** Targeting of proteins with polybasic motifs to the PM by PI4P and PI(4,5)P2. Representative images before and after rapamycin treatment, and dissociation index of cells transfected with the indicated GFP-tagged motifs, Lyn11-FRB-CFP and the indicated PJ construct. Lact-C2, lactadherin C2 domain (PS sensor). PJ, pseudojanine corresponds to an enzymatic chimera of inositol polyphosphate-5-phosphatase E (INPP5E), which converts PI(4,5)P2 to PI4P and the *S. cerevisiae* Sac1 phosphatase, which dephosphorylates PI4P. PJ-Sac, PJ-INPP5E or PJ-Dead correspond to the dead version of INPP5E on PJ construct, the dead version of Sac1 on PJ construct orthe dead version of INPP5E and Sac1 on PJ construct. Adapted from Heo et al., 2006 and Hammond et al., 2012.

probes.

$PI(3,4,5)P_3$ is a highly anionic phospholipid (net charge -7) localized at the PM. It is present in minute amount but its synthesis is acutely induced upon growth factor stimulation. Heo et *al.* reported that the stimulation of PI3Kinase activity at the PM increased $PI(3,4,5)P_3$ PM level, with a concomitant recruitment of the cationic probe Rin tail at this membrane. This suggested that the PM-associated $PI(3,4,5)P_3$ could be involved in PM MSC. The subcellular localization of cationic probes and the FRET signal of the MCS+ reporter were only slightly affected by LY294002 or wortmanin treatment, two pharmacological inhibitors which prevent $PI(3,4,5)P_3$ production by inhbiting PI3-Kinases. Therefore, similar to $PI(4,5)P_2$, $PI(3,4,5)P_3$ might also control PM MSC together with other anionic lipids. Application of PI3-kinase inhibitors coupled to PM-inducible recruitment of a 5-phosphatase (Inp54) concomitantly decreased $PI(4,5)P_2$ and $PI(3,4,5)P_3$ levels and induced the PM-dissociation of cationic probes (MARCKS-ED, Rin and Rit tail) but not that of membrane integrity sensors (Figure 13C-D). This indicated that $PI(4,5)P_2$ and $PI(3,4,5)P_3$ also act redundantly to regulate PM MSC. Altogether, $PI(4,5)P_2$ seems to be critical to define PM membrane surface charge in human cells but is not sufficient and acts redundantly with $PI(3,4,5)P_3$ and/or PI4P.

c. Evidence that PS contributes to the PM electrostatic field

PIPs are highly anionic but represent only about 1% of total phospholipids in living cells. Other less anionic lipids might also contribute to MSC, notably due to higher abundance. In animals, PS represents about 10 to 20% of PM-phospholipids but PS is less anionic than phosphoinositides (net charge -1). The pharmacological experiments described above from Yeung et al., (2006) (part II.A.) suggested that PS might take part in PM surface charge. However, the exact distribution of intracellular PS was unknown due to the lack of appropriate tools. Two years later[7], Yeung et *al.*, (2008) investigated the role of PS in MSC by setting up a specific intracellular PS probe. By contrast to the C2 domain of annexin-V, the C2 domain of bovine lactadherin synthase ($C2^{LACT}$) binds selectively to PS independently of calcium and can be used

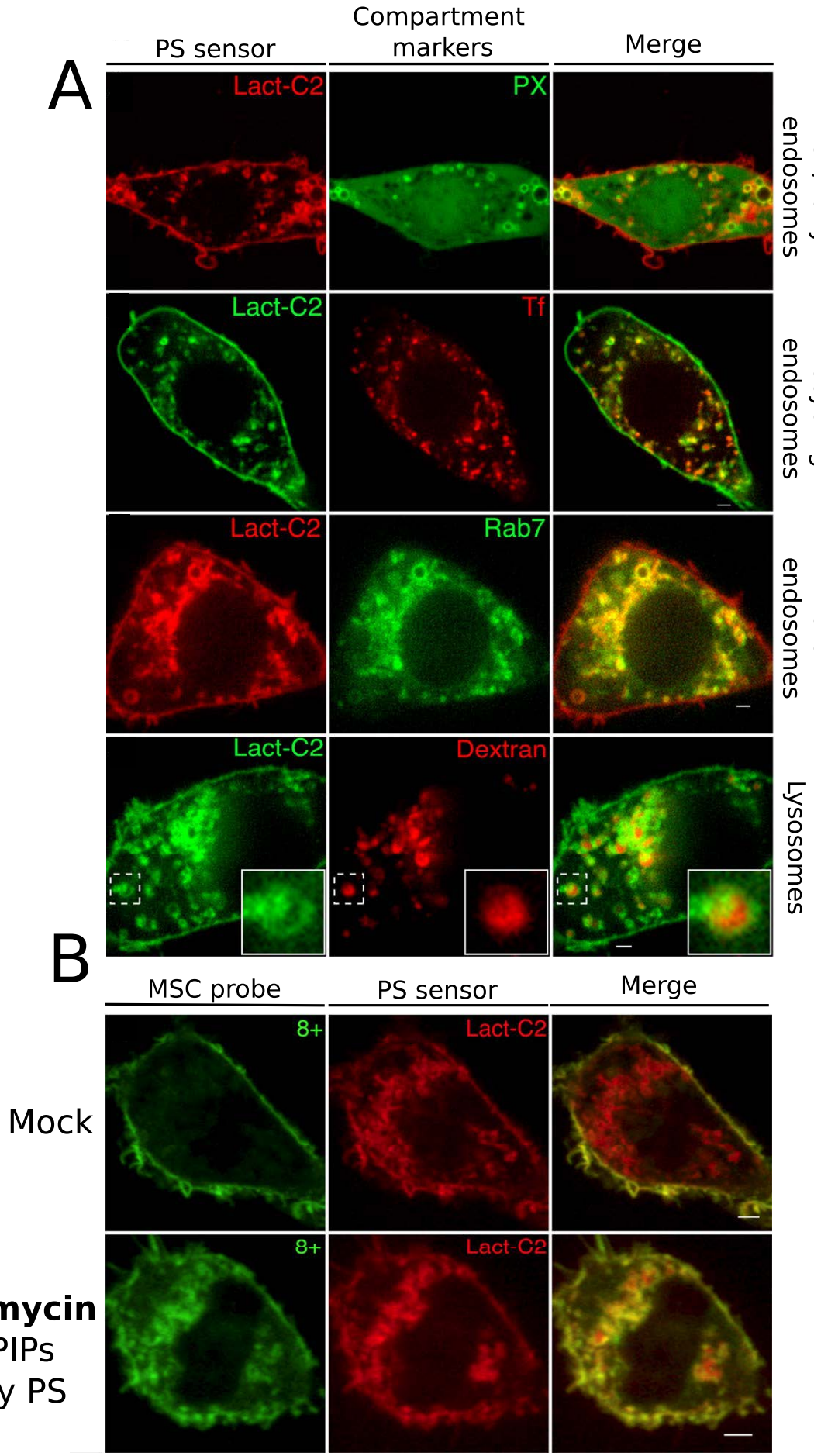

Figure 14. PS sensor localizes all-along the endocytic pathway and is required for plasma membrane surface charge. A, Macrophages co-expressing mRFP-Lact-C2 (PS sensor, left) and either GFP-PX or GFP-Rab7 and macrophages expressing GFP-Lact-C2 (left) were incubated with either rhodamine- transferrin or rhodamine-dextran under conditions that label preferentially endosomes and lysosomes, respectively. Inset shows a magnification of the area delimited by the dotted box, illustrating a Lact-C2-positive vesicle containing rhodamine-dextran in its lumen. Overlays of the red and green images are shown in right panels. **B,** Macrophages were co-transfected with mRFP-Lact-C2 (red) and the GFP-8+ surface charge probe (green). Images were acquired before (top) or following incubation in medium containing 2-deoxy-glucose and antimycin to deplete cellular ATP (bottom). Overlays of the two images are shown in the right panels. Scale bars, 2 µm. Adapted from Yeung et al., 2008.

as a genetically encoded PS sensor when fused to a fluorescent protein. Based on co-localization analyses and immunogold electron-mycroscopy, PS was found at the plasma membrane, endosomes and lysosomes and more enriched at the PM than in late endosomal compartments (Yeung et al., 2008; Fairn et al., 2011a) (Figure 14A).

To investigate the relative role of PS compared to PIPs in PM electrostatic field maintenance the authors inhibited ATP synthesis by using a concomitant treatment of antimycin and deoxyglucose. This treatment concomitantly inhibits mitochondrial respiration and glycolysis, thereby depleting cellular ATP. The rational of this experiment is the following: among other effects, ATP depletion in the cell should trigger the rapid depletion in phosphoinositides because in the absence of ATP, lipid kinases are not making any new PIPs, while lipid phosphatases are still constantly dephosphorylating these lipids. However, PS maintenance does not require a kinase and the PS pool should not be affected, at least under short-term treatment with antimycin. To verify this assumption Yeung et al., monitored the localization of $PI(4,5)P_2$ and $PI(3,4,5)P_3$ probes and that of their newly described PS sensor ($C2^{LACT}$) following antimycin treatment. Antimycin depleted PH-PLC and PH-AKT probes from the PM, but had no effect on $C2^{LACT}$, suggesting a decrease of cellular PIPs but not PS. Next, they examined the localization of the MSC probe K-Ras tail and found that following antimycin treatment, it was delocalized in intracellular compartments, although a portion was still associated with the PM (Figure 14B). This experiment showed that in the absence of PIP, the PM looses its electrostatic signature, which confirms the importance of phosphoinositides in this particular PM property (as described by Heo et al., (2006) and Hammond et al., (2012)). However, a portion of the K-Ras tail probe was retained at the PM in the absence of phosphoinositides, suggesting that other anionic lipids, likely PS, are involved in this PM electrostatics. Next, Yeung et al., investigated, in which cellular compartment K-Ras tail MCS sensors relocalized in the absence of PIPs (i.e. following antimycin treatment). In this condition, K-Ras tail resides almost exclusively in PS containing organelles (as labeled by $C2^{LACT}$, i.e. endosomes and lysosomes), showing a near perfect correlation between the putative presence of PS and negative charges (Figure 14B). Together, these results argue that (1), that PIPs are required for PM electrostatic field and (2) that PS might contribute to MSC both at the PM but also along the endocytic pathway (point discussed below).

Altogether, Yeung et al., suggested that PS is a regulator of the PM electrostatic field. However,

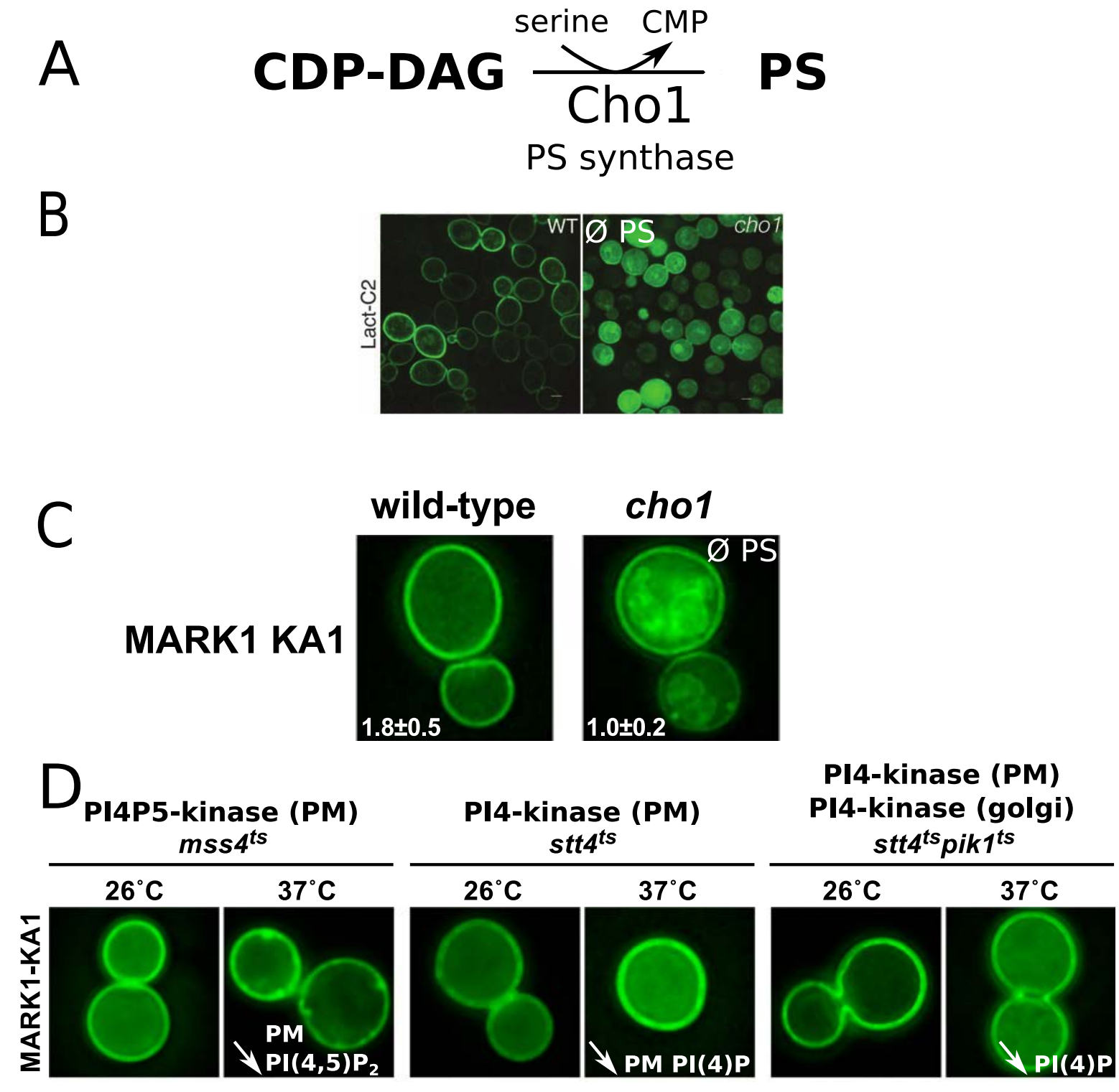

Figure 15. PS but not PIPs is required to maintain plasma membrane electrostatic field in yeast. A, Biosynthetic pathway of PS in yeast. **B,** Confocal images of wild-type *S. cerevisiae* (left) and a PS-deficient mutant (*cho1*) (right) expressing GFP–Lact-C2. Scale bars, 2 μm. Adapted from Yeung et al. 2008. **C,** GFP-fused KA1 domain from human MARK1 shows robust plasma membrane localization in *S. cerevisiae* cells, which is diminished in *cho1Δ* cells that lack PS. Mean fPM/fCyt ratios for each experiment (±standard deviation) are quoted in individual panels. **D,** Localization of the human MARK1 KA1 domain (fused to GFP) was analyzed in mss4ts cells, stt4ts cells, and stt4ts/pik1ts cells, grown to midlog phase, and then incubated for 40 min at either 26C or 37C before being examined by fluorescence microscopy. Images are representative of >90% of cells observed (from three experiments in each of which > 100 cells were analyzed). Levels of $PI(4,5)P_2$ are greatly reduced in mss4ts and stt4ts cells at the restrictive temperature. Plasma membrane and total PtdIns4P levels are greatly reduced at the restrictive temperature in stt4ts and stt4ts/pik1ts cells respectively. In no case did elevating the temperature above the restrictive temperature lead to a significant alteration of fPM/fCyt ratios, by contrast with the impaired plasma membrane localization seen in cho1Δ cells in C. Adapted from Moravcevic et al., 2010.

due to limitations in the pharmacological approaches described in the previous paragraph and the lack of direct evidence, it is still not fully demonstrated that PS indeed participate in PM electrostatics in mamalian cells. Loss of function experiments that would consist of depleting the PS cellular content and analyze its effect on MSC has not been conducted to my knowledge.

III. Anionic lipids in the maintenance of the PM electrostatics field in yeast

By contrast to mammals, yeast has a single PS synthase gene, called *cho1*. Cho1p has a different catalytic activity than the mamalian PSS1/PSS2 enzymes as it produces PS via a CDP-diacylglycerol:l-serine *O*-phosphatidyltransferase activity (Figure 15A). In laboratory conditions, when grown in rich medium, Cho1p is not critical for yeast viability. However, biochemically, the *cho1* mutant does not contain PS and the PS sensor $C2^{LACT}$ becomes cytosolic when expressed in *cho1*. While the catalytic activity of Cho1p is different than PSS1/PSS2, there are extensive paralellism between PS synthesis in yeast and animals: PS is produced in the ER and then transferred to the PM at membrane contact sites by evolutionary conserved proteins[19,20] (Maeda et al., 2013; Moser von Filseck et al., 2015). However, the site of PS subcellular accumulation are different in yeast and animals. In mammals, $C2^{LACT}$ localizes at the PM but also in PM-derived organelles along the endocytic pathway. In yeast however, $C2^{LACT}$ is exclusively localized at the PM and virtualy no intracellular compartments are labelled by this probe (Yeung et al., 2008; Moravcevic et al., 2010; Fairn et al., 2011b; Filseck et al., 2015; Maeda et al., 2013) (Figure 15B). This suggests that by contrast to animal cells, PS is predominantly accumulated at the PM in yeast, and therefore might have a predominant role for PM electrostatics.

The K-Ras based MSC probe is not restricted to the PM in *S. cerevisiae*. This prevented Yeung et al., to obtain direct comparison of MSC reporter localization in WT vs *cho1* mutant. However, in 2010, Moravcevic et *al.* identified a new MSC reporter by characterizing the Kinase associated 1 (KA1) domain. KA1 domains have been identified in both yeast and mammalian proteins involved in kinases regulation. Biochemical assay, crystallography and *in vivo* experiments define the KA1 domain as a membrane-associated domain that binds all acidic phospholipids,

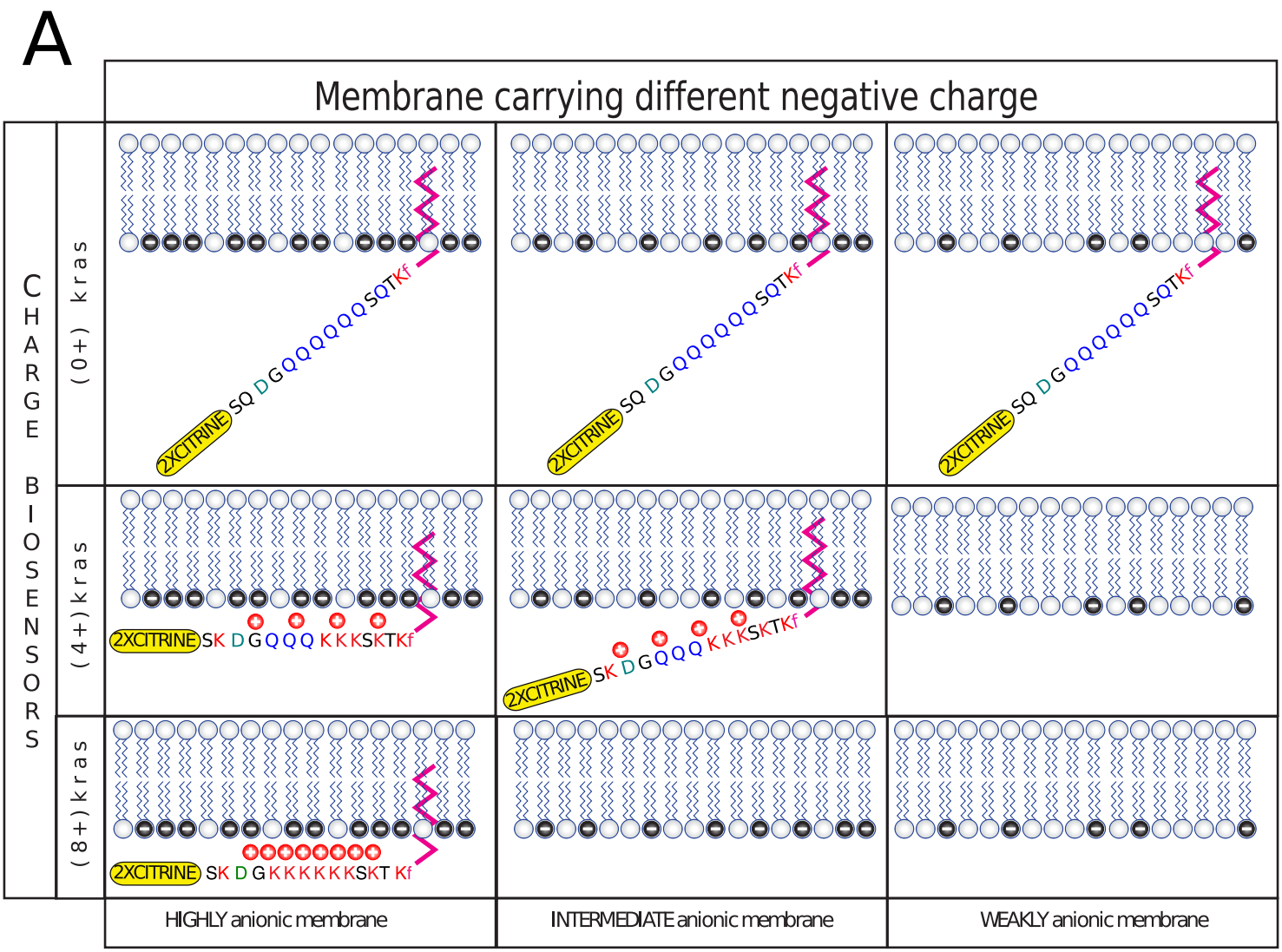

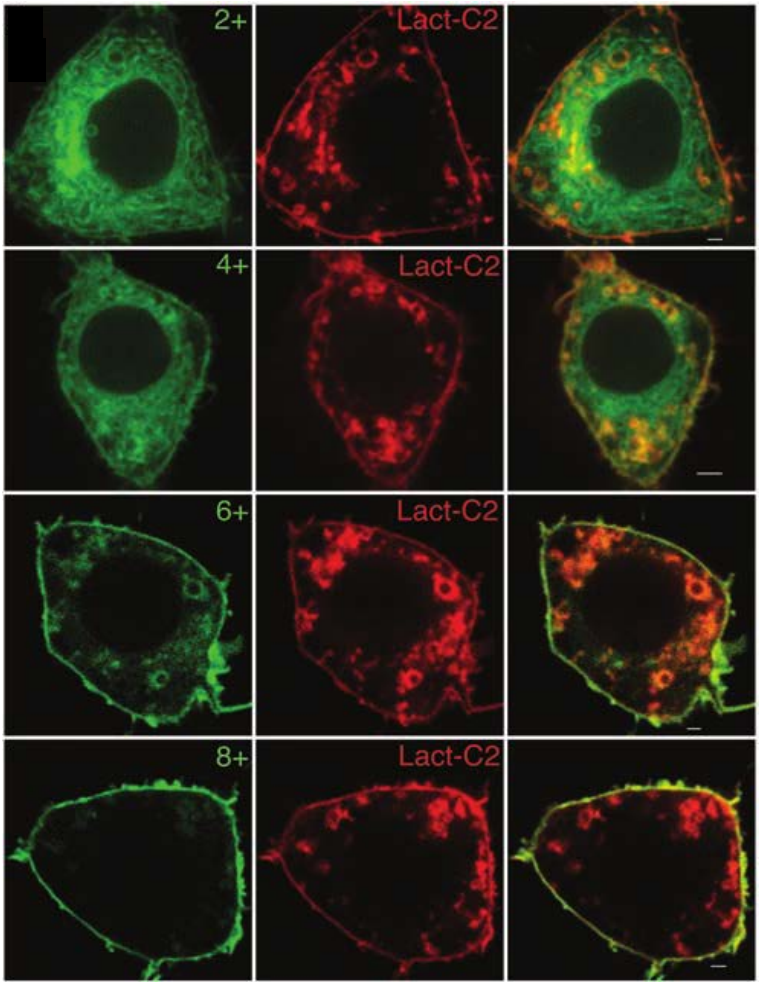

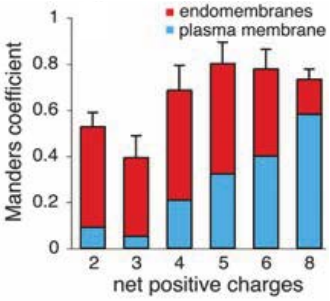

Figure 16. Membrane surface charge probes with intermediate charges localizes between the plasma membrane and endosomes and co-localized with PS sensor. A, Schematic representation of the principle of intermadiate charge sensors corresponding to mutated-K-ras C-terminal . In purple, lipid anchor; black neutral amino acids; red, positive amino acids; green, negative amino acids; 2xmCITRINE corresponds to fluorescent protein in tandem. The relative strength of the electrostatic interaction is represented by the angle between the sensor and the membrane. **B,** Macrophages cotransfected with mRFP–Lact- C2 (middle) and a series of GFP-tagged surface charge probes containing a farnesyl anchor and a cationic motif with 2 to 8 positive charges, as indicated (left). Overlays shown in the right. Quantification of colocalization of surface charge probes with Lact-C2. The Manders coefficient indicates the fraction of the surface charge probes that colocalize with mRFP–Lact- C2. The contribution to the overall Manders coefficient of the plasmalemma (blue) and of all intracellular endomembranes (red) is indicated. Adapted from Yeung et al., 2008.

regardless of their respective head group. Similarly, to the PS probe $C2^{LACT}$, KA1 domains localized strictly to the plasmalemma in yeast. Next, the authors addressed, whether PS, PIP or both participate in KA1 domains localization. In *cho1*, KA1 lost its specific PM localization (i.e. it became soluble and associated with a much broader membrane domain including both PM and intracellular compartments; Figure 15C). This results suggested a major contribution of PS in setting up PM surface charges in yeast. Thermo-sensitive mutations in the genes encoding the PI4-kinases that generate PI4P at the plasma membrane (Stt4p) and Golgi (Pik1p) deplete PI4P from these mutants at restrictive temperature. In the other hand, thermo-sensitive mutation in the only gene that codes for PI4P-5-kinase (Mss4p) inhibits $PI(4,5)P_2$ production. Mss4p mutant is depleted of $PI(4,5)P_2$ but not PI4P at restrictive temperature, while the double mutant stt4p;pik1p (that lack a PI4-kinase), lack both PI4P and $PI(4,5)P_2$. Surprisingly, KA1 domains remains strictly localized at the PM in all these yeast mutant strains (Figure 15D), suggesting that unlike in animals, PIPs do not play a major role in PM MSC and that PS is the major anionic lipids of the yeast plasmalemma inner leaflet (importantly, the yeast *S. cerevisiae* does not produce any $PI(3,4)P_2$ and $PI(3,4,5)P_3$, making PI4P and PI(4,5)P2 the only phosphoinositide at the cell surface). Altogether, these results suggest either no or minor role of PIPs in plasmalemma surface charge, while PS is the main anionic lipid driving the PM electrostatic potential in yeast.

IV. Membrane surface charges defines an electrostatic territory corresponding to PM-derived organelles

a. In mammals, endocytic compartments are electrostatic.

With the idea that not only the PM is an anionic membrane, Yeung et al., altered the strength of electrostatic associations (decrease of the Debey length) by changing the charges of the PBR of MSC reporters. To this end, they mutated the K-Ras tail by substituting its charged amino acids (i.e. Lysines) into neutral residues (i.e. Glutamine) to decrease its net positive charge. They obtained a set of probes containing from 0 to 8 positive charges called 0+ to 8+ (Figure 16A). In macrophages, 0+ sensor reports an intracellular localization that corresponds to the default

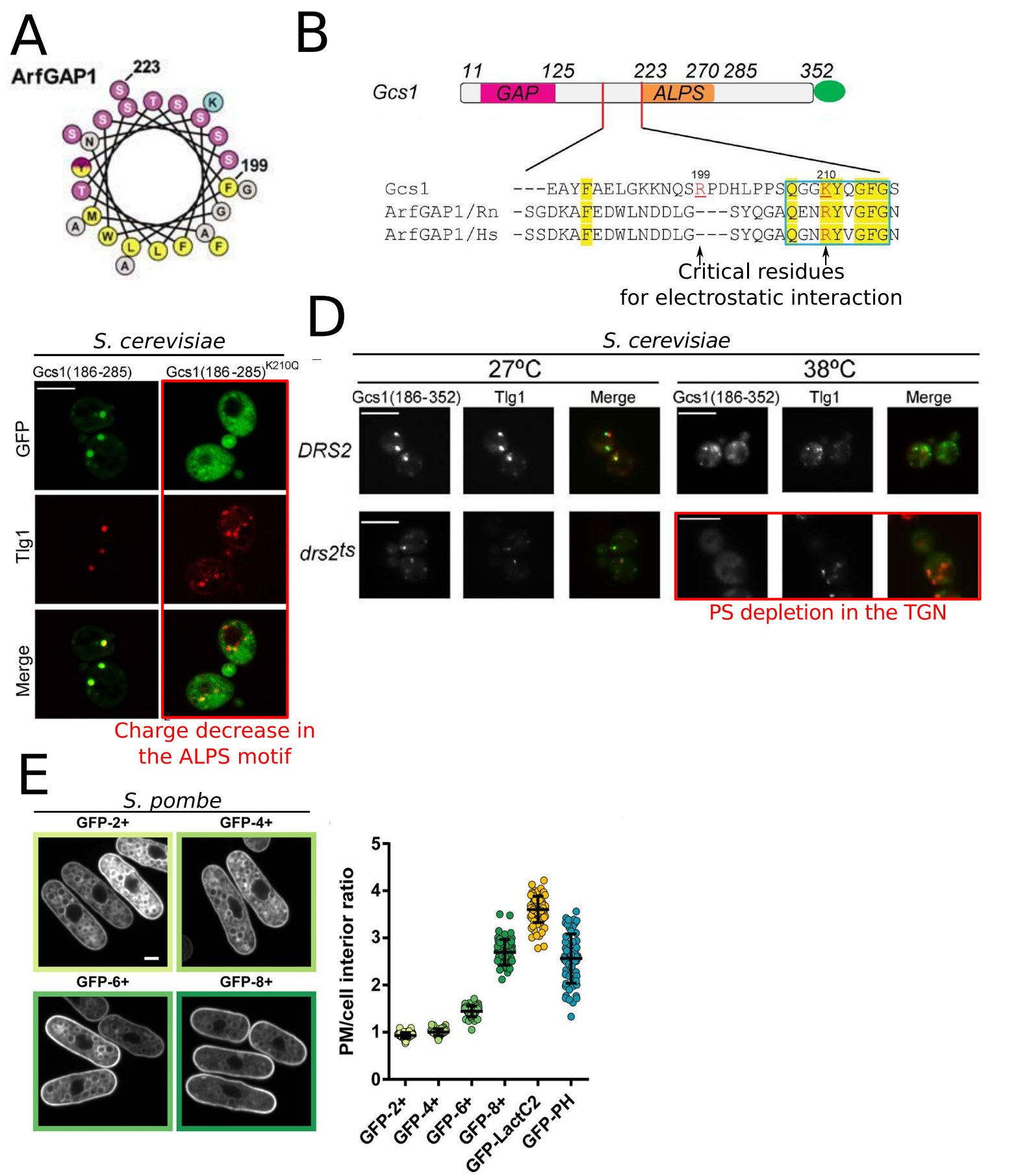

Figure 17. In yeasts, intracellular compartment are negatively charged. A, Schematic representation of the ALPS motif of ArfGAP1 obtain by Heliquest sofware, purple represents hydrophilic amino acids, yellow represents hydrophobic amino acids. **B,** Diagram of Gcs1. The positive charged resides Lysine at position 210 and Arginine at position 199 are highlighted in red. Conserved sequences between Gcs1 and mammalian ArfGAP1 are highlighted in yellow. **C,** Mutation of K210 in Gcs1 disrupts TGN/EE localization. GFP-tagged Gcs1(186–285) and Gcs1(186–285)K210Q expressed in WT cells and imaged relative to mCherry-Tlg1. **D,** Gcs1(186–352)-GFP localization was monitored in drs2 cells carrying wild-type DRS2 or a drs2 temperature-sensitive allele (drs2ts) grown at 27°C or shifted to 38°C for 1 h. Bars, 5 µm. **E,** Distribution of membrane charge probes GFP-2+, 4+, 6+, and 8+ expressed from an inducible pREP3X plasmid in wild-type *S. Pombe* cells. Quantification of plasma membrane enrichment over cell interior for membrane charge probes and charged lipid probes. Adapted from Bigay et al., 2005, Xu et al., 2013 and Haupt et al., 2017.

localization driven by the lipid anchor. However, the 8+ sensor reports PM-labeling as previously described. Intermediate charge sensors have dual-localization, at the PM and in other intracellular compartments. Therefore, the more cationic the sensor is, the more it reports PM-labeling and less an intracellular labeling. Conversely, neutral sensors are less localized at the PM and more in intracellular membranes. Therefore, sensors with intermediate charges (e.g. 4+) report the existence of intracellular compartments of intermediate charges, that are not as electronegative as the PM but that are not neutral either. Colocalization studies suggested that these compartment of intermediate electronegativity corresponds to endosomes (including early and late endosomes, as well as lysosomes; Figure 16B). In addition, MSC sensors relocalized to PS containing organelles in the absence of PIPs (i.e. following antimycin/deoxyglucose treatment), suggesting that PS is important for the electrostatic properties of endosomes.

While it is likely that PS contributes to the overall charge of PM-derived organelles in animals, it is worth noting that this conclusion is essentially based on correlations (i.e. colocalization between a PS sensor and a charge sensor in the absence of PIP) observed in antimycin treated cells. Depletion in cellular ATP is expected to have a myriad of effects on cell physiology, including stopping of all intracellular trafficking, kinases reactions and membrane potential. All this effects could also affect the localization of MSC in antimycin treated cells, independent of PS localization. Again, it would be interesting in the future to analyze the localization of MSC reporters in PS depleted cells.

b. Membrane electrostatic of intracellular compartments in yeast

In the yeast *Saccharomyces cerevisiea*, the $C2^{LACT}$ sensor is strictly localized at the PM, suggesting that the cell surface massively accumulates PS at the expense of its intracellular localization (Yeung et al. 2008; Filseck et al., 2015; Fairn et al., 2011a; Moravcevic et al., 2010). While this is an excellent argument for PS as a driver of PM electrostatics in this yeast species, it does not argue in favor of PS being important for intracellular compartments electrostatics. In the litterature, only one paper reported PS localization in intracellular compartments (Xu et al.,

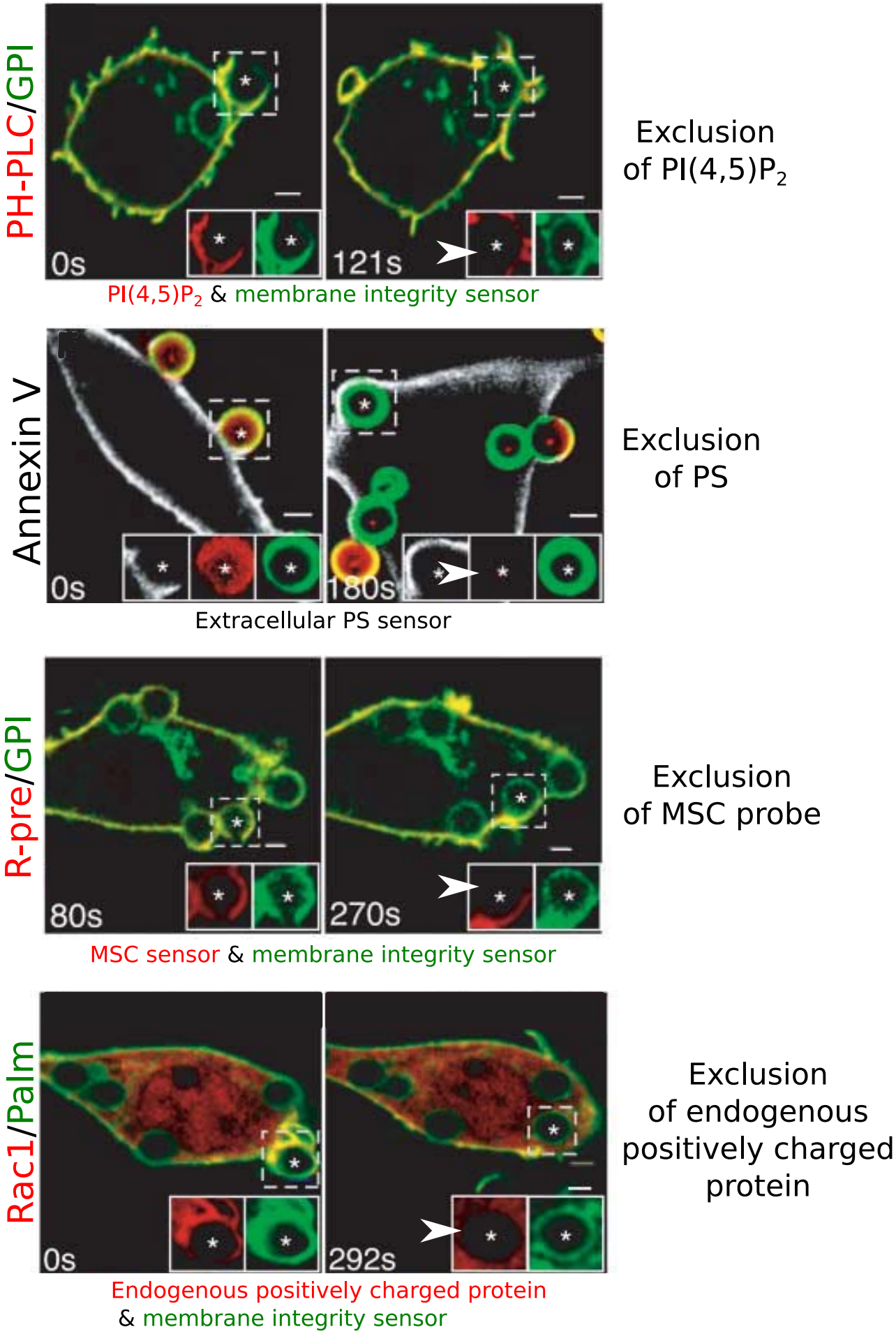

Figure 19. Lipid, charge and cationic protein redistribution during phagocytosis. From top to the bottom, redistribution of PH- PLCd and GPI-GFP during phagocytosis and distribution of PS (white) during phagocytosis. Green, total beads; red, extracellular beads. R-pre/GPI-GFP redistribution during phagocytosis. Asterisks indicate latex beads. Redistribution of Rac1 and Palm during phagocytosis in time course. Arrows indicate the absence of labelling by probes and protein. Adapted from Yeung et al., 2006.

2013). In this paper, Xu et al., used the $C2^{LACT}$ reporter and were able to detect it at the surface of the TGN. The reason for the discrepencies between the usualy reported localization of $C2^{LACT}$ in yeast and this study are unclear.

Xu et al., investigated the role of PS in defining the electrostatic field of the TGN (Xu et al., 2013). They identified a motif corresponding to an amphiphatic lipid packing sensor (ALPS) that are positively charge (+ALPS) in an ArfGAP protein (Gcs1). ALPS motifs are able to sense lipid packing defects that are present (notably) in highly curved membranes and are composed of an hydrophobic and of an hydrophilic face (Figure 17A-B). Because ALPS motifs are able to senses curved membranes (diameter 50nm), theirs localizations are restricted to the *cis*-golgi. Historically, the ALPS motif has been identified in the protein ArfGAP1 and is responsible for ArfGAP1 targetting and function in the cis-golgi for vesicular sorting. Colocalization analysis between the +ALPS motif and *trans*-golgi network (TGN; Tlg1 or Sec7) clearly demonstrates its localization beyond the Golgi. Mutations in the +ALPS positively charged amino acids restrict its localization to the *cis*-golgi *in vivo* (Figure 17C). In vitro experiments showed that +ALPS and mutated +ALPS bind more and less PS-containing liposomes, respectively; this result implied that charged amino acids could drive the +ALPS motif out of the Golgi. The authors speculated that the extended localization to the TGN of the +ALPS motif may be due to negative surface charges of this compartment and argued that the electrostatic territory is not limited to the PM in yeast. Consistent with this hypothesis, in their hand, $C2^{LACT}$ colocalized with the +ALPS motif which itself colocalized with TGN markers (Tgl1 and sec7). In addition, the localization of Gcs1P +ALPS motif was significantly affected in the *cho1Δ* mutant.

Drs2 is a P4-ATPase that is flipping PS from the luminal to the cytosolic leaflet of the TGN. In Drs2 thermo-sensitive mutant at restrictive temperature, the +ALPS localization was significantly dispersed throughout the cytoplasm (Figure 17D). Therefore, the authors proposed that Drs2-dependent PS flipping at the TGN induces negative charges on the surface of this compartment. This mechanism allows the specific recruitment of +ALPS motif containing ARF-GAP to the TGN, as they are both highly curved and electrostatic membranes. Because, the localization of the +ALPS motifs was unchanged in *vps34* and *fab1* mutants, which are impaired in PI3P and $PI(3,5)P_2$ synthesis, respectively, it is likely that intracellular phosphoinositides play a minor role in the electrostatic properties of this intracellular compartments (unfortunately, yeast mutants

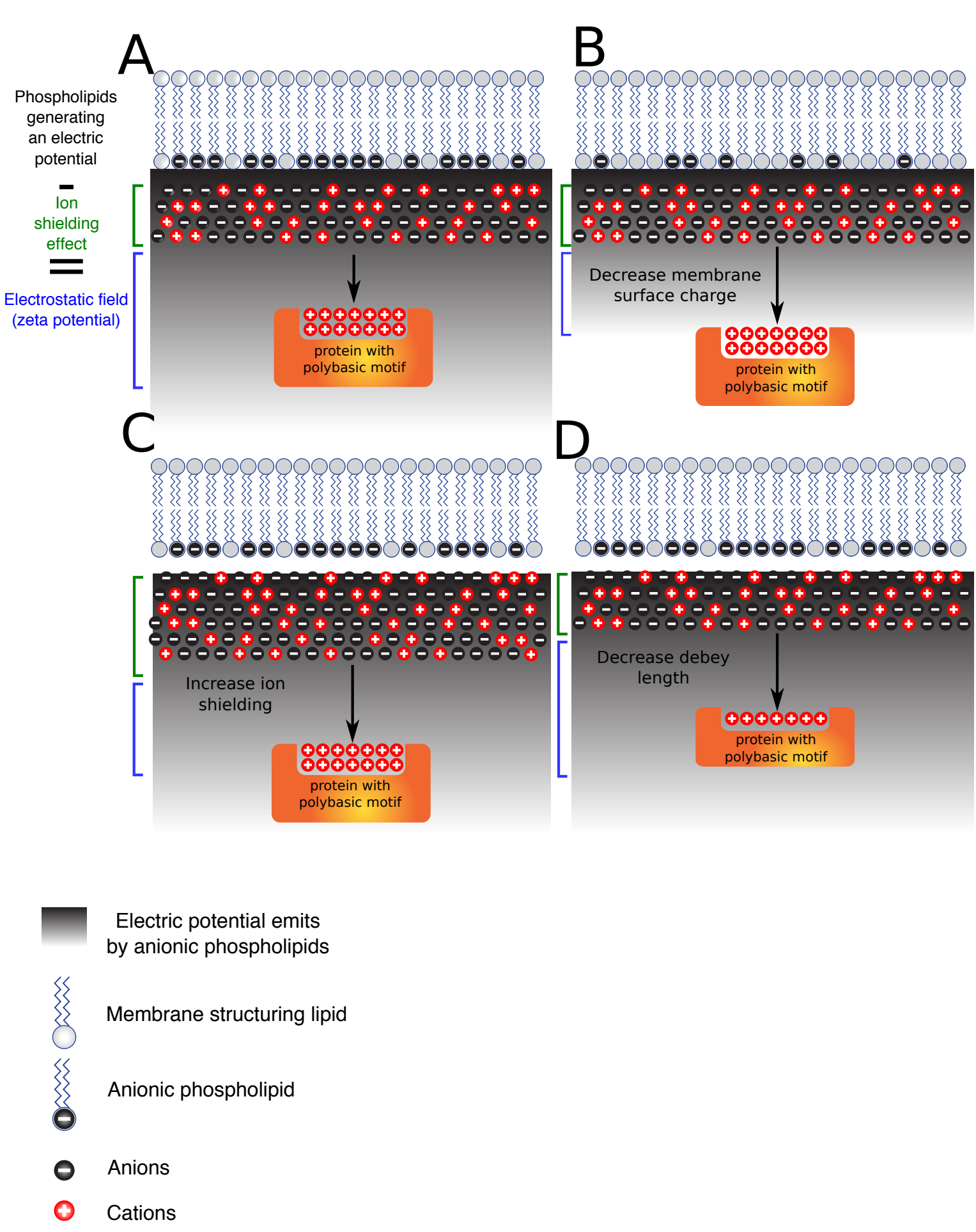

Figure 18. Schematic representation of the attraction strenght modulation. A, Schematic representation of attraction between negative membranes and positively charged protein by electrostatic interaction. **B,** Decrease of the electrostatic field by decreasing the electric potential emits by anionic lipids playing with anionic lipid concentration. **C,** Decrease of the electrostatic field by increasing the ion shielding effect by playing with ions concentration. **D,** Decrease of the strength of the attraction decreasing the number of psositive charge in the protein polycationic region The electric potential emits by anionic phospholipids in represented by black-gray-white gradient. The relative strength of the ion shielding effect and of the electrostatic field is represented by the lenght of the square bracket. The strength of attraction between membrane and protein is represented by a double arrow and is proportional to its length

lacking PI4P, such as *pik1*Δ, where not investigated).

In parallel, Haupt et al., 2017, have investigated the role of PS in defining the electrostatic field of intracellular compartment in *Schyzosaccharomyces pombe* (Haupt and Minc, 2017). In this system, $C2^{LACT}$ and MSC reporters (0+, 2+, 4+, 6+ and 8+) localization closely resemble the situation in animal, with a gradient of PS from the PM to intracellular compartments (Figure 17E-F). Therefore, similar to mammals, PS is likely involved in defining the electrostatics of PM-derived organelles in fission yeast.

Taken together the results presented above indicate that PS is likely the main anionic lipid that drives the membrane surface charge of the TGN and endocytic compartments of both animal and yeast systems. However, the contribution of phosphoinositides in maintaining the electrostatic propeties of endocytic compartments has not been dissected to date (with the exception of PI(3)P and $PI(3,5)P_2$ in yeast). To this end, the +ALPS motif may be used as a sensor of electrostatic curved membranes in futur experiments.

V. Why electrostatism?

The notion of electrostatic interaction is a basic concept corresponding to attraction through weak interactions (Wan Der Walls interactions) between negatively and positively charged molecules. Although “simple”, protein-lipid electrostatic interactions are an extremely powerful way to localize proteins, as they provide localization specificity (at least to some extent) and are highly reversible and amenable to regulations. The latter is particularly important in signaling, as a variation of the strength of electrostatic interaction between the membrane and the protein could lead to a rapid change in protein localization. In this part, I will review how the strenght of the electrostatic interaction may be modulated to regulate cell signaling. Cells have in their tool box three different ways to decrease or increase the recruitment of cationic proteins to the membrane through electrostatic interactions and thereby to modulate protein localization. This can be

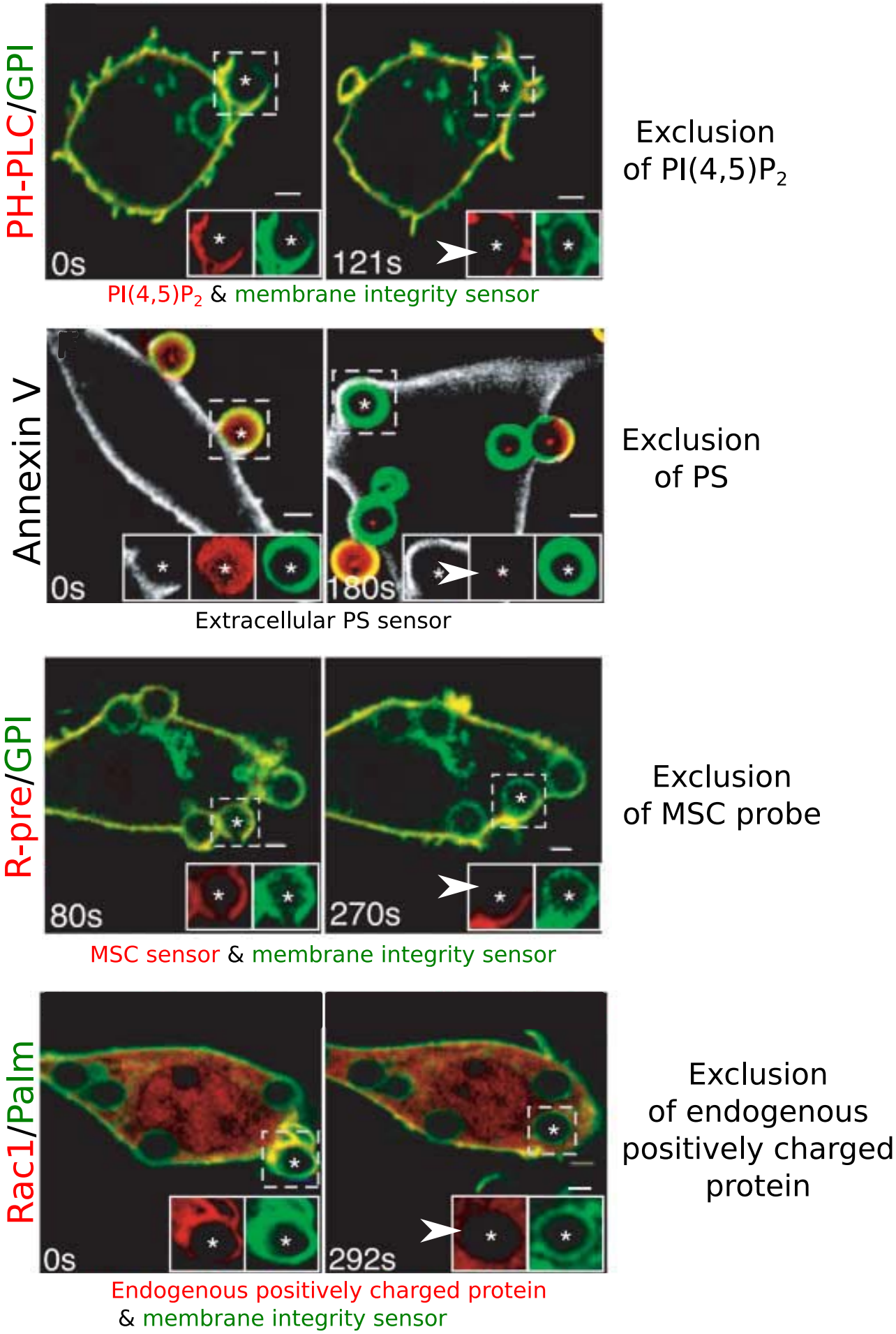

Figure 19. Lipid, charge and cationic protein redistribution during phagocytosis. From top to the bottom, redistribution of PH- PLCd and GPI-GFP during phagocytosis and distribution of PS (white) during phagocytosis. Green, total beads; red, extracellular beads. R-pre/GPI-GFP redistribution during phagocytosis. Asterisks indicate latex beads. Redistribution of Rac1 and Palm during phagocytosis in time course. Arrows indicate the absence of labelling by probes and protein. Adapted from Yeung et al., 2006.

achieved by adjusting i) the spatio-temporal control of anionic phospholipid enrichment (i.e. local production or hydrolysis of anionic lipids), ii) the net charge in the polybasic motif of the protein, and iii) the ion shielding effect (Figure 18). In a physiological context, the modulation of the electrostatic interactions between proteins and the cytosolic face of the plasma membrane have been implicated in numerous signalling processes influencing protein targeting, conformational changes and activity. Here, I will discuss some examples that illustrate these three different ways to modulate protein localization via modulation of electrostatic interaction

a. Tuning the electrostatic field by adjusting the spatio-temporal control of anionic phospholipid enrichment

i. Example 1: Anionic lipid remodeling controls protein dynamics during phagocytosis

In 2006, Yeung et *al.* took advantage of the extensive plasma membrane remodeling during phagocytosis to analyze how variation of membrane composition could control protein recruitment. In nascent phagosome, $PI(4,5)P_2$, PS and MSC probes (R-pre, K-Ras tail) were depleted but not membrane integrity sensors suggesting a local alteration of the electrostatic field. They speculated that these overall variation in PM charges may dynamicaly regulate the localization of phagosome regulators. The small GTPase Rac1 and K-Ras, which have a C-terminal PBR, are involved in cytoskeleton rearrangement and signal transduction, two processes crucial during phagocytosis (Leventis and Silvius, 1998). Both proteins are excluded from nascent autophagosomes, and as such, behave as MSC probes, providing a relevant physiological role to membrane electrostatics (Figure 19). Altogether, the tethering of important signaling molecules, including K-Ras and Rac1, can be modulated focally by localized changes in surface potential regulated by $PI(4,5)P_2$ and/or PS.

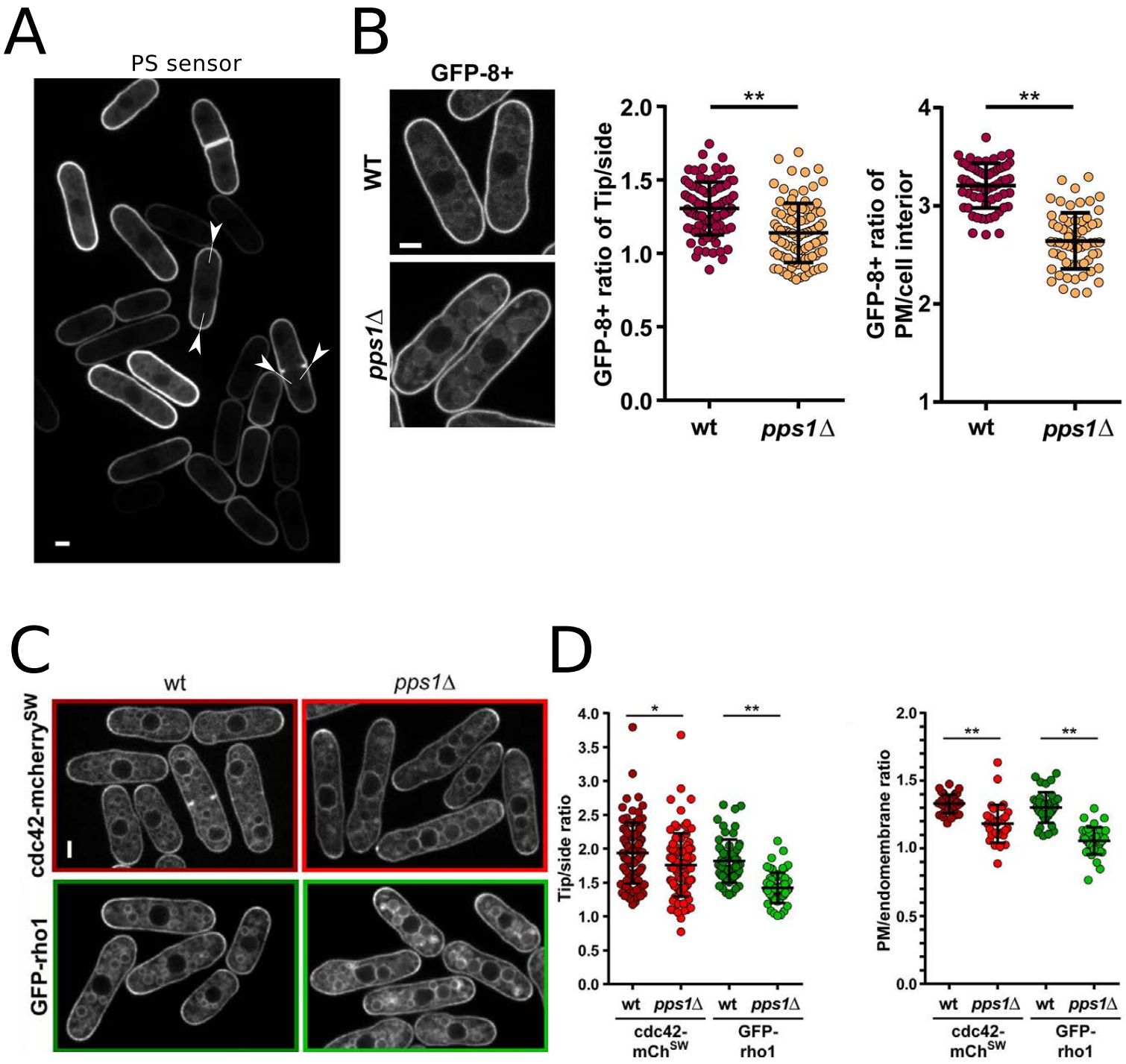

Figure 20. PS is differentialy partioned at the plasma membrane and regulates spatio-temporaly polarized proteins through electrostatic interaction in *S. pombe*. A, Distribution of GFP-LactC2 expressed from an inducible pREP3X plasmid in wild-type cells grown in EMM without thiamine for 48 h. Arrows indicate the enrichment of the PS sensor at the PM at different developmental stages. **B,** Comparison of GFP-8+ probe distribution expressed under the shk1 promotor in wild-type and pps1Δ cells. Left, representative images. Center, quantification of the tip:side ratio on the plasma membrane. Right, quantification of the plasma membrane/cell interior ratio. Scale bars: 2 µm. **C,** Distribution of cdc42-mcherrySW (top, red frames) and GFP-rho1 (bottom, green frames) in wild-type and pps1Δ cells. **D,**Tip:side ratio of cdc42-mcherrySW and GFP-rho1 in wild-type and pps1Δ cells (first graph, left). Plasma membrane: endomembrane ratio of cdc42-mcherrySW and GFP-rho1 in wild-type and pps1Δ cells (second graph, right). Adapted from Haupt et al., 2017.

ii. Example 2: Phosphatidylserine generates a charge gradient along the plasma membrane to coordinate proper polarity in yeast

In baker yeast (*Saccharomyces cerevisiae*), the PS probe $C2^{LACT}$ accumulates massively in the budding site of the yeast during division (Fairn et al., 2011b). Fairn et al., showed that the accumulation of PS at the bud neck is likely due to polarized secretion. This focal PS accumulation is required to polarize cdc42, a Rho GTPase involved in the control of cell division and polarity and that contains a polycationic C-terminal tail. In addition, the KA1 domain containing proteins Kcc4 and Gin4 are localized to the neck region of the growing bud via interaction with PS and this localization is required for proper cell division (Lemmon, 2008).

In fission yeast (*Schyzosaccharomyces pombe*) Haupt et al., monitored the distribution of the PS sensor GFP-$C2^{LACT}$. During interphase, PS sensors localized at the PM and to a lesser extent in intracellular compartments. Interestingly, $C2^{LACT}$ accumulated preferentialy at both cell tips in a polarized-manner. During mitosis, the PS sensor accumulated at the center of the cell at the zone of future cytokinesis and was enriched in region close to the constricting ring (Figure 20A). These results highlight a dynamic distribution of PS depending on the cell cycle status. By contrast to *S. cerevisiae*, in which PS polar accumulation was due to secretion (Fairn et al., 2011b), PS polarity in fission yeast is controled by actin-dependent endocytosis (Haupt and Minc, 2017). Importantly, the localization of the K-Ras based probe (8+) closely matched PS localization suggesting that PS is responsible for a polarized electrostatic field at the PM. Consistently, 8+ PM association and polarity was abolished in a PS synthase mutant (*pps1Δ*), suggesting that polarized PS localization is causal to the polarized electrostatic field in fission yeast (Figure 20B). Rho1 and cdc42, two PBR-containing RhoGTPases involved in cell polarity, are mispolarized in *pps1Δ*, which is consistent with the aberant cell shape and polarity defect of this mutant (Figure 20C). Altogether, these results support the existence of a gradient of negative charges along the plasma membrane that is driven by asymetric PS distribution and is required to define proper cell polarity over the cell cycle.

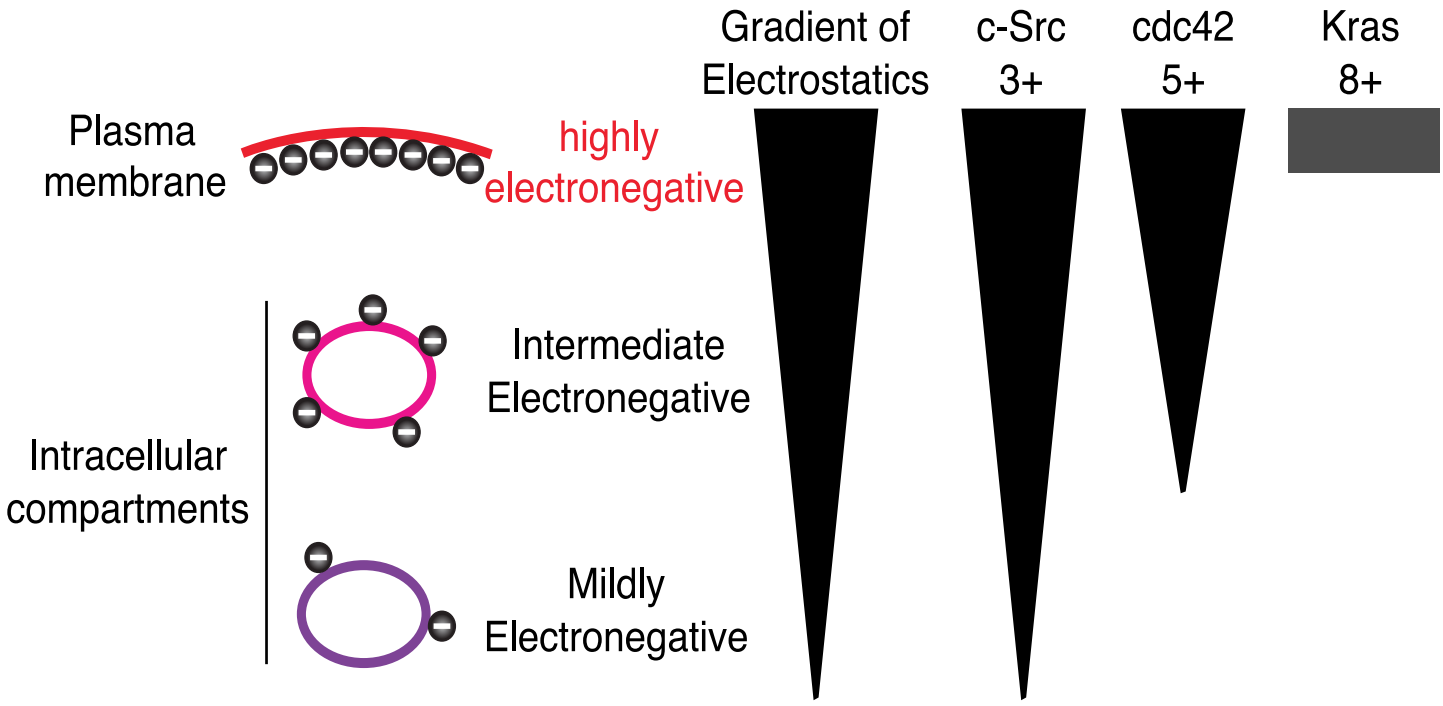

Figure 21. Schematic representation of the subcellular organisation of proteins containing polycationic regionsalong the electrostatic gradient. From the left to the right, representation of the negative charges compartimentalizationwithin cells, whcih generate the gradient of electrostatics and in turn localizes proteins into different intracellular compartments according to their positive charges.
.

b. Modulation of protein cationic regions to drive its own localization

i. Encoding cationic regions with a variety of charges

As mentioned previously, proteins with different charges will differentially localize in the electrostatic territory. Heo et al., generalized this concept as a main driver of small GTPase localization. From all small GTPases (including Ras, Rab, Arf, and Rho proteins), 48 plasma membrane-localized proteins were found[6]. Among these PM-localized small GTPases, 37 contain clusters of positively charged amino acids, indicating a high correlation between the presence of a PBR and plasma membrane localization. However, proteins with intermediate charges do not localize only to the PM and are also found in endosomes (which have intermediate electronegativity). For example, in animal cells, c-Src localizes to both the PM and endosomes and has a polybasic stretch of +5 adjacent to its N-terminal myristoylation anchor (Yeung et al., 2008). Similarly, cdc42 has a PBR of +3 and is not strictly localized at the PM. By contrast, K-Ras, Rho1 or Rac1 are more specific of the plasmalemma and have PBR of +8, +7 and +6, respectively (Figure 21) (Yeung et al., 2008). Therefore, variations in membrane electrostatics within the electrostatic territory is used by cells to drive protein localization in different subcellular compartments (including PM, endosomes and lysosomes localization) depending on the charge of the PBR.

ii. Postranslational modification on proteins and the electrostatic switch hypothesis

The « electrostatic switch » hypothesis was proposed by Stuart McLaughlin in 1995 (McLaughlin and Aderem, 1995). It postulates that phosphorylation of polybasic region(s) in membrane proteins should modify their net charges and may induce repulsion from the membrane (i.e. solubilization into the cytosol) or relocalization from the plasma membrane to intracellular compartments. This model is well documented for two proteins: myristoylated alanine-rich C-

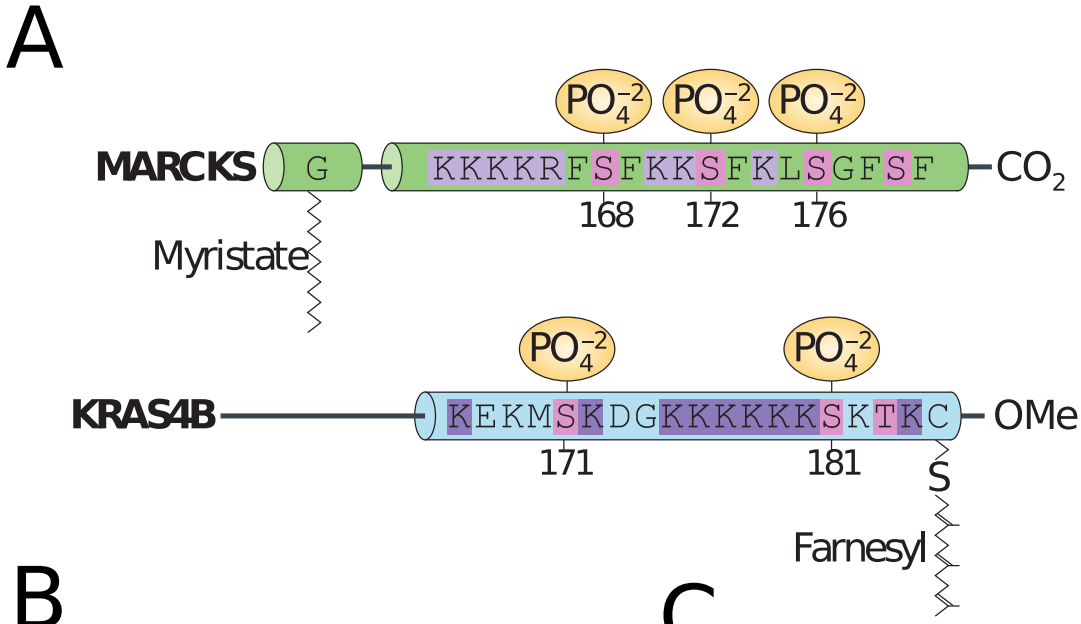

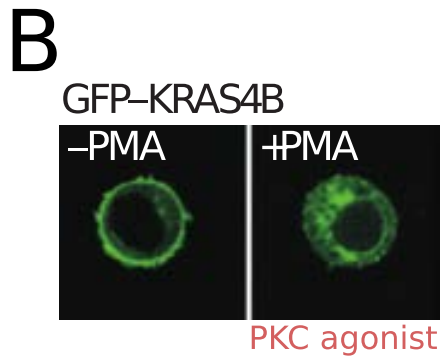

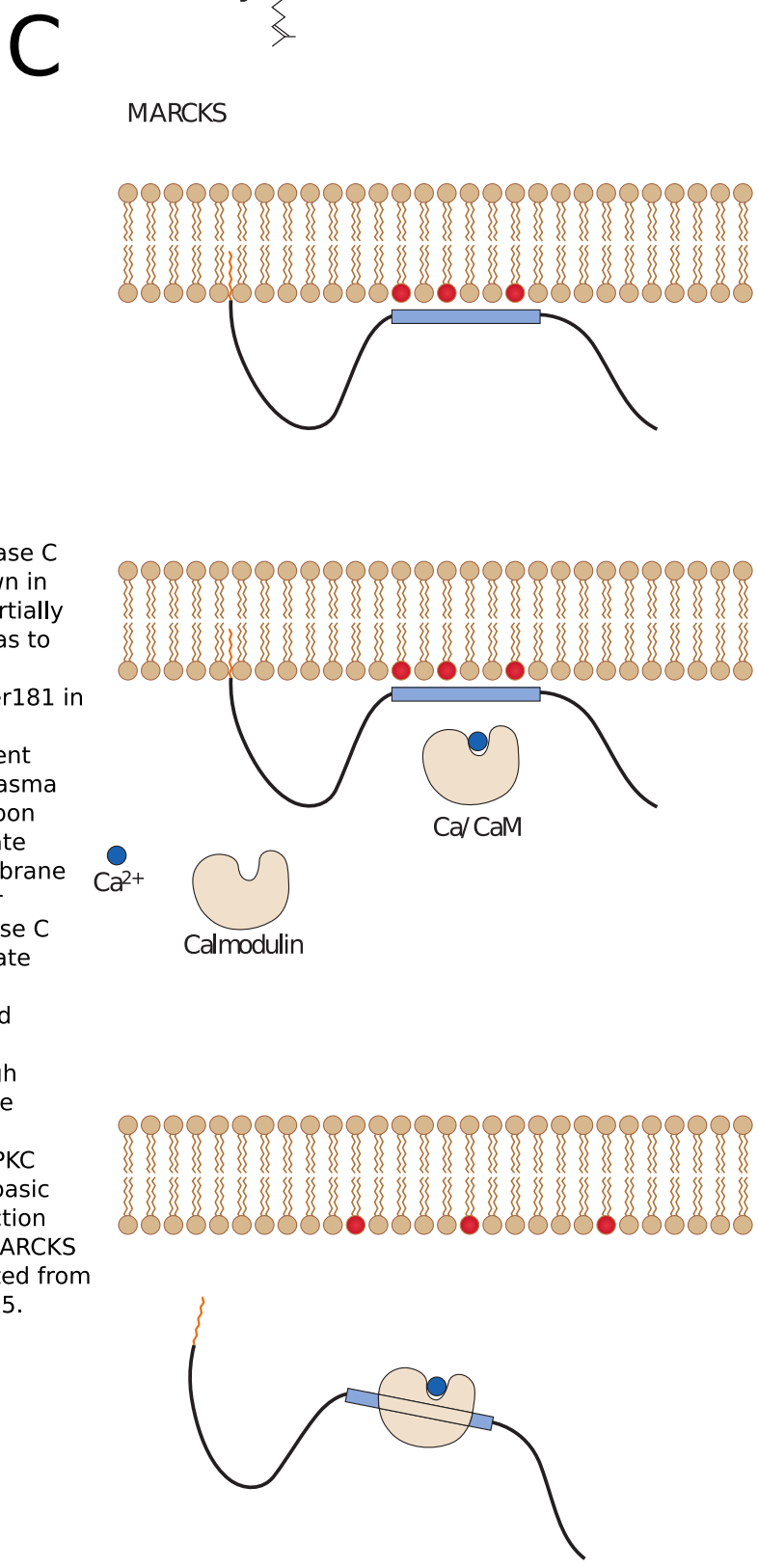

Figure 22. The electrostatic switch controls protein subcellular localization. A, The myristoylated Ala-rich C-kinase substrate (MARCKS) protein and KRAS4B are known to associate conditionally with the plasma membrane in a phosphorylation dependent manner. Protein kinase C (PKC)-induced phosphorylation of Ser residues (shown in pink) within the polybasic region of MARCKS/Kras partially neutralizes its positive charge and allow MARCKS/Kras to fall off the membrane in a process known as a myristoyl–electrostatic switch. Phosphorylation of Ser181 in KRAS4B promotes the dissociation of RAS from membranes. **B,** Images showing that green fluorescent protein (GFP)-bound KRAS4B dissociates from the plasma membrane and is internalized in live Jurkat T cells upon exposure to the PKC agonist phorbol myristate acetate (PMA). **C,** Top, MARCKS attaches to the plasma membrane of a quiescent cell (low free cytoplasmic intracellular calcium concentration ([Ca2+]) and low protein kinase C (PKC) activity) by two anchors, an N-terminal myristate (orange) and a basic 'effector domain' (blue), which sequesters three PIP2 molecules (lipids with red head groups). Middle, When the free cytoplasmic [Ca2+] increases, Ca/CaM binds to the basic cluster with high affinity and pulls it off the membrane, releasing three PIP2 molecules. Bottom, MARCKS bound to Ca/CaM translocates from the membrane to the cytoplasm. PKC phosphorylation of three serine residues within the basic effector domain also reduces its electrostatic interaction with the membrane and produces translocation of MARCKS from the plasma membrane to the cytoplasm. Adapted from Ahearn et al., 2010 and McLaughlin and Murray, 2005.

kinase substrate (MARCKS), which is an unstructured protein that regulates actin dynamics and the oncogenic version of K-Ras (K-Ras4B, hereafter referred to as K-Ras). MARCKS contains at its N-termini a myristoylation site that inserts hydrophobically the protein into the bilayer, and a conserved PBR (13 positive charges) located in the middle of the molecule that sticks electrostatically to the membrane (Figure 22A). K-Ras, as mentioned earlier, contains at its C-termini a PBR (8 positive charges) adjacent to a farnesylation site (Figure 22A). Both proteins are phosphorylated by the protein kinase C (PKC), which is involved in cell motility, phagocytosis, membrane trafficking and mitogenesis. Activation of PKC (for example by phorbol myristate acetate (PMA)) induces the subsequent phosphorylation of MARCKS and K-Ras and triggers their dissociation from the PM (McLaughlin and Murray, 2005) (Figure 22B). In both cases, MARCKS and K-Ras are phosphorylated on serine residues located within the PBR. Each phosphorylation carries two negative charges that decrease the relative positive charge in the PBR, destabilizing the interaction between the protein and the membrane. K-Ras is phosphorylated on two serine residues, which bring the net positive charge of the C-terminal tail from +8 to +4. As a consequence, K-Ras relocalizes to endosomes following PKC activation.

The case of MARCKS is a little bit more complex. Indeed, MARCKS is phosphorylated by PKC on three serine residues, which reduce the net charge of the PBR from +13 to +7. In this condition, MARCKS is solubilized into the cytosol. Such drastic change of localization cannot be explained solely by electrostatic repulsion, given that the phosphorylated PBR (+7) is still highly cationic. Indeed, phosphorylation of the PBR by PKC also induces calmodulin binding in the presence of calcium (McLaughlin and Murray, 2005). The current model is that going from +13 to +7, increases the on/off membrane binding rate of MARCKS, allowing interaction with calmodulin, which will then trigger MARCKS membrane desorption (Figure 22C). This is an elegant variation on the electrostatic switch hypothesis, because it has a switch like behavior (PM or cytosol) and is highly regulated as it requires both PKC activation, and the presence of calcium.

To conclude, cells can adjust the protein Debey length by using post-translational modification such as phosphorylation to regulate the subcellular localization of proteins.

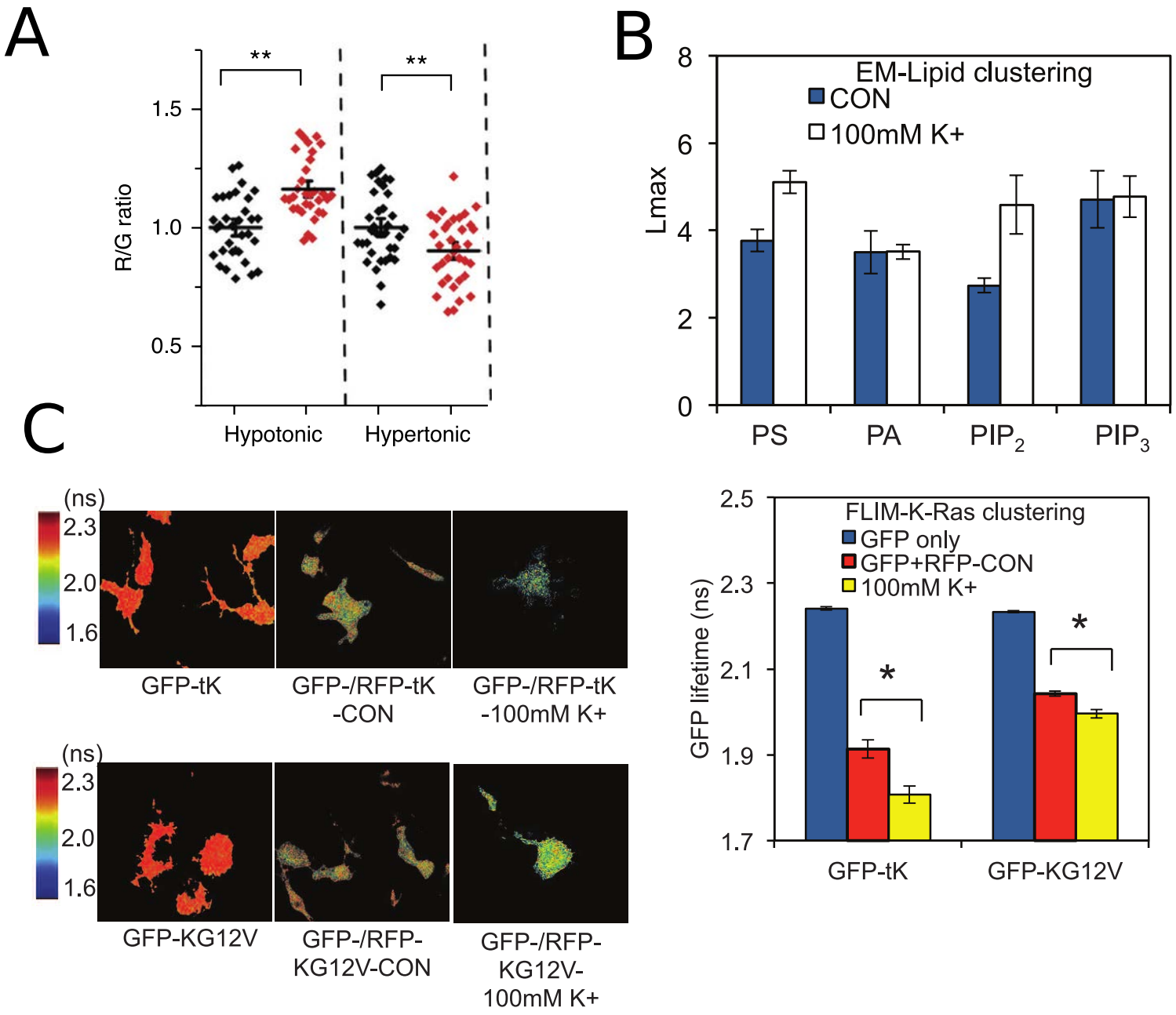

Figure 23. Variation in ion concentration leads to reorganization of membrane electrostatics. A, FRET efficiency of MCS+ in COS-7 cells before (black symbols) and after (red symbols) hypotonic (150 mM to 40 mM) and hypertonic (150 mM to 450 mM) treatments. FRET efficiencies were normalized to the mean of untreated cells. Each symbol is one measurement in one cell; horizontal and vertical bars represent mean and s.e.m., respectively. **B,** Quantification of the extent of nanoclustering of lipid probes for PS, PIP2, PA, or PIP3 in control and depolarized (100 mM [K+]) BHK cells. **C,** FLIM images of differentiated N2A cells expressing the FRET pairs: RFP/GFP-tK (tK is the polybasic C-terminal tail of Kras) or RFP/GFP– K-RasG12V (GFP-KG12V, represent the oncogenic version of Kras corresponding to a constitutive active form) and depolarized with 100 mM [K+] or 50 to 100 mM glutamate (Glu). Quantification of fluorescence lifetime of GFP–K- RasG12V or GFP-tK in N2A cells expressing the cognate RFP-FRET pair treated as in (A). Each data point is the mean (SEM) GFP lifetime measured in >60 individual cells. tK corresponds to the C-terminal tail of K-ras4B which interacts with anionic phospholipids. Adapted from Ma et al., 2017 and Zhou et al., 2015.

c. The ion shielding effect links membrane potential and membrane electrostatics and localy organize the plasma membrane electrostatic field

As mentioned in the introduction, the electrostatic field and membrane potential are two different concepts but are intimately link by the regulation of ions concentration. For example, application of buffers that lack Ca^{2+} and Mg^{2+} increase their ionic strength, which increases the presence of salt in the solution and in turn tunes the concentration of intracellular anions and cations. Applying such buffer to cells decreases the FRET efficiency of the MCS+ FRET-based sensor[29]. Conversely, treating cells with hypotonic solution results in an intracellular influx of water molecules reducing the concentration of ions in the cytoplasm and limiting the shielding effect of membrane surface charge. Consistently, hypotonic solution increases the FRET efficiency, while hypertonic solution decrease the FRET efficiency of the MCS+ probe[29] (Figure 23A). Taken together, these results indicate that a reduction of the ion shielding effect increases the apparent electrostatic potential of the membrane and suggest that the membrane potential may influence protein targeting by electrostatic interactions. Such example was recently documented by the group of John Hancock, which reported that membrane potential tunes K-Ras localization and activity (Zhou et al., 2015). Zhou et al., in 2015, investigated for the first time the link between membrane surface charges and the membrane potential. Treatment with exogenous extracellular potassium rapidly influences the membrane potential (within seconds) but also triggers changes in the plasma membrane dynamics of intracellular lipids, PS and $PI(4,5)P_2$ (i.e. the two key anionic lipids that maintain the PM electrostatic field). These changes in lipid localization are rapid (30s for PS, 5 min for $PI(4,5)P_2$) and consist in the relocalization of PS and $PI(4,5)P_2$ into nanoclusters at the cell surface. PS (and to a lesser extent $PI(4,5)P_2$, see next paragraph) nanoclustering locally creates electrostatic patches at the plasma membrane that attracts K-Ras via its PBR (Figure 23B). A string of paper from the same group had established earlier that accumulation of K-Ras into PM nanoclusters is necessary and sufficient for its activation (Zhou and Hancock, 2015). Indeed, they showed that modification of the membrane potential directly regulates K-Ras signaling output, such as MAP Kinase phosphorylation.

To date, this is the only paper describing a direct link *in vivo* between the membrane potential and surface charges through the regulation of ions concentration. Surprisingly, in this study,

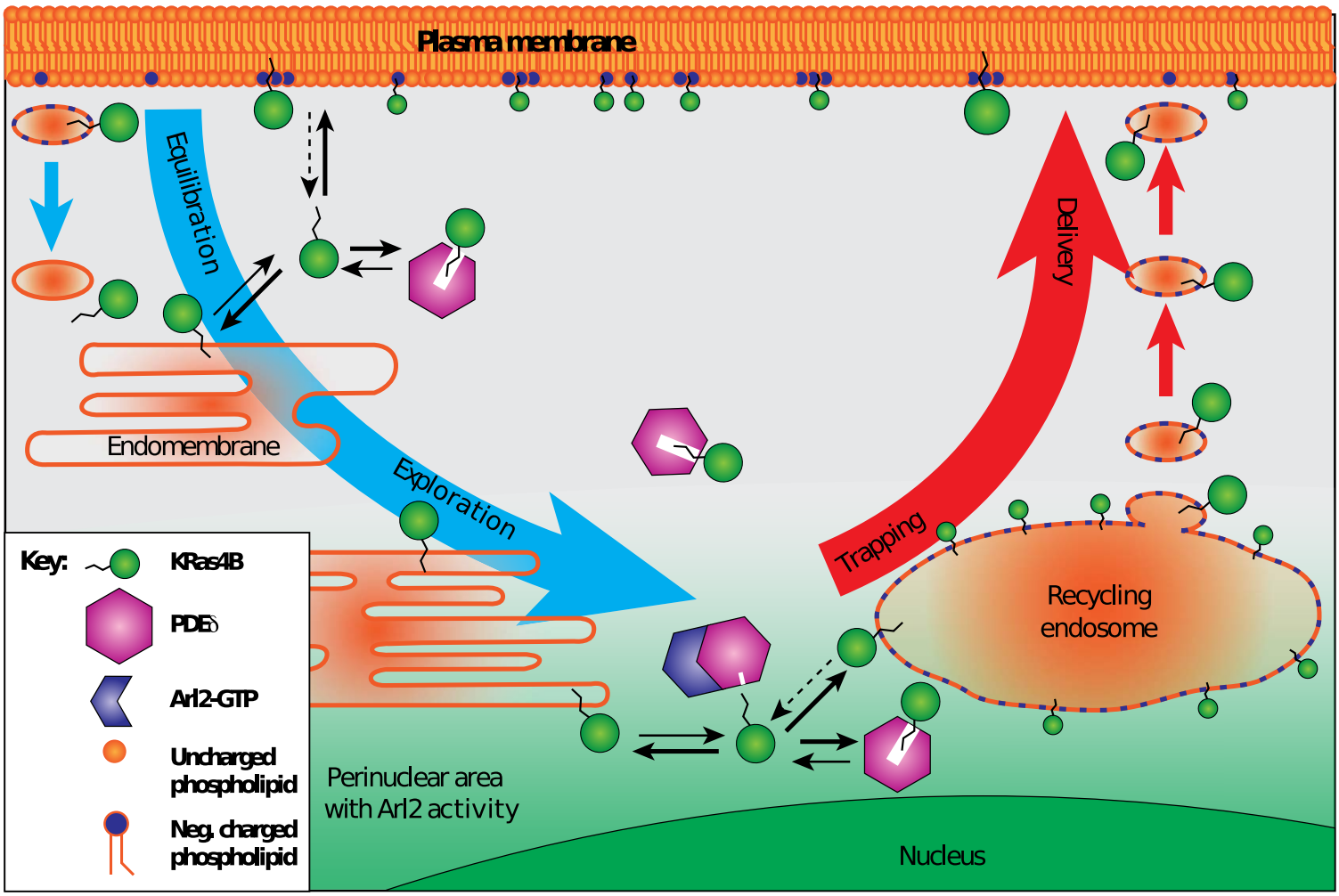

Figure 24. KRas4B localization cycle. KRas4B is lost (big blue arrow) from the plasma membrane (PM) by endocytosis (small blue arrow) and spontaneous dissociation. Endocytic vesicles lose their surface charge and let KRas4B dissociate into the cytosol from where it can bind to endomembranes or phosphodiesterase 6d (PDEd). Solubilizing KRas4B via PDEd enables subsequent Arf-like (Arl)2-GTP-mediated release in the perinuclear area (thick blue arrow), which is represented by a green gradient. This localized release concentrates KRas4B on perinuclear membranes. Here, KRas4B is trapped by the negatively charged recycling endosome (RE), from which directional vesicular transport brings it back to the plasma membrane (thick red arrow). This concerted cyclic process dynamically maintains KRas4B at the PM. The thickness of the black reaction arrows – connecting large KRas4B symbols – denotes the respective conversion rates between KRas4B binding states: cytosolic or bound to membranes or to PDEd. Adapted from Schmick et al., 2015.

changes in membrane potential do not modify overall the PM electrostatic field, but reorganize it within the plane of the PM. This spatial reorganization of the PM in turn affect signaling pathways (at least K-Ras, but likely others). It will be interesting in the future to understand the mechanisms that couple changes in membrane potential with local variations in lipid concentration at the PM.

VI. The limits of the electrostatic framework

a. Membrane targetting: a combination of electrostatic, hydrophobic interactions and trafficking.

Protein regions that interact with anionic membranes do not only rely on positively charged residues but also hydrophobic interactions (provided either by aromatic residues or a lipid anchor). For example, K-Ras farnesylation is required for its targeting to the plasma membrane, demonstrating that electrostatic interactions on their own are not sufficient for protein targeting.

In addition, the group of Philippe Bastiaens (Chandra et al., 2012) recently showed that K-Ras localization also depends on intracellular trafficking. Indeed, K-Ras PM targeting depends on PDEzeta and Arl2-GTP proteins(Chandra et al., 2012). Mechanistically, PDEzeta traps newly endocytosed K-Ras in the cytosol shielding its farnesyl anchor and PBR and preventing membrane interaction. PDEzeta interacts with Arl2-GTP on recycling endosomes. Arl2-GTP allows the dissociation of PDEzeta, which releases the farnesyl anchor from K-Ras and exposes its PBR. Because recycling endosomes are electrostatic, this allows stable membrane association of K-Ras on recycling endosomes and its subsequent trafficking to the PM (Figure 24).

Altogether, those findings support the notion that electrostatic interactions are not sufficient but are required for protein-membrane association. It seems that electrostatic interactions could act as a general and reversible targeting mechanisms that can be tweaked by additional regulatory mechanisms to fine-tune protein localization and dynamics.

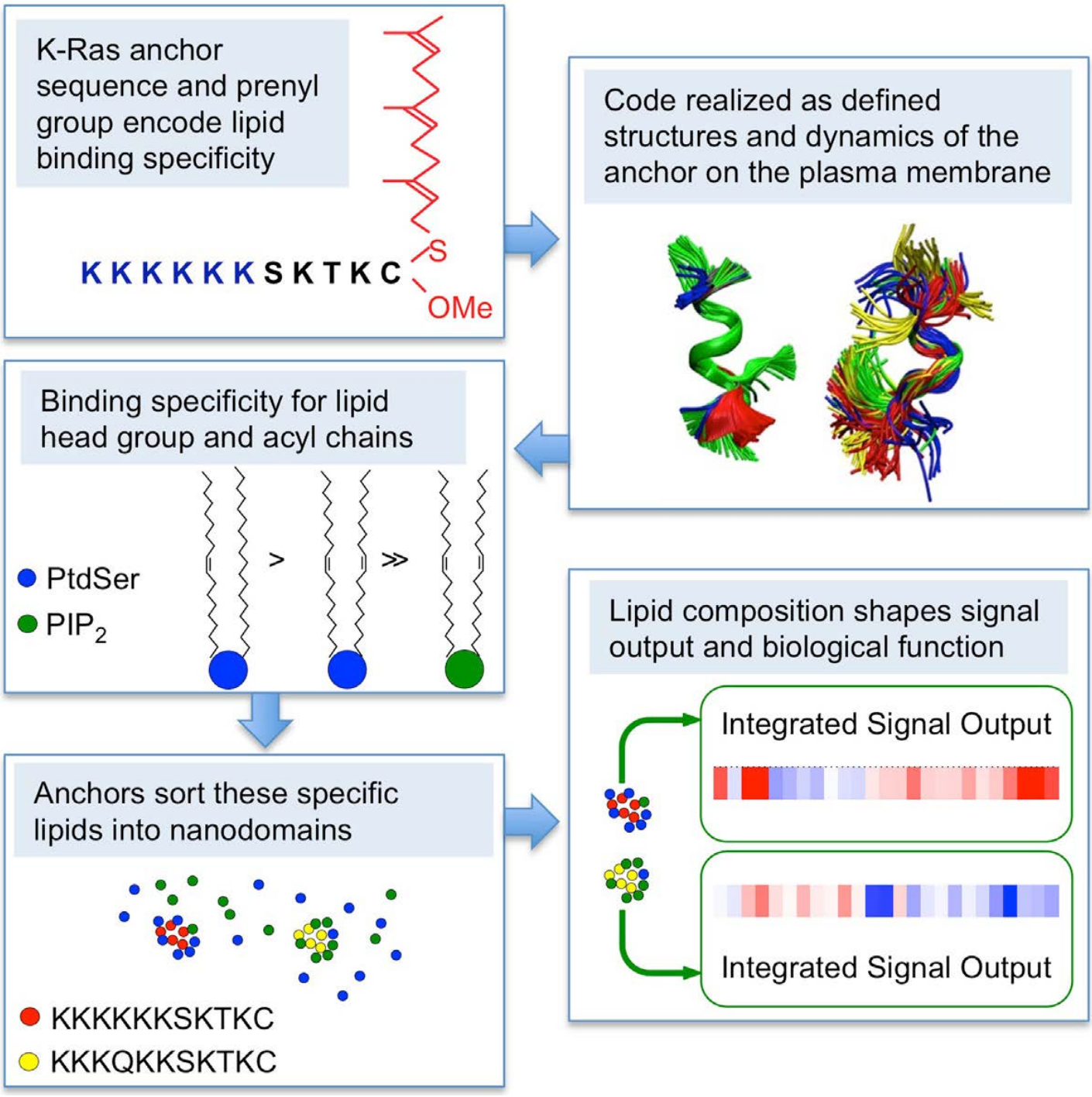

Figure 25. Selective interactions with lipids shapes Ras signaling output through formation of nanoclusters. The K-Ras C-terminal tail encodes previously unsuspected anionic lipid binding specificity according the sequence in its polybasic region and the anchor. Lipid selectivity is realized by defined conformational structures of the anchor. Lipid sorting capacity of the anchor is a key determinant of K-Ras signal output. Adapted from Zhou et al., 2017.

b. Polybasic regions may have specificity for lipid head group

It is clear from this introduction that K-Ras is by far the most studied protein that rely on electrostatic interaction for PM targeting. This is likely because K-Ras is mutated in 30% of all cancers, and is therefore highly relevant to human health. While it is very well established that the K-Ras C-terminal tail, which contains 8 Lysines (+8), interacts with the PM via electrostatic interactions, a recent paper from John Hancock's group revealed that this tail harbors some specificity *in vivo* for certain anionic lipids (Zhou et al., 2016).

The K-Ras C-terminal membrane anchor is also called the hyper-variable region (HRV) because other RAS proteins contain different lipid modifications (e.g. geranylgeranylation) and other amino acids sequence in their PBR tail. A recent study asked whether the HVR could be involved in K-Ras plasma membrane partitioning since it localizes to nanoclusters when activated and not when in resting conditions. Using electron microscopy spatial mapping, Zhou et al., showed that K-Ras tail interacts with selected species of phosphatidylserine and that single residue mutation, even when conserving the overall charge, influenced the lipid association in cells. Therefore, the authors postulated that there is a combinatorial lipid sorting code defined by the prenyl anchor and PBR sequence. K-Ras PBR is thought to be unstructured, it is therefore difficult to explain how small variations in the PBR sequence may affect the association with a specific type of lipid *in vivo*. All-atom molecular dynamics (MD) simulations found that K-Ras C-terminal tail (PBR + farnesyl moiety) is not completely disordered; rather it adopts a few relatively well-defined dynamic structures. The simulation found three main types of structural arrangements: D (disordered: no secondary structure), I (intermediate, with one or two helical turn) and O (ordered). Simulations determined that the free energy difference between the O and D state is relatively small (ΔG = -2.5 kcal/mol) and that therefore the three conformations observed in MD likely represent inter-converting equilibrium states. MD simulations of K-Ras C-terminal tail found 64% in the D state, 35% in the I state and 0% in the O state. Each structural group differed in the contribution of individual lysine residue to membrane binding via interaction with PS. For example, K177 interacts with PS in the I and D states but not in the O state, while K178 interacts similarly in all three. Therefore, mutations of K177 and K178 do not have the same effect on

membrane association (Figure 25). To conclude, although the polybasic regions that are adjacent to lipid anchors are mostly disordered, they actually sample several conformations. Therefore, the exact ordered of the amino acid sequence may influence lipid specificity, which is important for membrane binding. Overall, these slight variations may not have a strong impact for the selection of the membrane compartments but they may influence lateral segregation of proteins within the plane of the membrane.

I propose the following general framework for the localization of peripheral PBR-containing proteins: 1) hydrophobic anchor (lipid modification, aromatic residues) address the protein to membranes with limited specificity, 2) the polybasic region attracts the protein to a given membrane depending on its own debey length and the zeta potential of the membrane and 3) once addressed to the proper cellular compartment (e.g. plasma membrane) the nature and sequence of the PBR, together with the nature of the hydrophobic anchor, will define lipid preferences and influence the lateral segregation of the protein.

VII. General conclusion and problematic

To conclude, eukaryotic cells share common feature regarding the maintenance of the electrostatic field. Even though they are pluricellular (animals) or unicellular (yeast) organisms, it seems that eukaryotic cells have an electrostatic territory with the PM beeing the most electronegative compartment. However, differences exist concerning the lipids that are involved in the maintenance of the membrane surface charge notably at the plasmalemma. In yeast, PS is the major anionic lipid that drives plasma membrane surface charge, while PIPs are not required. In metazoans, PIPs are required to control PM MSC maintenance and several PIP species act redundantly to control PM electrostatics (Hammond et al. 2012; Dong et al. 2015; Heo et al. 2006). While direct evidence are still lacking to establish whether PS is involved in PM MSC in animals, pharmacological analyses suggest a role for PS in this property (Yeung et al., 2008; Ma et al., 2017). The plasma membrane is not the only electronegative membrane and PS bearing organelles are also electrostatics, which likely controls the localization of polybasic proteins with

different net positive charges.

In my PhD work, I analyzed how membrane electrostatics is organised in plants, using *Arabidopsis thaliana* as a model, in order to compare what are the similitudes and differences with other eukarytic systems.

I notably addressed the following questions:

1. How is the electrostatic field organized in plants?
2. How does it spatially organize compared to other eukaryotic organisms?
3. Which is (are) the anionic lipid(s) that is (are) required to maintain the electrostatic field on different organelle membranes?
4. What is (are) the function(s) of membrane electrostatics in signaling and plant development?

Athenstaedt, K., and Daum, G. (1999). Phosphatidic acid, a key intermediate in lipid metabolism. FEBS J. *266*, 1–16.

Balla, T. (2013). Phosphoinositides: Tiny Lipids With Giant Impact on Cell Regulation. Physiol. Rev. *93*, 1019–1137.

Bankaitis, V.A., Mousley, C.J., and Schaaf, G. (2010). The Sec14 superfamily and mechanisms for crosstalk between lipid metabolism and lipid signaling. Trends Biochem. Sci. *35*, 150–160.

Bigay, J., and Antonny, B. (2012). Curvature, Lipid Packing, and Electrostatics of Membrane Organelles: Defining Cellular Territories in Determining Specificity. Dev. Cell *23*, 886–895.

Bochud, A., and Conzelmann, A. (2015). The active site of yeast phosphatidylinositol synthase Pis1 is facing the cytosol. Biochim. Biophys. Acta BBA - Mol. Cell Biol. Lipids *1851*, 629–640.

Bohdanowicz, M., Schlam, D., Hermansson, M., Rizzuti, D., Fairn, G.D., Ueyama, T., Somerharju, P., Du, G., and Grinstein, S. (2013). Phosphatidic acid is required for the constitutive ruffling and macropinocytosis of phagocytes. Mol. Biol. Cell *24*, 1700–1712.

Chandra, A., Grecco, H.E., Pisupati, V., Perera, D., Cassidy, L., Skoulidis, F., Ismail, S.A., Hedberg, C., Hanzal-Bayer, M., Venkitaraman, A.R., et al. (2012). The GDI-like solubilizing factor PDEδ sustains the spatial organization and signalling of Ras family proteins. Nat. Cell Biol. *14*, 148–158.

Cho, K. -j., van der Hoeven, D., Zhou, Y., Maekawa, M., Ma, X., Chen, W., Fairn, G.D., and Hancock, J.F. (2015). Inhibition of acid sphingomyelinase depletes cellular phosphatidylserine and mislocalizes K-Ras from the plasma membrane. Mol. Cell. Biol.

Chung, J., Torta, F., Masai, K., Lucast, L., Czapla, H., Tanner, L.B., Narayanaswamy, P., Wenk, M.R., Nakatsu, F., and Camilli, P.D. (2015). PI4P/phosphatidylserine countertransport at ORP5- and ORP8-mediated ER–plasma membrane contacts. Science *349*, 428–432.

Fairn, G.D., Schieber, N.L., Ariotti, N., Murphy, S., Kuerschner, L., Webb, R.I., Grinstein, S., and Parton, R.G. (2011a). High-resolution mapping reveals topologically distinct cellular pools of phosphatidylserine. J. Cell Biol. *194*, 257–275.

Fairn, G.D., Hermansson, M., Somerharju, P., and Grinstein, S. (2011b). Phosphatidylserine is polarized and required for proper Cdc42 localization and for development of cell polarity. Nat. Cell Biol. *13*, 1424–1430.

Filseck, J.M. von, Čopič, A., Delfosse, V., Vanni, S., Jackson, C.L., Bourguet, W., and Drin, G. (2015). Phosphatidylserine transport by ORP/Osh proteins is driven by phosphatidylinositol 4-phosphate. Science *349*, 432–436.

Hammond, G.R.V., Schiavo, G., and Irvine, R.F. (2009). Immunocytochemical techniques reveal

multiple, distinct cellular pools of PtdIns4P and PtdIns(4,5)P2. Biochem. J. *422*, 23–35.

Hammond, G.R.V., Fischer, M.J., Anderson, K.E., Holdich, J., Koteci, A., Balla, T., and Irvine, R.F. (2012). PI4P and PI(4,5)P2 Are Essential But Independent Lipid Determinants of Membrane Identity. Science *337*, 727–730.

Hankins, H.M., Baldridge, R.D., Xu, P., and Graham, T.R. (2015). Role of flippases, scramblases, and transfer proteins in phosphatidylserine subcellular distribution. Traffic Cph. Den. *16*, 35.

Haupt, A., and Minc, N. (2017). Gradients of phosphatidylserine contribute to plasma membrane charge localization and cell polarity in fission yeast. Mol. Biol. Cell *28*, 210–220.

Heo, W.D., Inoue, T., Park, W.S., Kim, M.L., Park, B.O., Wandless, T.J., and Meyer, T. (2006). PI(3,4,5)P3 and PI(4,5)P2 Lipids Target Proteins with Polybasic Clusters to the Plasma Membrane. Science *314*, 1458–1461.

Hermansson, M., Hokynar, K., and Somerharju, P. (2011). Mechanisms of glycerophospholipid homeostasis in mammalian cells. Prog. Lipid Res. *50*, 240–257.

van der Hoeven, D., Cho, K. -j., Ma, X., Chigurupati, S., Parton, R.G., and Hancock, J.F. (2013). Fendiline Inhibits K-Ras Plasma Membrane Localization and Blocks K-Ras Signal Transmission. Mol. Cell. Biol. *33*, 237–251.

Jackson, C.L., Walch, L., and Verbavatz, J.-M. (2016). Lipids and Their Trafficking: An Integral Part of Cellular Organization. Dev. Cell *39*, 139–153.

Kim, Y.J., Guzman-Hernandez, M.L., and Balla, T. (2011). A Highly Dynamic ER-Derived Phosphatidylinositol-Synthesizing Organelle Supplies Phosphoinositides to Cellular Membranes. Dev. Cell *21*, 813–824.

Kim, Y.J., Guzman-Hernandez, M.-L., Wisniewski, E., and Balla, T. (2015). Phosphatidylinositol-Phosphatidic Acid Exchange by Nir2 at ER-PM Contact Sites Maintains Phosphoinositide Signaling Competence. Dev. Cell *33*, 549–561.

Klose, C., Surma, M.A., Gerl, M.J., Meyenhofer, F., Shevchenko, A., and Simons, K. (2012). Flexibility of a Eukaryotic Lipidome – Insights from Yeast Lipidomics. PLOS ONE *7*, e35063.

Lemmon, M.A. (2008). Membrane recognition by phospholipid-binding domains. Nat. Rev. Mol. Cell Biol. *9*, 99–111.

Leventis, P.A., and Grinstein, S. (2010). The Distribution and Function of Phosphatidylserine in Cellular Membranes. Annu. Rev. Biophys. *39*, 407–427.

Leventis, R., and Silvius, J.R. (1998). Lipid-Binding Characteristics of the Polybasic Carboxy-

Terminal Sequence of K-ras 4B. Biochemistry (Mosc.) *37*, 7640–7648.

Ma, Y., Yamamoto, Y., Nicovich, P.R., Goyette, J., Rossy, J., Gooding, J.J., and Gaus, K. (2017). A FRET sensor enables quantitative measurements of membrane charges in live cells. Nat. Biotechnol. *35*, 363–370.

Maeda, K., Anand, K., Chiapparino, A., Kumar, A., Poletto, M., Kaksonen, M., and Gavin, A.-C. (2013). Interactome map uncovers phosphatidylserine transport by oxysterol-binding proteins. Nature *501*, 257–261.

Mayinger, P. (2012). Phosphoinositides and vesicular membrane traffic. Biochim. Biophys. Acta BBA - Mol. Cell Biol. Lipids *1821*, 1104–1113.

McLaughlin, S. (1989). The Electrostatic Properties of Membranes. Annu. Rev. Biophys. Biophys. Chem. *18*, 113–136.

McLaughlin, S., and Aderem, A. (1995). The myristoyl-electrostatic switch: a modulator of reversible protein-membrane interactions. Trends Biochem. Sci. *20*, 272–276.

McLaughlin, S., and Murray, D. (2005). Plasma membrane phosphoinositide organization by protein electrostatics. Nature *438*, 605–611.

Moravcevic, K., Mendrola, J.M., Schmitz, K.R., Wang, Y.-H., Slochower, D., Janmey, P.A., and Lemmon, M.A. (2010). Kinase Associated-1 Domains Drive MARK/PAR1 Kinases to Membrane Targets by Binding Acidic Phospholipids. Cell *143*, 966–977.

Moser von Filseck, J., opi, A., Delfosse, V., Vanni, S., Jackson, C.L., Bourguet, W., and Drin, G. (2015). Phosphatidylserine transport by ORP/Osh proteins is driven by phosphatidylinositol 4-phosphate. Science *349*, 432–436.

Payrastre, B., Missy, K., Giuriato, S., Bodin, S., Plantavid, M., and Gratacap, M.-P. (2001). Phosphoinositides : key players in cell signalling, in time and space. Cell. Signal. *13*, 377–387.

Platre, M.P., and Jaillais, Y. (2017). Anionic lipids and the maintenance of membrane electrostatics in eukaryotes. Plant Signal. Behav. *12*, e1282022.

Sohn, M., Ivanova, P., Brown, H.A., Toth, D.J., Varnai, P., Kim, Y.J., and Balla, T. (2016). Lenz-Majewski mutations in PTDSS1 affect phosphatidylinositol 4-phosphate metabolism at ER-PM and ER-Golgi junctions. Proc. Natl. Acad. Sci. U. S. A. *113*, 4314.

Sousa, S.B., Jenkins, D., Chanudet, E., Tasseva, G., Ishida, M., Anderson, G., Docker, J., Ryten, M., Sa, J., Saraiva, J.M., et al. (2013). Gain-of-function mutations in the phosphatidylserine synthase 1 (PTDSS1) gene cause Lenz-Majewski syndrome. Nat. Genet. *46*, 70–76.

Xu, P., Baldridge, R.D., Chi, R.J., Burd, C.G., and Graham, T.R. (2013). Phosphatidylserine

flipping enhances membrane curvature and negative charge required for vesicular transport. J Cell Biol *202*, 875–886.

Yeung, T., Terebiznik, M., Yu, L., Silvius, J., Abidi, W.M., Philips, M., Levine, T., Kapus, A., and Grinstein, S. (2006). Receptor Activation Alters Inner Surface Potential During Phagocytosis. Science *313*, 347–351.

Yeung, T., Gilbert, G.E., Shi, J., Silvius, J., Kapus, A., and Grinstein, S. (2008). Membrane Phosphatidylserine Regulates Surface Charge and Protein Localization. Science *319*, 210–213.

Zhang, F., Wang, Z., Lu, M., Yonekubo, Y., Liang, X., Zhang, Y., Wu, P., Zhou, Y., Grinstein, S., Hancock, J.F., et al. (2014). Temporal Production of the Signaling Lipid Phosphatidic Acid by Phospholipase D2 Determines the Output of Extracellular Signal-Regulated Kinase Signaling in Cancer Cells. Mol. Cell. Biol. *34*, 84–95.

Zhou, Y., and Hancock, J.F. (2015). Ras nanoclusters: Versatile lipid-based signaling platforms. Biochim. Biophys. Acta BBA - Mol. Cell Res. *1853*, 841–849.

Zhou, Y., Wong, C.-O., Cho, K., Hoeven, D. van der, Liang, H., Thakur, D.P., Luo, J., Babic, M., Zinsmaier, K.E., Zhu, M.X., et al. (2015). Membrane potential modulates plasma membrane phospholipid dynamics and K-Ras signaling. Science *349*, 873–876.

Zhou, Y., Prakash, P., Liang, H., Cho, K.-J., Gorfe, A.A., and Hancock, J.F. (2016). Lipid-Sorting Specificity Encoded in K-Ras Membrane Anchor Regulates Signal Output. Cell.

B. RESULTS

Chapter I : A PtdIns(4)P-driven electrostatic field controls cell membrane identity and signalling in plants

HHS Public Access

Author manuscript

Nat Plants. Author manuscript; available in PMC 2016 December 20.

Published in final edited form as:

Nat Plants. ; 2: 16089. doi:10.1038/nplants.2016.89.

A PI4P-driven electrostatic field controls cell membrane identity and signaling in plants

Mathilde Laetitia Audrey Simon[1,*], **Matthieu Pierre Platre**[1,*], **Maria Mar Marquès-Bueno**[1], **Laia Armengot**[1], **Thomas Stanislas**[1], **Vincent Bayle**[1], **Marie-Cécile Caillaud**[1,#], and **Yvon Jaillais**[1,#]

[1]Laboratoire de Reproduction et Développement des Plantes, UMR 5667 CNRS/INRA/ENS-Lyon/ Université de Lyon, 46 allée d'Italie, 69364 Lyon Cedex 07, France

Abstract

Many signaling proteins permanently or transiently localize to specific organelles for function. It is well established that certain lipids act as biochemical landmarks to specify compartment identity. However, they also influence membrane biophysical properties, which emerge as important features in specifying cellular territories. Such parameters include the membrane inner surface potential, which varies according to the lipid composition of each organelle. Here, we found that the plant plasma membrane (PM) and the cell plate of dividing cells have a unique electrostatic signature controlled by phosphatidylinositol-4-phosphate (PI4P). Our results further reveal that, contrarily to other eukaryotes, PI4P massively accumulates at the PM, establishing it as a critical hallmark of this membrane in plants. Membrane surface charges control the PM localization and function of the polar auxin transport regulator PINOID, as well as proteins from the BRI1 KINASE INHIBITOR1 (BKI1)/MEMBRANE ASSOCIATED KINASE REGULATORs (MAKRs) family, which are involved in brassinosteroid and receptor-like kinase signaling. We anticipate that this PI4P-driven physical membrane property will control the localization and function of many proteins involved in development, reproduction, immunity and nutrition.

Each membrane compartment has a unique identity and thereby recruits a specific set of proteins[1–3]. It has been established for decades that these identities are acquired by the combined presence of specific lipid and protein molecules that act as biochemical landmark on each membrane. For example, small GTPases from the Rab and ADP ribosylation factor (ARF) family as well as Soluble N-ethylmaleimide-sensitive-factor Attachment protein

[#]Correspondence and requests for materials should be addressed to Y.J. (yvon.jaillais@ens-lyon.fr) and M.C.C (marie-cecile.caillaud@ens-lyon.fr).

[*]These authors contributed equally to this work

Author contributions: M.S., M.P. and M.C.C produced and imaged the lipid and MSC reporter lines, M.S., M.P., M.C.C and T.S. imaged the KA1^{MARK1} reporter in various tissues and plant systems, M.S. and M.P. carried out the PAO and WM experiments, V.B. performed the FRAP experiments and helped with image quantification and acquisition, M.C.C. performed cytokinesis and *N. Benthamiana* experiments, M.S., M.M.M.B and L.A. performed yeast and lipid overlay experiments, M.M.M.B and L.A. produced and imaged the MAKRs-cYFP lines, M.S. produced and phenotyped the *EXP7::PID* lines, M.S., M.P., M.C.C and Y.J. conceived the study and designed experiments, M.S., M.P., M.C.C. and Y.J. wrote the manuscript.

The authors declare no competing financial interests.

Receptor (SNARE) families are important components that contribute to membrane identity[1]. On the lipid side, major determinants that distinguish one membrane from another belong to the phosphatidylinositol phosphate family (also known as phosphoinositides or PIPs)[4]. These phospholipids have an inositol head group that can be phosphorylated at various positions on their polar head[4,5]. Many organelles contain a specific combination of phosphoinositides, which therefore attract proteins containing PIP-interacting stereospecific domains[3,5,6]. Furthermore, it is well established that phosphoinositide production, dynamics and localization are regulated by Rab, ARF and SNARE proteins and conversely, that the activity and localization of these regulators is under the control of PIPs[1].

More recently, it was also recognized that each membrane can additionally be distinguished by its own biophysical properties, including lipid packing, curvature and electrostatics[7]. While the importance of these parameters were acknowledged long ago by biophysicists using theoretical modeling and artificial membrane systems, tools to probe these particular membrane properties in vivo have only recently been developed and have seldom been used so far in plants. Plant membranes share many characteristics with other eukaryotes; nonetheless they have singular features, including the presence of unique lipids (e.g. phytosterols, highly polar phytosphingolipids, galactolipids)[8–10] and a drastically different endomembrane system (e.g. presence of chloroplasts, plasmodesmata, several vacuoles, a unique compartment that serves as trans-Golgi Network (TGN) and early endosome)[11–15].

Here, we began to address how membrane biophysical properties contribute to membrane identity in plants. In particular we analyzed the importance of membrane electrostatics in organelle identity and protein localization. Electrostatic interactions with negatively charged membrane contribute to the localization of many proteins containing polybasic clusters or cationic domains[16–18]. Membrane surface charges (MSC) are carried by anionic phospholipids[7,18]. MSC are not evenly distributed throughout the cell but they are rather organized in specific cellular territories[7,19]. How MSC are distributed and organized in plants is unknown. Using a set of surface charge biosensors, we found that the plant PM and the cell plate of dividing cells are highly electronegative as compared to endomembranes. Our results further revealed that the specific electrostatic field of the PM is lost upon chemical or genetic depletion of PI4P and that it contributes to the PM localization and function of several proteins involved in hormone and receptor-like kinase signaling.

Results

The plant PM has a specific electrostatic signature

In order to address the importance of membrane electrostatics in plants, we set out to map MSC in vivo, in Arabidopsis root epidermis. We raised a set of transgenic lines that constitutively express a mCITRINE (cYFP) fluorescent protein fused to a C-terminal farnesyl anchor in conjunction with an adjacent unstructured peptide of varying net positive charges (Extended Data Fig. 1)[16,19]. The least cationic probe (8Q-Farn, 0+) was localized in numerous endomembrane compartments (Fig. 1a, p and Extended Data Fig. 1). Increasing electrostatic interactions by the gradual addition of lysines (cationic charges) targeted the probes to the PM at the expense of endomembrane localization (Fig. 1a–e, p, Extended Data Fig. 1). Probes of intermediate charges (4+ to 6+) clearly associated with the PM and labeled

few endomembrane compartments (Fig. 1c–d, p and Extended Data Fig. 1), which presumably are of intermediate electronegativity (Fig. 1q and Extended Data Fig. 1). The most cationic probe (8K-Farn, 8+) was strictly localized at the PM (Fig. 1e, p and Extended Data Fig. 1). To confirm the importance of the charges in the localization of our biosensors, we substituted the lysines within the cationic stretch with either arginine (8R-Farn, 8+, Fig. 1f) or glutamic acid (6K2E, 4+; 7K1E, 6+, Fig. 1g–h). Consistently, the probes with identical net charges showed a similar localization (Fig. 1c–h, p).

Next, we tested the effect of adding an adjacent polybasic sequence to different lipid anchors (Extended Data Fig. 1). Probes that were either geranylgeranylated (8Q-Gege, 0+) or myristoylated (Myr-8Q, 0+) were mainly localized in endomembrane compartments (Fig. 1i–j, p, Extended Data Fig. 1). By contrast, the 8+ probes (8K-Gege and Myr-8K, 8+) were specifically localized to the PM, supporting the notion that strong electrostatic interactions provide PM specificity regardless of the lipid anchor (Fig. 1k–l, p, Extended Data Fig. 1). Next, we expressed two cationic amphipathic helices that do not rely on lipid anchors for membrane association (the synthetic KRΦ sequence, 8+ and the C-terminal tail of the human GTPase Rit (Rit-tail), 9+, Extended Data Fig. 1)[16,17]. Both probes were strictly localized to the PM (Fig. 1m–n, p). We also assayed the localization of the Kinase Associated-1 domains (KA1) of the human MARK1 ($KA1^{MARK1}$) and yeast Kcc4p proteins ($KA1^{Kcc4p}$)[20]. KA1 is a folded domain that lacks stereo-specificity and associates non-specifically with every anionic lipids[20,21]. Consistent with our peptide-based probes, both KA1 domains localized specifically to the PM (Fig. 1o, p and Extended Data Fig. 1). Altogether, our results indicate that the PM of Arabidopsis root epidermal cells has a strong electrostatic-field, a unique and intrinsic property of this membrane that contributes to its identity (Fig. 1q). Interestingly, both 8K-Farn and $KA1^{MARK1}$ MSC probes were insensitive to the cycling inhibitor Brefeldin A (BFA) (Extended Data Fig. 1), suggesting that high PM electrostatics does not require endocytic recycling. In addition, this property is not restricted to the root epidermis and was confirmed in other Arabidopsis cell types and in *Nicotiana benthamiana* (Extended Data Fig. 2).

PI4P is present early during cell plate formation, which correlates with the acquisition of a distinctive electrostatic state at the surface of this membrane

In animal cells, PM MSC are controlled by phosphatidylinositol-4,5-bisphosphate ($PI(4,5)P_2$), a phosphoinositide that localizes specifically at this membrane[3,17,21]. However, $PI(4,5)P_2$ is necessary but not sufficient to maintain PM electrostatics[17,21]. Indeed, depletion of $PI(4,5)P_2$ alone does not perturb PM MSC[17,21]. However, concomitant depletion of $PI(4,5)P_2$ together with phosphatidylinositol-4-phosphate (PI4P)[21] or phosphatidylinositol-3,4,5-bisphosphate ($PI(3,4,5)P_3$)[17] triggers loss of PM MSC. $PI(3,4,5)P_3$ does not exist in plants[3,22], but $PI(4,5)P_2$ and PI4P both localize at the PM[3,22–24] and are therefore potential anionic phospholipid candidates that might regulate PM electrostatics either alone or in combination. PI4P and $PI(4,5)P_2$ have both been reported to localize preferentially on the apical and basal poles of root epidermal cells rather than on their lateral sides[25,26]. To analyze whether the localization of our MSC reporters correlates with the reported polar localization of phosphoinositide reporters[25,26], we determined their polarity indices (Extended Data Fig. 3). However, contrarily to previous reports[25,26], our

analysis suggested that phosphoinositides reporters are not differentially localized as compared to non-polar controls (Extended Data Fig. 3). We favor the hypothesis that confocal images of root cells might be biased for apical/basal signal over lateral signal because of the topology of these cells (see Extended Data Fig. 3). Next, to analyze whether MSC could be regulated preferentially by PI4P and/or $PI(4,5)P_2$, we analyzed MSC and the localization of these phosphoinositides during cytokinesis. In tobacco BY-2 cells, PI4P is present early during cell plate formation, while $PI(4,5)P_2$ is recruited later[23,24]. We confirmed this observation using time-lapse imaging of Arabidopsis root meristem. To this end, we simultaneously localized our cYFP-tagged phosphoinositide sensors[22] with the red dye FM4-64 as a cell plate marker[13] or CENH3-RFP[27] as a chromosome marker (Extended Data Video 1 to 3). In addition, we concomitantly visualized a PI4P sensor in cyan ($2xCyPet\text{-}1xPH^{FAPP1}$) and a $PI(4,5)P_2$ sensor in yellow ($cYFP\text{-}2xPH^{PLC}$)[22] in the same roots and confirmed that PI4P is recruited to the cell plate much earlier than $PI(4,5)P_2$ (Fig. 1r and Extended Data Video 4 and 5). Next, we imaged our MSC sensor $cYFP\text{-}KA1^{MARK1}$ together with FM4-64, CENH3-RFP or $2xCHERRY\text{-}1xPH^{FAPP1}$ and found that our MSC probe is recruited to the cell plate at the same time as PI4P (Fig. 1s and Extended Data Video 3 and 6 to 8). Together, these results suggest that $PI(4,5)P_2$ is dispensable for the establishment of a high electrostatic field, at least at the cell plate. By contrast, PI4P accumulation correlates with high membrane electrostatics at the PM and cell plate, suggesting that it could be important for MSC.

PI4-Kinase activity is required to maintain PM surface charges

To test this importance of PI4P in membrane electrostatics, we used short-term treatment of phenylarsine oxide (PAO), a PI4-kinases (PI4Ks) inhibitor (Fig. 2a)[21,23,28]. We found that PAO triggers dissociation of PI4P-biosensors from the PM into the cytosol, while it had no or little effect on the PM localization of phosphatidylserine (PS) and $PI(4,5)P_2$ biosensors[19,22] (Fig. 2b–i and Extended Data Fig. 4). This later result suggested that short-term inhibition of PI4Ks did not have a strong impact on $PI(4,5)P_2$ synthesis, although we found, as expected, that longer-term PAO treatment dissociated partially $PI(4,5)P_2$ from the PM (Extended Data Fig. 4). Likewise, short-term PAO treatment in mammalian cells inhibits PI4P production without severely affecting $PI(4,5)P_2$ level[21]. Similar to PI4P biosensors, PAO triggered the dissociation from the PM of our MSC sensor $KA1^{MARK1}$ (Fig. 2f–g, j–o and t), in a time and dose-dependent manner. In addition, PAO also dissociated the MSC reporters Rit-Tail and KRΦ from the PM (Extended Data Fig. 4). These results suggest that PI4K activity plays a critical role in the PM electrostatic field. We confirmed these results using Wortmannin (WM), an inhibitor of PI3-kinases (PI3Ks) and PI4Ks at high concentration (>30 μM) but only of PI3Ks at low concentration (1 μM)(Fig. 2a)[29,30]. As a control, we also used LY294002 that inhibits PI3Ks but not PI4Ks (Fig. 2a)[31]. We exploit our lipid biosensors[22] to assess the effect of these drugs on PI3P, PI4P, $PI(4,5)P_2$ and PS (Extended data 4). Treatments at 30 μM WM dissociated both our PI4P biosensors and our MSC probe $KA1^{MARK1}$ from the PM (Fig. 2s–t and Extended Data Fig. 4), albeit less effectively than PAO, while they had no effect on the PM localization of $PI(4,5)P_2$ and PS sensors (Extended Data Fig. 4). However, neither LY294002 nor 1 μM WM dissociated $KA1^{MARK1}$ from the PM, confirming that PI4K but not PI3K activity is required for PM MSC (Fig. 2p–r, t and Extended Data Fig. 4). Live imaging in dividing cells together with

our pharmacological approaches suggest that PI4P, which is produced by PI4Ks, might be critical for PM electrostatics.

PI4P massively accumulates at the plant PM

$PI(4,5)P_2$ in mammals and PS in yeasts are major determinants of PM MSC[16,17,19–21]. In both cases, these lipids specifically localize at the PM, thereby providing a specific electrostatic signature to this membrane. In plants, PI4P accumulates at the PM and endomembranes, as visualized by the PI4P biosensor $1xPH^{FAPP1}$ (Fig. 2g)[22,23,32,33]. This raised the question of how PI4P might specifically control PM electrostatics while harboring such a binary localization. To probe whether PI4P preferentially accumulates at the PM, we compared the localization of three biosensors with increasing PI4P avidity. Increasing the number of PH^{FAPP1} domains increases the dwell time of the sensor in PI4P-riched membranes (Extended Data Fig. 5)[3,22], as confirmed by Fluorescent Recovery After Photobleaching (FRAP) experiments (Fig. 3a–c). Accordingly, $3xPH^{FAPP1}$, and to a lesser extent $2xPH^{FAPP1}$, preferentially localize to the PM rather than endosomes (Fig. 3d–f and i). Consistently, we previously found that PH^{OSBP}, another PI4P-binding protein, had a strict PM localization[22] (Fig 2g, i). To confirm these findings, we used the recently described P4M domain from the *Legionella pneumophila* SidM protein, which was elegantly demonstrated as an exquisitely specific PI4P biosensor in vivo[34]. In mammalian cells, $P4M^{SidM}$ highlights several PI4P pools, including a main pool in the Golgi/TGN, and two relatively minor pools at the PM and endolysosomes[34]. In contrast, $P4M^{SidM}$ was strictly localized at the PM in Arabidopsis and in *Nicotiana benthamiana* leaf epidermis (Fig. 3h–j and Extended Data Fig. 6). The localization of the PH domain of FAPP1 relies on coincidence binding with both PI4P as well as the ARF1 small GTPase[3,35]. In plants, ARF1 localizes to endosomes[36] and might account for the endomembrane localization of $1xPH^{FAPP1}$. However, the fact that $1xPH^{FAPP1}$ also accumulates at the PM in plants, a compartment that lacks the ARF1 proteins, further suggest that PI4P accumulates to a significant extent in this membrane. Moreover, PH^{FAPP1} has two distinct binding sites for PI4P and ARF1, which can be mutated independently to specifically impair binding with one or the other molecule in vitro[35]. We tested these mutants in vivo using transient expression in *N. benthamiana* leaf epidermis (Fig 3k–o). We found that mutants impaired in PI4P binding did not localized at the PM but in the cytosol as well as endomembranes, likely because of binding to ARF1 (Fig. 3l–m). On the contrary, PH^{FAPP1} version mutated in their ARF1-binding interface had a similar localization as $P4M^{SidM}$, being specifically localized at the PM and excluded from endomembranes (Fig. 3j and n–o). This result further exemplifies that PI4P is highly enriched at the PM in plants, which contrasts with other eukaryotic cells in which PI4P predominantly localizes to Golgi/TGN membranes and to a lesser extent at the PM[3].

The pool of PI4P at the PM controls the surface charge signature of this membrane

Next, we built a genetic system to specifically deplete the PM PI4P pool and test its importance in PM MSC. In this system, we fused the active or inactive (DEAD) catalytic domain of the yeast Sac1p protein (a PI4P phosphatase) with the MAP (Myristoylation And Palmitoylation) sequence, which induces PM targeting in plants (Fig 4a)[37]. To verify that our chimeric proteins were specifically targeted to the PM, we fused them to the cyan fluorescent protein mTURQUOISE2 and expressed them transiently in *N. Benthamiana*

(Fig. 4b–c). Next, we transiently co-expressed our chimeric enzymes together with our cYFP-tagged MSC probes or phosphoinositide markers. We found that MAP-SAC1, but not a catalytic mutant (MAP-SAC1^{DEAD}), displaced PI4P sensors to endosomes suggesting that our approach efficiently decreases PI4P concentration at the PM (Fig. 4d–e, i–j and n). However, we could not see any effects on the localization of our PI(4,5)P_2 biosensors (Fig. 4f, k and n). Importantly, we found that MAP-SAC1 perturbed the PM localization of the KA1^{MARK1} and 8K-Farn MSC markers, which were also found in endosomes in this condition (Fig 4g–h and l–n). This experiment confirms two predictions: i) PI4P are much more concentrated at the plant PM than in endosomes and PI4P binding proteins localize to endosomes only when PI4P concentration at the PM is reduced and ii) PM PI4Ps are required to establish the high electrostatic property of the PM as compared to endomembranes. Our data therefore suggest that in plants, PI4P will confer endosomal localization to proteins that bind concomitantly to PI4P and to another endosome-localized partner (e.g. ARF1). However, it will target strict PI4P-binders specifically to the PM. Together, our results establish PI4P as a hallmark of the plant PM and a driving force behind the PM electrostatic field.

The PM electrostatic field drives the localization and function of a subset of hormone signaling proteins

Next, we asked whether endogenous Arabidopsis proteins might rely on the PM electrostatic field for their localization. The auxin transport regulator PINOID (PID) binds anionic lipids in vitro[38,39] and is targeted to the PM via a polybasic unstructured loop within its kinase domain (PID membrane hook, PID^{MH}, 9+)[38]. The negative regulator of the brassinosteroid receptor kinase, BRI1 KINASE INHIBITOR1 (BKI1), relies on a lysine-arginine-rich membrane hook for PM localization and function[40,41]. We found that the cationic stretches in PID and BKI1 contribute to the interaction with anionic phospholipids in vitro and to their PM localization in yeast (Fig. 5a–b). Likewise, BKI1 family members (MEMBRANE ASSOCIATED KINASE REGULATORs, MAKR1 to MAKR4[40]) also interacted with anionic lipids in vitro (Fig. 5a and Extended Data Fig. 7). Next, we took advantage of the yeast *cho1Δ* mutant, which is impaired in PS biosynthesis[19] and therefore lacks a strong PM electrostatic field[20]. As a result of this loss of PM MSC in *cho1Δ*, endomembranes become more electronegative than the PM and cationic proteins relocalize to endomembranes at the expense of their PM localization[20] (Extended Data Fig. 8). We confirmed that PID, BKI1 and MAKR1 to MAKR4 localized in endomembrane rather than the PM in *cho1Δ*, while they associated with the PM in WT yeasts (Fig. 5b and Extended Data Fig. 8). In planta, MAKR1 to MAKR4 also associated with the PM via their polybasic N-termini (Extended Data Fig. 9). Next, we visualized MAKR2-cYFP and PID-YFP under the control of their endogenous promoter and found that they were targeted to the PM, although PID was also present in endomembrane compartments[42] (Fig. 5c). These results are consistent with the notion that PID, MAKR2 and possibly other family members might localize to the PM by reading out its electrostatic field. Consistently, PID and MAKR2 localization were sensitive to PAO (Fig. 5c), indicating that their localization rely on PI4K activity.

Next, we tested the functional requirement of PID targeting at the PM by electrostatics. We took advantages of the PID^{9Q} membrane hook mutant (0+, Fig. 6a) that localizes to

endosomes but not at the PM (Fig. 6b). We adopted a gain-of-function strategy by specific overexpression of PID-cYFP (9+) in root-hair cells, which inhibits root hair elongation[43,44] (Fig. 6c, h). By contrast, PID^{9Q}-cYFP (0+) overexpression in these cells had elongated root hairs (Fig. 6d, h). This phenotype resembled wild type (WT), PID^{D205N}-cYFP (kinase-dead) and $2xcYFP^{8K\text{-}Farn}$ control root hairs (8+, Fig. 6f), although they were slightly shorter (Fig. 6h). Because the membrane hook is in PID kinase domain (Fig. 6a), we could not exclude that the 9Q mutations might alter kinase activity, thereby preventing its function. We added a 5K3Q-Farn tail (5+, Extended Data Fig. 1) at the C-terminus of cYFP to target PID^{9Q} back at the PM and endosomes (Fig. 6e). This construct induced a short root hair phenotype that was statistically different from PID^{9Q} overexpression (Fig. 6e, h), suggesting that PID^{9Q} is a functional kinase and that, similar to BKI1[40,41], PID PM association by its cationic membrane hook is required for its function. This result further confirmed that PID is active at the PM rather than endomembranes[39].

Discussion

In this study we found that PI4P biosensors accumulate specifically at the PM in various cell types and in two plant species (i.e. *Arabidopsis thaliana* and *Nicotiana benthamiana*). Previous studies, using the PH domain of FAPP1, identified a pool of PI4P in endomembranes[22,23]. We show that PH^{FAPP1} localization in endomembranes is due to coincidence binding of this domain with endosomal ARF1. This raised the question whether PI4P does accumulate in endosomes in plants. Multiple lines of evidence suggest that it does: i) PI4Kβs localize in endosomes[45,46] and ii) several Arabidopsis proteins that bind PI4P also localize in endomembranes[47,48]. However, similar to PH^{FAPP1}, these proteins also bind both PI4P and endosomal small GTPases[47,48]. In addition, we show that PI4P-binding domains that localizes specifically to the PM, also localizes to endomembranes upon depletion of the PI4P PM pool. This experiment suggests that there are two PI4P pools in plant cells that compete for the localization of PI4P-binding proteins: a major pool at the PM and a minor pool in endosomes (Fig. 4o). As a result, proteins that bind only to PI4P localize to the PM, while proteins that bind concomitantly to PI4P and an endomembrane protein are targeted to intracellular compartments. This organization of PI4P in two quantitatively different pools might therefore allow differential targeting of PI4P-binding proteins based on whether or not they bind additional molecules. It is important to bear in mind that PI4P biosensors can only associate with lipids that are not constantly occupied by endogenous PI4P-binding proteins (i.e. ‘unoccupied’ PI4P pool)[3]. It is therefore possible that a massive pool of PI4P is present in endomembranes but not available to target lipid sensors to this compartment (i.e. ‘occupied’ PI4P pool)[49]. However, such occupied PI4P pool does not generate negative membrane charges, and is therefore not relevant for the generation of membrane electrostatic fields. In any case, in plant cells, the localization of ‘unoccupied’ PI4P that are labeled by biosensors, is drastically different from other eukaryotes, in which relatively equal pools of PI4P are detected at the PM and endomembrane inner surfaces[3].

We found that accumulation of PI4P at the PM is essential to generate a high electrostatic field at this membrane. Our analyses in dividing cells suggest that $PI(4,5)P_2$ is dispensable for PM MSC. As such, PM MSC is differentially regulated in plants and animals[17,19,21]. In the latter, $PI(4,5)P_2$ is required for the PM electrostatic field, but PI4P and/or $PI(3,4,5)P_3$ are

also important for the generation of high PM MSC[17,21]. By contrast, in plants, loss of PM PI4P is sufficient to perturb membrane electrostatic properties. However, we cannot exclude that other anionic phospholipids such as PS or phosphatidic acid (PA) might also contribute to the PM electrostatic field. PA is not normally present at the PM in yeast and animal cells[3], but it has been visualized in this membrane in plant tip-growing cells[50]. Given that PA has two net negative charges, it could also be important for PM MSC. PS is the major anionic phospholipid at the yeast PM[20], but is also involved in PM electrostatics in animals[19], in a non-redundant manner with phosphoinositides[17,21]. Future studies will reveal whether PA and/or PS are involved, together with PI4P, in PM MSC.

We described several proteins involved in auxin, brassinosteroid and/or RLK signaling that rely on PM MSC for localization and function. There is a broad signaling potential behind this electrostatic localization mechanism[18], since these interactions might be rapidly modulated by variations in: lipid composition (e.g. activation of phospholipases), the local cytosolic environment (e.g. ion influx) or modification of the protein itself. For example, phosphorylation of a conserved tyrosine within BKI1 membrane hook triggers PM dissociation[40], likely by acting as an electrostatic switch[18]. Here, we provide several examples of MSC effectors in Arabidopsis, but we expect that many more proteins will rely on this particular PM physical property for localization and function.

Methods

Growth condition and plant materials

The following transgenic lines: *pUBQ10::cYFP-1xPH^{FAPP1}*, *pUBQ10::cYFP-2xPH^{FAPP1}*, *pUBQ10::cYFP-PH^{OSBP}*, *pUBQ10::cYFP-2xPH^{PLC}*, *pUBQ10::2xCHERRY-1xPH^{FAPP1}*, *pUBQ10::2xCyPet-1xPH^{FAPP1}*, *35S::CENH3-RFP, 35S::EGFP-Lti6b; 35S::EGFP-aqPIP2a; PIN2::PIN2-EGFP* (Gift from Ben Scheres, Wageningen University, Netherland) and *pPID::PID-YFP* (Gift from Jiří Friml, Institute of Science and Technology, Austria) were described before[22,27,36,42,51]. Arabidopsis Col0 accession were grown in soil under long-day conditions at 21°C and 70% humidity.

Root imaging and image quantification

Plant growth—For root imaging, seedlings were grown vertically on MS medium (pH 5.7) containing 0.8% plant agar (Duchefa, http://www.duchefa-biochemie.nl/) in the absence of sucrose, with continuous daylight for 6–9 days.

Microscopy setup—Plant imaging was performed on an inverted Zeiss microscope (AxioObserver Z1, Carl Zeiss Group, http://www.zeiss.com/) equipped with a spinning disk module (CSU-W1-T3, Yokogawa, www.yokogawa.com) and a ProEM+ 1024B camera (Princeton Instrument, http://www.princetoninstruments.com/) using a 63x Plan-Apochromat objective (numerical aperture 1.4, oil immersion). GFP was excited with a 488 nm laser (150mW) and fluorescence emission was filtered by a 525/50 nm BrightLine® single-band bandpass filter (Semrock, http://www.semrock.com/). YFP/cYFP were excited with a 515nm laser (60mW) and fluorescence emission was filtered by a 578/105 nm BrightLine® single-band bandpass filter (Semrock, http://www.semrock.com/), CyPet/

mTURQUOISE2 were excited with a 445nm laser (80mW) and fluorescence emission was filtered by a 482/35 nm BrightLine® single-band bandpass filter (Semrock, http://www.semrock.com/), CHERRY/RFP were excited with a 561nm laser (80mW) and fluorescence emission was filtered by a 609/54 nm BrightLine® single-band bandpass filter (Semrock, http://www.semrock.com/). All imaging experiments were performed with spinning disk confocal except FM-64 colocalizations, which were performed on an inverted Zeiss CLSM710 confocal microscope (time lapse of cell division, Extended Data Video 1, 2 and 6) or inverted Zeiss CLSM780 confocal microscope (BFA experiments of Extended Data Figure 1, Sigma, www.sigmaaldrich.com) and images from Extended Figure 1 which were acquired on an inverted Zeiss CLSM710 confocal microscope as previously described[22].

For quantitative imaging, pictures of epidermal root meristem cells were taken with detector settings optimized for low background and no pixel saturation. Care was taken to use similar confocal settings when comparing fluorescence intensity. Pseudo-colored images were obtained using the “Green Fire Blue” look-up-table (LUT) of Fiji software (http://www.fiji.sc/).

Time lapse imaging of cell division in root meristem—Five days old Arabidopsis seedlings were transferred in a chambered cover glass (Lab-Tek II, http://www.thermoscientific.com), which contained 1.5 ml of MS medium (pH 5.7) containing 0.8% plant agar (Duchefa, http://www.duchefa-biochemie.nl/) in the absence of sucrose. Epidermal cells in the meristematic region of the root were subjected to time-lapse imaging with spinning disk confocal microscope, except for FM4-64 (Life Technologies, http://www.thermofisher.com/) colocalization. Colocalization analysis of cYFP-biosensor with FM4-64 was performed on an inverted Zeiss CLSM710 confocal microscope using a 63x Plan-Apochromat objective (numerical aperture 1.4, oil immersion). Counter-staining of the plasma membrane was obtained by incubating roots with 1 μM FM4-64 solution during the entire time course. cYFP and FM4-64 were excited with a 515 nm laser and detected with microscope settings described in[44]. Two or three roots were observed simultaneously and images were collected at different *Z*-positions every 3 min (spinning disk) or 4 min (CLSM). All the Time-lapse were adjusted for growth using the Template Matching and Slice Alignment (ImageJ Plugins, https://sites.google.com/site/qingzongtseng/template-matching-ij-plugin). In figure 1, t=0 min was determined as the frame preceding the first image with cell plate labeling in the PI4P reporter channel (t=3 min).

Quantification of the number of intracellular compartments (“spots”) per cell—The intracellular compartments (“spots”) per cell were counted in a double blind setup. 100 cells were counted per condition, in at least 20 independent roots imaged over the course of at least 3 independent experiments. For the MAP-SAC1 experiments in agro-infiltrated *Nicotiana Benthamiana* leaves quantifications were performed by counting the number of cells with endomembrane labeling (presence of cytosolic “spots”) and the number of cells showing only PM labeling. Minimums of 100 cells were counted in each condition over the course of at least three independent experiments.

PAO, WM and LY294002 treatments and dissociation index—7-day old transgenic lines (cYFP-1xPH^{FAPP1}, cYFP-C2^{Lact}, cYFP-2xPH^{PLC}, cYFP-KA1^{MARK1}, cYFP-2xFYVE^{HRS}, pMAKR2::MAKR2-cYFP and pPID::PID-YFP or the following F2 crosses 2xCHERRY-C2^{Lact}xcYFP-1xPH^{FAPP1}; cYFP-2xPH^{PLC}x2xCyPet-1xPH^{FAPP1}; cYFP-KA1^{MARK1}x2xCHERRY-1xPH^{FAPP1}) were incubated in wells containing 30 μM or 60 μM PAO (Sigma, www.sigmaaldrich.com, PAO stock solution at 60 mM in DMSO), 1 μM or 30 μM PAO (Sigma, www.sigmaaldrich.com, WM stock solution at 30 mM in DMSO), 50 μM LY294002 (Cayman chemical, https://www.caymanchem.com, LY29002 stock solution at 50 mM in DMSO), or a volume of DMSO equivalent to the highest drug concentration used in each case (mock treatment) during the indicated time. Roots were imaged within a 10 min time frame window around the indicated time. The PAO, WM and LY29002 effects on the localization of our biosensors were analyzed by calculating the "dissociation index" for each reporter protein[21]. First, we calculated "indexMock": the ratio between the fluorescence intensity (Mean Grey Value function of Fiji software) measured in two elliptical region of interest (ROIs) from the plasma membrane region (one at the apical/basal PM region and one in the lateral PM region) and two elliptical ROIs in the cytosol in the mock condition. "IndexMock" was quantified in 150 cells over three independent replicates (50 cells per replicate). Next, we measured a similar ratio in drug treated seedlings ("indexDrug"). "indexDrug" was also quantified in 150 cells over three independent replicates (50 cells per replicate). The dissociation index is the ratio of (indexMock)/(indexPAO). This dissociation index reveals the degree of relocalization of the fluorescent reporters from the plasma membrane to the cytosol, between the mock and drug treated conditions.

For the quantification of the PAO effect on PID-YFP and MAKR2-cYFP localization, we did not use a dissociation index, because the localization of these two proteins was already high in the cytosol even in the absence of PAO. Therefore, to reflect the variability associated with protein localization, we scored, in a double blind setup, the number of cells in which PID-YFP or MAKR2-cYFP were associated or not with the PM in the mock and PAO treated conditions. In Figure 5, these scores are given as the number of cells with protein at the PM over the total number of cells (mock condition) and the number of cells with no protein at the PM over the total number of cells (PAO-treated condition).

FRAP experiment—Fluorescence in a rectangle region of interest (ROIs) (50 μm^2, 15μm long), in the plasma membrane region, was bleached in root optical section by four successive scans at full laser power (150W) using the ilas^2 FRAP module (Roper scientific, http://www.biovis.com/ilas.htm) of our spinning disk microscope. Fluorescence recovery was subsequently analyzed in the bleached ROIs and in controlled ROIs (rectangle with the same dimension, in unbleached area). FRAP was recorded continuously during 90s with a delay of 0.3s between frames. Fluorescence intensity data were normalized as previously described[37]. For visualization, kymographs were obtained using the kymograph function of the Metamorph software.

Extended Data

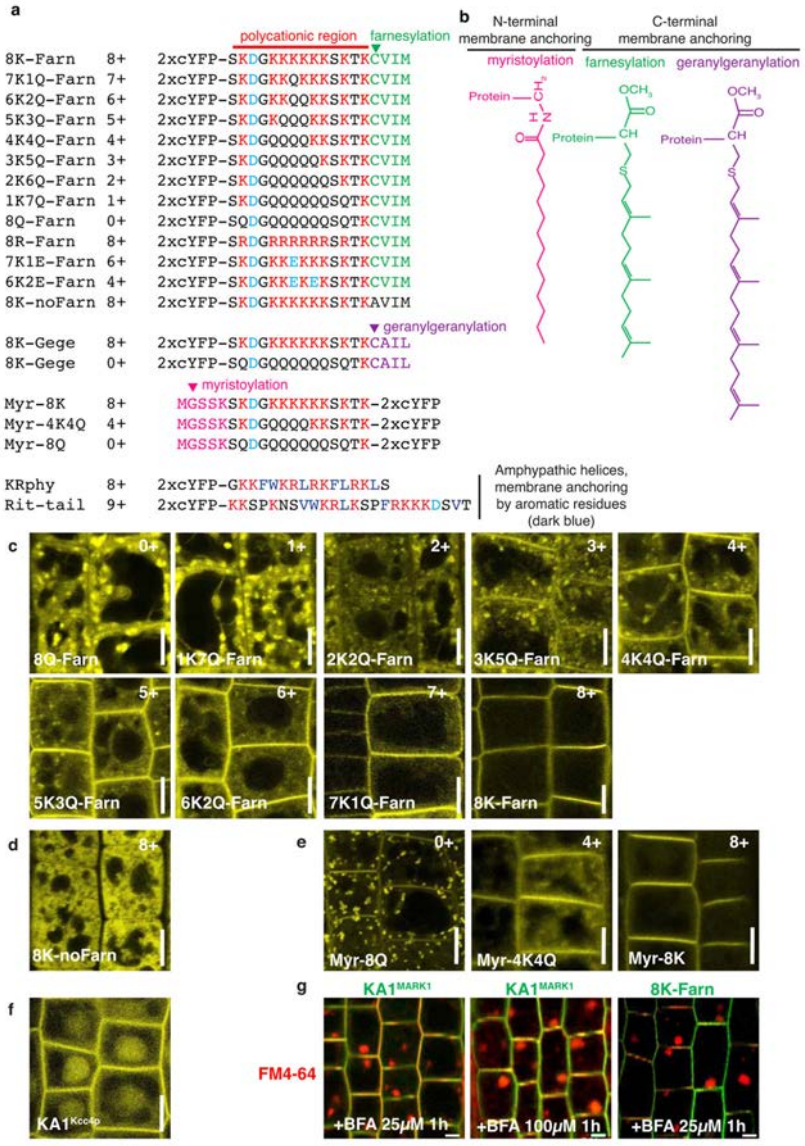

Extended Data Figure 1. Construction of membrane surface charge (MSC) probes and additional MSC reporters confirming the high electronegativity of the plasma membrane in plants

a) Sequence alignment between the different MSC probes showing the polybasic stretch in each construct (or the associated mutations) and their respective net positive charges. Cationic residues (K, R) are in red, acidic residues (E, D) in light blue, hydrophobic and aromatic residues in the amphipatic helixes Rit-tail and KRphy are in dark blue (F, W, L, V), the C-terminal farnesylation sequence CVIM (CxxM box) is in green, the C-terminal geranylgeranylation sequence CAIL (CxxL box) is in purple and, the N-terminal myristoylation sequence MGSSK is in pink.

b) Schematic representation of the lipid modifications used in our MSC probes: myristoyl (pink, N-terminal modification, covalently linked to the second glycine), farnesyl (green, C-terminal modification, covalently linked to the cysteine in the CxxM motif) and geranylgeranyl (purple, C-terminal modification, covalently linked to the cysteine in the CxxL motif).

c–f) Representative confocal images of root epidermal cells expressing the indicated MSC probe. All the constructs are expressed by the *pUBQ10* promoter and are fused with cYFP at their N-terminus, except the myristoylated constructs, which are fused with cYFP at their C-terminus. bars, 5μm.

c) Localization of the full collection of farnesylated probes from 8Q-Farn (0+) to 8K-Farn (8+). The farnesylated MSC probes are based on the C-terminal tail of the human small GTPase K-Ras4B[19]. K-Ras is targeted to the PM via a C-terminal farnesyl anchor in conjunction with an adjacent unstructured polybasic peptides made of 8 lysines. Our bioprobes consist of a fusion between a tandem repeat mCITRINE fluorescent protein (cYFP) and the K-Ras C-terminal tail, in which we modified the net positive charges via site directed mutagenesis of the lysine stretch. The least cationic probe (0+), in which 8 lysines have been substituted by glutamine (8Q-Farn), is localized in numerous endomembrane compartments. This suggests that farnesylation of the 8Q-probe is sufficient to provide membrane anchoring in the absence of its adjacent lysines and that this probe, which is targeted mainly by hydrophobic interactions, confers targeting to intracellular membranes. The gradual addition of cationic charges should increase electrostatic interactions with anionic lipids and thereby shift the probes localization toward more negatively charged membranes. Indeed, we observed that the more cationic the probe is, the more it is targeted to the PM at the expense of endomembrane localization.

d) The cysteine in the CxxM motif of 8K-Farn was substituted by an alanine thereby prohibiting C-terminal addition of a farnesyl lipid anchor (8K-noFarn). This non-farnesylated probe failed to associate with any membrane and was fully soluble, despite being strongly cationic (8+). This suggests that electrostatic interactions by themselves are not sufficient for membrane targeting and that stable membrane association requires some type of hydrophobic interactions.

e) Localization of the Myr-8Q (0+), Myr-4K4Q (4+) and Myr-8K (8+) probes. Note that, by contrast with the 8Q-Farn (Extended Data Fig. 1c, top left pannel) and 8Q-Gege probes (see main Fig. 1i), the Myr-8Q probe is already partly associated with the PM in the absence of electrostatic interactions. This showed that these different lipid anchors have different intrinsic targeting properties but that they each failed to provide PM specificity on their own. Nonetheless, like for the farnesylated reporters, the gradual addition of net positive charges next to the myristoyl modification gradually increases PM association: Myr-4K4Q (4+) has an intermediate PM/endomembrane localization and Myr-8K is specifically localized at the PM. Together, our results support the notion that strong electrostatic interactions provide PM specificity regardless of the lipid anchor type.

f) Localization of the $KA1^{Kcc4p}$ reporter at the PM and in the nucleus. Similar to $KA1^{MARK1}$, $KA1^{Kcc4p}$ is specifically localized at the PM and not in endomembrane compartments, confirming that this specific localization at the cell surface is a property of the KA1 domain in general rather than a specific feature of the MARK1 protein. However, unlike KA^{MARK1}, $KA1^{Kcc4p}$ was also partly localized in the cytosol and the nucleus, which

makes this domain less convenient as a MSC readout. For this reason, from now on, we decided to use the KA1^{MARK1} domain in subsequent experiments.

g) Sensitivity of KA1^{MARK1} (left and middle panel) and 8K-Farn (8+ probe, right panel) to 90 min of BFA treatment at the indicated concentration. To show that BFA was active during our treatment we used the endocytic tracer FM4-64 and found that it was accumulated in BFA bodies at both 25 μM and 100 μM of BFA. FM4-64 was used at 1 μM and added 10 min prior confocal observations in the continuous presence of BFA.

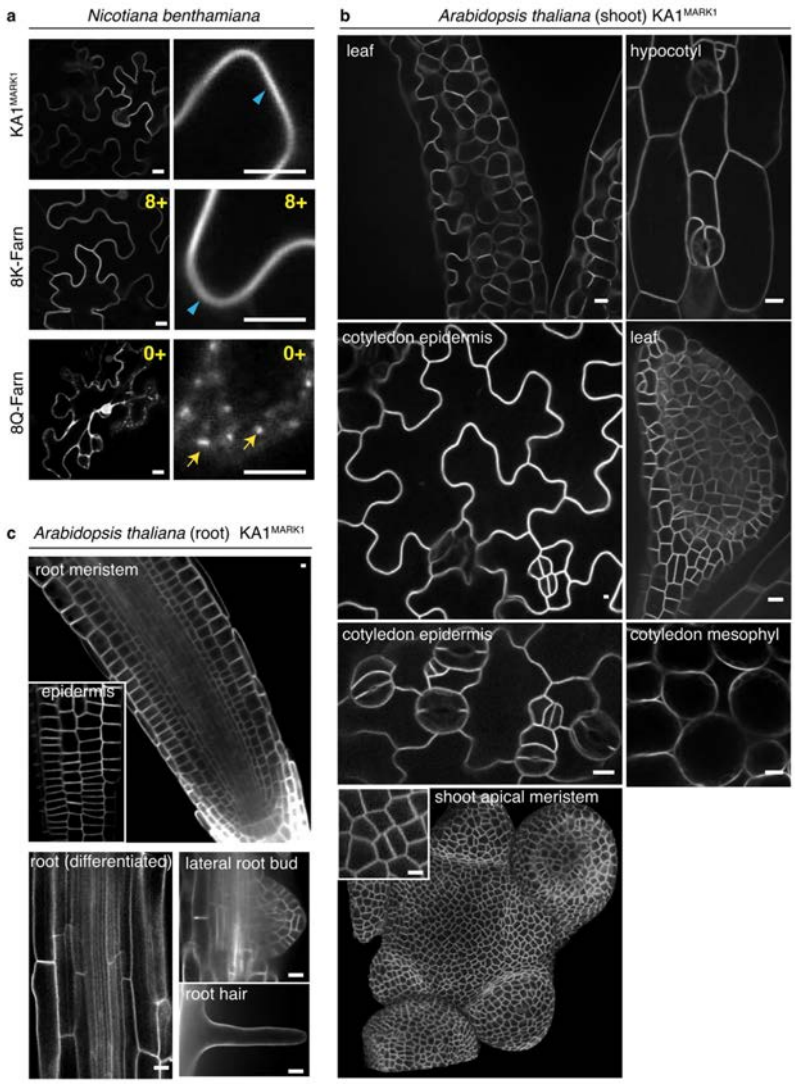

Extended Data Figure 2. The high electronegativity of the PM is a common feature of many cell types and at least two plant species

a) Localization of KA1^{MARK1}, 8K-Farn (8+), 8Q-Farn (0+) in transiently transformed *N. benthamiana* leaves. Blue arrowheads show PM localization and yellow arrows show endomembrane localization. **b–c)** Confocal picture of **b)** the shoot and **c)** the root of transgenic Arabidopsis lines stably expressing cYFP-KA1^{MARK1}. Scale bars, 10 μm.

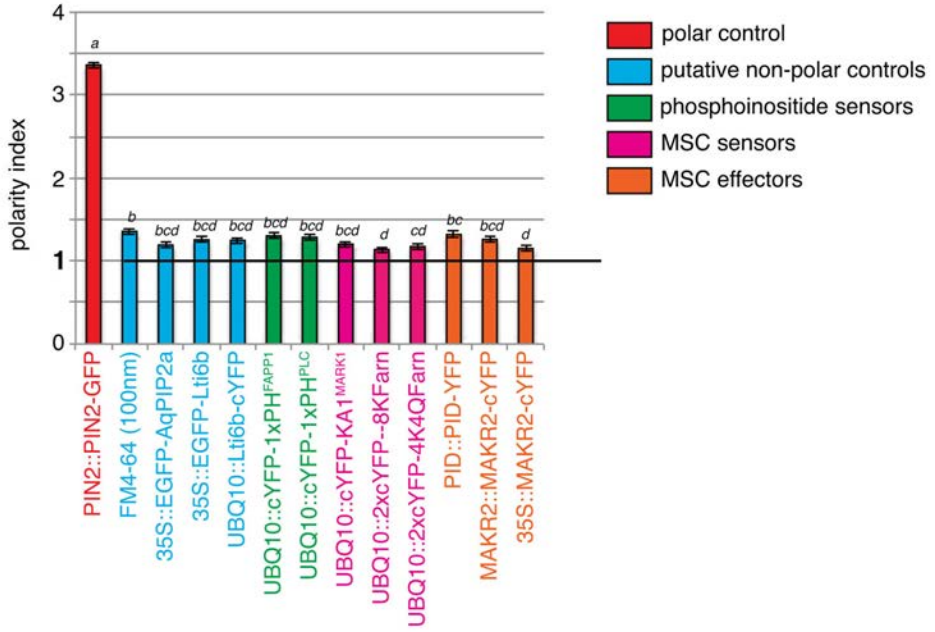

Extended Data Figure 3. Polarity indices in Arabidopsis root epidermis of various fluorescent PM proteins

Charts showing the polarity index for each fusion protein indicated at the bottom. Different italicized-letters indicate significant differences among means (*P<0.0001,* Tukey's test). Note that only PIN2-GFP (red) is significantly different from all the other genotypes. The polarity indices of phosphoinositide (green) and MSC (pink) sensors fluctuate between 1.2 and 1.4, which is close to the numbers reported for PI4P and PI(4,5)P_2 reporters[20]. However, we found that expected non-polar controls (blue), including the lipid dye FM4-64 and plasma membrane proteins Lti6b and PIP2a aquaporin (aqPIP2a) have similar polarity indices. Therefore, we could not detect significant statistical differences between our phosphoinositides or MSC sensors and expected non-polar controls. Although we cannot exclude that these non-polar control are in fact polar, we favor the hypothesis that confocal images of root cells might be biased for apical/basal signal over lateral signal because of the topology of these cells. First, the apical pole of one cell is tighlty juxtaposed to the basal pole of its neighbouring cell, which tend to enhance the apparent apical/basal signal over the lateral one. In addition, pinhole-based microscopes have high thickness of the z-sections. As a result, the z resolution is much lower than x and y resolution, so the volume collected by the microscope is not an isodiametric cube but cuboid; therefore a straight membrane in z will appear stronger than a curved one - which is the case of the apical and basal root membranes compared to the lateral membranes. Therefore we concluded that phosphoinositides and PM MSC are likely not polar in Arabidopsis root epidermis.

Method for quantification of polarity index. 7 days old transgenic lines were analyzed to determine the "Polarity index" in root tip epidermis. "Polarity index" is the ratio between the fluorescence intensity (Mean Grey Value function of Fiji software) measured at the PM apical/basal side and PM lateral sides (Line width=3). We selected only cells for which the PM at each pole (apical, basal and laterals) were easily viewable and we selected cells that were entering elongation (at least as long as wide, but no more than twice as long as wide).

Quantification was conducted in 100 cells over more than 15 independent plants. This Polarity index reveals the degree of polarity of the fluorescent reporters between the apical/basal side and lateral sides of the PM.

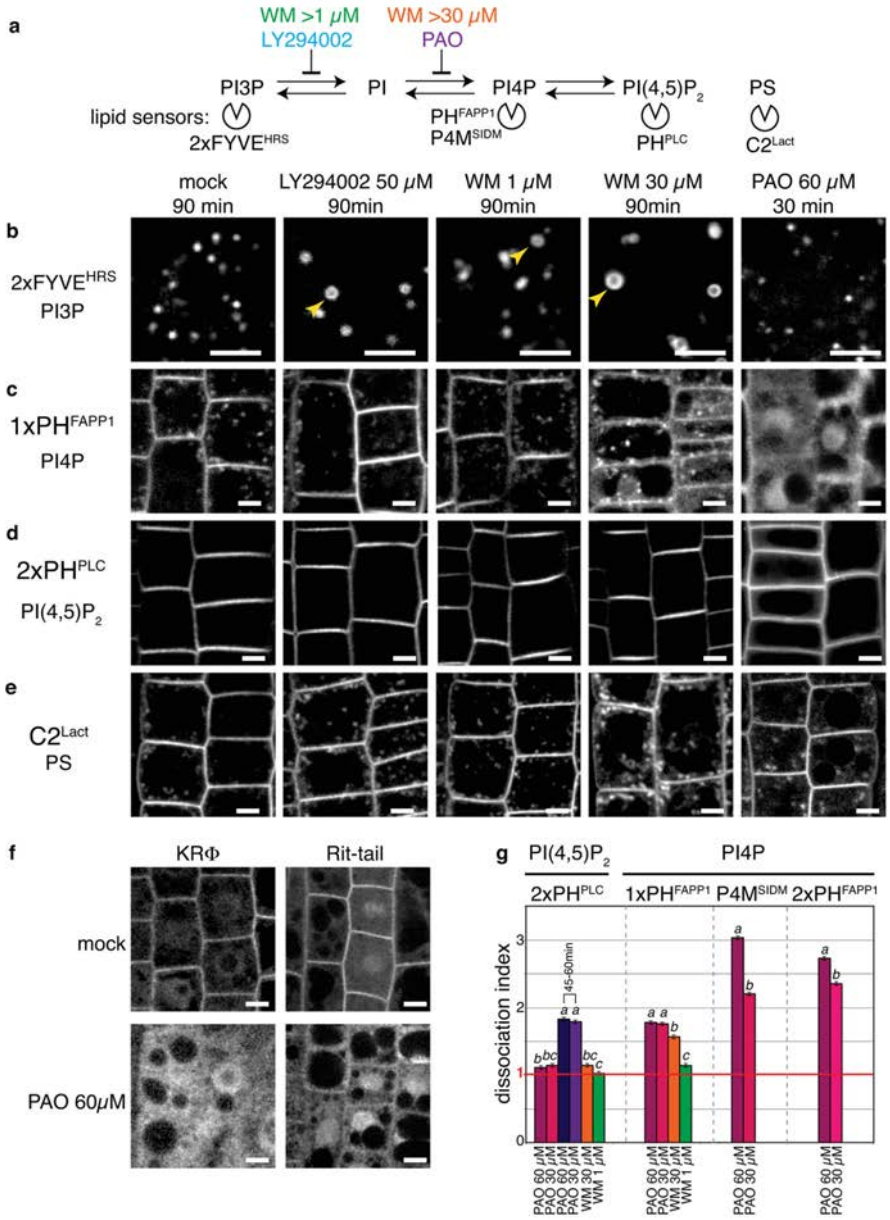

Extended Data Figure 4. Sensitivity of phosphoinositides and MSC sensors to PI3K and PI4K inhibitors

a) Schematic representation of the action of the drugs used to perturb phosphoinositides production and lipid sensors used as read-out. **b–e**) Confocal pictures of Arabidopsis root epidermis from the genotype indicated on the left, treated with the drug concentration indicated at the top for 90 min (mock, LY294002 and WM) or 30 min (PAO).

b) cYFP-2xFYVE^{HRS}. As reported previously, 90 min of PI3K inhibition leads to swelling of late endosomes labelled by the PI3P sensors 2xFYVE^{HRS}, rather than a release of the probe into the cytoplasm[21]. Yellow arrowheads show enlarged endosomes. Endosome swelling suggested that WM and LY294002 are active, although we noticed that WM had a more drastic effect at 30 μM than 1 μM. On the other hand, PAO treatment had no effect on 2xFYVE^{HRS}-labelled endosomes.

c) cYFP-1xPH^{FAPP1}. PI3K inhibition by LY294002 and 1 μM WM had no effect on 1xPH^{FAPP1} localization. However PI3K and PI4K inhibition by 30 μM WM partially released 1xPH^{FAPP1} into the cytosol and PI4K inhibition by PAO fully solubilized this PI4P sensor. In the 60 μM 30 min PAO treatment (right) both the PM and endosomal pools of 1xPH^{FAPP1} were solubilized. This result is surprising given that the endosomal pool of 1xPH^{FAPP1} can rely only on ARF1-binding for endomembrane localization (See Fig. 3 of main text). The PH domain of FAPP1 interacts specifically with GTP-loaded ARF1[22] and it is possible that PI4K inhibition inhibits ARF1 activation. For example, the ARF GTPase Activating Protein (ARF-GAP) VAN3, which binds ARF1 in Arabidopsis, has a PI4P-binding PH domain and its GAP activity is enhanced by PI4P[23].

d) cYFP-2xPH^{PLC}. Only PAO 60 μM 30 min (right) had a slight effect on the PM localization of the PI(4,5)P_2 bionsensor 2xPH^{PLC}, which becomes significant after prolonged treatment (45 to 60 min of 60 μM PAO, see **g**).

e) cYFP-C2^{Lact}. Inhibition of PI3K and/or PI4K had no effect on the PM localization of the PS bionsensor C2^{Lact}. However, we noticed that 60 μM PAO for 30 min (right) decreased the number of endomembrane compartments labeled by this probe, suggesting some impact of PI4K activity on the intracellular localization of PS.

f) Confocal picture of Arabidopsis root epidermis from the genotype indicated at the top, treated with the drug concentration indicated on the left for 30 min.

g) Dissociation index (mean ±SEM) for the genotype and drug concentration indicated at the bottom. All treatments were performed during 30 min, except when indicated otherwise. Different italicized-letters indicate significant differences among means (*P<0.0001,* Kruskal Wallis test); only different treatments with the same genotype were compared (separated by grey-dashed lines). Scale bars in b to f, 5 μm.

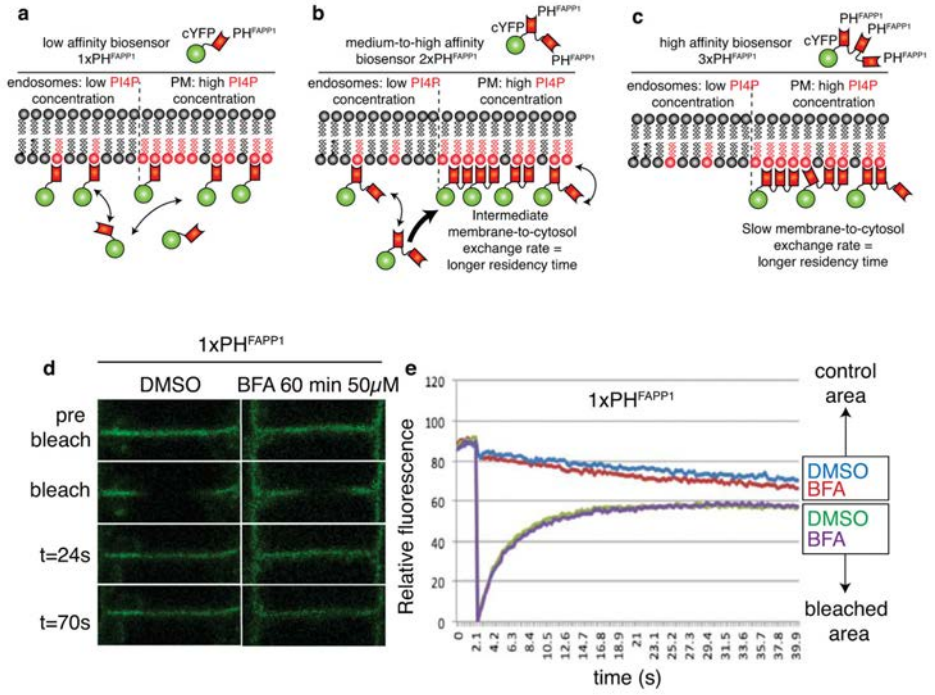

Extended Data Figure 5. 2x and 3xPH^{FAPP1} have longer residency time at the PM than 1xPH^{FAPP1}

High affinity lipid binding domains (LBDs) are expected to localize more specifically to the membrane compartment that accumulates the most its cognate lipid, while lower affinity LBDs are more likely to have a broader localization domain (**a–c**). Low affinity sensors (here 1xPH^{FAPP1}) are less efficient in discriminating between two membranes with two different concentrations of their targeted lipid species (here PI4P) and as a result they might be targeted to both of these membranes (**a**). By contrast, high affinity sensors (2xPH^{FAPP1} and 3xPH^{FAPP1}) will have increased dwell time at the membrane that is the most enriched in the targeted lipid and they will accumulate preferentially in this compartment (**b and c**). In other words, high affinity sensors work like a “Velcro fastener”: they will grab more strongly to a surface with more spikes (in this case the spikes being PI4P). In order to confirm that our PH^{FAPP1}-based sensors behaves according to the scenario explained above, we performed a FRAP experiment (See main Fig. 3a to c). This analysis showed that the recovery was much faster in the case of 1xPH^{FAPP1} and kymographic analysis showed that the recovery of fluorescence has an oval shape, indicating recovery from both the side (i.e. the PM) and the cytosol (Fig. 3a–c of the main text). This result is compatible with the idea that 1xPH^{FAPP1} has a fast exchange rate between the PM and the cytosol. On the contrary, in the case of 2xPH^{FAPP1} and 3xPH^{FAPP1} the recovery was slower and kymographic analysis (Fig. 3b of the main text) showed that the recovery of fluorescence is centripetal (triangle shape). 1xPH^{FAPP1} localizes at the PM and in endomembranes, while 2x and 3xPH^{FAPP1} are not (or less) present in intracellular compartments. Therefore, it is conceivable that the fast recovery of the 1xPH^{FAPP1} reporter might come from fast endocytic recycling that is not happening in the case of the 2x and 3xPH^{FAPP1} proteins. To exclude this possibility, we tested whether pharmacological inhibition of protein recycling by BFA had any impact on

the recovery time of the 1xPH^{FAPP1} construct and (**d–e**). We found that cYFP-1xPH^{FAPP1} had similar recovery time in the presence or absence of BFA (100 μM 60 min). These results are consistent with the notion that the 2xPH^{FAPP1} and 3xPH^{FAPP1} sensors have a longer residency time at the PM than 1xPH^{FAPP1} and repopulate the bleached area by lateral diffusion with their cognate lipids.

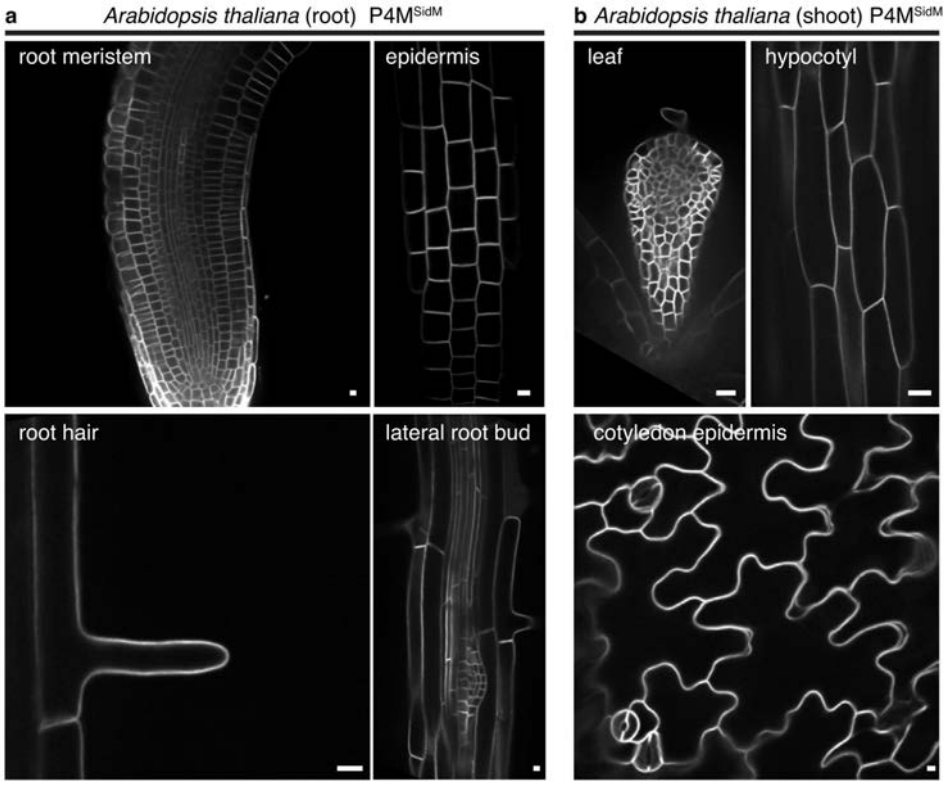

Extended Data Figure 6. P4M^{SidM} is specifically localized to the PM in various cell types in Arabidopsis

Confocal pictures of **a)** the root and **b)** the shoot of transgenic Arabidopsis lines stably expressing cYFP-P4M^{SidM}. Scale bars, 10 μm.

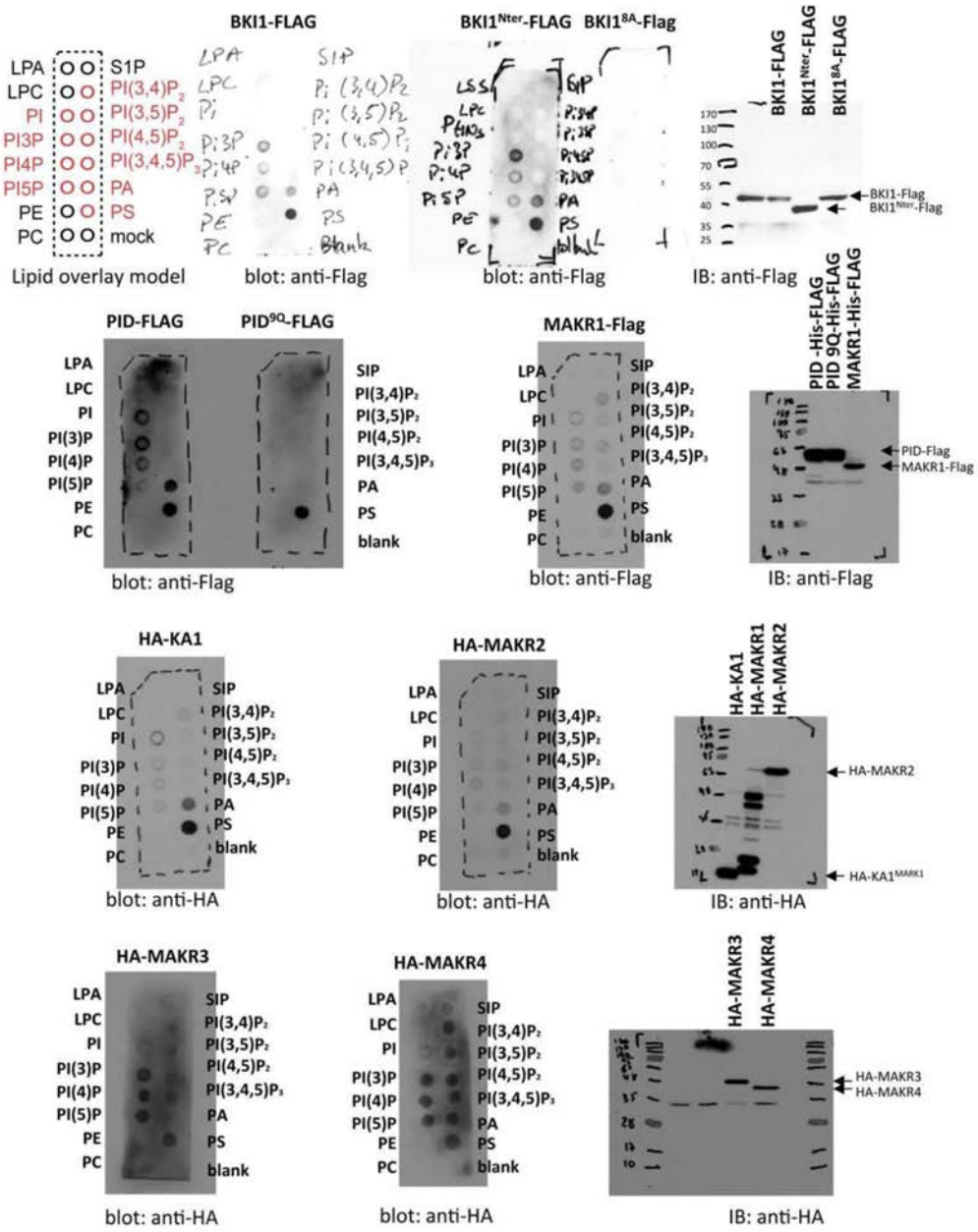

Extended Data Figure 7. Full scan of lipid-protein overlay experiments and associated western blots

Full scan of lipid overlay assays presented in the main Figure 5a, and their associated western blots. Top left is shown the position of the different lipids spotted on each membrane: Lysophosphatidic acid (LPA), Lysophosphocholine (LPC), Phosphatidylinositol (PI), Phosphatidylinositol-3-phosphate (PI3P), Phosphatidylinositol-4-phosphate (P4P), Phosphatidylinositol-5-phosphate (PI5P), Phosphatidylethanolamine (PE), Phosphatidylcholine (PC), Sphingosine 1-Phosphate (S1P), Phosphatidylinositol-3,4-bisphosphate ($PI(3,4)P_2$), Phosphatidylinositol-3,5-bisphosphate ($PI(3,5)P_2$), Phosphatidylinositol-4,5-bisphosphate ($PI(4,5)P_2$), Phosphatidylinositol-3,4,5-trisphosphate

($PI(3,4,5)P_3$), Phosphatidic acid (PA), Phosphatidylserine (PS) and mock. Anionic phospholipids are indicated in red.

Note that with this in vitro interaction technique, we systematically found a stronger signal with PS and to a lesser extent with PA. This was also the case for HA-$KA1^{MARK1}$ which is known to bind PS, PA and $PI(4,5)P_2$ with similar binding affinities in Surface Plasmon Resonance experiments[2]. It is important to point out that these fat blots experiments are qualitative rather than quantitative. The main point of these experiments is to show that PID, BKI1 and MAKR1 to MAKR4 are indeed able to bind anionic phospholipids in vitro, and that this binding relies on their respective membrane hook (for PID and BKI1). We do not think that these experiments faithfully pin point particular lipid preferences. In fact, we expect PID, BKI1 and MAKR1 to MAKR4 to rely on membrane surface charges (non specific electrostatic interactions) in vivo and we therefore concentrated our experiments using in vivo assays (see yeast and in planta experiments).

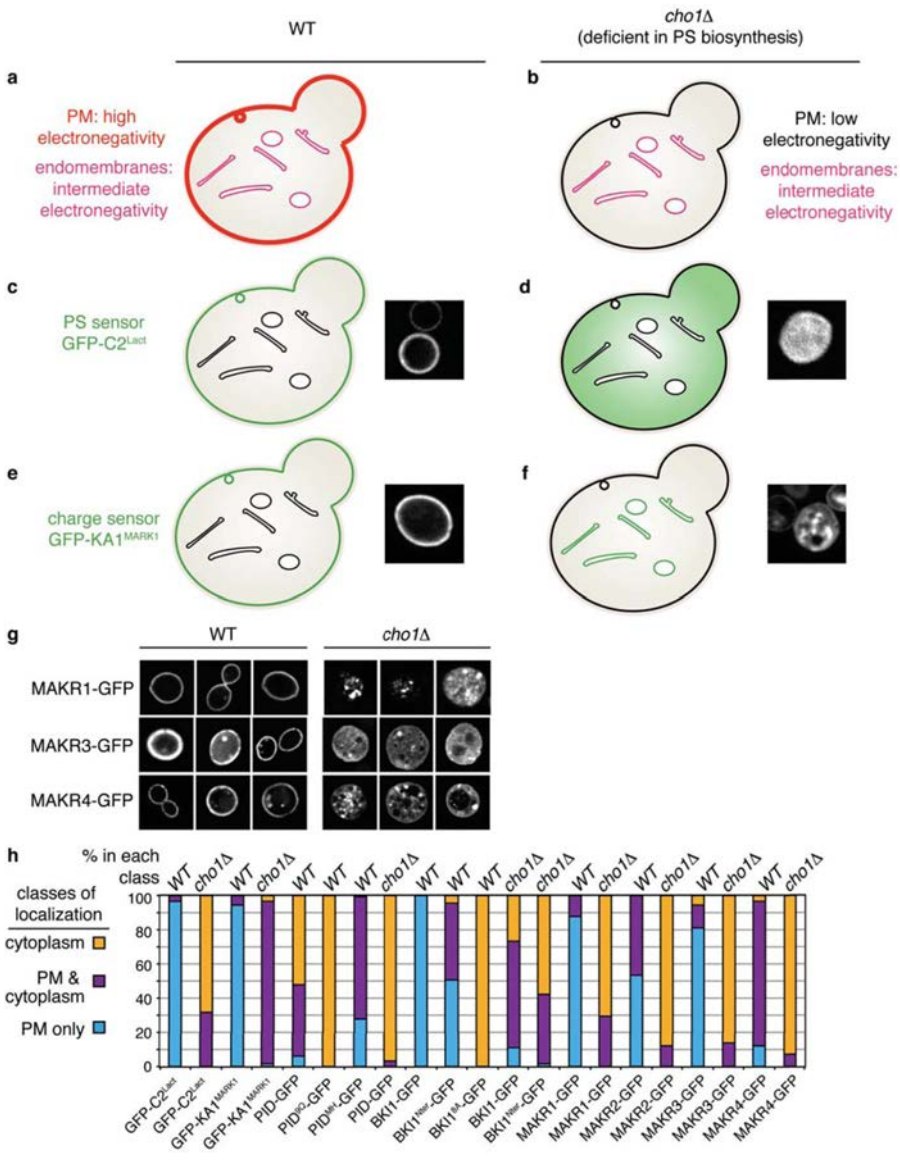

Extended Data Figure 8. Using the *cho1Δ* yeast mutant to test the requirement of PM MSC for protein localization

a) In yeast, the PM is highly electronegative, mainly due to the presence of phosphatidylserine (PS), which massively accumulates in this membrane[3]. Endomembrane compartments are of intermediate electronegativity, likely because of the marginal presence anionic lipids in these compartments (e.g. PI4P in the Golgi, PI3P in endosomes). **b)** The yeast *cho1Δ* mutant is impaired in PS biosynthesis and therefore lacks a strong PM electrostatic field[2,3]. As a result of this loss of PM MSC, endomembranes become more electronegative than the PM in *cho1Δ* and cationic proteins relocalize to endomembranes at the expense of the PM[2]. This situation is exemplified by the localization of GFP-$C2^{Lact}$ **(c and d)**, a PS biosensor[3], and GFP-$KA1^{MARK1}$ **(e and f)**, a MSC reporter[2]. **c)** GFP-$C2^{Lact}$ is specifically localized at the PM in yeast[3] confirming that the main pool of this lipid is in this

membrane. **d)** On the contrary, GFP-C2^{Lact} is soluble in the *cho1Δ*. This soluble GFP-C2^{Lact} is a localization by default in the absence of PS to target this sensor to membranes. **e)** GFP-KA1^{MARK1} is localized at the PM in yeast[2], confirming that the PM is highly electronegative in this system. **f)** GFP-KA1^{MARK1} is sensitive to PS depletion and relocalizes to endomembranes in the *cho1Δ*, which become more electronegative than the PM in this mutant[2]. Therefore, the *cho1Δ* mutant assay allows discriminating between proteins that are targeted to the PM by specific interactions with PS (e.g. C2^{Lact}) or by reading-out the PS-dependent PM MSC (e.g. KA1^{MARK1}). Proteins that specifically interact with PS are solubilized in *cho1Δ*, while MSC effector proteins are depleted from the PM and relocalize to endomembranes.

g) Three representative images showing the localization of the indicated constructs in WT and *cho1Δ* yeast. **h)** Quantification of localization of the indicated construct in yeast. Cytoplasm = cytosol and/or endomembrane (n=300 cells). The localization quantification was performed using three categories according on the fluorescence expression pattern, “Plasma membrane”, “Cytoplasm” and “Plasma membrane and Cytoplasm”. Here, we took cytoplasm in a broad sense, including both soluble proteins (see for example localization of BKI1^{8A}-GFP in WT yeast or localization of the PS sensor GFP-C2^{Lact} in *cho1Δ*) but also proteins associated with endomembranes (see for example localization of GFP-KA1^{MARK1} in *cho1Δ*). For each GFP-tagged proteins, three independent experiments were performed and the localization was recorded in 100 yeasts in each experiment (300 cells total).

Note that PID-GFP has a dual localization in yeast at the PM and in endomembrane compartments. PID^{MH}-GFP is more specifically localized at the PM than full length PID-GFP, while PID^{9Q}-GFP is localized in endomembrane compartments but not at the PM. These results suggest that in yeast PID likely has two localization sequences, one PM targeting sequence that corresponds to PID^{MH} and a second, so far unknown sequence, that targets PID to endomembranes. The situation is likely similar in planta, since PID-cYFP has a dual PM and endosomal localization, while PID^{9Q}-cYFP localizes only to endosomes but not at the PM (see Fig. 5c and 6b of the main text).

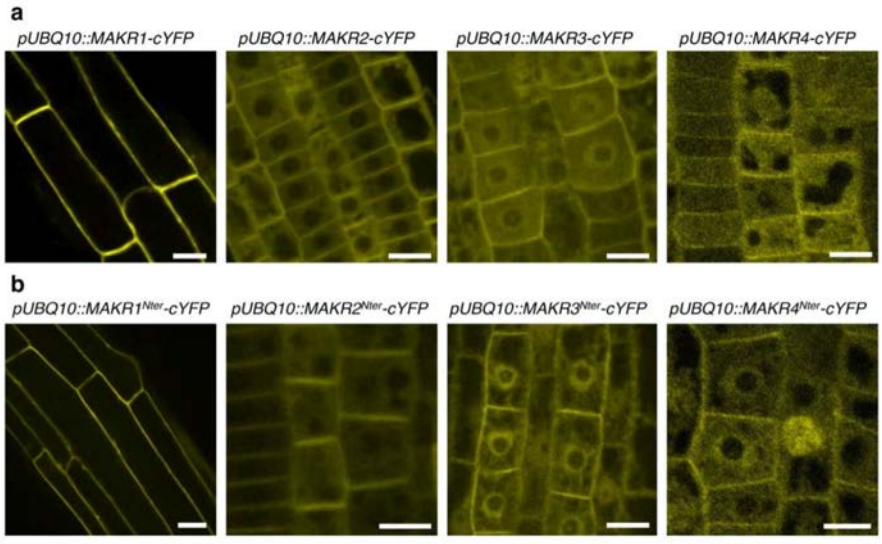

Extended Data Figure 9. Localization of MAKR1 to MAKR4 and their respective C-terminal deletion in Arabidopsis root

a) Representative images of full length MAKR1 to MAKR4 localization in roots of stably transformed transgenic Arabidopsis lines. **b)** Representative images of MAKR1 to MAKR4 N-terminus localization in root of stably transformed transgenic Arabidopsis lines. Note that, similar to BKI1, all the MAKR proteins are localized to the PM and cytoplasm. Furthermore, in some cases they are also present in the nucleus (see for example MAKR3 or MAKR4). Nuclear localization has also been reported for GFP-MAKR4 but the functional significance of this localization is currently unknown[24]. Scale bars, 10 μm.

Supplementary Material

Refer to Web version on PubMed Central for supplementary material.

Acknowledgments

We thank M. Dreux, O. Hamant, G. Vert, T. Vernoux, S. Mongrand, A. Martiniere-Delaunay and the SiCE group for discussions and comments, J. Chory for initial support and discussions, S. Grinstein, M. Lemmon, G. Hammond, J. Friml, J. Goedhart, B. Scheres for reagents, A. Lacroix and J. Berger for plant care and PLATIM for help with imaging. Y.J. is funded by ERC n°3363360-APPL and Marie Curie Action, n°PCIG-GA-2011-303601, under FP/2007-2013. This work was initially supported by grants from the US National Institutes of Health (GM094428) and the Howard Hughes Medical Institute to Joanne Chory and a fellowship from the H.M. Kirby foundation to Y.J. M.S is funded by a PhD fellowship from the French ministry of education. T.S is supported by ERC grant n °615739-MechanoDevo to Olivier Hamant.

References

1. Jean S, Kiger AA. Coordination between RAB GTPase and phosphoinositide regulation and functions. Nature reviews Molecular cell biology. 2012; 13:463–470. DOI: 10.1038/nrm3379 [PubMed: 22722608]
2. Holthuis JC, Levine TP. Lipid traffic: floppy drives and a superhighway. Nature reviews. Molecular cell biology. 2005; 6:209–220. DOI: 10.1038/nrm1591 [PubMed: 15738987]
3. Platre MP, Jaillais Y. Guidelines for the Use of Protein Domains in Acidic Phospholipid Imaging. Methods Mol Biol. 2016; 1376:175–194. DOI: 10.1007/978-1-4939-3170-5_15 [PubMed: 26552684]
4. Balla T. Phosphoinositides: tiny lipids with giant impact on cell regulation. Physiological reviews. 2013; 93:1019–1137. DOI: 10.1152/physrev.00028.2012 [PubMed: 23899561]
5. Kutateladze TG. Translation of the phosphoinositide code by PI effectors. Nature chemical biology. 2010; 6:507–513. DOI: 10.1038/nchembio.390 [PubMed: 20559318]
6. Lemmon MA. Membrane recognition by phospholipid-binding domains. Nature reviews. Molecular cell biology. 2008; 9:99–111. DOI: 10.1038/nrm2328 [PubMed: 18216767]
7. Bigay J, Antonny B. Curvature, lipid packing, and electrostatics of membrane organelles: defining cellular territories in determining specificity. Developmental cell. 2012; 23:886–895. DOI: 10.1016/j.devcel.2012.10.009 [PubMed: 23153485]
8. Cacas JL, et al. Revisiting Plant Plasma Membrane Lipids in Tobacco: A Focus on Sphingolipids. Plant physiology. 2016; 170:367–384. DOI: 10.1104/pp.15.00564 [PubMed: 26518342]
9. Grosjean K, Mongrand S, Beney L, Simon-Plas F, Gerbeau-Pissot P. Differential effect of plant lipids on membrane organization: specificities of phytosphingolipids and phytosterols. The Journal of biological chemistry. 2015; 290:5810–5825. DOI: 10.1074/jbc.M114.598805 [PubMed: 25575593]
10. Botte CY, Marechal E. Plastids with or without galactoglycerolipids. Trends in plant science. 2014; 19:71–78. DOI: 10.1016/j.tplants.2013.10.004 [PubMed: 24231068]

11. Boutte Y, Moreau P. Modulation of endomembranes morphodynamics in the secretory/retrograde pathways depends on lipid diversity. Current opinion in plant biology. 2014; 22:22–29. DOI: 10.1016/j.pbi.2014.08.004 [PubMed: 25233477]
12. Surpin M, Raikhel N. Traffic jams affect plant development and signal transduction. Nature reviews. Molecular cell biology. 2004; 5:100–109. DOI: 10.1038/nrm1311 [PubMed: 15040443]
13. Dettmer J, Hong-Hermesdorf A, Stierhof YD, Schumacher K. Vacuolar H+-ATPase activity is required for endocytic and secretory trafficking in Arabidopsis. The Plant cell. 2006; 18:715–730. DOI: 10.1105/tpc.105.037978 [PubMed: 16461582]
14. Grison MS, et al. Specific membrane lipid composition is important for plasmodesmata function in Arabidopsis. The Plant cell. 2015; 27:1228–1250. DOI: 10.1105/tpc.114.135731 [PubMed: 25818623]
15. Bayer EM, Mongrand S, Tilsner J. Specialized membrane domains of plasmodesmata, plant intercellular nanopores. Frontiers in plant science. 2014; 5:507. [PubMed: 25324854]
16. Yeung T, et al. Receptor activation alters inner surface potential during phagocytosis. Science. 2006; 313:347–351. DOI: 10.1126/science.1129551 [PubMed: 16857939]
17. Heo WD, et al. PI(3,4,5)P3 and PI(4,5)P2 lipids target proteins with polybasic clusters to the plasma membrane. Science. 2006; 314:1458–1461. DOI: 10.1126/science.1134389 [PubMed: 17095657]
18. McLaughlin S, Murray D. Plasma membrane phosphoinositide organization by protein electrostatics. Nature. 2005; 438:605–611. DOI: 10.1038/nature04398 [PubMed: 16319880]
19. Yeung T, et al. Membrane phosphatidylserine regulates surface charge and protein localization. Science. 2008; 319:210–213. DOI: 10.1126/science.1152066 [PubMed: 18187657]
20. Moravcevic K, et al. Kinase associated-1 domains drive MARK/PAR1 kinases to membrane targets by binding acidic phospholipids. Cell. 2010; 143:966–977. DOI: 10.1016/j.cell.2010.11.028 [PubMed: 21145462]
21. Hammond GR, et al. PI4P and PI(4,5)P2 are essential but independent lipid determinants of membrane identity. Science. 2012; 337:727–730. DOI: 10.1126/science.1222483 [PubMed: 22722250]
22. Simon ML, et al. A multi-colour/multi-affinity marker set to visualize phosphoinositide dynamics in Arabidopsis. The Plant journal: for cell and molecular biology. 2014; 77:322–337. DOI: 10.1111/tpj.12358 [PubMed: 24147788]
23. Vermeer JE, et al. Imaging phosphatidylinositol 4-phosphate dynamics in living plant cells. The Plant journal: for cell and molecular biology. 2009; 57:356–372. DOI: 10.1111/j.1365-313X.2008.03679.x [PubMed: 18785997]
24. van Leeuwen W, Vermeer JE, Gadella TW Jr, Munnik T. Visualization of phosphatidylinositol 4,5-bisphosphate in the plasma membrane of suspension-cultured tobacco BY-2 cells and whole Arabidopsis seedlings. The Plant journal: for cell and molecular biology. 2007; 52:1014–1026. DOI: 10.1111/j.1365-313X.2007.03292.x [PubMed: 17908156]
25. Tejos R, et al. Bipolar Plasma Membrane Distribution of Phosphoinositides and Their Requirement for Auxin-Mediated Cell Polarity and Patterning in Arabidopsis. The Plant cell. 2014; 26:2114–2128. DOI: 10.1105/tpc.114.126185 [PubMed: 24876254]
26. Ischebeck T, et al. Phosphatidylinositol 4,5-bisphosphate influences PIN polarization by controlling clathrin-mediated membrane trafficking in Arabidopsis. The Plant cell. 2013; 25:4894–4911. DOI: 10.1105/tpc.113.116582 [PubMed: 24326589]
27. Caillaud MC, et al. Subcellular localization of the Hpa RxLR effector repertoire identifies a tonoplast-associated protein HaRxL17 that confers enhanced plant susceptibility. The Plant journal: for cell and molecular biology. 2012; 69:252–265. DOI: 10.1111/j.1365-313X.2011.04787.x [PubMed: 21914011]
28. Balla A, Tuymetova G, Tsiomenko A, Varnai P, Balla T. A plasma membrane pool of phosphatidylinositol 4-phosphate is generated by phosphatidylinositol 4-kinase type-III alpha: studies with the PH domains of the oxysterol binding protein and FAPP1. Molecular biology of the cell. 2005; 16:1282–1295. DOI: 10.1091/mbc.E04-07-0578 [PubMed: 15635101]
29. Delage E, Ruelland E, Guillas I, Zachowski A, Puyaubert J. Arabidopsis type-III phosphatidylinositol 4-kinases beta1 and beta2 are upstream of the phospholipase C pathway

triggered by cold exposure. Plant & cell physiology. 2012; 53:565–576. DOI: 10.1093/pcp/pcs011 [PubMed: 22318862]

30. Jaillais Y, Fobis-Loisy I, Miege C, Rollin C, Gaude T. AtSNX1 defines an endosome for auxin-carrier trafficking in Arabidopsis. Nature. 2006; 443:106–109. DOI: 10.1038/nature05046 [PubMed: 16936718]
31. Fujimoto M, Suda Y, Vernhettes S, Nakano A, Ueda T. Phosphatidylinositol 3-kinase and 4-kinase have distinct roles in intracellular trafficking of cellulose synthase complexes in Arabidopsis thaliana. Plant & cell physiology. 2015; 56:287–298. DOI: 10.1093/pcp/pcu195 [PubMed: 25516570]
32. Thole JM, Vermeer JE, Zhang Y, Gadella TW Jr, Nielsen E. Root hair defective4 encodes a phosphatidylinositol-4-phosphate phosphatase required for proper root hair development in Arabidopsis thaliana. The Plant cell. 2008; 20:381–395. DOI: 10.1105/tpc.107.054304 [PubMed: 18281508]
33. Munnik T, Nielsen E. Green light for polyphosphoinositide signals in plants. Current opinion in plant biology. 2011; 14:489–497. DOI: 10.1016/j.pbi.2011.06.007 [PubMed: 21775194]
34. Hammond GR, Machner MP, Balla T. A novel probe for phosphatidylinositol 4-phosphate reveals multiple pools beyond the Golgi. The Journal of cell biology. 2014; 205:113–126. DOI: 10.1083/jcb.201312072 [PubMed: 24711504]
35. He J, et al. Molecular basis of phosphatidylinositol 4-phosphate and ARF1 GTPase recognition by the FAPP1 pleckstrin homology (PH) domain. The Journal of biological chemistry. 2011; 286:18650–18657. DOI: 10.1074/jbc.M111.233015 [PubMed: 21454700]
36. Xu J, Scheres B. Dissection of Arabidopsis ADP-RIBOSYLATION FACTOR 1 function in epidermal cell polarity. The Plant cell. 2005; 17:525–536. DOI: 10.1105/tpc.104.028449 [PubMed: 15659621]
37. Martiniere A, et al. Cell wall constrains lateral diffusion of plant plasma-membrane proteins. Proceedings of the National Academy of Sciences of the United States of America. 2012; 109:12805–12810. DOI: 10.1073/pnas.1202040109 [PubMed: 22689944]
38. Zegzouti H, et al. Structural and functional insights into the regulation of Arabidopsis AGC VIIIa kinases. The Journal of biological chemistry. 2006; 281:35520–35530. DOI: 10.1074/jbc.M605167200 [PubMed: 16973627]
39. Barbosa IC, Schwechheimer C. Dynamic control of auxin transport-dependent growth by AGCVIII protein kinases. Current opinion in plant biology. 2014; 22:108–115. DOI: 10.1016/j.pbi.2014.09.010 [PubMed: 25305415]
40. Jaillais Y, et al. Tyrosine phosphorylation controls brassinosteroid receptor activation by triggering membrane release of its kinase inhibitor. Genes & development. 2011; 25:232–237. DOI: 10.1101/gad.2001911 [PubMed: 21289069]
41. Belkhadir Y, Jaillais Y. The molecular circuitry of brassinosteroid signaling. The New phytologist. 2015; 206:522–540. DOI: 10.1111/nph.13269 [PubMed: 25615890]
42. Michniewicz M, et al. Antagonistic regulation of PIN phosphorylation by PP2A and PINOID directs auxin flux. Cell. 2007; 130:1044–1056. DOI: 10.1016/j.cell.2007.07.033 [PubMed: 17889649]
43. Lee SH, Cho HT. PINOID positively regulates auxin efflux in Arabidopsis root hair cells and tobacco cells. The Plant cell. 2006; 18:1604–1616. DOI: 10.1105/tpc.105.035972 [PubMed: 16731587]
44. Marques-Bueno MM, et al. A versatile Multisite Gateway-compatible promoter and transgenic line collection for cell type-specific functional genomics in Arabidopsis. The Plant journal: for cell and molecular biology. 2016; 85:320–333. DOI: 10.1111/tpj.13099 [PubMed: 26662936]
45. Kang BH, Nielsen E, Preuss ML, Mastronarde D, Staehelin LA. Electron tomography of RabA4b- and PI-4Kbeta1-labeled trans Golgi network compartments in Arabidopsis. Traffic. 2011; 12:313–329. DOI: 10.1111/j.1600-0854.2010.01146.x [PubMed: 21134079]
46. Preuss ML, et al. A role for the RabA4b effector protein PI-4Kbeta1 in polarized expansion of root hair cells in Arabidopsis thaliana. The Journal of cell biology. 2006; 172:991–998. DOI: 10.1083/jcb.200508116 [PubMed: 16567499]

47. Antignani V, et al. Recruitment of PLANT U-BOX13 and the PI4Kbeta1/beta2 phosphatidylinositol-4 kinases by the small GTPase RabA4B plays important roles during salicylic acid-mediated plant defense signaling in Arabidopsis. The Plant cell. 2015; 27:243–261. DOI: 10.1105/tpc.114.134262 [PubMed: 25634989]

48. Naramoto S, et al. Phosphoinositide-dependent regulation of VAN3 ARF-GAP localization and activity essential for vascular tissue continuity in plants. Development. 2009; 136:1529–1538. DOI: 10.1242/dev.030098 [PubMed: 19363154]

49. Heilmann M, Heilmann I. Plant phosphoinositides-complex networks controlling growth and adaptation. Biochimica et biophysica acta. 2015; 1851:759–769. DOI: 10.1016/j.bbalip.2014.09.018 [PubMed: 25280638]

50. Potocky M, et al. Live-cell imaging of phosphatidic acid dynamics in pollen tubes visualized by Spo20p-derived biosensor. The New phytologist. 2014; 203:483–494. DOI: 10.1111/nph.12814 [PubMed: 24750036]

51. Cutler SR, Ehrhardt DW, Griffitts JS, Somerville, Random CR. GFP::cDNA fusions enable visualization of subcellular structures in cells of Arabidopsis at a high frequency. Proceedings of the National Academy of Sciences of the United States of America. 2000; 97:3718–3723. [PubMed: 10737809]

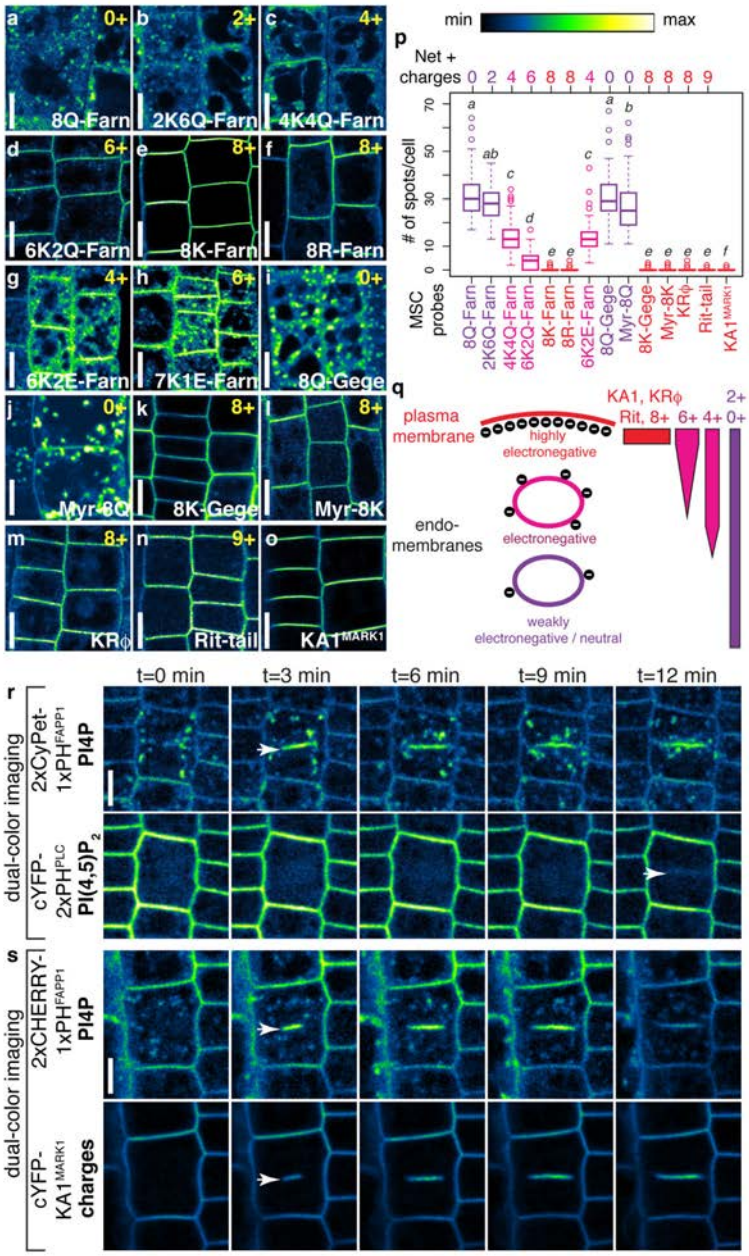

Fig. 1. The plant PM and the cell plate are highly electronegative, a property that correlates with PI4P localization

a–o) Confocal pictures of MSC probes in Arabidopsis root epidermis. Probes are indicated at the bottom and net charges at the top. **p)** Tukey boxplot showing the distribution of intracellular compartments (spots) per cell for each MSC reporter. Different italicized-letters indicate significant differences among means (*P<0.0001,* Kruskal-Wallis test). **q)** Schematic representation of MSC organization in plants. **r–s)** Dual-color imaging during cytokinesis in Arabidopsis root epidermis. Plants co-expressing: **r)** 2xCyPet-1xPH^{FAPP1} (top) and cYFP-2xPH^{PLC} (bottom) or **s)** 2xCHERRY-1xPH^{FAPP1} (top) and cYFP-KA^{MARK1} (bottom).

Confocal images are color-coded with respect to pixel intensity based on the scale shown in the top right corner. Scale bars, 5 μm.

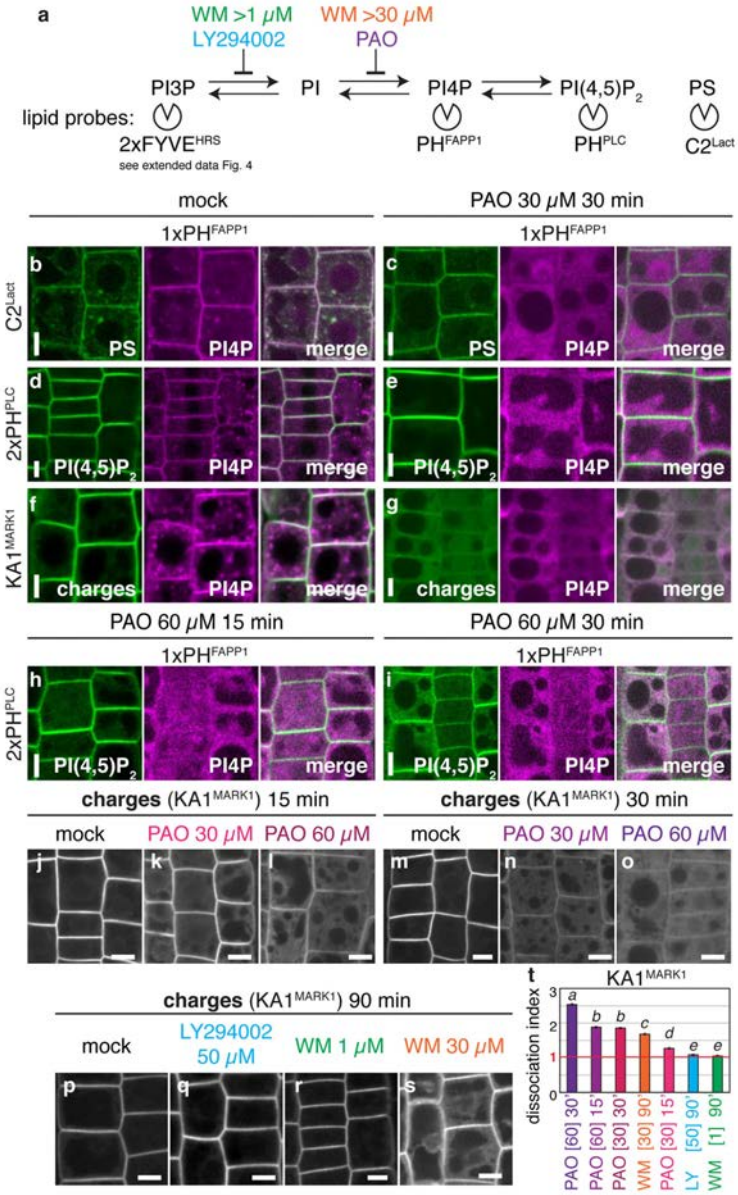

Fig. 2. PI4K activity is required to maintain the PM electrostatic signature

a) Schematic representation of the drugs used to perturb phosphoinositides production and lipid sensors used as read-out. **b–i)** Dual-color imaging of plants treated with the indicated time and drug concentration. PS, $PI(4,5)P_2$ and MSC reporters are pseudo-colored in green (left), $1xPH^{FAPP1}$ are pseudo-colored in purple (middle). Colocalizations are showed in white in the merged channel (right). **b–c**) Plants co-expressing $2xCHERRY\text{-}C2^{Lact}$ and $cYFP\text{-}1xPH^{FAPP1}$. **d–e** and **h–i**) Plants co-expressing $cYFP\text{-}2xPH^{PLC}$ and $2xCyPet\text{-}1xPH^{FAPP1}$. **f–g)** Plants co-expressing $cYFP\text{-}KA1^{MARK1}$ and $2xCHERRY\text{-}1xPH^{FAPP1}$. **j–s)** Confocal pictures of $cYFP\text{-}KA1^{MARK1}$ MSC reporter treated with the indicated time and drug concentration and **t)** corresponding dissociation index

(mean ±SEM). Different italicized-letters indicate significant differences among means (*P<0.0001,* Kruskal-Wallis test).

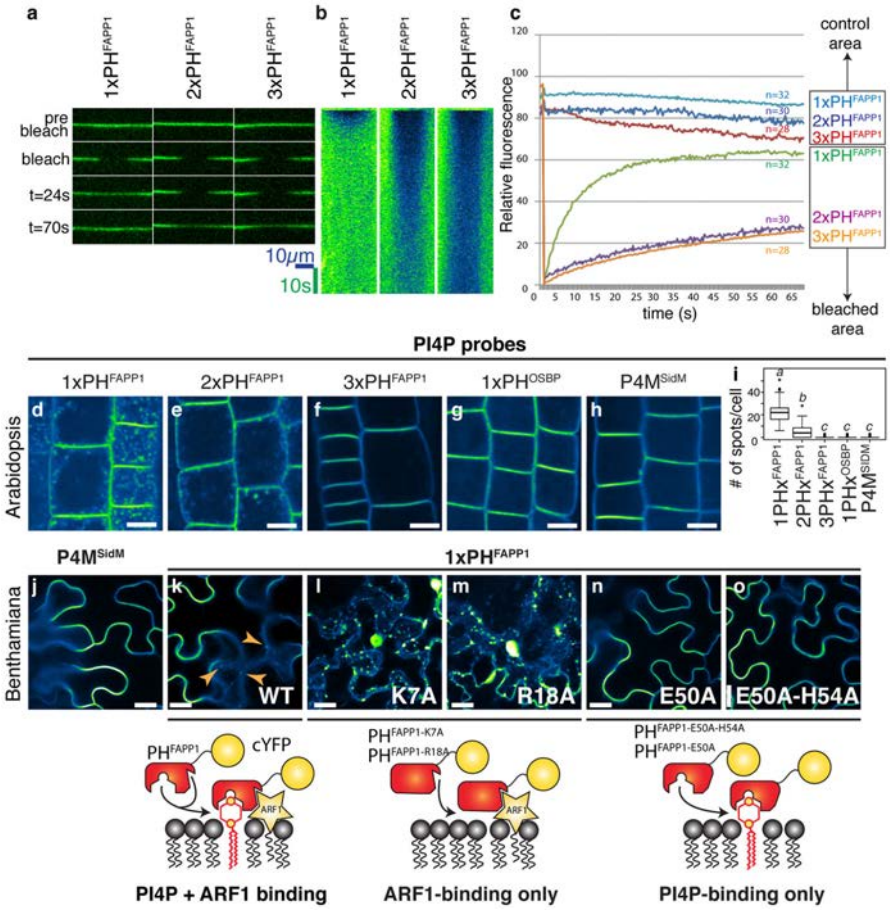

Fig. 3. PI4P is a hallmark of the plant PM

a–c) FRAP analyses of 1x, 2x and 3xPH^{FAPP1} sensors. **a)** Representative confocal pictures, **b)** kymograms of protein diffusion within the PM and **c)** trace of fluorescence intensity during FRAP analyses. **d–h)** Confocal pictures of PI4P probes in Arabidopsis root epidermis. Probes are indicated at the top. Scale bars, 5 μm. **i)** Tukey boxplot showing the distribution of intracellular compartments (spots) per cell for each PI4P reporter. Different italicized-letters indicate significant differences among means (*P<0.0001,* Kruskal-Wallis test). **j–o)** Confocal pictures of PI4P probes in *Nicotiana benthamiana* leaf epidermis. Probes are indicated at the top and mutations in PH^{FAPP1} at the bottom. Bottom panels show schematic representations of PH^{FAPP1} membrane recruitment mechanism according to the different mutations used. Orange arrowheads indicate endosomal localization of 1xPH^{FAPP1}. Scale bars, 20 μm.

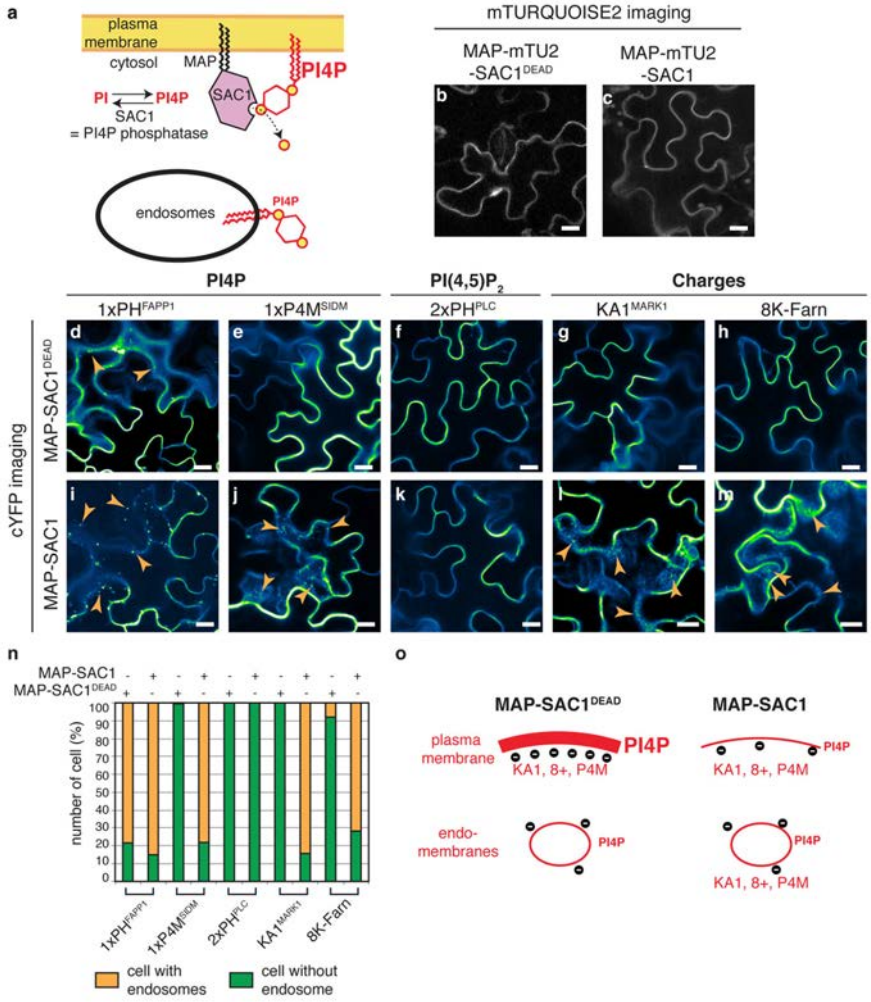

Fig. 4. PM PI4P drives the electrostatic field of the cell membrane

a) Schematic representation of the genetic system used to specifically deplete PM PI4P. **b–c**) mTURQUOISE2 imaging of MAP-mTU2-SAC1^{DEAD} (**b**) and MAP-mTU2-SAC1 (**c**) in *Nicotiana benthamiana* leaf epidermis. **d–m**) cYFP imaging of the lipid or MSC reporter indicated at the top in *Nicotiana benthamiana* leaf epidermis, co-expressed with MAP-mTU2-SAC1^{DEAD} (**d–h**) or MAP-mTU2-SAC1 (**i–m**). **n**) Quantification of localization observed in d–m. **o**) Schematic representation of PI4P and MSC organization in non-perturbed cells (left) or cells with reduced PM PI4P (right). Scale bars, 20 μm.

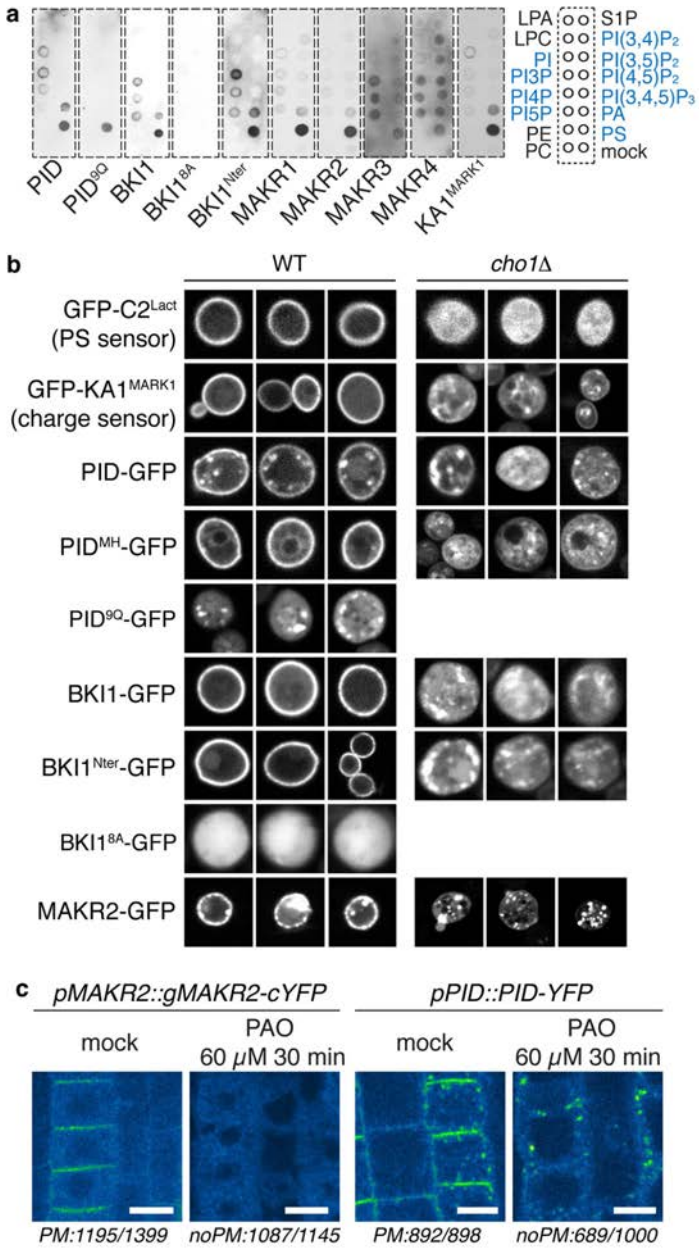

Fig. 5. PINOID and BKI1/MAKRs are effectors of the PM electrostatic field

a) Lipid overlay assays with recombinant PID-Flag, PID^{9Q}-FLAG, BKI1-Flag, BKI1^{8A}-Flag, BKI1^{Nter}-Flag, MAKR1-Flag, HA-MAKR2, HA-MAKR3, HA-MAKR4 and the HA-KA1^{MARK1} control. Anionic lipids are indicated in blue. **b)** Three representative confocal pictures showing the localization of the indicated GFP-fused protein in WT and *cho1Δ* yeast. **c)** Representative images in mock or PAO treated plants. Numbers at the bottom indicates the proportion of cells with signal at the PM or not. Scale bars, 5 μm.

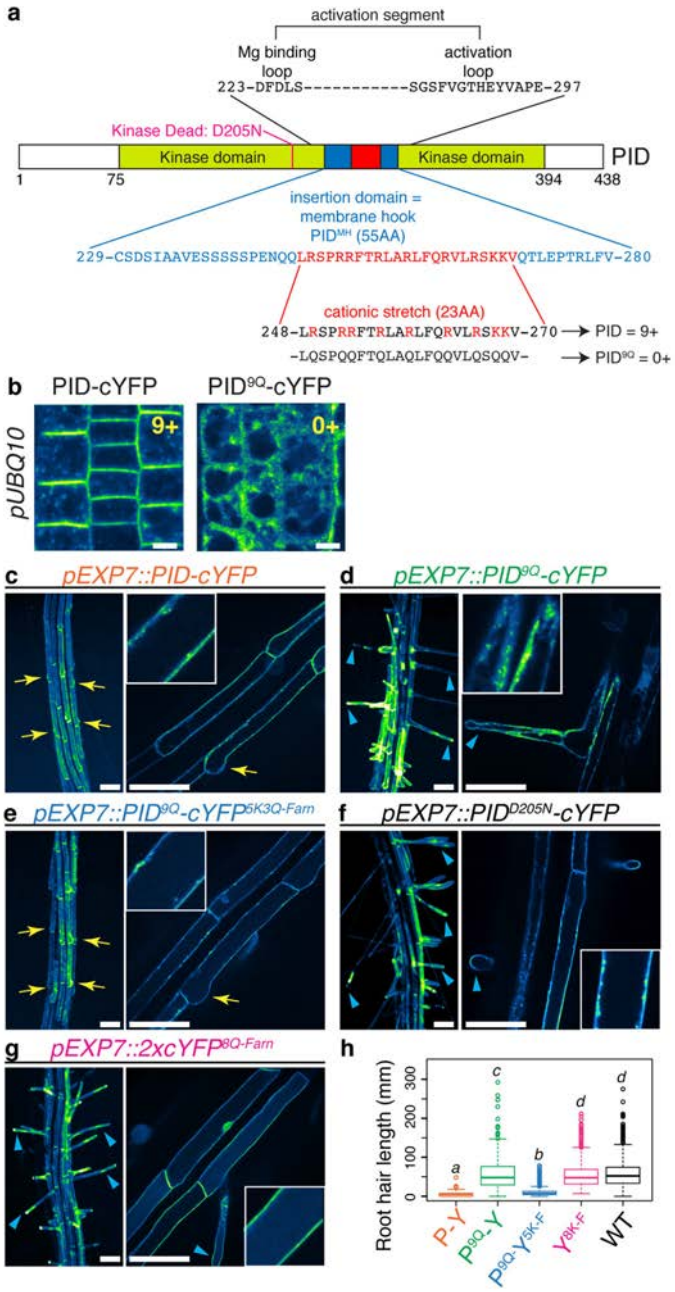

Fig. 6. PM targeting by PID cationic membrane hook is required for function

a) Schematic representation of the PID protein. **b)** Confocal picture of *pUBQ10::PID-cYFP* and *pUBQ10::PID^{9Q}–cYFP* in Arabidopsis root meristem epidermis. Scale bars, 5μm. **c–g)** Representative picture of root hair phenotypes (left) and localization of the indicated construct (right). Each picture was taken with identical setting indicating that each transgenic line expressed comparable level of PID protein. Blue arrowheads indicate elongated root hairs and yellow arrows indicate root hairs with inhibited growth. Scale bars, 100 μm. **h)** Tukey boxplot showing the quantification of root hair length in the following

lines: *pEXP7::PID-cYFP* (P-Y, orange); *pEXP7::PID^{9Q}-cYFP* (P^{9Q}-Y); *pEXP7::PID^{9Q}-cYFP$^{5K3Q\text{-}Farn}$* (P^{9Q}-Y$^{5K\text{-}F}$); *pEXP7::2x-cYFP$^{8K\text{-}Farn}$* (Y$^{8K\text{-}F}$) and WT. Different italicized-letters indicate significant differences among means (*P<0.0001,* Kruskal-Wallis test).

Chapter II : Combinatorial PA, PS and PI4P cooperation determines the electrostatic territory in plants

Title:

Combinatorial PA, PS and PI4P cooperation determines the electrostatic territory in plants

Matthieu Pierre Platre[1], Mehdi Doumane[1], Vincent Bayle[1], Mathilde Laetitia Audrey Simon[1], Lilly Maneta-Peyret[2], Laetitia Fouillen[2], Thomas Stanislas[1], Laia Armengot[1], Přemysl Pejchar[3], Marie-Cécile Caillaud[1], Martin Potocký[3], Alenka Čopič[4], Patrick Moreau[2,5], Yvon Jaillais[1]#

[1]Laboratoire Reproduction et Développement des Plantes, Université de Lyon, ENS de Lyon, UCB Lyon 1, CNRS, INRA, F-69342 Lyon, France.

[2]UMR 5200 Membrane Biogenesis Laboratory, CNRS-University of Bordeaux, Bâtiment A3 - INRA Bordeaux Aquitaine, 71 Avenue Edouard Bourlaux- CS 20032, 33140 Villenave d'Ornon, France.

[3]Institute of Experimental Botany, Czech Academy of Sciences, 16502 Prague 6 - Lysolaje, Czech Republic

[4]Institut Jacques Monod, CNRS, UMR 7592, Université Paris Diderot, Sorbonne Paris Cité, F-75013 Paris, France.

[5]Bordeaux Imaging Center, UMS 3420 CNRS, US4 INSERM, University of Bordeaux, 33000 Bordeaux, France.

Corresponding author, lead contact: yvon.jaillais@ens-lyon.fr

Abstract

Membrane surface charge is critical for the transient, yet specific recruitment of proteins with polybasic regions to certain organelles. In all eukaryotes, the plasma membrane (PM) is the most electronegative compartment of the cell, which specifies its identity. As such, membrane electrostatics is a central parameter in signaling, intracellular trafficking and polarity. Here, we explore which are the lipids that control membrane electrostatics using plants as a model. We show that phosphatidic acidic (PA), phosphatidylserine (PS) and phosphatidylinositol-4-phosphate (PI4P) are separately required to generate the distinctively high PM electrostatic field. In addition, we reveal the existence of an electrostatic territory that is organized as a gradient along the endocytic pathway and is controlled by PS/PI4P combination. Altogether, we propose that combinatorial lipid composition of the cytosolic leaflet of cellular organelles not only defines the plant electrostatic territory but also distinguishes different compartments within this territory by specifying their varying surface charges.

Introduction

An evolutionarily conserved feature of cellular organelles is the distinct phospholipid composition of their membranes, which is essential to specify their identity and function. Within the endomembrane system of eukaryotic cells, the existence of two major lipid territories has been postulated, one characterized by membranes with lipid packing defects, and the other defined by membrane surface charges (Bigay and Antonny, 2012). These two lipid territories correspond roughly to two dynamic membrane-recycling systems; one centered on the endoplasmic reticulum (ER) and that includes membranes from the ER, the nuclear envelope and the *cis*-Golgi, and the other centered on the plasma membrane (PM) and that comprises the *trans*-Golgi, the *trans*-Golgi Network (TGN), the PM and endosomes (Jackson et al., 2016). In the later, referred to as the electrostatic territory, anionic membranes recruit proteins with polybasic regions to their surface and as such participate in the localization of a large number of cellular factors along the endocytic pathway (Jackson et al., 2016). In mammalian cells, the anionic phospholipid phosphatidylserine (PS) is enriched in these so-called PM-derived organelles and was proposed to act as a landmark of the electrostatic territory (Bigay and Antonny, 2012; Jackson et al., 2016; Yeung et al., 2008). However, this model, which is speculated to be a conserved feature of eukaryotic cells, was only tested *in vitro* in cultured human cells, notably in macrophages (Yeung et al., 2008; Yeung et al., 2009), and was not yet challenged in loss-of-function experiments with genetic and/or pharmacological depletion of cellular PS.

A second characteristic of the electrostatic territory lays in the finding that it is not uniformly organized across all PM-derived organelles (Platre and Jaillais, 2017; Yeung et al., 2006). Rather, the inner leaflet of the PM is the most electronegative cytosolic-facing membrane across eukaryotes, including yeasts, animals and plants (Platre and Jaillais, 2017). This PM electrostatic signature is critical for cell signaling as it enables to specifically recruit proteins to the PM., such as e.g., small GTPases, kinases, or kinase regulators (Barbosa et al., 2016; Heo et al., 2006; Moravcevic et al., 2010; Simon et al., 2016; Yeung et al., 2006). While the PM high electronegative property is conserved across eukaryotes, the lipids that generate its surface charges are not (Platre and Jaillais, 2017). Indeed, PS massively accumulates at the PM in yeasts, thereby defining its electronegative signature (Haupt and Minc, 2017; Moravcevic et al., 2010). In animal cells, phosphatidylinositol-4,5-bisphosphate ($PI(4,5)P_2$) is a major driver of PM electrostatics but acts redundantly with both phosphatidylinositol-4-phosphate (PI4P) and

phosphatidylinositol-3,4,5-trisphosphate PI(3,4,5)P_3 (Dong et al., 2015; Hammond et al., 2012; Heo et al., 2006). In addition to these phosphoinositides, PS was also proposed to regulate the surface charge of the PM in animal cells (Ma et al., 2017; Yeung et al., 2008).

We recently showed that in plants, PI4P massively accumulates at the PM (Simon et al., 2014; Simon et al., 2016). Because PI4P represents about 80% of plant phosphoinositides, its accumulation at the PM is critical to define the electrostatic signature of the plant plasmalemma (Simon et al., 2016). Thereby, by contrast to human cells, in which several phosphoinositides cooperate to regulate PM surface charges, a single phosphoinositide species is critical to maintain PM electrostatics in plants (Platre and Jaillais, 2017). Thus, we wondered whether other anionic phospholipids could be involved in the generation of an electrostatic territory. We therefore studied the potential roles of PS and phosphatidic acid (PA), which are two anionic phospholipids that are relatively abundant in plant membranes. To address whether they could control PM electrostatics, we first analyzed their subcellular localization using genetically encoded biosensors. We further used these sensors to validate pharmacological and genetic approaches designed to perturb the production of these lipids. We demonstrate that PA and PS act in concert with PI4P to generate the distinctively high PM electrostatic field. In addition, we reveal the existence of an electrostatic gradient along the endocytic pathway, being the highest at the PM, intermediate in early endosomes/*trans*-Golgi Network (EE/TGN) and lowest in late endosomes (LE). We further show that PS, in combination with PI4P, organizes this intracellular electrostatic gradient.

Results

PA accumulates at the PM cytosolic leaflet in *Arabidopsis* root epidermis

PA is an anionic phospholipid, which accumulates in the sub apical region of the PM cytosolic leaflet in tobacco pollen tubes (Potocky et al., 2014). To analyze whether PA could also localize at the PM in *Arabidopsis* sporophytic tissues, and thereby may contribute to PM electrostatics, we raised transgenic *Arabidopsis* lines stably expressing mCITRINE-tagged variants of the recently developed "*PA biosensor with superior sensitivity*" (mCITRINE-1xPASS and mCITRINE-2xPASS) (Lu et al., 2016; Zhang et al., 2014) under the control of the mild ubiquitous promoter of the *UBIQUITIN10* (*UBQ10*) gene. This PA probe is based on the PA-binding motif of the yeast Spo20p protein, with an extra nuclear export signal (NES) to exclude the fusion protein from the nucleus and increase the accessibility of the probe to the cytosol (Lu et al., 2016; Zhang et al., 2014). Both mCITRINE-1xPASS and mCITRINE-2xPASS sensors were targeted to the PM in

Arabidopsis, including root and shoot tissues (Figure 1A, Figure S1A and S1B). We noticed that these PA probes localized early at the cell plate (Video S1) and colocalized with the endocytic dye FM4-64 (Figure S1C), one of the earlier marker incorporated into the membrane of this compartment (Dettmer et al., 2006). Furthermore, mCITRINE-2xPASS localized on the flank region of growing root hairs (Video S2), in a pattern that closely resembled the localization of PA sensor in growing tobacco pollen tubes (Potocky et al., 2014). While both PA sensors localized at the PM, mCITRINE-1xPASS was also cytosolic, while mCITRINE-2xPASS accumulated in the nucleus (Figure 1A). This suggests that in mCITRINE-2xPASS, the NES is not as efficient as in the mCITRINE-1xPASS probe. Consistently, the mCITRINE-1xPASS probe for which the NES is mutated (1xPASS^{NESmut}) localized at the PM, the cytosol and in the nucleus (Figure 1A). It is unclear what the significance of the nuclear localization of the probe is. Indeed, it might reflect uncontrolled diffusion from the cytosol into the nucleus or trapping of the probe in the nucleus by nuclear PA. Of note, for all three transgenic lines (mCITRINE-1xPASS, mCITRINE-1xPASS^{NESmut}, mCITRINE-2xPASS), we observed some variability on the intensity of PM labeling between different roots. Although the cause of this variability is currently unknown, it might arise from different stress status of individual roots or cells since PA metabolism is well known to be under tight environmental control (Testerink and Munnik, 2011). Nonetheless, the three aforementioned probes are targeted to the PM of root meristematic cells (Figure 1A), suggesting local enrichment of PA in this membrane even in normal growing conditions (i.e. non-stressed).

The PA-binding motif of Spo20p was extensively validated as a sensor *in vivo* in animal cells (Bohdanowicz et al., 2013; Zhang et al., 2014), as well as in pollen tube (Potocky et al., 2014). However, *in vitro*, PA binding was also shown to be dependent on the local lipid environment of the probe (i.e. local surface charges) (Horchani et al., 2014; Kassas et al., 2017). In order to validate the PA sensor specificity *in planta*, we first expressed mCITRINE-1xPASS mutant versions (L67P single mutant, K66E-K68E double mutants and K66E-K68E-K71E-K73E quadruple mutants), which were previously shown to impair PA binding (Potocky et al., 2014). mCITRINE-1xPASS$^{K66E\text{-}K68E}$ (1xPASS$^{K>E\ double}$) retained a faint PM labeling, while mCITRINE-1xPASS^{L67P} and mCITRINE-1xPASS$^{K66E\text{-}K68E\text{-}K71E\text{-}K73E}$ (1xPASS$^{K>E\ quadruple}$) were fully soluble, suggesting that lipid binding is required for the PM localization of the 1xPASS probe (Figure 1A). Diacylglycerol kinases (DGK) are the major PA producing enzymes at the PM of animal cells with constitutively elevated PA level (Bohdanowicz et al., 2013). We therefore analyzed the effect of R59949 and R59022, two inhibitors of DGK activity, on the localization of PA

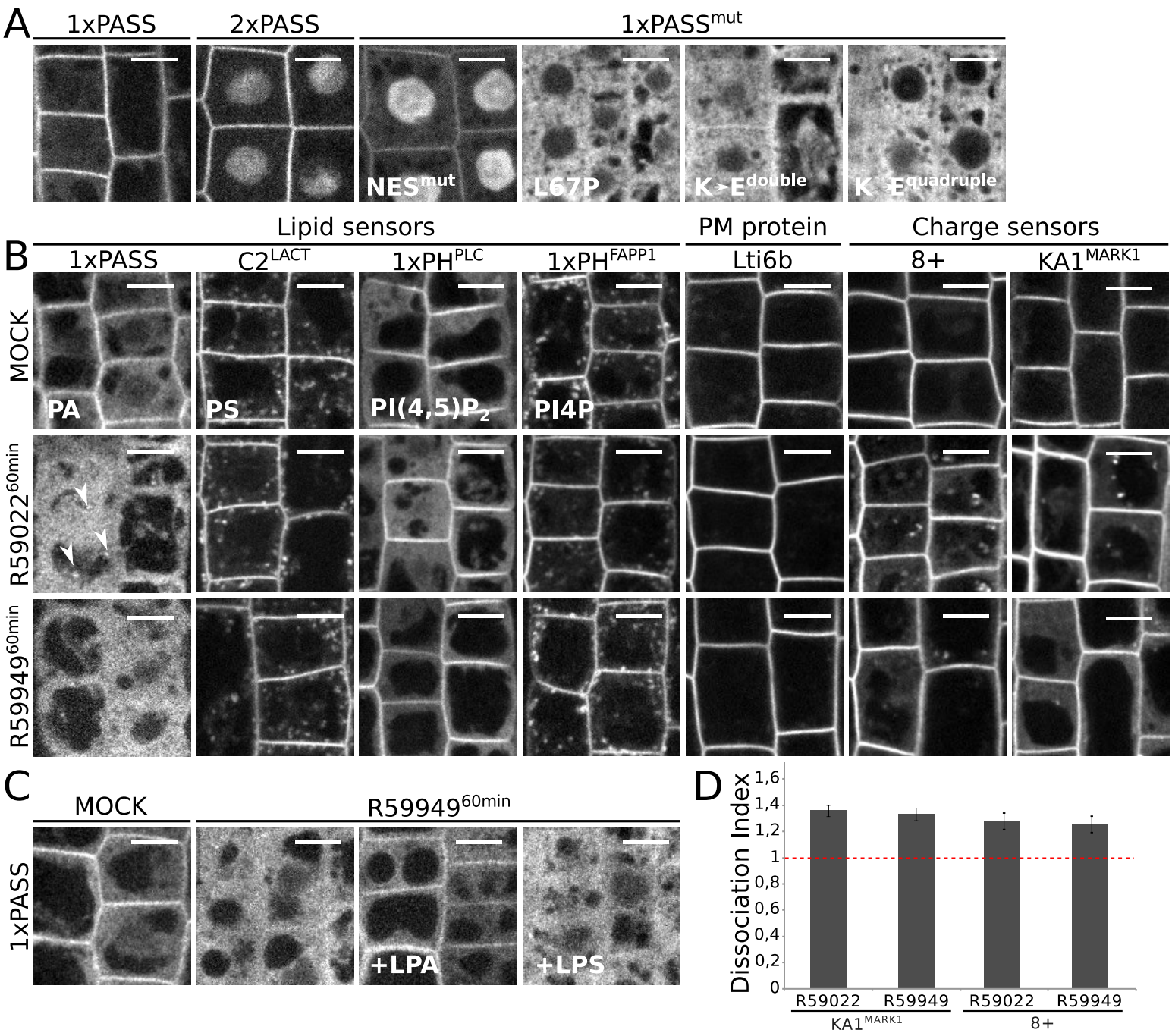
A
1xPASS
2xPASS
1xPASS^mut
NES^mut
L67P
K➔E^double
K➔E^quadruple
B
Lipid sensors
PM protein
Charge sensors
1xPASS
C2^LACT
1xPH^PLC
1xPH^FAPP1
Lti6b
8+
KA1^MARK1
MOCK
R59022^60min
R59949^60min
PA
PS
PI(4,5)P2
PI4P
C
MOCK
R59949^60min
1xPASS
+LPA
+LPS
D
Dissociation Index
1,6
1,4
1,2
1
0,8
0,6
0,4
0,2
0
R59022
R59949
R59022
R59949
KA1^MARK1
8+

Figure_1

Figure 1. DAG Kinase-dependent accumulation of phosphatidic acid at the PM is required to maintain the electrostatic field of the PM cytosolic leaflet. A, Confocal images of *Arabidopsis* root epidermis expressing from left to right, mCITRINE-1xPASS, mCITRINE-2xPASS, mCITRINE-1xPASS^{NESmut}, mCITRINE-1xPASS^{L67P}, mCITRINE-1xPASS$^{K66E\text{-}K68E}$ (K→E double), and mCITRINE-1xPASS$^{K66E\text{-}K68E\text{-}K71E\text{-}K73E}$ (K→E quadruple). **B**, Confocal images of plants expressing from left to right, PA, PS, PI(4,5)P_2 and PI4P sensors (mCITRINE-1xPASS, mCITRINE-C2^{LACT}, mCITRINE-1xPH^{PLC}, mCITRINE-1xPH^{FAPP1}), plasma membrane-associated protein (EGFP-Lti6b) and charge sensors (mCITRINE$^{8K\text{-}Farn}$ (8+), mCITRINE-KA1^{MARK1}), in mock conditions (top), plants treated with 12.5µM R59022 (middle) or 12.5µM R59949 (bottom) for 60 min. Arrows highlight the presence of spots. **C**, Confocal images of *Arabidopsis* root epidermis expressing mCITRINE-1xPASS upon concomitant lysoPA (LPA) or lysoPS (LPS) and R59949(12.5 µM) treatment for 60min. From left to right, mock, R59949alone, R59949+ LPA, and R59949+ LPS. **D,** Quantification of the mCITRINE-KA1^{MARK1} and mCITRINE$^{8K\text{-}Farn}$ dissociation index (mean ±s.e.m), upon R59022 and R59949 treatment (n=150 cells 12.5µM, 60min). Scale bars, 5 µm.

reporters. Both inhibitors induced the release of mCITRINE-1xPASS and mCITRINE-2xPASS PA probes from the PM into the cytosol and nucleus, respectively (Figure 1B and S1D). These results suggest that DGKs are required to maintain PA production at the plant PM. To confirm that the dissociation of mCITRINE-1xPASS was caused by inhibition of PA production in R59949 treated seedling, we performed add-back experiments by supplementing the root with exogenous lysophosphatidic acid (LPA) or lysophosphatidylserine (LPS) as control. We used lysophospholipids since they have identical head groups as PA/PS but are more soluble than phospholipids and as such are more likely to reach the cytosolic leaflet of cellular membranes (Moser von Filseck et al., 2015). We found that upon inhibition of endogenous PA production by R59949, mCITRINE-1xPASS was maintained at the PM in presence of an exogenous supply of LPA but not in the presence of LPS (Figure 1C). Moreover, in the presence of either R59949 or R59022, reporters for PI4P, PI(4,5)P_2 and PS anionic phospholipids (mCITRINE-1xPH^{FAPP1}, mCITRINE-1xPH^{PLC} and mCITRINE-C2^{Lact} respectively (Simon et al., 2014; Simon et al., 2016)), were still localized at the PM (Figure 1B). Altogether, these results indicated that the PM localization of the mCITRINE-1xPASS and mCITRINE-2xPASS probes are largely driven by DGK-synthesized PA, rather than by a general requirement of these probes for anionic phospholipids. In addition, both R59949 and R59022 treatments had no impact on the localization of EGFP-Lti6b (Figure 1B), a control protein with two transmembrane segments and very short cytosolic tails, whose localization is not regulated by anionic lipids (Cutler et al., 2000). Altogether, these results validate the specificity of our PA probes and suggest that PA accumulates in the cytosolic leaflet of the plant PM. It is therefore possible that this anionic lipid participates in the control of PM electrostatics.

PA contributes to PM cytosolic leaflet surface charges

We next asked whether PA could participate in the electrostatic property of the PM. We took advantage of DGK inhibitors to reduce the level of PA at the PM and analyze the impact of this pharmacological inhibition on the localization of membrane surface charge reporters. We used two types of membrane charge reporters that we previously validated *in planta* (Simon et al., 2016). The first probe, mCITRINE$^{8K\text{-}Farn}$ corresponds to two mCITRINE fluorescent proteins fused in tandem, which localize in electrostatic membranes thanks to the combinatorial effects of a polycationic region (with 8 net positive charges, +8) and an adjacent farnesyl lipid anchor, which provides hydrophobic anchoring (Haupt and Minc, 2017; Platre and Jaillais, 2017; Simon et al., 2016; Yeung et al., 2008; Yeung et al., 2006). The second probe corresponds to the KA1 domain of the human protein MARK1, which is a folded unit known to interact non-

stereospecifically with all anionic phospholipids (Hammond et al., 2012; Moravcevic et al., 2010; Platre and Jaillais, 2017; Simon et al., 2016). We found that in PA depleted condition, charge sensors (mCITRINE$^{8K\text{-}Farn}$ and mCITRINE-KA1^{MARK1} probes) were released into the cytosol and endosomes (Figure 1B and D). Endosome labelling was more prominent with R59022 than R59949 treatment and correlated with the concomitant accumulation of mCITRINE-1xPASS in similar compartments (see arrows, Figure 1B). Together, our results suggest that PA contributes to the electrostatic properties of the plasmalemma cytosolic leaflet.

PS accumulates on the cytosolic leaflet of PM and PM-derived organelles

To evaluate the potential function of PS in membrane electrostatics, we studied its sub-cellular distribution using genetically encoded biosensors that report the localization of PS in inner membrane leaflets. We used the stereospecific PS-binding C2 domain of bovine Lacthaderin (C2^{LACT}) and the pleckstrin homology (PH) domain of human EVECTIN2 (PH^{EVCT2}). These probes were extensively validated as calcium-independent PS reporters (Chung et al., 2015; Haupt and Minc, 2017; Moravcevic et al., 2010; Moser von Filseck et al., 2015; Simon et al., 2016; Uchida et al., 2011; Yeung et al., 2008; Yeung et al., 2009) (Figure S2A and S2B). We raised transgenic *Arabidopsis* plants that stably express fluorescent fusions with either C2^{LACT}, or 2xPH^{EVCT2} under the control of the *UBQ10* promoter. As we previously reported for mCITRINE-C2^{LACT} in root epidermis (Simon et al., 2016), we found that the C2^{LACT} domain was localized at the PM and in multiple intracellular compartments in all cell types analyzed, including both shoot and root tissues (Figure 2A and Figure S2C-J). We noticed that in tip growing cells such as root hairs and pollen tubes, C2^{LACT}, was localized to the shank region of the plasma membrane and intracellular compartments and accumulated in the inverted cone region at their very tip (Video S3 and S4, respectively), a region known for active endocytic and exocytic activities (Noack and Jaillais, 2017). In addition, the mCITRINE-2xPH^{EVCT2} reporter showed a similar localization pattern as mCITRINE-C2^{LACT} and, consistently, tdTOMATO-2xPH^{EVCT2} extensively colocalized with mCITRINE-C2^{LACT} (Figure S2C). However, similarly to animal cells (Chung et al., 2015; Uchida et al., 2011; Yeung et al., 2008), we noticed that mCITRINE-C2^{LACT} PM localization was more pronounced than that of mCITRINE-2xPH^{EVCT2}/tdTOMATO-2xPH^{EVCT2}.

Next, we analyzed in which endomembrane structures the C2^{LACT} probe localized. We crossed the mCITRINE-C2^{LACT} reporter line with various red-fluorescent membrane markers lines or imaged it in conjunction with red-fluorescent dyes (Figure 2A). mCITRINE-C2^{LACT} extensively

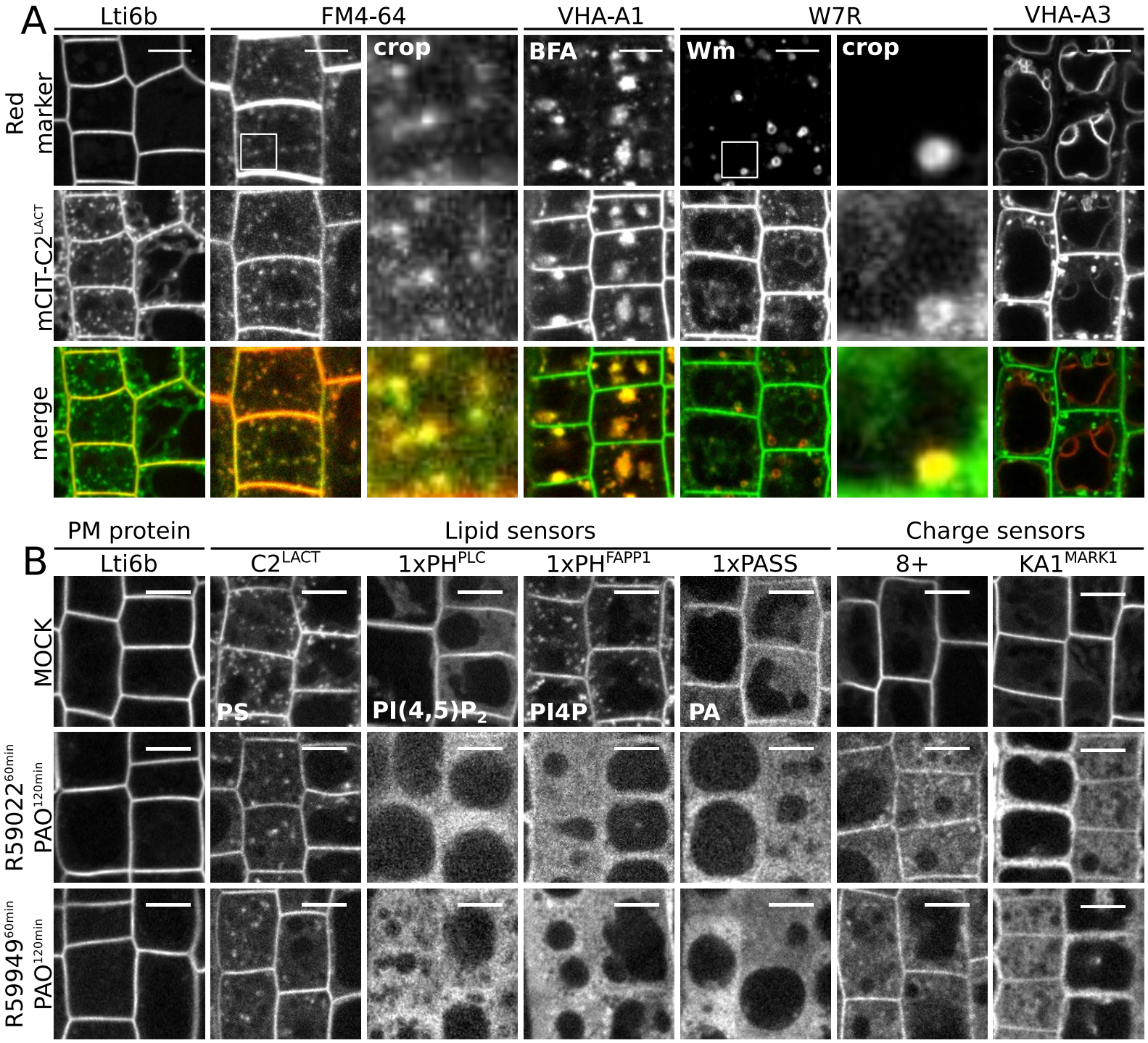
A
Lti6b
FM4-64
VHA-A1
W7R
VHA-A3
Red marker
mCIT-C2LACT
merge
crop
BFA
Wm
crop
B
PM protein
Lipid sensors
Charge sensors
Lti6b
C2LACT
1xPHPLC
1xPHFAPP1
1xPASS
8+
KA1MARK1
MOCK
PS
PI(4,5)P2
PI4P
PA
R59022 60min PAO 120min
R59949 60min PAO 120min

Figure_2

Figure 2. Phosphatidylserine accumulates at the PM and along the endocytic pathway and is sufficient to maintain negative charges at the PM cytosolic leaflet. **A)** Confocal images of *Arabidopsis* root epidermis co-expressing a red fluorescence marker (top), mCITRINE-$C2^{LACT}$ (middle), and corresponding merge (bottom). Top images correspond to (from left to right): Lti6b-2xmCHERRY (PM marker), FM4-64 (endocytic tracer, 1µM, 60 min), VHA-A1-mRFP1 (EE/TGN marker) in the presence of brefeldinA (BFA, 25µM, 60min), W7R (LE marker) treated with 30µM wortmannin (Wm, 30µM, 90min), VHA-A3-mRFP1 (tonoplast marker). **B,** Confocal images of plants expressing from left to right, EGFP-Lti6b, mCITRINE-$C2^{LACT}$ (PS), mCITRINE-$1xPH^{PLC}$ ($PI(4,5)P_2$), mCITRINE-PH^{FAPP1} (PI4P), mCITRINE-1xPASS (PA), mCITRINE$^{8K\text{-}Farn}$ (membrane charge) and mCITRINE-$KA1^{MARK1}$ (membrane charge), in mock conditions (top), plants pre-treated with 30µM PAO for 60 min and then concomitantly treated with 12.5µM R59022 and 30µM PAO for 60 min (middle), plants pre-treated with 30µM PAO for 60 min and then concomitantly treated with 12.5µM R59949and 30µM PAO for 60 min (bottom). Scale bars, 5 µm.

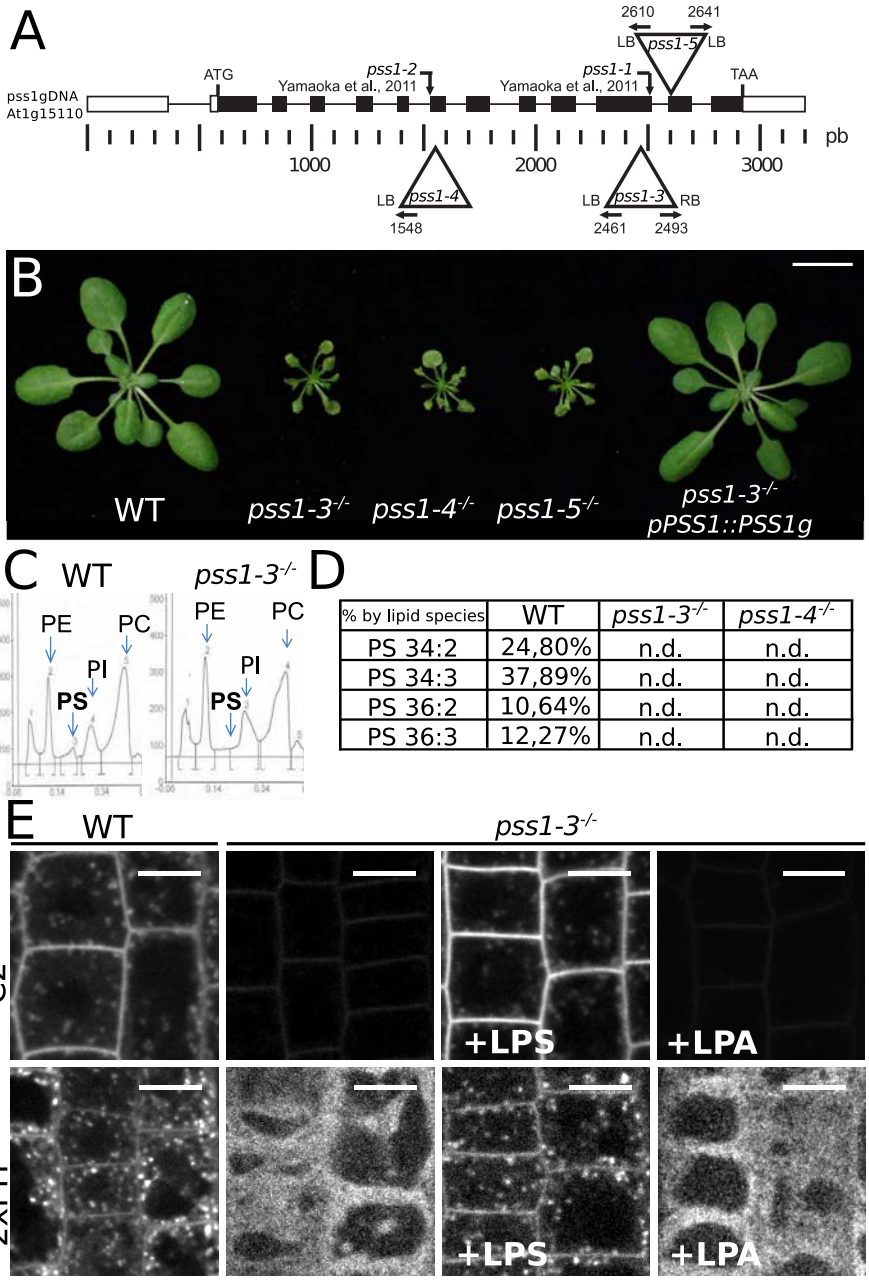

% by lipid species	WT	*pss1-3*$^{-/-}$	*pss1-4*$^{-/-}$
PS 34:2	24,80%	n.d.	n.d.
PS 34:3	37,89%	n.d.	n.d.
PS 36:2	10,64%	n.d.	n.d.
PS 36:3	12,27%	n.d.	n.d.

Figure_3

Figure 3. PSS1 is required for PS biosynthesis and plant growth. A, Schematic representation of T-DNA insertions in *PSS1*. LB, left border; RB, right border; numbers indicate the position of border/*PSS1* junctions. **B,** Rosette phenotype of *pss1* mutants compared to the wild type. From left to right, wild type (WT, Col0), *pss1-3*$^{-/-}$, *pss1-4*$^{-/-}$, *pss1-5*$^{-/-}$ and *pss1-3*$^{-/-}$ expressing *pPSS1::PSS1g*. Scale bar, 2 cm. **C,** High performance thin layer chromatography (HPTLC) assay showing a representative quantification of the phospholipids phosphatidylcholine (PC), phosphatidylethanolamine (PE), phosphatidylinositol (PI) and phosphatidylserine (PS) in WT and *pss1-3*$^{-/-}$ seedlings. **D**, Table showing the percentage of the four major PS species in WT, *pss1-3*$^{-/-}$ and *pss1-4*$^{-/-}$ quantified by LC-MS/MS. n.d., non-detected. For an extended table of the molecular composition of PC/PE/PI/PS species, see table S1. **E**, Confocal images of *Arabidopsis* root epidermis expressing mCITRINE-C2^{LACT} (top) and mCITRINE-2xPH^{EVCT2} (bottom), from left to right in WT, *pss1-3*$^{-/-}$, *pss1-3*$^{-/-}$ supplemented with 54µM lysoPS (LPS) or LysoPA (LPA) for 60 min. Scale bars, 5 µm.

colocalized with the plasmalemmal marker Lti6b-2xmCHERRY (Elsayad et al., 2016), confirming that this PS sensor accumulates at the PM (Figure 2A). We also found that mCITRINE-C2^{LACT} was localized along the endocytic pathway. Indeed, mCITRINE-C2^{LACT} colocalized with the endocytic tracer FM4-64 and its localization was sensitive to both the fungal toxin brefeldinA (BFA) and wortmannin (Wm, Figure 2A), two drugs that affects the morphology of early and late endocytic compartments, respectively (Bayle et al., 2017; Dettmer et al., 2006; Geldner et al., 2009; Jaillais et al., 2008; Jaillais et al., 2006). Finally, we observed in few meristematic cells (14.3% s.e.m. ±2.73, n=458 cells) that mCITRINE-C2^{LACT} colocalized with the tonoplast marker VHA-A3-mRFP1 (Figure 2A) (Dettmer et al., 2006). We also found that mCITRINE-C2^{LACT} localized early on forming cell plate during cytokinesis, together with FM4-64 and PI4P (Figure S2K and Video S5). Therefore, PS accumulation at the cell plate together with PA and PI4P correlates with the acquisition of the cell plate electrostatic identity (Simon et al., 2016). Together, our results suggest that PS accumulates at the PM and cell plate, as well as in PM-derived organelles.

PS is sufficient to maintain negative surface charges on the PM cytosolic leaflet

Next, we addressed whether PS contributes to PM electrostatics. Because there is no chemical compound known to directly inhibit PS production, we tested whether PS could be involved in PM electrostatics by depleting all other anionic phospholipids from this membrane through chemical inhibition. We previously validated the use of PAO, a PI4-Kinase inhibitor, to interfere with PM phosphoinositides production (Simon et al., 2016). We showed that short-term treatment (15-30 min) significantly depletes PI4P but not PI(4,5)P_2 pools, while longer treatment (>60 min) affects the synthesis of both lipids (Simon et al., 2016). In order to concomitantly deplete the plant PM from PA, PI4P and PI(4,5)P_2, leaving PS as the sole anionic lipid in this membrane, we used a combination of R59949 or R59022 (60 min, as described in Figure 1) and prolonged PAO treatment (120 min). This treatment efficiently displaced PI4P, PI(4,5)P_2 and PA sensors from the PM to the cytosol, while the PM localization of EGFP-Lti6b and mCITRINE-C2^{LACT} were largely unaffected by this treatment (Figure 2B). As expected, a proportion of mCITRINE$^{8K\text{-}Farn}$ and mCITRINE-KA1^{MARK1} charge reporters were found in the cytosol in this condition (Figure 2B). However, surprisingly, both charge reporters retained a degree of PM localization that can be attributed to PS, the only remaining anionic lipid in this membrane. Given the physiological importance of PA, PI4P and PI(4,5)P_2, this concomitant treatment is expected to have pleiotropic detrimental effects on plant cell biology, notably inhibiting various intracellular trafficking pathways such as endocytosis and exocytosis as well

as signaling pathways. Nonetheless, in this condition, PS appears to be sufficient to maintain a certain degree of surface charges at the PM.

phosphatidylserine synthase1 mutants do not produce any PS but are viable

In order to analyze the impact of PS depletion on membrane surface charges, we characterized mutants in the *PHOSPHATIDYLSERINE SYNTHASE1* (*PSS1*) gene (Yamaoka et al., 2011). We isolated three *pss1* alleles that we named *pss1-3*; *pss1-4* and *pss1-5* (Figure 3A). These three alleles expressed no detectable full length *PSS1* cDNA (Figure S3C), and segregated as single recessive mutants without any distorted segregation (Figure S3A). All three alleles showed the same sporophytic phenotype, the *pss1* mutants being severely dwarf both at the shoot and root level (Figure 3B, S3F-I). In addition, these mutants were sterile and had to be propagated as heterozygous. Next, we introduced a wild type copy of the *PSS1* gene in the *pss1-3* allele, which fully complemented the *pss1-3* shoot phenotypes (Figure 3B, S3D and F). High performance thin layer chromatography (HPTLC) and LC-MS/MS lipidomic analyses showed that *pss1-3* and *pss1-4* sporophytes do not produce any PS (Figure 3C-D and table S1). Importantly, these analyses suggested that both alleles had only minor changes in their overall phospholipid content (Figure 3C, S3B and table S1). To confirm these biochemical analyses, we introgressed mCITRINE-C2^{LACT} and mCITRINE-2xPH^{EVCT2} into the *pss1-3* mutant. By contrast to the wild type situation, we could detect only a faint signal for mCITRINE-C2^{LACT} in *pss1-3*, suggesting that in the absence of PS, mCITRINE-C2^{LACT} is unstable in plant cells (Figure 3E). Consistently, exogenously treating mCITRINE-C2^{LACT}/*pss1-3*$^{-/-}$ seedlings for one hour with LPS, but not LPA, fully complemented mCITRINE-C2^{LACT} fluorescence signal intensity and localization at the PM and intracellular compartments (Figure 3E). In addition, the mCITRINE-2xPH^{EVCT2} probe was fully soluble in *pss1-3*, as expected for a PS-depleted mutant and this localization was rescued by one hour LPS add back experiments but not by exogenous treatment with LPA (Figure 3E). Furthermore, both root and shoot phenotypes were partially rescued by exogenous treatment with LPS (Figure S3E-I). Together, our biochemical, cell biological and phenotypical analyses suggest that *pss1-3* and *pss1-4* mutants do not produce any PS, which seems dispensable for gametogenesis and embryonic development but is absolutely required for normal post-embryonic plant development and sporophyte fertility. In addition, this PS-depleted mutant further validates the specificity of our PS-binding probes C2^{LACT} and 2xPH^{EVCT2}.

PS is required for surface charges of the PM cytosolic leaflet

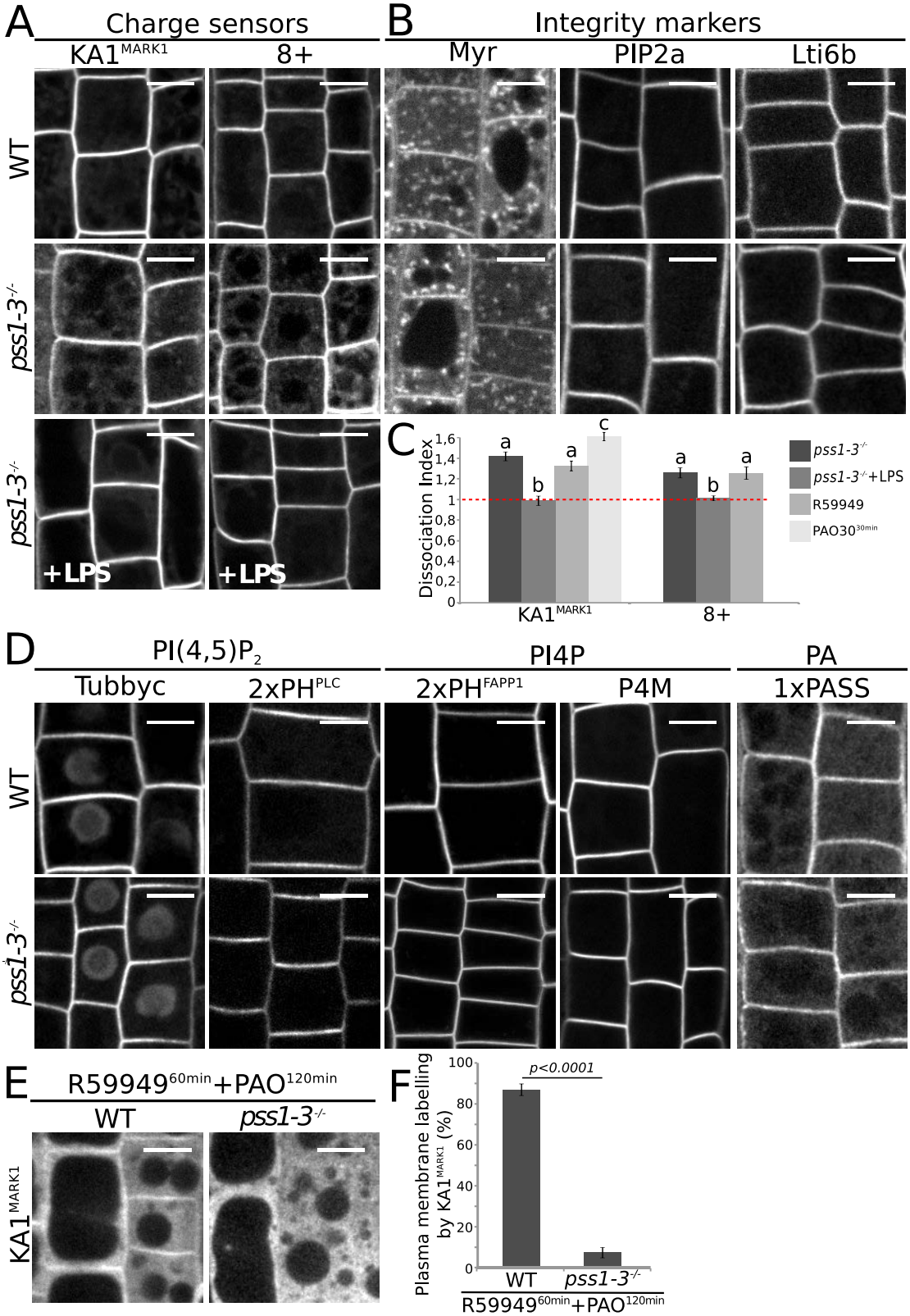
A
Charge sensors
KA1MARK1
8+
B
Integrity markers
Myr
PIP2a
Lti6b
WT
pss1-3-/-
pss1-3-/-
+LPS
+LPS
C
Dissociation Index
1,6
1,4
1,2
1
0,8
0,6
0,4
0,2
0
a
b
a
c
a
b
a
KA1MARK1
8+
pss1-3-/-
pss1-3-/-+LPS
R59949
PAO3030min
D
PI(4,5)P2
PI4P
PA
Tubbyc
2xPHPLC
2xPHFAPP1
P4M
1xPASS
WT
pss1-3-/-
E
R59949 60min+PAO120min
WT
pss1-3-/-
KA1MARK1
F
p<0.0001
Plasma membrane labelling by KA1MARK1 (%)
100
80
60
40
20
0
WT
pss1-3-/-
R59949 60min+PAO120min

Figure_4

Figure 4. PS contributes to PM surface charges but is not required for the localization of other anionic phospholipids. A, Confocal images of *Arabidopsis* root epidermis expressing, mCITRINE-KA1^{MARK1} (left, KA1^{MARK1}), mCITRINE$^{8K\text{-}Farn}$ (right, 8+) in WT (top), *pss1-3*$^{-/-}$ (middle), and *pss1-3*$^{-/-}$ supplemented with 54µM lysoPS (LPS) for 60 min (bottom). B, Confocal images of *Arabidopsis* root epidermis expressing PM integrity markers Myr-mCITRINE (myristoylation, Myr), EGFP-PIP2a and EGFP-Lti6b in WT (top) and *pss1-3*$^{-/-}$ (bottom). **C**, Quantification (mean ±s.e.m, n=150 cells) of mCITRINE-KA1^{MARK1} (left) and mCITRINE-8K^{Farn} (8+, right) dissociation index in *pss1-3*$^{-/-}$, *pss1-3*$^{-/-}$ supplemented with 54µM LPS for 60 min, 12.5µM R59949 for 60 min (same data set as in Figure 1D) and 30µM PAO for 30 min. Different letters indicate significant differences among means (p-value=0.05, Kruskal-Wallis bilateral test) **D**, Confocal images of *Arabidopsis* root epidermis expressing from left to right, PI(4,5)P_2 sensors (mCITRINE-TUBBY-C (P15Y) and mCITRINE-2xPH^{PLC} (P24Y)), PI4P sensors (mCITRINE-2xPH^{FAPP1} (P21Y) and mCITRINE-P4M^{SidM}) and PA sensor (mCITRINE-1xPASS) in WT (top) and *pss1-3*$^{-/-}$ (bottom). **E**, Confocal images of WT (left) and *pss1-3*$^{-/-}$ (right) root epidermis expressing mCITRINE-KA1^{MARK1} pre-treated with 30µM PAO for 60 min and then concomitantly treated with 12.5µM R59949 and 30µM PAO for 60 min. **F,** Quantification (mean ±s.e.m) of the percentage of cells with mCITRINE-KA1^{MARK1} at the PM in WT (left, n=887cells) and *pss1-3*$^{-/-}$ (right, n=806 cells) (same treatment as in E). Statistical analysis was performed using the non-parametric Wilcoxon-Mann-Whitney test (p-value=0.05). Scale bars, 5 µm.

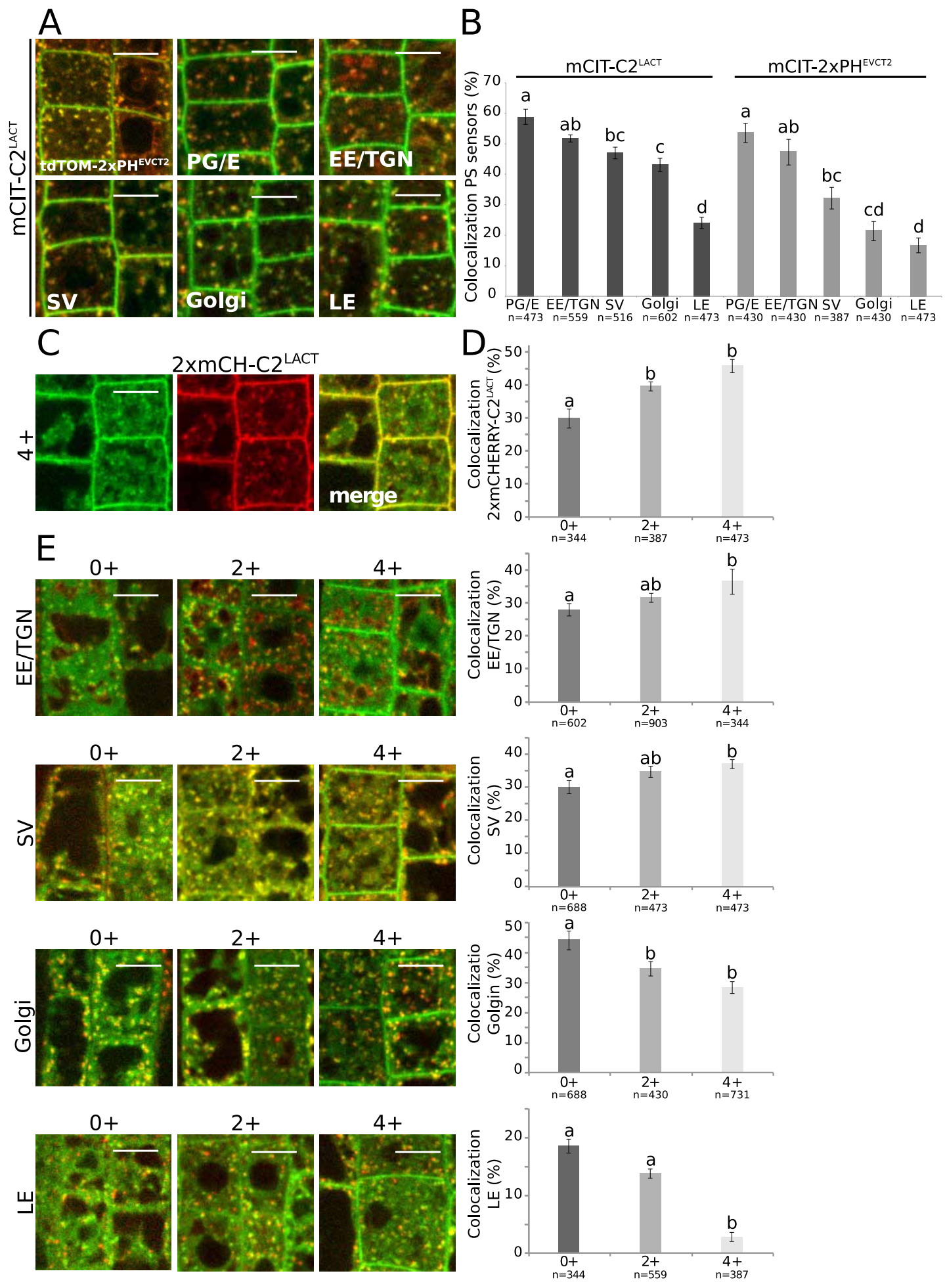
A
mCIT-C2LACT
tdTOM-2xPHEVCT2
PG/E
EE/TGN
SV
Golgi
LE
B
mCIT-C2LACT
mCIT-2xPHEVCT2
Colocalization PS sensors (%)
PG/E n=473
EE/TGN n=559
SV n=516
Golgi n=602
LE n=473
PG/E n=430
EE/TGN n=430
SV n=387
Golgi n=430
LE n=473
C
2xmCH-C2LACT
4+
merge
D
Colocalization 2xmCHERRY-C2LACT (%)
Colocalization EE/TGN (%)
Colocalization SV (%)
Colocalizatio Golgin (%)
Colocalization LE (%)
0+
2+
4+
E
EE/TGN
SV
Golgi
LE

Figure_5

Figure 5. A PS gradient along the endocytic pathway correlates with a gradient of electrostatics. A, Merged confocal images of *Arabidopsis* root epidermis of plants co-expressing mCITRINE-C2^{LACT} with tdTOMATO-PH^{EVCT2} (top left), W25R post-Golgi endosomal/endosomes (PG/E) marker (top middle), W13R early endosomal (EE/TGN) marker (top right), W24R secretory vesicle (SV) marker (bottom left), W18R Golgi marker (bottom middle), W7R late endosomal (LE) marker (bottom right). **B,** Quantification of the percentage of compartments labelled by PS sensors (mCITRINE-C2^{LACT} and mCITRINE-2xPH^{EVCT2}) that also contain compartment markers (same as above-mentioned), n=(387, 602) cells (mean ±s.e.m, percentage of colocalization). Different letters indicate significant differences among means (p value= 0.05, Kruskal-Wallis bilateral test) **C,** Confocal images of plants co-expressing mCITRINE$^{4K4Q\text{-}Farn}$ (left) and 2xmCHERRY-C2^{LACT} (middle) and merge channel (right). **D**, Quantification (mean ±s.e.m) of the percentage of compartments labelled by PS sensors (2xmCHERRY-C2^{LACT}) that also contain membrane charge reporters (mCITRINE$^{8Q\text{-}Farn}$ (0+), 2xmCITRINE$^{2K6Q\text{-}Farn}$ (2+) and 2xmCITRINE$^{4K4Q\text{-}Farn}$ (4+)), n=(387, 602) cells. Different letters indicate significant differences among means (p value= 0.05, Kruskal-Wallis bilateral test), **E,** Merged confocal images (left) and colocalization quantification (mean ±s.e.m, right) of plants co-expressing mCITRINE$^{8Q\text{-}Farn}$ (0+, left), mCITRINE$^{2K6Q\text{-}Farn}$ (2+, middle) and mCITRINE$^{4K4Q\text{-}Farn}$ (4+, right) with, from top to bottom, W13R (EE/TGN), W24R (SV), W18R (Golgi) and W7R (LE) markers, n=(344, 688) cells. Different letters indicate significant differences among means (p value= 0.15, Kruskal-Wallis bilateral test). In each graph, "n" represents the estimated number of cells sampled in each condition. Scale bars, 5 µm.

Next, we analyzed the localization of our membrane charge reporters in *pss1-3* mutant background. Both mCITRINE$^{8K\text{-}Farn}$ and mCITRINE-KA1^{MARK1} retained a certain degree of PM localization in *pss1-3*, but also relocalized in the cytosol and were found in intracellular compartments (Figure 4A and C). Quantification showed that the PM dissociation of mCITRINE-KA1^{MARK1} was weaker in *pss1-3* than upon PI4P depletion (i.e. PAO treatment), and similar as upon PA depletion (i.e. R59022) (Figure 4C). We next investigated whether loss of PS could be the primary cause behind these defects in PM electrostatics. First, we found that membrane charge reporters strict PM localization was fully restored by short-term (one hour) add-back experiment with LPS (Figure 4A and 4C). Second, since we previously showed that PI4P and PA regulate PM electrostatics, we next asked whether loss of PS might affect PM anionic phospholipid subcellular distribution. Interestingly, the PM localization of PI(4,5)P_2, PI4P and PA sensors were not affected in *pss1-3* (Figure 4D). In addition, by introgressing in *pss1-3* various control fluorescent markers of the PM (Figure 4B) and intracellular compartments (Figure S4), we could not detect any phenotype suggesting general defects in PM protein localization, membrane organization, and/or compartments morphogenesis.

As described above, PS is presumably the last remaining anionic phospholipid at the PM following depletion of cellular PI4P/PI(4,5)P_2/PA using a combination of PAO and R59949 treatment. If this assumption is correct, the vast majority of anionic phospholipids should be removed from the PM in the *pss1* mutant following this treatment, which should therefore trigger a full dissociation from the PM of our mCITRINE-KA1^{MARK1} membrane charge reporter. Concomitant PAO/R59949 treatment in *pss1-3*, indeed induced a complete loss of PM localization of mCITRINE-KA1^{MARK1}, which became fully soluble in the cytosol (Figure 4E and F). This experiment demonstrates that PM localization of mCITRINE-KA1^{MARK1} in wild-type plants following concomitant PAO/R59949 treatment can be attributed to PS. Altogether, our results show that PS is not directly involved in the PM localization of other anionic lipids, but contribute to PM surface charges.

PS localization correlates with that of electrostatic compartments

Because PS was proposed to be an important component of the electrostatic territory (Bigay and Antonny, 2012; Jackson et al., 2016), we next asked whether PS could also participate in membrane surface charges of intracellular compartments. To this end, we first mapped PS intracellular localization using quantitative colocalization analyses (see Fig S5 for a description of the method). In accordance with the BFA and Wm sensitivity we previously reported (Figure 2A), both the mCITRINE-C2^{LACT} and mCITRINE-2xPH^{EVCT2} probes localized in post-

Golgi/endosomal (PG/E) compartments (Figure 5A and 5B). Interestingly, we found that both PS probes accumulated according to a concentration gradient, which is higher in early endocytic compartments (including EE/TGN and secretory vesicles (SV)), intermediate in the Golgi apparatus (Golgi) and lower in late endosomes (LE) (Figure 5B).

Next, we addressed which intracellular compartments were electronegative. To this end, we used charge reporters that are hydrophobically-anchored to membrane via a farnesyl moiety and that have an adjacent unstructured peptide of net varying charges (from +0 to +8) (Simon et al., 2016). A neutral version of the probe (+0, 8Q-Farn) is localized only by the intrinsic properties of the farnesyl lipid anchor, independently of membrane electrostatics. The gradual addition of positive charges by substitution of neutral glutamines into cationic lysines gradually increases the avidity of the probes for anionic membranes. As a result, a probe with intermediate charges (e.g. 4K4Q-Farn, 4+) resides in compartments that are electronegative indistinctively of whether they are highly negatively charged or not (Haupt and Minc, 2017; Platre and Jaillais, 2017; Simon et al., 2016; Yeung et al., 2008; Yeung et al., 2006). By contrast, a probe that is strongly cationic (e.g. 8K-Farn, 8+) is greatly stabilized in highly anionic membranes such as the PM and is not found on compartments of intermediate electronegativity. We therefore reasoned that if PS contributes to the electrostatic properties of intracellular compartments, it should accumulate in compartments that are electronegative. To test this idea, we crossed the mCITRINE$^{4K4Q\text{-}Farn}$ (4+) reporter with the 2xmCHERRY-C2^{LACT} sensor and confirmed that both probes colocalized (Figure 5C). In addition, we found that 2xmCHERRY-C2^{LACT} colocalized preferentially with mCITRINE$^{4K4Q\text{-}Farn}$ (4+) (which labels electrostatic compartments) rather than mCITRINE$^{8Q\text{-}Farn}$ (0+) (which localization is charge independent) (Figure 5D). We next performed quantitative colocalization assay between intracellular compartment markers and charge reporters containing a gradual increase in net positive charges (0+, 2+ and 4+) in order to test the relative contribution of their positive charges on their intracellular distribution. We did not use probes with higher net positive charges than 4+, because the mCITRINE$^{6K2Q\text{-}Farn}$ (6+) seldom localizes in intracellular compartments and mCITRINE$^{8K\text{-}Farn}$ (8+) is strictly localized at the PM (Simon et al., 2016). We found that addition of positive charges gradually increased the proportion of the probes in EE/TGN and SV at the expense of their Golgi and late endosomes localization (Figure 5E). Therefore, the endomembrane system is organized according to an electrostatic gradient that is the highest at the PM, intermediate in early endocytic compartments, and low in the Golgi and late endosomes. This electrostatic gradient correlates with the PS concentration gradient, which suggests that PS might be involved in defining this electrostatic territory.

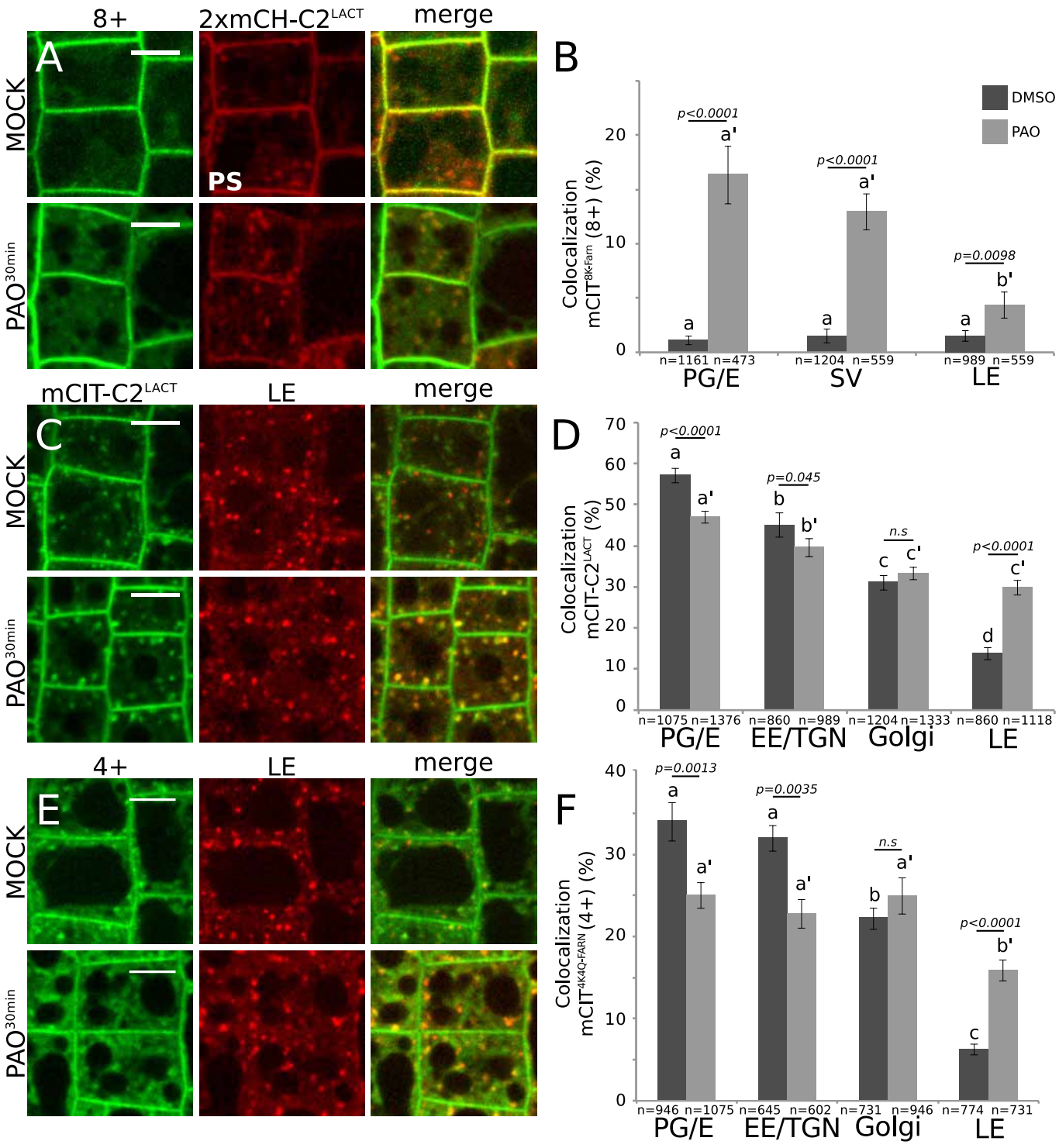
8+
2xmCH-C2LACT
merge
A
MOCK
PS
PAO30min
B
DMSO
PAO
p<0.0001
a'
p<0.0001
a'
p=0.0098
b'
a
a
a
Colocalization mCIT8kFarn (8+) (%)
20
10
0
n=1161 n=473
n=1204 n=559
n=989 n=559
PG/E
SV
LE
mCIT-C2LACT
LE
merge
C
MOCK
PAO30min
D
p<0.0001
a
a'
p=0.045
b
b'
n.s
c
c'
p<0.0001
c'
d
Colocalization mCIT-C2LACT (%)
70
60
50
40
30
20
10
0
n=1075 n=1376
n=860 n=989
n=1204 n=1333
n=860 n=1118
PG/E
EE/TGN
Golgi
LE
4+
LE
merge
E
MOCK
PAO30min
F
p=0.0013
a
a'
p=0.0035
a
a'
n.s
b
a'
p<0.0001
b'
c
Colocalization mCIT4K4Q-FARN (4+) (%)
40
30
20
10
0
n=946 n=1075
n=645 n=602
n=731 n=946
n=774 n=731
PG/E
EE/TGN
Golgi
LE

Figure_6

Figure 6. PS and PI4P cooperate to control endosome electrostatics. A, Confocal images of plants co-expressing mCITRINE$^{8K\text{-}Farn}$ (8+) with mCHERRY-C2^{LACT} in mock (top) and PAO (60µM, 30 min, bottom) treated conditions. **B,** Quantification (mean ±s.e.m) of the percentage of compartments labelled by mCITRINE$^{8K\text{-}Farn}$ (8+) that also contain W25R (PG/E), W24R (SV), and W7R (LE) in presence or absence of PAO (60µM, 30 min) n=(478, 1204) cells **C,** Confocal images of plants co-expressing mCITRINE-C2^{LACT} with W7R (LE) in mock (top) and PAO (60µM, 30 min, bottom) conditions. **D,** Quantification (mean ±s.e.m) of the percentage of compartments labelled by mCITRINE-C2^{LACT} that also contain W25R (PG/E), W13R (EE/TGN), W18R (Golgi), and W7R (LE) in presence or absence of PAO (60µM, 30 min), n=(860, 1376) cells. **E,** Confocal images of plants co-expressing mCITRINE$^{4K4Q\text{-}Farn}$ (4+) with W7R (LE) in mock (top) and PAO (60µM, 30 min, bottom) conditions. **F,** Quantification (mean ±s.e.m) of the percentage of compartments labelled by mCITRINE$^{4K4Q\text{-}Farn}$ (4+), that also contain W25R (PG/E), W13R (EE/TGN), W18R (Golgi), and W7R (LE) in presence or absence of PAO (60µM, 30 min) n=(602, 1075) cells. In graph B, D and F, different letters indicate significant differences among means (normal letters for DMSO comparison and letters with a prime symbol for PAO comparison, p value=0.05, Kruskal-Wallis bilateral test). Statistical difference between each sample is indicated by the p value at the top of each compared conditions (p-value=0.05, non-parametric Wilcoxon-Mann-Whitney test, non-significant (n.s.)). “n” represents the estimated number of cells sampled in each condition. Scale bars, 5 µm.

Membrane surface charge probes relocalize to PS-bearing organelle in the absence of PI4P

Next, to grasp whether intracellular PS could control the electrostatic properties of intracellular membrane compartments, we inhibited PI4P synthesis using a 30 minutes PAO treatment (Simon et al., 2016) and asked where the mCITRINE$^{8K\text{-}Farn}$ (8+) relocalized inside the cell. Interestingly, following PAO treatment, mCITRINE$^{8K\text{-}Farn}$ was observed on the surface of PS bearing organelles, being mainly localized in early endocytic compartments and to a lower extent in late endosomes (Figure 6A-B and S6A-C). These results suggest that in the absence of PI4P, which is required for the distinctively high PM electrostatic signature (Simon et al., 2016), strongly cationic membrane surface charge reporters (such as the mCITRINE$^{8K\text{-}Farn}$ reporter) localize inside the cell according to the PS concentration gradient.

We previously noticed that PI4-kinase inhibition by PAO affects PS intracellular distribution (Simon et al., 2016). We therefore analyzed quantitatively PS subcellular localization in the absence or presence of PAO. We found that PAO treatment attenuated the gradient of PS as visualized by mCITRINE-C2^{LACT} (Figure 6D). In particular, PAO treatment increased the localization of mCITRINE-C2^{LACT} in late endosomes (Figure 6C-D). Strikingly, the electrostatic gradient, as visualized by the mCITRINE$^{4K4Q\text{-}Farn}$ (4+) charge reporter was similarly affected by PAO treatment, with an increased localization of the reporter in late endosomes (Figure 6E-F and S6D-G). These results further confirm that charge reporter localization coincides with the presence of PS at the surface of intracellular membranes and support the notion that PS contributes overall to the establishment of the plant electrostatic territory at the surface of the PM cytosolic leaflet and along the endocytic pathway. In addition, we also noticed that PAO treatment decreased the accumulation of the mCITRINE$^{4K4Q\text{-}Farn}$ (4+) probe in early endosomes (Figure 6F), while PS localization in this compartment was only mildly affected by this treatment (Figure 6D). PAO affects PI4P production, a lipid that is present in EE/TGN albeit to a lower extent than the PM (Simon et al., 2016). Loss of PI4P may therefore impact the electrostatic properties of EE and may explain the decreased accumulation of the mCITRINE$^{4K4Q\text{-}Farn}$ (4+) probe in this compartment. As such, PI4P likely acts in combination with PS to specify the intermediate electronegativity of EE/TGN.

Discussion

Here, we addressed which organelles are found in the electrostatic territory in plants and what are the anionic lipids that control this territory. Similar to previously published models, we found that the plant electrostatic territory corresponds to PM-derived organelles (Bigay and Antonny, 2012; Jackson et al., 2016). However, interestingly, we noticed that not all membranes in this territory are equally anionic. Rather, we revealed the existence of an electrostatic gradient, which is at its highest at the PM, intermediate in early endosomes and low in late endosomes. This electrostatic gradient is set up by various anionic phospholipid combinations. The concomitant accumulation of PA, PS and PI4P drives the very high electrostatic field of the PM. However, PS accumulation extends beyond the PM as it accumulates along the endocytic pathway according to a concentration gradient. This PS cellular distribution resembles that of animal cells, and contrast to that of yeast, in which PS massively accumulates at the PM (Moravcevic et al., 2010; Moser von Filseck et al., 2015; Yeung et al., 2008). Furthermore, like in animals, the PS subcellular distribution in plants closely matches the electrostatic gradient, suggesting that PS is likely instrumental in setting up the electrostatic territory. In this scenario, PS and PI4P, which are found in the EE/TGN, drive the intermediate electrostatic property of this compartment. However, PS is also present in LE, where it may contribute to the weak electrostatic field of the late endocytic pathway. Phosphatidylinositol-3-phosphate (PI3P) and phosphatidylinositol 3,5-bisphosphate ($PI(3,5)P_2$), are also enriched in LE (Noack and Jaillais, 2017), but are extremely rare lipids, which is consistent with the weak electronegativity of these compartments.

PS as a general landmark of electrostatic membranes

The idea of two membrane territories, with distinct lipid compositions, as a fundamental organizing principle of the endomembrane system of eukaryotic cells was first proposed by Antonny and colleagues (Bigay and Antonny, 2012). These two lipid territories correspond roughly to ER and PM-derived membranes, and are defined by opposite physicochemical parameters (Bigay and Antonny, 2012; Jackson et al., 2016). The cytosolic leaflet of ER derived membranes is characterized by its low electrostatic property (as the vast majority of anionic phospholipids in the ER are orientated toward the lumen) and by its high occurrence of lipid packing defects, which are promoted by unsaturated lipids and the presence of small lipid head groups (Bigay and Antonny, 2012). By contrast, PM-derived organelles have few packing defects but are electrostatic, as they accumulate anionic phospholipids. PS is localized in PM-

derived organelles in mammalian cells and may thereby contribute to the electrostatic properties of these compartments (Yeung et al., 2008). However, the importance of PS in mediating membrane surface charges along the animal endocytic pathway was deduced from pharmacological approaches that are known to also affect other cellular lipids (Ma et al., 2017; Yeung et al., 2008). Here, we combined pharmacological and genetic approaches to demonstrate that in plants PS is both necessary to establish the PM electrostatic signature and sufficient to maintain a certain degree of surface charges at the PM. Thus our results further consolidate the notion that PS is an important lipid across eukaryotes to establish the electrostatic territory (Jackson et al., 2016; Platre and Jaillais, 2017). However, by contrast to the proposed model, we further demonstrated that PS does not act alone in this process but rather do so in concert with PI4P and PA.

Plants cells have significant PA levels in their plasma membrane, which is required to maintain the electrostatic properties of the PM cytosolic leaflet

It is well established that PA acts as a lipid messenger in plants, notably in response to the environment (Testerink and Munnik, 2011). In fact, almost every environmental stress triggers PA production within minutes, including abiotic stresses (e.g. cold, heat, drought, wounding, salinity) and biotic interactions (Testerink and Munnik, 2011). This rapid induction happens mostly at the PM and is regulated by direct production of PA by Phospholipase D (PLD) and/or by diacylglycerol phosphorylation by DGKs (Testerink and Munnik, 2011). Interestingly, in the present study, we found that the plant PM has significant PA level, as visualized by the recruitment of PA-binding sensors, even when plants are grown in optimal conditions. Plasma membrane recruitment of a PA reporter was previously observed in sub-domain of tobacco pollen tubes plasmalemma (Potocky et al., 2014) and seems to be extendable to most of the tissues we observed in *Arabidopsis*. In animals, most cells have minute amount of PA at the PM and PA sensors are not recruited to the PM in resting conditions (Bohdanowicz et al., 2013). By contrast, phagocytic cells, such as macrophages and immature dendritic cells, have relatively high level of PA in their PM (Bohdanowicz et al., 2013). This unusual concentration of PA allows these cells to have constitutive membrane ruffling in order to scan their environment, which is required for immune surveillance. These phagocytic cells maintain their elevated PA level at the PM via DGK activity (Bohdanowicz et al., 2013). Similarly, we found that in plants a DGK activity is required to sustain the level of PA at the PM. Pharmacological inhibition of DGK activities not only solubilizes PA sensors but also impacts PM electrostatic properties. Using similar approaches, it was recently shown that PA plays a

role in the PM targeting of the D6-PROTEIN KINASE (D6PK) (Barbosa et al., 2016), an AGC kinase involved in polar auxin transport (Armengot et al., 2016). The localization of D6PK is dependent on both PI4P, PI(4,5)P_2 and PA, suggesting that a combination of phosphoinositides and PA is responsible for its localization rather than a single phospholipid species (Barbosa et al., 2016). Here, we obtained similar results with several independent generic membrane surface charge reporters, suggesting that the requirement for several anionic phospholipids may not be an intrinsic property of D6PK but rather a more general feature of the electrostatic field of the plant PM. In addition, this further suggests that our results are not just limited to our synthetic charge reporters, but are relevant for the localization of endogenous *Arabidopsis* proteins, and point toward a more general requirement of PI4P/PA/PS combination for the localization of many proteins in plants.

In most eukaryotic cells, PM electrostatics seems to be extremely robust, as the loss of one anionic phospholipid species has little impact on the overall charge of the PM. For example in animal cells, acute depletion of PI(4,5)P_2 has no effect on the PM electrostatic field, since charges from PI4P and PI(3,4,5)P_3 are sufficient to maintain PM electrostatics (Hammond et al., 2012; Heo et al., 2006). Similarly in yeast, inhibition of PI4P and PI(4,5)P_2 synthesis does not impact PM electrostatics significantly (Moravcevic et al., 2010). By contrast in plants, we found that the individual loss of PI4P, PS and PA directly impact PM electrostatics. While they are all anionic phospholipids, they have radically different turnover. Indeed, PS is a relatively stable phospholipid, while PI4P and PA have a high turnover rate. One may speculates that PS ensures a stable PM electrostatic field, while spatiotemporal variations in PI4P and/or PA may directly impact PM surface charges. As such, PM electrostatics in plants may be particularly prone to respond to environmental changes. It will be an exciting future direction to understand how environmental stresses impact membrane electrostatics, what are the contributions of individual lipids in these variations and how this might impact signaling, intracellular trafficking and cellular polarity.

Acknowledgements

We thank A. Martinière-Delaunay, O. Hamant, M. Dreux and the SiCE group for discussions and comments, G. Du, T. Taguchi, S. Grinstein, B. Kost and addgene for providing plasmids, N. Geldner, K. Schumacher, I. Moore, D. Ehrhardt, the GABI-KAT, and the NASC collection for providing transgenic *Arabidopsis* lines, A. Lacroix, J. Berger and P. Bolland for plant care, J.C. Mulatier for help in preparing lipids and PLATIM for help with imaging. Y.J. is funded by ERC

no. 3363360-APPL under FP/2007-2013. M.D. and M.S are funded by a PhD fellowship from the French Ministry of Higher Education. T.S is supported by ERC grant no. 615739-MechanoDevo to O. Hamant. P.P and M.P. are supported by the Czech Science Foundation grant no. 17-27477S. Lipidomic analyses were performed on the Bordeaux Metabolome Facility-MetaboHUB (ANR-11-INBS-0010).

Author contributions:

M.P.P. was responsible of all experiments described in the manuscript except the following: production and imaging of the *PDF1*-driven PS reporter line (T.S.), lipid measurements (L.M-P., L.F. and P.M.); time-lapse imaging of cytokinesis/root hair (M.D. and M.C.C.) and pollen tube (P.P. and M.P.). V.B. helped with image quantification and acquisition, L.A. helped with yeast and lipid overlay experiments; A.C. helped with LPS/LPA addback experiments, M.S. participated in the production of membrane charge reporter lines. M.P.P., and Y.J. conceived the study, designed experiments and wrote the manuscript and all the authors discussed the results and commented on the manuscript.

References

Alberti, S., Gitler, A.D., and Lindquist, S. (2007). A suite of Gateway cloning vectors for high-throughput genetic analysis in Saccharomyces cerevisiae. Yeast *24*, 913-919.

Armengot, L., Marques-Bueno, M.M., and Jaillais, Y. (2016). Regulation of polar auxin transport by protein and lipid kinases. Journal of experimental botany *67*, 4015-4037.

Barbosa, I.C., Shikata, H., Zourelidou, M., Heilmann, M., Heilmann, I., and Schwechheimer, C. (2016). Phospholipid composition and a polybasic motif determine D6 PROTEIN KINASE polar association with the plasma membrane and tropic responses. Development *143*, 4687-4700.

Bayle, V., Platre, M.P., and Jaillais, Y. (2017). Automatic Quantification of the Number of Intracellular Compartments in Arabidopsis thaliana Root Cells. Bio-protocol *7*.

Bigay, J., and Antonny, B. (2012). Curvature, lipid packing, and electrostatics of membrane organelles: defining cellular territories in determining specificity. Developmental cell *23*, 886-895.

Bloch, D., Pleskot, R., Pejchar, P., Potocky, M., Trpkosova, P., Cwiklik, L., Vukasinovic, N., Sternberg, H., Yalovsky, S., and Zarsky, V. (2016). Exocyst SEC3 and Phosphoinositides Define Sites of Exocytosis in Pollen Tube Initiation and Growth. Plant physiology *172*, 980-1002.

Bohdanowicz, M., Schlam, D., Hermansson, M., Rizzuti, D., Fairn, G.D., Ueyama, T., Somerharju, P., Du, G., and Grinstein, S. (2013). Phosphatidic acid is required for the constitutive ruffling and macropinocytosis of phagocytes. Molecular biology of the cell *24*, 1700-1712, S1701-1707.

Chung, J., Torta, F., Masai, K., Lucast, L., Czapla, H., Tanner, L.B., Narayanaswamy, P., Wenk, M.R., Nakatsu, F., and De Camilli, P. (2015). INTRACELLULAR TRANSPORT. PI4P/phosphatidylserine countertransport at ORP5- and ORP8-mediated ER-plasma membrane contacts. Science *349*, 428-432.

Cutler, S.R., Ehrhardt, D.W., Griffitts, J.S., and Somerville, C.R. (2000). Random GFP::cDNA fusions enable visualization of subcellular structures in cells of Arabidopsis at a high frequency. Proceedings of the National Academy of Sciences of the United States of America *97*, 3718-3723.

Dettmer, J., Hong-Hermesdorf, A., Stierhof, Y.D., and Schumacher, K. (2006). Vacuolar H+-ATPase activity is required for Endocytic and secretory trafficking in Arabidopsis. The Plant cell *18*, 715-730.

Dong, W., Zhang, X., Liu, W., Chen, Y.J., Huang, J., Austin, E., Celotto, A.M., Jiang, W.Z., Palladino, M.J., Jiang, Y.*, et al.* (2015). A conserved polybasic domain mediates plasma membrane targeting of Lgl and its regulation by hypoxia. The Journal of cell biology *211*, 273-286.

Elsayad, K., Werner, S., Gallemi, M., Kong, J., Sanchez Guajardo, E.R., Zhang, L., Jaillais, Y., Greb, T., and Belkhadir, Y. (2016). Mapping the subcellular mechanical properties of live cells in tissues with fluorescence emission-Brillouin imaging. Science signaling *9*, rs5.

French, A., Ubeda-Tomas, S., Holman, T.J., Bennett, M.J., and Pridmore, T. (2009). High-throughput quantification of root growth using a novel image-analysis tool. Plant physiology *150*, 1784-1795.

Geldner, N., Denervaud-Tendon, V., Hyman, D.L., Mayer, U., Stierhof, Y.D., and Chory, J. (2009). Rapid, combinatorial analysis of membrane compartments in intact plants with a multicolor marker set. Plant Journal *59*, 169-178.

Gietz, R.D., Schiestl, R.H., Willems, A.R., and Woods, R.A. (1995). Studies on the transformation of intact yeast cells by the LiAc/SS-DNA/PEG procedure. Yeast *11*, 355-360.

Hammond, G.R., Fischer, M.J., Anderson, K.E., Holdich, J., Koteci, A., Balla, T., and Irvine, R.F. (2012). PI4P and PI(4,5)P2 are essential but independent lipid determinants of membrane identity. Science *337*, 727-730.

Haupt, A., and Minc, N. (2017). Gradients of phosphatidylserine contribute to plasma membrane charge localization and cell polarity in fission yeast. Molecular biology of the cell *28*, 210-220.

Heape, A.M., Juguelin, H., Boiron, F., and Cassagne, C. (1985). Improved one-dimensional thin-layer chromatographic technique for polar lipids. J Chromatogr *322*, 391-395.
Heo, W.D., Inoue, T., Park, W.S., Kim, M.L., Park, B.O., Wandless, T.J., and Meyer, T. (2006). PI(3,4,5)P3 and PI(4,5)P2 lipids target proteins with polybasic clusters to the plasma membrane. Science *314*, 1458-1461.
Horchani, H., de Saint-Jean, M., Barelli, H., and Antonny, B. (2014). Interaction of the Spo20 membrane-sensor motif with phosphatidic acid and other anionic lipids, and influence of the membrane environment. PloS one *9*, e113484.
Jackson, C.L., Walch, L., and Verbavatz, J.M. (2016). Lipids and Their Trafficking: An Integral Part of Cellular Organization. Developmental cell *39*, 139-153.
Jaillais, Y., Fobis-Loisy, I., Miege, C., and Gaude, T. (2008). Evidence for a sorting endosome in Arabidopsis root cells. The Plant journal : for cell and molecular biology *53*, 237-247.
Jaillais, Y., Fobis-Loisy, I., Miege, C., Rollin, C., and Gaude, T. (2006). AtSNX1 defines an endosome for auxin-carrier trafficking in Arabidopsis. Nature *443*, 106-109.
Jaillais, Y., Hothorn, M., Belkhadir, Y., Dabi, T., Nimchuk, Z.L., Meyerowitz, E.M., and Chory, J. (2011). Tyrosine phosphorylation controls brassinosteroid receptor activation by triggering membrane release of its kinase inhibitor. Genes & development *25*, 232-237.
Kassas, N., Tanguy, E., Thahouly, T., Fouillen, L., Heintz, D., Chasserot-Golaz, S., Bader, M.F., Grant, N.J., and Vitale, N. (2017). Comparative Characterization of Phosphatidic Acid Sensors and Their Localization during Frustrated Phagocytosis. The Journal of biological chemistry *292*, 4266-4279.
Klahre, U., and Kost, B. (2006). Tobacco RhoGTPase ACTIVATING PROTEIN1 spatially restricts signaling of RAC/Rop to the apex of pollen tubes. The Plant cell *18*, 3033-3046.
Kost, B., Spielhofer, P., and Chua, N.H. (1998). A GFP-mouse talin fusion protein labels plant actin filaments in vivo and visualizes the actin cytoskeleton in growing pollen tubes. The Plant journal : for cell and molecular biology *16*, 393-401.
Lu, M., Tay, L.W., He, J., and Du, G. (2016). Monitoring Phosphatidic Acid Signaling in Breast Cancer Cells Using Genetically Encoded Biosensors. Methods Mol Biol *1406*, 225-237.
Ma, Y., Yamamoto, Y., Nicovich, P.R., Goyette, J., Rossy, J., Gooding, J.J., and Gaus, K. (2017). A FRET sensor enables quantitative measurements of membrane charges in live cells. Nat Biotechnol *35*, 363-370.
Macala, L.J., Yu, R.K., and Ando, S. (1983). Analysis of brain lipids by high performance thin-layer chromatography and densitometry. Journal of lipid research *24*, 1243-1250.
Moravcevic, K., Mendrola, J.M., Schmitz, K.R., Wang, Y.H., Slochower, D., Janmey, P.A., and Lemmon, M.A. (2010). Kinase associated-1 domains drive MARK/PAR1 kinases to membrane targets by binding acidic phospholipids. Cell *143*, 966-977.
Moser von Filseck, J., Copic, A., Delfosse, V., Vanni, S., Jackson, C.L., Bourguet, W., and Drin, G. (2015). INTRACELLULAR TRANSPORT. Phosphatidylserine transport by ORP/Osh proteins is driven by phosphatidylinositol 4-phosphate. Science *349*, 432-436.
Noack, L.C., and Jaillais, Y. (2017). Precision targeting by phosphoinoistides: how PIs direct endomembrane trafficking in plants. . Current opinion in plant biology *40*.
Platre, M.P., and Jaillais, Y. (2017). Anionic lipids and the maintenance of membrane electrostatics in eukaryotes. Plant signaling & behavior *12*, e1282022.
Potocky, M., Pleskot, R., Pejchar, P., Vitale, N., Kost, B., and Zarsky, V. (2014). Live-cell imaging of phosphatidic acid dynamics in pollen tubes visualized by Spo20p-derived biosensor. The New phytologist *203*, 483-494.
Samalova, M., Fricker, M., and Moore, I. (2006). Ratiometric fluorescence-imaging assays of plant membrane traffic using polyproteins. Traffic *7*, 1701-1723.
Schindelin, J., Arganda-Carreras, I., Frise, E., Kaynig, V., Longair, M., Pietzsch, T., Preibisch, S., Rueden, C., Saalfeld, S., Schmid, B*., et al.* (2012). Fiji: an open-source platform for biological-image analysis. Nature methods *9*, 676-682.

Simon, M.L., Platre, M.P., Assil, S., van Wijk, R., Chen, W.Y., Chory, J., Dreux, M., Munnik, T., and Jaillais, Y. (2014). A multi-colour/multi-affinity marker set to visualize phosphoinositide dynamics in Arabidopsis. The Plant journal : for cell and molecular biology *77*, 322-337.
Simon, M.L., Platre, M.P., Marques-Bueno, M.M., Armengot, L., Stanislas, T., Bayle, V., Caillaud, M.C., and Jaillais, Y. (2016). A PtdIns(4)P-driven electrostatic field controls cell membrane identity and signalling in plants. Nat Plants *2*, 16089.
Testerink, C., and Munnik, T. (2011). Molecular, cellular, and physiological responses to phosphatidic acid formation in plants. Journal of experimental botany *62*, 2349-2361.
Uchida, Y., Hasegawa, J., Chinnapen, D., Inoue, T., Okazaki, S., Kato, R., Wakatsuki, S., Misaki, R., Koike, M., Uchiyama, Y.*, et al.* (2011). Intracellular phosphatidylserine is essential for retrograde membrane traffic through endosomes. Proceedings of the National Academy of Sciences of the United States of America *108*, 15846-15851.
Yamaoka, Y., Yu, Y., Mizoi, J., Fujiki, Y., Saito, K., Nishijima, M., Lee, Y., and Nishida, I. (2011). PHOSPHATIDYLSERINE SYNTHASE1 is required for microspore development in Arabidopsis thaliana. The Plant journal : for cell and molecular biology *67*, 648-661.
Yeung, T., Gilbert, G.E., Shi, J., Silvius, J., Kapus, A., and Grinstein, S. (2008). Membrane phosphatidylserine regulates surface charge and protein localization. Science *319*, 210-213.
Yeung, T., Heit, B., Dubuisson, J.F., Fairn, G.D., Chiu, B., Inman, R., Kapus, A., Swanson, M., and Grinstein, S. (2009). Contribution of phosphatidylserine to membrane surface charge and protein targeting during phagosome maturation. The Journal of cell biology *185*, 917-928.
Yeung, T., Terebiznik, M., Yu, L., Silvius, J., Abidi, W.M., Philips, M., Levine, T., Kapus, A., and Grinstein, S. (2006). Receptor activation alters inner surface potential during phagocytosis. Science *313*, 347-351.
Zhang, F., Wang, Z., Lu, M., Yonekubo, Y., Liang, X., Zhang, Y., Wu, P., Zhou, Y., Grinstein, S., Hancock, J.F.*, et al.* (2014). Temporal production of the signaling lipid phosphatidic acid by phospholipase D2 determines the output of extracellular signal-regulated kinase signaling in cancer cells. Molecular and cellular biology *34*, 84-95.

CONTACT FOR REAGENT AND RESOURCE SHARING

Further information and requests for resources and reagents should be directed to and will be fulfilled by the Lead Contact, Yvon Jaillais (yvon.jaillais@ens-lyon.fr)

EXPERIMENTAL MODEL AND SUBJECT DETAILS

Growth condition and plant materials. *Arabidopsis thaliana* Col-0 accession was used as wild type (WT) reference background throughout this study. Plants were grown in soil under long-day conditions at 21°C and 70% humidity and in vitro on Murashige and Skoog (MS) Basal Medium supplemented with 0.8% plant agar (pH 5.7) in continuous light conditions at 21°C.
Tobacco *(Nicotiana tabacum* cv. Samsun) pollen was cultivated on the rich medium solidified with 0.25% (w/v) phytagel according to Kost et al. (1998).

Plant transformation and selection. Each construct was transformed into C58 GV3101 Agrobacterium strain and selected on YEB media (5g/L beef extract; 1g/L yeast extract; 5g/L peptone; 5g/L sucrose; 15g/L bactoagar; pH 7.2) supplemented with antibiotics (Spectinomycin, Gentamycin). After two days of growth at 28°C, bacteria were collected using a single-use cell scraper, re-suspended in about 200mL of transformation buffer (10mM MgCl2; 5% sucrose; 0.25% silweet) and plants were transformed by dipping.
Primary transformants (T1) were selected in vitro on the appropriate antibiotic/herbicide (glufosinate for mCITRINE, hygromycin for mCHERRY-tagged proteins). Approximately 20 independent T1s were selected for each line. In the T2 generation at least 3 independent transgenic lines were selected using the following criteria when possible: i) good expression level in the root for detection by confocal microscopy, ii) uniform expression pattern, iii) single insertion line (1 sensitive to 3 resistant segregation ratio) and, iv) line with no obvious abnormal developmental phenotypes. Lines were rescreened in T3 using similar criteria as in T2 with the exception that we selected homozygous lines (100% resistant). At this step, we selected one transgenic line for each PS and PA biosensor that were used for further analyses and crosses.

Pollen expression vector was transferred into tobacco pollen grains germinating on solid culture medium by particle bombardment as described previously (Bloch et al., 2016). Particles were coated with 1 µg of DNA.

Microscopy setup. All imaging experiments were performed with the following spinning disk confocal microscope set up, except when indicated otherwise (see bellow): inverted Zeiss microscope (AxioObserver Z1, Carl Zeiss Group, http://www.zeiss.com/) equipped with a spinning disk module (CSU-W1-T3, Yokogawa, www.yokogawa.com) and a ProEM+ 1024B camera (Princeton Instrument, http://www.princetoninstruments.com/) using a 63x Plan- Apochromat objective (numerical aperture 1.4, oil immersion). GFP

was excited with a 488 nm laser (150mW) and fluorescence emission was filtered by a 525/50 nm BrightLine® single-band bandpass filter (Semrock, http://www.semrock.com/). YFP/mCITRINE were excited with a 515 nm laser (60mW) and fluorescence emission was filtered by a 578/105nm BrightLine® single-band bandpass filter (Semrock, http://www.semrock.com/), CHERRY/RFP were excited with a 561nm laser (80mW) and fluorescence emission was filtered by a 609/54 nm BrightLine® single-band bandpass filter (Semrock, http://www.semrock.com/). 488 or 515 nm laser and 561 nm laser were used to excite GFP or YFP/mCITRINE and RFP/mCHERRY, respectively. For quantitative imaging, pictures of epidermal root meristem cells were taken with detector settings optimized for low background and no pixel saturation. Care was taken to use similar confocal settings when comparing fluorescence intensity or for quantification. Yeasts were visualized by spinning disk microscopy using 100X objective (Plan-apochromatic, numerical aperture 1.46) and 488nm laser.

mCITRINE-C2^{LACT} imaging of shoot tissues were performed on a Leica SP8 up-right confocal microscope (Leica, Wetzlar, Germany), with a water immersion objective (HCX IRAPO L 25x/0.95 W), and a 488 nm led laser. Fluorescence emission was detected at 525-600nm.

Colocalization between mCITRINE-C2^{LACT} and VHA-A3-RFP, were acquired on an inverted Zeiss CLSM710 confocal microscope as previously described (Simon et al., 2014).

For pollen tube live-cell imaging, 6-9-h-old pollen tubes were observed using a spinning-disc confocal microscope (Yokogawa CSU-X1 on Nikon Ti-E platform) equipped with a 60X Plan Apochromat objective (WI; numerical aperture = 1.2) and an Andor Zyla sCMOS camera. Laser excitation at 488 nm together with a 542/27-nm single-band filter (Semrock Brightline) were used for fluorescence collection of YFP.

Transformation and protein localization in yeast. Both, WT strain BY4743 Ref. YSC1050 (Thermo scientific, http://www.thermoscientific.fr/) and *cho1Δ* Ref. YSC6275-201917366 clone ID 37756 (Thermo scientific, http://www.thermoscientific.fr/) were grown at 30°C with YPD media and transformed using the Li-Ac mediated yeast transformation method described in (Gietz et al., 1995). Transformed yeasts were grown in YPD –Leu media at 30°C for 3-5 days.

METHODS DETAILS

Time lapse imaging. Time lapse imaging of cell division and root hair growth were performed as described (Doumane et al., 2017). In brief, five days old Arabidopsis seedlings were transferred in a chambered cover glass (Lab-Tek II, http:// www.thermoscientific.com), which contained 1.5 ml of MS medium (pH 5.7) containing 0.8% plant agar (Duchefa, http://www.duchefa-biochemie.nl/) in the absence of sucrose. Epidermal cells in the meristematic region of the root (to image cytokinesis) or growing root hairs were subjected to time-lapse imaging with spinning disk confocal microscope.

Two or three roots were observed simultaneously and images were collected at different Z-positions every 3 min (cytokinesis) or every 5 minutes (root hair).

Shoot apical meristem imaging. To access the inflorescence meristem, flowers and floral buds were dissected out and imaged on a Leica SP8 up-right confocal microscope (Leica, Wetzlar, Germany). Fluorescence emission was detected at 525-600 nm in sequential line scanning mode with a line average of 4 and stacks of serial optical sections were generated. Projections of the signal in the L1 layer were obtained using MorphoGraphX software (http://www.mpipz.mpg.de/MorphoGraphX) (Barbier de Reuille et al., 2015), according to parameter describe in MorphoGraphX User manual (http://www.mpipz.mpg.de/4085950/MGXUserManual.pdf).

FM4-64, BFA, WM, PAO, R59022, R59949 treatments. The plasma membrane and endosomes of 5 to 7-day old transgenic lines expressing mCITRINE-C2^{LACT} were stained by incubating roots with 1 µM FM4-64 (thermofisher scientific, https://www.thermofisher.com) liquid MS solution for 60 min. Lines co-expressing mCITRINE-C2^{LACT} and VHA-A1-RFP were incubated in wells containing 25 µM Brefeldin A (BFA, Sigma, www.sigmaaldrich.com, BFA stock solution at 50 mM in DMSO) liquid MS solution for 60 min. Lines co-expressing mCITRINE-C2^{LACT} and W7R were incubated in wells containing 30 µM Wortmannin (Sigma, www.sigmaaldrich.com, WM stock solution at 30 mM in DMSO) liquid MS solution for 90 min. Lines co-expressing mCITRINE-C2^{LACT} with compartment markers (W25R, W13R, W18R, W7R) and 2xmCITRINE$^{8K\text{-}FARN}$ (8+) with compartment markers (W25R, W34R W7R) and 2xmCITRINE$^{4K4Q\text{-}FARN}$ (4+) with compartment markers (W25R, W13R, W18R, W7R) were incubated in wells containing 60 µM PAO (Sigma, www.sigmaaldrich.com, PAO stock solution at 60 mM in DMSO) liquid MS solution for 30 minutes. Lines expressing (Lti6b-GFP, mCITRINE-C2^{LACT}, mCITRINE-1xPH^{PLC}, mCITRINE-1xPH^{FAPP1}, mCITRINE-1xPASS, mCITRINE-2xPASS, mCITRINE-KA1^{MARK1}, 2xmCITRINE$^{8K\text{-}FARN}$ (8+)) were incubated in wells containing 12.5 µM R59022 or R59949 (Sigma, www.sigmaaldrich.com, stock solution at 25 mM in DMSO) liquid MS solution. For concomitant treatment (PAO and R599022) lines expressing (Lti6b-GFP, mCITRINE-C2^{LACT}, mCITRINE-1xPH^{PLC}, mCITRINE-1xPH^{FAPP1}, mCITRINE-1xPASS, mCITRINE-KA1^{MARK1}, 2xmCITRINE$^{8K\text{-}FARN}$ (8+)) were incubated in wells containing first liquid MS solution with PAO at 30 µM for 60 min and then were transferred into wells containing liquid MS solution with PAO at 30 µM and R59949 at 12.5 µM for 60 min. For each treatment, the mock condition corresponds to incubation of plants in well supplemented with a volume of DMSO equivalent to the highest drug concentration used and for the same time as the actual treatment. Roots were imaged within a 10-minute time frame window around the indicated time.

Subcellular and phenotype complementation with lysophospholipids. For complementation of the subcellular localization of PA sensor, 5 to 7-day old transgenic lines expressing mCITRINE-1xPASS were concomitantly treated with R59949 and lysophosphatidic acid (LPA, 54µM) or lysophosphatidylserine (LPS, 54µM) for 60 min in 12-well plates. For complementation of the subcellular localization of PS sensors, 8 to 12-day old transgenic lines expressing mCITRINE-C2^{LACT} or mCITRINE-2xPH^{EVCT2} in

pss1-3$^{-/-}$ were treated with LPA or LPS at 54µM for 60 min in 12-well plates. For complementation of the root growth rate, plants grown for 8 days on MS plates were transferred to plate containing control media (BSA only) or media supplemented with BSA + LPS at 2.47µM for 3 days (LPS:BSA molar ratio 4:1). Root size was quantified each day following the procedure described below. For complementation of the rosette size, plants were grown for 8 days on MS plates, transferred on control media (BSA only) or LPS media (see above) for 6 days, and then transferred to soil for 8 days. Finally, plants were imaged and rosette size (see bellow).

Co-localization Analysis. For quantitative co-localisation, we used an object-based analysis method (OBA). OBA is used to determine the centroid of each spot (intracellular compartment) and to compare their respective localization. Co-localization between the two structures is validated if the distance between the two centroids is below the optical resolution (Bolte and Cordelieres, 2006). The OBA was performed as followed; first the intracellular compartments were automatically detected in each channel applying a "DoG" filter with a sigma of 3 in order to improve the localization of each spots increasing the Gaussian fitting, and then a "Triangle" thresholding was applied (Bayle et al., 2017). Next, with binary images obtained we used JACoP plugin on Fiji (Bolte and Cordelieres, 2006) to acquire quantitative data of the co-localization with the following parameters: minimum size of 3µm^2 and maximum size of 20µm^2. To allow high throughput data processing, this analysis pipeline has been automatized on a Fiji macro. The percentage of colocalization always corresponds to the proportion of spots in the yellow channel that colocalize with spots in the red channel, except when 2xmCHERRY-C2^{LACT} was used (Figure 5D), in which case the percentage of colocalization corresponds to the proportion of spots in the red channel (2xmCHERRY-C2^{LACT}) that colocalize with spots in the yellow channel (membrane charge reporters mCITRINE$^{4K4Q\text{-}FARN}$ (4+), mCITRINE$^{2K6Q\text{-}FARN}$ (2+), 2xmCITRINE$^{8Q\text{-}FARN}$ (0+)). In other words, the percentage of colocalization corresponds to the number of spot detected in the yellow channel (mCITRINE-C2^{LACT}, mCITRINE-PH^{EVCT2}, mCITRINE$^{8K\text{-}FARN}$ (8+), mCITRINE$^{4K4Q\text{-}FARN}$ (4+), mCITRINE$^{2K6Q\text{-}FARN}$ (2+), 2xmCITRINE$^{8Q\text{-}FARN}$ (0+)), colocalizing with spots detected in the red channel (compartment markers) divided by the total number of spots detected in the yellow channel and multiplied by hundred. In order to avoid artefacts due to low number of spots detected in one of the channels, a ratio was applied. This ratio corresponds to the number of spots detected in "Image A" divided by the number of spots detected in "Image B". If the ratio was either above 2 or below 0.5 the corresponding results were discarded. This rule was not applied for colocalization with 2xmCITRINE$^{8K\text{-}FARN}$ (8+) that is massively localized at the PM and seldom in intracellular compartments (justifying a low number of spots detected in yellow channel). Co-localization was quantified in at least 8 independent roots for untreated conditions in duplicates (Figure 5). For treated conditions (Figure 6), triplicate experiments were performed and at least 15 independent roots were analyzed for quantification in mock conditions and treated conditions. To estimate the approximate number of cells present in one image, we counted the number of cells in 14 independent roots. We found an average of 43 cells per root image (meristematic/elongation zone of root epidermal cells). This allowed us to estimate the number of cells that were used for each colocalization analysis (Figure 5 and 6).

Dissociation index. The effects of PAO, R59022 and R59949 and PS depletion (and LPS add-back in the *pss1-3*$^{-/-}$) on the localization of our charge biosensor mCITRINE-KA1^{MARK1} were analyzed by calculating the "dissociation index". First, we calculated "indexMock": the ratio between the fluorescence intensity (Mean Grey Value function of Fiji software) measured in two elliptical region of interest (ROIs) from the plasma membrane region (one at the apical/basal PM region and one in the lateral PM region) and two elliptical ROIs in the cytosol in the mock condition. "IndexMock" was quantified in 150 cells over three independent replicates (50 cells per replicate). Next, we measured a similar ratio in perturbed conditions ("indexExp"). "indexExp" was also quantified in 150 cells over three independent replicates (50 cells per replicate). The dissociation index is the ratio of (indexMock)/(indexExp). This dissociation index reveals the degree of relocalization of the fluorescent reporters from the plasma membrane to the cytosol, between the mock and perturbed conditions (pharmacological treatment or mutant).
In figure 4F, the percentage of cell with mCITRINE-KA1^{MARK1} at the plasma membrane was counted by hand, by counting the number of cell with visible plasma membrane labeling and the total number of cells in each condition. Triplicate experiments were performed and at least 15 independent roots were analyzed.

Quantification of the root length and root growth rate. The root length was determined on 12-day-old vertically grown seedlings and measured by hands using FIJI software. For the root growth rate, plants were transferred in plates supplemented with BSA only or BSA+LPS and scanned each day with an EPSON scanner perfection V300 PHOTO at 800 dpi for the next three days. Images scanned at different time points were stacked using "Images to stack" function of the Fiji software with the "Copy (Center)" method and analyzed using RootTrace. To allow high throughput data analyses, the process has been automatized on a Fiji macro. The starting point for quantification corresponds to the size of the root when the plants were transferred into media supplemented with LPS. The corresponding root growth rate represents the growth of the root for each day in millimeters.

Quantification of the rosette area. 8 days after transferring plants into soil, rosettes were imaged using a CANON EOS 450D with a SIGMA DC 18-50mm 1:2.8 EX MACRO lens at 278 pixels/cm. Fiji was used to apply an auto threshold "Percentile white" on images to obtain white rosette on black background. Then, the "wand (tracing) tool" on Fiji was used to identify the rosette rims, allowing measurement of the rosette area with Fiji measure tools (Ctrl+M).

Genotyping and characterization of *pss1* T-DNA insertion lines.
Characterization of pss1 T-DNA insertions: *pss1-3*$^{-/-}$*(GABI_166G10), pss1-4*$^{-/-}$ *(GABI_613C03), pss1-5*$^{-/-}$ *(GABI_217D10)* were produced by the GABI-KAT consortium (Kleinboelting et al., 2012) and provided by the NASC (http://arabidopsis.info/BasicForm). gDNA was extracted from wild type, *pss1-3*$^{-/-}$*, pss1-4*$^{-/-}$*, pss1-5*$^{-/-}$ plants using Edwards buffer and PCR and border sequencing were performed with primers starting by "Geno" in the resource table section Oligonucleotides.

PSS1 transcript expression by RT-PCR: total mRNA was extracted from wild type, *pss1-1*$^{-/-}$, *pss1-3*$^{-/-}$, *pss1-4*$^{-/-}$ and *pss1-5*$^{-/-}$ using Sigma-Aldrich Spectrum™ Plant Total RNA Kit and cDNA was produced using Invitrogen, SuperScript™ VILO™ cDNA Synthesis Kit. The expression of *PSS1* and the ubiquitous *TCTP* transcripts was tested with by PCR using primers starting with "RT" in the resource table section Oligonucleotides.

pss1 segregation analysis: In order to analyze the segregation of *pss1-3*, *pss1-4*, *pss1-5* T-DNA lines*;* seeds from self-fertilized *pss1-3*, *pss1-4*, *pss1-5* heterozygous plants were grown on plate containing the antibiotic sulfadiazine. Wild type plants (sulfadiazine sensitive plants) were counted after 12 days and resistant plants (heterozygous and homozygous) were transferred to soil. 20 days later, homozygous and heterozygous *pss1* plants were identified based on their rosette phenotype and counted.

Cloning

Preparation of gateway compatible entry clones (entry vector):

Published gateway compatible entry vectors are listed in the recombinant DNA table.

PA biosensors:

The 1xPASS and 2xPASS sequences were amplified from *pEGFP-C1-1xPASS* and *2xPASS-pEGFP-C1* plasmids (gift from Gangwei Du) (Bohdanowicz et al., 2013; Zhang et al., 2014). Gateway compatible PCR products were introduced into pDONRP2R-P3 vectors by BP recombination using the following primers: *PASS-P2RP3_R* and *PASS-P2RP3wSTOP_R* to give *1xPASS/pDONR P2RP3* and *PASS-P2RP3_R and 2xPASS-B3wstop*_R to give *2xPASS/pDONR P2RP3.*

Mutations in PASS were obtained by successive site directed mutagenesis using the following partially overlapping forward (FP) and reverse (RP) primers:

NESmut_F and NESmut_R using *1xPASS/pDONRP2RP3* as template to give *1xPASS*$^{\overline{NESmut}}$*/pDONR P2RP3*

PASSmut(L67P)_F and PASSmut(L67P)_R using *1xPASS/pDONRP2RP3* as template to give *1xPASS*$^{(L67P)}$*/pDONR P2RP3*

PASSmut(K66E&K68E)_F and PASSmut(K66E&K68E)_R using *1xPASS/pDONRP2RP3* as template to give *1xPASS*$^{(K66E,K68E)}$*/pDONR P2RP3*

PASSmut(K71E&K73E)_F and PASSmut(K71E&K73E)_R using *1xPASS*$^{(K66E,K68E)}$*/pDONRP2RP3* as template to give *1xPASS*$^{(K66E,K68E,\overline{K71E,K73E})}$*/pDONR P2RP3*

PS biosensors:

The PH^{EVCT2} sequence was amplified from *pEGFP-C1-1xPH*^{EVCT2} plasmid (Tomohiko Taguchi) (Uchida et al., 2011). Gateway compatible PCR products were introduced into *pDONRP2R-P3* or *pDONR221* vectors by BP recombination using the following primers: *EVECTIN2-P2RP3_F* and *EVECTIN2-P2RP3_R* or *1xPH-EVCT2-p221wSTOP_F* and

1xPH-EVCT2-p221wSTOP_R to give *1xPH^{EVCT2}/pDONRP2RP3* or *1xPH^{EVCT2}/pDONR221, respectively*.
To produce *2xPH^{EVCT2}/pDONRP2RP3,* the *1xPH^{EVCT2}/pDONR P2RP3* plasmid was amplified using *BackBone_1xPH-EVECT_F* and BackBone_1xPH-EVECT_R primers and 1xPH^{EVCT2} was amplified using *INSERT-PH-EVECT2_F* and *INSERT-PH-EVECT2_F* primers. Both PCR products were assembled by Gibson cloning (New England biolabs, https://www.neb.com/) to give *2xPH^{EVCT2}/pDONRP2RP3.*

For the cloning of Lat52:YFP-C2^{LACT}, C2^{LACT} sequence flanked by NgoMIV/ApaI sites was amplified from Lact-C2-GFP-p416 plasmid (Addgene #22853) by PCR using specific primers Lact-C2_F and Lact-C2_R. Amplified products were introduced into the multiple cloning sites of pollen expression vectors *pWEN240* using NgoMIV/ApaI restriction enzyme sites. The pWEN240 vector (Klahre and Kost, 2006) was kindly provided by Prof. Benedikt Kost (University of Erlangen-Nuremberg, Erlangen, Germany).

PSS1 genomic sequence:
PSS1 promoter and gene were amplified from gDNA extracted from *Arabidopsis thaliana* wild type plants (Col0 ecotype) using Edwards buffer. The entire genomic fragment (promoter+gene) was amplified using gateway compatible primers *promPSS1-p221_F* and *gPSS1-p221_R,* and the corresponding PCR product was introduced into the *pDONR221* vector by BP recombination to give *promPSS1-PSS1g/pDONR221*

Promoters and fluorescent protein (entry vector):
PDF1 promoter was amplified by PCR from Col0 genomic DNA with the following primers, *PDF1_F* and *PDF1_R* and introduced into the *pENTR5'-TOPO-TA* vector by TOPO cloning (life technologies www.lifetechnologies.com/) to give *PDF1prom/pENTRE5'*.

Construction of destination clones (destination vector):
Published destination vectors are listed in the recombinant DNA table.
Binary destination vectors for plant transformation were obtained using the multisite LR recombination system (life technologies, http://www.thermofisher.com/) using the *pB7m34GW* (basta resistant) and *pH7m34GW* (hygromycin resistant) (Karimi et al., 2007) as destination vectors. All *mCITRINE*-containing clones are in *pB7m34GW* and all *mCHERRY*-containing clones are in *pH7m34GW* to produce the following destination vectors: *pPSS1::PSS1g/pB7m34GW, pUBQ10::mCITRINE-2xPASS/pB7m34GW, pUBQ10::2xmCHERRY-C2^{LACT}/pH7m34GW, pUBQ10::GVG-mCITRINE-C2^{LACT}/pB7m34GW, PDF1::mCITRINE-C2^{LACT}/pB7m34GW, pUBQ10::mCITRINE-2xPH^{EVCT2}/pB7m34GW, pUBQ10::tdTOMATO-2xPH^{EVCT2}/pH7m34GW, pUBQ10::mCITRINE-1xPASS/pB7m34GW, pUBQ10::mCITRINE-1xPASS^{NESmut}/pB7m34GW, pUBQ10::mCITRINE-1xPASS^{L67P}/pB7m34GW, pUBQ10::mCITRINE-1xPASS^{K66E,K68E}/pB7m34GW and pUBQ10::mCITRINE-1xPASS^{K66E,K68E,R71E,K73E}/pB7m34GW.* 1xPH^{EVCT2} was recombined with *pAG425GPD-EGFP-ccdb* (addgene clone #14322, gift of Susan Lindquist) destination vector for N-terminal GFP tagging.

Recombinant protein expression and lipid-protein overlay assays:
The expression plasmid (*pTNT::HA-C2^{LACT}*) was used as DNA template for *in vitro* transcription and translation using the TNT® SP6 High-Yield Wheat Germ Protein Expression System (Promega, www.promega.com), following manufacturer's instructions. 5µl of the total reaction were used to analyze protein expression levels by western-blot using 1:1000 anti-HA (www.boehringer-ingelheim.com) primary antibodies and 1:5000 secondary anti-mouse (GE Healthcare Life Sciences, http://www.gelifesciences.com/) antibody. The lipid overlay assays were performed as follow: nitrocellulose membranes containing immobilized purified lipids (PIPstrip P-6001, Echelon Bioscience, http://echelon-inc.com/) were incubated for 1h in blocking solution (TBST (50 mM Tris, 150 mM NaCl, 0,05% Tween 20, pH 7.6) + 3% BSA). Membranes were then incubated for 2h with 10mL of blocking solution containing 40 µl of in vitro synthesized proteins. After three washing steps using blocking solution, membranes were incubated for 2h at room temperature with primary antibodies diluted in blocking solution, rinsed three times with blocking solution and incubated for 1h at room temperature with the secondary antibody also diluted in blocking solution. Antibodies and dilutions are the same as described above.

Lipid quantification (HPTLC and LC-MS/MS)

Lipid extraction
Leaves of 28-day old plants (0.1-1g fresh weight) were collected in glass tubes; 2 ml of preheated isopropanol were added and tubes were heated at 70°C for 20 min to inhibit phospholipase D activity. 6 ml of chloroform/methanol 2/1 (v/v) were added and lipid extraction was completed at room temperature. The organic phases were transferred to new glass tubes. Then 1.5 ml of H_2O was added to the organic phases and tubes were vortexed and centrifuged at 2000rpm; the organic phases were transferred to new glass tubes, evaporated and the lipids were resuspended in the appropriate volume of chloroform/methanol 2/1, v/v, in order to obtain the same concentration according to the initial seedlings fresh weight.

High performance thin layer chromatography (HPTLC)
Lipids were deposited on HPTLC plates (Silica gel 60G F_{254} glass plates Merck Millipore) together with external pure lipid standards (Avanti lipids). Plates were developed according to Heape et al (1985). Following chromatography, the lipids were charred for densitometry according to Macala et al. (1983). Briefly, plates were dipped into a 3% cupric acetate (w/v)-8% orthophosphoric acid (v/v) solution in H_2O and heated at 110°C for 30min. Plates were scanned at 366 nm using a CAMAG TLC scanner 3. 8 independent samples were quantified for *pss1-3* and *pss1-4* and 6 samples for col0.

LC-MS/MS
For the analysis of phospholipids by LC-MS/MS, phospholipid extracts were dissolved in 100 µL of eluent A (isopropanol/methanol/water 5/1/4 + 0.2% formic acid + 0.028% NH_3) containing synthetic internal lipid standards (PS 17:0/17:0; PE 17:0/17:0; PI 17:0/14:1 and PC 17:0/14:1 from Avanti Polar Lipids). LC-MS/MS (multiple reaction monitoring mode) analyses were performed with a model QTRAP 5500 (ABSciex) mass spectrometer coupled to a liquid chromatography system (Ultimate 3000; Dionex).

Analyses were performed in the negative (PS, PS, PI) and positive (PC) modes with fast polarity switching (50 ms); nitrogen was used for the curtain gas (set to 15), gas 1 (set to 20), and gas 2 (set to 0). Needle voltage was at -4500 or +5500 V without needle heating; the declustering potential was adjusted between -160 and -85 V or set at +40 V. The collision gas was also nitrogen; collision energy varied from -48 to -62 eV and +47 eV on a compound-dependent basis. Reverse-phase separations were performed at 50°C on a Luna C8 150x1 mm column with 100-Å pore size and 5-µm particles (Phenomenex). The gradient elution program was as follows: 0min, 30%B (isopropanol + 0.2%formic acid + 0.028%NH_3); 5min, 50% B; 30 min, 80% B; 31 to 41 min, 95% B. The flow rate was set at 40 mL/min, and 3mL sample volumes were injected. The areas of LC peaks were determined using MultiQuant software (version 2.1; ABSciex) for relative phospholipid quantification. Quantification of molecular phospholipids species were performed on five independent samples for *pss1-3* and *pss1-4* and ten independent samples for Col0.

QUANTIFICATION AND STATISTICAL ANALYSES.

Quantitative co-localization results were statistically compared using the Kruskal-Wallis bilateral test (p-value=0.05) using XLstat software (http://www.xlstat.com/). Pairwise comparisons between groups were performed according to Steel-Dwass-Critchlow-Fligner procedure (different letters indicate statistical difference between samples) (Hollander and Wolfe, 1999). For quantitative co-localization results of Figure 5E we used the bilateral test Kruskal-Wallis test (p-value=0.15) using XLstat software (http://www.xlstat.com/). Pairwise comparisons between groups was performed according to Dunn procedure (different letters indicate statistical difference between samples). Statistical analyses between two samples were performed using the non-parametric Wilcoxon-Mann-Whitney test (p-value=0.05).

METHODS
RESOURCES TABLE

REAGENTS and RESOURCES	SOURCE	IDENTIFIER
Bacterial and Virus Strains		
DH5a Competent Cells	ThermoFisher Scientific	Cat#18265017
Agrobacterium tumefaciens: C58 GV3101		N/A
Chemicals, Peptides, and Recombinant Proteins		
FM4-64	ThermoFisher Scientific	T13320
Wortmannin	Sigma-Aldrich	W1628
Brefeldin A (BFA)	Sigma-Aldrich	B7651
R59022	Sigma-Aldrich	D5919
R59949	Sigma-Aldrich	D5794
Phenylarsine oxide (PAO)	Sigma-Aldrich	P3075
BSA fatty acyl free	Sigma-Aldrich	A8806
HA-C2^{LACT}	this study	N/A
Lyso Phosphatidylserine 18:1	Avanti Polar Lipids	858143
Lyso Phosphatidic acid 18:1	Avanti Polar Lipids	857130
Experimental Models: Organisms/Strains		
Col 0 (*A. thaliana* accession)	NASC	NASC# N1092
Yeast (BY4743)	ThermoFisher Scientific	YSC1050
Δcho1 (YSC6275-201917366)	ThermoFisher Scientific	37756
pUBQ10::mCITRINE-1xPH^{FAPP1} (P5Y)	Simon et al., 2014, NASC	NASC# N2105607
pUBQ10::mCITRINE-2xPH^{FAPP1} (P21Y)	Simon et al., 2014, NASC	NASC# N2105612
pUBQ10::mCITRINE-P4M^{SidM}	Simon et al., 2016, NASC	NASC# N2107346
pUBQ10::mCITRINE-1xPH^{PLC} (P14Y)	Simon et al., 2014, NASC	NASC# N2105609
pUBQ10::mCITRINE-2xPH^{PLC} (P24Y)	Simon et al., 2014, NASC	NASC# N2105613
pUBQ10::mCITRINE-tubbyc (P15Y)	Simon et al., 2014, NASC	NASC# N2105610
pUBQ10::mCITRINE-C2^{LACT}	Simon et al., 2016, NASC	NASC# N2107347
pUBQ10::2xmCHERRY-C2^{LACT}	This study	N/A

PDF1::mCITRINE-C2^{LACT}	This study	N/A
pUBQ10::mCITRINE-2xPH^{EVCT2}	This study	N/A
pUBQ10::tdTOMATO -2xPH^{EVCT2}	This study	N/A
pUBQ10::mCITRINE-1xPASS	This study	N/A
pUBQ10::mCITRINE-1xPASS^{NESmut}	This study	N/A
pUBQ10::mCITRINE-1xPASS^{L67P}	This study	N/A
pUBQ10::mCITRINE-1xPASS^{K66E,K68E}	This study	N/A
pUBQ10::mCITRINE-1xPASS ^{K66E,K68E,R71E,K73E}	This study	N/A
pUBQ10::mCITRINE-2xPASS	This study	N/A
pUBQ10::mCITRINE-KA1^{MARK1}	Simon et al., 2016, NASC	NASC# N2107345
pUBQ10::2xmCITRINE-8K-Farn (8+)	Simon et al., 2016, NASC	NASC# N2107342
pUBQ10::2xmCITRINE-4K4Q-Farn (4+)	Simon et al., 2016, NASC	NASC# N2107343
pUBQ10::2xmCITRINE-2K6Q-Farn (2+)	Simon et al., 2016, NASC	N/A
pUBQ10::2xmCITRINE-0K8Q-Farn (0+)	Simon et al., 2016, NASC	NASC# N2107344
35S::EGFP-Lti6b	Cutler et., 2000, NASC	NASC# N84726
pUBQ10::Lti6b-2xmCHERRY	Elsayad et al., 2016	N/A
35S::EGFP-aqPIP2a	Cutler et., 2000, NASC	NASC# N84725
pUBQ10::myri-2xmCITRINE	Simon et al., 2016	N/A
W7R – mCHERRY-RABF2a	Geldner et al., 2011, NASC	NASC# N781672
W13R – mCHERRY-VTI12	Geldner et al., 2011, NASC	NASC# N781675
W18R – mCHERRY-Got1p	Geldner et al., 2011, NASC	NASC# N781676
W24R – mCHERRY-RABA5d	Geldner et al., 2011, NASC	NASC# N781678
W34R – mCHERRY-RABA1e	Geldner et al., 2011, NASC	NASC# N781683
W25R – mCHERRY-D1	Geldner et al., 2011, NASC	NASC# N781679
VHA-A1-mRFP1	Dettmer et al., 2006	N/A
VHA-A3-mRFP1	Dettmer et al., 2006	N/A
Sec-RFP	Samalova et al., 2006, NASC	NASC# N799370
pss1-3	*GABI_166G10*	NASC# N415922
pss1-4	*GABI_613C03*	NASC# N458779
pss1-5	*GABI_217D10*	NASC# N420782

pPSS1::PSS1g/pss1-3	This study	N/A
pAG425-GPD::EGFP-C2^{LACT}	Simon et al., 2016	N/A
pAG425-GPD::EGFP-1xPH^{EVCT2}	This study	N/A
Oligonucleotides		
Geno-pss1_LP2 GGGGCAGAACAAAGATGAAAG	IDTDNA	N/A
Geno-pss1_RP2 TCATGGTAGGTATCTGGGCAG	IDTDNA	N/A
Geno-LBGABI-SEQ ATATTGACCATCATACTCATTGC	IDTDNA	N/A
Geno-RBGABI-SEQ ATATTGACCATCATACTCATTGC	IDTDNA	N/A
RT-pss1-1_LP *TCTGGATCTTCCATGTCCAAG*	IDTDNA	N/A
RT-pss1-1_RP *TTCTTTGGGTGCTTTCAATTG*	IDTDNA	N/A
RT-TCTP-F *GTTGAACCCTCCTTGTAGTAAG*		
RT-TCTP-R *GTTGAACCCTCCTTGTAGTAAGC*	IDTDNA	N/A
NES-PASS-P2RP3_R *GGGGACAGCTTTCTTGTACAAAGT GGCTTCTCGAGCGAACAGCAATG AATTAGCC*	IDTDNA	N/A
TOMATO-p221_F *GGGGACAAGTTTGTACAAAAAAGC AGGCTTAACCATGGTGAGCAAGG GCGAGGAGGTC*	IDTDNA	N/A
TOMATO-p221_R *GGGGACCACTTTGTACAAGAAAG CTGGGTACTTGTACAGCTCGTCCA TGCCGTA*	IDTDNA	N/A
NES-PASS-P2RP3wSTOP_F GGGGACAACTTTGTATAATAAAGT TGCTTAACTAGTCTTAGTGGCGTC ATCGAACCG	IDTDNA	N/A
2xPASS-B3wstop_R GGGGACAACTTTGTATAATAAAGT TGCTTATCTAGATCCGGTGGATCC TTAACT	IDTDNA	N/A
EVECTIN2-P2RP3_F *GGGGACAGCTTTCTTGTACAAAGT GGCTACCCAGATCTCGATGGCGT TTGTGAAGA*	IDTDNA	N/A
EVECTIN2-P2RP3_R *GGGGACAACTTTGTATAATAAAGT TGCTAGGGATCCCTAGTTTGTCCT AGAATCT*	IDTDNA	N/A
INSERT-PH-EVECT2_F *CAAGATTCTAGGACAAACGTCGAC*	IDTDNA	N/A

GGTACCATGGCG		
INSERT-PH-EVECT2_R GTATAATAAAGTTGCTAGCTAGTTT GTCCTAGAATCTTGGAGTGTAAAT TTC	IDTDNA	N/A
BackBone_1xPH-EVECT_F TAGCTAGCAACTTTATTATACAAAG	IDTDNA	N/A
BackBone_1xPH-EVECT_R GTTTGTCCTAGAATCTTGGAG		
NESmut_R TGATATCAGCACCTGCTGCTTTCA AGGCTAATTCATTGCTGTTCG	IDTDNA	N/A
NESmut_F TAGCCTTGAAAGCAGCAGGTGCT GATATCAACAAGACAGAATCTAGA ATGG	IDTDNA	N/A
1xPASSmut(L67P)_R CCTCAAGGATTTAGGCTTCACATG TAGCCTATCACGTCTTCTGC	IDTDNA	N/A
1xPASSmut(L67P)_F GCTACATGTGAAGCCTAAATCCTT GAGGAATAAAATCCAC	IDTDNA	N/A
1xPASSmut(K66E & K68E)_R TCAAGGATTCAAGCTCCACATGTA GCCTATCACGTCTTCTGCTTCCTG	IDTDNA	N/A
1xPASSmut(K66E & K68E)_F GGCTACATGTGGAGCTTGAATCCT TGAGGAATAAAATCCACAAACAAC TTCACC	IDTDNA	N/A
1xPASSmut(R71E & K73E)_R GTTGTTTGTGGATTTCATTCTCCAA GGATTCAAGCTCCACATGTAGCC	IDTDNA	N/A
1xPASSmut(R71E & K73E)_F GAGCTTGAATCCTTGGAGAATGAA ATCCACAAACAACTTCACCCAAAC TGTCGG	IDTDNA	N/A
1xPH-EVCT2-p221wSTOP_F GGGGACAAGTTTGTACAAAAAAGC AGGCTTAACCATGGCGTTTGTGAA GAGTGGCTG	IDTDNA	N/A
1xPH-EVCT2-p221wSTOP_R GGGGACCACTTTGTACAAGAAAG CTGGGTACTAGTTTGTCCTAGAAT CTTGGAGTG	IDTDNA	N/A
promPSS1-p221_F GGGGACAAGTTTGTACAAAAAAGC AGGCTTATAGTGCTTTTTAATTGTA TTCGCAGT	IDTDNA	N/A
gPSS1-p221_R GGGGACCACTTTGTACAAGAAAG	IDTDNA	N/A

CTGGGTACAAAAAAAAACCACAATGGCATTTCA		
Lact-C2_F ATAGCCGGCTGCACTGAACCCCTAGG	Sigma-Aldrich	N/A
Lact-C2_R ATAGGGCCCCTAACAGCCCAGCAGCTC	Sigma-Aldrich	N/A
Recombinant DNA		
Empty gateway entry vector: pDONR221	thermofisher	cat# 12536017
Empty gateway entry vector: pDONR P4P1R	thermofisher	cat# 12537023
Empty gateway entry vector: pDONR P2RP3	thermofisher	cat# 12537023
Empty gateway destination vector: pB7m34GW	Karimi et al., 2007	N/A
Empty gateway destination vector: pH7m34GW	Karimi et al., 2007	N/A
Empty gateway destination vector: pAG425GPD-EGFP-ccdb	Alberti et al., 2007	addgene clone #14322
Empty gateway destination vector: pTNT-HA-ccdb	Simon et al., 2016	N/A
Cloning vector: pWEN240	Klarhe and Kost 2006	N/A
Gateway entry vector (promoter): UBQ10prom/pDONR P4P1R	Jaillais et al., 2011, NASC	NASC# N2106315
Gateway entry vector (promoter): PDF1prom/ pENTR5'	This study	N/A
Gateway entry vector (fluorescent protein): mCITRINEnoSTOP/pDONR221	Simon et al., 2014, NASC	NASC# N2106287
Gateway entry vector (fluorescent protein): 2xmCHERRYnoSTOP/pDONR221	Simon et al., 2014, NASC	N/A
Gateway entry vector (fluorescent protein): tdTOMATOnoSTOP/pDONR221	This study	N/A
Gateway entry vector (lipid binding domain): 1xPASS/pDONR P2RP3	This study	N/A
Gateway entry vector (lipid binding domain): 2xPASS/pDONR P2RP3	This study	N/A
Gateway entry vector (lipid binding domain): 1xPASS^{NESmut}/pDONR P2RP3	This study	N/A

Gateway entry vector (lipid binding domain): 1xPASS^{L67P}/pDONR P2RP3	This study	N/A
Gateway entry vector (lipid binding domain): 1xPASS^{K66E,K68E}/pDONR P2RP3	This study	N/A
Gateway entry vector (lipid binding domain): 1xPASS^{K66E,K68E,R71E,K73E} /pDONR P2RP3	This study	N/A
Gateway entry vector (lipid binding domain): 1xPH^{EVCT2}/pDONR P2RP3	This study	N/A
Gateway entry vector (lipid binding domain): 1xPH^{EVCT2}/pDONR 221	This study	N/A
Gateway entry vector (lipid binding domain): 2xPH^{EVCT2}/pDONR P2RP3	This study	N/A
Gateway entry vector (lipid binding domain): 1xC2^{LACT}/pDONR P2RP3	Simon et al., 2016	N/A
Gateway entry vector (lipid binding domain): 1xC2^{LACT}/pDONR 221	Simon et al., 2016	N/A
Gateway entry vector (PSS1 promotor and gDNA): promPSS1-PSS1g/pDONR 221	This study	N/A
Gateway destination vector (for plant transformation): pUBQ10::2xmCHERRY-C2^{LACT}/pH7m34GW	This study	N/A
Gateway destination vector (for plant transformation): PDF1::mCITRINE-C2^{LACT}/pB7m34GW	This study	N/A
Gateway destination vector (for plant transformation): pUBQ10::mCITRINE-2xPH^{EVCT2}/pB7m34GW	This study	N/A
Gateway destination vector (for plant transformation): pUBQ10::2xmCHERRY - 2xPH^{EVCT2}/pH7m34GW	This study	N/A
Gateway destination vector (for plant transformation): pUBQ10::mCITRINE-1xPASS/pB7m34GW	This study	N/A
Gateway destination vector (for plant transformation): pUBQ10::mCITRINE-1xPASS^{NESmut}/pB7m34GW	This study	N/A
Gateway destination vector (for plant transformation): pUBQ10::mCITRINE-1xPASS^{L67P}/pB7m34GW	This study	N/A

Gateway destination vector (for plant transformation): pUBQ10::mCITRINE-1xPASS^{K66E,K68E}/pB7m34GW	This study	N/A
Gateway destination vector (for plant transformation): pUBQ10::mCITRINE-1xPASS ^{K66E,K68E,R71E,K73E}/pB7m34GW	This study	N/A
Gateway destination vector (for plant transformation): pUBQ10::mCITRINE-2xPASS/pB7m34GW	This study	N/A
Gateway destination vector (for plant transformation): promPSS1-PSS1g/ pB7m34GW	This study	N/A
Gateway destination vector (for yeast transformation): pAG425GPD-EGFP-C2^{LACT}	Simon et al., 2016	N/A
Gateway destination vector (for yeast transformation): pAG425GPD-EGFP-1xPH^{EVCT2}	This study	N/A
Gateway destination vector (for in vitro transcription/translation): HA-C2^{LACT}/pTNT	This study	N/A
Pollen transformation vector (for transient transformation): Lat52::YFP-C2^{LACT}/pWEN240	This study	N/A
Vector used as PCR template: Lact-C2-GFP-p416	Yeung et al., 2006	Addgene #22853
Vector used as PCR template: pEGFP-C1-1xPASS	Zhang et al., 2014	N/A
Vector used as PCR template: 2xPASS-pEGFP-C1	Zhang et al., 2014	N/A
Vector used as PCR template: pEGFP-C1-1xPH^{EVCT2}	Uchida et al., 2011	N/A
Software and Algorithms		
FIJI	Schindelin et al., 2012	https://fiji.sc/
RootTrace	French et al., 2009	http://www.plant-image-analysis.org/software/roottrace
JACoP	Bolte et al., 2006	https://imagej.nih.gov/ij/plugins/track/jacop.html
SiCE SpotDetectorV3	Jaillais's lab	http://www.ens-

		lyon.fr/RDP/SiCE/METHODS_files/SiCE%20SpotDetectorV3.ijm
RootgrowthrateMacro	Jaillais's lab	N/A
ColocalizationMacro	Jaillais's lab	N/A
SpotdescriptorMacro	Jaillais's lab	N/A
Other		
Invitrogen™ SuperScript™ VILO™ cDNA Synthesis Kit	Fischer Scientific	11754-050
Spectrum™ Plant Total RNA Kit	Sigma-Aldrich	STRN250
Corning® Costar® TC-Treated Multiple Well Plates	Sigma-Aldrich	CLS3513
Gibson Assembly® Cloning Kit	NEB	E5510S

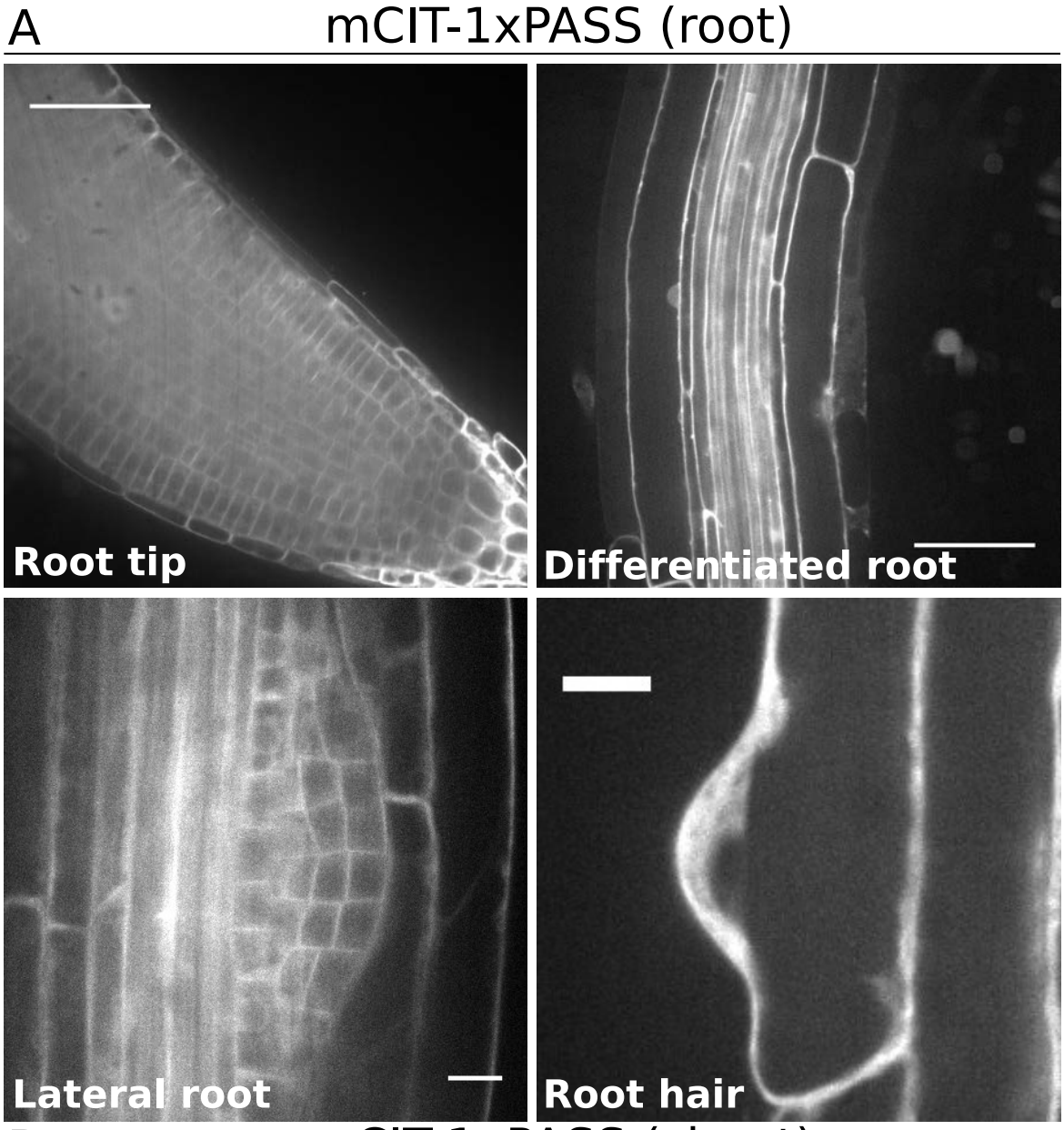
A
mCIT-1xPASS (root)
Root tip
Differentiated root
Lateral root
Root hair
B
mCIT-1xPASS (shoot)
Cotyledons
Leaf
Hypocotyl
C
mCIT-1xPASS
FM4-64
merge
D
mCIT-2xPASS
MOCK
R59022 60min
R59949 60min

Figure_S1

Figure S1 (Related to Figure 1). PA sensors localize at the plasma membrane in different cell types. A, Confocal images of plants expressing mCITRINE-1xPASS in different root tissues: root tip (top left), differentiated cells (top right), lateral root primordium (bottom left) and bulging root hair (bottom right). **B**, Confocal images of plants expressing mCITRINE-1xPASS in different shoot tissues: cotyledons (left), leaf (middle) and hypocotyl (right). **C**, Confocal images of *Arabidopsis* root epidermis stained by FM4-64 (1µM, 60min) and expressing mCITRINE-1xPASS showing co-labelling at the cell plate. **D**, Confocal images of plant expressing mCITRINE-2xPASS in control condition (right), or following DGK inhibition by R59022 (12.5µM, 60 min, middle) or R59949(12.5µM, 60 min, right).

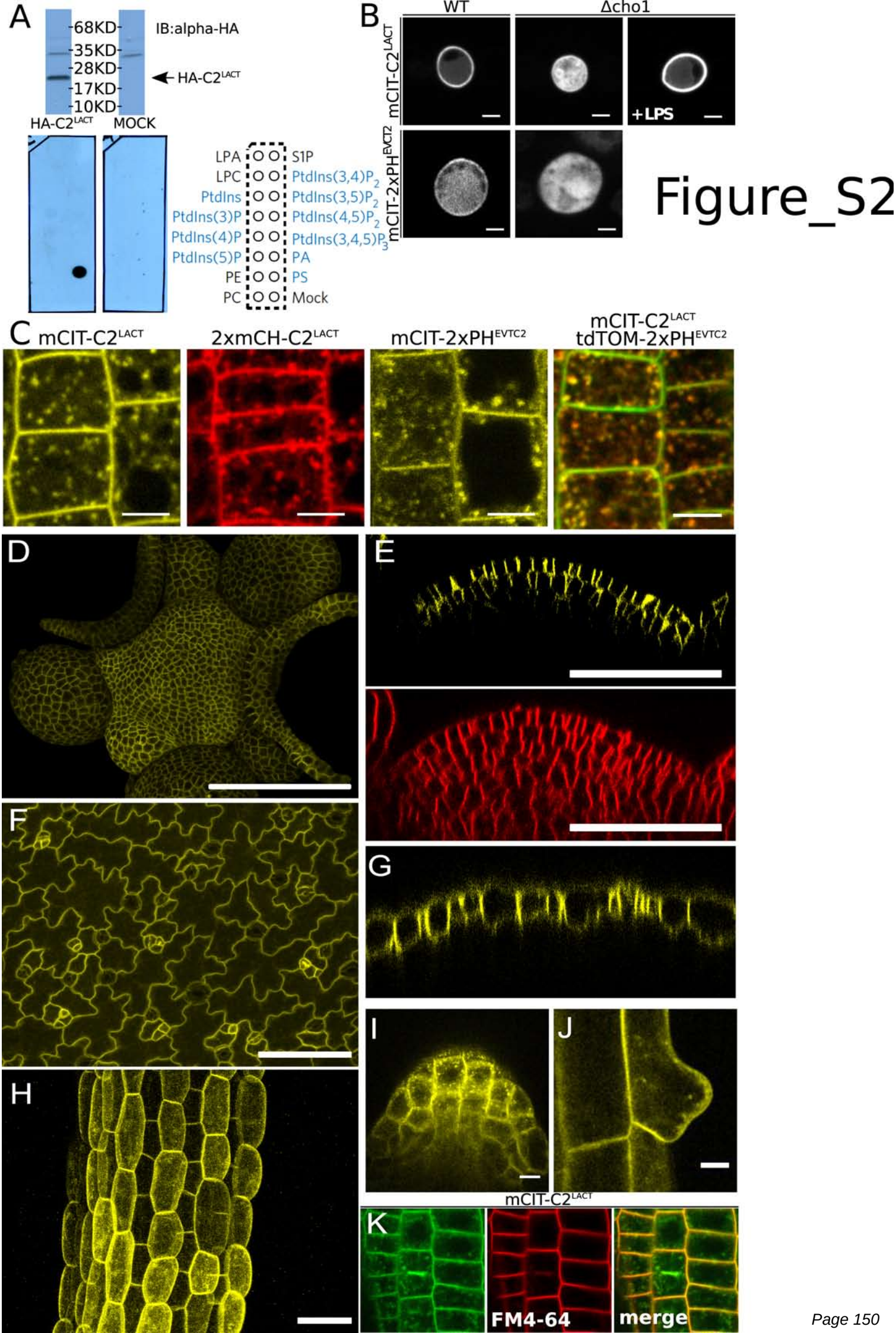
A
68KD
35KD
28KD
17KD
10KD
IB:alpha-HA
HA-C2LACT
HA-C2LACT
MOCK
LPA
LPC
PtdIns
PtdIns(3)P
PtdIns(4)P
PtdIns(5)P
PE
PC
S1P
PtdIns(3,4)P2
PtdIns(3,5)P2
PtdIns(4,5)P2
PtdIns(3,4,5)P3
PA
PS
Mock
B
WT
Δcho1
mCIT-C2LACT
+LPS
mCIT-2xPHEVTC2
C
mCIT-C2LACT
2xmCH-C2LACT
mCIT-2xPHEVTC2
mCIT-C2LACT
tdTOM-2xPHEVTC2
D
E
F
G
H
I
J
mCIT-C2LACT
K
FM4-64
merge

Figure_S2

Figure S2 (Related to Figure 2). Characterization of PS sensors localization in different cell types.

Although the C2 domain of Lacthaderin has been extensively used as a PS reporter, we verified the PS-binding selectivity of our construct, which differs from published reporters in its linker sequence between the $C2^{LACT}$ domain and the fluorescent proteins. All our constructs were obtained using recombination-based cloning. We can therefore switch tags and expression systems while keeping the linker sequence constant. First, we found that in vitro translated HA-$C2^{LACT}$ specifically binds to PS in lipid-protein overlay assays (Fig. S2A), confirming previous binding assays performed with liposomes (Yeung et al., 2008). Second, we tested the localization and PS sensitivity of our $C2^{LACT}$ construct in vivo using recombinant expression in wild type and *cho1Δ* yeast strains, the latter being deficient for PS biosynthesis (Fig. S2B). As we previously reported (Simon et al., 2016), our $C2^{Lact}$-GFP construct localizes at the plasma membrane (PM) in WT yeasts and is soluble in the absence of PS in the *cho1Δ* mutant (Fig. S2B). In addition, the soluble localization of $C2^{LACT}$ in *cho1Δ* is rescued by one hour of exogenous treatment with lysoPS (LPS), confirming that our construct behaves as previously described $C2^{LACT}$ probes (Maeda et al., 2013; Moser von Filseck et al., 2015; Yeung et al., 2008). Together, these results validate the PS-selectivity of our $C2^{Lact}$ construct. Furthermore, we verified that it colocalizes with another PS binding protein, the PH domain of human EVECTIN2 (PH^{EVCT2}), which has also been used as a PS reporter in vivo. In *Arabidopsis* root epidermis, mCITRINE-2xPH^{EVCT2} showed a similar localization pattern as the $C2^{LACT}$ reporter and mCHERRY-2xPH^{EVCT2} extensively colocalizes with mCITRINE-$C2^{LACT}$ (Fig S2C). Similar to $C2^{LACT}$, we validated our PS PH^{EVCT2} probe specificity using heterologous expression in WT and *cho1Δ*mutant yeast (Fig. S2B). Together, these approaches validated $C2^{LACT}$ as a *bona fide* PS reporter in plants.

A, Western blot showing expression of recombinant HA-$C2^{LACT}$ (top), lipid overlay assay performed with HA-$C2^{LACT}$ (bottom left), empty vector (bottom middle) and scheme showing the position of the different lipid species spotted on the membrane (bottom right), anionic lipids are highlighted in blue. **B**, Confocal images of yeast expressing GFP-$C2^{LACT}$ upper panel and GFP-1xPH^{EVCT2}. Left pictures correspond to wild type background, middle to *Δcho1* yeast strain depleted of PS and right *Δcho1* yeast strain complemented with LPS (54µM 60 min). Scale bars, 5 µm. **C**, Confocal images of plants expressing PS sensors. From left to right, mCITRINE-$C2^{LACT}$, 2xmCHERRY-$C2^{LACT}$ and mCITRINE-2xPH^{EVCT2} and plants co-expressing, 2xmCHERRY-2xPH^{EVCT2} with mCITRINE-$C2^{LACT}$. Scale bars, 5 µm. **D-H**, Plant expressing mCITRINE-$C2^{LACT}$ driven by the shoot- and L1-specific *PDF1* promoter in different shoot tissues. **D**, top view of the shoot apical meristem, **E**, Cross-section in the central zone of the shoot apical meristem (top) and FM4-64 staining for 60 min (bottom), **F**, cotyledon epidermis and **G**, a cross-section in cotyledons epidermis **H**, Z-projection of z-stacks taken in the hypocotyl. **I-J**, Confocal images of UBQ10prom::mCITRINE-$C2^{LACT}$ in lateral root primordium (**I**) and in bulging root hair (**J**). **K**, Confocal images of *Arabidopsis* root epidermis stained by FM4-64 (1µM, 60min) and expressing mCITRINE-$C2^{LACT}$ showing co-labelling at the cell plate. Scale bars, 5 µm.

A

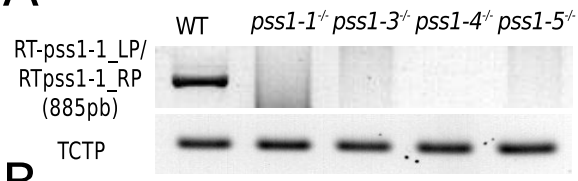

B

% of plant	WT	Heterozygous	Homozygous
pss1-3 (n=419)	28%	47%	26%
pss1-4 (n=402)	28%	50%	22%
pss1-5 (n=305)	27%	49%	24%

C

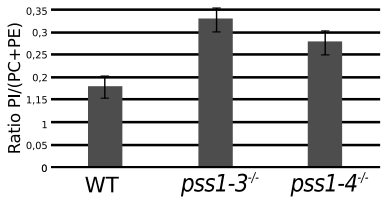

D

E

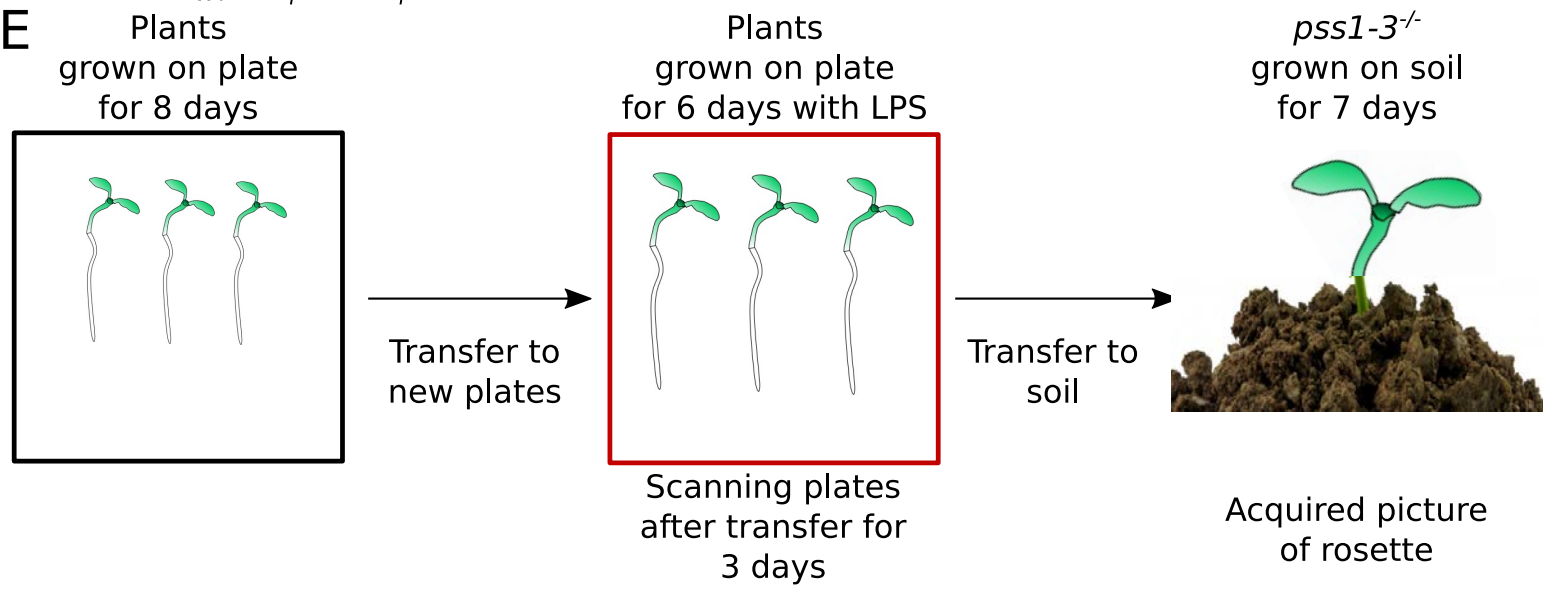

Figure_S3

F

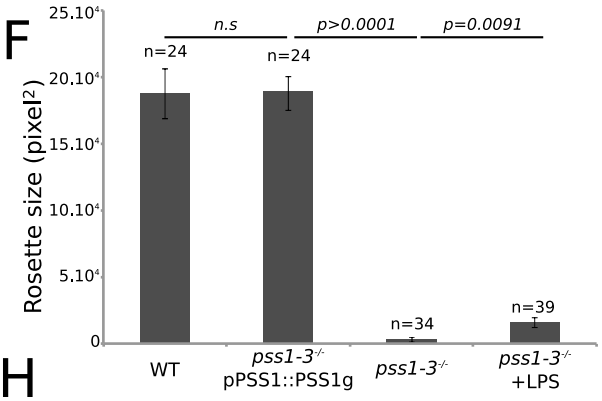

G

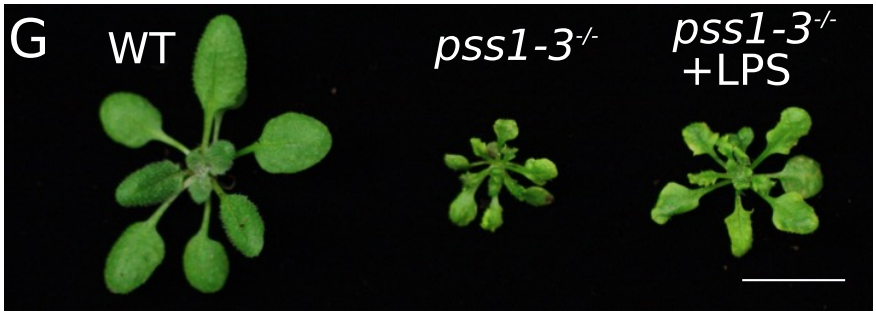

H

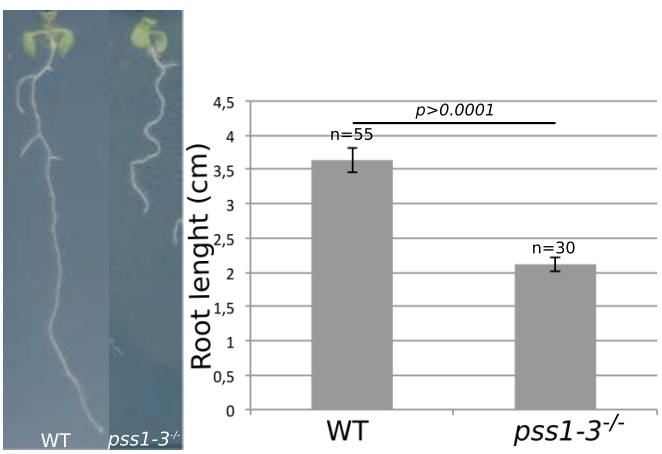

I

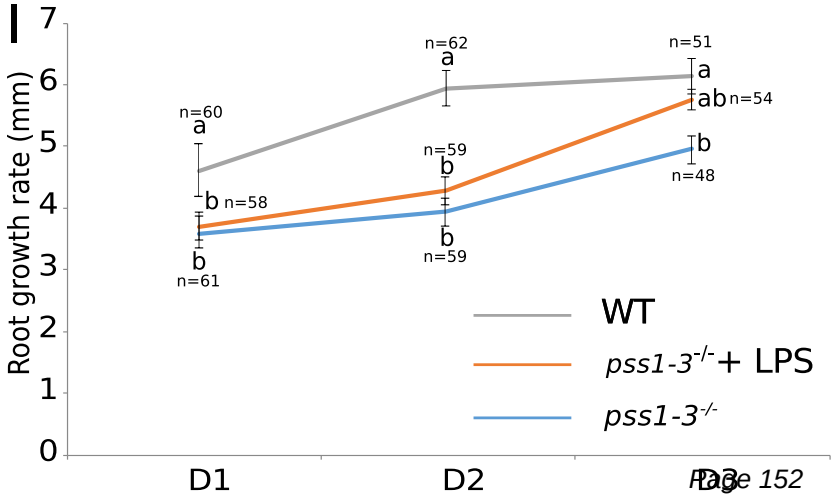

Figure S3 (Related to Figure 3). Characterization of *pss1* mutants. A, RT-PCR analysis of *PSS1* transcript in WT and *pss1* mutant showing the absence of full length *PSS1* transcript in *pss1-1* to *pss1-4* alleles. The bottom row shows expression of ubiquitously express *TCTP* gene in both WT and *pss1* mutants. **B**, Segregation analysis from *pss1* heterozygous plants for *pss1-3*, *pss1-4* and *pss1-5*, in percentage. **C,** Quantification of the ratio of PI/(PC+PE) in WT and *pss1* mutants. This ratio was obtained by measuring the area bellow the pics corresponding to PI, PE and PC for each genotype (WT, n=6; *pss1-3*, n=8 and *pss1-4*, n=8). This analysis shows that *pss1* mutants have a slight elevation in their total PI content at the expense of PC and PE. **D**, Comparison of 45 day-old plants between a wild type plant (left), a *pss1-3*$^{+/-}$ heterozygous plant (Het, middle) and *pss1-3*$^{-/-}$ homozygous plant complemented by transgenic expression of a *PSS1* genomic fragment (*pPSS1::PSS1g*). **E,** Schematic representation of the procedure to complement plants with LPS in order to quantify the root growth rate and the rosette area. **F,** Quantification of the rosette area (mean ±s.e.m in pixel^2) of wild type plants, *pss1-3*$^{-/-}$ mutants expressing *pPSS1::PSS1g*, *pss1-3*$^{-/-}$ mutants and *pss1-3*$^{-/-}$ mutants treated with exogenous LPS at 2.47µM. Statistical difference between each sample is indicated by the p value at the top of each compared conditions (p-value=0.05, non-parametric Wilcoxon-Mann-Whitney test, non-significant (n.s.)). “n” correspond to the number of plants used. **G**, Picture showing the rosette of 21-day-old wild type plants, *pss1-3*$^{-/-}$ and *pss1-3*$^{-/-}$ supplemented with LPS for 6 days. (see Fig S3G). **H**, Picture showing 12 days-old seedlings of wild type (left) and *pss1-3*$^{-/-}$ (right) plants. Statistical difference between each sample is indicated by the p value at the top of each compared conditions (p-value=0.05, non-parametric Wilcoxon-Mann-Whitney test). “n” correspond to the number of plants used. **I**, Quantification (mean ±s.e.m in mm) of root growth for 3 days in wild type, *pss1-3*$^{-/-}$ and *pss1-3*$^{-/-}$ supplemented with LPS at 2.47µM. D1-D2-D3 correspond to one, two or three days after LPS treatment, respectively. Different letters indicates statistical difference between samples (p value=0.05, Kruskal-Wallis bilateral test). “n” correspond to the number of plants used.

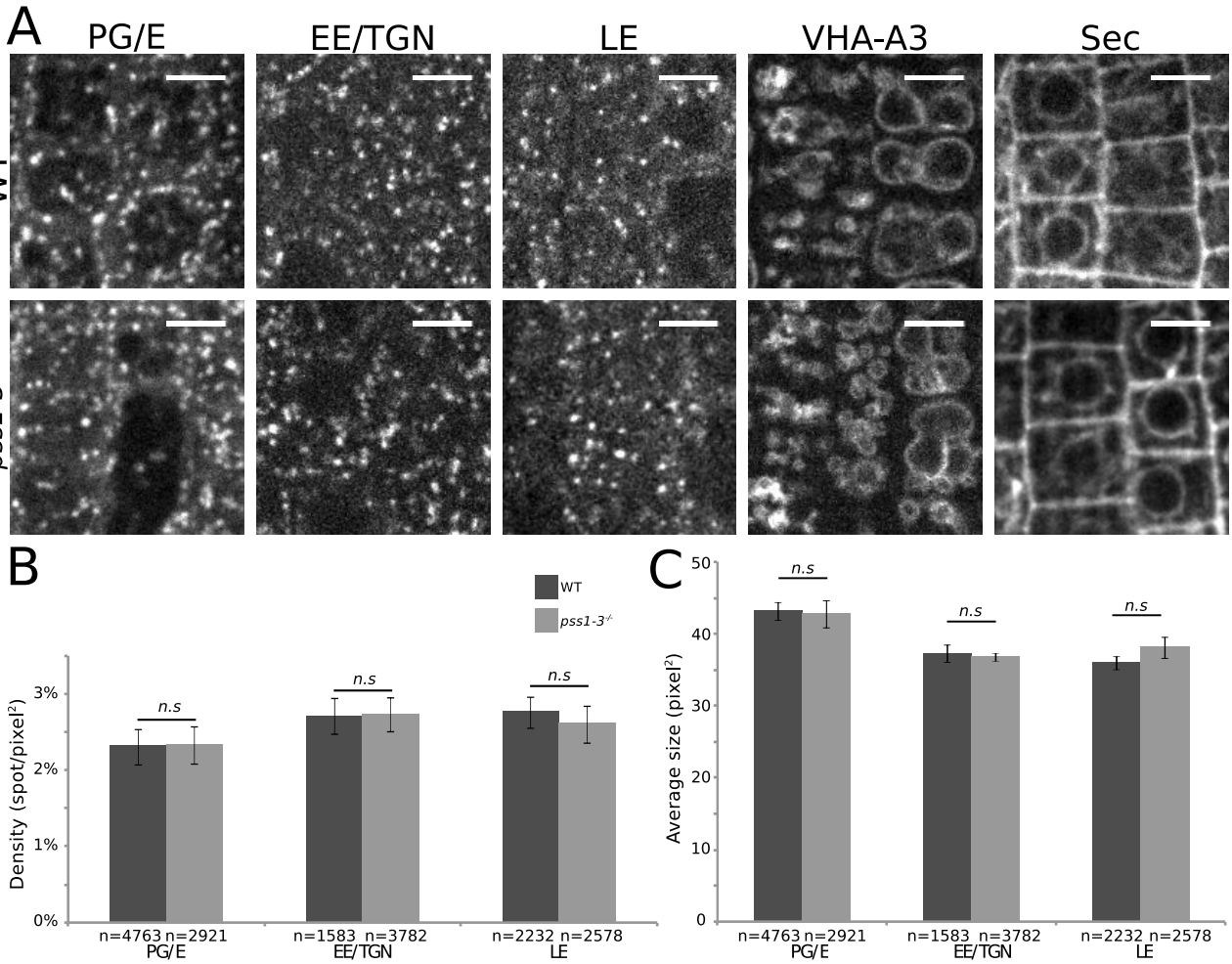
A
PG/E
EE/TGN
LE
VHA-A3
Sec
WT
pss1-3-/-
B
WT
pss1-3-/-
Density (spot/pixel²)
3%
2%
1%
0%
n.s
n.s
n.s
n=4763 n=2921
PG/E
n=1583 n=3782
EE/TGN
n=2232 n=2578
LE
C
Average size (pixel²)
50
40
30
20
10
0
n.s
n.s
n.s
n=4763 n=2921
PG/E
n=1583 n=3782
EE/TGN
n=2232 n=2578
LE

Figure_S4

Figure S4 (Related to Figure 4). Intracellular compartmentalization is not affected in *pss1-3*$^{-/-}$. A, From the left to the right, plants expressing W25R (post-Golgi/endosomal (PG/E)), W13R (Early endosomes/*trans*-Golgi network (EE/TGN)), W7R (Late endosomes (LE)), VHA-A3-RFP (tonoplast), and Sec-RFP (secretion) in wild type plant (upper panel) and in *pss1-3*$^{-/-}$ (lower panel). **B,** Quantification (mean ±s.e.m, number of spots per pixel^2) of the density of intracellular compartments labeled by W25R (PG/E), W13R (EE/TGN), W7R (LE) in wild type and *pss1-3*$^{-/-}$**. C,** Quantification (mean ±s.e.m, size in pixel^2) of the average size of intracellular compartments labeled by W25R (PG/E), W13R (EE/TGN), W7R (LE) in wild type and *pss1-3*$^{-/-}$**.** Statistical difference between each sample is indicated by the p value at the top of each compared conditions (p-value=0.05, non-parametric Wilcoxon-Mann-Whitney test, non-significant (n.s.)). "n" represents the number of spots sampled in each condition. Scale bars, 5 µm.

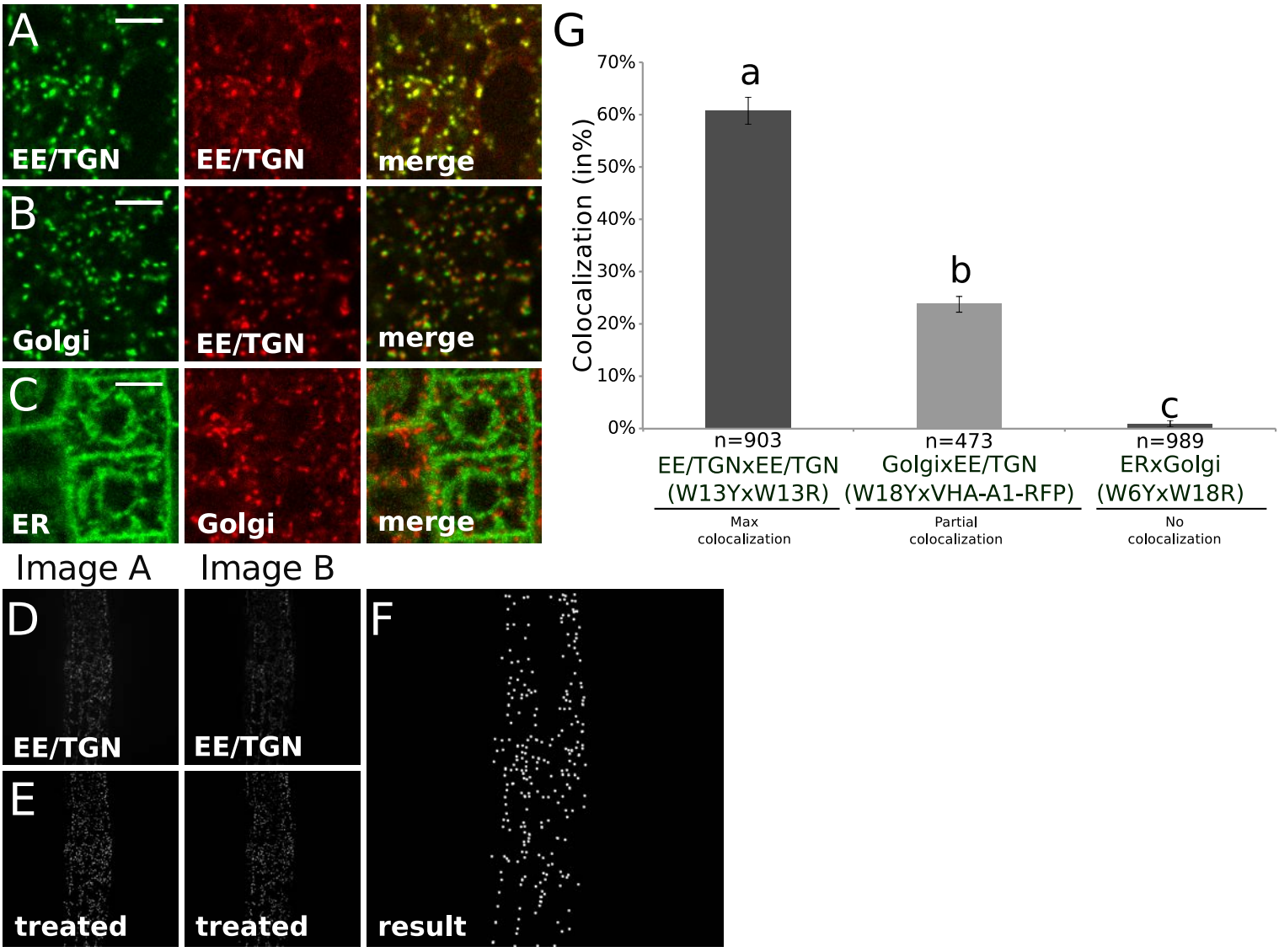
A
EE/TGN
EE/TGN
merge
B
Golgi
EE/TGN
merge
C
ER
Golgi
merge
G
Colocalization (in%)
70%
60%
50%
40%
30%
20%
10%
0%
a
b
c
n=903
EE/TGNxEE/TGN
(W13YxW13R)
n=473
GolgixEE/TGN
(W18YxVHA-A1-RFP)
n=989
ERxGolgi
(W6YxW18R)
Max colocalization
Partial colocalization
No colocalization
Image A
Image B
D
EE/TGN
EE/TGN
E
treated
treated
F
result

Figure_S5

Figure S5 (Related to Figure 5). Validation of the quantitative colocalization methods used in this study. A, Confocal images of plant co-expressing EE/TGN marker W13Y (left) and W13R (middle) and the corresponding merge (right). **B**, Confocal images of plant co-expressing Golgi marker W18Y (left) and early endosomal marker VHA-A1-RFP (middle) and the corresponding merge (right). **C**, Confocal images of plant co-expressing endoplasmic reticulum marker W6Y (left) and Golgi marker W18R (middle) and the corresponding merge (right). **D**, Raw images of plant co-expressing EE/TGN marker W13Y (left, Image A) and W13R (right, Image B). **E**, Image processing applying a DoG filter with a sigma of 3 and a triangle thresholding for the corresponding image A (left) and B (middle). **F**, Each white spots indicate colocalization between spots issue from the treated image A and B. **G**, Quantification (mean ±s.e.m) of the percentage of colocalization of the indicated yellow wave line (WnY) with red wave line (WnR). Statistical analysis was performed using the non-parametrical Kruskal-Wallis test (p-value=0.05) and pairwise comparisons between groups was performed according to Steel-Dwass-Critchlow-Fligner procedure (a, b, c indicate statistical difference between samples). "n" represents the estimated number of cells sampled in each condition. Scale bars, 5 µm.

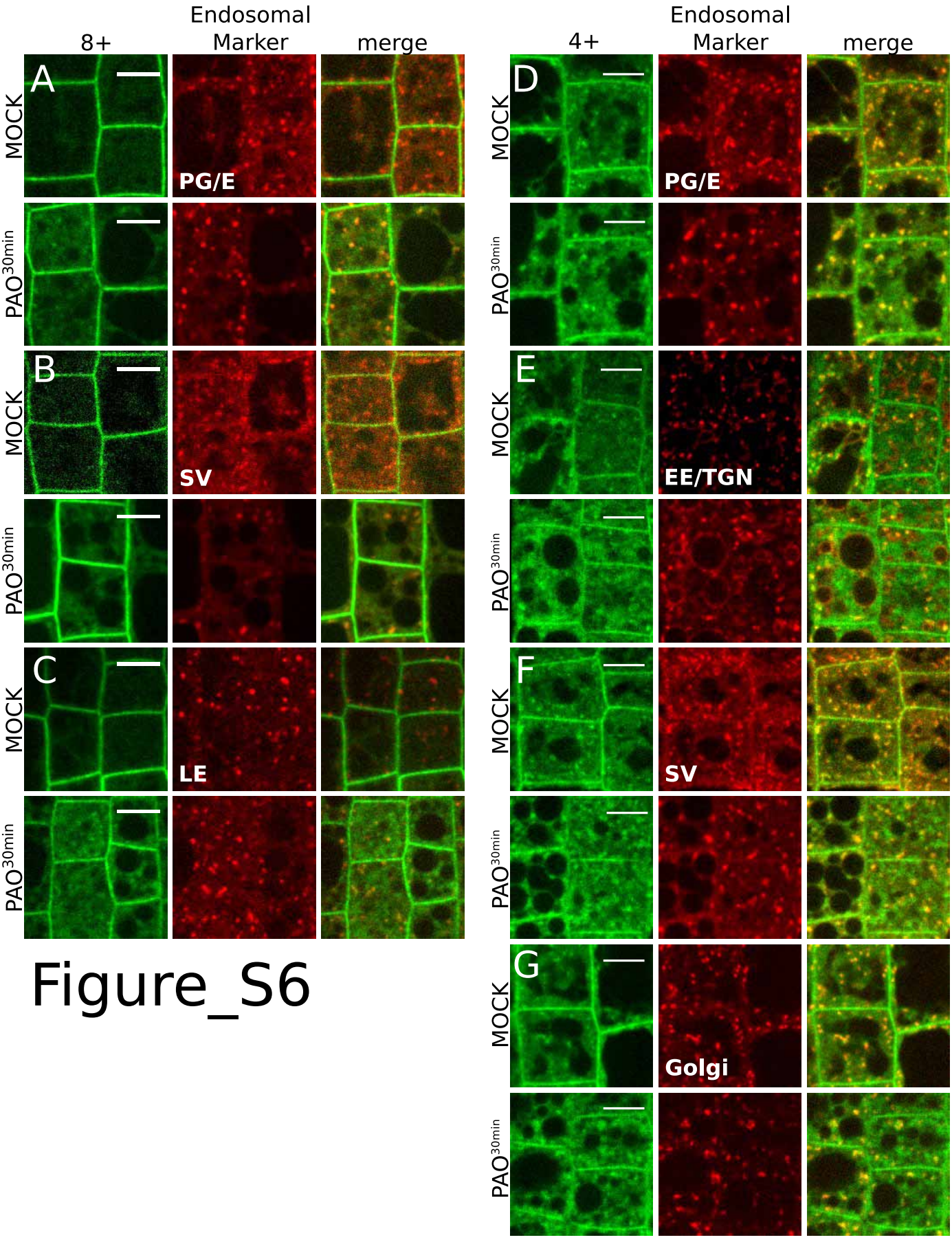
8+
Endosomal Marker
merge
4+
Endosomal Marker
merge
A
B
C
D
E
F
G
MOCK
PAO30min
PG/E
SV
LE
EE/TGN
Golgi

Figure_S6

Figure S6 (Related to Figure 6). Effect of PAO on membrane charge sensor localization. A, Plant co-expressing mCITRINE$^{8K\text{-}Farn}$ (left) and W25R post-Golgi/endosomal marker (middle), and the corresponding merge (right) in mock condition (top) and upon 60µM PAO treatment for 30 min (bottom). **B**, Plant co-expressing mCITRINE$^{8K\text{-}Farn}$ (8+, left) and W24R secretory vesicle marker (middle), and the corresponding merge (right) in mock condition (top) upon 60µM PAO treatment for 30 min (bottom). **C**, Plant co-expressing mCITRINE$^{8K\text{-}Farn}$ (8+, left) and W7R late endosomal marker (middle), and the corresponding merge (right) in mock condition (top) upon 60µM PAO treatment for 30 min (bottom).**D**, Plant co-expressing mCITRINE$^{4K4Q\text{-}Farn}$ (4+, left) and W25R post-Golgi/endosomal marker (middle), and the corresponding merge (right) in mock condition (top) and upon 60µM PAO treatment for 30 min (bottom). **E**, Plant co-expressing mCITRINE$^{4K4Q\text{-}Farn}$ (left) and W24R secretory vesicle marker (middle), and the corresponding merge (right) in mock condition (top) and upon 60µM PAO treatment for 30 min (bottom). **F**, Plant co-expressing mCITRINE$^{4K4Q\text{-}Farn}$ (4+, left) and VHA-A1-RFP early endosomal marker (middle), and the corresponding merge (right) in mock condition (top) and upon 60µM PAO treatment for 30 min (bottom). **G**, Plant co-expressing mCITRINE$^{4K4Q\text{-}Farn}$ (4+, left) and W18R Golgi marker (middle), and the corresponding merge (right) in mock condition (top panel) and upon 60µM PAO treatment for 30 min (bottom). Scale bars, 5 µm.

Chapter III : A tunable lipid rheostat steers Rho-mediated auxin signalling

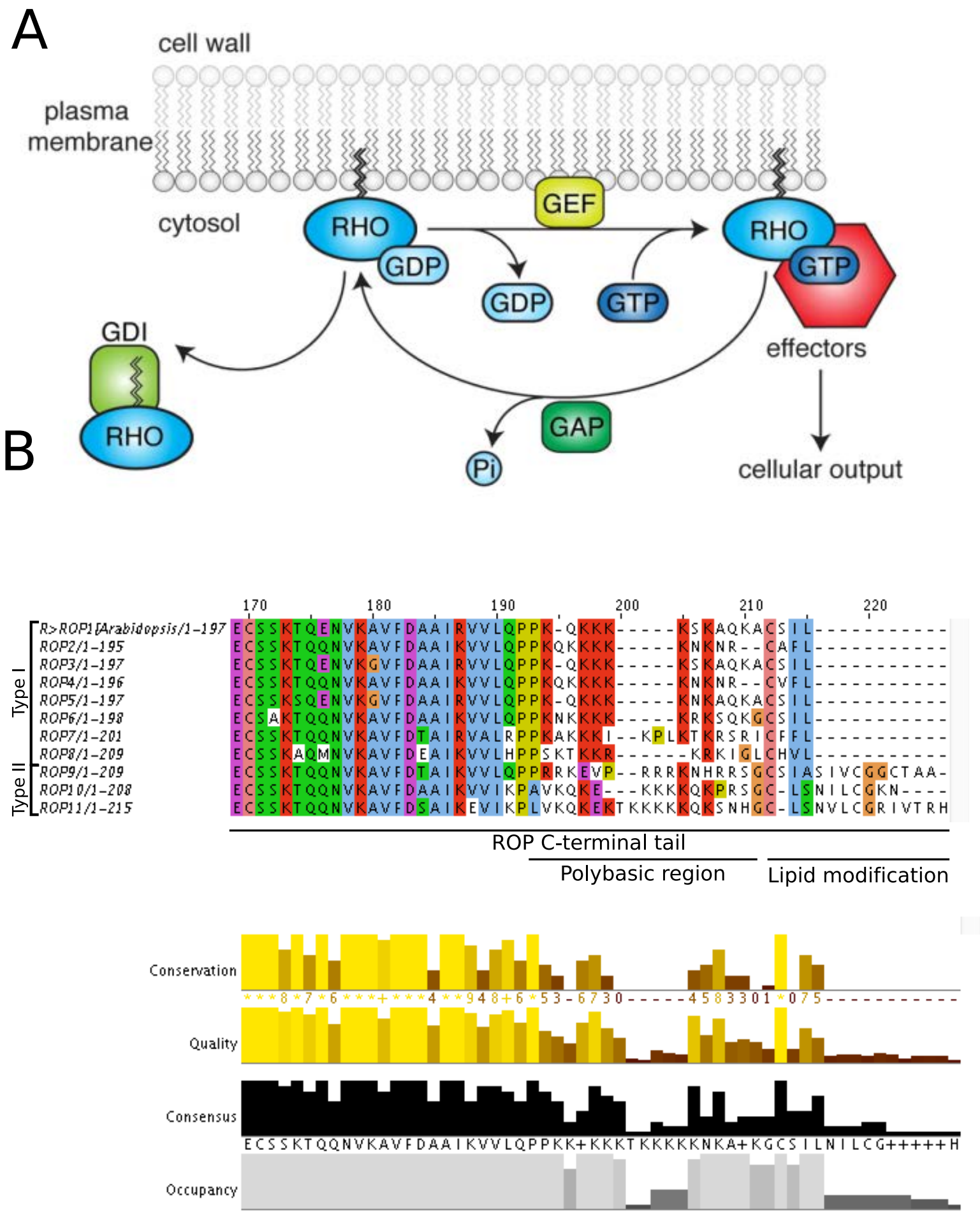

Figure 26. RhoGTPase family in plants. A, Schematic representation of the GTP/GDP cycle of the GTPase. **B,** Alignment of the C-terminal tail of ROP family members that allowed to determine their affiliation according to their lipid modification. Alignment was generated from Jalview using WSclustal.

a. General introduction on Rho of plant GTPases.

Small GTPase proteins are involved in a wide range of processes such as signal transduction, cell proliferation, cytoskeletal organization, and intracellular membrane trafficking in eukaryotic cells (Etienne-Manneville and Hall, 2002). The Arabidopsis genome contains 93 genes that encode small GTP-binding protein homologs. Phylogenetic analysis of these genes shows that plants contain Rab, Rho, Arf, and Ran GTPases, but no Ras GTPases compare to yeast and mammals (Vernoud, 2003). Plant Rho GTPases are called Rho-Of-Plant (ROP) (but are sometime also referred to as RAC proteins, notably in plant other than Arabidopsis such as Tobacco or Rice). They function as molecular switches that cycle between GTP-bound state (so called “active” form) to GDP-bound state (so called “inactive” form). In the active state, they interact with target proteins that are called effectors to promote downstream signal processing. The cycle is highly regulated by three classes of protein: i) ROP guanine nucleotide exchange factors (GEFs) catalyze nucleotide exchange and mediate activation; ii) GTPase-activating proteins (GAPs) stimulate GTP hydrolysis and thereby promote the GDP-bound state, leading to inactivation (Wu et al., 2011) and iii) guanine nucleotide exchange inhibitors (GDIs) extract the inactive GTPase from membranes (Figure 26A). In Arabidopsis, the ROP family contains 11 members divided into two classes based on their C-terminal tail sequence: ROP-type I from ROP1 to ROP8 and ROP-type II from ROP9 to ROP11 (Figure 26B-C). The Arabidopsis genome encodes fourteen ROPGEFs, six ROPGAPs and three ROPGDIs to regulate the GDP-GTP cycle. All ROP are prenylated (geranylgeranylation) at their C terminus, and this is required for function and localization at the plasma membrane(Sorek et al., 2011) (Figure 26C).

ROPs are central regulators controlling a plethora of signaling events involved in growth and developmental aspects but also plant defense responses. ROPs regulate cell growth, morphogenesis and polarity of highly polarized cells notably the pollen tube, root hairs, pavement cells but also root epidermal cell during the gravitropic response. At the cellular level, ROPs tune cytoskeleton organization of F-actin and microtubules and intracellular membrane trafficking such as endocytosis and exocytosis to establish proper growth, cell polarity and morphogenesis (Nagawa et al., 2010; Paciorek et al., 2005; Chen et al., 2012; Lin et al., 2012; Nagawa et al., 2012; Robert et al., 2010; Xu et al., 2014; Xu et al., 2010; Stanislas et al., 2015). Translation reinitiation requires

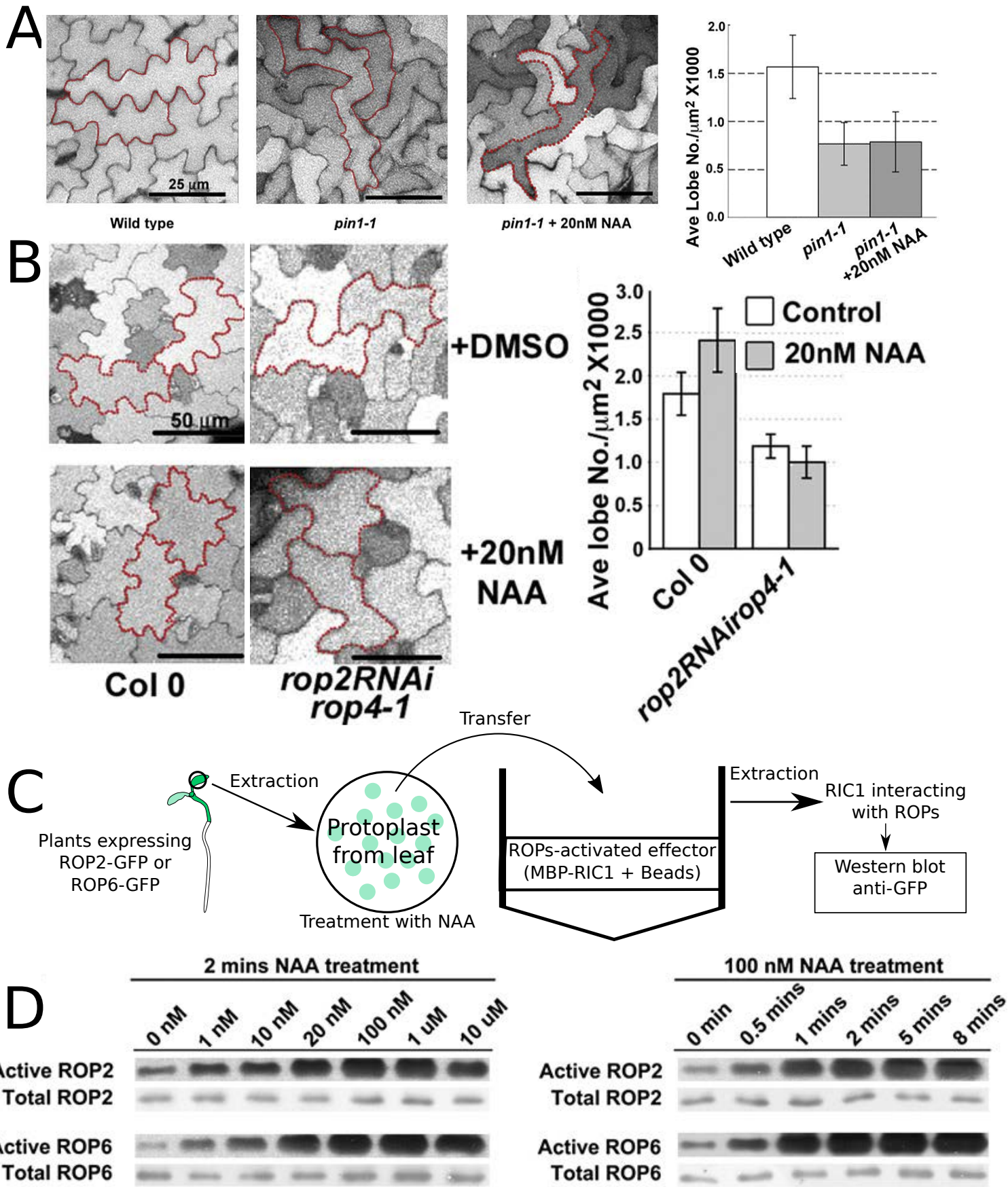

Figure 27. Auxin signaling pathway in pavement cells (PC) is controled by ROPs **A,** PC shapes in wild-type (left) and *pin1-1* mutant (middle). *pin1-1* PCs were slender with few lobes, a phenotype similar to a *rop2-1rop4-1* double knockout mutant (see Panel B). 20 nM NAA was unable to rescue *pin1-1* phenotype in PCs (right). **B,** Auxin increased interdigitation of WT but not in the *ROP2RNAi rop4-1*. Seedlings were cultured in liquid MS with or without 20 nM NAA, and cotyledon PCs were imaged 4 days after stratification. Quantitative analysis of PC interdigitation. The degree of interdigitation was quantified by determining the density of lobes for each PC (Figure S1A). Data are mean lobe number per mm^2 ± SD (n > 400 cells from three individual plants). **C,** Schematic representation of the procedure allowing to quantify the amount activated ROP in presence of auxin analog NAA. **D,** Auxin dosage responses of ROP2 and ROP6 activation. Protoplasts from leaves of transgenic GFP-ROP2 or -ROP6 seedlings were treated with the indicated concentrations of NAA for 2 min (left), or treated with 100 nM NAA for the indicated times (right). GTP-bound active GFP-ROP2 or -ROP6 and total GFP-ROP2 or -ROP6 (GDP and GTP forms). Results from one out of five independent experiments with similar results are shown. ROP2 and ROP6 experiments were conducted in parallel under identical conditions. Adapted from Xu et al., 2010.

ROP2 activity since auxin activates ROPs to promote target of rapamycin (TOR) activation. Among many function, the TOR pathway is critically required for translation reinitiation of mRNAs encoding proteins such as transcription factors, protein kinases and growth factors (Schepetilnikov et al., 2017). Moreover, ROP2 is involved in light-auxin transduction signal by inducing TOR activation, which in turn controls cell cycle transcription factors (Li et al., 2017b). ROPs also regulate the activity of plasma membrane-associated NADPH oxidase complexes, resulting in the production of reactive oxygen species and thereby modulating plants defense responses (Choudhury et al., 2017). In parallel, ROPs activate the abscisic acid hormonal signaling pathway acting in the negative regulation of stomatal closure upon stresses (Choudhury et al., 2017). Auxin acts in several signaling pathways upstream of ROP activation. In the next paragraph, I will detail the role of auxin upstream of ROP activation in two different developmental processes, the pavement cell morphogenesis and the gravitropic response.

b. ROPGTPase as a central regulator of the ‘non-genomic’ auxin signaling pathway

Auxin has been described to be perceived through TIR1/AFB receptors into the nucleus where it controls various developmental aspects. This pathway corresponds to the so called “genomic” auxin pathway. However, during the last decade, a second pathway, which relies on auxin perception at the plasma membrane and involves receptor like kinases have been uncovered. This second pathway mediate rapid cellular responses in the absence of transcription and translation corresponding to the so called “non-genomic” auxin pathway (Perrot-Rechenmann, 2010). Here, I will focus on the “non-genomic” auxin pathway since ROP signaling occurs at the plasma membrane.

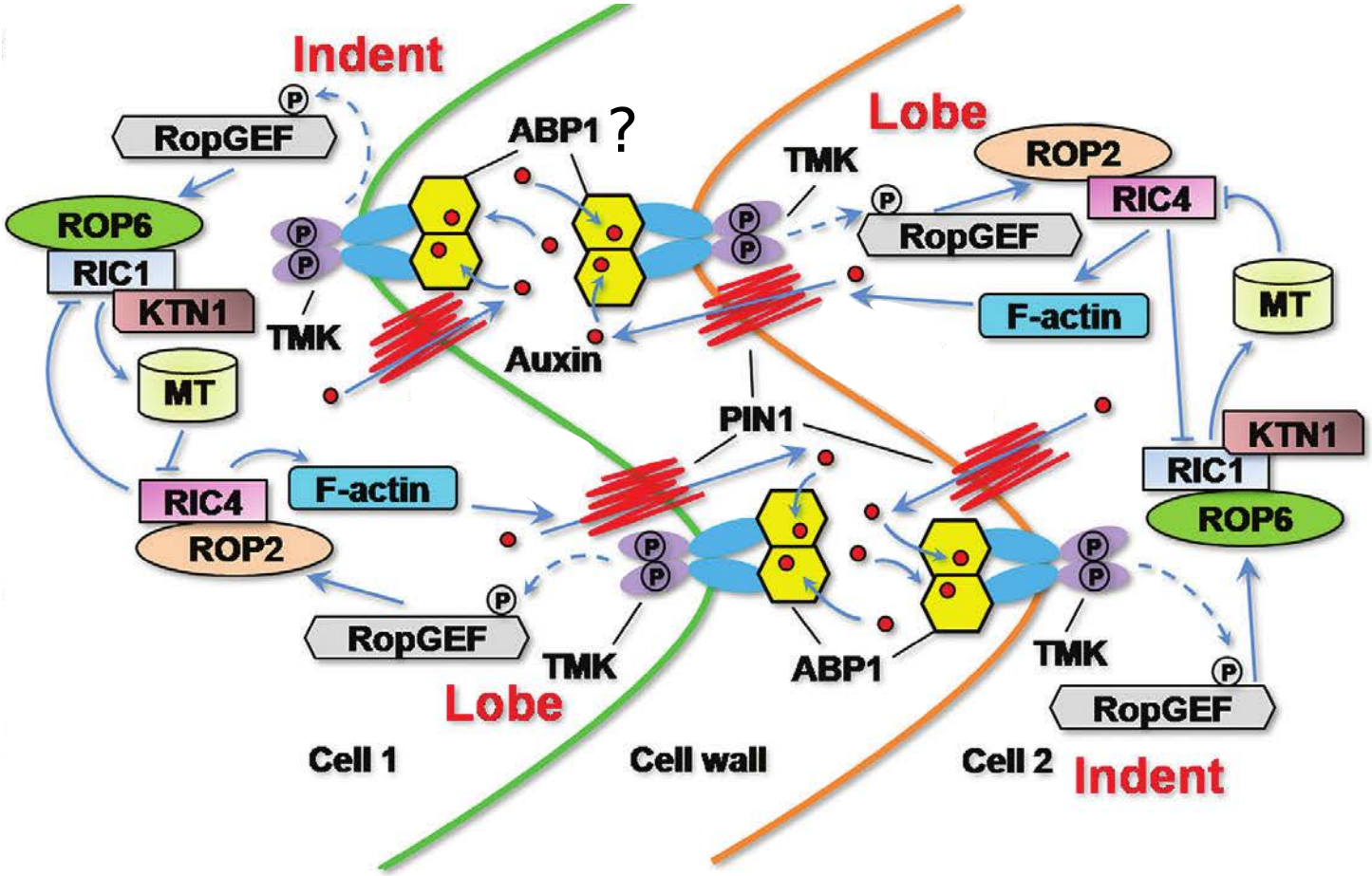

Figure 28. A working model for auxin control of pavement cells interdigitated pattern Control of interdigitated pattern through both inter- and intracellular coordination of the ROP2 and ROP6 pathways. On one hand, interdigitated growth of PCs is regulated by an auxin-dependent self-organizing mechanism. Auxin activates the ROP2 pathway via the cell surface ABP1–TMK auxin receptor complex and subsequent downstream RopGEF. The ROP2–RIC4 pathway exports auxin to locally amplify extracellular auxin through the ROP2–PIN1 positive feedback loop. PIN1-exported auxin at the lobe sites can diffuse across the cell wall to coordinately activate ROP6–RIC1 at the complementary indenting site through another ABP1–TMK auxin receptor complex. Mutual inhibition of the ROP2 and ROP6 pathways maintains ROP polarity and promotes lobe protrusion and neck indentation. According to controversial role of ABP1 in the litterature I choose to omit its role and discuss its involvement in the "non-genomic" auxin signaling pathway. Adapted from Chen et al., 2015.

i. Auxin influence the interdigitating status of leaf pavement cells

Leaf growth is controlled by interdigitated epidermal cells named pavement cells (PCs). Interdigitated-growth requires cell polarization that forms lobes and necks allowing the establishment of an epidermal jigsaw-puzzle pavement. Addition of exogenous auxin promotes lobe formation in a dose-dependent manner, while auxin biosynthesis mutants present a decrease of lobes that can be rescue by adding exogenous auxin (Xu et al., 2014; Xu et al., 2010 ; Figure 27B). Auxin can be transported actively across cells and tissues by specialized plasma membrane-associated protein, such as auxin influx or efflux carriers. Overexpression of an intracellular auxin-efflux carrier (PIN1) increases the presence of auxin in PCs that positively regulates the number of lobes formation (Guo et al., 2015; Li et al., 2017a). Loss-of-function *pin1* mutant also presents an altered PC phenotype that cannot be rescue by exogenous auxin treatment (Xu et al 2010) (Figure 27A). In addition, inhibition of polar auxin transport by 1-N-Naphthylphthalamic acid (NPA) affects wild-type pavement cell morphology (Ringli et al., 2008; Xu et al., 2014). This result suggests that PIN1-mediated polar auxin transport is critical for PC shape-establishment and acts as a modular regulator of leaf cell morphogenesis.

ii. Auxin activates ROPs to orchestrate cytoskeletal rearrangement required to establish pavement cell polarity.

Rho-like guanosine triphosphatases (GTPase) of plants (ROP) such as ROP2/ ROP4 and ROP6 are activated by auxin (Craddock et al., 2012) (Yang and Lavagi, 2012; Schepetilnikov, 2017; Xu et al., 2010). The subcellular organization of ROP2 and ROP6 is different since ROP2 accumulates slightly more in the intracellular side of the lobes than in the necks, while ROP6 accumulates preferentially in the neck (Fu et al., 2005). However, both ROP2 and ROP6 gain-of-function experiments show a loss of the jigsaw-puzzle shape of the PCs by a reduction in their number of lobes and necks (Fu et al., 2002; Lin et al., 2013; Fu et al., 2009; Poraty-Gavra et al., 2013). Despite *rop2* and *rop6* and *rop2*/*rop4* mutants present similar phenotypes, a reduction in their number of

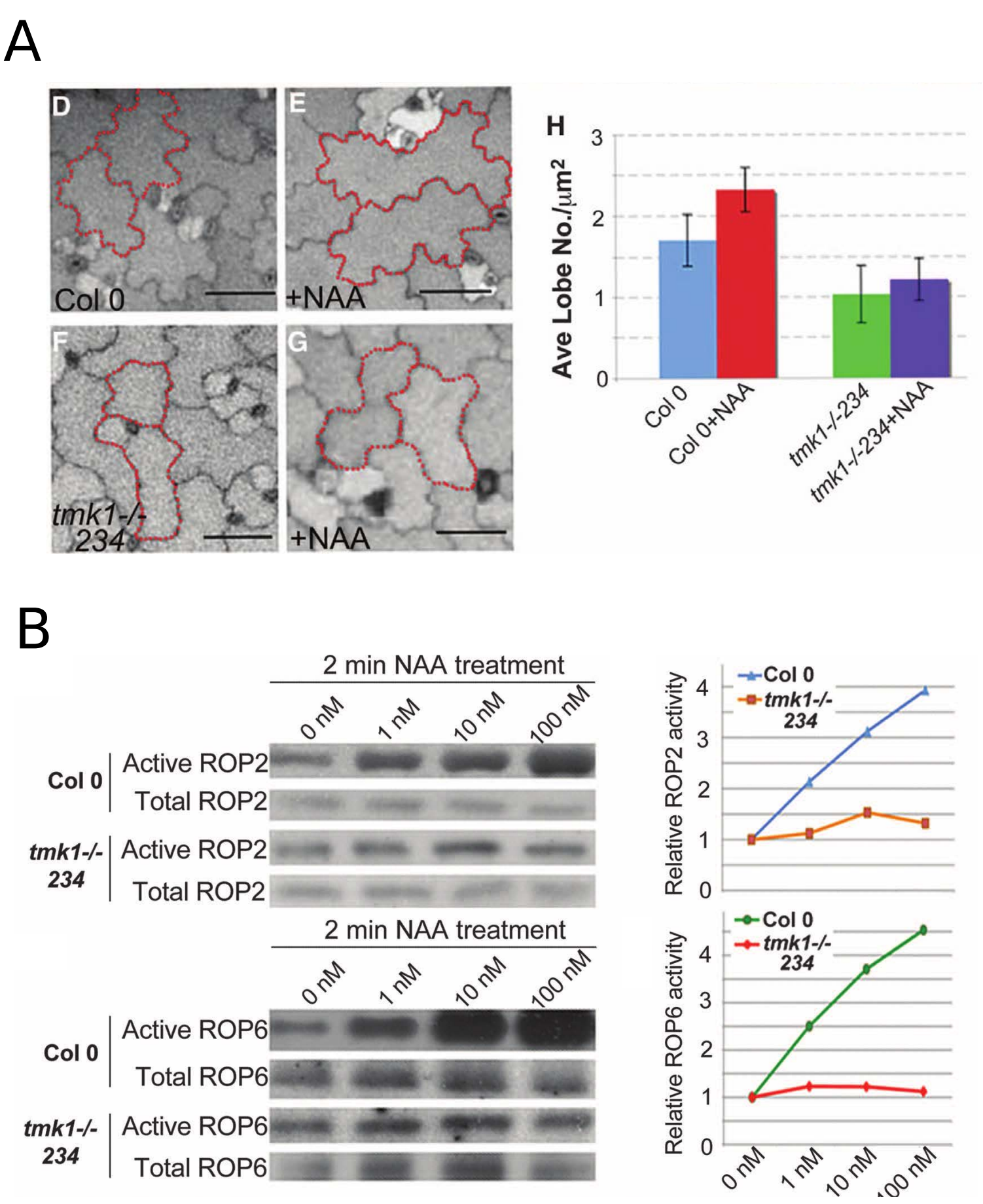

Figure 29. TMKs activate ROPs to regulate pavement cell morphogenesis A, Pavement cell phenotype of the wild type with (D) or without (E) auxin (20 nM NAA) treatment, and *tmk1*$^{-/-}$*;tmk234* quadruple mutant with (F) or without (G) auxin (20 nM NAA) treatment. Scale bars, 10 mm. The degree of pavement cell interdigitation was quantified by determining the average number of lobes per square micrometer of pavement cells (Ave Lobe No./mm2) (H). Error bars indicate SD. **B,** Upper panel, ROP2 activation by auxin in the wild type and the *tmk1*$^{-/-}$*;tmk234* mutant was analyzed by pull-down assay. Quantification of relative active GFP-ROP2 level (amount of GTP-bound GFP-ROP2 divided by amount of total GFP-ROP2) to control (as "1") is shown (B). Lower panel, ROP6 activation by auxin in the wild type and the *tmk1*$^{-/-}$*;tmk234* mutant was tested (left) and quantified (right) as above. Adapted from Xu et al., 2014.

lobes and necks, they act on cytoskeleton dynamics in different ways (Fu et al., 2005) (Figure 27B). ROP2 interacts with ROP INTERACTIVE CRIB MOTIF-CONTAINING PROTEIN4 (RIC4), an effector that drives actin assembly in the lobe region, promoting targeted exocytosis and/or endocytosis events required for cellular outgrowth. On the contrary, RIC1, a ROP6 downstream effector, promotes microtubule bundling between necks. Microtubules orient cellulose synthase activity, leading to a local thickening of cell wall between neck and thereby restricting growth (Sampathkumar et al., 2014; Fu et al., 2005; Fu et al., 2009; Lin et al., 2013; Nagawa et al., 2012). RIC1 controls microtubule organization by interacting directly with KATANIN (KAT), a microtubule-severing enzyme (Lin et al., 2013) (Figure 28).

Auxin rapidly induces ROP2 and ROP6 activity (i.e. promotes their GTP-associated form), which triggers their interaction with downstream effectors (Wu et al., 2011; Wu et al., 2011; Xu et al., 2010) (Figure 27C). In the presence of auxin, activated ROP2 interacts with RIC4 that stabilizes actin and decrease PIN1 internalization in the lobe region. A reduction of PIN1 endocytosis rate consequently accumulates PIN1 in the lobe region that seems to be required for normal pavement cell shape establishment (Nagawa et al., 2012) (Figure 28). The proposed model suggests that PIN1 exports auxin preferentially in the lobe region, which in turn activates ROP2, which itself promotes PIN1 localization in lobes. This double positive feedback loop may act as a self-organizing system in the establishment of polar PIN1 distribution in PCs and subsequent lobe outgrowth.

iii. TRANSMEMBRANE RECEPTOR KINASEs (TMKs) act upstream of ROP signaling in the “non-genomic” auxin signaling pathway

The receptor like kinases (RLK) from the TRANSMEMBRANE RECEPTOR KINASEs (TMKs) family (TMK1 to TMK4) have been proposed to act upstream of ROP2/ROP6 activation (Xu et al., 2014; Xu et al., 2010). Multiple combination-mutants in TMK genes present altered PCs shape that cannot be rescued by auxin treatment (Xu et al., 2014) (Figure 29A). In the quadruple *tmk1234* mutants, the ROP2 effector RIC4 is mislocalized in the cytosol, while ROP6 effector RIC1

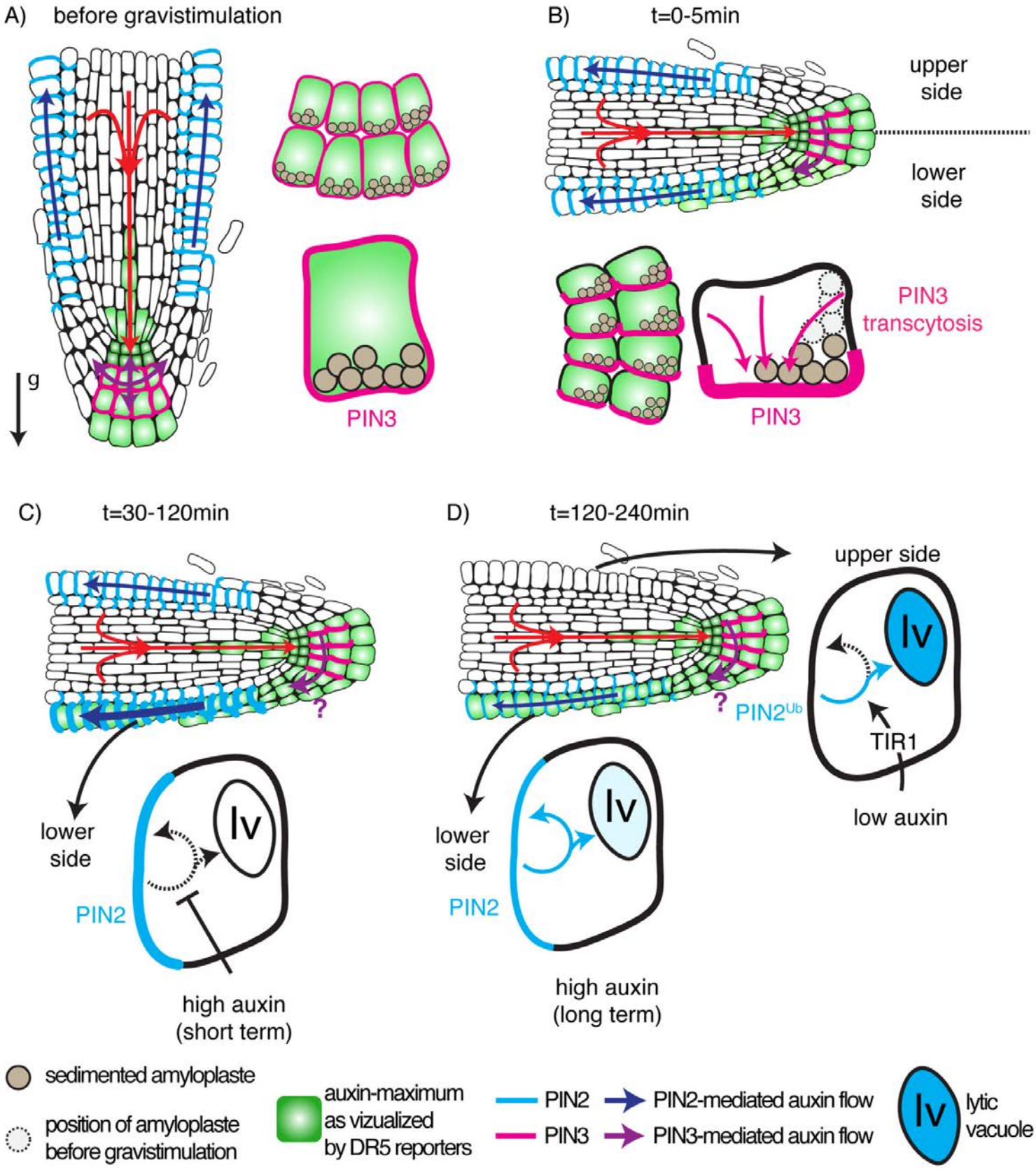

Figure 30. Auxin fluxes and PIN trafficking during the gravitropic root response. **A,** Auxin fluxes and PIN2/PIN3 localization in the primary root tip before gravistimulation. Note the position of sedimented amyloplasts in the collumela. The arrow with the 'g' letter indicates the gravity vector. **B,** Auxin fluxes and PIN2/PIN3 localization in the primary root tip from 0 to 30 min after gravistimulation. Note the movement of amyloplasts according to the new gravity vector, which triggers PIN3 transcytosis to the lower part of the cell and initiates the establishment of an asymmetric auxin maximum between the upper and lower part of the root. **C,** Auxin fluxes and PIN2/PIN3 localization in the primary root tip from 30 to 120 min after gravistimulation. High auxin in the lower part of the root inhibits PIN2 endocytosis, which promotes its localization at the plasma membrane and reinforce asymmetric auxin localization. Accumulation of auxin on the lower part of the root locally inhibits cell elongation, which triggers root bending. **D,** Auxin fluxes and PIN2/PIN3 localization in the primary root tip from 120 to 240 min after gravistimulation. Inhibition of endocytosis by auxin is transient and PIN2 endocytosis is re-established in the lower part of the root. In the meantime, low auxin on the upper part of the root triggers PIN2 degradation in a TIR1/AFBs-dependent manner. Note that the times indicated are compiled between those reported by Band et al., 2012 and Baster et al., 2013, but may vary according to the experimental setup and are only indicative. It is unknown at what point during the gravitropic response PIN3 localization is reset to apolar, hence the purple question mark in C and D. Adapted from Armengot et al., 2016.

association with microtubule is impaired. Together, these results suggest that TMKs act upstream of ROPs. Importantly, auxin-induced activation of both ROP2 and ROP6 is lost in *tmk1234* mutant, demonstrating the importance of this receptor kinase family for auxin-induced activation of ROPs (Figure 29B). TMKs likely control downstream signaling components by phosphorylation. However TMK substrates are currently unknown but could be ROPGTPases themselves or ROP-GUANINE EXCHANGE FACTOR (ROP-GEF) proteins (Miyawaki and Yang, 2014).

iv. "Non-genomic" auxin signaling pathway regulates the gravitropic response through ROPGTPase

Root gravitropism response is an important feature for plants to adapt themselves to their environment. Root gravitropism response can be defined as the capacity of the root to be constantly aligned according to the gravity vector. Auxin has been proposed to be a major regulator in gravitropism perception. Both, "genomic" and "non-genomic" auxin signaling pathways are involved in this response. Here, I report only the involvement of the "non-genomic" auxin signaling pathway. Active auxin transport modulates auxin enrichment in some regions with the possibility to generate an auxin maximum and minimum. When the root is aligned according to the gravity vector, auxin is transported equally to both side of the root tip. However, when the root is not aligned, auxin is differentially transported. Auxin is accumulated in the basal part of the root tip creating an auxin maximum in this region and an auxin minimum in the upper part (Figure 30). Auxin accumulation and depletion in those two regions set up a differential growth, promoting the inhibition and activation of elongation growth, respectively. This differential growth leads to root bending and to the realigment of the root tip according to the gravity vector (Figure 30). The molecular mechanisms behind root gravitropism have been intensely studied during the last decade (Armengot et al., 2016). PIN proteins (which are auxin efflux carriers), notably, PIN2 and PIN3 are key regulator of the gravitropic response. PIN1 transports auxin from the root top to the root tip through the vascular tissue to reach specialized cells corresponding to the collumela region.

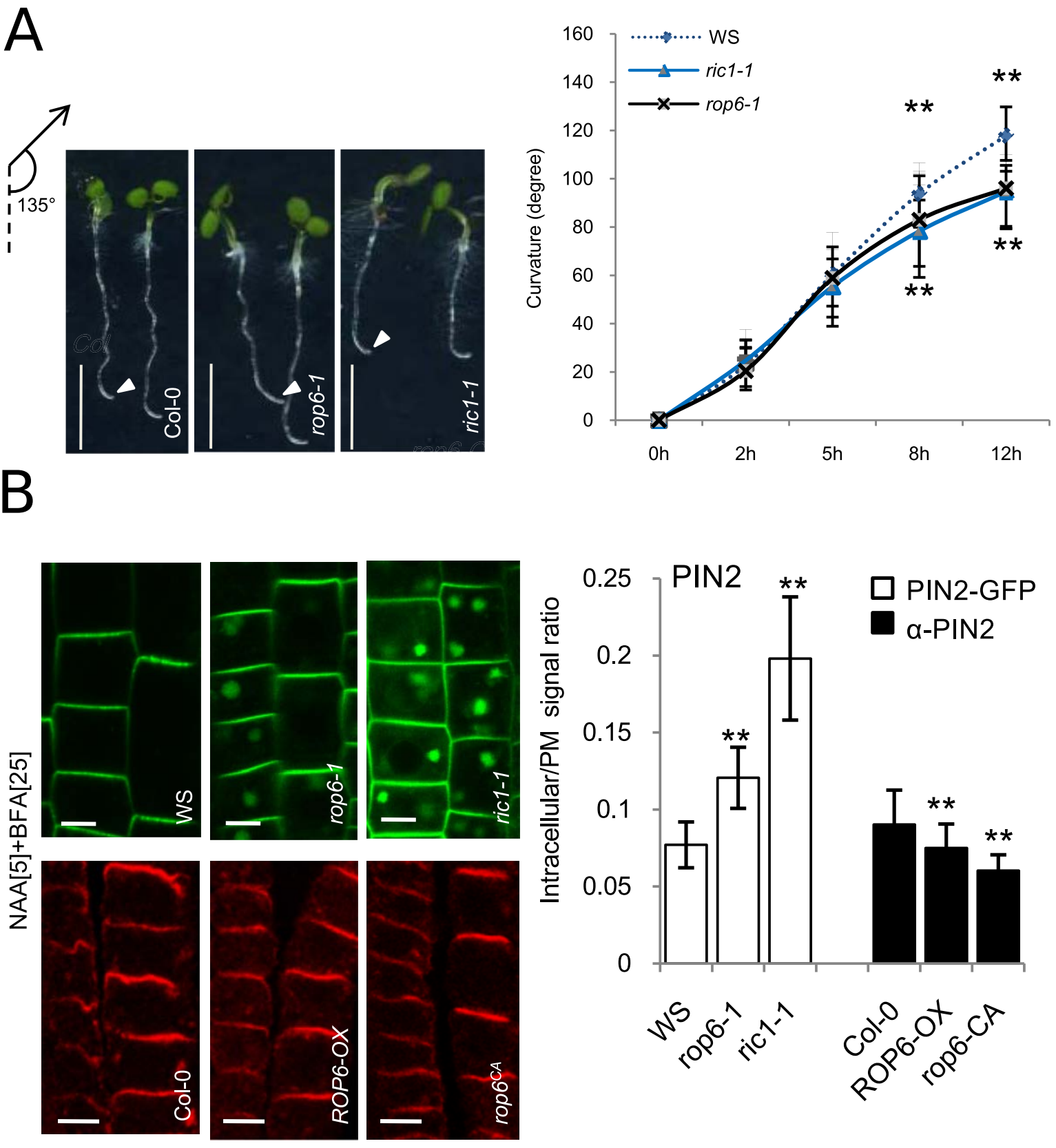

Figure 31. ROP6 controls gravitropism response through the inhibition of PIN2 endocytosis. A, *rop6-1* and *ric1-1* mutants were less sensitive to gravitropic stimulation. The arrowheads highlight the reorientation angle. Scale bar represents 2 mm. The value was the average angle of roots after 2 hr, 5 hr, 8 hr, and 12 hr of 135 reorientation growth (n > 30). **B,** *rop6-1* and *ric1-1* were less sensitive to auxin, whereas ROP6-OX and rop6CA were more sensitive to the inhibitory auxin effect on endocytosis. Col-0, rop6-1, ric1-1 (all in PIN2-GFP background), ROP6-OX (a-PIN2), and rop6CA (a-PIN2) were pretreated with NAA (5 mM, 30 min), and then were cotreated with NAA (5 mM) and BFA (25 mM) for 90 min. GFP is green and a-PIN2 is red. Scale bar represents 5 µm. Adapted from Chen et al., 2012.

Collumela cells contain amyloplast, which sediment according to the gravity. In non-gravi-stimulated root, amylopasts are sedimented on the basal part of the collumela cells. PIN3, which is expressed in these cells, is non-polar and distribute auxin on both sides of the root(Figure 30). Gravitropism stimulation induces the sedimentation of amyloplasts toward the new basal part of the cells[31]. This sedimenting amyloplast induces a signal, which is perceived and transduce by largely unknown molecular components that ultimately leads to PIN3 repolarization toward the new basal pole of the cell (Figure 30). This response happens within minutes after gravistimulation. PIN3 polarization leads to preferential auxin transport toward the basal part of the root, generating an epidermal auxin maximum on the lower side of the root and as a consequence a depletion of auxin in the upper side[31]. Accumulation of auxin promotes the inhibition of endocytosis which is required for epidermal PIN2 accumulation at the basal part of the root and thereby amplify the asymmetric auxin accumulation between the two root sides (Paciorek et al., 2005; Robert et al., 2010). A 'non-genomic' pathway, resembling the pathway described above for PCs establishment and regulated by ROP6, is involved in the inhibition of endocytosis by auxin (Chen et al., 2012; Lin et al., 2012). *rop6* and its effector *ric1* mutants present similar defects in the gravitropic response, with a slow gravitropic response kinetic (Figure 31A). Concomitant treatment of auxin (which inhibits endocytosis) and brefeldin A (BFA) (which aggregates all internalized membrane within the so called BFA bodies) allowed to evaluate the rate of PIN2 internalization by counting the number of BFA bodies. Following auxin and BFA treatment, PIN2 is more internalized into BFA bodies in rop6 and ric1 loss-of-function mutants, showing an insensitivity toward auxin for both mutants (Figure 31B). Furthermore, ROP6 and RIC1 gain-of-functions are more sensitive to auxin mediated inhibition of PIN2 endocytosis. Consequently, ROP6 and RIC1 gain-of-function bend faster than their wild type counterpart during gravitropism assay (Chen et al., 2012; Lin et al., 2012). SPIKE1 (SPK1) has been identified to act upstream of ROP6 in this pathway (Lin et al., 2012). SPK1 is a Rho guanine nucleotide exchange (ROP-GEF) that is able to activate ROPGTPase through it GEF activity (Basu et al., 2008). *spk1* mutants share similar gravitropic phenotypes with *rop6/ric1* mutants: slow gravitropic bending kinetic and auxin insensitivity (PIN2 being still internalized into BFA bodies upon concomitant BFA/auxin treatment). Moreover, in vivo data based on förster resonance energy transfer (FRET) analysis and Co-IP show that SPK1 directly interacts with the GDP bound form of ROP6, indicating that SPK1 may activate ROP6 by promoting its GDP to GTP conversion. Depending on the study, SPK1 has been found to localized

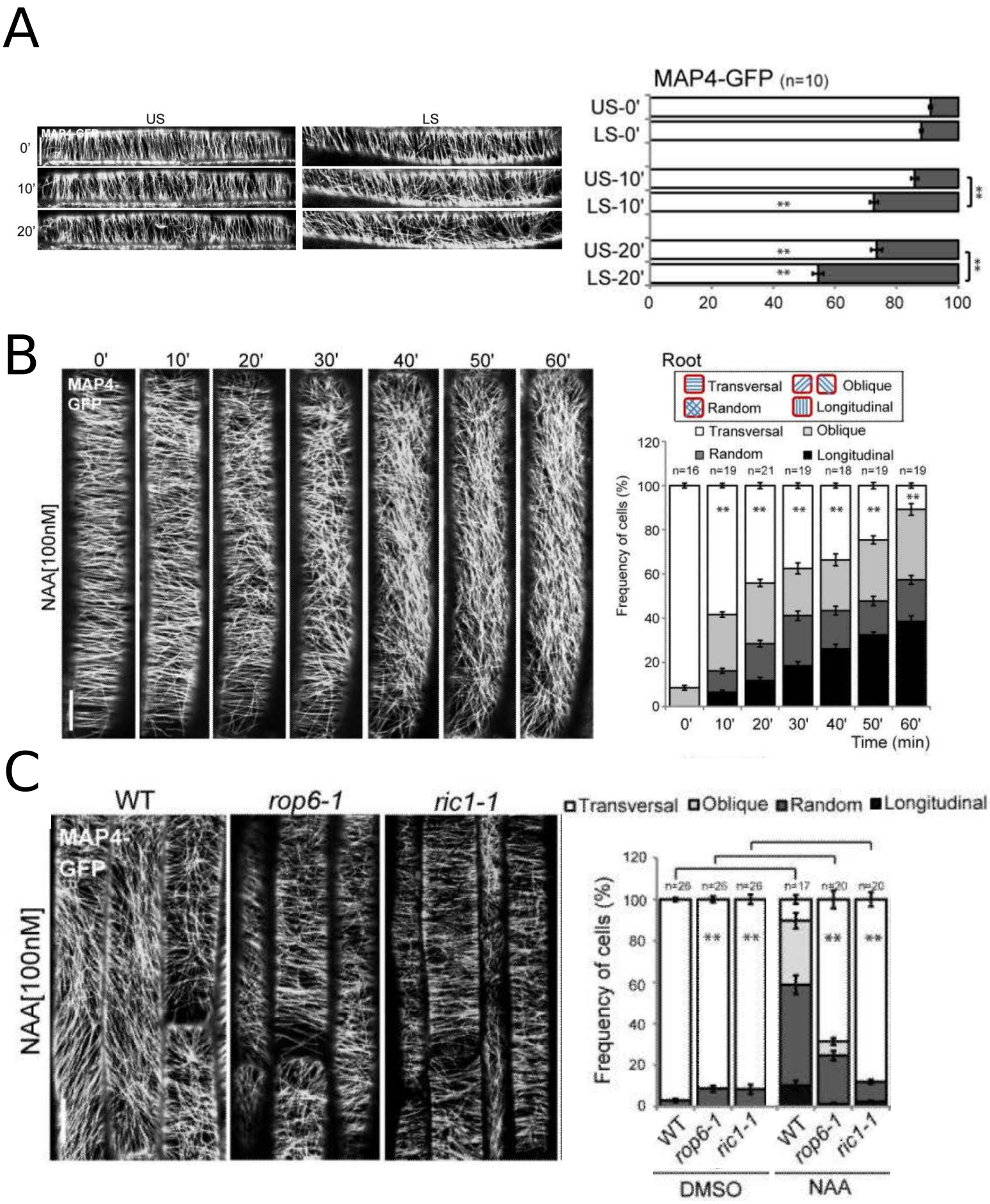

Figure 32. ROP6 controls microtubulule orientation. A, Rearrangement of MTs at the lower side (LS) compared with the upper side (US) of 90° reoriented roots of WT expressing MAP4-GFP). Two different types of MTs orientation (90±30° or 0-60°/ 120-180°) were quantified. Student's T-test was calculated for the MAP4-GFP visualization of MTs category of transversal MTs in comparison to each 0' time point and calculated for transversal MTs in the LS in comparison of the US at each time point (** $p<0.001$). **B,** Orientation in roots by time-lapse imaging following 100 nM NAA or 10 µM IAA treatment. The cartoon illustrates the four categories of MTs orientation. **C,** MTs orientation and quantification in roots of WT, *rop6-1*, *ric1-1*, following 60 min of DMSO or 100 nM NAA application. Adapted from Chen et al., 2015.

at the plasma membrane (PM) or the endoplasmic reticulum (ER). It is difficult to reconcile SPK1 localization at the ER with its function as a GEF for ROP6 at the PM, but we could hypothesize a role for ER-PM contact site in ROP signaling regulation.

To conclude, ROPs act on the "non-genomic" auxin signaling pathway by regulating endocytosis and cytoskeleton dynamics in both pavement cell and root.

v. Auxin controls microtubule organization during the gravitropic response, which may impact differential cell elongation

As aforementioned, the "non-genomic" auxin signaling pathway is involved in root gravitropism through the inhibition of endocytosis. As such, it increases the presence of auxin in the basal part of root, which in turn down regulates cell expansion, leading to root bending. Importantly, cell expansion requires ordered cytoskeleton arrangement (Perrot-Rechenmann C, et al., 2010). A study from the Perrot-Rechenmann and from Friml labs investigated in 2014 the molecular mechanisms linking the regulation of cell expansion and microtubule (MT) organization by the signaling molecule auxin. In Arabidopsis thaliana root epidermal cells, exogenous application of auxin or redistribution of endogenous auxin upon gravitropism induces rapid microtubule reorientation (i.e. roughly 30 to 120 min) from transversal to longitudinal, which is coherent with the inhibition of cell expansion (Figure 32A). In pavement cells, the canonical pathway controls cell morphogenesis through microtubule organization that relies on auxin-promoting ROP6-RIC1 interaction triggering KATANIN-dependent microtubule severing. Consistently, this pathway has been investigated in root during gravitropism response. In elongated root epidermal cells, microtubule orientation in *rop6* and *ric1* mutants are slightly affected compared to the wild type situation arguing for a role of this pathway in the regulation of cytoskeleton arrangement. Exogenous auxin treatment triggers MT arrangement in wild type but slightly affects MT alignment in *rop6* and *ric1* mutants, respectively, suggesting that auxin acts through this pathway to regulate cell expansion (Figure 32B). The latest component of the pathway, KATANIN (KAT), has not been tested in elongated root epidermal cells, however similar results as *rop6* and *ric1* mutants have been observed in

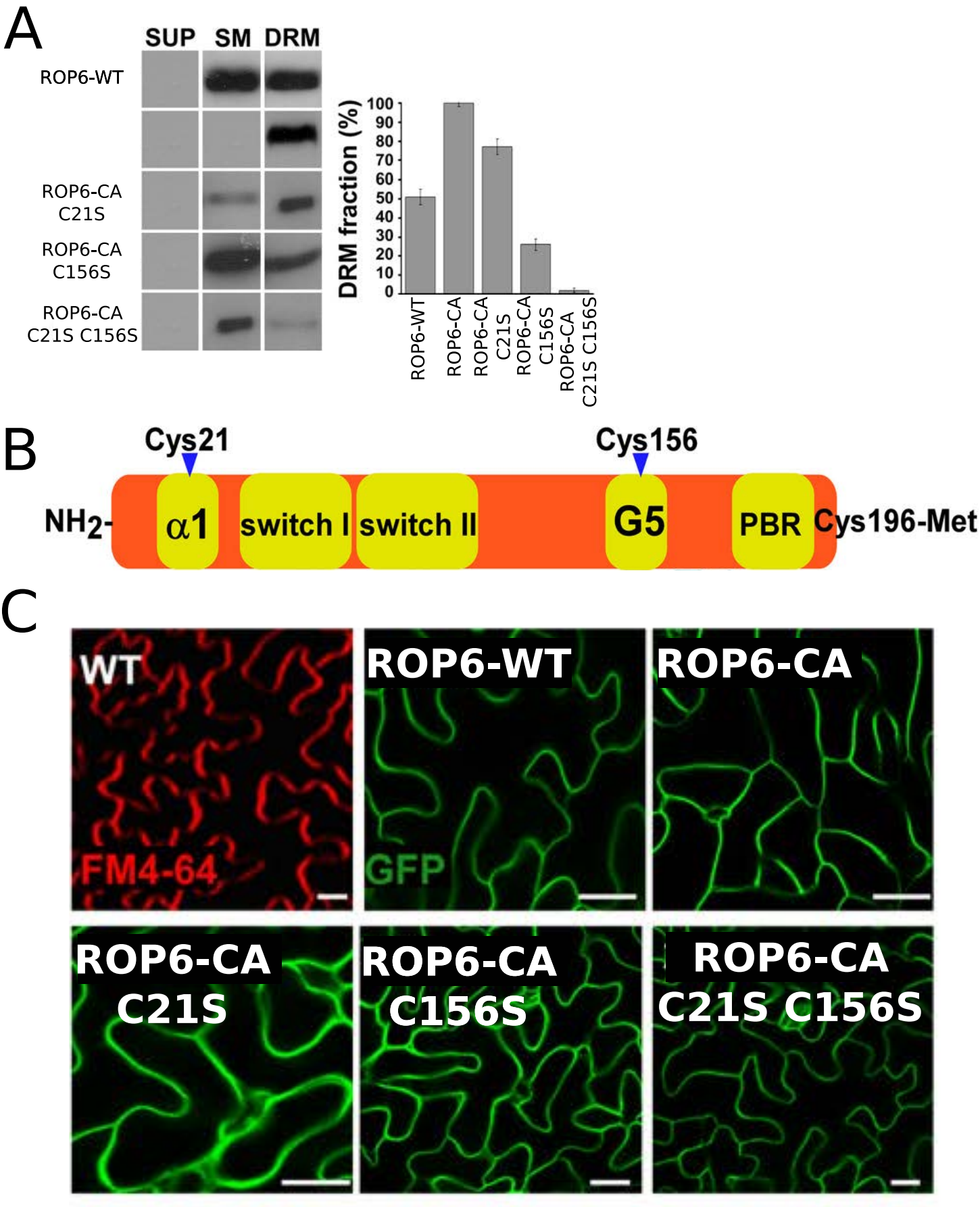

Figure 33. ROP6 signaling occurs in specialized regions of the plasma membrane by transient acylation. A, Protein immunoblots showing distribution of His6-GFP-ROP6 WT and mutants between soluble and membrane, DRM, and SM fractions. Error bars represent standard error (SE). **B,** A scheme of Arabidopsis ROP6 highlighting C21, C156, and the prenylated CaaL box C196. **C,** Confocal images showing subcellular localization of His6-GFP-ROP6 (ROP6-WT, CA, C21S, and C156S single and double mutants). WT-FM4-64 labeled nontransgenic wild-type (WT) plants. Bars correspond to 20 µm.SM, soluble membrane; DRM, detergent resistant membrane. C#S, indicates mutation of a cysteine into a serine and the number the postion of the correponding amino acid. Adapted from Sorek et al., 2010.

elongated hypocotyl. These results generalized the auxin signaling pathway organizing the cytoskeleton in root epidermal cells and suggest a role for “non-genomic” auxin signaling in cell expansion (Chen and Yang, 2014).However, the causal effect between microtubule orientation and differential cell elongation was not demonstrated in this study, which was criticized by some authors. Tobias Baskin reported few weeks later that the experiments performed by Chen et al., did not supported the hypothesis that microtubules drive growth inhibition (Baskin, 2015). All along the paper, no cell expansion data was presented showing directly that microtubule reorientation leads to inhibition of cell expansion. In fact, it is possible that auxin-mediated growth inhibition could drive microtubules to reorient, and not the contrary. Altogether, the idea that auxin regulates microtubule orientation by a “non-genomic” pathway involving ROP6/RIC1/KAT in different cell type is robust, however the direct role of microtubule reorientation in auxin-mediated growth arrest is not solidly established.

Furthermore, Sassi et al., (2014), showed that auxin, via the ROP6/RIC1/KAT pathway, regulates cortical microtubule, which affect the anisotropy of cellulose microfibrils orientation and tissue mechanics (Sassi et al., 2014). Microfibrils orientation impact directly cellulose deposition and consequently cell wall property, which is required to determined organ growth direction. However, it is difficult to directly compare the results from Chen et al., with those of Sassi et al., because they look at different cell types (root meristem and hypocotol v.s. shoot apical meristem, respectively) and different time points (30 to 120min v.s. 1 to 3 days, respectively). In any case, the pathway ROP6/RIC1/KAT seems to be a master regulator of microtubule organization, which dictates cell wall deposition and in turn control organ growth and organization.

To conclude, root gravitropic response is tightly controlled by auxin signaling that orchestrates two cellular processes corresponding to the inhibition of endocytosis and cytoskeleton organization in order to regulate cell expansion.

vi. Activated ROPs are localized in the so called detergent resistant membrane (DRM) to trigger proper signaling

ROPs activation requires the switch from GDP to GTP to interact with downstream effectors and trigger signal transduction. Shaul Yalovsky's lab in 2010 addressed how activated ROPs behaves at the plasma membrane. They showed that the constitutive active version of ROP6 (ROP6-CA) is locked in its GTP form and interact persistently with effectors. Biochemical experiment allowing to fractionate membrane into two different pools corresponding to soluble membrane (SM, non-ordered membrane) and detergent resistant membrane (DRM, ordered membrane or raft) depending on lipid enrichment (Stanislas et al., 2015) showed that ROP6-CA localized in DRM while ROP6 localized into SM (Figure 33A). This argue that ROP6 is associated with specialized region of the plasma membrane when activated. The association with DRM required strong interaction between lipids and proteins such as hydrophobic interaction. The C-terminal tail of ROPs contain a prenylation site, which presents low affinity for DRM (Melkonian et al., 1999). Moreover, only activated-ROP6 is associated with DRM, which favors for a transient lipid modification on ROP6. Using gas chromatography-coupled mass spectrometry, Sorek et al., identified two cysteine residues that can be S-acylated and which corresponds to transient lipid modification in the G domain of the GTPase (Figure 33B). Overexpression of ROP6-CA leads to squared pavement cells compare to the wild type control, in which pavement cells have a typical jigsaw puzzle shape with lobes and indentations. Mutations in both ROP6 cysteines prevent S-acylation and abrogate the squared pavement cells phenotype associated with ROP6 overexpression (Figure 33C). Consistently biochemical membrane fractionation prevents this ROP6-CA cysteine mutants to associate with DRM. Taken together, these results show that activated-ROP6 require transient S-acylation for proper addressing at the plasma membrane into DRM likely to interact with downstream effectors(Sorek et al., 2010). As mentioned previously, "non-genomic" auxin signaling at the plasma membrane activates ROPs (notably ROP2, ROP4 and ROP6) (Chen et al., 2012; Lin et al., 2012; Xu et al., 2014; Xu et al., 2010; Schepetilnikov, et al., 2017; Li et al., 2017). In this chapter, we addressed the link between auxin-mediated ROP activation and its partitioning at the plasma membrane as well as some mechanistic aspect behinds this partitioning and role(s) in signaling and development.

Armengot, Laia, Maria Mar Marquès-Bueno, and Yvon Jaillais. 2016. "Regulation of Polar Auxin Transport by Protein and Lipid Kinases." Journal of Experimental Botany 67(14): 4015–37.

Baskin, T.I. (2015). Auxin inhibits expansion rate independently of cortical microtubules. Trends Plant Sci. *20*, 471–472.

Basu, D., Le, J., Zakharova, T., Mallery, E.L., and Szymanski, D.B. (2008). A SPIKE1 signaling complex controls actin-dependent cell morphogenesis through the heteromeric WAVE and ARP2/3 complexes. Proc. Natl. Acad. Sci. U. S. A. *105*, 4044–4049.

Chen, J., and Yang, Z. (2014). Novel ABP1-TMK auxin sensing system controls ROP GTPase-mediated interdigitated cell expansion in Arabidopsis. Small GTPases.

Chen, X., Naramoto, S., Robert, S., Tejos, R., Löfke, C., Lin, D., Yang, Z., and Friml, J. (2012). ABP1 and ROP6 GTPase Signaling Regulate Clathrin-Mediated Endocytosis in Arabidopsis Roots. Curr. Biol. *22*, 1326–1332.

Choudhury, F.K., Rivero, R.M., Blumwald, E., and Mittler, R. (2017). Reactive oxygen species, abiotic stress and stress combination. Plant J. *90*, 856–867.

Craddock, C., Lavagi, I., and Yang, Z. (2012). New insights into Rho signaling from plant ROP/Rac GTPases. Trends Cell Biol. *22*, 492–501.

Etienne-Manneville, S., and Hall, A. (2002). Rho GTPases in cell biology. Nature *420*, 629.

Fu, Y., Li, H., and Yang, Z. (2002). The ROP2 GTPase Controls the Formation of Cortical Fine F-Actin and the Early Phase of Directional Cell Expansion during Arabidopsis Organogenesis. Plant Cell Online *14*, 777–794.

Fu, Y., Gu, Y., Zheng, Z., Wasteneys, G., and Yang, Z. (2005). Arabidopsis Interdigitating Cell Growth Requires Two Antagonistic Pathways with Opposing Action on Cell Morphogenesis. Cell *120*, 687–700.

Fu, Y., Xu, T., Zhu, L., Wen, M., and Yang, Z. (2009). A ROP GTPase Signaling Pathway Controls Cortical Microtubule Ordering and Cell Expansion in Arabidopsis. Curr. Biol. *19*, 1827–1832.

Guo, X., Qin, Q., Yan, J., Niu, Y., Huang, B., Guan, L., Li, Y., Ren, D., Li, J., and Hou, S. (2015). TYPE-ONE PROTEIN PHOSPHATASE4 Regulates Pavement Cell Interdigitation by Modulating PIN-FORMED1 Polarity and Trafficking in Arabidopsis. Plant Physiol. *167*, 1058–1075.

Li, C., Lu, H., Li, W., Yuan, M., and Fu, Y. (2017a). A ROP2-RIC1 pathway fine-tunes microtubule reorganization for salt tolerance in Arabidopsis. Plant Cell Amp Environ. *40*, 1127–1142.

Li, X., Cai, W., Liu, Y., Li, H., Fu, L., Liu, Z., Xu, L., Liu, H., Xu, T., and Xiong, Y. (2017b). Differential TOR activation and cell proliferation in Arabidopsis root and shoot apexes. Proc. Natl. Acad. Sci. *114*, 2765–2770.

Lin, D., Nagawa, S., Chen, J., Cao, L., Chen, X., Xu, T., Li, H., Dhonukshe, P., Yamamuro, C., Friml, J., et al. (2012). A ROP GTPase-Dependent Auxin Signaling Pathway Regulates the Subcellular Distribution of PIN2 in Arabidopsis Roots. Curr. Biol. *22*, 1319–1325.

Lin, D., Cao, L., Zhou, Z., Zhu, L., Ehrhardt, D., Yang, Z., and Fu, Y. (2013). Rho GTPase Signaling Activates Microtubule Severing to Promote Microtubule Ordering in Arabidopsis. Curr. Biol. *23*, 290–297.

Melkonian, K.A., Ostermeyer, A.G., Chen, J.Z., Roth, M.G., and Brown, D.A. (1999). Role of Lipid Modifications in Targeting Proteins to Detergent-resistant Membrane Rafts MANY RAFT PROTEINS ARE ACYLATED, WHILE FEW ARE PRENYLATED. J. Biol. Chem. *274*, 3910–3917.

Miyawaki, K.N., and Yang, Z. (2014). Extracellular signals and receptor-like kinases regulating ROP GTPases in plants. Front. Plant Sci. *5*.

Nagawa, S., Xu, T., and Yang, Z. (2010). RHO GTPase in plants: Conservation and invention of regulators and effectors. Small GTPases *1*, 78–88.

Nagawa, S., Xu, T., Lin, D., Dhonukshe, P., Zhang, X., Friml, J., Scheres, B., Fu, Y., and Yang, Z. (2012). ROP GTPase-Dependent Actin Microfilaments Promote PIN1 Polarization by Localized Inhibition of Clathrin-Dependent Endocytosis. PLOS Biol. *10*, e1001299.

Paciorek, T., Zažímalová, E., Ruthardt, N., Petrášek, J., Stierhof, Y.-D., Kleine-Vehn, J., Morris, D.A., Emans, N., Jürgens, G., Geldner, N., et al. (2005). Auxin inhibits endocytosis and promotes its own efflux from cells. Nature *435*, 1251–1256.

Perrot-Rechenmann, C. (2010). Cellular Responses to Auxin: Division versus Expansion. Cold Spring Harb. Perspect. Biol. *2*, a001446.

Poraty-Gavra, L., Zimmermann, P., Haigis, S., Bednarek, P., Hazak, O., Stelmakh, O.R., Sadot, E., Schulze-Lefert, P., Gruissem, W., and Yalovsky, S. (2013). The Arabidopsis Rho of Plants GTPase AtROP6 Functions in Developmental and Pathogen Response Pathways. Plant Physiol. *161*, 1172–1188.

Ringli, C., Bigler, L., Kuhn, B.M., Leiber, R.-M., Diet, A., Santelia, D., Frey, B., Pollmann, S., and Klein, M. (2008). The Modified Flavonol Glycosylation Profile in the Arabidopsis rol1 Mutants Results in Alterations in Plant Growth and Cell Shape Formation. Plant Cell Online *20*, 1470–1481.

Robert, S., Kleine-Vehn, J., Barbez, E., Sauer, M., Paciorek, T., Baster, P., Vanneste, S., Zhang, J., Simon, S., Čovanová, M., et al. (2010). ABP1 Mediates Auxin Inhibition of Clathrin-Dependent Endocytosis in Arabidopsis. Cell *143*, 111–121.

Sampathkumar, A., Krupinski, P., Wightman, R., Milani, P., Berquand, A., Boudaoud, A., Hamant, O., Jönsson, H., and Meyerowitz, E.M. (2014). Subcellular and supracellular mechanical stress prescribes cytoskeleton behavior in Arabidopsis cotyledon pavement cells. eLife *3*, e01967.

Sassi, M., Ali, O., Boudon, F., Cloarec, G., Abad, U., Cellier, C., Chen, X., Gilles, B., Milani, P., Friml, J., et al. (2014). An Auxin-Mediated Shift toward Growth Isotropy Promotes Organ Formation at the Shoot Meristem in Arabidopsis. Curr. Biol. *24*, 2335–2342.

Schepetilnikov, M., Makarian, J., Srour, O., Geldreich, A., Yang, Z., Chicher, J., Hammann, P., and Ryabova, L.A. (2017). GTPase ROP2 binds and promotes activation of target of rapamycin, TOR, in response to auxin. EMBO J. *36*, 886–903.

Sorek, N., Segev, O., Gutman, O., Bar, E., Richter, S., Poraty, L., Hirsch, J.A., Henis, Y.I., Lewinsohn, E., Jürgens, G., et al. (2010). An S-Acylation Switch of Conserved G Domain Cysteines Is Required for Polarity Signaling by ROP GTPases. Curr. Biol. *20*, 914–920.

Sorek, N., Gutman, O., Bar, E., Abu-Abied, M., Feng, X., Running, M.P., Lewinsohn, E., Ori, N., Sadot, E., Henis, Y.I., et al. (2011). Differential Effects of Prenylation and S-Acylation on Type I and II ROPS Membrane Interaction and Function. Plant Physiol. *155*, 706–720.

Stanislas, T., Hüser, A., Barbosa, I.C.R., Kiefer, C.S., Brackmann, K., Pietra, S., Gustavsson, A., Zourelidou, M., Schwechheimer, C., and Grebe, M. (2015). *Arabidopsis* D6PK is a lipid domain-dependent mediator of root epidermal planar polarity. Nat. Plants *1*, nplants2015162.

Vernoud, V. (2003). Analysis of the Small GTPase Gene Superfamily of Arabidopsis. PLANT Physiol. *131*, 1191–1208.

Wu, H., Hazak, O., Cheung, A.Y., and Yalovsky, S. (2011). RAC/ROP GTPases and Auxin Signaling. Plant Cell *23*, 1208.

Xu, T., Wen, M., Nagawa, S., Fu, Y., Chen, J.-G., Wu, M.-J., Perrot-Rechenmann, C., Friml, J., Jones, A.M., and Yang, Z. (2010). Cell Surface- and Rho GTPase-Based Auxin Signaling Controls Cellular Interdigitation in Arabidopsis. Cell *143*, 99–110.

Xu, T., Dai, N., Chen, J., Nagawa, S., Cao, M., Li, H., Zhou, Z., Chen, X., Rycke, R.D., Rakusová, H., et al. (2014). Cell Surface ABP1-TMK Auxin-Sensing Complex Activates ROP GTPase Signaling. Science *343*, 1025–1028.

Yang, Z., and Lavagi, I. (2012). Spatial control of plasma membrane domains: ROP GTPase-based symmetry breaking. Curr. Opin. Plant Biol. *15*, 601–607.

Title: A tunable lipid rheostat steers Rho-mediated auxin signalling

Matthieu Pierre Platre[1], Vincent Bayle[1], Laia Armengot[1], Maria Mar Marques-Bueno[1], Audrey Creff[1], Lili Maneta-Peyret[2], Jean-Bernard Fiche[3], Mathilde Laetitia Audrey Simon[1], Marcelo Nolmann[3], Christine Miège[1], Patrick Moreau[2,4], Alexandre Martinière-Delaunay[5] and Yvon Jaillais[1#]

[1]Laboratoire Reproduction et Développement des Plantes, Université de Lyon, ENS de Lyon, UCB Lyon 1, CNRS, INRA, F-69342 Lyon, France.

[2]UMR 5200 Membrane Biogenesis Laboratory, CNRS-University of Bordeaux, Bâtiment A3 - INRA Bordeaux Aquitaine, 71 Avenue Edouard Bourlaux- CS 20032, 33140 Villenave d'Ornon, France.

[3]Centre de Biochimie Structurale, CNRS UMR5048, INSERM U1054, Université de Montpellier, 29 Rue de Navacelles, 34090, Montpellier, France

[4]Bordeaux Imaging Center, UMS 3420 CNRS, US4 INSERM, University of Bordeaux, 33000 Bordeaux, France.

[5]Biochimie et Physiologie Moléculaire des Plantes, UMR5004, INRA/CNRS/Montpellier SupAgro/Université Montpellier, 34060 Montpellier, France

Corresponding author: yvon.jaillais@ens-lyon.fr

Summary paragraph (max 200 words)

Rho GTPases are universal regulators of cytoskeleton dynamics and intracellular trafficking, which control the morphology, movement and behaviour of cells and organisms[1]. To do so, they integrate signalling pathways at the cell surface into various cellular outputs. However, it is still unclear how spatially localized activation of Rho GTPases is accomplished. In plants, ROP (RHO-OF-PLANTS) GTPases transduce auxin signalling at the plasma membrane (PM) to regulate cell and organ shape[2-9]. Here, we show that the anionic phospholipid phosphatidylserine is a rate-limiting regulator of ROP6 signalling. Using super-resolution single particle tracking, we found that phosphatidylserine forms stable assembly platforms at the PM that stabilise ROP6 into nanoclusters following auxin treatment. This immobilization of ROP6 via direct ROP/phosphatidylserine interaction is required for downstream auxin signalling. Furthermore, we found that auxin-dependent variations in the PM phosphatidylserine content tune ROP6 signalling intensity. Our results demonstrate that phosphatidylserine acts as a developmentally-controlled lipid rheostat that regulates cellular auxin sensitivity and plant development.

Phosphatidylserine (PS) is an anionic phospholipid that contributes around 2 to 5% of total phospholipid at the plant PM[10]. PS is synthesized by a single enzyme in Arabidopsis, called PHOSPHATIDYLSERINE SYNTHASE1 (PSS1)[11]. We recently showed that *pss1* knock-out mutants are not able to produce any PS but are viable, albeit sterile[12]. *pss1* mutants were dwarf with curled and twisted leaves (Fig S1a)[12]. In wild type (WT) plants, leaf epidermal pavement cells have a characteristic jigsaw-puzzle shape[2]. This organization was dramatically altered in *pss1* mutants, which exhibited squared cells,

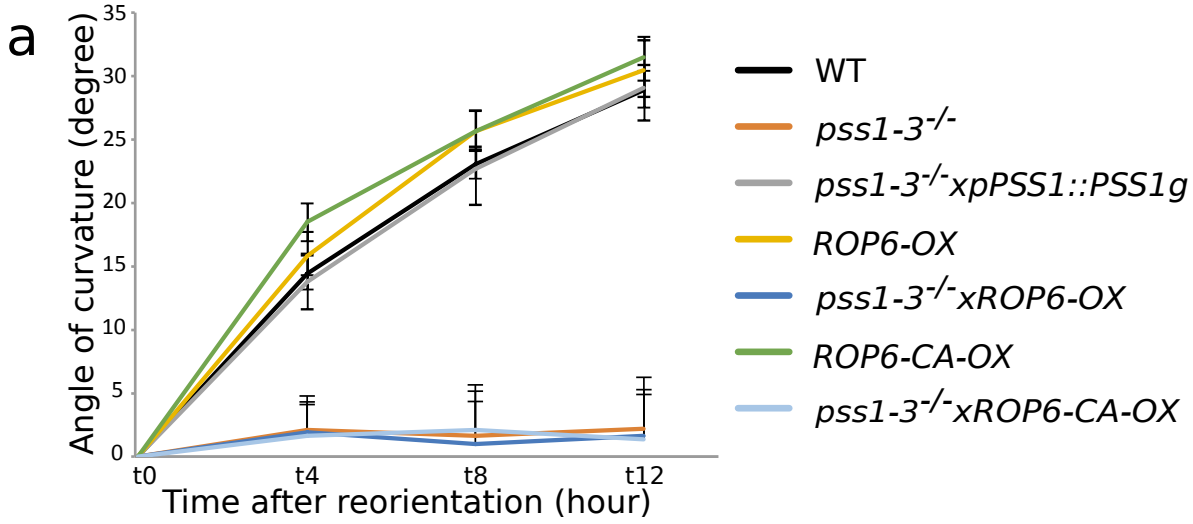
a
Angle of curvature (degree)
0
5
10
15
20
25
30
35
t0
t4
t8
t12
Time after reorientation (hour)
WT
pss1-3-/-
pss1-3-/-xpPSS1::PSS1g
ROP6-OX
pss1-3-/-xROP6-OX
ROP6-CA-OX
pss1-3-/-xROP6-CA-OX

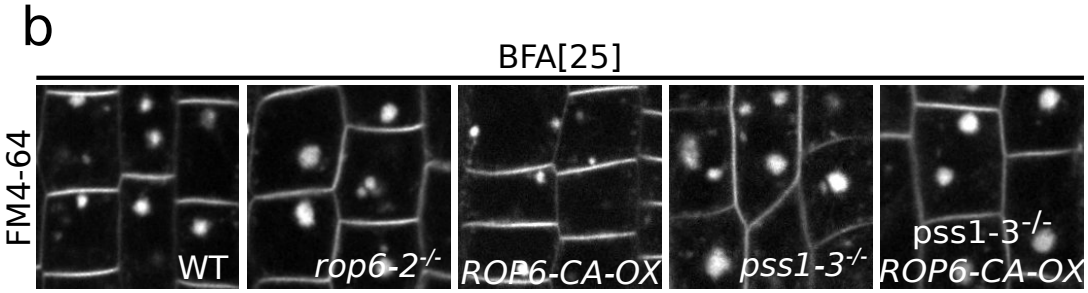
b
BFA[25]
FM4-64
WT
rop6-2-/-
ROP6-CA-OX
pss1-3-/-
pss1-3-/-
ROP6-CA-OX

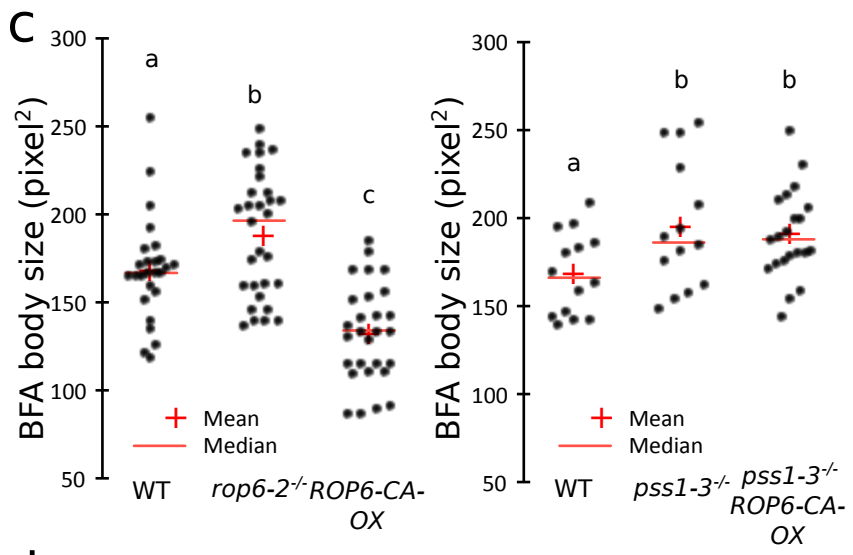
c
BFA body size (pixel2)
50
100
150
200
250
300
a
b
c
Mean
Median
WT
rop6-2-/-
ROP6-CA-OX
a
b
b
Mean
Median
WT
pss1-3-/-
pss1-3-/-
ROP6-CA-OX

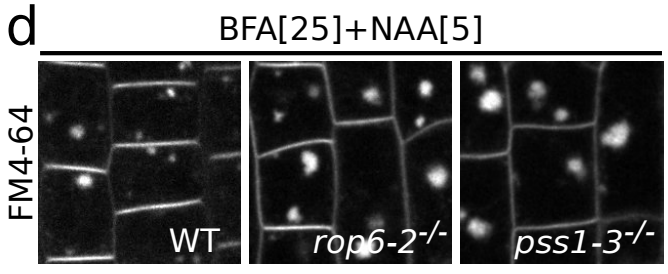
d
BFA[25]+NAA[5]
FM4-64
WT
rop6-2-/-
pss1-3-/-

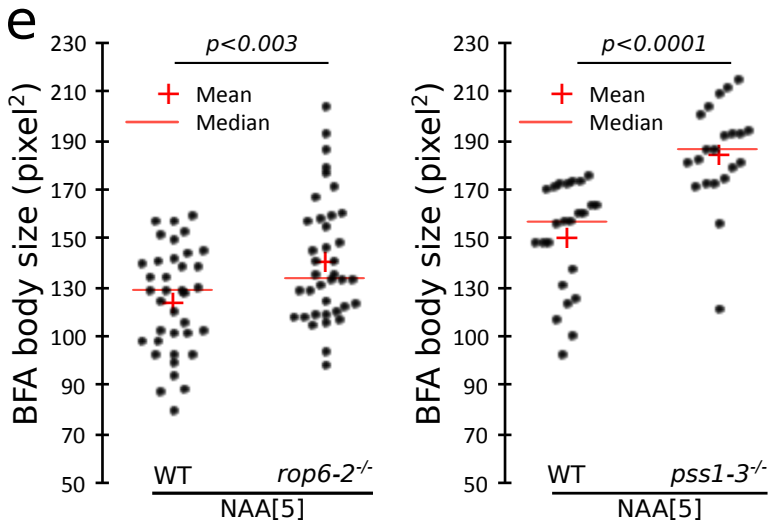
e
BFA body size (pixel2)
50
70
90
100
130
150
170
190
210
230
p<0.003
Mean
Median
WT
rop6-2-/-
NAA[5]
p<0.0001
Mean
Median
WT
pss1-3-/-
NAA[5]

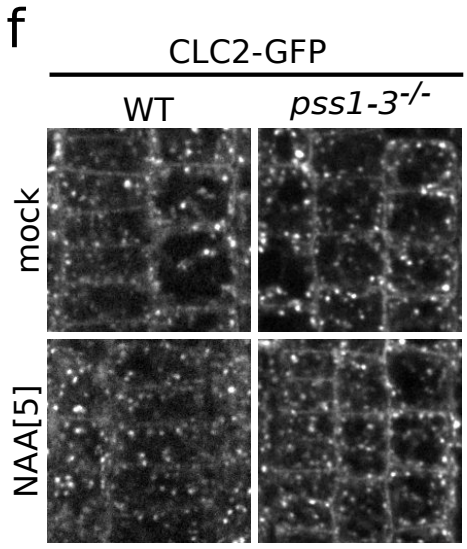
f
CLC2-GFP
WT
pss1-3-/-
mock
NAA[5]

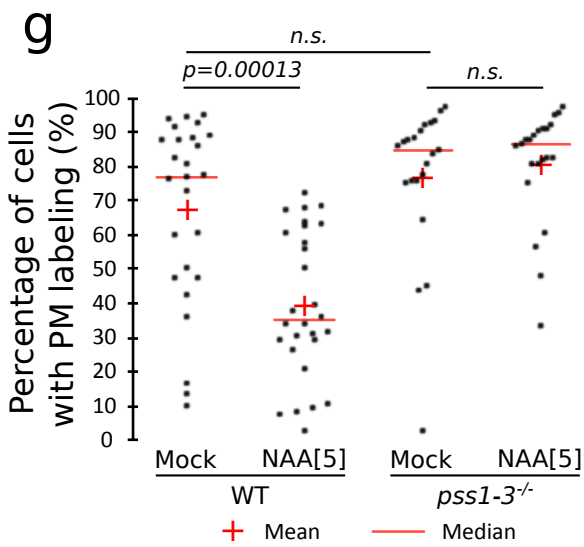
g
Percentage of cells with PM labeling (%)
0
10
20
30
40
50
60
70
80
90
100
n.s.
p=0.00013
n.s.
Mock
NAA[5]
Mock
NAA[5]
WT
pss1-3-/-
Mean
Median

Figure 1. The ROP6-dependent auxin signalling pathway is deficient in PS-less mutant. (a) Quantification of the gravitropic response in the genotypes indicated on the right. Error bars represent SEM. (b-e) Confocal images of epidermal root cells stained by FM4-64 and (b) treated with BFA, or (d) NAA and BFA, and (c and e) related quantification of the BFA body size. Letters indicate statistical difference. (f) CLC2-GFP localization in the presence and absence of NAA in WT and *pss1-3*, and (g) related quantification. For statistical analyses details see, Sup_Data_Sheet_1.

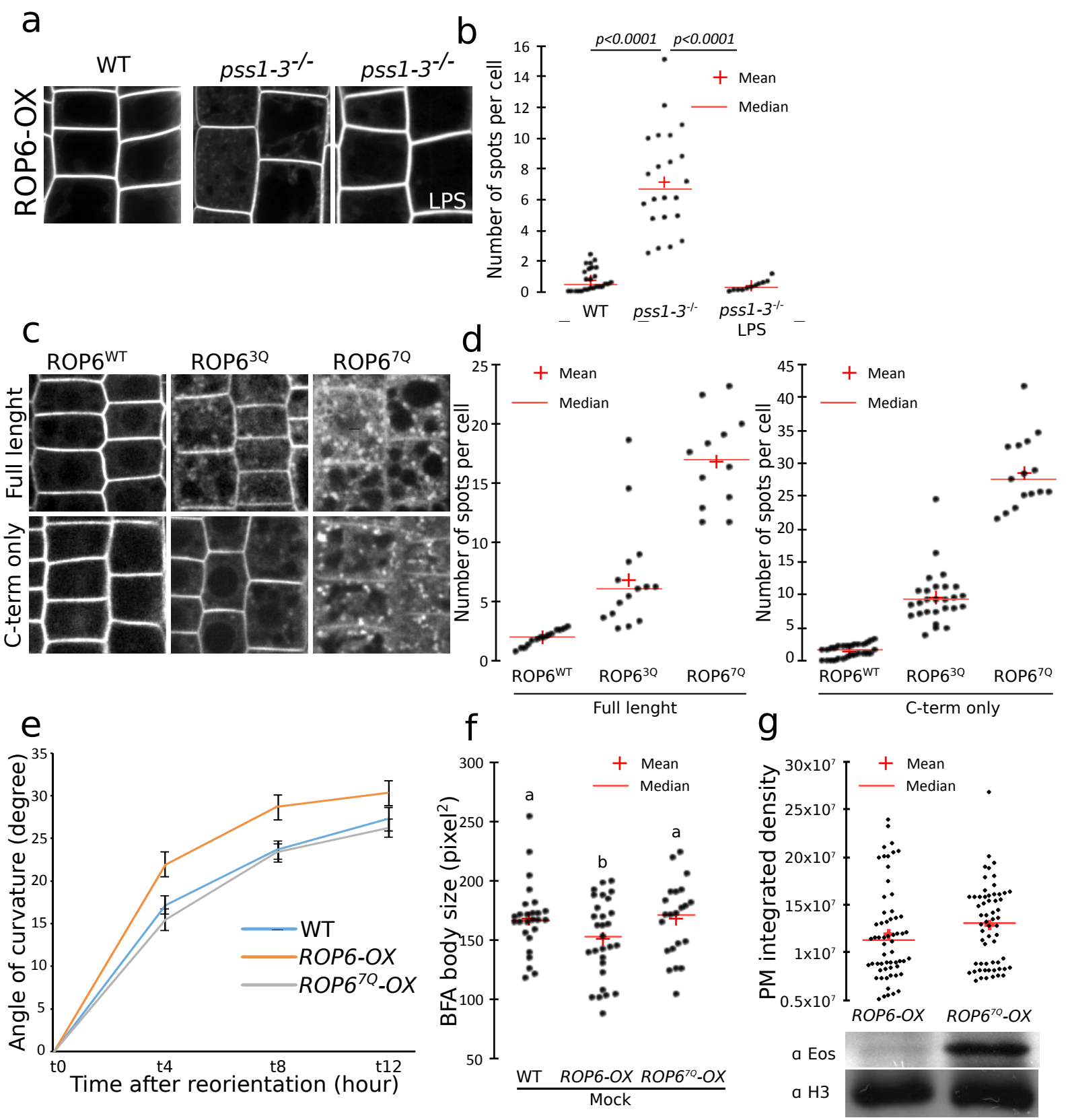
a
WT
pss1-3-/-
pss1-3-/-
ROP6-OX
LPS
b
p<0.0001
p<0.0001
Mean
Median
Number of spots per cell
WT
pss1-3-/-
pss1-3-/-
LPS
c
ROP6WT
ROP63Q
ROP67Q
Full lenght
C-term only
d
Mean
Median
Number of spots per cell
ROP6WT
ROP63Q
ROP67Q
Full lenght
C-term only
e
Angle of curvature (degree)
WT
ROP6-OX
ROP67Q-OX
t0
t4
t8
t12
Time after reorientation (hour)
f
Mean
Median
BFA body size (pixel2)
a
b
a
WT
ROP6-OX
ROP67Q-OX
Mock
g
Mean
Median
PM integrated density
ROP6-OX
ROP67Q-OX
α Eos
α H3

Figure 2. ROP6 polybasic region is required for ROP6 localization and function. (a) Confocal images of *GFP-ROP6-OX* in WT, *pss1-3*$^{-/-}$ and *pss1-3*$^{-/-}$ complemented with lysophosphatidylserine (LPS), and (b) related quantification of the number of spots per cells. (c) Confocal images of *ROP6prom::mCITRINE-ROP6*, *ROP6prom::mCITRINE-ROP6*^{3Q}, *ROP6prom::mCITRINE-ROP6*^{7Q}, *UBQ10prom::mCITRINE-ROP6-C-term*, *UBQ10prom::mCITRINE-ROP6*^{3Q}*-C-term*, *UBQ10prom::mCITRINE-ROP6*^{7Q}*-C-term*, and (d) related quantification of the number of spots per cells. (e) Quantification of gravitropic response in WT, *mEos-ROP6-OX* and *mEos-ROP6*^{7Q}*-OX*. Error bars represent SEM. (f) related quantification of BFA body size. (g) Related quantification of integrated density at the plasma membrane and related western blot. Letter indicates statistical difference. For statistical analyses details see, Sup_Data_Sheet_2.

with less lobes and indentations (Fig. S1b-c). In addition, *pss1* mutants had aberrant root hair morphology (Fig. S1d-e) and positioning (Fig. S1f-g), and showed defects in root gravitropism (Fig 1a, S1h-i). All these traits are regulated by ROP GTPases[2-4,8,13,14], notably ROP2, 4 and 6, indicating that PS may be involved in ROP signalling.

To further address the function of *PSS1* in ROP signalling, we focused on the root gravitropic response. *ROP6* is involved in root gravitropism, with *rop6* loss-of-function mutants responding more slowly to gravitropism than their wild type counterpart and *ROP6* gain-of-function mutants responding faster[3,4,8]. We tested the genetic interaction between *pss1-3* and *ROP6* gain-of-function mutants, since they have opposite gravitropic phenotype (Fig. 1a). We confirmed that lines overexpressing either mEos-ROP6 (*ROP6-OX*) or constitutively active GTP-locked GFP-ROP6 (*ROP6-CA-OX*) bent faster than WT (Fig 1a). By contrast *pss1-3xROP6-OX* and *pss1-3xROP6-CA-OX* double mutants had the same phenotype than the *pss1-3* single mutant (Fig 1a), suggesting that *PSS1* is required for *ROP6* activity during gravitropism. During root gravitropism, ROP6 acts downstream of auxin to regulate endocytosis and microtubule orientation[3,4,8,15]. We quantified cellular endocytic activity by analysing the size of the intracellular compartments labelled by the endocytic tracer FM4-64 following treatment with the fungal toxin BrefeldinA (BFA)[16]. Quantification of the size of BFA-bodies showed that *rop6-2*, a loss-of-function allele, had bigger BFA bodies than the WT, while ROP6-CA had smaller BFA-bodies (Fig. 1b-c). These results are consistent with previously published results showing that ROP6 is a negative regulator of endocytosis[3,4] and validate our quantitative assay. Similar to *rop6-2*, *pss1-3* showed enlarged FM4-64-stained BFA-bodies, a phenotype that was not rescued in *pss1-3xROP6-CA* double mutant (Fig. 1b-c, S2a-b). Auxin inhibits endocytosis[8,16,17], and co-treatment of roots with BFA and the synthetic auxin 1-naphthaleneacetic acid (NAA) induces small BFA bodies (Fig. 1d-e). Similar to *rop6-2*[3,4] and by contrast to wild-type

plants, auxin failed to inhibit endocytosis in *pss1-3* (Fig. 1d-e, S2a-e). Furthermore, CLATHRIN-LIGHT-CHAINE2 (CLC2)-GFP PM association was insensitive to auxin treatment in *pss1-3* (Fig. 1f-g), a phenotype again shared with *rop6* mutant[3]. In addition, we found that auxin-mediated microtubule reorientation was abolished in *pss1-3* mutants (Fig S2f-g), as reported for *rop6-1*[15]. Together, our genetic and cell biological analyses suggest that *PSS1* is required for auxin-mediated ROP6 signalling during root gravitropism.

PS is known to regulate the localization of many small GTPases in mammals and yeasts, including K-Ras and Cdc42[18-22], which belong to the Ras and Rho superfamily, respectively. We therefore analysed GFP-ROP6-OX localization in *pss1-3*. GFP-ROP6-OX localized strictly at the PM of epidermal cells in both WT and *pss1-3* roots (Fig. 2a-b). However, we noticed that GFP-ROP6-OX also labelled intracellular compartments in *pss1-3*, albeit weakly (Fig. 2a-b). This phenotype was rescued by exogenous treatment with lysophosphatidylserine (LPS; Fig. 2a-b)[12]. The PS-dependent localization of ROP6 reminded us of the localization of membrane surface charge (MSC) sensors, which localization relies on membrane electrostatics[12,23]. Consistently, full-length recombinant ROP6 protein interacted with all anionic phospholipids in protein-lipid overlay experiments, including PS (Fig. S3). ROP6, like MSC sensors, possess in its C-terminus a polybasic region (PBR) adjacent to a prenylation site (i.e. geranylgeranylation) (Fig. S3). Substitution of seven lysine residues into neutral glutamine in ROP6 PBR ($ROP6^{7Q}$) abolished *in vitro* interaction with all anionic lipids (Fig. S3). In planta, diminishing the net positive charges of mCITRINE-ROP6 PBR gradually increased its localization in intracellular compartments at expense of its PM localization (Fig. 2c-d). We obtained similar results when we expressed only the C-terminal tail of ROP6 (PBR +

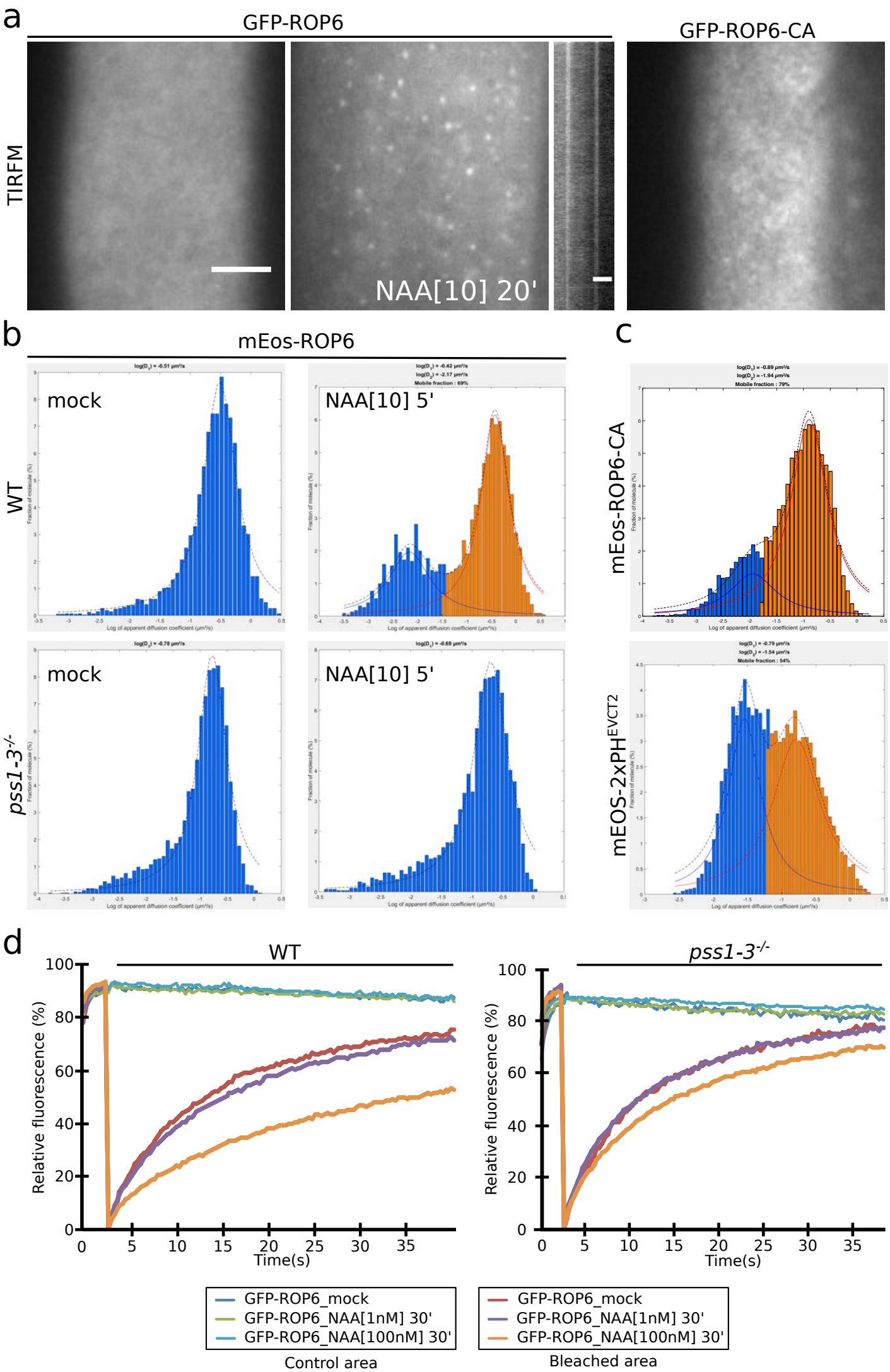
a
GFP-ROP6
GFP-ROP6-CA
TIRFM
NAA[10] 20'
b
mEos-ROP6
c
WT
mock
NAA[10] 5'
pss1-3-/-
mock
NAA[10] 5'
mEos-ROP6-CA
mEOS-2xPHEVCT2
d
WT
pss1-3-/-
Relative fluorescence (%)
Time(s)
GFP-ROP6_mock
GFP-ROP6_NAA[1nM] 30'
GFP-ROP6_NAA[100nM] 30'
Control area
GFP-ROP6_mock
GFP-ROP6_NAA[1nM] 30'
GFP-ROP6_NAA[100nM] 30'
Bleached area

Figure 3. Auxin triggers PS-dependent nanoclustering of activated-ROP6. (a) Confocal images obtained by TIRFM of GFP-ROP6-OX in the absence and presence of NAA and representative kymograph upon NAA treatment and, TIRFM image of GFP-ROP6-CA-OX (Timelapse: 3min, time frame: 500ms). (b) Quantification of the percentage of mEos-ROP6-OX molecules according to their log of apparent diffusion coefficient obtained by analysing sptPALM tracks in WT and *pss1-3*$^{-/-}$ in the presence and absence of NAA. (c) Quantification of the percentage of mEos-ROP6-OX and mEos-2xPH^{EVCT2} molecules according to their log of apparent diffusion coefficient obtained by analysing sptPALM tracks. (d) Traces of fluorescence intensity or ROP6-GFP-OX during FRAP analyses in WT and *pss1-3*$^{-/-}$ in the presence and absence of NAA. Scale bars, 5 μm and 1 μm.

geranylgeranylation site, Fig. 2c-d and S3). ROP6^{7Q} failed to induce overexpression phenotypes to the same extent as WT ROP6 (Fig. 2e-f and S4) and to complement *rop6-2* (Fig. S5). Note that for each ROP6^{7Q} line, we selected transgenics that had very strong expression level in order to have similar levels of ROP6 protein at the PM (Fig. 2.g, S4 and S5). Together, our results show that ROP6 PBR is required for interaction with anionic lipids, ROP6 localization and function.

GFP-ROP6 is still mainly localized at the PM in *pss1-3* (Fig. 2a) and ROP6^{7Q} is not functional even when overexpressed and present at a similar amount than WT ROP6 at the PM. This suggested that ROP6 PM localization is not sufficient for function and that electrostatic interaction may additionally regulate ROP6 signalling. PS promotes K-Ras localization into PM nanoclusters, which are required for K-Ras signalling[19,20,24]. K-Ras is an oncogenic small GTPase that, like ROP6, contains a polycationic C-terminal tail adjacent to a prenylation site (i.e. farnesylation)[19]. Because ROP6 was previously shown to localize in membrane domains upon activation[13], we addressed whether PS could be involved in ROP6 partitioning at the PM. To this end, we analysed ROP6 localization and membrane dynamics using total internal reflexion fluorescence microscopy (TIRFM), super-resolution single particle tracking photoactivated localization microscopy (sptPALM) and fluorescence recovery after photobleaching (FRAP). In TIRFM, GFP-ROP6 was mostly localized uniformly at the PM, while ROP6-CA additionally resided in diffraction-limited spots present in the plane of the PM (Fig 3a). A similar spotty localization was observed for GFP-ROP6 upon auxin treatment, suggesting that ROP6 is confined to particular membrane domains when activated either genetically (i.e. ROP6-CA) or by endogenous activators (i.e. auxin; Fig 3a). Kymograph analyses suggested that these spots where immobile at the PM (Fig 3a). Consistently, sptPALM experiments showed that mEos-

ROP6^{CA} coexisted as two separable populations with distinct dynamics (Fig. 3c): a fast-diffusible fraction, whose diffusion coefficient was similar to the mobile protein mEos-Lti6b, and a slow-diffusible fraction, which diffuses similarly as the immobile aquaporin mEos-PIP2a[25] (Fig. S6). By contrast, mEos-ROP6 was present as a single population at the PM, which corresponded to the fast-diffusible fraction observed with mEos-ROP6^{CA} (Fig. 3b-c). Importantly, short-term auxin treatment triggered the apparition of a second population of mEos-ROP6, which was immobile and correspond to the slow-diffusible population observed with mEos-ROP6^{CA} (Fig. 3b-c). Finally, GFP-ROP6^{CA} showed delayed fluorescence recovery as compared to GFP-ROP6 in FRAP experiments, which was consistent with the notion that a proportion of GFP-ROP6^{CA} was immobile (Figure S6). Again, auxin treatment induced a comparable delay in the fluorescence recovery of GFP-ROP6 as observed with GFP-ROP6^{CA} (Fig. 3d).

Next, we tested the impact of *pss1* loss-of-function on ROP6 PM dynamics, using sptPALM and FRAP assays. We found that ROP6 PM dynamics was not affected in *pss1-3* in the absence of treatment, but that auxin failed to induce ROP6 slow-diffusible fraction (Fig. 3b) and only caused mild delay in fluorescence recovery in FRAP experiment when compared to the WT situation (Fig. 3d). Together, these results strongly support the notion that ROP6 is immobilized in PM nanodomains upon activation, notably following auxin treatment, and that ROP6/PS interaction is required for ROP6 immobilization. It was recently shown that PS may be immobilized within the plane of the PM of Chinese Hamster Ovary cells[26]. We thus analysed the dynamics of the PS reporter mEos-2xPH^{EVCT2} by sptPALM analyses. Similar to activated mEos-ROP6, this PS-binding domain was present at the PM as a slow- and a fast-diffusible population (Fig. 3c). The presence of an immobile fraction suggested that at least a portion of PS is not moving within the plane of the plant PM and could therefore contribute to ROP6 nanoclustering.

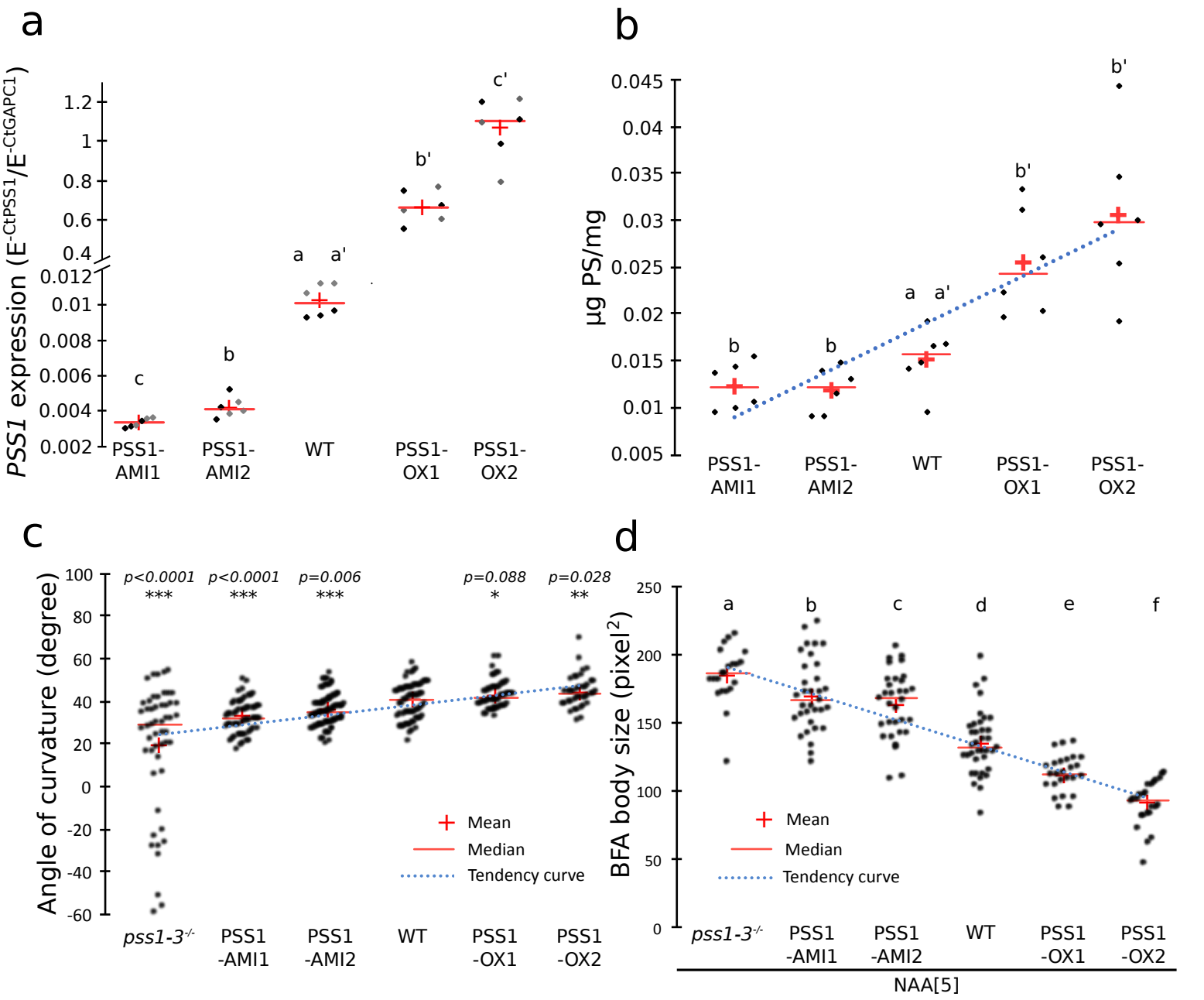
a
PSS1 expression (E-CtPSS1/E-CtGAPC1)
1.2
1
0.8
0.6
0.4
0.012
0.01
0.008
0.006
0.004
0.002
c
b
a
a'
b'
c'
PSS1-AMI1
PSS1-AMI2
WT
PSS1-OX1
PSS1-OX2
b
µg PS/mg
0.045
0.04
0.035
0.03
0.025
0.02
0.015
0.01
0.005
b
b
a
a'
b'
b'
PSS1-AMI1
PSS1-AMI2
WT
PSS1-OX1
PSS1-OX2
c
Angle of curvature (degree)
100
80
60
40
20
0
-20
-40
-60
p<0.0001 ***
p<0.0001 ***
p=0.006 ***
p=0.088 *
p=0.028 **
Mean
Median
Tendency curve
pss1-3-/-
PSS1-AMI1
PSS1-AMI2
WT
PSS1-OX1
PSS1-OX2
d
BFA body size (pixel2)
250
200
150
100
50
0
a
b
c
d
e
f
Mean
Median
Tendency curve
pss1-3-/-
PSS1-AMI1
PSS1-AMI2
WT
PSS1-OX1
PSS1-OX2
NAA[5]
e
Elongation
Meristem
C2LACT
2xPHEVCT2
f
DMSO
NAA[10]
C2LACT
2xPHEVCT2
g
Dissociation Index
3
2,5
2
1,5
1
0,5
p<0.0001
p<0.0001
Mean
Median
DMSO
NAA
DMSO
NAA
C2LACT
2xPHEVCT2

Figure 4. PS concentration tunes ROP6 signaling. qRT-PCR analysis of *PSS1* expression (a) and quantification of the PS content by HPTLC (b) in the genotypes indicated at bottom. Letter indicates statistical difference compared to the WT. Quantification of the gravitropic response 8 hours after gravistimulation (c, the p-value indicates differences compared to the WT) and the size of FM4-64-stained BFA bodies in the presence of NAA (d, letters indicate statistical differences). (e) Confocal images of mCITRINE-$C2^{LACT}$ and mCITRINE-$2xPH^{EVCT2}$ root epidermis in the meristematic and elongation zone. (f) Confocal images of mCITRINE-$C2^{LACT}$ and mCITRINE-$2xPH^{EVCT2}$ epidermal root cells in the absence and presence of NAA and (g) related association index. For statistical analysis details see, Sup_Data_Sheet_3.

To explore whether PS could tune auxin signalling via manipulation of ROP6 nanoclustering, we experimentally manipulated the plant PS content by either overexpressing *PSS1* or reducing its level using artificial microRNAs. These plants expressed more or less *PSS1* as compared to the WT control and had elevated or attenuated PS production, respectively (Fig. 4a-b). Next, we evaluated the impact of these genetic manipulations on ROP6 signalling. Lines with reduced PS content had stunted ROP6 signalling, as measured by a slow gravitropic response and decreased auxin-mediated inhibition of endocytosis (Fig. 4b-d, S7). By contrast, but similar to ROP6-OX plants, lines with heightened PS content bent faster than WT plants in gravitropic assays and had a pronounced inhibition of endocytosis upon auxin treatment (Fig. 4b-d, S7). Together, these results suggest that the cellular PS level might act like a rheostat to tune ROP6 signalling outputs. (*Note that we are now addressing the impact of these genetic manipulation of the PS content on ROP6 nanoclustering. These experiments are on-going and could not be included in this version of the thesis, but will be performed prior to submission of the manuscript*).

We next analysed whether the PS level at the PM may vary *in vivo* during development, thereby providing a physiological relevance to the "PS-rheostat" hypothesis. We previously validated the use of two PS reporter lines[12,23] expressing mCITRINE-C2^{LACT} and mCITRINE-2xPH^{EVCT2}. Both reporters are localized at the PM and in endosomes, with mCITRINE-C2^{LACT} PM localization being more pronounced[12]. Although the reasons for the slightly different localization of these sensors is still unclear, we found in both cases that their PM localization was markedly more pronounced in meristematic root tissues than in cells undergoing differentiation (Fig. 4e, S8). This developmental gradient coincided with the accumulation of auxin at the root tip[8] and raised the possibility that PS PM

localization may be under the control of auxin. Consistently, relatively short auxin treatment (60 min NAA) increased the level of both PS sensors at the PM at the expense of its intracellular localization (Fig. 4f-g). Together, our results suggest that the relative PS concentration at the PM varies during plant root development. In addition, auxin itself appears as one of the factors involved in adjusting the PS-PM content, whether directly or not, remains an open question. As the PS concentration directly manipulates ROP6 signalling output, our work exemplify a yet uncharacterized mode of feedback regulation of auxin on its own signalling pathway[8]. Modelling experiments on K-Ras showed that GTPase nanoclustering acts as an analogue-digital-analogue circuit relay for high-fidelity signal transduction across the PM[24]. We propose that *in vivo* variations of the PS-PM concentration may act like a digital gain to adjust the sensitivity of ROP6-nanoswitch activation and hence auxin action in a cell-context dependent manner.

Acknowledgements

We thank O. Hamant, M. Dreux and the SiCE group for discussions and comments, T. Stanislas for help with root hair phenotyping, S. Bednarek, S. Yalovsky, B. Scheres and the NASC collection for providing transgenic *Arabidopsis* lines, A. Lacroix, J. Berger and P. Bolland for plant care, J.C. Mulatier for help in preparing lipids and PLATIM for help with imaging. Y.J. is funded by ERC no. 3363360-APPL under FP/2007-2013. M.S was funded by a PhD fellowship from the French Ministry of Higher Education. Lipidomic analyses were performed on the Bordeaux Metabolome Facility-MetaboHUB (ANR-11-INBS-0010).

Author contributions:

M.P.P. generated all transgenic material, and was responsible for all experiments. V.B., M.P.P. and A.M-D. conceived and performed super-resolution imaging. L.M-P and P.M. performed lipid measurements. M.P.P and L.A. performed lipid overlay experiments. M.M.M-B., C.M. and M.S. assisted with phenotyping, J-B.F. and M.N. designed the sptPALM analyses pipeline, M.P.P., and Y.J. conceived the study, designed experiments and wrote

the manuscript and all the authors discussed the results and commented on the manuscript.

References

1 Etienne-Manneville, S. & Hall, A. Rho GTPases in cell biology. *Nature* **420**, 629-635, doi:10.1038/nature01148 (2002).

2 Xu, T. *et al.* Cell surface- and rho GTPase-based auxin signaling controls cellular interdigitation in Arabidopsis. *Cell* **143**, 99-110, doi:10.1016/j.cell.2010.09.003 (2010).

3 Chen, X. *et al.* ABP1 and ROP6 GTPase signaling regulate clathrin-mediated endocytosis in Arabidopsis roots. *Current biology : CB* **22**, 1326-1332, doi:10.1016/j.cub.2012.05.020 (2012).

4 Lin, D. *et al.* A ROP GTPase-dependent auxin signaling pathway regulates the subcellular distribution of PIN2 in Arabidopsis roots. *Current biology : CB* **22**, 1319-1325, doi:10.1016/j.cub.2012.05.019 (2012).

5 Xu, T. *et al.* Cell surface ABP1-TMK auxin-sensing complex activates ROP GTPase signaling. *Science* **343**, 1025-1028, doi:10.1126/science.1245125 (2014).

6 Li, X. *et al.* Differential TOR activation and cell proliferation in Arabidopsis root and shoot apexes. *Proceedings of the National Academy of Sciences of the United States of America* **114**, 2765-2770, doi:10.1073/pnas.1618782114 (2017).

7 Schepetilnikov, M. *et al.* GTPase ROP2 binds and promotes activation of target of rapamycin, TOR, in response to auxin. *The EMBO journal* **36**, 886-903, doi:10.15252/embj.201694816 (2017).

8 Armengot, L., Marques-Bueno, M. M. & Jaillais, Y. Regulation of polar auxin transport by protein and lipid kinases. *Journal of experimental botany* **67**, 4015-4037, doi:10.1093/jxb/erw216 (2016).

9 Sassi, M. *et al.* An auxin-mediated shift toward growth isotropy promotes organ formation at the shoot meristem in Arabidopsis. *Current biology : CB* **24**, 2335-2342, doi:10.1016/j.cub.2014.08.036 (2014).

10 Lynch, D. V. & Steponkus, P. L. Plasma Membrane Lipid Alterations Associated with Cold Acclimation of Winter Rye Seedlings (Secale cereale L. cv Puma). *Plant physiology* **83**, 761-767 (1987).

11 Yamaoka, Y. *et al.* PHOSPHATIDYLSERINE SYNTHASE1 is required for microspore development in Arabidopsis thaliana. *The Plant journal : for cell and molecular biology* **67**, 648-661, doi:10.1111/j.1365-313X.2011.04624.x (2011).

12 Platre MP *et al.* Combinatorial PA, PS and PI4P cooperation determines the electrostatic territory in plants. (Submitted).

13 Sorek, N. *et al.* An S-acylation switch of conserved G domain cysteines is required for polarity signaling by ROP GTPases. *Current biology : CB* **20**, 914-920, doi:10.1016/j.cub.2010.03.057 (2010).

14 Stanislas, T. *et al.* Arabidopsis D6PK is a lipid domain-dependent mediator of root epidermal planar polarity. *Nature Plants* (2015).

15 Chen, X. *et al.* Inhibition of cell expansion by rapid ABP1-mediated auxin effect on microtubules. *Nature* **516**, 90-93, doi:10.1038/nature13889 (2014).
16 Paciorek, T. *et al.* Auxin inhibits endocytosis and promotes its own efflux from cells. *Nature* **435**, 1251-1256, doi:10.1038/nature03633 (2005).
17 Robert, S. *et al.* ABP1 mediates auxin inhibition of clathrin-dependent endocytosis in Arabidopsis. *Cell* **143**, 111-121, doi:10.1016/j.cell.2010.09.027 (2010).
18 Yeung, T. *et al.* Membrane phosphatidylserine regulates surface charge and protein localization. *Science* **319**, 210-213, doi:10.1126/science.1152066 (2008).
19 Zhou, Y. *et al.* Lipid-Sorting Specificity Encoded in K-Ras Membrane Anchor Regulates Signal Output. *Cell* **168**, 239-251 e216, doi:10.1016/j.cell.2016.11.059 (2017).
20 Zhou, Y. *et al.* SIGNAL TRANSDUCTION. Membrane potential modulates plasma membrane phospholipid dynamics and K-Ras signaling. *Science* **349**, 873-876, doi:10.1126/science.aaa5619 (2015).
21 Haupt, A. & Minc, N. Gradients of phosphatidylserine contribute to plasma membrane charge localization and cell polarity in fission yeast. *Molecular biology of the cell* **28**, 210-220, doi:10.1091/mbc.E16-06-0353 (2017).
22 Fairn, G. D., Hermansson, M., Somerharju, P. & Grinstein, S. Phosphatidylserine is polarized and required for proper Cdc42 localization and for development of cell polarity. *Nature cell biology* **13**, 1424-1430, doi:10.1038/ncb2351 (2011).
23 Simon, M. L. *et al.* A PtdIns(4)P-driven electrostatic field controls cell membrane identity and signalling in plants. *Nat Plants* **2**, 16089, doi:10.1038/nplants.2016.89 (2016).
24 Tian, T. *et al.* Plasma membrane nanoswitches generate high-fidelity Ras signal transduction. *Nature cell biology* **9**, 905-914, doi:10.1038/ncb1615 (2007).
25 Hosy, E., Martiniere, A., Choquet, D., Maurel, C. & Luu, D. T. Super-resolved and dynamic imaging of membrane proteins in plant cells reveal contrasting kinetic profiles and multiple confinement mechanisms. *Molecular plant* **8**, 339-342, doi:10.1016/j.molp.2014.10.006 (2015).
26 Raghupathy, R. *et al.* Transbilayer lipid interactions mediate nanoclustering of lipid-anchored proteins. *Cell* **161**, 581-594, doi:10.1016/j.cell.2015.03.048 (2015).

Growth condition and plant materials. Arabidopsis thaliana Col-0 accession was used as wild type (WT) reference background throughout this study. Plants were grown in soil under long-day conditions at 21°C and 70% humidity and in vitro on Murashige and Skoog (MS) Basal Medium supplemented with 0.8% plant agar (pH 5.7) in continuous light conditions at 21°C. Every plant used for experiments are homozygous lines or F2 crosses.

Microscopy setup. All imaging experiments were performed with the following spinning disk confocal microscope set up, except when indicated otherwise (see bellow): inverted Zeiss microscope (AxioObserver Z1, Carl Zeiss Group, http://www.zeiss.com/) equipped with a spinning disk module (CSU-W1-T3, Yokogawa, www.yokogawa.com) and a ProEM+ 1024B camera (Princeton Instrument, http://www.princetoninstruments.com/) using a 63x Plan-Apochromat objective (numerical aperture 1.4, oil immersion). GFP was excited with a 488nm laser (150mW) and fluorescence emission was filtered by a 525/50 nm BrightLine® single-band bandpass filter (Semrock, http://www.semrock.com/). YFP/mCITRINE were excited with a 515nm laser (60mW) and fluorescence emission was filtered by a 578/105nm BrightLine® single-band bandpass filter (Semrock, http://www.semrock.com/). 488 or 515 nm lasers were used to excite GFP or YFP/mCITRINE. For quantitative imaging, pictures of epidermal root meristem cells were taken with detector settings optimized for low background and no pixel saturation. Care was taken to use similar confocal settings when comparing fluorescence intensity or for quantification. TIRF microscopy was done using an objective-based azimuthal ilas2 TIRF microscope (Roper Scientific) with 100x Apo NA 1.46 Oil objective. Angle was set up as resulting in minimum background. The images were acquired mode at 200 ms exposure time per frame (500ms for kymograph analysis).

sptPALM. Single particle tracking were done with a Zeiss Elyra PS1 system with 100x Apo NA 1.46 Oil objective. mEOS was photoconverted using 0.05% 405nm laser power and resulting photoconverted fluorophores were excited using 561nm laser (5%). Lasers power were adjusted to have significant number of tracks without too high density to facilitate further analysis. 10000 images time series were recorded at 50 frames per second (20ms exposure time) on a 256 x 256 pixels region of interest. High density tracking analysis was made using MTT algorithm (Sergé et al., 2008) and further computational analysis of tracks were made using CBS sptPALM analyser (Fiche et al., unpublished).

FRAP experiment. Fluorescence in a rectangle ROI (50 μm^2, 15 µm long), in the plasma membrane region, was bleached in the root optical section by four successive scans at full laser power (150 W) using the iLas2 FRAP module (Roper scientific, http://www.biovis.com/ilas.htm) of our spinning disc microscope. Fluorescence recovery was subsequently analysed in the bleached ROIs and in controlled ROIs (rectangle with the same dimension in unbleached area). FRAP was recorded continuously during 90 s with a delay of 0.3 s between frames. Fluorescence intensity data were normalized as previously described (Martinière et al., 2012). At least 27 ROIs have been used for quantification in three independent experiments.

FM4-64, BFA, NAA and LPS treatments. For endocytosis rate evaluation, the plasma membrane and endosomes of 5 to 12-days old transgenic lines were stained by incubating roots with 1 µM FM4-64 (thermofisher scientific, https://www.thermofisher.com) concomitantly with Brefeldin A at 25 µM (BFA, Sigma, www.sigmaaldrich.com, BFA stock

solution at 50 mM in DMSO) in liquid MS solution for 60 min. For the auxin analog, Naphthaleneacetic acid (NAA) effect on the endocytosis rate, plants were pretreated with NAA for 30 minutes at 5 µM (Sigma, http://www.sigmaaldrich.com/, NAA stock at 10 mM) and then the plasma membrane and endosomes of 5 to 12-days old transgenic lines were stained by incubating roots with 1 µM FM4-64 concomitantly with Brefeldin A at 25 µM and NAA at 5 µM in liquid MS solution for 60 min. For PIN2 endocytosis evaluation in the different genotypes 7 to 12-days old transgenic lines expressing PIN2-GFP, were treated with BFA at the indicated time and concentration in 12-well plates. For NAA effect on endocytosis, PIN2-GFP expressing lines were pretreated with NAA at 10 µM for 30 minutes and then concomitantly treated with NAA at 10 µM and BFA at 50 µM for 1 hour in 12-well plates. For NAA effect on PS biosensors mCITRINE-$C2^{LACT}$ and mCITRINE-$2xPH^{EVCT2}$, 5 to 7-day old seedlings were treated with 10 µM NAA for 1 hour. For NAA effect on microtubule orientation, 5 to 7-day old seedling expressing MAP65-GFP were treated with NAA at 5 µM for 30 minutes. For complementation of the subcellular localization of ROP6-GFP in *pss1-3* mutant, 12 days old transgenic lines expressing ROP6-GFP were treated with lysophosphatidylserine (LPS, 54µM) for 60 min in 12-well plates. Plants observed in TIRFM was treated with 10µM for 20 minutes For SptPALM experiment, seedlings roots were incubated 20’ in mock condition medium prior to 10µM NAA treatment for 5 minutes. For FRAP experiment, NAA was applied at 1nM and 100nM for 10 minutes. For each treatment, the mock condition corresponds to incubation of plants in well supplemented with a volume of DMSO equivalent to the highest drug concentration used and for the same time as the actual treatment. Roots were imaged within a 5-minutes time frame window around the indicated time.

CLONING

Preparation of gateway compatible entry clones (entry vector):
Published gateway compatible entry vectors are listed in the recombinant DNA table (Chapter III).

ROP6

The ROP6 promotor was amplified from gDNA extracted using Edwards buffer. Gateway compatible PCR products were introduced into pDONRP4R-P1 vectors by BP recombination using the following primers: *ROP6prom_F* and *ROP6prom_R* to give *ROP6pom/pDONRP4RP1*.

The ROP6 genomic encoded sequence was amplified from gDNA extracted using Edwards buffer. Gateway compatible PCR products were introduced into pDONRP2R-P3 vectors by BP recombination using the following primers: *ROP6-B2R* and *ROP6-B3w3'UTR* to give *ROP6g/pDONRP2RP3.*
Mutation in ROP6g was obtained by successive site directed mutagenesis using the following partially overlapping forward (F) and reverse (R) primers:
ROP6-CA-fw and ROP6-CA-Rev using ROP6g/pDONRP2RP3 as template to give ROP6g-CA/pDONRP2RP3.
Mutations in ROP6g-PBR were obtained by ligation using the following 5’-phosphorylated primers :
ROP6g-7Q_F and ROP6g-7Q_R using ROP6g/pDONRP2RP3 as template to give $ROP6g^{7Q}$/pDONRP2RP3.

ROP6g-3Q_F and ROP6g-3Q_R using ROP6g/pDONRP2RP3 as template to give ROP6g^{3Q}/pDONRP2RP3.

The ROP6 cDNA sequence was amplified from cDNA produced by RT-PCR. Gateway compatible PCR products were introduced into pDONRP221 vectors by BP recombination using the following primers: *ROP6-B1* and *ROP6-B2wSTOP* to give *ROP6cDNA/pDONRP221*.
Mutations in ROP6cDNA-PBR was obtained by partially overlapping strategy and ligation using the following phosphorylated primers:
ROP6g-7Q_F and ROP6g-7Q_R using ROP6cDNA/pDONRP221 as template to give ROP6^{7Q}cDNA/pDONRP221.

The ROP6 C-terminal tail, wild type and mutated ones were generated using ligation using the following 5'phosphorylated primers:
ROP6C-term_F and ROP6Cterm_R using mCITRINE/pDONRP2RP3 as template to give ROP6-C-term/pDONRP221.
ROP6-3Q-C-term_F and ROP6-3QCterm_R using mCITRINE/pDONRP2RP3 as template to give ROP6^{3Q}-C-term/pDONRP221.
ROP6-7Q-C-term_F and ROP6-7QCterm_R using mCITRINE/pDONRP2RP3 as template to give ROP6^{7Q}-C-term/pDONRP221.

PSS1

The PSS1 cDNA sequence was amplified from cDNA produced by RT-PCR. Gateway compatible PCR products were introduced into pDONRP221 vectors by BP recombination using the following primers: *PSS1-OX_F* and *PSS1-OX_R* to give *PSS1cDNA/pDONRP221*.
PSS1 artificial microRNAs were generated using WMD3-Web MicroRNA designer (Ossowski Stephan, Fitz Joffrey, Schwab Rebecca, Riester Markus and Weigel Detlef, personal communication). The PSS1-AMI1_B1_B2 and PSS1-AMI2_B1_B2 were produced by IDT to be introduced into pDONRP221 vectors by BP recombination.

mEos

The mEosFP sequence was amplified from mEosFP plasmid (Mathur et al., 2010). Gateway compatible PCR products were introduced into pDONRP221 vectors by BP recombination using the following primers: *mEos_B1_F* and *mEos_B1_R* to give *mEosFP/pDONRP221*.

Construction of destination clones (destination vector):

Published and used destination vectors are listed in the recombinant DNA table (Chapter III). Binary destination vectors for plant transformation were obtained using the multisite LR recombination system (life technologies, http://www.thermofisher.com/) using the *pB7m34GW* (basta resistant) or *pK7m34GW* (Kanamycin resistant) (Karimi et al., 2007) as destination vectors. *pROP6prom::mCITRINE-ROP6g/pB7m34GW, pROP6prom::mCITRINE-ROP6g^{3Q}/pB7m34GW, pROP6prom::mCITRINE-ROP6g^{7Q}/pB7m34GW, 2x35sprom::mEOS-ROP6g/pB7m34GW, 2x35sprom::mEOS-ROP6g^{3Q}/pB7m34GW, 2x35sprom::mEOS-ROP6g^{7Q}/pB7m34GW, 2x35sprom::mEOS-*

ROP6g-CA/pB7m34GW, 2x35sprom::mEOS-ROP6g^{7Q}-CA/pB7m34GW UBQ10prom::mCITRINE-ROP6-C-term/pB7m34GW, UBQ10prom::mCITRINE-ROP6^{3Q}-C-term/pB7m34GW, UBQ10prom::mCITRINE-ROP6^{7Q}-C-term/pB7m34GW, 2x35sprom::mEOS-2xPH-^{EVCT2}/pB7m34GW, promUBQ10::PSS1-OX1-mCITRINE/pB7m34GW, promUBQ10::PSS1-OX2-mCITRINE/pB7m34GW, promUBQ10::PSS1-AMI1/pK7m34GW, promUBQ10::PSS1-AMI2/pK7m34GW

Recombinant protein expression and lipid-protein overlay assays. The expression plasmid (pTNT::HA-ROP6cDNA and pTNT::HA-ROP6^{7Q}cDNA) was used as DNA template for in vitro transcription and translation using the TNT® SP6 High-Yield Wheat Germ Protein Expression System (Promega, www.promega.com), following manufacturer's instructions. 5µl of the total reaction were used to analyze protein expression levels by western-blot using 1:1000 anti-HA (www.boehringer-ingelheim.com) primary antibodies and 1:5000 secondary anti-mouse (GE Healthcare Life Sciences, http://www.gelifesciences.com/) antibody. The lipid overlay assays were performed as follow: nitrocellulose membranes containing immobilized purified lipids (PIPstrip P-6001, Echelon Bioscience, http://echelon-inc.com/) were incubated for 1h in blocking solution (TBST (50 mM Tris, 150 mM NaCl, 0,05% Tween 20, pH 7.6) + 3% BSA). Membranes were then incubated for 2h with 10mL of blocking solution containing 40 µl of in vitro synthesized proteins. After three washing steps using blocking solution, membranes were incubated for 2h at room temperature with primary antibodies diluted in blocking solution, rinsed three times with blocking solution and incubated for 1h at room temperature with the secondary antibody also diluted in blocking solution. Antibodies and dilutions are the same as described above.

qRT-PCR. Total RNA was extracted using the Spectrum Plant Total RNA Kit (Sigma). Total RNAs were digested with Turbo DNA-free DNase I (Ambion) according to the manufacturer's instructions. RNA was reverse transcribed using the SuperScript VILO cDNA Synthesis Kit (Invitrogen) according to the manufacturer's protocol. PCR reactions were performed in an optical 396-well plate in theQuantStudio 6 Flex Real-Time PCR System (Applied Biosystems), using FastStart Universal SYBR Green Master (Rox) (Roche), in a final volume of 10 µl, according to the manufacturer's instructions. The following standard thermal profile was used for all PCR reactions: 95 °C for 10 min, 40 cycles of 95 °C for 10 s, and 60 °C for 30 s. Data were analysed using the StepOne Software v2.2 (Applied Biosystems). As a reference, primers for the GAPC1 cDNA were used. PCR efficiency (*E*) was estimated from the data obtained from standard curve amplification using the equation $E=10^{-1/slope}$. Expression levels are presented as $E^{-CtPSS1}$ / $E^{-CtGAPC1}$.

LIPID QUANTIFICATION (HPTLC)

Lipid extraction. 12 days old seedlings (0.1-1g fresh weight) were collected in glass tubes; 2 ml of preheated isopropanol were added and tubes were heated at 70°C for 20 min to inhibit phospholipase D activity. 6 ml of chloroform/methanol 2/1 (v/v) were added and lipid extraction was completed at room temperature. The organic phases were transferred to new glass tubes. Then 1.5 ml of H2O was added to the organic phases and tubes were vortexed and centrifuged at 2000rpm; the organic phases were transferred to new glass tubes, evaporated and the lipids were resuspended in the appropriate volume of chloroform/methanol 2/1, v/v, in order to obtain the same concentration according to the initial seedlings fresh weight.

High performance thin layer chromatography (HPTLC). Lipids were deposited on HPTLC plates (Silica gel 60G F254 glass plates Merck Millipore) together with external pure lipid standards (Avanti lipids). Plates were developed according to (Heape et al., 1985). Following chromatography, the lipids were charred for densitometry according to (Macala et al., 1983). Briefly, plates were dipped into a 3% cupric acetate (w/v)-8% orthophosphoric acid (v/v) solution in H2O and heated at 110°C for 30min. Plates were scanned at 366 nm using a CAMAG TLC scanner 3. 6 independent samples were quantified for wild type, PSS1-AMI1, PSS1-AMI2, PSS1-OX1 and PSS1-OX2 plants.

Western blot. 20µl of the total reaction were used to analyze protein expression levels by western-blot using 1:2000 anti-Eos and 1:10000 anti H3 (www.boehringer-ingelheim.com) primary antibodies incubated overnight at 4°C. 1:5000 secondary anti-rabbit-HRP antibody was applied at room temperature for 1 hour (www.thermofisher.com). For revelation ECL prime was applied for 30 seconds.

QUANTIFICATION

Association Index. The effects of NAA on the localization of our PS biosensors mCITRINE-$C2^{LACT}$ and mCITRINE-2xPH^{EVCT2} were analyzed by calculating the "Association index". First, we calculated "indexMock": the ratio between the fluorescence intensity (Mean Grey Value function of Fiji software) measured in two elliptical region of interest (ROIs) from the plasma membrane region (one at the apical/basal PM region and one in the lateral PM region) and two elliptical ROIs in the cytosol in the mock condition. "IndexMock" was quantified in 150 cells over three independent replicates (50 cells per replicate). Next, we measured a similar ratio in perturbed conditions ("indexExp"). "indexExp" was also quantified in 150 cells over three independent replicates (50 cells per replicate). The dissociation index is the ratio of (indexMock)/(indexExp). This dissociation index reveals the degree of relocalization of the fluorescent reporters from the cytosol to the plasma membrane, between the mock and perturbed conditions.

BFA body size. BFA body size was quantified on at least 14 roots in three independent experiments using a macro in ImageJ. Threshold was determined, images harboring less than ten BFA bodies were removed from the analysis as well as images issue from misshapen root cells. Per root an average of 38 BFA bodies was detected representing at least 532 BFA bodies quantified per conditions.

Gravitropic response and gravitropic defect. 7-8 days old seedlings were subjected to 135° angle for 12 hours. Every 4 hours, plates were scanned with EPSON scanner perfection V300 PHOTO at 800 dpi. Each plate at the different time points were cropped and aligned using "Template Matching and Slice Alignment" plugin on FIJI to obtain a timelapse for 12h. To allow high throughput data analyses, the process has been automatized on a Fiji macro. To quantify the average root angle of curvature RootTrace software was used (French et al., 2009). The horizontal and vertical growth index were calculated on 12 days old seedlings of pss1-$3^{-/-}$, pss1-$4^{-/-}$ and pss1-$5^{-/-}$ mutant plants (Grabov et al., 2005) using FIJI.

Microtubules orientation. Microtubule arrays were acquired on 12 days old seedlings in the transition zone of root cells. The average orientation was calculated on at least 28 cells of 13 roots in two independent experiments using FibriTool software (Boudaoud et al., 2014) on Fiji.

Spot number. The number of spot was calculated using SiCESpotDetector.ijm plugin (Bayle et al., 2017)

(http://www.enslyon.fr/RDP/SiCE/METHODS_files/SiCE%20SpotDetectorV3.ijm) on 5 to 7-days old transgenic plants expressing ROP6, ROP6^{3Q}, ROP6^{7Q} full length fused to mCITRINE exppressed by its own promotor or the ROP C-terminal wild type, 3Q and 7Q fused to mCITRINE expressed under the *UBQ10prom*. In the case of plants expressing ROP6-GFP in pss1-3$^{-/-}$ mutant and LPS complementation, the number of spots was determined by eyes (because the plugin described above was not sensitive enough to detect ROP6 spots in the *pss1* mutant).

Plasma membrane intensity. 5 to 7-days old transgenic lines was used to quantified the plasma membrane intensity according to the integrated density. The integrated density average was measured from 60 plasma membranes issue of three roots using a line of three pixels and the "Measure" plugin in Fiji.

Lateral root density. 12 days old seedlings were used for quantification for the complementation assay, plates were scanned with EPSON scanner perfection V300 PHOTO at 800 dpi. A ratio of the number of lateral root divided by the root length was applied in order to calculate the lateral root density. At least 67 plants were analyzed in two independent experiments.

Pavement cell circularity. Stage 3 leafs of 28 days old plants were used for pavement cell circularity quantification. For image acquisition, adaxial leaf epidermis was printed on tepid agar at 3% poured on a coverslip. 5 days after printing, pavement cell edges was observed on the slip using Zeiss IMAGER M5 AXIO optical microscope with 40x/0.75 Zeiss EZ.plan-NEOFLUAR objective with DIC illumination. At least 79 pavement cells of 5 independent leafs were analysed with Fiji using the circularity measurement.

Root hair phenotype and initiation site ratio. Root hair phenotyping and initiation site was performed by hand on 5 days old seedlings on at least 7 plants representing 336 root hairs for phenotyping and 48 for initiation site in two independent experiments. In order to determine the initiation site ratio, the length of the root hair initiation site from the basal side divided by the total length of the trichoblast were measured. For image acquisition, plants were set up between slip and coverslip containing water and observed using Zeiss IMAGER M5 AXIO optical microscope with 40x/0.75 Zeiss EZ.plan-NEOFLUAR objective.

STATISTICAL ANALYSES

Each sample were subjected to four different normality tests (Jarque-Bera, Lilliefors, Anderson-Darling and Shapiro-Wilk), sample were considered as a Gaussian distribution when at least one test was significant. Consequently, parametric or non-parametric test were performed. For parameric test, an ANOVA was performed coupled to a Fisher test in order to proceed to pairwise comparison between samples (confidence index, 95% or 90% in the case of gravitropism experiment). Statistical analyses between two samples were performed using the Student t-test (p-value=0.05 or 0.10 in the case of gravitropism experiment). For non-parametric test, results were statistically compared using the Kruskal-Wallis bilateral test (p-value=0.05) using XLstat software (http://www.xlstat.com/). Pairwise comparisons between groups were performed according to Steel-Dwass-Critchlow- Fligner procedure (different letters indicate statistical difference between samples) (HOLLANDER and WOLFE, 1999). Statistical analyses between two samples were performed using the non- parametric Wilcoxon-Mann-Whitney test (p-value=0.05).

OLIGONUCLEOTIDES TABLE:

ROP6prom_R	ttttttgtacaaacttgcctttctctccttcttcaaacttc
ROP6prom_F	gtatagaaaagttgctaacaagctttcagaaaagaggatg
ROP6-B2R	ggggacagctttcttgtacaaagtggctatgagtgcttcaaggtttatcaagtg
ROP6-B3w3'UTR	ggggacaactttgtataataaagttgccttaagacaattggtgtgaatctagg
ROP6-B1	ggggacaagtttgtacaaaaaagcaggcttaatgagtgcttcaaggtttatcaagtg
ROP6-B2wSTOP	ggggaccactttgtacaagaaagctgggtatcagagtatagaacaacctttctgag
ROP6g-7Q_R	/5phos/gctgctgctggttttttggtggctggagaacgac
ROP6g-7Q-Fw	/5phos/agcagcaacaatctcagaaaggttgttctatactc
ROP6-CA_F	gtcggcgacgttgctgttggaaagacttgtc
ROP6-CA-Rev	tccaacagcaacgtcgccgacagtgacacacttgataaacc
ROP6-C-term_R	/5phos/ctcttcttcttcttcttgttttttggagccactttgtacaagaaagttgaacgagaaacg
ROP6-C-term_F	/5phos/aaaatctcagaaaggttgttctatactctaagcaactttattatacaaagttggc
ROP6-7Q-C-term_R	/5phos/gctgctgctggttttttggagccactttgtacaagaaagttgaacg
ROP6-7Q-C-term_F	/5phos/agcagcaacaatctcagaaaggttgttctatactctaagc
ROP6-3Q-C-term_R	/5phos/gcttctgcttctgcttgttttttggagccactttgtacaagaaagttgaacg
ROP6-3Q-C-term_F	/5phos/agaaatctcagaaaggttgttctatactctaagcaactttattatacaaagttggc
ROP6g-3Q_F	ccaaaaaacaagcagaagcagaagcagaaatctcagaaaggttgttc
ROP6g-3Q_R	gagatttctgcttctgcttctgcttgttttttggtggctggagaacgacc
mEos_B1_F	ggggacaagtttgtacaaaaaagcaggcttaatgagtgcgattaagccagacatgaag
mEos_B2_R	ggggaccactttgtacaagaaagctgggtattatcgtctggcattgtcaggcaatc
PSS1-AMI1_B1_B2	Acaagtttgtacaaaaaagcaggctcaaacacacgctcggacgcatattacacatgttcatac acttaatactcgctgttttgaattgatgttttaggaatatatatgtaga**taataatgatgcgcttaa cgt**tcacaggtcgtgatatgattcaattagcttccgactcattcatccaaataccgagtcgccaa aattcaaactagactcgttaaatgaatgaatgatgcggtagacaaattggatcattgattctcttt ga**acgttaagcgcatcattatta**tctctcttttgtattccaattttcttgattaatctttcctgcaca aaaacatgcttgatccactaagtgacatatatgctgccttcgtatatatagttctggtaaaattaac attttgggtttatctttatttaaggcatcgccatgacccagctttcttgtacaaagtggt
PSS1-AMI2_B1_B2	acaagtttgtacaaaaaagcaggctcaaacacacgctcggacgcatattacacatgttcatac acttaatactcgctgttttgaattgatgttttaggaatatatatgtaga**tttaacgtctcttttgcgc gc**tcacaggtcgtgatatgattcaattagcttccgactcattcatccaaataccgagtcgccaaa attcaaactagactcgttaaatgaatgaatgatgcggtagacaaattggatcattgattctctttg a**gcgcgcaaaagagacgttaaa**tctctcttttgtattccaattttcttgattaatctttcctgcac aaaaacatgcttgatccactaagtgacatatatgctgccttcgtatatatagttctggtaaaattaa catttgggtttatctttatttaaggcatcgccatgacccagctttcttgtacaaagtggt
PSS1-OX_F	ggggacaagtttgtacaaaaaagcaggcttaaccatggaacccaatgggtacaggaaa
PSS1-OX_R	ggggaccactttgtacaagaaagctgggtaacgtctcttttgcgcgaggatcttct

LINES TABLE:

Lines	Sources	Used in figure(s) and panel(s)
pss1-3	Chapitre 3	Fig., 1.a-b, 1.d-g. Fig., 2.a-b. Fig., 3. Fig., 4.c-d. Fig., S1.a-i.
pss1-1	Chapitre 3	Fig., S1.a-i
pss1-4	Chapitre 3	Fig., S1.a-i
pss1-5	Chapitre 3	Fig., S1.a-i
pss1-3xpPSS1::PSS1g	Chapitre 3	Fig., 1.a. Fig., S1.b-c
2x35s::GFP-ROP6	Yalovski et al., 2005	Fig., S1.b-c. Fig., 3.a.d.

*pss1-3*x2x35s::GFP-ROP6	This study	Fig., 2.a-b. Fig., 3.
2x35s::GFP-ROP6-CA	Yalovski et al., 2005	Fig., 1.a. Fig., S1.b-c. Fig., 3.a.
*pss1-3*x2x35s::GFP-ROP6-CA	This study	Fig., 1.a.
rop6-2	Lin et al., 2012	Fig., 1.b-e. Fig., Fig., S1.b-c. Fig., S2.c-d. Fig., S5.b-d
2x35s::mEos-ROP6g (line #2) 10	This study	Fig., 1.a.
*pss1-3*x2x35s::mEos-ROP6g (line #2) 10	This study	Fig., 1.a.
*pss1-3*x2x35s::mEos-ROP6g (line #1) 13	This study	Fig., 3.b.
pCLC2::CLC2-GFP	Konopka et al., 2008	Fig., 1.f-g
rop6-2xpROP6::mCITRINE-ROP6g (line #1) (1)	This study	Fig., 2.c-d. Fig., S5.a-d
*rop6-2*xpROP6::mCITRINE-ROP6g (line #2) (7)	This study	Fig., S5.c.
*rop6-2*xpROP6::mCITRINE-ROP6g^{3Q}	This study	Fig., 2.c-d.
rop6-2xpROP6::mCITRINE-ROP6g^{7Q} (line #1) (4)	This study	Fig., S5.a, S5.d.
rop6-2xpROP6::mCITRINE-ROP6g^{7Q} (line #2) (13)	This study	Fig., 2.c-d. Fig., S5.a-d.
rop6-2xpROP6::mCITRINE-ROP6g^{7Q} (line #3) (18)	This study	Fig., S5.a, S5.c.
pUBQ10::mCITRINE-ROP6-C-term	This study	Fig., 2.c-d.
pUBQ10::mCITRINE-ROP6^{3Q}-C-term	This study	Fig., 2.c-d.
pUBQ10::mCITRINE-ROP6^{7Q}-C-term	This study	Fig., 2.c-d.
2x35s::mEos-ROP6g (line #1) (13)	This study	Fig., 2.e-f. Fig., 3.b. Fig., S4.a-b.
2x35s::mEos-ROP6g^{7Q} (line #1) (2)	This study	Fig., 2.e-f. Fig., S4.a-b.
2x35s::mEos-ROP6g-CA (line #1) (1)	This study	Fig., 3.b. Fig., S4.a-d.
2x35s::mEos-ROP6g-CA (line #2) (16)	This study	Fig., S4.a.c-d.
2x35s::mEos-ROP6g^{7Q}-CA (line #1) (2)	This study	Fig., S4.a-d.
2x35s::mEos-ROP6g^{7Q}-CA (line #2) (10)	This study	Fig., S4.a.c-d.
2x35s::mEos-2xPH^{EVCT2}	This study	Fig., 3.c.
pUBQ10::PSS1-AMI1	This study	Fig., 4.a-d. Fig., S7.a-c.
pUBQ10::PSS1-AMI2	This study	Fig., 4.a-d. Fig., S7.a-c.
pUBQ10::PSS1-OX1	This study	Fig., 4.a-d. Fig., S7.a-c.
pUBQ10::PSS1-OX2	This study	Fig., 4.a-d. Fig., S7.a-c.
pUBQ10::mCITRINE-	Simon et al. 2016	Fig., 4.e-g.

$C2^{LACT}$		
pUBQ10::mCITRINE-$2xPH^{EVCT2}$	Chapitre 3	Fig., 4.e-g.
MAP65-1::GFP-MAP65-1	Lucas et al., 2011	Fig., S2.f-g.
pss1-3xMAP65-1::GFP-MAP65-1	This study	Fig., S2.f-g.
PIN2::PIN2-GFP	Xu et al., 2005	Fig., S2.c-e.
pss1-3xPIN2::PIN2-GFP	This study	Fig., S2.c-e.
*rop6-2*xPIN2::PIN2-GFP	This study	Fig., S2.c-d.
pUBQ10::Lti6b-mEOS	This study	Fig., S6
pUBQ10::PIP2a-mEOS	Martinière et al., 2012	Fig., S6

Bayle, V., Platre, M.P., and Jaillais, Y. (2017). Automatic Quantification of the Number of Intracellular Compartments in Arabidopsis thaliana Root Cells. Bio-Protoc. *7*.

Boudaoud, A., Burian, A., Borowska-Wykręt, D., Uyttewaal, M., Wrzalik, R., Kwiatkowska, D., and Hamant, O. (2014). FibrilTool, an ImageJ plug-in to quantify fibrillar structures in raw microscopy images. Nat. Protoc. *9*, 457–463.

French, A., Ubeda-Tomás, S., Holman, T.J., Bennett, M.J., and Pridmore, T. (2009). High-Throughput Quantification of Root Growth Using a Novel Image-Analysis Tool. Plant Physiol. *150*, 1784–1795.

Grabov, A., Ashley, M. k., Rigas, S., Hatzopoulos, P., Dolan, L., and Vicente-Agullo, F. (2005). Morphometric analysis of root shape. New Phytol. *165*, 641–652.

Heape, A.M., Juguelin, H., Boiron, F., and Cassagne, C. (1985). Improved one-dimensional thin-layer chromatographic technique for polar lipids. J. Chromatogr. *322*, 391–395.

HOLLANDER, M., and WOLFE, D.A. (1999). Nonparametric Statistical Methods (New York: John Wiley & Sons).

Karimi, M., Depicker, A., and Hilson, P. (2007). Recombinational Cloning with Plant Gateway Vectors. Plant Physiol. *145*, 1144–1154.

Macala, L.J., Yu, R.K., and Ando, S. (1983). Analysis of brain lipids by high performance thin-layer chromatography and densitometry. J. Lipid Res. *24*, 1243–1250.

Martinière, A., Lavagi, I., Nageswaran, G., Rolfe, D.J., Maneta-Peyret, L., Luu, D.-T., Botchway, S.W., Webb, S.E.D., Mongrand, S., Maurel, C., et al. (2012). Cell wall constrains lateral diffusion of plant plasma-membrane proteins. Proc. Natl. Acad. Sci. *109*, 12805–12810.

Mathur, J., Radhamony, R., Sinclair, A.M., Donoso, A., Dunn, N., Roach, E., Radford, D., Mohaghegh, P.S.M., Logan, D.C., Kokolic, K., et al. (2010). mEosFP-Based Green-to-Red Photoconvertible Subcellular Probes for Plants. Plant Physiol. *154*, 1573–1587.

Sergé, A., Bertaux, N., Rigneault, H., and Marguet, D. (2008). Dynamic multiple-target tracing to probe spatiotemporal cartography of cell membranes. Nat. Methods *5*, 687–694.

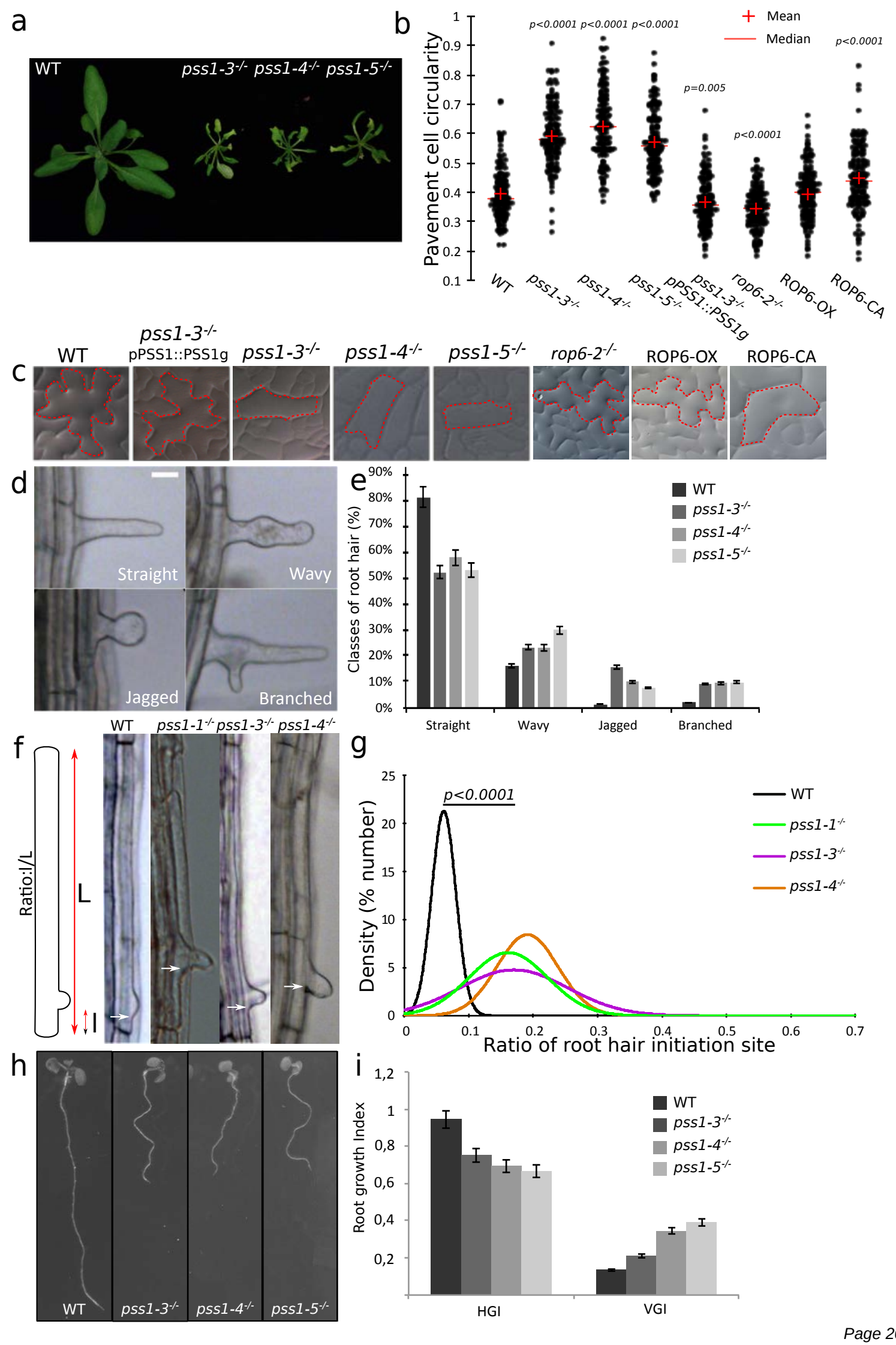
a
WT
pss1-3-/- pss1-4-/- pss1-5-/-
b
Mean
Median
Pavement cell circularity
p<0.0001 p<0.0001 p<0.0001
p=0.005
p<0.0001
p<0.0001
WT
pss1-3-/-
pss1-4-/-
pss1-5-/-
pPSS1::PSS1g
pss1-3-/-
rop6-2-/-
ROP6-OX
ROP6-CA
c
WT
pss1-3-/- pPSS1::PSS1g
pss1-3-/-
pss1-4-/-
pss1-5-/-
rop6-2-/-
ROP6-OX
ROP6-CA
d
Straight
Wavy
Jagged
Branched
e
Classes of root hair (%)
WT
pss1-3-/-
pss1-4-/-
pss1-5-/-
Straight
Wavy
Jagged
Branched
f
WT
pss1-1-/-
pss1-3-/-
pss1-4-/-
Ratio:l/L
L
l
g
p<0.0001
Density (% number)
WT
pss1-1-/-
pss1-3-/-
pss1-4-/-
Ratio of root hair initiation site
h
WT
pss1-3-/-
pss1-4-/-
pss1-5-/-
i
Root growth Index
WT
pss1-3-/-
pss1-4-/-
pss1-5-/-
HGI
VGI

Extended Data Figure 1. PS-less mutants share ROPs-associated phenotypes. (a) Picture of WT, *pss1-3*$^{-/-}$, *pss1-4*$^{-/-}$ and *pss1-5*$^{-/-}$ rosette at 21 days after germination (DAG). (b) Quantification of the pavement cells circularity of WT, *pss1-3*$^{-/-}$, *pss1-4*$^{-/-}$, *pss1-5*$^{-/-}$, *pss1-3*$^{-/-}$ x*pPSS1::PSS1g*, *rop6-2*$^{-/-}$, *GFP-ROP6-OX* and *GFP-ROP6-CA-OX*. (c) Picture showing pavement cells shape of WT, *pss1-3*$^{-/-}$, *pss1-4*$^{-/-}$, *pss1-5*$^{-/-}$, *pss1-3*$^{-/-}$x*pPSS1::PSS1g*, *rop6-2*$^{-/-}$, *ROP6-OX* and *ROP6-CA*. (d) Picture of representative root hair shape observed in *pss1* mutants and classification in straight, wavy, bulged and branched phenotypic categories. Quantification of root hair shape phenotypes in WT, *pss1-3*$^{-/-}$, *pss1-4*$^{-/-}$, *pss1-5*$^{-/-}$ according to the classification. (f) Representation of root hair initiation site ratio calculation and picture of WT, *pss1-3*$^{-/-}$, *pss1-4*$^{-/-}$ and *pss1-5*$^{-/-}$ root hairs initiation site. Arrows indicate the root initiation site. (g) Quantification of the root hair initiation site ratio in WT, *pss1-3*$^{-/-}$, *pss1-4*$^{-/-}$, *pss1-5*$^{-/-}$. (h) Picture showing defect of gravitropism perception in *pss1-3*$^{-/-}$, *pss1-4*$^{-/-}$, *pss1-5*$^{-/-}$, compared to the WT at 12 DAG. (i) Quantification of horizontal growth index (HGI) and vertical growth index (VGI) in WT, *pss1-3*$^{-/-}$, *pss1-4*$^{-/-}$ and *pss1-5*$^{-/-}$ at 12 DAG. For statistical analysis details see, Sup_Data_Sheet_4.

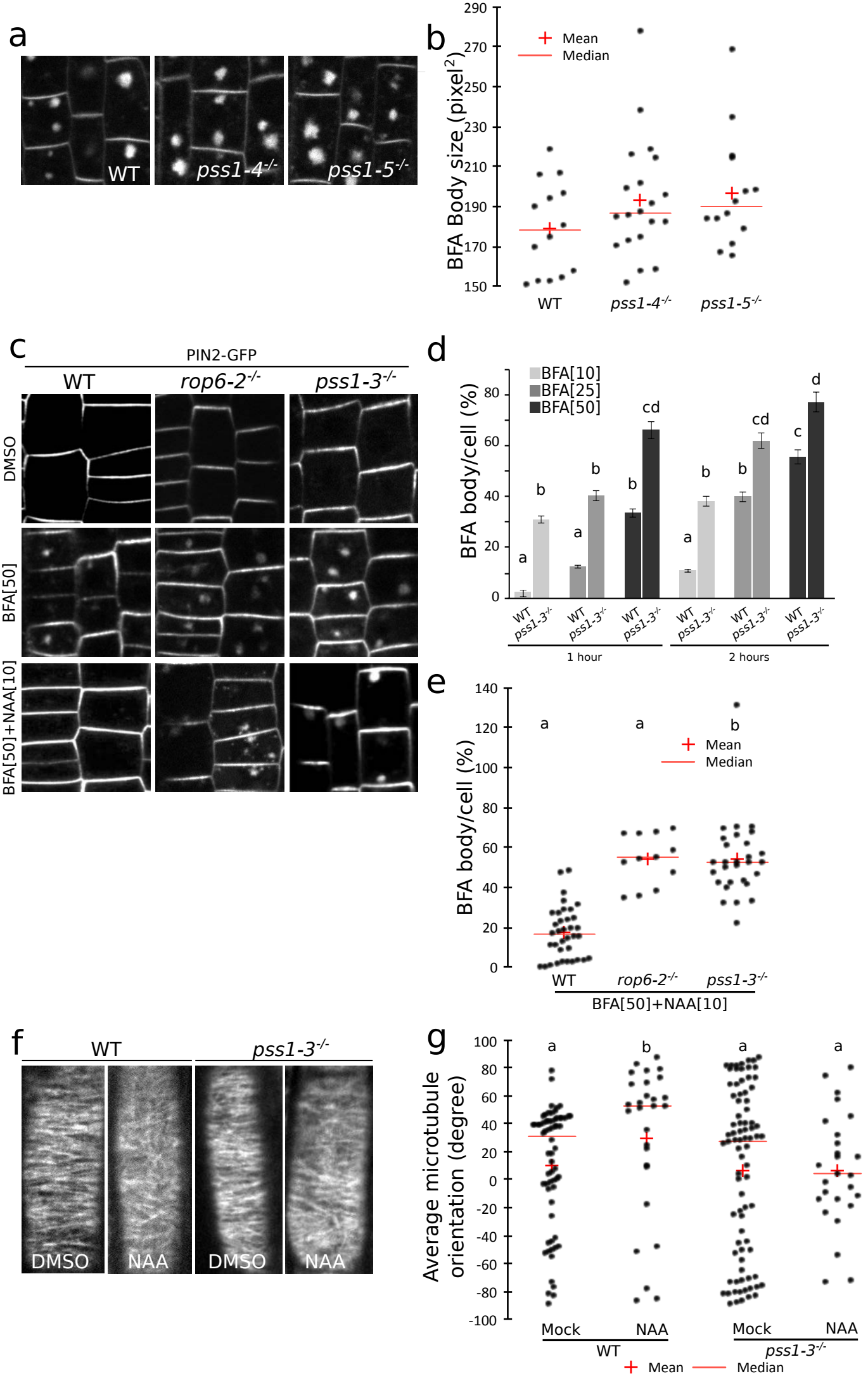
a
WT
pss1-4-/-
pss1-5-/-
b
BFA Body size (pixel2)
290
270
250
230
210
190
170
150
Mean
Median
WT
pss1-4-/-
pss1-5-/-
c
PIN2-GFP
WT
rop6-2-/-
pss1-3-/-
DMSO
BFA[50]
BFA[50]+NAA[10]
d
BFA body/cell (%)
BFA[10]
BFA[25]
BFA[50]
a
b
a
b
b
cd
a
b
b
cd
c
d
WT
pss1-3-/-
1 hour
2 hours
e
BFA body/cell (%)
a
a
b
Mean
Median
WT
rop6-2-/-
pss1-3-/-
BFA[50]+NAA[10]
f
WT
pss1-3-/-
DMSO
NAA
DMSO
NAA
g
Average microtubule orientation (degree)
a
b
a
a
Mock
NAA
Mock
NAA
WT
pss1-3-/-
Mean
Median

Extended Data Figure 2. ROP6-dependent auxin signaling pathway is defective in *pss1* mutant. (a) Confocal images of WT, *pss1-4*$^{-/-}$, *pss1-5*$^{-/-}$ epidermal root cells stained by FM4-64 and concomitantly treated with BFA. (b) Quantification of the BFA body size in WT, *pss1-4*$^{-/-}$, *pss1-5*$^{-/-}$. Confocal images of 12 days old seedlings expressing PIN2-GFP in WT, *rop6-2*$^{-/-}$, *pss1-3*$^{-/-}$ (upper panel), treated with BFA (middle panel) and concomitantly with BFA and NAA (lower panel). (c) Quantification of PIN2-positive BFA body number per cell express in percentage in WT, *rop6-2*$^{-/-}$ and *pss1-3*$^{-/-}$ concomitantly treated with BFA and NAA. Letters indicate statistical difference. (e) Quantification of PIN2-positive BFA body number per cell express in percentage in WT and *pss1-3*$^{-/-}$ treated with BFA at different time and concentration. Letters indicate statistical difference. (f) Confocal images of 12 days old seedlings expressing MAP65-GFP in WT and *pss1-3*$^{-/-}$ in presence and absence of NAA. (g) Quantification of the average microtubule orientation in WT and *pss1-3*$^{-/-}$ in presence and absence of NAA. Letters indicate statistical difference. For statistical analysis details see, Sup_Data_Sheet_5.

a

C-terminal tail

ROP6 PPKNKKKKKRKSQKGCSIL

ROP6^{3Q} PPKNKQKQKQKSQKGCSIL

ROP6^{7Q} PPKNQQQQQQQSQKGCSIL

*

b

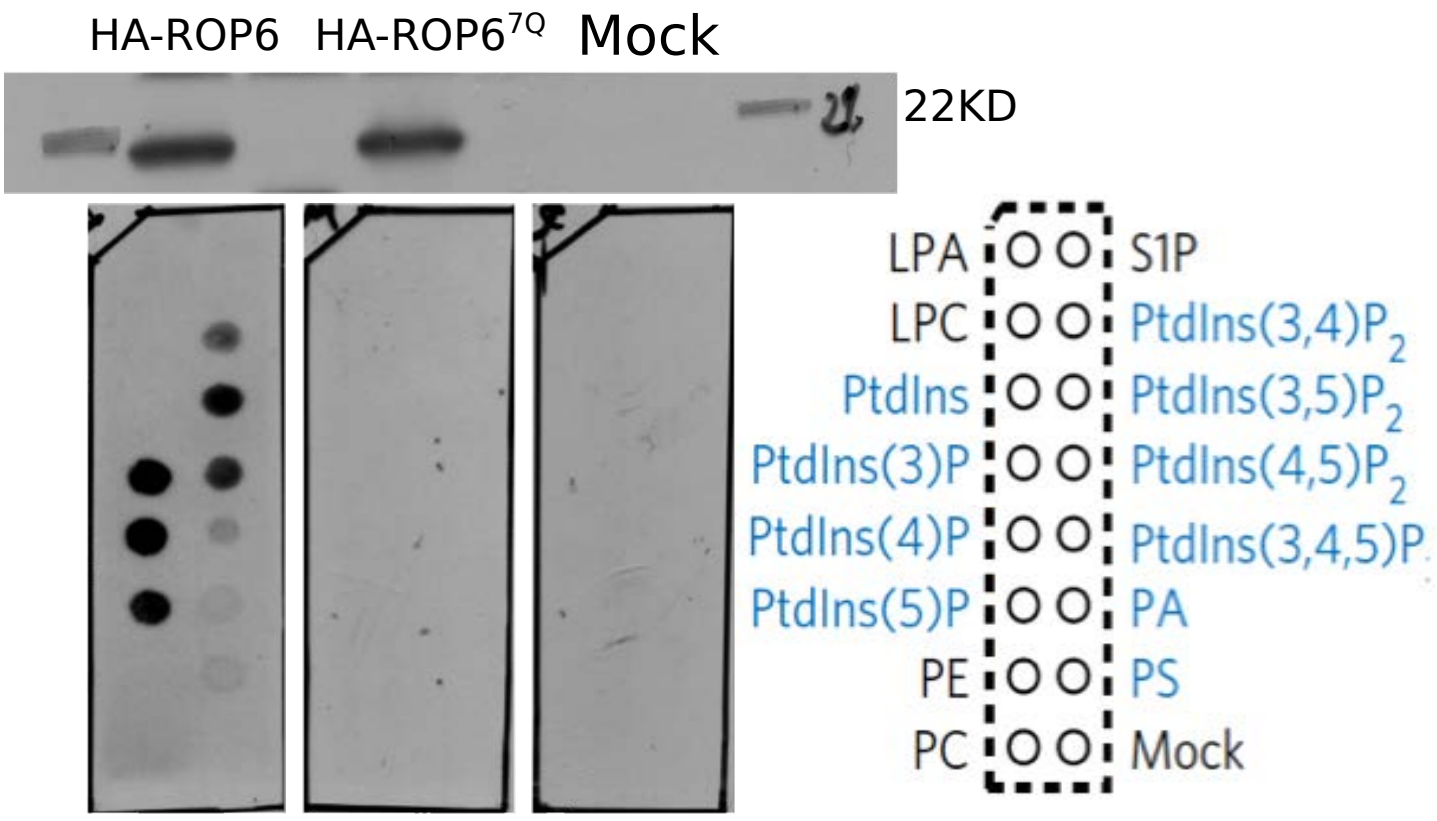

Extended Data Figure 3. ROP6 polybasic region interacts with anionic phospholipids. (a) Sequence of ROP6, ROP6^{3Q}, ROP6^{7Q} C-terminal tail. Asterisk indicates the cysteine required for prenylation (b) Western blot showing expression of recombinant HA-ROP6cDNA and HA-ROP6^{7Q}cDNA (top), lipid overlay assay performed with HA-ROP6cDNA and HA-ROP6^{7Q}cDNA (bottom left), empty vector (bottom middle) and scheme showing the position of the different lipid species spotted on the membrane (bottom right), anionic lipids are highlighted in blue.

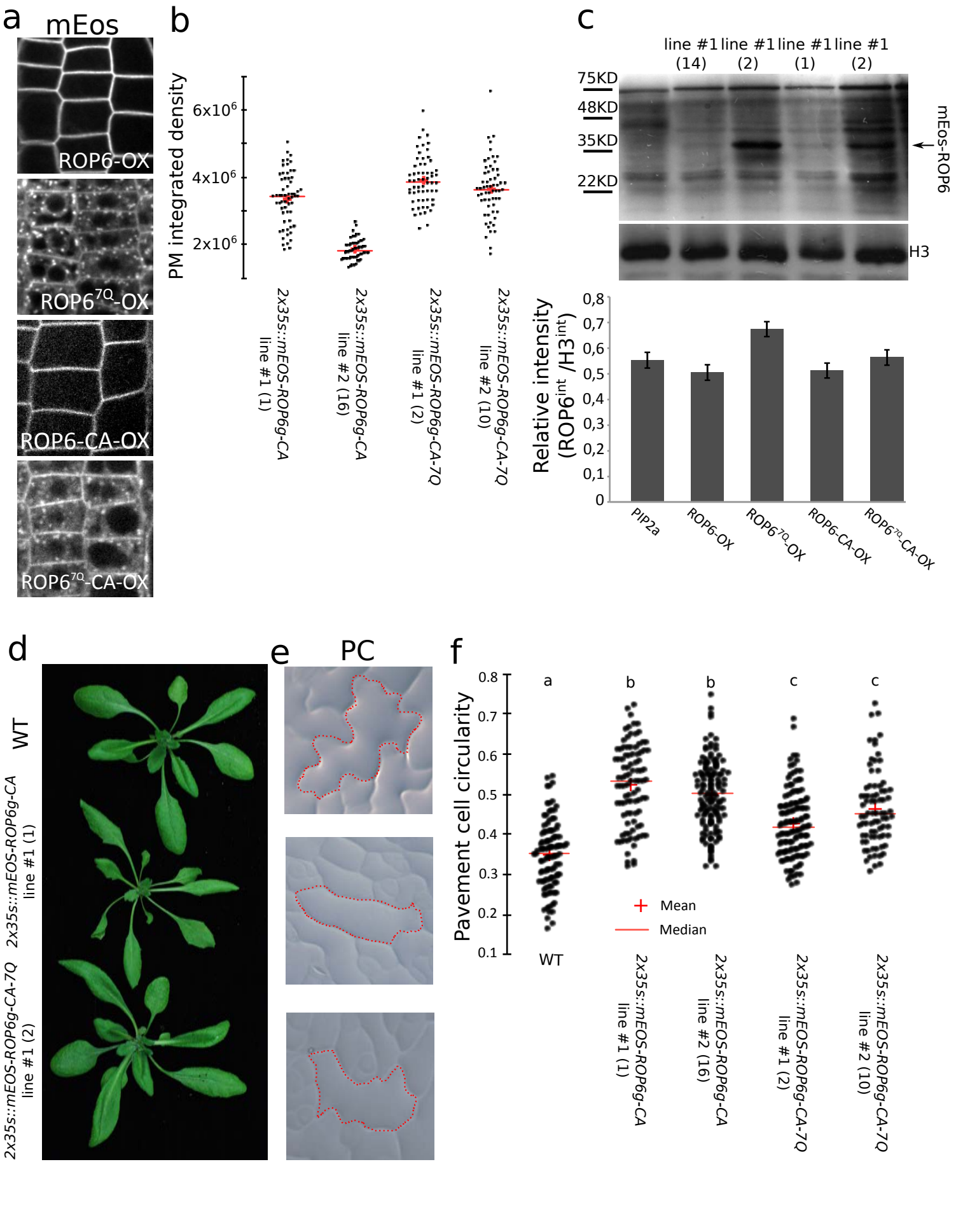
a
mEos
ROP6-OX
ROP6^{7Q}-OX
ROP6-CA-OX
ROP6^{7Q}-CA-OX
b
PM integrated density
6x10^6
4x10^6
2x10^6
2x35s::mEOS-ROP6g-CA line #1 (1)
2x35s::mEOS-ROP6g-CA line #2 (16)
2x35s::mEOS-ROP6g-CA-7Q line #1 (2)
2x35s::mEOS-ROP6g-CA-7Q line #2 (10)
c
line #1 (14)
line #1 (2)
line #1 (1)
line #1 (2)
75KD
48KD
35KD
22KD
mEos-ROP6
H3
Relative intensity (ROP6^{int} /H3^{int})
0,8
0,7
0,6
0,5
0,4
0,3
0,2
0,1
0
PIP2a
ROP6-OX
ROP6^{7Q}-OX
ROP6-CA-OX
ROP6^{7Q}-CA-OX
d
WT
2x35s::mEOS-ROP6g-CA line #1 (1)
2x35s::mEOS-ROP6g-CA-7Q line #1 (2)
e
PC
f
Pavement cell circularity
0.8
0.7
0.6
0.5
0.4
0.3
0.2
0.1
a
b
b
c
c
Mean
Median
WT
2x35s::mEOS-ROP6g-CA line #1 (1)
2x35s::mEOS-ROP6g-CA line #2 (16)
2x35s::mEOS-ROP6g-CA-7Q line #1 (2)
2x35s::mEOS-ROP6g-CA-7Q line #2 (10)

Extended Data Figure 4. The polybasic region is required for full ROP6 activity when overexpressed. (a) Confocal images of 7 days old seedlings overexpressing mEos-ROP6-CA, mEos-ROP6^{7Q}-CA, mEos-ROP6-OX, mEos-ROP6^{7Q}-OX (b) Quantification of the plasma membrane integrated intensity in 7 days old seedlings overexpressing mEos-ROP6-CA, mEos-ROP6^{7Q}-CA, mEos-ROP6-OX, mEos-ROP6^{7Q}-OX (n=60). (c) Western blot oon protein extracted of plant espressing *PIP2a-mEos*, *mEos-ROP6-OX line #1 (14)*, *mEos-ROP6^{7Q}-OX line #1 (2)*, *mEos-ROP6-CA-OX line #1 (1)* and *mEos-ROP6^{7Q}-CA-OX line #1 (2)* (upper panel), quantity of protein loaded (middle panel) and the related quantification(lower panel). (d) Picture of the rosette at 28 days after germination of WT, *mEos-ROP6-CA-OX*, *mEos-ROP6^{7Q}-CA-OX* plants and (e) the related pavement cell shape. (f) Quantification of the pavement cells circularity of WT, *mEos-ROP6-CA-OX*, *mEos-ROP6^{7Q}-CA-OX*. Letters indicate statistical difference. For statistical analysis details see, Sup_Data_Sheet_6.

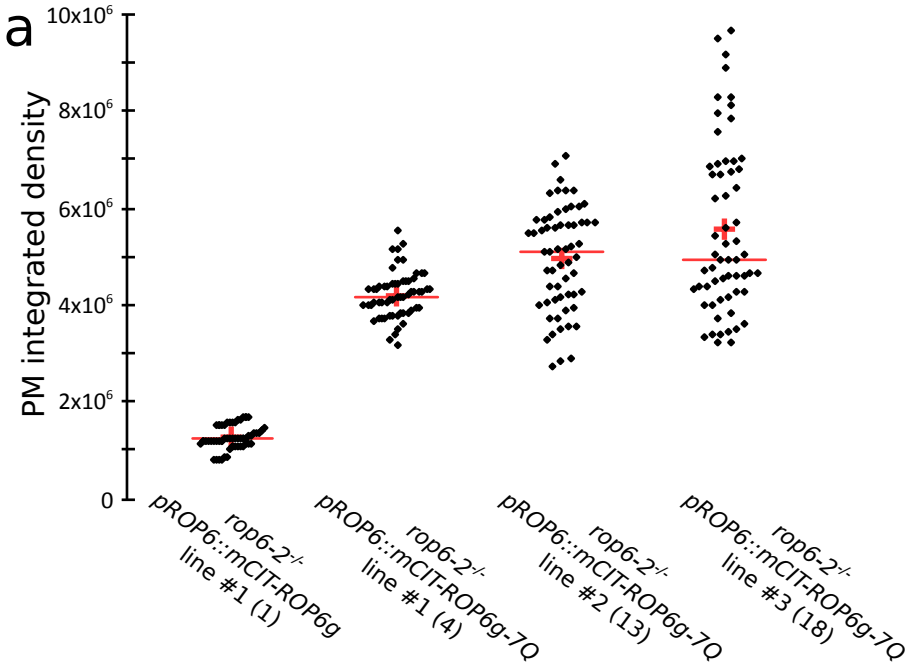
a
PM integrated density
10x10⁶
8x10⁶
6x10⁶
4x10⁶
2x10⁶
0
pROP6::mCIT-ROP6g line #1 (1)
rop6-2-/-
pROP6::mCIT-ROP6g-7Q line #1 (4)
pROP6::mCIT-ROP6g-7Q line #2 (13)
pROP6::mCIT-ROP6g-7Q line #3 (18)

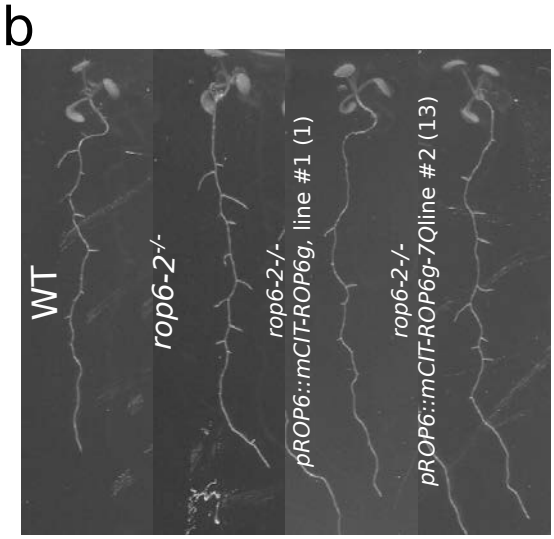
b
WT
rop6-2-/-
rop6-2-/- pROP6::mCIT-ROP6g, line #1 (1)
rop6-2-/- pROP6::mCIT-ROP6g-7Qline #2 (13)

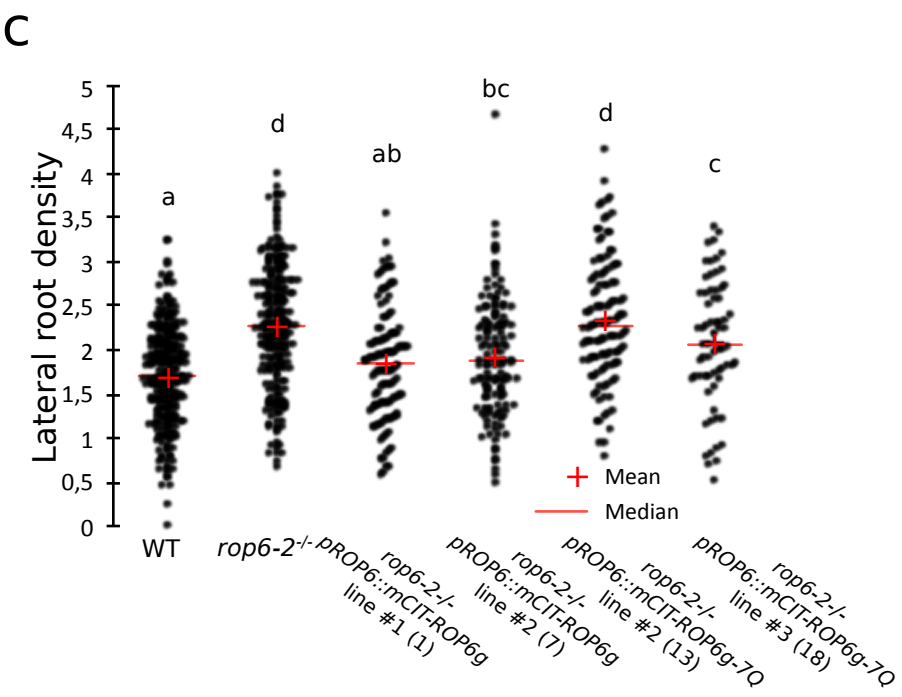
c
Lateral root density
5
4,5
4
3,5
3
2,5
2
1,5
1
0,5
0
a
d
ab
bc
d
c
Mean
Median
WT
rop6-2-/-
pROP6::mCIT-ROP6g line #1 (1)
pROP6::mCIT-ROP6g line #2 (7)
pROP6::mCIT-ROP6g-7Q line #2 (13)
pROP6::mCIT-ROP6g-7Q line #3 (18)

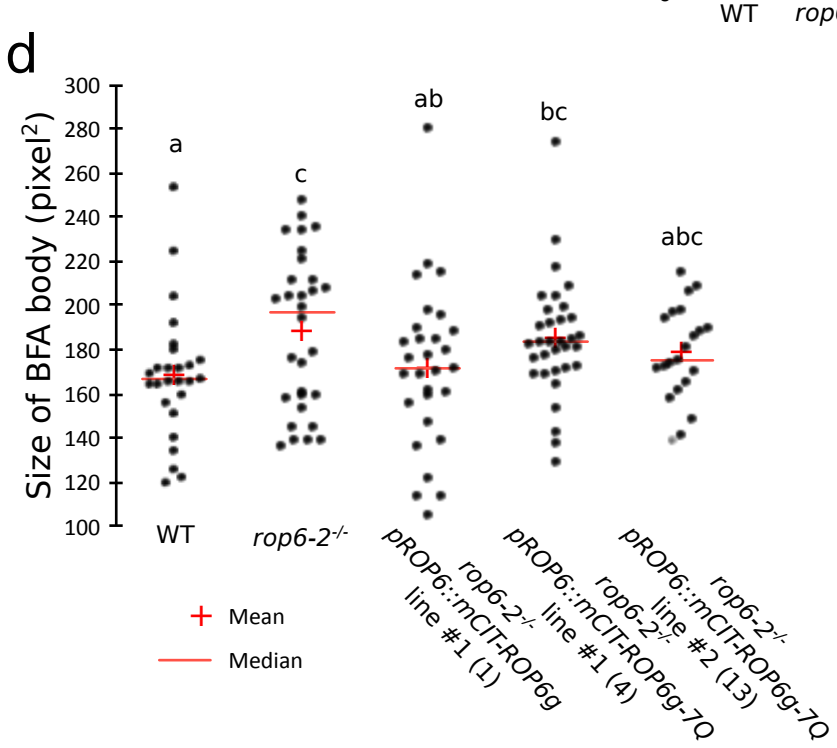
d
Size of BFA body (pixel²)
300
280
260
240
220
200
180
160
140
120
100
a
c
ab
bc
abc
Mean
Median
WT
rop6-2-/-
pROP6::mCIT-ROP6g line #1 (1)
pROP6::mCIT-ROP6g-7Q line #1 (4)
pROP6::mCIT-ROP6g-7Q line #2 (13)
pROP6::mCIT-ROP6g-7Q line #3 (18)

Extended Data Figure 5. The ROP6 polybasic region is required to complement *rop6-2*. (a) Quantification of the plasma membrane integrated intensity in 7 days old seedlings expressing *mCITRINE-ROP6* and *mCITRINE-ROP6*^{7Q} driven by its own promotor in *rop6-2*$^{-/-}$ background (n=60). (b) Images of 12 days old seedlings of plants expressing *mCITRINE-ROP6* and *mCITRINE-ROP6*^{7Q} driven by its own promotor in *rop6-2*$^{-/-}$ background showing lateral root formation and (c) the related quantification of the lateral root density. Letters indicate statistical difference. (d) Quantification of BFA body size in *mCITRINE-ROP6* and *mCITRINE-ROP6*^{7Q} lines driven by its own promotor in *rop6-2*$^{-/-}$ background. Letters indicate statistical difference. For statistical analysis details see, Sup_Data_Sheet_7.

a

PIP2a-mEOS

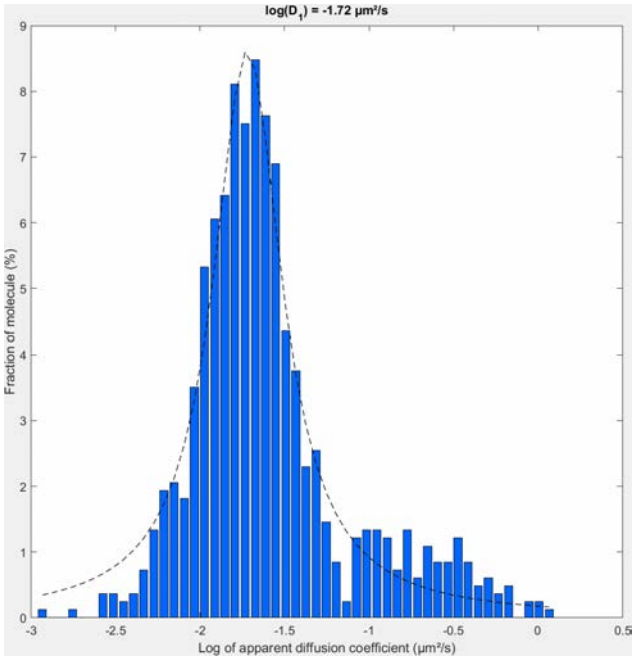

Lti6b-mEOS

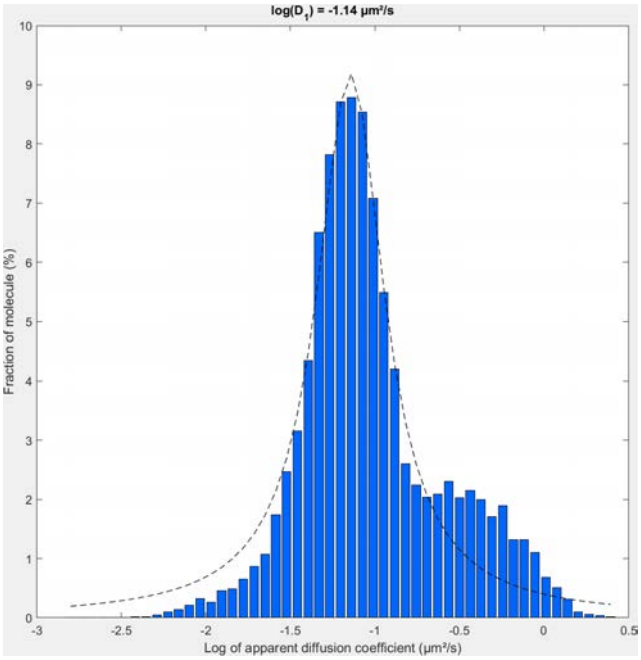

b

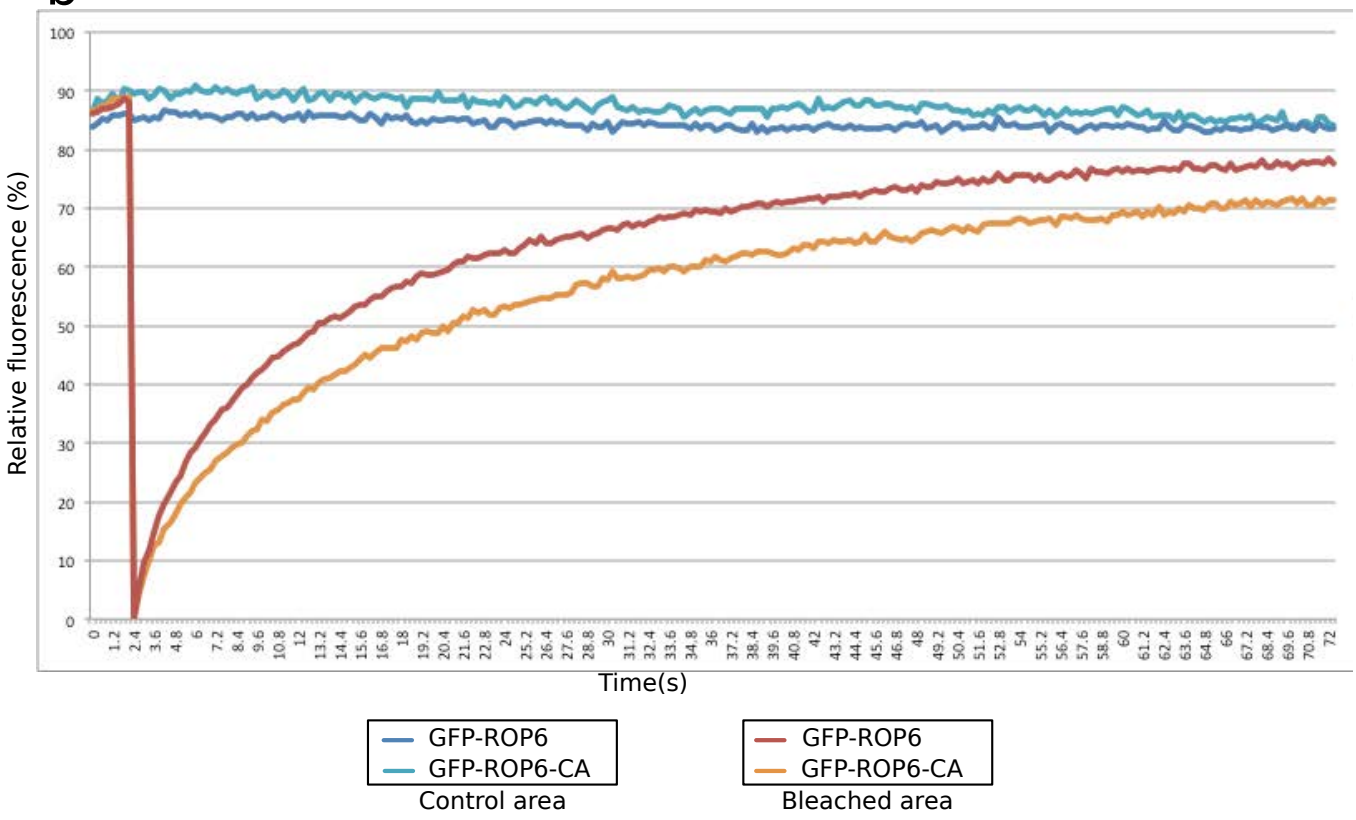

Extended Data Figure 6. Coefficient diffusion of low and fast-diffusible fraction and ROP6-CA diffusion. (a) Quantification of the percentage of Lti6b-mEos (left) and PIP2a-mEos (right) molecules according to their log of apparent diffusion coefficient obtained by analysing SptPALM tracks. (b) Traces of fluorescence intensity or GFP-ROP6 and GFP-ROP6-CA during FRAP analyses in WT plants.

a

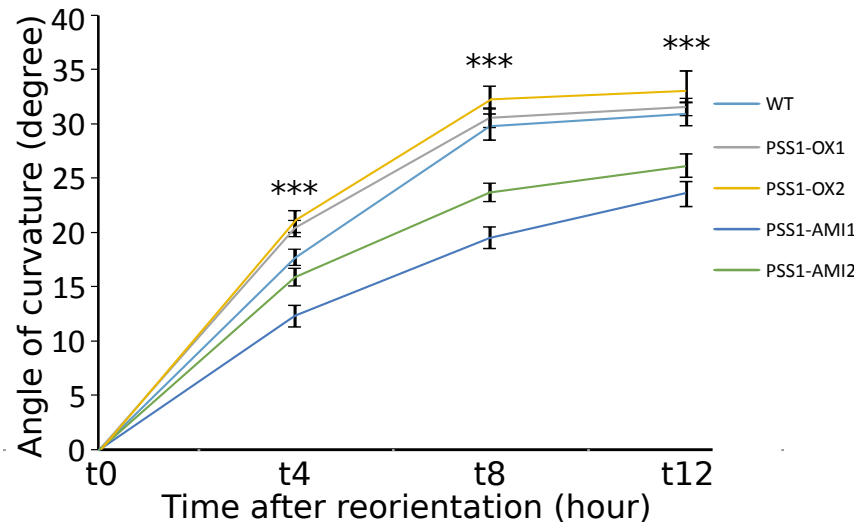
Angle of curvature (degree)
40
35
30
25
20
15
10
5
0
t0
t4
t8
t12
Time after reorientation (hour)
***
***
***
WT
PSS1-OX1
PSS1-OX2
PSS1-AMI1
PSS1-AMI2

b

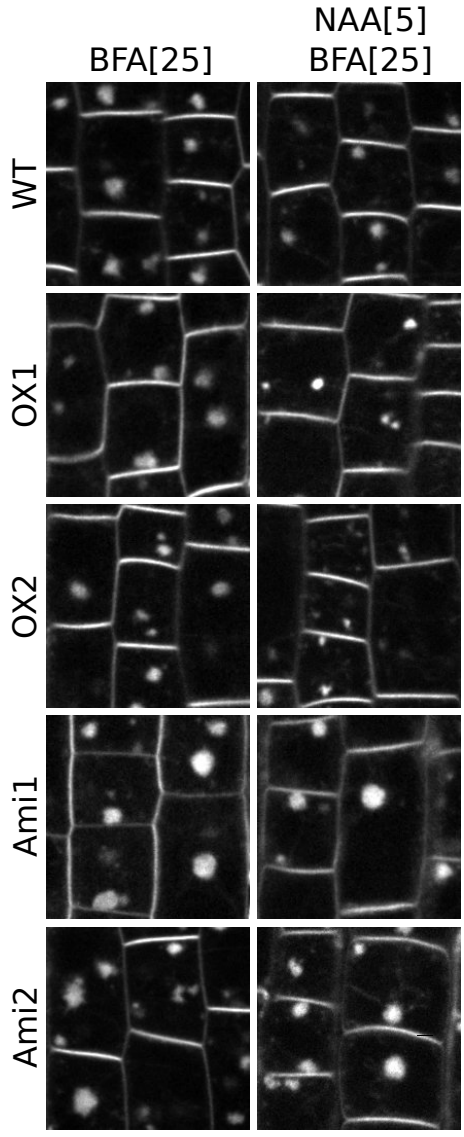
BFA[25]
NAA[5]
BFA[25]
WT
OX1
OX2
Ami1
Ami2

c

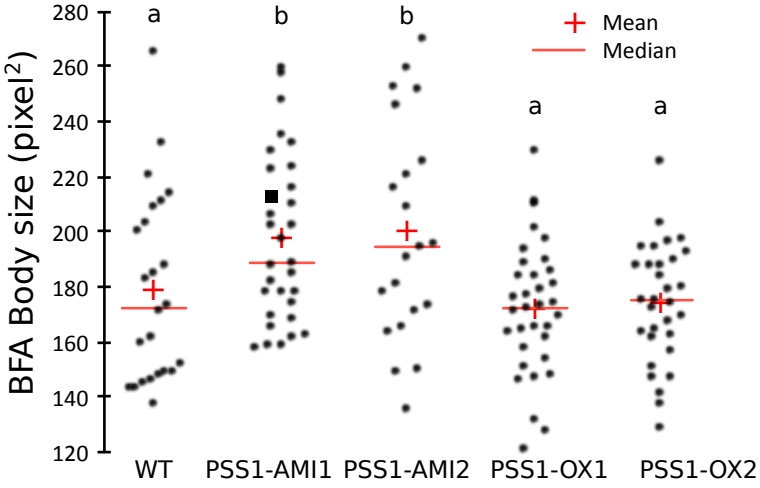
BFA Body size (pixel²)
280
260
240
220
200
180
160
140
120
a
b
b
a
a
Mean
Median
WT
PSS1-AMI1
PSS1-AMI2
PSS1-OX1
PSS1-OX2

Extended Data Figure 7. PS concentration affects endocytosis and gravitropic response in a dose dependent manner. (a) Quantification of gravitropic response in WT, *PSS1-AMI1*, *PSS1-AMI2*, *PSS1-OX1* and *PSS1-OX2*. 8 days old seedlings were rotated to 135°, and root tropic bending curvatures were measured at intervals of 4 hr. Stars indicated significant differences between WT and other genotypes at different time points. Error bars represent SEM. (b) Confocal images of 7-days-old seedlings of WT, *PSS1-AMI1*, *PSS1-AMI2*, *PSS1-OX1* and *PSS1-OX2* epidermal root cells stained by FM4-64 and concomitantly treated with BFA or BFA and NAA. (c) Quantification of the BFA body of WT, *PSS1-AMI1*, *PSS1-AMI2*, *PSS1-OX1* and *PSS1-OX2*. For statistical analysis details see, Sup_Data_Sheet_8.

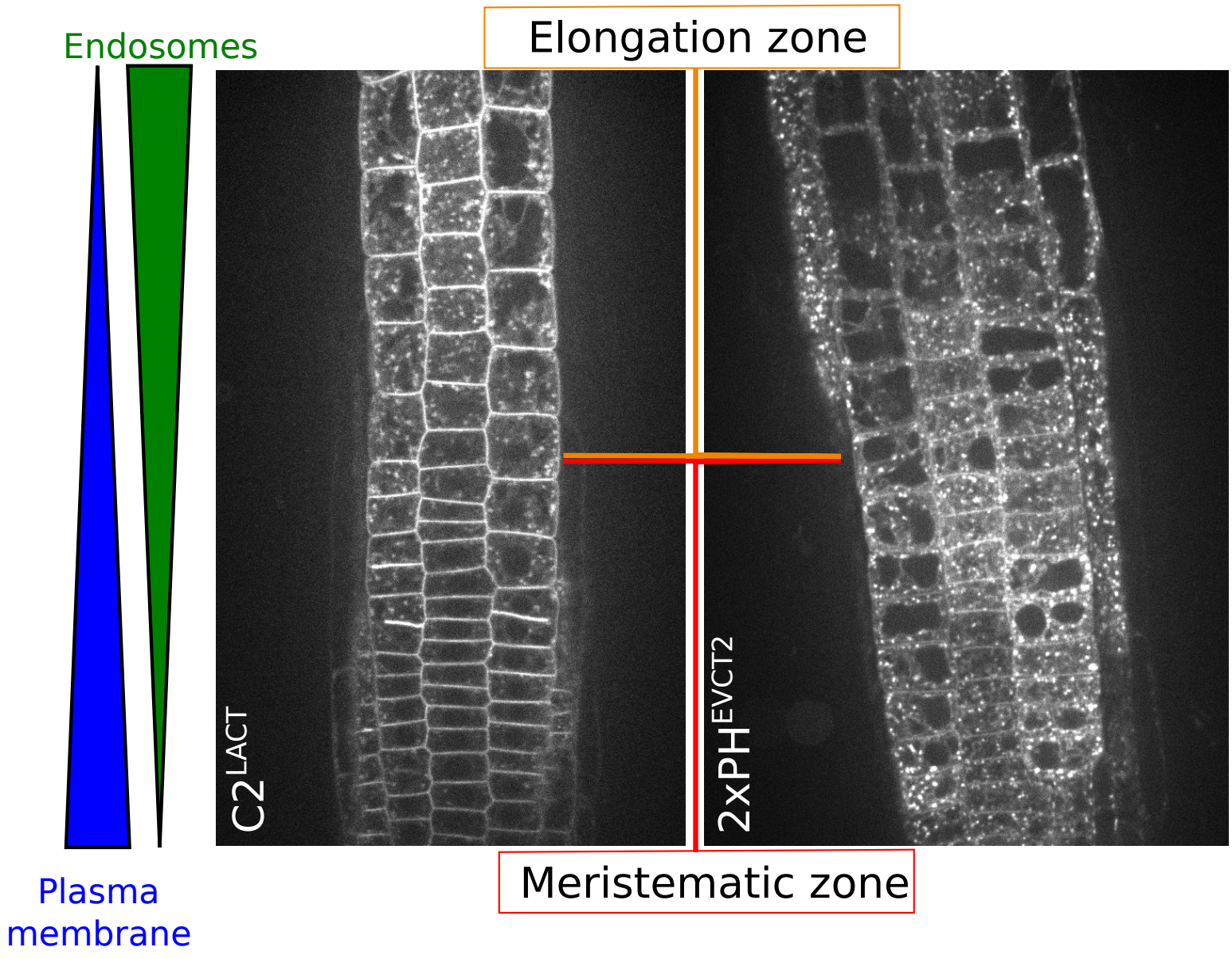
Endosomes
Elongation zone
C2LACT
2xPHEVCT2
Meristematic zone
Plasma membrane

Extended Data Figure 8. The plasma membrane PS association in the epidermal root cells tip correlates the auxin development gradient. From, the left to the right, gradient showing the preferential association of PS reporters, mCITRINE-$C2^{LACT}$ (left) and mCITRINE-$2xPH^{EVCT2}$ (right) with the plasma membrane and endosomes. For both PS sensors, the plasma membrane vs endosomes labelling is more pronounced in the meristematic zone compared to the elongation zone.

SUP_DATA_Sheet_1

Fig. 1.a

Variable\Test	Shapiro-Wilk	Anderson-Darling	Lilliefors	Jarque-Bera
1142-10	0,071	0,167	0,754	0,178
846-23	**0,001**	**0,005**	**0,023**	< **0,0001**
PSS1-3	**0,009**	**0,005**	**0,001**	0,214
PSS1-3x1142-10	**0,004**	**0,001**	**0,031**	0,178
PSS1-3xROP6-CA	**0,001**	**0,002**	**0,001**	< **0,0001**
ROP6-CA	0,185	0,342	0,717	0,475
WT	**0,040**	**0,020**	**0,032**	0,080

Test interpretation:
H0: The variable from which the sample was extracted follows a Normal distribution.
Ha: The variable from which the sample was extracted does not follow a Normal distribution.
As the computed p-value is greater than the significance level alpha=0,05, one cannot reject the null hypothesis H0.

T4

Variable	Observations	Obs. with missing data	Obs. without missing data	Minimum	Maximum	Mean	Std. deviation
WT	42	0	42	14,200	55,300	29,807	9,172
ROP6-CA	39	0	39	19,600	52,300	35,782	9,469

Mann-Whitney test / Two-tailed test:

U	525
U (standardized)	-2,774
Expected value	819,000
Variance (U)	11191,736
p-value (Two-tailed)	0,006
alpha	0,05

The p-value is computed using an exact method. Time elapsed: 0.000000s.

Variable	Observations	Obs. with missing data	Obs. without missing data	Minimum	Maximum	Mean	Std. deviation
WT	42	0	42	14,200	55,300	29,807	9,172
PSS1-3x1142-10	61	0	61	-46,600	47,100	18,131	21,939

Mann-Whitney test / Two-tailed test:

U	1670
U (standardized)	2,607
Expected value	1281,000
Variance (U)	22201,439
p-value (Two-tailed)	0,009
alpha	0,05

The p-value is computed using an exact method. Time elapsed: 0.000000s.

Variable	Observations	Obs. with missing data	Obs. without missing data	Minimum	Maximum	Mean	Std. deviation
WT	42	0	42	14,200	55,300	29,807	9,172
846-23	34	0	34	9,900	81,200	31,262	12,740

Mann-Whitney test / Two-tailed test:

U	701
U (standardized)	-0,131
Expected value	714,000
Variance (U)	9161,873
p-value (Two-tailed)	0,896
alpha	0,05

The p-value is computed using an exact method. Time elapsed: 0.000000s.

Variable	Observations	Obs. with missing data	Obs. without missing data	Minimum	Maximum	Mean	Std. deviation
WT	42	0	42	14,200	55,300	29,807	9,172
PSS1-3xROP6-CA	64	0	64	-51,300	49,400	16,136	22,858

Mann-Whitney test / Two-tailed test:

U	1912
U (standardized)	3,666
Expected value	1344,000
Variance (U)	23965,826
p-value (Two-tailed)	0,000
alpha	0,05

The p-value is computed using an exact method. Time elapsed: 0.000000s.

Variable	Observations	Obs. with missing data	Obs. without missing data	Minimum	Maximum	Mean	Std. deviation
WT	42	0	42	14,200	55,300	29,807	9,172
PSS1-3	50	0	50	-36,600	48,200	20,052	17,996

Mann-Whitney test / Two-tailed test:

U	1424
U (standardized)	2,928
Expected value	1050,000
Variance (U)	16273,746
p-value (Two-tailed)	0,003
alpha	0,05

The p-value is computed using an exact method. Time elapsed: 0.000000s.

Variable	Observations	Obs. with missing data	Obs. without missing data	Minimum	Maximum	Mean	Std. deviation
WT	42	0	42	14,200	55,300	29,807	9,172
1142-10	30	0	30	19,200	58,200	33,583	9,872

Mann-Whitney test / Two-tailed test:

U	478,500
U (standardized)	-1,725
Expected value	630,000
Variance (U)	7664,507
p-value (Two-tailed)	0,085
alpha	0,05

The p-value is computed using an exact method. Time elapsed: 0.000000s.

Variable\Test	Shapiro-Wilk	Anderson-Darling	Lilliefors	Jarque-Bera
1142-10	0,606	0,595	0,437	0,637
846-23	**0,000**	**< 0,0001**	**< 0,0001**	**< 0,0001**
PSS1-3	**0,003**	**0,003**	0,051	0,129
PSS1-3x1142-10	**0,002**	**0,001**	**0,007**	0,191
PSS1-3xROP6-CA	**0,001**	**0,001**	**0,015**	**0,003**
ROP6-CA	0,256	0,511	0,851	0,507
WT	0,325	0,210	0,271	0,620

Test interpretation:
H0: The variable from which the sample was extracted follows a Normal distribution.
Ha: The variable from which the sample was extracted does not follow a Normal distribution.
As the computed p-value is greater than the significance level alpha=0,05, one cannot reject the null hypothesis H0.

T8

Variable	Observations	Obs. with missing data	Obs. without missing data	Minimum	Maximum	Mean	Std. deviation
WT	39	0	39	25,700	52,400	38,438	6,889
PSS1-3xROP6-CA	70	0	70	-66,300	59,400	15,811	28,761

Mann-Whitney test / Two-tailed test:

U	2195
U (standardized)	5,244
Expected value	1365,000
Variance (U)	25023,261
p-value (Two-tailed)	< 0,0001
alpha	0,05

The p-value is computed using an exact method. Time elapsed: 0.000000s.

Variable	Observations	Obs. with missing data	Obs. without missing data	Minimum	Maximum	Mean	Std. deviation
WT	39	0	39	25,700	52,400	38,438	6,889
ROP6-CA	40	0	40	26,200	63,200	42,863	10,037

Mann-Whitney test / Two-tailed test:

U	575
U (standardized)	-2,005
Expected value	780,000
Variance (U)	10398,228
p-value (Two-tailed)	0,045
alpha	0,05

The p-value is computed using an exact method. Time elapsed: 0.000000s.

Variable	Observations	Obs. with missing data	Obs. without missing data	Minimum	Maximum	Mean	Std. deviation
846-23	35	0	35	26,000	89,200	40,237	13,477
WT	39	0	39	25,700	52,400	38,438	6,889

Mann-Whitney test / Two-tailed test:

U	623,500
U (standardized)	-0,633
Expected value	682,500
Variance (U)	8529,987
p-value (Two-tailed)	0,526
alpha	0,05

The p-value is computed using an exact method. Time elapsed: 0.000000s.

Variable	Observations	Obs. with missing data	Obs. without missing data	Minimum	Maximum	Mean	Std. deviation
WT	39	0	39	25,700	52,400	38,438	6,889
PSS1-3x1142-10	64	0	64	-50,900	49,400	17,273	27,050

Mann-Whitney test / Two-tailed test:

U	1995
U (standardized)	5,076
Expected value	1248,000
Variance (U)	21630,337
p-value (Two-tailed)	< 0,0001
alpha	0,05

The p-value is computed using an exact method. Time elapsed: 0.000000s.

Variable	Observations	Obs. with missing data	Obs. without missing data	Minimum	Maximum	Mean	Std. deviation
WT	39	0	39	25,700	52,400	38,438	6,889
PSS1-3	51	0	51	-58,600	54,800	19,565	29,477

Mann-Whitney test / Two-tailed test:

U	1448
U (standardized)	3,689
Expected value	994,500
Variance (U)	15082,008
p-value (Two-tailed)	0,000
alpha	0,05

The p-value is computed using an exact method. Time elapsed: 0.000000s.

Variable	Observations	Obs. with missing data	Obs. without missing data	Minimum	Maximum	Mean	Std. deviation
1142-10	28	0	28	29,100	63,400	43,425	8,705
WT	39	0	39	25,700	52,400	38,438	6,889

Mann-Whitney test / Two-tailed test:

U	720,500
U (standardized)	2,212
Expected value	546,000
Variance (U)	6187,136
p-value (Two-tailed)	0,027
alpha	0,05

The p-value is computed using an exact method. Time elapsed: 0.000000s.

Variable\Test	Shapiro-Wilk	Anderson-Darling	Lilliefors	Jarque-Bera
1142-10	**0,011**	**0,042**	0,134	**0,043**
846-23	0,050	**0,027**	**0,009**	0,340
PSS1-3	**0,003**	**0,002**	**0,015**	0,128
PSS1-3x1142-10	**0,002**	**0,000**	**0,000**	0,178
PSS1-3xROP6-CA	**0,001**	**0,001**	**0,025**	**0,008**
ROP6-CA	0,327	0,432	0,404	0,572
WT	0,174	0,200	0,324	0,070

Test interpretation:
H0: The variable from which the sample was extracted follows a Normal distribution.
Ha: The variable from which the sample was extracted does not follow a Normal distribution.
As the computed p-value is greater than the significance level alpha=0,05, one cannot reject the null hypothesis H0.

T12

Variable	Observations	Obs. with missing data	Obs. without missing data	Minimum	Maximum	Mean	Std. deviation
WT	42	0	42	23,400	76,200	44,219	9,871
ROP6-CA	37	0	37	32,900	76,000	48,684	10,571

Mann-Whitney test / Two-tailed test:

U	587,500
U (standardized)	-1,857
Expected value	777,000
Variance (U)	10358,361
p-value (Two-tailed)	0,063
alpha	0,05

The p-value is computed using an exact method. Time elapsed: 0.000000s.

Variable	Observations	Obs. with missing data	Obs. without missing data	Minimum	Maximum	Mean	Std. deviation
WT	42	0	42	23,400	76,200	44,219	9,871
PSS1-3x1142-10	64	0	64	-62,500	61,800	17,877	28,832

Mann-Whitney test / Two-tailed test:

U	2333,500
U (standardized)	6,388
Expected value	1344,000
Variance (U)	23966,913
p-value (Two-tailed)	< 0,0001
alpha	0,05

The p-value is computed using an exact method. Time elapsed: 0.000000s.

Variable	Observations	Obs. with missing data	Obs. without missing data	Minimum	Maximum	Mean	Std. deviation
WT	42	0	42	23,400	76,200	44,219	9,871
846-23	38	0	38	24,800	75,500	46,618	13,622

Mann-Whitney test / Two-tailed test:

U	786
U (standardized)	-0,111
Expected value	798,000
Variance (U)	10771,864
p-value (Two-tailed)	0,912
alpha	0,05

The p-value is computed using an exact method. Time elapsed: 0.000000s.

Variable	Observations	Obs. with missing data	Obs. without missing data	Minimum	Maximum	Mean	Std. deviation
WT	42	0	42	23,400	76,200	44,219	9,871
PSS1-3xROP6-CA	70	0	70	-66,300	59,400	15,811	28,761

Mann-Whitney test / Two-tailed test:

U	2556
U (standardized)	6,524
Expected value	1470,000
Variance (U)	27682,399
p-value (Two-tailed)	< 0,0001
alpha	0,05

The p-value is computed using an exact method. Time elapsed: 0.000000s.

Variable	Observations	Obs. with missing data	Obs. without missing data	Minimum	Maximum	Mean	Std. deviation
WT	42	0	42	23,400	76,200	44,219	9,871
PSS1-3	54	0	54	-57,300	61,400	20,070	30,089

Mann-Whitney test / Two-tailed test:

U	1749,500
U (standardized)	4,542
Expected value	1134,000
Variance (U)	18332,130
p-value (Two-tailed)	< 0,0001
alpha	0,05

The p-value is computed using an exact method. Time elapsed: 0.000000s.

Variable	Observations	Obs. with missing data	Obs. without missing data	Minimum	Maximum	Mean	Std. deviation
WT	42	0	42	23,400	76,200	44,219	9,871
1142-10	31	0	31	30,600	83,600	48,274	13,480

Mann-Whitney test / Two-tailed test:

U	550
U (standardized)	-1,122
Expected value	651,000
Variance (U)	8027,885
p-value (Two-tailed)	0,262
alpha	0,05

The p-value is computed using an exact method. Time elapsed: 0.000000s.

Test interpretation:
H0: The difference of location between the samples is equal to 0.
Ha: The difference of location between the samples is different from 0.
As the computed p-value is lower than the significance level alpha=0,05, one should reject the null hypothesis H0, and accept the alternative hypothesis Ha.

Fig. 1.c

Variable\Test	Shapiro-Wilk	Anderson-Darling	Lilliefors	Jarque-Bera
WT_ROP6	0,272	0,143	0,349	0,482
rop6-2	0,137	0,197	0,398	0,545
ROP6-CA	0,669	0,755	0,784	0,777
WT_PSS1	0,189	0,256	0,285	0,568
PSS1-3	0,140	0,190	0,375	0,538
PSS1-3xROP6-CA	0,622	0,367	0,452	0,929

Test interpretation:
H0: The variable from which the sample was extracted follows a Normal distribution.
Ha: The variable from which the sample was extracted does not follow a Normal distribution.
As the computed p-value is greater than the significance level alpha=0,05, one cannot reject the null hypothesis H0.

Variable	Categories	Counts
Genotype	PSS1-3	14
	PSS1-3xROP6-CA	21
	WT	14

Variable	Categories	Counts
Genotype	ROP6-CA	28
	WT	26
	rop6-2	30

Genotype / Fisher (LSD) / Analysis of the differences between the categories with a confidence interval of 95% (BFA_SIZE):

Contrast	Difference	Standardized difference	Critical value	Pr > Diff	Significant
rop6-2 vs ROP6-CA	56,251	7,403	1,981	**< 0,0001**	Yes
rop6-2 vs WT	20,116	2,596	1,981	**0,011**	Yes
WT vs ROP6-CA	36,135	4,588	1,981	**< 0,0001**	Yes
LSD-value :			14,103		

Category	LS means	Standard error	Lower bound (95%)	Upper bound (95%)	Groups	
rop6-2	188,211	5,279	177,752	198,670	A	
WT	168,095	5,671	156,860	179,329		B
ROP6-CA	131,959	5,465	121,133	142,786		C

Genotype / Fisher (LSD) / Analysis of the differences between the categories with a confidence interval of 95% (BFA_SIZE):

Contrast	Difference	Standardized difference	Critical value	Pr > Diff	Significant
PSS1-3 vs WT	26,855	2,377	1,990	**0,020**	Yes
PSS1-3 vs PSS1-3xROP6-CA	4,946	0,479	1,990	0,633	No
PSS1-3xROP6-CA vs WT	21,909	2,124	1,990	**0,037**	Yes
LSD-value :			18,361		

Category	LS means	Standard error	Lower bound (95%)	Upper bound (95%)	Groups	
PSS1-3	205,843	7,990	189,942	221,744	A	
PSS1-3xROP6-CA	200,897	6,524	187,914	213,880	A	
WT	178,988	7,990	163,087	194,889		B

Fig. 1.e

Variable\Test	Shapiro-Wilk	Anderson-Darling	Lilliefors	Jarque-Bera
WT_ROP6	0,450	0,586	0,835	0,568
ROP6-2	0,285	0,330	0,239	0,392
WT-PSS1	**0,007**	**0,005**	**0,012**	0,230
PSS1	**0,046**	0,156	0,107	**0,008**

Test interpretation:
H0: The variable from which the sample was extracted follows a Normal distribution.
Ha: The variable from which the sample was extracted does not follow a Normal distribution.
As the computed p-value is greater than the significance level alpha=0,05, one cannot reject the null hypothesis H0.

Variable	Observations	Obs. with missing data	Obs. without missing data	Minimum	Maximum	Mean	Std. deviation
WT-PSS1	24	0	24	102,200	175,762	150,661	21,986
PSS1	21	0	21	120,860	214,976	184,316	20,807

t-test for two independent samples / Two-tailed test:

95% confidence interval on the difference between the means:
[-46,578 ; -20,731 [

Difference	-33,654
t (Observed value)	-5,252
|t| (Critical value)	2,017
DF	43
p-value (Two-tailed)	< 0,0001
alpha	0,05

Test interpretation:
H0: The difference between the means is equal to 0.
Ha: The difference between the means is different from 0.

As the computed p-value is lower than the significance level alpha=0,05, one should reject the null hypothesis H0, and accept the alternative hypothesis Ha.

Variable	Observations	Obs. with missing data	Obs. without missing data	Minimum	Maximum	Mean	Std. deviation
WT_ROP6	37	0	37	79,537	158,636	124,343	21,585
ROP6-2	38	0	38	98,435	203,583	140,827	25,346

t-test for two independent samples / Two-tailed test:

95% confidence interval on the difference between the means:
[-27,332 ; -5,636 [

Difference	-16,484
t (Observed value)	-3,029
|t| (Critical value)	1,993
DF	73
p-value (Two-tailed)	0,003
alpha	0,05

Test interpretation:
H0: The difference between the means is equal to 0.
Ha: The difference between the means is different from 0.
As the computed p-value is lower than the significance level alpha=0,05, one should reject the null hypothesis H0, and accept the alternative hypothesis Ha.

Fig. 1.g

Variable\Test	Shapiro-Wilk	Anderson-Darling	Lilliefors	Jarque-Bera
WT	**0,009**	**0,012**	0,052	0,292
WT_NAA	0,068	0,092	0,332	0,557
PSS1-3	**0,000**	**< 0,0001**	**0,000**	**< 0,0001**
PSS1-3_NAA	**0,000**	**< 0,0001**	**< 0,0001**	**0,000**

Test interpretation:
H0: The variable from which the sample was extracted follows a Normal distribution.
Ha: The variable from which the sample was extracted does not follow a Normal distribution.
As the computed p-value is greater than the significance level alpha=0,05, one cannot reject the null hypothesis H0.

Variable	Observations	Obs. with missing data	Obs. without missing data	Minimum	Maximum	Mean	Std. deviation
WT	26	0	26	9,524	95,000	67,528	26,733
PSS1-3	21	0	21	2,703	97,500	77,138	22,475

Mann-Whitney test / Two-tailed test:

U	220,500
U (standardized)	-1,113
Expected value	273,000
Variance (U)	2183,747
p-value (Two-tailed)	0,266
alpha	0,05

The p-value is computed using an exact method. Time elapsed: 0.000000s.

Variable	Observations	Obs. with missing data	Obs. without missing data	Minimum	Maximum	Mean	Std. deviation
PSS1-3	21	0	21	2,703	97,500	77,138	22,475
PSS1-3_NAA	22	0	22	33,333	97,436	80,463	16,506

Mann-Whitney test / Two-tailed test:

U	214
U (standardized)	-0,401
Expected value	231,000
Variance (U)	1693,360
p-value (Two-tailed)	0,688
alpha	0,05

The p-value is computed using an exact method. Time elapsed: 0.000000s.

Variable	Observations	Obs. with missing data	Obs. without missing data	Minimum	Maximum	Mean	Std. deviation
WT	26	0	26	9,524	95,000	67,528	26,733
WT_NAA	28	0	28	2,778	72,000	39,513	21,472

Mann-Whitney test / Two-tailed test:

U	585,500
U (standardized)	3,826
Expected value	364,000
Variance (U)	3336,412

p-value (Two-tailed)	0,00013
alpha	0,05

The p-value is computed using an exact method. Time elapsed: 0.000000s.

Test interpretation:
H0: The difference of location between the samples is equal to 0.
Ha: The difference of location between the samples is different from 0.
As the computed p-value is lower than the significance level alpha=0,05, one should reject the null hypothesis H0, and accept the alternative hypothesis Ha.

SUP_Data_Sheet_2

Fig. 2.b

Variable\Test	Shapiro-Wilk	Anderson-Darling	Lilliefors	Jarque-Bera
WT	**0,027**	**0,035**	**0,029**	0,504
PSS1-3	0,189	0,333	0,671	0,325
PSS1-3_LPS	0,086	0,177	0,583	0,248

Test interpretation:
H0: The variable from which the sample was extracted follows a Normal distribution.
Ha: The variable from which the sample was extracted does not follow a Normal distribution.
As the computed p-value is greater than the significance level alpha=0,05, one cannot reject the null hypothesis H0.

Variable	Observations	Obs. with missing data	Obs. without missing data	Minimum	Maximum	Mean	Std. deviation
PSS1-3	22	0	22	2,548	15,077	7,222	3,284
PSS1-3_LPS	11	0	11	0,037	1,174	0,372	0,339

t-test for two independent samples / Two-tailed test:

95% confidence interval on the difference between the means:
[4,810; 8,891 [

Difference	6,850
t (Observed value)	6,847
|t| (Critical value)	2,040
DF	31
p-value (Two-tailed)	< 0,0001
alpha	0,05

Variable	Observations	Obs. with missing data	Obs. without missing data	Minimum	Maximum	Mean	Std. deviation
WT	26	0	26	0,000	2,438	0,754	0,751
PSS1-3	22	0	22	2,548	15,077	7,222	3,284

t-test for two independent samples / Two-tailed test:

95% confidence interval on the difference between the means:
[-7,802 ; -5,135 [

Difference	-6,469
t (Observed value)	-9,765
|t| (Critical value)	2,013
DF	46
p-value (Two-tailed)	< 0,0001
alpha	0,05

Test interpretation:
H0: The difference between the means is equal to 0.
Ha: The difference between the means is different from 0.

As the computed p-value is lower than the significance level alpha=0,05, one should reject the null hypothesis H0, and accept the alternative hypothesis Ha.

Fig. 2.d

Full lengh

Variable\Test	Shapiro-Wilk	Anderson-Darling	Lilliefors	Jarque-Bera
ROP6	0,694	0,772	0,730	0,689
ROP6-3Q	**0,014**	**0,035**	0,068	**0,014**
ROP6-7Q	0,610	0,837	0,936	0,709

Test interpretation:
H0: The variable from which the sample was extracted follows a Normal distribution.
Ha: The variable from which the sample was extracted does not follow a Normal distribution.
As the computed p-value is greater than the significance level alpha=0,05, one cannot reject the null hypothesis H0.

Variable	Categories	Counts
Genotype	ROP6	14
	ROP6-3Q	15
	ROP6-7Q	12

Genotype / Fisher (LSD) / Analysis of the differences between the categories with a confidence interval of 95% (NB/Cell):

Contrast	Difference	Standardized difference	Critical value	Pr > Diff	Significant
ROP6-7Q vs ROP6	14,945	11,028	2,024	**< 0,0001**	Yes
ROP6-7Q vs ROP6-3Q	10,015	7,506	2,024	**< 0,0001**	Yes
ROP6-3Q vs ROP6	4,930	3,851	2,024	**0,000**	Yes
LSD-value:			2,547		

Category	LS means	Standard error	Lower bound (95%)	Upper bound (95%)	Groups		
ROP6-7Q	16,874	0,994	14,861	18,887	A		
ROP6-3Q	6,859	0,890	5,058	8,660		B	
ROP6	1,929	0,921	0,065	3,792			C

C-term

Variable\Test	Shapiro-Wilk	Anderson-Darling	Lilliefors	Jarque-Bera
ROP6	0,470	0,668	0,831	0,662
ROP6-3Q	0,991	0,981	0,998	0,853
ROP6-7Q	0,226	0,275	0,286	0,403

Test interpretation:
H0: The variable from which the sample was extracted follows a Normal distribution.
Ha: The variable from which the sample was extracted does not follow a Normal distribution.
As the computed p-value is greater than the significance level alpha=0,05, one cannot reject the null hypothesis H0.

Variable	Categories	Counts
Genotype	ROP6	28
	ROP6-3Q	27
	ROP6-7Q	15

Genotype / Fisher (LSD) / Analysis of the differences between the categories with a confidence interval of 95% (NB/Cell):

Contraste	Différence	Différence standardisée	Valeur critique	Pr > Diff	Significatif

ROP6-7Q vs ROP6	27,082	23,474	1,996	**< 0,0001**	Yes
ROP6-7Q vs ROP6-3Q	19,036	16,394	1,996	**< 0,0001**	Yes
ROP6-3Q vs ROP6	8,046	8,273	1,996	**< 0,0001**	Yes
LSD-value :			1,923		

Category	LS means	Standard error	Lower bound (95%)	Upper bound (95%)	Groups		
ROP6-7Q	28,583	0,931	26,725	30,441	A		
ROP6-3Q	9,547	0,694	8,162	10,932		B	
ROP6	1,501	0,681	0,141	2,861			C

Fig. 2.e

T4

Variable\Test	Shapiro-Wilk	Anderson-Darling	Lilliefors	Jarque-Bera
ROP6-7Q-OX	**0,006**	**0,004**	**0,009**	0,231
ROP6-OX	0,137	0,142	0,189	0,323
WT	0,180	0,286	0,158	0,413

Test interpretation:
H0: The variable from which the sample was extracted follows a Normal distribution.
Ha: The variable from which the sample was extracted does not follow a Normal distribution.
As the computed p-value is greater than the significance level alpha=0,05, one cannot reject the null hypothesis H0.

Variable	Categories	Counts
Genotype	ROP6-7Q-OX	45
	ROP6-OX	37
	WT	45

Genotype / Fisher (LSD) / Analysis of the differences between the categories with a confidence interval of 90% (Angle):

Contrast	Difference	Standardized difference	Critical value	Pr > Diff	Significant
ROP6-OX vs ROP6-7Q-OX	5,942	3,745	1,657	**0,000**	Oui
ROP6-OX vs WT	3,402	2,144	1,657	**0,034**	Oui
WT vs ROP6-7Q-OX	2,540	1,685	1,657	**0,094**	Oui
LSD-value :			2,498		

Category	LS means	Standard error	Lower bound (95%)	Upper bound (95%)	Groups		
ROP6-OX	35,362	1,175	33,414	37,310	A		
WT	31,960	1,066	30,194	33,726		B	
ROP6-7Q-OX	29,420	1,066	27,654	31,186			C

T8

Variable\Test	Shapiro-Wilk	Anderson-Darling	Lilliefors	Jarque-Bera
WT	0,352	0,276	0,275	0,415
ROP6-OX	**0,009**	**0,031**	0,087	0,145
ROP6-7Q-OX	0,504	0,496	0,591	0,548

Test interpretation:
H0: The variable from which the sample was extracted follows a Normal distribution.
Ha: The variable from which the sample was extracted does not follow a Normal distribution.
As the computed p-value is greater than the significance level alpha=0,05, one cannot reject the null hypothesis H0.

Variable	Categories	Counts
Genotype	ROP6-7Q-OX	42
	ROP6-OX	43
	WT	49

Genotype / Fisher (LSD) / Analysis of the differences between the categories with a confidence interval of 90% (Angle):

Contrast	Difference	Standardized difference	Critical value	Pr > Diff	Significant
ROP6-OX vs ROP6-7Q-OX	4,790	3,268	1,657	**0,001**	Oui
ROP6-OX vs WT	3,646	2,583	1,657	**0,011**	Oui
WT vs ROP6-7Q-OX	1,144	0,805	1,657	0,422	Non
LSD-value :			2,261		

Category	LS means	Standard error	Lower bound (95%)	Upper bound (95%)	Groups	
ROP6-OX	42,128	1,030	40,421	43,835	A	
WT	38,482	0,965	36,883	40,081		B
ROP6-7Q-OX	37,338	1,043	35,611	39,065		B

T12

Variable\Test	Shapiro-Wilk	Anderson-Darling	Lilliefors	Jarque-Bera
ROP6-7Q-OX	**0,020**	**0,032**	0,159	0,215
ROP6-OX	0,245	0,304	0,498	0,295
WT	0,695	0,728	0,734	0,603

Variable	Categories	Counts
Genotype	ROP6-7Q-OX	50
	ROP6-OX	43
	WT	65

Genotype / Fisher (LSD) / Analysis of the differences between the categories with a confidence interval of 90% (Angle):

Contrast	Difference	Standardized difference	Critical value	Pr > Diff	Significant
ROP6-OX vs ROP6-7Q-OX	3,582	2,120	1,655	**0,036**	Oui
ROP6-OX vs WT	1,702	1,066	1,655	0,288	Non
WT vs ROP6-7Q-OX	1,880	1,230	1,655	0,220	Non
LSD-value :			2,358		

Modalité	Moyennes estimées	Erreur standard	Borne inférieure (90%)	Borne supérieure (90%)	Groupes	
ROP6-OX	43,774	1,239	41,724	45,824	A	
WT	42,072	1,008	40,405	43,740	A	B
ROP6-7Q-OX	40,192	1,149	38,291	42,093		B

Fig. 2.f

Variable\Test	Shapiro-Wilk	Anderson-Darling	Lilliefors	Jarque-Bera
WT	**0,009**	**0,005**	0,052	**0,011**
ROP6-7Q-OX	0,762	0,604	0,335	0,787
ROP6-OX	0,176	0,379	0,724	0,552

Test interpretation:
H0: The variable from which the sample was extracted follows a Normal distribution.
Ha: The variable from which the sample was extracted does not follow a Normal distribution.
As the computed p-value is greater than the significance level alpha=0,05, one cannot reject the null hypothesis H0.

Categories	Counts	Comptages
Genotype	ROP6-7Q-OX	22
	ROP6-OX	29
	WT	26

Genotype / Fisher (LSD) / Analysis of the differences between the categories with a confidence interval of 95% (BFA_SIZE):

Contrast	Difference	Standardized difference	Critical value	Pr > Diff	Significant
WT vs ROP6-OX	17,194	2,539	1,973	**0,012**	Yes
WT vs ROP6-7Q-OX	0,656	0,090	1,973	0,928	No
ROP6-7Q-OX vs ROP6-OX	16,537	2,332	1,973	**0,021**	Yes
LSD-value :			10,099		

Category	LS means	Standard error	Lower bound (95%)	Upper bound (95%)	Groups	
WT	168,095	4,918	158,391	177,798	A	
ROP6-7Q-OX	167,438	5,347	156,890	177,986	A	
ROP6-OX	150,901	4,657	141,713	160,088		B

SUP_Data_Sheet_3

Fig. 4.a

Variable\Test	Shapiro-Wilk	Anderson-Darling	Lilliefors	Jarque-Bera
PSS1-AMI1	0,653	0,644	0,715	0,740
PSS1-AMI2	0,802	0,704	0,835	0,787
WT	0,145	0,184	0,383	0,671
PSS1-OX1	0,815	0,839	0,832	0,811
PSS1-OX2	0,336	0,343	0,374	0,668

Test interpretation:
H0: The variable from which the sample was extracted follows a Normal distribution.
Ha: The variable from which the sample was extracted does not follow a Normal distribution.
As the computed p-value is greater than the significance level alpha=0,05, one cannot reject the null hypothesis H0.

Variable	Categories	Counts
Genotype	PSS1-AMI1	6
	PSS1-AMI2	6
	PSS1-OX1	6
	PSS1-OX2	6
	WT	6

Genotype / Fisher (LSD) / Analysis of the differences between the categories with a confidence interval of 95% (Value):

Contrast	Difference	Standardized difference	Critical value	Pr > Diff	Significant
WT vs PSS1-AMI1	0,007	18,736	2,131	**< 0,0001**	Yes
WT vs PSS1-AMI2	0,006	16,343	2,131	**< 0,0001**	Yes
PSS1-AMI2 vs PSS1-AMI1	0,001	2,394	2,131	**0,030**	Yes
LSD-value:			7,846E-4		

Category	LS means	Standard error	Lower bound (95%)	Upper bound (95%)	Groups		
WT	0,010	0,000	0,010	0,011	A		
PSS1-AMI2	0,004	0,000	0,004	0,005		B	
PSS1-AMI1	0,003	0,000	0,003	0,004			C

Genotype / Fisher (LSD) / Analysis of the differences between the categories with a confidence interval of 95% (Value):

Contrast	Difference	Standardized difference	Critical value	Pr > Diff	Significant
PSS1-OX2 vs WT	1,057	17,945	2,131	**< 0,0001**	Yes
PSS1-OX2 vs PSS1-OX1	0,398	6,760	2,131	**< 0,0001**	Yes
PSS1-OX1 vs WT	0,659	11,185	2,131	**< 0,0001**	Yes
LSD-value:			0,125		

Category	LS means	Standard error	Lower bound (95%)	Upper bound (95%)	Groups		
PSS1-OX2	1,067	0,042	0,978	1,155	A		
PSS1-OX1	0,669	0,042	0,580	0,758		B	
WT	0,010	0,042	-0,079	0,099			C

Fig. 4.b

Variable\Test	Shapiro-Wilk	Anderson-Darling	Lilliefors	Jarque-Bera
PSS1-AMI1	0,286	0,285	0,368	0,692
PSS1-AMI2	0,405	0,481	0,591	0,739
WT	0,705	0,542	0,616	0,798
PSS1-OX1	0,369	0,416	0,546	0,711
PSS1-OX2	0,912	0,780	0,726	0,886

Test interpretation:
H0: The variable from which the sample was extracted follows a Normal distribution.
Ha: The variable from which the sample was extracted does not follow a Normal distribution.
As the computed p-value is greater than the significance level alpha=0,05, one cannot reject the null hypothesis H0.

Variable	Categories	Counts
Genotype	PSS1-AMI1	6
	PSS1-AMI2	6
	WT	6

Genotype / Fisher (LSD) / Analysis of the differences between the categories with a confidence interval of 90% (Value):

Contrast	Difference	Standardized difference	Critical value	Pr > Diff	Significant
WT vs PSS1-AMI2	0,003	2,017	1,753	**0,062**	Yes
WT vs PSS1-AMI1	0,003	1,808	1,753	**0,091**	Yes
PSS1-AMI1 vs PSS1-AMI2	0,000	0,209	1,753	0,837	No
LSD-value:			0,003		

Category	LS means	Standard error	Lower bound (90%)	Upper bound (90%)	Groups	
WT	0,015	0,001	0,013	0,017	A	
PSS1-AMI1	0,012	0,001	0,010	0,014		B
PSS1-AMI2	0,012	0,001	0,010	0,014		B

Genotype / Fisher (LSD) / Analysis of the differences between the categories with a confidence interval of 90% (Value):

Contrast	Difference	Standardized difference	Critical value	Pr > Diff	Significant
PSS1-OX2 vs WT	0,015	4,273	1,753	**0,001**	Yes
PSS1-OX2 vs PSS1-OX1	0,005	1,405	1,753	0,180	No
PSS1-OX1 vs WT	0,010	2,868	1,753	**0,012**	Yes
LSD-value:			0,006		

Category	LS means	Standard error	Lower bound (90%)	Upper bound (90%)	Groups	
PSS1-OX2	0,031	0,003	0,026	0,035	A	
PSS1-OX1	0,025	0,003	0,021	0,030	A	
WT	0,015	0,003	0,011	0,020		B

Fig. 4.c

Variable\Test	Shapiro-Wilk	Anderson-Darling	Lilliefors	Jarque-Bera
PSS1-3	**< 0,0001**	**< 0,0001**	**0,000**	**0,015**
PSS1-AMI1	0,511	0,628	0,585	0,496
PSS1-AMI2	0,625	0,622	0,498	0,660
WT	**0,004**	**0,039**	0,196	**< 0,0001**
PSS1-OX1	**0,037**	0,066	0,253	0,096
PSS1-OX2	0,077	0,265	0,341	**0,005**

Test interpretation:
H0: The variable from which the sample was extracted follows a Normal distribution.
Ha: The variable from which the sample was extracted does not follow a Normal distribution.

As the computed p-value is lower than the significance level alpha=0,05, one should reject the null hypothesis H0, and accept the alternative hypothesis Ha.

Variable	Categories	Counts
Genotype	PSS1-AMI1	57
	PSS1-AMI2	77
	PSS1-OX1	52
	PSS1-OX2	40
	PSS1-3	51
	WT	65

Variable	Observations	Obs. with missing data	Obs. without missing data	Minimum	Maximum	Mean	Std. deviation
WT	65	0	65	21,700	84,400	40,511	10,160
PSS1-AMI1	57	0	57	17,600	50,400	32,584	7,797

Mann-Whitney test / Two-tailed test:

U	2712
U (standardized)	4,408
Expected value	1852,500
Variance (U)	37973,113
p-value (Two-tailed)	< 0,0001
alpha	0,1

The p-value is computed using an exact method. Time elapsed: 0.000000s.

Variable	Observations	Obs. with missing data	Obs. without missing data	Minimum	Maximum	Mean	Std. deviation
WT	65	0	65	21,700	84,400	40,511	10,160
PSS1-3	51	0	51	-58,600	54,800	19,565	29,477

Mann-Whitney test / Two-tailed test:

U	2470,500
U (standardized)	4,520
Expected value	1657,500
Variance (U)	32319,138
p-value (Two-tailed)	< 0,0001
alpha	0,1

The p-value is computed using an exact method. Time elapsed: 0.000000s.

Variable	Observations	Obs. with missing data	Obs. without missing data	Minimum	Maximum	Mean	Std. deviation
WT	65	0	65	21,700	84,400	40,511	10,160
PSS1-AMI2	77	0	77	20,100	53,800	35,794	7,661

Mann-Whitney test / Two-tailed test:

U	3174
U (standardized)	2,748
Expected value	2502,500
Variance (U)	59637,042
p-value (Two-tailed)	0,006
alpha	0,1

The p-value is computed using an exact method. Time elapsed: 0.000000s.

Variable	Observations	Obs. with missing data	Obs. without missing data	Minimum	Maximum	Mean	Std. deviation
WT	65	0	65	21,700	84,400	40,511	10,160
PSS1-OX2	40	0	40	31,000	69,500	44,470	7,546

Mann-Whitney test / Two-tailed test:

U	967,500
U (standardized)	-2,191
Expected value	1300,000
Variance (U)	22964,405
p-value (Two-tailed)	0,028
alpha	0,1

The p-value is computed using an exact method. Time elapsed: 0.000000s.

Variable	Observations	Obs. with missing data	Obs. without missing data	Minimum	Maximum	Mean	Std. deviation
WT	65	0	65	21,700	84,400	40,511	10,160
PSS1-OX1	52	0	52	32,900	61,500	43,167	6,579

Mann-Whitney test / Two-tailed test:

U	1378,500
U (standardized)	-1,706
Expected value	1690,000
Variance (U)	33233,554
p-value (Two-tailed)	0,088
alpha	0,1

The p-value is computed using an exact method. Time elapsed: 0.000000s.

Fig. 4.c

Variable\Test	Shapiro-Wilk	Anderson-Darling	Lilliefors	Jarque-Bera
DMSO_C2LACT	**0,047**	0,423	0,713	**0,043**
NAA_C2LACT	**0,037**	0,057	**0,035**	**0,022**
DMSO_EVCT2	0,102	**0,018**	**0,023**	0,125
NAA_EVCT2	**< 0,0001**	**< 0,0001**	**< 0,0001**	**0,000**

Test interpretation:
H0: The variable from which the sample was extracted follows a Normal distribution.
Ha: The variable from which the sample was extracted does not follow a Normal distribution.

As the computed p-value is lower than the significance level alpha=0,05, one should reject the null hypothesis H0, and accept the alternative hypothesis Ha.

Variable	Observations	Obs. with missing data	Obs. without missing data	Minimum	Maximum	Mean	Std. deviation
DMSO	150	0	150	0,607	1,338	0,990	0,125
NAA	150	0	150	0,880	2,136	1,242	0,206

Mann-Whitney test / Two-tailed test:

U	2520
U (standardized)	-11,620
Expected value	11250,000

Variance (U)	564375,000
p-value (Two-tailed)	< 0,0001
alpha	0,05

The p-value is computed using an exact method. Time elapsed: 0.000000s.

Variable	Observations	Obs. with missing data	Obs. without missing data	Minimum	Maximum	Mean	Std. deviation
DMSO	150	0	150	1,027	2,538	1,571	0,253
NAA	150	0	150	1,242	2,949	1,943	0,318

Mann-Whitney test / Two-tailed test:

U	3900
U (standardized)	-9,783
Expected value	11250,000
Variance (U)	564375,000
p-value (Two-tailed)	< 0,0001
alpha	0,05

The p-value is computed using an exact method. Time elapsed: 0.000000s.

SUP_Data_Sheet_4

Fig.S1.b

Variable\Test	Shapiro-Wilk	Anderson-Darling	Lilliefors	Jarque-Bera
WT	**< 0,0001**	**0,000**	**0,009**	**< 0,0001**
PSS1-3	0,242	0,127	0,199	0,380
PSS1-4	0,276	0,245	0,217	0,299
PSS1-5	**0,007**	**0,003**	**0,003**	**0,046**
PSS1-3_COMP	**0,009**	**0,015**	**0,013**	**0,002**
rop6-2	0,728	0,935	0,839	0,662
ROP6-OX	0,754	0,610	0,606	0,494
ROP6-CA	0,067	0,143	0,433	0,074

Test interpretation:
H0: The variable from which the sample was extracted follows a Normal distribution.
Ha: The variable from which the sample was extracted does not follow a Normal distribution.
As the computed p-value is greater than the significance level alpha=0,05, one cannot reject the null hypothesis H0.

Variable	Observations	Obs. with missing data	Obs. without missing data	Minimum	Maximum	Mean	Std. deviation
WT	154	4	150	0,222	0,713	0,395	0,089
PSS1-3	154	4	150	0,264	0,908	0,592	0,104
PSS1-4	154	4	150	0,368	0,925	0,626	0,118
PSS1-5	154	4	150	0,375	0,874	0,571	0,105
PSS1-3_COMP	154	4	150	0,184	0,676	0,366	0,084
rop6-2	154	7	147	0,181	0,510	0,344	0,069
ROP6-OX	154	0	154	0,183	0,663	0,397	0,087
ROP6-CA	154	3	151	0,171	0,829	0,448	0,109

Variable	Observations	Obs. with missing data	Obs. without missing data	Minimum	Maximum	Mean	Std. deviation
WT	150	0	150	0,222	0,713	0,395	0,089
ROP6-CA	151	0	151	0,171	0,829	0,448	0,109

Mann-Whitney test / Two-tailed test:

U	7726
U (standardized)	-4,766
Expected value	11325,000
Variance (U)	570002,801
p-value (Two-tailed)	< 0,0001
alpha	0,05

The p-value is computed using an exact method. Time elapsed: 0.000000s.

Variable	Observations	Obs. with missing data	Obs. without missing data	Minimum	Maximum	Mean	Std. deviation
WT	150	0	150	0,222	0,713	0,395	0,089
ROP6-OX	154	0	154	0,183	0,663	0,397	0,087

Mann-Whitney test / Two-tailed test:

U	11083,500
U (standardized)	-0,608
Expected value	11550,000
Variance (U)	587098,793
p-value (Two-tailed)	0,543
alpha	0,05

The p-value is computed using an exact method. Time elapsed: 0.000000s.

Variable	Observations	Obs. with missing data	Obs. without missing data	Minimum	Maximum	Mean	Std. deviation
WT	150	0	150	0,222	0,713	0,395	0,089
rop6-2	147	0	147	0,181	0,510	0,344	0,069

Mann-Whitney test / Two-tailed test:

U	14582,500
U (standardized)	4,807
Expected value	11025,000
Variance (U)	547569,984
p-value (Two-tailed)	< 0,0001
alpha	0,05

The p-value is computed using an exact method. Time elapsed: 0.000000s.

Variable	Observations	Obs. with missing data	Obs. without missing data	Minimum	Maximum	Mean	Std. deviation
WT	150	0	150	0,222	0,713	0,395	0,089
PSS1-COMP	150	0	150	0,184	0,676	0,366	0,084

Mann-Whitney test / Two-tailed test:

U	13347,500
U (standardized)	2,791
Expected value	11250,000
Variance (U)	564370,109
p-value (Two-tailed)	0,005
alpha	0,05

The p-value is computed using an exact method. Time elapsed: 0.000000s.

Variable	Observations	Obs. with missing data	Obs. without missing data	Minimum	Maximum	Mean	Std. deviation
WT	150	0	150	0,222	0,713	0,395	0,089
PSS1-5	150	0	150	0,375	0,874	0,571	0,105

Mann-Whitney test / Two-tailed test:

U	2118
U (standardized)	-12,155

Expected value	11250,000
Variance (U)	564370,610
p-value (Two-tailed)	< 0,0001
alpha	0,05

The p-value is computed using an exact method. Time elapsed: 0.000000s.

Variable	Observations	Obs. with missing data	Obs. without missing data	Minimum	Maximum	Mean	Std. deviation
WT	150	0	150	0,222	0,713	0,395	0,089
PSS1-4	150	0	150	0,368	0,925	0,626	0,118

Mann-Whitney test / Two-tailed test:

U	1338
U (standardized)	-13,193
Expected value	11250,000
Variance (U)	564370,610
p-value (Two-tailed)	< 0,0001
alpha	0,05

The p-value is computed using an exact method. Time elapsed: 0.000000s.

Variable	Observations	Obs. with missing data	Obs. without missing data	Minimum	Maximum	Mean	Std. deviation
WT	150	0	150	0,222	0,713	0,395	0,089
PSS1-3	150	0	150	0,264	0,908	0,592	0,104

Mann-Whitney test / Two-tailed test:

U	1752
U (standardized)	-12,642
Expected value	11250,000
Variance (U)	564366,848
p-value (Two-tailed)	< 0,0001
alpha	0,05

The p-value is computed using an exact method. Time elapsed: 0.000000s.

Test interpretation:
H0: The difference of location between the samples is equal to 0.
Ha: The difference of location between the samples is different from 0.
As the computed p-value is lower than the significance level alpha=0,05, one should reject the null hypothesis H0, and accept the alternative hypothesis Ha.

Fig.S1.e

	Straight	Wavy	Jagged	Branched	Total
WT	637	124	8	14	783
pss1-3	501	222	148	86	957
pss1-4	467	186	78	74	805
pss1-5	290	163	40	52	545

Fig.S1.g

Variable\Test	Shapiro-Wilk	Anderson-Darling	Lilliefors	Jarque-Bera
WT	0,087	0,074	0,073	0,286
PSS1-1	**0,048**	**0,030**	**0,039**	0,190
PSS1-3	**0,001**	**0,001**	**0,013**	**0,002**
PSS1-4	**< 0,0001**	**0,001**	**0,021**	**0,000**

Variable	Categories	Counts
Genotype	PSS1-1	48
	PSS1-3	109
	PSS1-4	136
	WT	137

Variable	Observations	Obs. with missing data	Obs. without missing data	Minimum	Maximum	Mean	Std. deviation
WT	137	0	137	0,027	0,117	0,059	0,016
PSS1-1	48	0	48	0,097	0,305	0,191	0,047

Mann-Whitney test / Two-tailed test:

U	3
U (standardized)	0,000
Expected value	3288,000
Variance (U)	101928,000
p-value (Two-tailed)	< 0,0001
alpha	0,05

The p-value is computed using an exact method. Time elapsed: 0.000000s.

Variable	Observations	Obs. with missing data	Obs. without missing data	Minimum	Maximum	Mean	Std. deviation
WT	137	0	137	0,027	0,117	0,059	0,016
PSS1-3	109	0	109	0,033	0,454	0,188	0,085

Mann-Whitney test / Two-tailed test:

U	441
U (standardized)	0,000
Expected value	7466,500
Variance (U)	307370,917
p-value (Two-tailed)	< 0,0001
alpha	0,05

The p-value is computed using an exact method. Time elapsed: 0.000000s.

Variable	Observations	Obs. with missing data	Obs. without missing data	Minimum	Maximum	Mean	Std. deviation
WT	137	0	137	0,027	0,117	0,059	0,016
PSS1-4	136	0	136	0,034	0,452	0,160	0,061

Mann-Whitney test / Two-tailed test:

U	491
U (standardized)	0,000
Expected value	9316,000
Variance (U)	425430,667
p-value (Two-tailed)	< 0,0001
alpha	0,05

The p-value is computed using an exact method. Time elapsed: 0.000000s.

Test interpretation:
H0: The difference of location between the samples is equal to 0.
Ha: The difference of location between the samples is different from 0.

As the computed p-value is lower than the significance level alpha=0,05, one should reject the null hypothesis H0, and accept the alternative hypothesis Ha.
The risk to reject the null hypothesis H0 while it is true is lower than 0,01%.

Fig.S1.i

Variable	Categories	Counts

Genotype	WT	44
	PSS1-3	45
	PSS1-4	9
	PSS1-5	5

SUP_Data_Sheet_5

Fig. S3.b

Variable	Categories	Counts
Genotype	PSS1-4	20
	PSS1-5	14
	WT	14

Fig. S3.d

Variable\Test	Shapiro-Wilk	Anderson-Darling	Lilliefors	Jarque-Bera
WT	0,781	0,560	0,663	0,952
PSS1-3	0,775	0,560	0,553	0,798
WT_NAA	0,119	0,174	0,295	0,660
PSS1-NAA	0,358	0,365	0,478	0,564
WT_ROP6	0,598	0,568	0,652	0,682
ROP6-2	0,250	0,402	0,626	0,657

Test interpretation:
H0: The variable from which the sample was extracted follows a Normal distribution.
Ha: The variable from which the sample was extracted does not follow a Normal distribution.

As the computed p-value is lower than the significance level alpha=0,05, one should reject the null hypothesis H0, and accept the alternative hypothesis Ha.

Variable	Categories	Counts
Ecotype	PSS1-3	10
	PSS1-NAA	29
	ROP6-2_NAA	12
	WT	11
	WT_NAA	36
	WT_ROP6	13

Genotype / Fisher (LSD) / Analysis of the differences between the categories with a confidence interval of 95% (BFA_Body):

Contrast	Difference	Standardized difference	Critical value	Pr > Diff	Significant
PSS1-3 vs WT_NAA	0,587	11,401	1,983	**< 0,0001**	Yes
PSS1-3 vs WT_ROP6	0,525	8,659	1,983	**< 0,0001**	Yes
PSS1-3 vs PSS1-NAA	0,219	4,150	1,983	**< 0,0001**	Yes
PSS1-3 vs ROP6-2_NAA	0,218	3,539	1,983	**0,001**	Yes
PSS1-3 vs WT	0,208	3,297	1,983	**0,001**	Yes
WT vs WT_NAA	0,380	7,648	1,983	**< 0,0001**	Yes
WT vs WT_ROP6	0,317	5,374	1,983	**< 0,0001**	Yes
WT vs PSS1-NAA	0,012	0,229	1,983	0,819	No
WT vs ROP6-2_NAA	0,011	0,179	1,983	0,859	No
ROP6-2_NAA vs WT_NAA	0,369	7,680	1,983	**< 0,0001**	Yes
ROP6-2_NAA vs WT_ROP6	0,306	5,313	1,983	**< 0,0001**	Yes
ROP6-2_NAA vs PSS1-NAA	0,001	0,019	1,983	0,985	No
PSS1-NAA vs WT_NAA	0,368	10,234	1,983	**< 0,0001**	Yes
PSS1-NAA vs WT_ROP6	0,305	6,352	1,983	**< 0,0001**	Yes
WT_ROP6 vs WT_NAA	0,062	1,339	1,983	0,183	No
LSD-value :			0,067		

Category	LS means	Standard error	Lower bound (95%)	Upper bound (95%)	Groups		
PSS1-3	0,759	0,046	0,668	0,849	A		
WT	0,551	0,043	0,465	0,637		B	
ROP6-2_NAA	0,540	0,042	0,458	0,623		B	
PSS1-NAA	0,539	0,027	0,486	0,592		B	
WT_ROP6	0,234	0,040	0,155	0,313			C
WT_NAA	0,171	0,024	0,124	0,219			C

Fig. S3.e

Variable\Test	Shapiro-Wilk	Anderson-Darling	Lilliefors	Jarque-Bera
WT_BFA10_1h	**< 0,0001**	**< 0,0001**	**< 0,0001**	0,169
PSS1-3_BFA10_1h	0,812	0,657	0,463	0,831
WT_BFA25_1h	0,213	0,194	0,183	0,676
PSS1-3_BFA25_1h	0,875	0,668	0,633	0,934
WT_BFA50_1h	**0,017**	**0,018**	**0,014**	0,608
PSS1-3_BFA50_1h	0,809	0,566	0,580	0,941
WT_BFA10_2h	0,196	0,208	0,187	0,655
PSS1-3_BFA10_2h	0,615	0,684	0,749	0,763
WT_BFA25_2h	0,203	0,202	0,411	0,640
PSS1-3_BFA25_2h	0,687	0,617	0,544	0,747
WT_BFA50_2h	0,499	0,523	0,627	0,753
PSS1-3_BFA50_2h	0,123	0,122	0,150	0,504

Test interpretation:

H0: The variable from which the sample was extracted follows a Normal distribution.

Ha: The variable from which the sample was extracted does not follow a Normal distribution.

As the computed p-value is lower than the significance level alpha=0,05, one should reject the null hypothesis H0, and accept the alternative hypothesis Ha.

Variable	Categories	Counts
Treatment	PSS1-3_BFA10_1h	8
	PSS1-3_BFA10_2h	6
	PSS1-3_BFA25_1h	10
	PSS1-3_BFA25_2h	8
	PSS1-3_BFA50_1h	7
	PSS1-3_BFA50_2h	13
	WT_BFA10_1h	11
	WT_BFA10_2h	12
	WT_BFA25_1h	8
	WT_BFA25_2h	6
	WT_BFA50_1h	9
	WT_BFA50_2h	18

Genotype / Fisher (LSD) / Analysis of the differences between the categories with a confidence interval of 95% (BFA_Body):

Contrast	Difference	Standardized difference	Critical value	Pr > Diff	Significant
PSS1-3_BFA50_2h vs WT_BFA	0,746	15,585	1,983	**< 0,0001**	Yes
PSS1-3_BFA50_2h vs WT_BFA	0,661	14,137	1,983	**< 0,0001**	Yes
PSS1-3_BFA50_2h vs WT_BFA	0,646	12,308	1,983	**< 0,0001**	Yes
PSS1-3_BFA50_2h vs PSS1-3_	0,461	8,772	1,983	**< 0,0001**	Yes
PSS1-3_BFA50_2h vs WT_BFA	0,434	8,558	1,983	**< 0,0001**	Yes
PSS1-3_BFA50_2h vs PSS1-3_	0,390	6,755	1,983	**< 0,0001**	Yes
PSS1-3_BFA50_2h vs WT_BFA	0,370	6,407	1,983	**< 0,0001**	Yes
PSS1-3_BFA50_2h vs PSS1-3_	0,367	7,468	1,983	**< 0,0001**	Yes
PSS1-3_BFA50_2h vs WT_BFA	0,215	5,043	1,983	**< 0,0001**	Yes
PSS1-3_BFA50_2h vs PSS1-3_	0,151	2,884	1,983	**0,005**	Yes
PSS1-3_BFA50_2h vs PSS1-3_	0,108	1,980	1,983	0,050	No
PSS1-3_BFA50_1h vs WT_BFA	0,638	11,286	1,983	**< 0,0001**	Yes
PSS1-3_BFA50_1h vs WT_BFA	0,553	9,948	1,983	**< 0,0001**	Yes
PSS1-3_BFA50_1h vs WT_BFA	0,538	8,893	1,983	**< 0,0001**	Yes
PSS1-3_BFA50_1h vs PSS1-3_	0,352	5,823	1,983	**< 0,0001**	Yes

PSS1-3_BFA50_1h vs WT_BFA	0,325	5,522	1,983	**< 0,0001**	Yes
PSS1-3_BFA50_1h vs PSS1-3_	0,281	4,324	1,983	**< 0,0001**	Yes
PSS1-3_BFA50_1h vs WT_BFA	0,261	4,016	1,983	**0,000**	Yes
PSS1-3_BFA50_1h vs PSS1-3_	0,259	4,491	1,983	**< 0,0001**	Yes
PSS1-3_BFA50_1h vs WT_BFA	0,106	2,037	1,983	**0,044**	Yes
PSS1-3_BFA50_1h vs PSS1-3_	0,043	0,711	1,983	0,479	No
PSS1-3_BFA25_2h vs WT_BFA	0,595	10,952	1,983	**< 0,0001**	Yes
PSS1-3_BFA25_2h vs WT_BFA	0,510	9,560	1,983	**< 0,0001**	Yes
PSS1-3_BFA25_2h vs WT_BFA	0,495	8,469	1,983	**< 0,0001**	Yes
PSS1-3_BFA25_2h vs PSS1-3_	0,309	5,292	1,983	**< 0,0001**	Yes
PSS1-3_BFA25_2h vs WT_BFA	0,282	4,970	1,983	**< 0,0001**	Yes
PSS1-3_BFA25_2h vs PSS1-3_	0,238	3,774	1,983	**0,000**	Yes
PSS1-3_BFA25_2h vs WT_BFA	0,218	3,456	1,983	**0,001**	Yes
PSS1-3_BFA25_2h vs PSS1-3_	0,216	3,890	1,983	**0,000**	Yes
PSS1-3_BFA25_2h vs WT_BFA	0,063	1,270	1,983	0,207	No
WT_BFA50_2h vs WT_BFA10	0,532	11,887	1,983	**< 0,0001**	Yes
WT_BFA50_2h vs WT_BFA10	0,447	10,260	1,983	**< 0,0001**	Yes
WT_BFA50_2h vs WT_BFA25	0,432	8,696	1,983	**< 0,0001**	Yes
WT_BFA50_2h vs PSS1-3_BFA	0,246	4,957	1,983	**< 0,0001**	Yes
WT_BFA50_2h vs WT_BFA50	0,219	4,594	1,983	**< 0,0001**	Yes
WT_BFA50_2h vs PSS1-3_BFA	0,175	3,178	1,983	**0,002**	Yes
WT_BFA50_2h vs WT_BFA25	0,155	2,814	1,983	**0,006**	Yes
WT_BFA50_2h vs PSS1-3_BFA	0,153	3,310	1,983	**0,001**	Yes
PSS1-3_BFA25_1h vs WT_BFA	0,379	7,424	1,983	**< 0,0001**	Yes
PSS1-3_BFA25_1h vs WT_BFA	0,294	5,881	1,983	**< 0,0001**	Yes
PSS1-3_BFA25_1h vs WT_BFA	0,279	5,037	1,983	**< 0,0001**	Yes
PSS1-3_BFA25_1h vs PSS1-3_	0,094	1,688	1,983	0,094	No
PSS1-3_BFA25_1h vs WT_BFA	0,067	1,240	1,983	0,218	No
PSS1-3_BFA25_1h vs PSS1-3_	0,023	0,373	1,983	0,710	No
PSS1-3_BFA25_1h vs WT_BFA	0,002	0,041	1,983	0,968	No
WT_BFA25_2h vs WT_BFA10	0,377	6,350	1,983	**< 0,0001**	Yes
WT_BFA25_2h vs WT_BFA10	0,292	4,994	1,983	**< 0,0001**	Yes
WT_BFA25_2h vs WT_BFA25	0,277	4,385	1,983	**< 0,0001**	Yes
WT_BFA25_2h vs PSS1-3_BFA	0,091	1,444	1,983	0,152	No
WT_BFA25_2h vs WT_BFA50	0,064	1,041	1,983	0,300	No
WT_BFA25_2h vs PSS1-3_BFA	0,020	0,297	1,983	0,767	No
PSS1-3_BFA10_2h vs WT_BFA	0,357	6,012	1,983	**< 0,0001**	Yes
PSS1-3_BFA10_2h vs WT_BFA	0,272	4,651	1,983	**< 0,0001**	Yes
PSS1-3_BFA10_2h vs WT_BFA	0,257	4,068	1,983	**< 0,0001**	Yes
PSS1-3_BFA10_2h vs PSS1-3_	0,071	1,126	1,983	0,263	No
PSS1-3_BFA10_2h vs WT_BFA	0,044	0,716	1,983	0,476	No
WT_BFA50_1h vs WT_BFA10	0,312	5,949	1,983	**< 0,0001**	Yes
WT_BFA50_1h vs WT_BFA10	0,228	4,418	1,983	**< 0,0001**	Yes
WT_BFA50_1h vs WT_BFA25	0,213	3,745	1,983	**0,000**	Yes
WT_BFA50_1h vs PSS1-3_BFA	0,027	0,475	1,983	0,636	No
PSS1-3_BFA10_1h vs WT_BFA	0,286	5,258	1,983	**< 0,0001**	Yes
PSS1-3_BFA10_1h vs WT_BFA	0,201	3,763	1,983	**0,000**	Yes
PSS1-3_BFA10_1h vs WT_BFA	0,186	3,177	1,983	**0,002**	Yes
WT_BFA25_1h vs WT_BFA10	0,100	1,838	1,983	0,069	No
WT_BFA25_1h vs WT_BFA10	0,015	0,282	1,983	0,778	No
WT_BFA10_2h vs WT_BFA10	0,085	1,738	1,983	0,085	No
LSD-value :			0,077		

Category	LS means	Standard error	Lower bound (95%)	Upper bound (95%)	Groups				
PSS1-3_BFA50_2h	0,770	0,032	0,706	0,835	A				
PSS1-3_BFA50_1h	0,662	0,044	0,574	0,750	A	B			
PSS1-3_BFA25_2h	0,619	0,041	0,537	0,701		B	C		
WT_BFA50_2h	0,556	0,028	0,501	0,610			C		
PSS1-3_BFA25_1h	0,403	0,037	0,330	0,477				D	
WT_BFA25_2h	0,401	0,048	0,306	0,495				D	
PSS1-3_BFA10_2h	0,381	0,048	0,286	0,475				D	
WT_BFA50_1h	0,337	0,039	0,259	0,414				D	
PSS1-3_BFA10_1h	0,310	0,041	0,228	0,392				D	
WT_BFA25_1h	0,124	0,041	0,042	0,206					E
WT_BFA10_2h	0,109	0,034	0,042	0,176					E
WT_BFA10_1h	0,024	0,035	-0,046	0,094					E

Fig. S3.g

Variable\Test	Shapiro-Wilk	Anderson-Darling	Lilliefors	Jarque-Bera
WT_DMSO	0,187	0,156	**0,043**	0,258
PSS1-3_DMSO	**0,000**	**0,000**	**0,001**	0,163
PSS1-3_NAA	0,760	0,845	0,945	0,914
WT_NAA	**0,001**	**0,000**	**0,001**	0,103

Test interpretation:
H0: The variable from which the sample was extracted follows a Normal distribution.
Ha: The variable from which the sample was extracted does not follow a Normal distribution.

As the computed p-value is lower than the significance level alpha=0,05, one should reject the null hypothesis H0, and accept the alternative hypothesis Ha.

Variable	Categories	Counts
Genotype	PSS1-3_DMSO	82
	PSS1-3_NAA	26
	WT_DMSO	64
	WT_NAA	28

Genotype / Fisher (LSD) / Analysis of the differences between the categories with a confidence interval of 95% (AVERAGE_ORT_MT):

Contraste	Différence	Différence standardisée	Valeur critique	Pr > Diff	Significatif
WT_NAA vs PSS1-3_NAA	23,858	1,694	1,653	**0,092**	Yes
WT_NAA vs PSS1-3_DMSO	23,586	2,084	1,653	**0,038**	Yes
WT_NAA vs WT_DMSO	19,935	1,702	1,653	**0,090**	Yes
WT_DMSO vs PSS1-3_NAA	3,923	0,326	1,653	0,745	No
WT_DMSO vs PSS1-3_DMSO	3,651	0,423	1,653	0,673	No
PSS1-3_DMSO vs PSS1-3_NAA	0,272	0,023	1,653	0,981	No
LSD-value :			13,343		

Modalité	Moyennes estimées	Erreur standard	Borne inférieure (90%)	Borne supérieure (90%)	Groupes	
WT_NAA	29,966	9,770	13,819	46,112	A	
WT_DMSO	10,031	6,462	-0,649	20,710		B
PSS1-3_DMSO	6,380	5,709	-3,055	15,815		B
PSS1-3_NAA	6,108	10,139	-10,648	22,864		B

SUP_Data_Sheet_6

Fig. S4.f

Variable\Test	Shapiro-Wilk	Anderson-Darling	Lilliefors	Jarque-Bera
1139-1-10	0,258	0,301	0,551	0,333
1139-16	0,553	0,465	0,462	0,975
1140-2	0,399	0,779	0,929	0,323
1140-10	**0,005**	**0,012**	**0,028**	**0,022**

Test interpretation:
H0: The variable from which the sample was extracted follows a Normal distribution.
Ha: The variable from which the sample was extracted does not follow a Normal distribution.

As the computed p-value is lower than the significance level alpha=0,05, one should reject the null hypothesis H0, and accept the alternative hypothesis Ha.

Variable	Observations	Obs. with missing data	Obs. without missing data	Minimum	Maximum	Mean	Std. deviation
1139-16	136	0	136	0,320	0,750	0,499	0,086
1140-10	79	0	79	0,309	0,726	0,464	0,094

Mann-Whitney test / Two-tailed test:

U	6732
U (standardized)	3,092
Expected value	5372,000
Variance (U)	193383,010
p-value (Two-tailed)	0,002
alpha	0,05

The p-value is computed using an exact method. Time elapsed: 0.000000s.

Variable	Observations	Obs. with missing data	Obs. without missing data	Minimum	Maximum	Mean	Std. deviation
1139-16	136	0	136	0,320	0,750	0,499	0,086
1140-2	124	0	124	0,275	0,688	0,427	0,084

Mann-Whitney test / Two-tailed test:

U	12230
U (standardized)	6,270
Expected value	8432,000
Variance (U)	366777,475
p-value (Two-tailed)	< 0,0001
alpha	0,05

The p-value is computed using an exact method. Time elapsed: 0.000000s.

Variable	Observations	Obs. with missing data	Obs. without missing data	Minimum	Maximum	Mean	Std. deviation
1139-1-10	94	0	94	0,321	0,721	0,522	0,101
1140-10	79	0	79	0,309	0,726	0,464	0,094

Mann-Whitney test / Two-tailed test:

U	4981,500
U (standardized)	3,864
Expected value	3713,000
Variance (U)	107671,759
p-value (Two-tailed)	0,000
alpha	0,05

The p-value is computed using an exact method. Time elapsed: 0.000000s.

Variable	Observations	Obs. with missing data	Obs. without missing data	Minimum	Maximum	Mean	Std. deviation
1139-1-10	94	0	94	0,321	0,721	0,522	0,101
1140-2	124	0	124	0,275	0,688	0,427	0,084

Mann-Whitney test / Two-tailed test:

U	8856
U (standardized)	6,564
Expected value	5828,000
Variance (U)	212714,731
p-value (Two-tailed)	< 0,0001
alpha	0,05

The p-value is computed using an exact method. Time elapsed: 0.000000s.

Variable	Observations	Obs. with missing data	Obs. without missing data	Minimum	Maximum	Mean	Std. deviation
WT	102	0	102	0,163	0,546	0,348	0,085
1140-2	124	0	124	0,275	0,688	0,427	0,084

Mann-Whitney test / Two-tailed test:

U	3299,500
U (standardized)	-6,182
Expected value	6324,000
Variance (U)	239248,051
p-value (Two-tailed)	< 0,0001
alpha	0,05

The p-value is computed using an exact method. Time elapsed: 0.000000s.

Variable	Observations	Obs. with missing data	Obs. without missing data	Minimum	Maximum	Mean	Std. deviation
WT	102	0	102	0,163	0,546	0,348	0,085
1139-16	136	0	136	0,320	0,750	0,499	0,086

Mann-Whitney test / Two-tailed test:

U	1491,500
U (standardized)	-10,357
Expected value	6936,000
Variance (U)	276277,360
p-value (Two-tailed)	< 0,0001
alpha	0,05

The p-value is computed using an exact method. Time elapsed: 0.000000s.

Variable	Observations	Obs. with missing data	Obs. without missing data	Minimum	Maximum	Mean	Std. deviation
WT	102	0	102	0,163	0,546	0,348	0,085
1139-1-10	94	0	94	0,321	0,721	0,522	0,101

Mann-Whitney test / Two-tailed test:

U	954
U (standardized)	-9,678
Expected value	4794,000
Variance (U)	157398,108
p-value (Two-tailed)	< 0,0001
alpha	0,05

The p-value is computed using an exact method. Time elapsed: 0.000000s.

SUP_Data_Sheet_7

Fig. S5.c

Variable\Test	Shapiro-Wilk	Anderson-Darling	Lilliefors	Jarque-Bera
WT	0,912	0,602	0,223	0,775
rop6-2	0,323	0,475	0,548	0,484
ROP6-1	0,318	0,372	0,509	0,451
ROP6-7	**0,036**	0,556	0,362	**0,001**
ROP6-7Q-13	0,606	0,460	0,515	0,442
ROP6-7Q-18	0,270	0,424	0,384	0,464

Test interpretation:
H0: The variable from which the sample was extracted follows a Normal distribution.

Ha: The variable from which the sample was extracted does not follow a Normal distribution.
As the computed p-value is greater than the significance level alpha=0,05, one cannot reject the null hypothesis H0.

Variable	Observations	Obs. with missing data	Obs. without missing data	Minimum	Maximum	Mean	Std. deviation
WT	267	0	267	0,000	3,241	1,708	0,564
rop6-2	243	0	243	0,659	4,008	2,267	0,686
ROP6-1	116	0	116	0,570	3,541	1,836	0,633
ROP6-7	136	0	136	0,493	4,651	1,914	0,660
ROP6-7Q-13	117	0	117	0,793	4,271	2,333	0,696
ROP6-7Q-18	67	0	67	0,518	3,399	2,069	0,709

Genotype / Fisher (LSD) / Analysis of the differences between the categories with a confidence interval of 95% (LR_density):

Contrast	Difference	Standardized difference	Critical value	Pr > Diff	Significant
ROP6-7Q-13 vs WT	0,625	8,736	1,962	**< 0,0001**	Yes
ROP6-7Q-13 vs ROP6-1	0,498	5,881	1,962	**< 0,0001**	Yes
ROP6-7Q-13 vs ROP6-1	0,419	5,150	1,962	**< 0,0001**	Yes
ROP6-7Q-13 vs ROP6-7Q-18	0,264	2,666	1,962	**0,008**	Yes
ROP6-7Q-13 vs rop6-2	0,066	0,905	1,962	0,365	No
rop6-2 vs WT	0,559	9,778	1,962	**< 0,0001**	Yes
rop6-2 vs ROP6-1	0,432	5,925	1,962	**< 0,0001**	Yes
rop6-2 vs ROP6-7	0,354	5,113	1,962	**< 0,0001**	Yes
rop6-2 vs ROP6-7Q-18	0,198	2,222	1,962	**0,027**	Yes
ROP6-7Q-18 vs WT	0,361	4,097	1,962	**< 0,0001**	Yes
ROP6-7Q-18 vs ROP6-1	0,234	2,359	1,962	**0,019**	Yes
ROP6-7Q-18 vs ROP6-7	0,156	1,615	1,962	0,107	No
ROP6-7 vs WT	0,206	3,026	1,962	**0,003**	Yes
ROP6-7 vs ROP6-1	0,078	0,958	1,962	0,338	No
ROP6-1 vs WT	0,128	1,777	1,962	0,076	No
LSD-value :			0,11		

Category	LS means	Standard error	Lower bound (95%)	Upper bound (95%)	Groups			
ROP6-7Q-13	2,333	0,060	2,216	2,450	A			
rop6-2	2,267	0,041	2,186	2,349	A			
ROP6-7Q-18	2,069	0,079	1,915	2,224		B		
ROP6-7	1,914	0,055	1,805	2,022		B	C	
ROP6-1	1,836	0,060	1,718	1,953			C	D
WT	1,708	0,039	1,630	1,785				D

Fig. S5.d

Variable\Test	Shapiro-Wilk	Anderson-Darling	Lilliefors	Jarque-Bera
WT	**0,030**	**0,018**	**0,027**	0,060
rop6-2	**0,040**	0,053	0,112	0,326
ROP6-1	0,227	0,325	0,570	0,246
ROP6-7Q-4	**0,026**	**0,035**	0,195	**0,001**
ROP6-7Q-13	0,855	0,936	0,930	0,756

Test interpretation:
H0: The variable from which the sample was extracted follows a Normal distribution.
Ha: The variable from which the sample was extracted does not follow a Normal distribution.
As the computed p-value is greater than the significance level alpha=0,05, one cannot reject the null hypothesis H0.

Variable	Observations	Obs. with missing data	Obs. without missing data	Minimum	Maximum	Mean	Std. deviation
WT	26	0	26	118,908	254,357	168,095	29,508
rop6-2	30	0	30	136,829	247,720	188,211	35,432
ROP6-1	29	0	29	104,594	280,063	171,756	36,640
ROP6-7Q-4	33	0	33	129,226	274,000	184,455	26,672
ROP6-7Q-13	21	0	21	138,811	215,387	178,217	21,536

Genotype / Fisher (LSD) / Analysis of the differences between the categories with a confidence interval of 95% (BFA_SIZE):

Contrast	Difference	Standardized difference	Critical value	Pr > Diff	Significant
rop6-2 vs WT	20,116	2,431	1,978	**0,016**	Yes
rop6-2 vs 1151-1	16,454	2,046	1,978	**0,043**	Yes
rop6-2 vs 1154-13	9,994	1,137	1,978	0,257	No
rop6-2 vs 1154-4	3,756	0,482	1,978	0,631	No
1154-4 vs WT	16,360	2,020	1,978	**0,045**	Yes
1154-4 vs 1151-1	12,698	1,615	1,978	0,109	No
1154-4 vs 1154-13	6,238	0,724	1,978	0,471	No
1154-13 vs WT	10,122	1,117	1,978	0,266	No
1154-13 vs 1151-1	6,460	0,730	1,978	0,467	No
1151-1 vs WT	3,662	0,439	1,978	0,661	No
LSD-value :			15,037		

Category	LS means	Standard error	Lower bound (95%)	Upper bound (95%)	Groups		
rop6-2	188,211	5,638	177,059	199,363	A		
1154-4	184,455	5,376	173,822	195,088	A	B	
1154-13	178,217	6,739	164,888	191,546	A	B	C
1151-1	171,756	5,735	160,414	183,099		B	C
WT	168,095	6,057	156,115	180,074			C

SUP_Data_Sheet_8

Fig. S7.a.

T4

Variable\Test	Shapiro-Wilk	Anderson-Darling	Lilliefors	Jarque-Bera
WT	**0,004**	**0,039**	0,196	**< 0,0001**
rop6-2	0,953	0,880	0,913	0,985
PSS1-AMI1	0,511	0,628	0,585	0,496
PSS1-AMI2	0,625	0,622	0,498	0,660
PSS1-OX1	**0,037**	0,066	0,253	0,096
PSS1-OX2	0,077	0,265	0,341	**0,005**

Test interpretation:
H0: The variable from which the sample was extracted follows a Normal distribution.
Ha: The variable from which the sample was extracted does not follow a Normal distribution.
As the computed p-value is greater than the significance level alpha=0,05, one cannot reject the null hypothesis H0.

Variable	Categories	Counts
Genotype	PSS1-AMI1	62
	PSS1-AMI2	70
	PSS1-OX1	53
	PSS1-OX2	38
	PSS1-WT	61

Genotype / Fisher (LSD) / Analysis of the differences between the categories with a confidence interval of 90% (Angle):

Contrast	Difference	Standardized difference	Critical value	Pr > Diff	Significant
PSS1-OX1 vs PSS1-AMI1	8,178	6,277	1,649	**< 0,0001**	Yes
PSS1-OX1 vs PSS1-AMI2	5,605	4,420	1,649	**< 0,0001**	Yes
PSS1-OX1 vs PSS1-WT	5,221	3,992	1,649	**< 0,0001**	Yes
PSS1-OX1 vs PSS1-OX2	1,072	0,724	1,649	0,470	No
PSS1-OX2 vs PSS1-AMI1	7,106	4,952	1,649	**< 0,0001**	Yes
PSS1-OX2 vs PSS1-AMI2	4,533	3,230	1,649	**0,001**	Yes
PSS1-OX2 vs WT	4,149	2,883	1,649	**0,004**	Yes
WT vs PSS1-AMI1	2,957	2,354	1,649	**0,019**	Yes
WT vs PSS1-AMI2	0,383	0,314	1,649	0,754	No
PSS1-AMI2 vs PSS1-AMI1	2,573	2,119	1,649	**0,035**	Yes
LSD-value :			1,942		

Category	LS means	Standard error	Lower bound (90%)	Upper bound (90%)	Groups		
PSS1-OX1	33,625	0,957	32,047	35,202	A		
PSS1-OX2	32,553	1,130	30,689	34,416	A		
WT	28,403	0,892	26,932	29,874		B	
PSS1-AMI2	28,020	0,832	26,647	29,393		B	
PSS1-AMI1	25,447	0,884	23,988	26,906			C

T8

Variable\Test	Shapiro-Wilk	Anderson-Darling	Lilliefors	Jarque-Bera
WT	**0,043**	**0,020**	0,052	0,355
PSS1-AMI1	**0,015**	**0,020**	**0,014**	0,228
PSS1-AMI2	0,347	0,451	0,673	0,429
PSS1-OX1	0,890	0,918	0,960	0,798
PSS1-OX2	0,826	0,874	0,821	0,767

Test interpretation:
H0: The variable from which the sample was extracted follows a Normal distribution.
Ha: The variable from which the sample was extracted does not follow a Normal distribution.
As the computed p-value is greater than the significance level alpha=0,05, one cannot reject the null hypothesis H0.

Variable	Categories	Counts
Genotype	PSS1-AMI1	57
	PSS1-AMI2	77
	PSS1-OX1	52
	PSS1-OX2	40
	WT	65

Genotype / Fisher (LSD) / Analysis of the differences between the categories with a confidence interval of 90% (Angle):

Contrast	Difference	Standardized difference	Critical value	Pr > Diff	Significant
PSS1-OX2 vs PSS1-AMI1	11,886	7,197	1,649	**< 0,0001**	Yes
PSS1-OX2 vs PSS1-AMI2	8,676	5,560	1,649	**< 0,0001**	Yes
PSS1-OX2 vs WT	3,959	2,461	1,649	**0,014**	Yes
PSS1-OX2 vs PSS1-OX1	1,303	0,774	1,649	0,440	No
PSS1-OX1 vs PSS1-AMI1	10,583	6,892	1,649	**< 0,0001**	Yes
PSS1-OX1 vs PSS1-AMI2	7,374	5,131	1,649	**< 0,0001**	Yes
PSS1-OX1 vs WT	2,657	1,783	1,649	**0,075**	Yes
WT vs PSS1-AMI1	7,927	5,455	1,649	**< 0,0001**	Yes
WT vs PSS1-AMI2	4,717	3,498	1,649	**0,001**	Yes
PSS1-AMI2 vs PSS1-AMI1	3,209	2,294	1,649	**0,022**	yes
LSD-value :			2,128		

Category	LS means	Standard error	Lower bound (90%)	Upper bound (90%)	Groups			
PSS1-OX2	44,470	1,266	42,382	46,558	A			
PSS1-OX1	43,167	1,110	41,336	44,999	A			
WT	40,511	0,993	38,873	42,149		B		
PSS1-AMI2	35,794	0,912	34,289	37,298			C	
PSS1-AMI1	32,584	1,061	30,835	34,333				D

T12

Variable\Test	Shapiro-Wilk	Anderson-Darling	Lilliefors	Jarque-Bera
WT	0,357	0,742	0,973	0,531
PSS1-AMI1	0,362	0,304	0,090	0,516
PSS1-AMI2	**0,033**	**0,017**	**0,006**	0,276
PSS1-OX1	0,534	0,394	0,438	0,660
PSS1-OX2	0,928	0,878	0,485	0,954

Test interpretation:
H0: The variable from which the sample was extracted follows a Normal distribution.
Ha: The variable from which the sample was extracted does not follow a Normal distribution.
As the computed p-value is greater than the significance level alpha=0,05, one cannot reject the null hypothesis H0.

Variable	Categories	Counts
Ecotype	AMI1	60
	AMI2	82
	OX1	42
	OX2	39
	WT	67

Genotype / Fisher (LSD) / Analysis of the differences between the categories with a confidence interval of 90% (Angle):

Contrast	Difference	Standardized difference	Critical value	Pr > Diff	Significant
PSS1-OX2 vs PSS1-AMI1	8,529	4,848	1,649	**< 0,0001**	Yes
PSS1-OX2 vs PSS1-AMI2	7,008	4,212	1,649	**< 0,0001**	Yes
PSS1-OX2 vs WT	3,576	2,076	1,649	**0,039**	Yes
PSS1-OX2 vs PSS1-OX1	0,479	0,252	1,649	0,801	No
PSS1-OX1 vs PSS1-AMI1	8,050	4,678	1,649	**< 0,0001**	Yes
PSS1-OX1 vs PSS1-AMI2	6,529	4,022	1,649	**< 0,0001**	Yes
PSS1-OX1 vs WT	3,097	1,840	1,649	**0,067**	Yes
WT vs PSS1-AMI1	4,953	3,258	1,649	**0,001**	Yes
WT vs PSS1-AMI2	3,432	2,436	1,649	**0,015**	Yes
PSS1-AMI2 vs PSS1-AMI1	1,521	1,047	1,649	0,296	No
LSD-value :			2,203		

Category	LS means	Standard error	Lower bound (90%)	Upper bound (90%)	Groups		
PSS1-OX2	45,236	1,370	42,977	47,495	A		
PSS1-OX1	44,757	1,320	42,580	46,934	A		
WT	41,660	1,045	39,936	43,383		B	
PSS1-AMI2	38,228	0,945	36,670	39,786			C
PSS1-AMI1	36,707	1,104	34,885	38,528			C

Fig. S7.c.

Variable\Test	Shapiro-Wilk	Anderson-Darling	Lilliefors	Jarque-Bera
WT	0,133	0,228	0,467	0,486
PSS1-AMI1	0,528	0,784	0,827	0,604

PSS1-AMI2	0,442	0,490	0,629	0,545

Test interpretation:
H0: The variable from which the sample was extracted follows a Normal distribution.
Ha: The variable from which the sample was extracted does not follow a Normal distribution.
As the computed p-value is greater than the significance level alpha=0,05, one cannot reject the null hypothesis H0.

Variable	Categories	Counts
Ecotype	PSS1-AMI1	31
	PSS1-AMI2	21
	PSS1-OX1	34
	PSS1-OX2	31
	WT	24

Ecotype / Fisher (LSD) / Analysis of the differences between the categories with a confidence interval of 95% (BFA_SIZE):

Contrast	Difference	Standardized difference	Critical value	Pr > Diff	Significant
AMI2 vs OX1-8	27,702	3,371	1,978	**0,001**	Yes
AMI2 vs OX2-10	25,753	3,077	1,978	**0,003**	Yes
AMI2 vs WT	21,136	2,389	1,978	**0,018**	Yes
AMI2 vs AMI1	2,757	0,329	1,978	0,742	No
AMI1 vs OX1-8	24,945	3,392	1,978	**0,001**	Yes
AMI1 vs OX2-10	22,996	3,057	1,978	**0,003**	Yes
AMI1 vs WT	18,379	2,283	1,978	**0,024**	Yes
WT vs OX1-8	6,566	0,832	1,978	0,407	No
WT vs OX2-10	4,617	0,573	1,978	0,567	No
OX2-10 vs OX1-8	1,948	0,265	1,978	0,791	No
LSD-value:			14,203		

Category	LS means	Standard error	Lower bound (95%)	Upper bound (95%)	Groups	
AMI2	199,997	6,462	187,218	212,776	A	
AMI1	197,240	5,319	186,722	207,758	A	
WT	178,860	6,045	166,907	190,814		B
OX2-10	174,243	5,319	163,726	184,761		B
OX1-8	172,295	5,079	162,252	182,338		B

C. DISCUSSION AND PERSPECTIVES

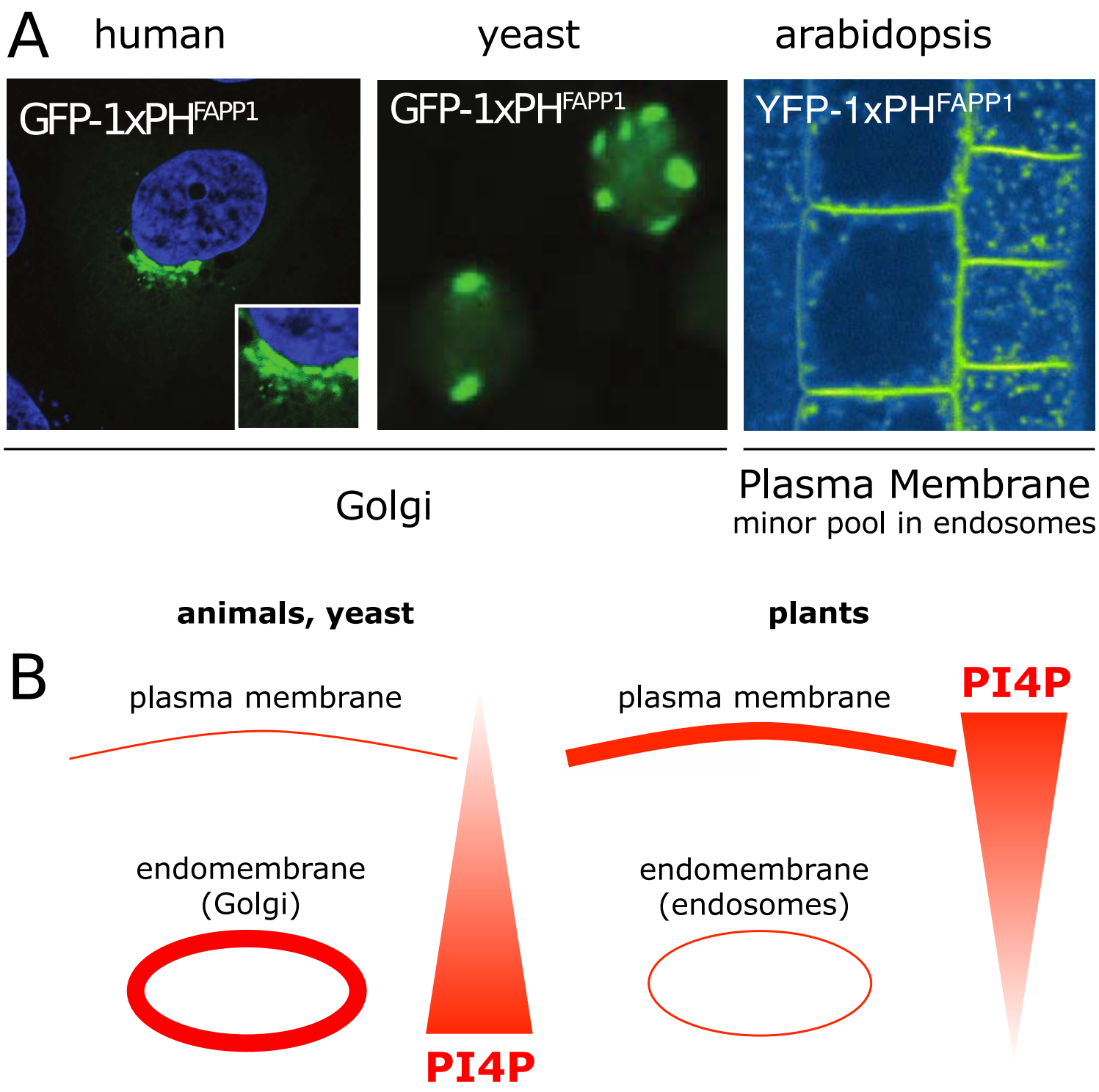

Figure 34. PI4P in plants is organized in an inverted gradient compared to other eukaryotic cells. A, From the left to the right, Huh-7 cells, yeast and Arabidopsis plant expressing the PI4P sensor 1xPH^{FAPP1}. **B**, Schematic representation of PI4P gradient in animals and yeast and in plants. Images issues from, Simon, Platre et al., 2014.

I. The membrane electrostatic field

In the first and second chapter of this manuscript, I demonstrated that the plasma membrane harbors a special feature as the most electrostatic compartment in plant cells. This unique property requires the cooperativity of three lipid species, PI(4)P, PS and PA. Nonetheless, other intracellular membranes are anionic. The enrichment of PS and PI(4)P into specific subcellular compartments dictates the gradient of electrostatics along the endocytic pathway. Here, I discuss how each lipid is involved in the maintenance of the electrostatic field in plant cells. Then, I discuss some reasons why lipid cooperativity might be a powerful system to regulate signaling.

a. Maintenance of the electrostatic field

i. By phosphatidylinositol 4-phosphate

PI(4)P is the most important anionic lipid setting up plasma membrane electrostatic field. Even though, in plant cells (i.e. rye leaf), PI represents only about 2% of total plasma membrane phospholipids and, PS and PA about 5% (Lynch and Steponkus, 1987), PI4P contains more negative charges than PS and PA (3 vs 1 and 2, respectively, Figure 6B). Moreover, PI(4)P accounts for about 80% of total phosphoinositides. Regarding the head group size, PI(4)P presents more steric hindrance as compared to PS and PA. As a consequence, the phosphorylated inositol group is more exposed to the cytosolic leaflet. According to several independent PI(4)P biosensors (i.e. PH^{FAPP1}, PH^{OSBP}, $P4M^{SidM}$) and genetic approaches, PI(4)P massively accumulates at the plasma membrane and is present to a lesser extent at the *trans*-Golgi network/early endosomes (TGN/EE) and Golgi. The major contribution of PI(4)P to PM electrostatics could be explained by three major points, i) its higher anionic property despite being present in a lesser extent, ii) its steric hindrance and iii) its massive accumulation at the plasma membrane.

In plants, PI4P massively accumulates at the plasma membrane, while in yeast and mammals PI(4)P is predominantly enriched in the Golgi and to a lesser extent at the plasma membrane (Hammond et al., 2014)(Simon et al., 2014)(Figure 34). In plants, alteration of the PI(4)P

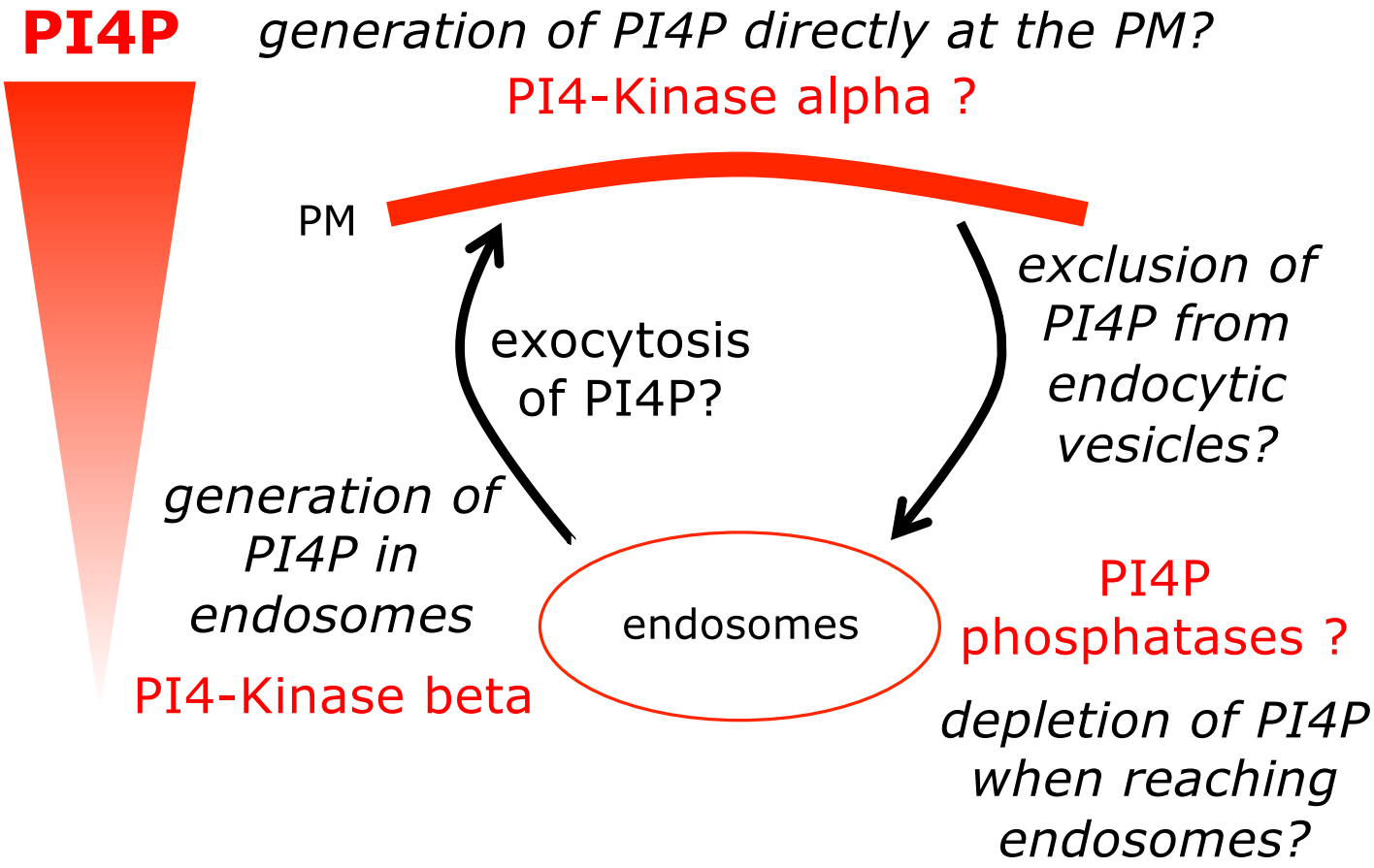

Figure 35. Schematic representation of the different hypotheses for the establishment of the PI4P gradient in plants. The triangle indicates the PI4P gradient. PM, plasma membrane.

gradient between PM and TGN/EE mislocalized MSC probes into endosomes. This suggests that the maintenance of the PI(4)P gradient is required to maintain the high PM electrostatics. An interesting question could be how does this gradient is maintained?

Similar to yeast and mammals, plant PIPs derive from PI that is synthetized in the ER. PI is then phosphorylated by lipid kinases to generate PIPs, which can in turn be dephosphorylated by lipid phosphatases. To date, three kinases and one phosphatase acting on PI4P turnover have been identified and localized in different subcellular compartments. From PI, PI(4) kinase β1 and β2 generate PI(4)P in TGN/EE compartments (Kang et al., 2011; Preuss et al., 2006). Root hair defective 4 (RHD4)/Suppressor of actin7 (SAC7) acts as a PI4 phosphatase generating PI from PI(4)P in EE/TGN (Thole et al., 2008). A scenario, could be that PI4 kinase β1 and β2 generate PI(4)P in TGN/EE and RHD4/SAC7 reduces PI4P concentration to maintain a low level of PI4P in endosomes. This scenario would explain how TGN/EE membranes accumulate low levels of PI(4)P, but does not explain how is the high PI(4)P concentration maintained. The PI4 kinase α1 is homologous to the yeast Stt4p protein, which produces PI(4)P at the PM. It has been proposed to localize at the PM in Arabidopsis (Okazaki et al., 2015). It is therefore likely that PI4 kinase α1 contribute to PI(4)P production at the plant PM, although this has not been demonstrated so far (Figure 35). In addition, such scenario does not consider exocytosis or endocytosis that could be also a powerful lever to maintain PI(4)P gradient.

PI(4)P is generated both at the PM and TGN/EE, however, membrane exchange is highly controlled by exocytosis/endocytosis events between those two organelles. A plausible hypothesis could be that newly generated PI(4)P in TGN/EE reaches rapidly the plasma membrane by exocytosis enriching the PM in PI(4)P. Consistent with this hypothesis, PI4K β 1 is localized in secretory vesicles of the TGN (Kang et al., 2011). Then, to prevent its enrichment in endosomes, PI(4)P could be excluded from endocytic events acting in combination with the TGN/EE-localized RHD4/SAC7 phosphatase (Figure 35). Consistently, double mutants PI4 kinases β1 and β2 or single mutant RHD4/SAC7 present defect in exocytosis (Kang et al., 2011; Preuss et al., 2006; Thole et al., 2008). However, less is known about the PM-associated PI(4)P, since PI(4) kinase α1 homozygous mutants are lethal (L. Noack personal communication). Non-viability of PI(4) kinase α1 mutant is in accordance with the utmost importance of PI(4)P in setting up the PM electrostatic field.

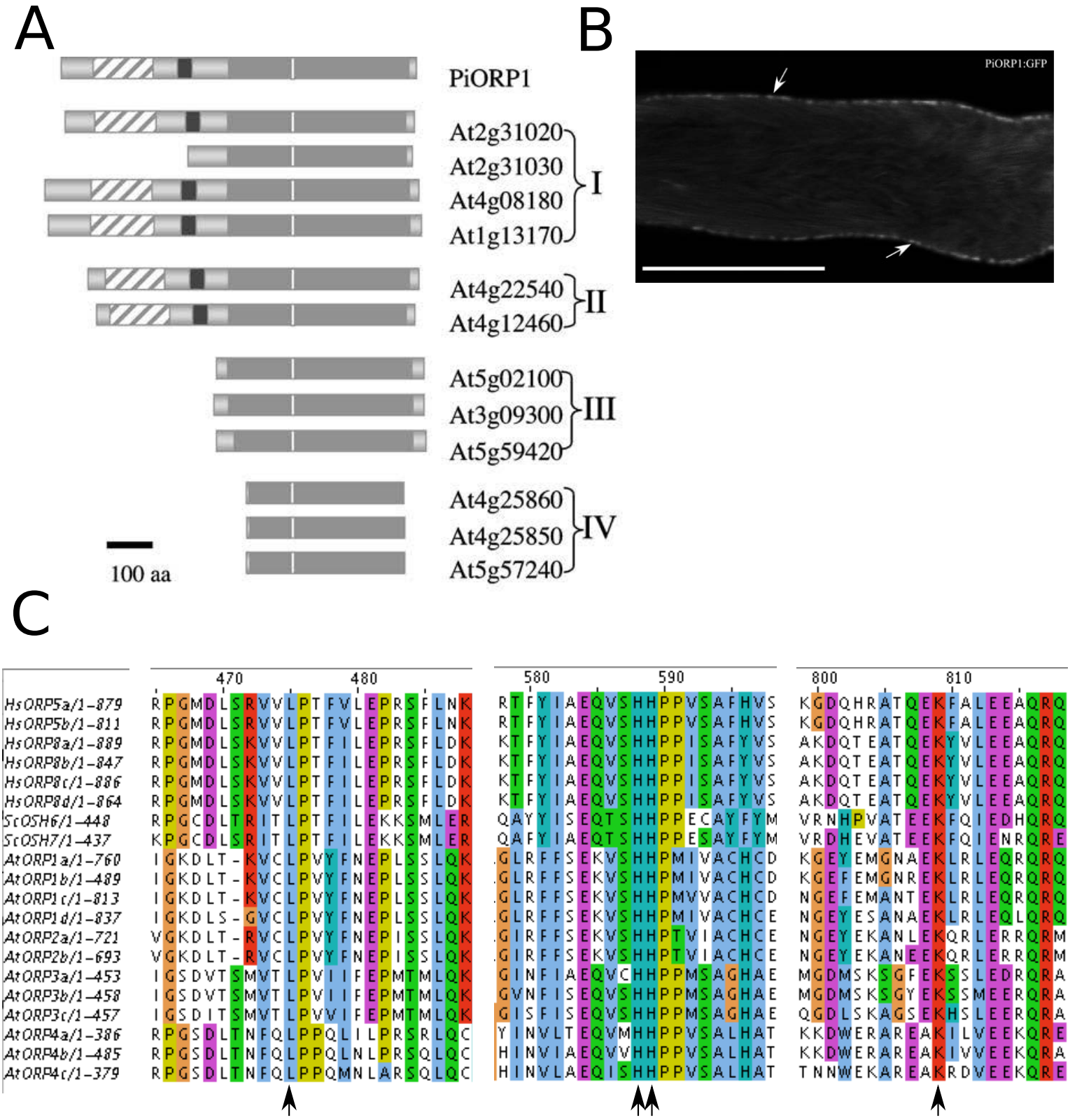

Figure 36. Schematic representation of the domain structures of ORP1 from Petunia inflata (Pi) and the 12 ORPs of Arabidopsis. A, The diagonally striped boxes indicate the PH domains, the dark gray shaded boxes indicate the oxysterol-binding domains and the black boxes represent coiled coil regions. Proteins are aligned by a highly conserved protein sequence (EQVSHHPP) indicated by the white box in the oxysterol-binding domain. ORPs fall into four distict subgroups, designated I, II, III and IV. **B,** Confocal image of GFP:PiORP in the subapical shank a growing pollen tube. Pollen tube is a cell specific type required to deliver the male gametophyte to the ovule for fecundation. Scale bar, 10 µm. **C,** Alignment of ORP/Osh from yeast, human and plants showing conserved residues critical for PI(4)P/PS counter transport indicated by an arrow. Alignment was performed using Jalview and ClustalWS procedure. Sc, *Saccharomyces cerevisiae*; Hs, *Homo sapiens*; At, *Arabidopsis thaliana.*

This hypothetic model favors massive PM-PI(4)P enrichment but may require down-regulation/feedbacks in order to balance the system. To date, no phosphatases have been identified at the PM to decrease PI(4)P enrichment in plants. An alternative way has been highlighted in yeast and mammals based on counter-transport between PM and ER at contact sites as mentioned in I/d/ii/2 relying on ORP/Osh proteins (Figure 9D). Briefly, PS is generated in the ER and transported to the PM, while PI(4)P is transported back from the PM to the ER where it is hydrolyzed by Sac1 to generate PI. Arabidopsis genome contains 12 genes encoding ORP/Osh proteins (Skirpan et al., 2006) (Figure 36A). This could be an elegant hypothesis, in which PI(4)P degradation would not require trafficking through endosomal compartments to be degraded. In addition, removal of PI(4)P could be an early signal for setting up endocytosis.

A way to investigate the role of PI4 kinases and phosphatases in the PI4P electrostatic field could be to introgress our set of PI(4)P biosensors in mutant backgrounds. Preliminary results, showed that PI4 kinases β1 and β2 and RHD4 are not required to maintain PM electrostatics since membrane surface charge sensors stay localized at the plasma membrane in the corresponding mutants. This suggests that exocytosis have a minor role in setting up the plasma membrane electrostatic field. The lethality of the PI(4) kinase α1 mutant makes it impossible to directly analyze MSC reporter localization in this background, but inducible down regulation (for example using artificial microRNAs) could be one way to get around this problem. Moreover, in order to investigate PI(4)P turnover, introgression of PI(4)P probes in ORP/Osh mutants could be interesting. As aforementioned, our hypothesis implies exclusion of PI(4)P from endocytic event. Using TIRF microscopy on plants co-expressing GFP-CLATHRIN LIGHT CHAIN 2 (CLC2) and Red-PI(4)P sensors would allow to appreciate the spatial organization of both markers but also their overlapping region. Preliminary result suggest that PI4P is weakly associated with clathrin foci since the Pearson coefficient between CLC2 and PI(4)P sensor is very low. This suggest that PI4P, if involved in setting up clathrin-dependent endocytosis machinery, may be required as an early signal. Determination of the spatio-temporal organization at the plasma membrane of clathrin-dependent endocytosis machinery ADAPTATOR 2μ (AP2μ), CLC2 and DYNAMIN-RELATED PROTEIN 1a (Drp1a) using TIRF could be an elegant way to characterize the contribution of PI4 kinases or PI4 phosphates on setting up clathrin-dependent endocytosis. To conclude, PI(4) kinase α1 activity and exclusion of PI(4)P from endocytic events may drive the PI(4)P enrichment at the PM, which is itself critical for setting up the PM electrostatic field.

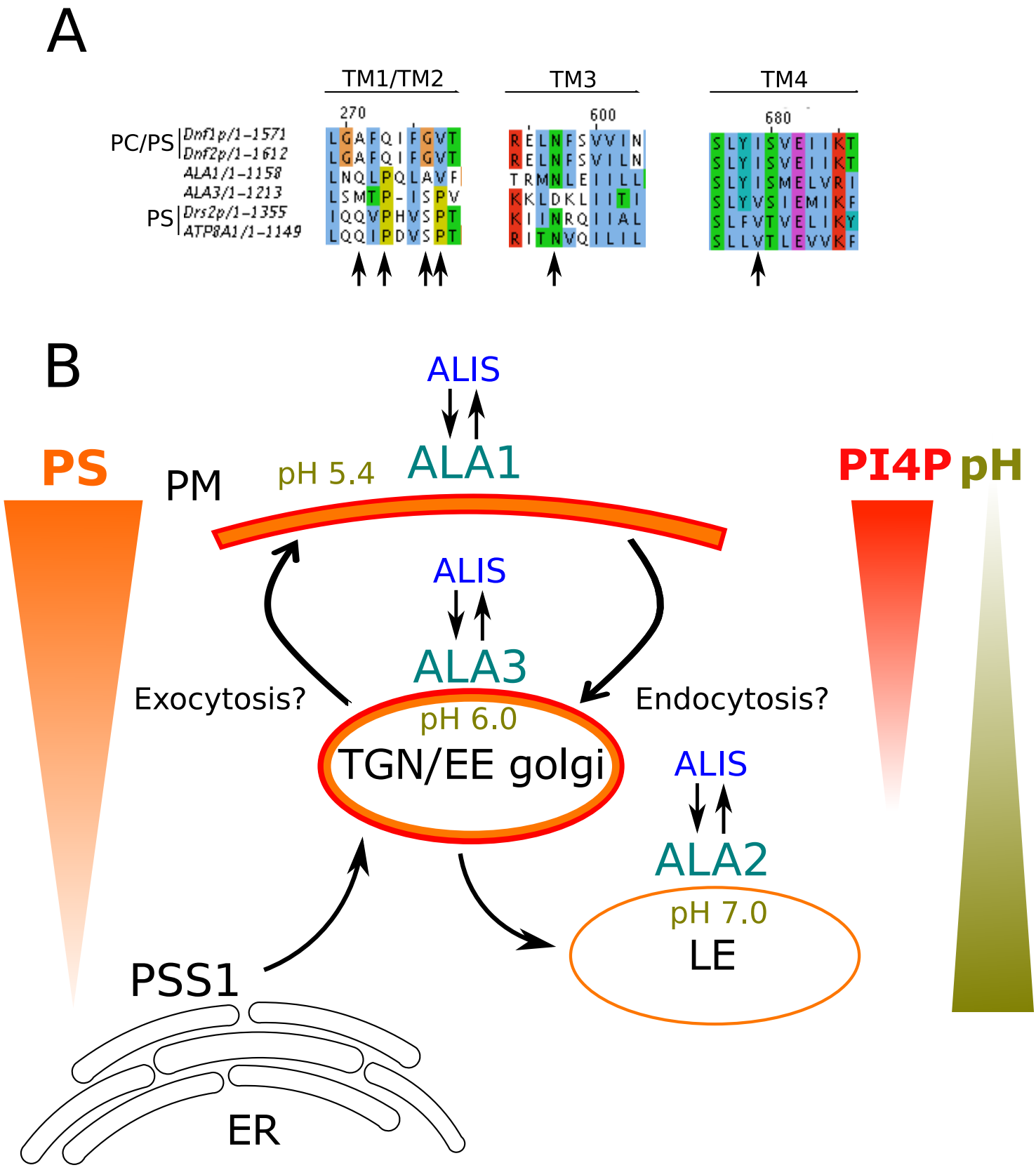

Figure 37. Schematic representation of the hypotheses for the establisment of the PS gradient by flippases. **A,** Alignment of Dnf1p, Dnf2p**,** Drs2p, ATP8ap PC/PS and PS-specific flippase proteins from yeast, respectively, with AtALA1 and AtALA3 flippase from Arabidopsis. Conserved residues for PS and/or PC flipping in TM are indicated by an arrow. **B,** The orange, red and green triangle indicate the PS, PI4P and pH gradient along the endocytic pathway. Arrows between compartments indicate the exocytosis and endocytosis. Arrows between ALA and ALIS indicate the hypothesis of a transient association regulating ALA activity. PI4P gradient is represented since PI4P may be required for flippase activity. PM, plasma membrane; TGN/EE, trans-golgi network/early endosomes; LE, late endosomes;ER, endoplasmic reticulum; ALA, aminophospholipid ATPase; ALIS, ALA interacting subunit; PSS1, phosphatidylserine synthase 1; TM, transmembrane.

ii. By phosphatidylserine

Compared to PI4P or PA, PS seems to be required across all eukaryotes to maintain plasma membrane electrostatic field. In addition, in mammals, yeasts and plants, PS-driven electrostatic field is not limited to the PM and is extended to PM-derived organelles. In mammals and plants, PS distribution correlates with the distribution of the electrostatic gradient all along the endocytic pathway. A remaining question, could be how does this gradient of PS is maintained? Below, I discuss possible mechanisms that could be involved in setting up the PS gradient in plants in order to maintain the electrostatic field.

In mammals, yeasts and plants, the cytosolic PS reporter (LactC2) reports mainly a plasmalemma localization, and it localizes to a lesser extend to endosomes. In mammals, this notion is sustained by colocalization analysis and immunogold labelling. In yeast, this observation stays circumstantial (Xu et al., 2013), but is supported by early biochemical studies indicating that the transition from early to late endosomes/lysosomes is associated with a decrease in PS (Leventis and Grinstein, 2010). PS content within the vacuole was estimated at <5%, markedly lower than that of the PM (30%), (Leventis and Grinstein, 2010). The PS enrichment observed in the cell surface and the gradient in the endocytic membranes cannot be attributed to a regulation by PS synthesis because PSS enzymes reside in the ER. However, “flip flop” mechanisms could be a powerful system to adjust PS concentration in the cytosolic face of organelles. Flippases transport PS from the extracellular or the luminal leaflet of an organelle to the cytosolic side and scramblases in both directions (Figure 9C). Flippases are eukaryotic P4-ATPases (type 4 P-type ATPases) activated by phosphorylation-triggered ATP cycle (Andersen et al., 2016). Scramblases activity depends on Ca^{2+} and has been assigned in mammals to early cell death response signaling. I favor the hypothesis that one-way flippases could be involved in the regulation of PS enrichment in different organelles since scramblases function to randomize or reduce the asymmetry of phospholipids in membranes.

The Arabidopsis genome contains 12 genes encoding for aminophospholipid flippases (ALAs) and are localized in the endomembrane system including the plasma membrane (PM), *trans*-Golgi network/early endosomes (TGN/EE), prevacuolar compartment (PVC) and endoplasmic reticulum (ER); (Botella et al., 2016; López-Marqués et al., 2010, 2012; McDowell et al., 2015; Poulsen et al., 2015) (Figure 37B). However, their proper subcellular localization and activity

depends on 5 ALA interacting β-subunits named ALIS. ALAs must interact with ALIS subunits to be extracted from the ER and addressed at a specific compartment (Costa et al., 2016; López-Marqués et al., 2010). Among the 12 identified flippases, only one flippase, ALA1 has been described to be able to flip PS (Gomès et al., 2000; López-Marqués et al., 2012). By bioinformatics analysis based on two papers from Todd Graham identifying critical residues for flippase substrate specificity (Baldridge and Graham, 2012, 2013) and personal communication (López-Marqués), I identified three putative PS-flippases, ALA1, ALA2 and ALA3 (Gomès et al., 2000; López-Marqués et al., 2012; McDowell et al., 2013)(Figure 37A). ALA1 is localized at the ER and PM, ALA2 at the ER and PVC and ALA3 at the ER, Golgi and TGN/EE. Localization of ALAs in the ER could be explained by the fact that PS is generated at the lumen of the ER and has to be flipped to the cytosolic face to exit the ER. Indeed,flippases are involved in vesicular sorting in yeasts and mammals (Sebastian et al., 2012). However, in all the experiments, ALAs were transiently overexpressed in *Nicotiana benthamiana*. Therefore, their ER localization could be due to side effect of overexpression and transient assays. Consistent with PS subcellular distribution, hypothetical PS-flippases are spread all along the endocytic pathway. In yeast, the exposition of PS to the TGN/EE cytosolic leaflet is prevented by knocking out the PS specific flippase TGN/EE-associated DRS2p, suggesting that PS is oriented to the luminal side of organelle membrane in the absence of flippases.

A scenario could be that PS is generated in the lumen of the ER and reaches the *cis*-Golgi by vesicular trafficking, it flips in the TGN and it is then rapidly delivered to the plasma membrane by exocytosis (still facing the cytosol). This is in agreement with the PS localization in Golgi, TGN/EE, recycling endosomes, and plasma membrane. PS would then be internalized by endocytosis and all along the endocytic pathway via a passive process to generate the PS gradient. A plausible hypothesis to regulate the concentration through the activity of flippases could be by the transient association of a specific ALA interacting β-subunits at different compartments (Figure 37B). Another hypothesis for flippase activity regulation could rely on PI(4)P, since in yeast DRS2p (in partnership with cdc50p, the yeast homolog of ALIS), is activated by PI(4)P to promote PS flipping (Azouaoui et al., 2017). As PI(4)P is present in the cytosolic face of the PM, TGN/EE and Golgi, it could activate constitutively flippases to enrich PS in these compartments and thereby sustain the PS localization according to the PI(4)P gradient (Simon, Platre et al., 2014; Figure 37B). The latest hypothesis, could rely on luminal pH value that could regulate the proton concentration, which in turn modulates the ATP

dependent activity of flippases (Figure 37B). Of note, for the later hypothesis, flippase dependent-pH activity showed no significant variation in the interval from pH 6.5 to pH 9.0 *in vitro* (Coleman et al., 2012). However, the luminal pH in plant endocytic compartments is much more acidic (from 6 to 7) and organized in a reverse gradient all along the endocytic pathway (increasing as compartment mature) (Martiniere et al., 2013) but this observation stays highly correlative.

Plant ORP/Osh could be involved in PS enrichment at the plasma membrane but also in endosomes. As mentioned above, the arabidopsis genome contains 12 genes encoding ORP proteins organized in four classes (Skirpan et al., 2006) (Figure 36A). In mammals, critical residues allowing PS and PI(4)P exchange have been identified and rely on a pleckstrin homology (PH) domain and an oxysterol binding domain named oxysterol binding protein related domain (ORD). In plants, the first two classes, ORP type 1 and ORP type 2, contain a PH and ORD domains for every isoform with the exception of the second isoform in the first class (Figure 36A). In petunia, one ORP1 harboring a PH and ORD domains has been identified and localized to the plasma membrane (Figure 36A and B). I identified by bioinformatics analyses that five ORP/Osh proteins contain a PH and ORD and carry as well as critical amino acids required for PS/P(4)P counter-transport. In yeast, the PH domain is not required for PM PS/PI(4)P counter transport. We could consider that other Arabidopsis ORP/Osh could participate in this process but also at different contact sites since the twelve AtORPs harbor critical residues (Figure 37). This suggests that ORP/Osh could be involved in lipid homeostasis and the establishment of the PS gradient (Figure 37). A hypothesis could be that in order to keep the PS gradient, ORPs localized preferentially where PS is more enriched, e.g. PM, TGN/EE and Golgi (Matteis et al., 2017; Sohn et al., 2016). Such scenario would also fit with the low PI(4)P concentration in endosomes since ORP could insure the decrease of PI(4)P in endosomes and Golgi (in conjugation with a PI(4)-phosphatase in the ER). Again, it could be interesting to express PS and PI(4)P sensors crossed with endomembrane markers in the five ORP mutant backgrounds to establish their role in lipid homeostasis.

To tackle those hypothesis, introgression of our lines co-expressing intermediate charge sensors (e.g. 0+, 2+, 4+ and 6+) or PS sensor crossed with endomembrane markers in ALA1, ALA2, ALA3 and the six ORP/Osh mutant backgrounds should highlight ALA/ORP involvement in PS and electrostatic gradient maintenance. In conclusion, the ORP protein family and ALA PS-

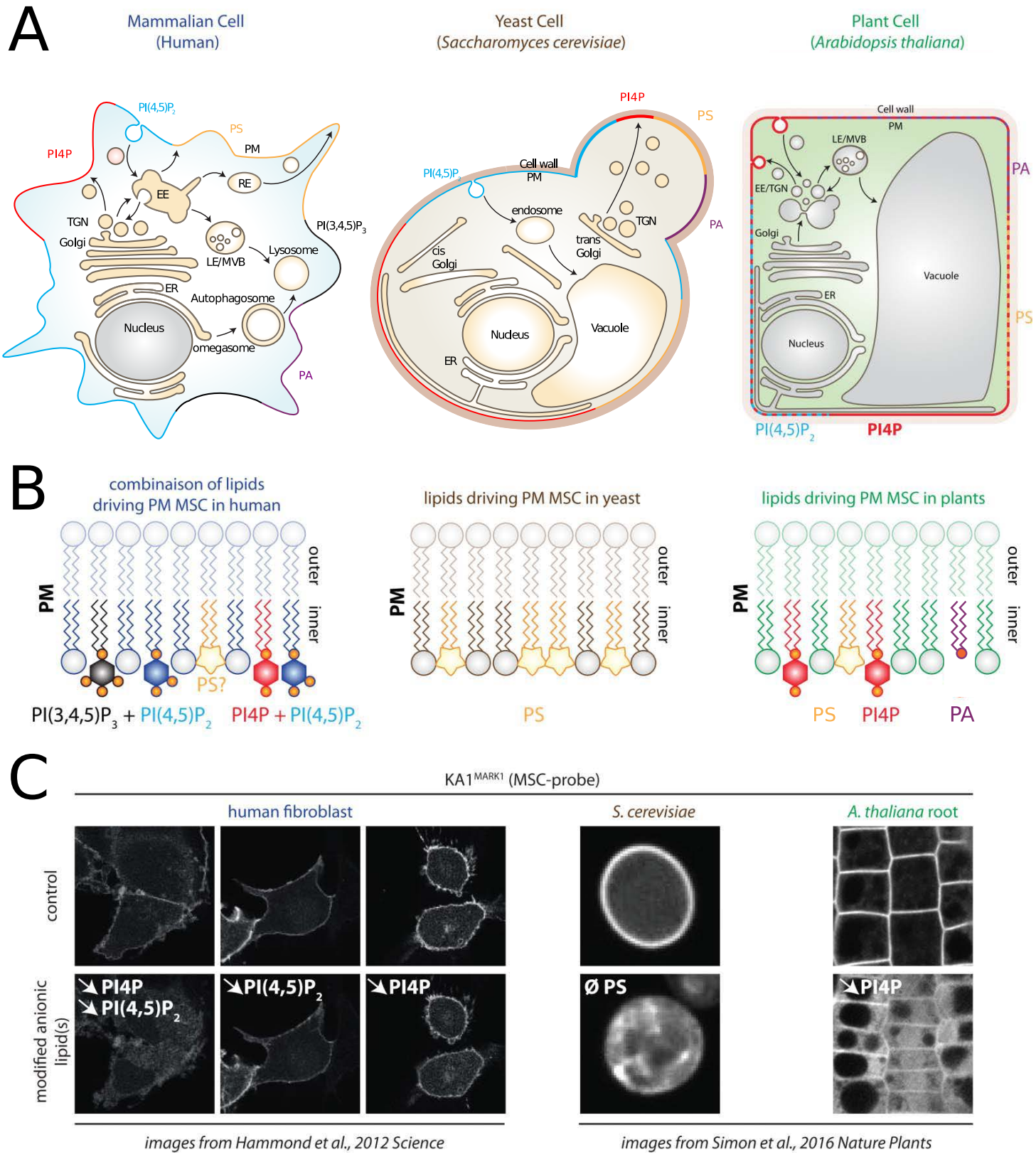

Figure 38. Summary of PM-associated anionic phospholipids in yeast animal and plant cells and their contribution to the PM electrostatic field. A, Schematic representation of human, yeast and plant cells. Anionic phospholipids that localize at the cell surface are indicated for each cell type. For clarity, PI3P, PI5P and PI(3,4)P_2 have been omitted, although they have been shown to localize at the plasma membrane in animal cells at very low quantity and /or upon specific stimuli. **B,** Schematic representation of the anionic lipids required for plasma membrane MSC in mammals (left), yeast (middel), ans plant (right). **C,** Confocal pictures showing the localization of KA1 domain of MARK1 in human fibroblast cells (left), S. cerevisiae (middel) and A. thaliana root epidermis (right).Top panels are control cells and bottom panels show conditions in which anionic phospholipids have been genetically or chemically perturbed. The targeted lipid(s) is indicated in white (downward pointing arrows indicate the reduction in the given lipid content and Ø total absence of the lipid). EE, early endosome; LE, late endosome; RE, recycling endosomes; TGN, trans golgi network; ER, Endoplasmic reticulum; MSC, membrane surface charge. Pictures of fibroblasts are from Hammond et al., and picture from yeasts and plants are from Simon et al. Adapted from Platre and Jaillais, 2016.

flippases may drive the gradient of electrostatics in plants (and perhaps in other eukaryotic systems).

iii. By phosphatidic acid

Compared to other anionic lipids discussed above, PA was not previously involved in the establishment of the plasma membrane electrostatic field. We showed that in plants, PA produced at the PM by diacylglycerol kinases (DGKs) is required for PM electrostatics. However, this result should be considered with care since it relies only on a pharmacological approach that could induce side effects.

As mentioned in the introduction, PA accumulates at the plasma membrane in a constitutive manner in phagocytic cells through a constitutive DGK activity (Bohdanowicz et al., 2013). The inner surface potential is altered during phagocytosis (Yeung et al., 2006). It would therefore be interesting to address whether variation in PA might also alter membrane electrostatics in macrophages, during phagocytosis. Moreover, another interesting point could be to investigate whether PA is involved in PM-targeting of K-Ras, since PA has been demonstrated to be involved in its regulation (Zhang and Du, 2009). In yeast, PA accounts about 12% of total lipids (which is highly elevated compared to other anionic phospholipids) and is localized at the plasma membrane. It would also be interesting to address whether PA might participate to the PM electrostatic field in yeast. To sum up, our results suggest that PA is important for PM electrostatics in plants, and I believe this could pave the way to future studies in other organisms, in which PA might also be an important driver of the PM electrostatic field.

Phosphatidic acid is a particular phospholipid not only because of its phospholipid backbone property but also by its involvement in a wide range of biological processes such as plant stress signaling, defense and development. PA is a critical molecule in response to stresses, it acts as a rapid second messenger (within second-minutes) for biotic stress (senescence/cell death) and for abiotic stress (drought, freezing, cold, salinity, wounding, and responses to the stress hormones ABA and ethylene). Stress responses induce PA generation through activation of either PLD, the PLC/DGK pathway, or both (Arisz et al., 2013; Li et al., 2009; Mishkind et

al., 2009; Testerink and Munnik, 2005, 2011). The PLD pathway utilizes preferentially phosphatidylcholine (PC) or phosphatidylethanolamine (PE) as substrates, while the PLC/DGK pathway necessitates PIPs (Figure 10B). The Arabidopsis genome encodes twelve phospholipase D (PLD), which are soluble or associated with membranes (mainly the plasma membrane) (Hong et al., 2010; Qin and Wang, 2002), and seven diacylglycerol kinases (DGK) predicted to be localized in the inner leaflet of the plasma membrane, EE/TGN, nucleus and cytosol (Gómez-Merino et al., 2004, 2005). Under stress conditions, PA could be a modulator of PM electrostatic field. In particular, the PLD pathway could be involved in the modulation of the PM electrostatic field since neutral phospholipids (i.e. PC, PE) are converted into anionic PA (Ruelland, 2002). First, it could be relevant to confirm that PA contributes to the PM electrostatic field by genetic approaches, using for example mutants in PM-associated DGKs. However, the Arabidopsis genome has seven DGKs, which makes genetic approach difficult. To overcome this drawback, an alternative way could be to express the catalytic domain of PHOSPHATIDIC ACID PHOSPHOHYDROLASE 1 (PAH1) from Arabidopsis fused to a myristoylation and palmitoylation (MAP) sequence for plasma membrane targeting to induce specific PA-PM depletion (similar to our MAP-SAC1 strategy used in chapter 1 of the thesis, Simon et al., Nature Plants). As PA is involved in early stress responses, creating a FRET-based PA sensor would be useful to investigate PM-PA variation under stress responses in a sensitive manner.

b. Why does a cooperation of three anionic lipids sustain the plasma membrane electrostatic field in plants?

Eukaryotic cells share the same similarity for plasma membrane property but this feature is not only powered by different anionic lipids but also maintained by different combinatorial systems (Figure 38). By contrast to other eukaryotes, plant PM-electrostatics maintenance system relies on three independent anionic lipids, PI(4)P, PA and PS, acting in cooperation (Figure 38). The biochemical meaning of cooperation is defined as a “phenomenon displayed by systems involving identical or near-identical elements, which act dependently of each other, relative to a hypothetical standard non-interacting system in which the individual elements are acting independently”. This definition is supported by experiments showing that PI(4)P, PS and PA act to maintain the PM electrostatics in an independent-manner. This notion implies also that

each actor requires feedbacks from the others to make the most of cooperation. Even if PI(4)P, PS and PA are not directly metabolically linked some feedbacks exist between them. PI(4)P is directly degraded by PLC to produce DAG, the substrate of DGKs, which are PA-generating enzymes (Ruelland, 2002). As previously described, lipid exchange between organelles links PI(4)P, PS and PA and could be more directly involved in feedbacks (Figure 7C and 9D). I favored the hypothesis that lipid exchange could be involved in lipid homeostasis, notably with PI(4)P as a central regulator. In animals, Nir2 links PI(4)P and PA metabolism between the endoplasmic reticulum and the plasma membrane, while ORP/Osh links PI(4)P and PS metabolism between the ER/PM and ER/Golgi (Chung et al., 2015; Filseck et al., 2015; Kim et al., 2015; Sohn et al., 2016). In plants, Nir2 homologs have never been found. However, by bioinformatics analyses, I identified a protein named SHOOT GRAVITROPIC RESPONSE 2 (SGR2) (Kato et al., 2002), a phospholipase-like protein that contains a DDHD domain which is critical for Nir2 activity and binds PI(4)P (Inoue et al., 2012) and which may be involved in PA/PI(4)P homeostasis.

Above, I discussed the electrostatic field as a mechanism to differentiate the subcellular compartments in order to regulate cell organization. However, the plasma membrane is a large interface in cells, which is itself organized. It is then highly probable that electrostatic field is not homogeneously organized within the plasma membrane (Bücherl et al., 2017; Gronnier et al., 2017; Zhou and Hancock, 2015). The presence of three anionic lipids may allow to create PM domains with a large spectrum of electrostatics properties. One may speculate that four different situations could exist: exclusion of anionic lipids, presence of one, two or three types of anionic lipids. Partitioning the PM in several platforms depending on electrostatics and lipid composition could trigger different signaling pathways. For example, a specific platform could be created in response to hormone or stress to recruit specific proteins and trigger proper signaling (Zhou and Hancock, 2015; Zhou et al., 2015). The organization of the plasma membrane in such domains may be particularly prone to respond to developmental and environmental changes. Analyzing the set of charge anionic lipid sensors using TIRF and/or super-resolution microscopy would allow to describe the spatial patterning of those regions at the plasma membrane in different conditions. The FRET-based sensor from Ma et al., 2017, could also help to decipher the plasma membrane electrostatic field organization during developmental and environmental changes. In accordance with the hypotheses made above, ORP/Osh or flippases proteins could be involved in this regulation and it could be relevant to introgress the MCS FRET-based sensor into those mutant backgrounds.

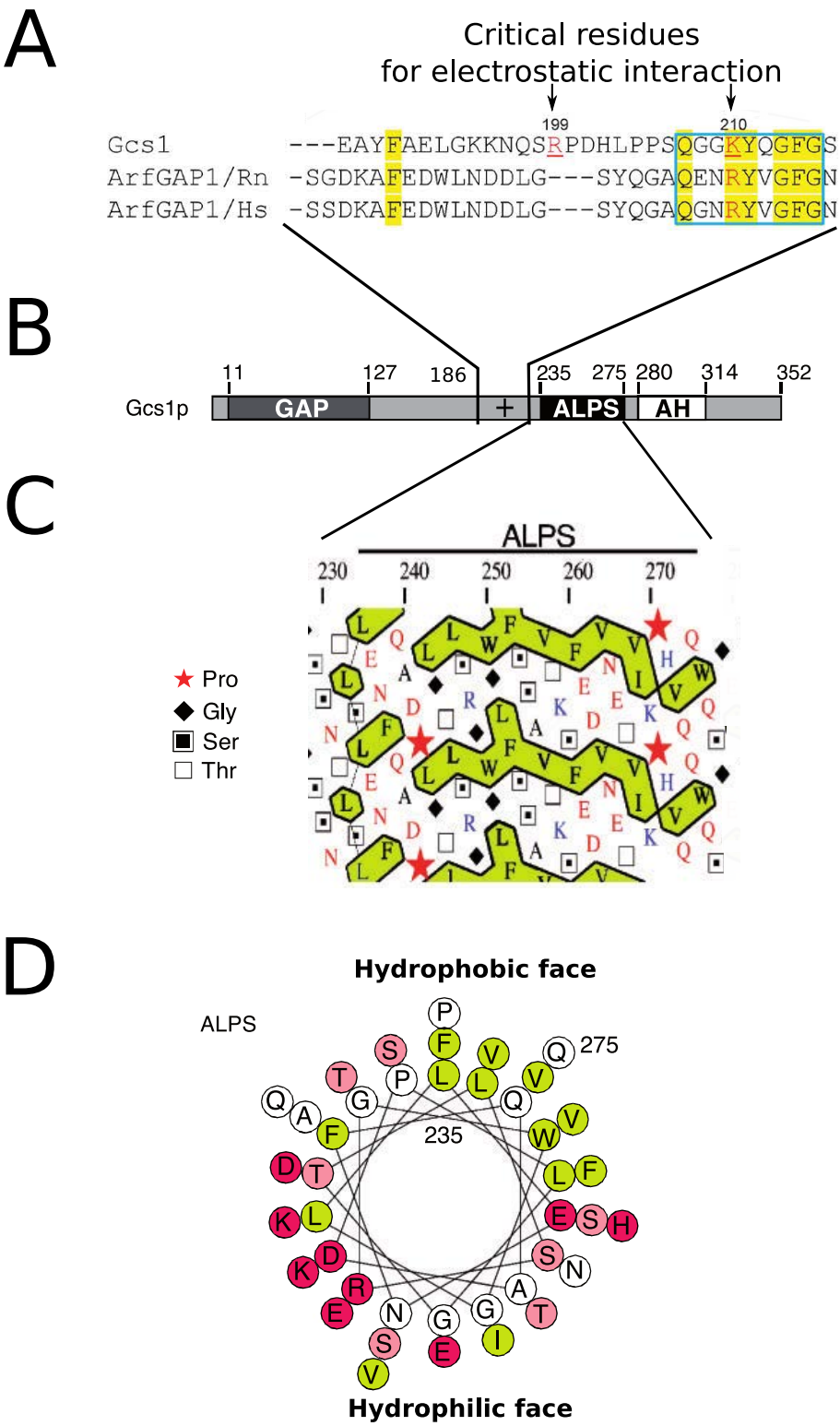

Figure 39. Description of the +ALPS motif of Gcs1. A, Alignment of Gcs1 and ArfGAP1 region prior to ALPS motif corresponding to the "+" sequence in Gcs1 which is necessary for the electrostatic interaction. The positive charged residues, lysine (K) at position 210 and arginine (R) at position 199 are highlighted in red. Conserved sequences between Gcs1 and mammalian ArfGAP1 are highlighted in yellow. **B,** Diagram of Gcs1 **C,** Gcs1 (230-275) corresponding to the ALPS motif, schematic representation of the hydrophobic cluster analysis (HCA) showing ALPS highly hydrophobic face in green. **D,** Schematic representation of the ALPS alpha helix composed of an hydrophobic and hydrophilic face from pepwheel software. Hydrophobic amino acids are represented in green and hydrophilic in red and pink. AH, amphipathic helix. Adapted from Zendeh-boodi et al., 2013 and Xu et al., 2013

c. PS and PI(4)P sustain the gradient of electrostatics all along the endocytic pathway

Our data suggest that in plants PS and PI(4)P are required to establish a gradient of electrostatic along the endocytic pathway. However, PS involvement in this feature is rather correlative and the implication of PI(4)P is only based on a pharmacologic approach using a set of K-Ras mutated tail markers (0+, 2+ and 4+, nested K-Ras markers). Furthermore, to date, we have not demonstrated the importance of endosome electrostatics for the localization and/or function of endogenous plant proteins.

To further demonstrate the relative importance of PI(4)P and PS in endosome electrostatics, it would be important to cross the nested K-Ras markers into the *pss1* and *pi4kbeta1beta2* mutants (the PI4Ks that localizes at TGN/endosomes). I started these crosses, but to obtain the right genotypes is a time-consuming process, since it requires to introgress each K-Ras marker (0+ to 8+, 5 lines) crossed with each compartment marker (5 wave line each: total of 25 lines) into the *pss1* mutant and *pi4kbeta1beta2* double mutant. In addition, while K-Ras mutated tail markers are useful, they also have limitations. Indeed, their localization is dependent on both charges and its lipid anchor, and markers with intermediate charges (4+) bind to both highly electrostatic and mildly electrostatic membranes (Figure 16A). As such, their localization in the electrostatic territory is not clear-cut and subsequent analyses with these markers systematically require extensive quantitative analyses. To circumvent these potential problems, I designed a biosensor dedicated to probing electrostatic properties of endosomal membranes. To this end, I decided to use the positively charged amphipathic lipid packing sensor motif of the yeast GROWTH COLD SENSITIVE 1 (GCS1) protein (called +ALPS; Figure 39)(Xu et al., 2013). As explained in the introduction (see part IV/b; Figure 17), the +ALPS motifs may act as sensors of negatively charged and curved membranes. In yeast, ALPS motifs localize preferentially in the Golgi, however, the +ALPS motif of GCS1 localizes out of the Golgi in the electrostatic territory (i.e. TGN). My preliminary results show that in plants the $+ALPS^{GCS1}$ strongly colocalize with EE/TGN endosomes and to a lesser extent with late endosomal compartments (data not shown), which is in accordance with our map of the electrostatic territory based on our nested K-Ras markers. In order to validate this sensor, I made mutations in the critical positive residues (which I called -ALPS) and crossed this line with red intracellular compartment markers. Consistently, -ALPS is less associated with EE/TGN

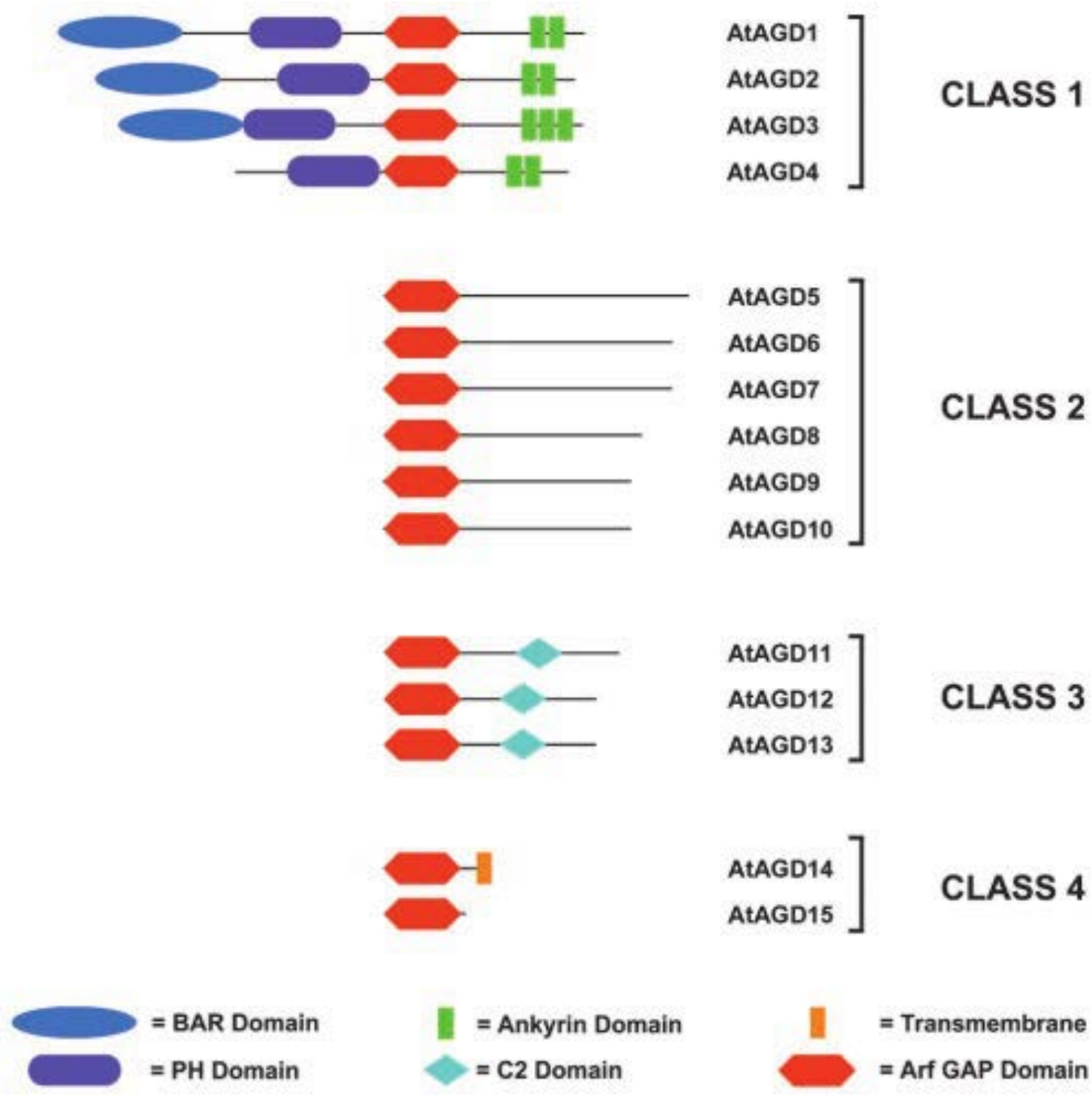

Figure 40. ArfGAP proteins of Arabidopsis. AtAGD proteins were identified using BLASTP with the AGD of ASAP1 (GenBankaccessionno.NP_060952). Domains within the AtAGD sequences were detected using SMART (Letunic et al., 2002). Adapted from Skirpan et al., 2006.

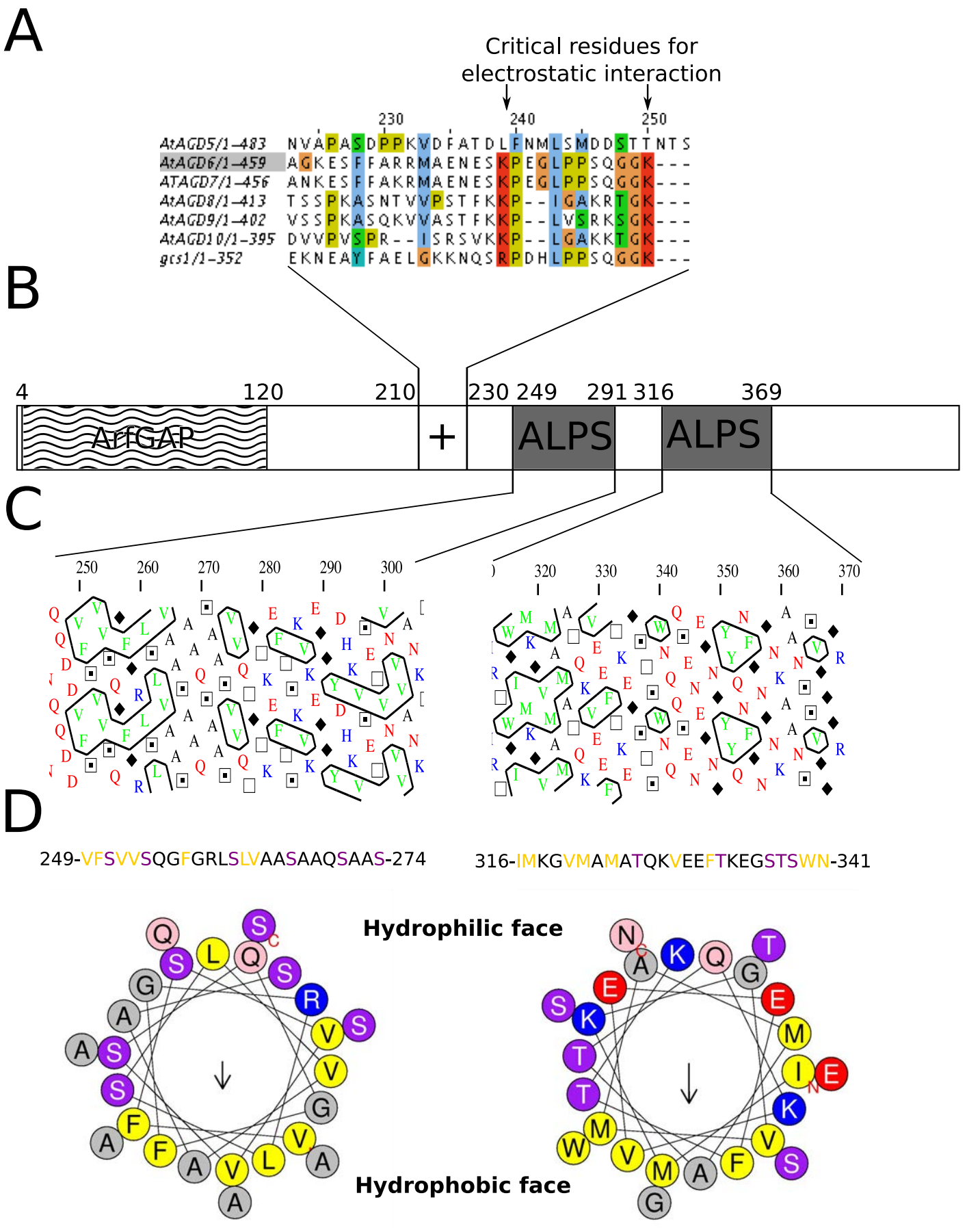

Figure 41. Description of the +ALPS motif of one of AGD type II, AGD6. A, Alignment of Gcs1 and AGD type II region prior to ALPS motif corresponding to the "+" sequence in Gcs1 which allows electrostatic interaction. The positive charged resides Lysine at position 210 and Arginine at position 199 are highlighted in red. Note that AGD5 contains also a +ALPS motif later in the sequence. **B,** Diagram of AGD6 **C,** Schematic representation of AGD6 ALPS motifs by hydrophobic cluster analysis (HCA) showing ALPS highly hydrophobic face in green. **D,** Schematic representation of the ALPS alpha helix composed of an hydrophobic and hydrophilic face generated from HeliQuest. Hydrophobic amino acids are represented in yellow and hydrophilic in purple and pink.

endosomes (data not shown). This result suggests that our sensor might function as a good read-out of the electrostatic properties of intracellular compartments and further confirm that EE/TGN are more negatively charged than other intracellular compartments. In addition, depletion of PI(4)P by PAO decreased the +ALPS motif localization in EE/TGN, arguing that PI(4)P may contribute to establish the electrostatic property of the EE/TGN. Moreover, to determine the respective contribution of PS, the same experiment could be performed using the PS-less mutant. By comparison to the nested K-Ras marker experiments, this would require much less crosses into the PS/PI(4)P mutants (for example only +ALPS/-ALPS crossed with a red TGN-marker). It has also the advantage to report only changes in endosome electrostatics but not PM electrostatics (while the 4+ reporter is sensitive to changes in surface charges in both PM and endosomes). However, +ALPS is also likely dependent on membrane curvature and this could be a limitation of this sensor. Indeed, changes in the localization of the +ALPS sensor can never be pinned down to changes in electrostatic only, since it could also arise from changes in membrane shape/curvature. To conclude, like all biosensors, the +ALPS motif have some limitations but I think it is complementary with the nested K-Ras marker set.

Mining the Arabidopsis genome for the presence of protein with +ALPS motifs, I identified that type II ARF-GAP (AGD) proteins contain a putative +ALPS motif (Figure 40 and 41). Several of these AGD proteins were previously localized in EE/TGN in plant cells. It would therefore be interesting in future experiments to test the functionality of type-II AGD +ALPS motifs and whether or not the localization of these AGD proteins rely on PS/PI(4)P-dependent TGN/endosome electrostatics. Furthermore, this would demonstrate the importance of the electrostatic properties of the EE/TGN for the localization of endogenous plant proteins.

II. ROPs nanoclustering

In this part, I will focus on the third results chapter of the thesis, which focuses on ROP signaling. I found that auxin triggers activated-ROP6 nanoclustering in a PS-dependent manner through electrostatic interactions. However, how is this process mechanistically controlled remain an exciting issue to explore in the future. In addition, what is the function of Rho-GTPase nanoclustering?

a. How are PS platforms set up?

We observed that PS is segregated at the plasma membrane into two different subpopulations, a mobile and an immobile fraction, the later likely corresponding to immobile nanoclusters enriched in PS. Raghupathy et al., in 2015, proposed a general model for PM nanoclustering, which involves transbilayer interactions (also referred to as interdigitation) and that specifically involves PS (Raghupathy et al., 2015). Interdigitation involves interaction between exoplasmic acyl chain (from the outer leaflet) and intracellular acyl chain (from the inner leaflet). They found that outer-leaflet long-acyl-chain and inner-leaflet PS-containing saturated long-acyl-chain in conjugation with cholesterol are pivotal in generating actin-dependent nanoclusters (Figure 42A). Modeling experiments suggest that immobilization of a lipid on one side of the membrane is sufficient to generate nanoscale platforms on the other side. In this case, the authors proposed that PS interacts with actin (or actin regulating proteins), which immobilizes PS and therefore allow the formation of immobile nanoclusters of glycosylphosphatidylinositol (GPI) anchored proteins on the outer leaflet. By extension, we may speculate that PS could also act in similar fashion to generate nanoclusters in plant cells. One possibility would be through interactions with actin. However, I believe that the situation in plants may be reversed as compared to animals. Indeed, a key feature of the modeling results from Raghupathy et al., is that immobilization of lipid molecules on either side of the membrane may trigger immobilization on the other side. It is well known that, in plants, the cell wall confines the diffusion of molecules that stick out of the membrane (for example receptor kinases, (Martinière et al., 2012)). On the plasma membrane outer leaflet of plant cells, GIPC (glycosyl-inositolphosphoryl-ceramides) are the most abundant lipids. GIPC is also the most important lipid on earth (Mongrand S. personal communication). They have large head groups that are predicted to extend into the cell wall and may therefore have a limited diffusion. In addition, they are sphingolipids with very long chains, which could be involved in transbilayer coupling with inner leaflet phospholipids. One could speculate that this system may allow the formation of stable PS nanoclusters in the cytosolic plasma membrane leaflet (Figure 42B).

To tackle those hypothesis, we could treat plant with metazachlor, which inhibits the production of very long chain sphingolipid (Wattelet-Boyer et al., 2016), and analyze its impact on the behavior of our PS sensor (and mEos-ROP6) using super resolution microscopy. We could also use mutants involved in GIPC biosynthesis (such as for example IPCS enzymes, Y.Boutté

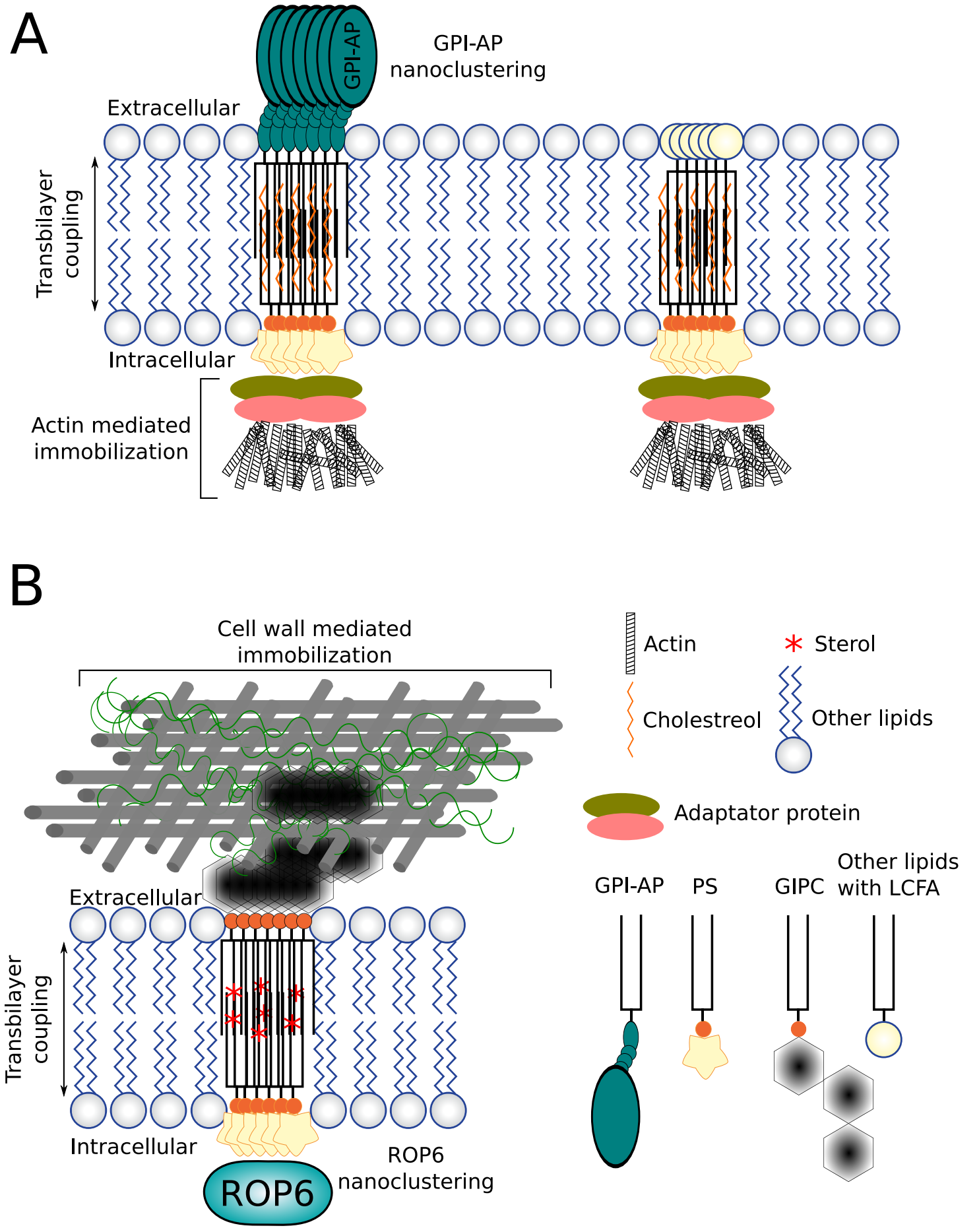

Figure 42. Model of PS-dependent nanoclustering based on transbilayer coupling in mammals and a speculative model in plants. A, Transbilayer interactions between outer-leaflet long-acyl-chain-containing lipids and inner-leaflet phosphatidylserine are pivotal in generating actin-dependent nanoclusters of membrane lipid-anchored proteins in mammals. **B,** Speculative model in plants. Transbilayer interactions between GIPC outer-leaflet long-acyl-chain and inner-leaflet phosphatidylserine generates nanoclusters of ROP6. GPI-AP, glycosylphosphatidylinositol anchor protein, GIPC, glycosyl inositol phospho ceramide, PS, phosphatidylserine, LCFA, long chain fatty acid. Adapted from Raghupathy et al., 2015.

personal communication). This experiment will allow to address, at least in part, whether interdigitation could play a role in PS-nanoclustering, and what could be the role of very long chain sphingolipids in this process. To tackle the importance of PS in this process, it would be interesting to add back PS with different acyl chain (lengthwise but also with different saturation degree) in the *pss1* mutant and then address mEos-PH^{EVCT2} and mEOS-ROP6 dynamics by sptPALM microscopy. Cholesterol has a central role in the interdigitation process and stabilizes nanoclusters in animals (Raghupathy et al., 2015). In plants, sterols are required for REMORIN nanoclusters (Gronnier et al., 2017) and for ROPs localization (Stanislas et al., 2015) acting with other anionic lipids such as PI(4)P and PI(4,5)P_2, respectively. To determine the role of sterol in PS immobilization and ROP6 signaling, we could apply 3-β-hydroxysterol-specific fluorescent probe filipin III (Stanislas et al., 2015) to appreciate the colocalization with PS sensors and ROP6, for example in TIRF microscopy. In addition, we could use pharmacological approaches to deplete the sterol pool (e.g. with Methyl-β-cyclodextrin) or inhibit sterol synthesis (e.g. with fenpropimorph, (Gronnier et al., 2017)) and analyze their respective effects on PS and ROP6 membrane dynamics.

b. How is ROPs nanoclustering regulated?

In the scenario presented above, PS nanoclusters are prepatterned prior to ROP6 activation and its subsequent recruitment into these nanoclusters, raising the question how does auxin trigger ROP6 clustering?

ROPs possess a polybasic region (PBR) which interacts through electrostatic interactions with anionic phospholipids. Because auxin induces PS localization at the PM (Figure 4 of the paper presented in chapter 3), it may increase the local concentration of PS in nanoclusters, boosting their electronegativity, and thereby recruiting ROP6. It would therefore be interesting to address PS dynamics at the PM in response to auxin. However, ROP6 nanoclustering is a fast response (within 5 minutes of auxin treatment) of the “non-genomic” auxin signaling pathway. It is therefore unlikely that an increase of PS into nanoclusters would be the trigger of ROP6 clustering as this would imply that proteins involved in PS clustering are very early targets of auxin (earlier than ROP6). Nevertheless, in such hypothesis, PM-associated PS flippases could get activated in the presence of auxin, promoting PS enrichment in nanocluster. ALA1 is

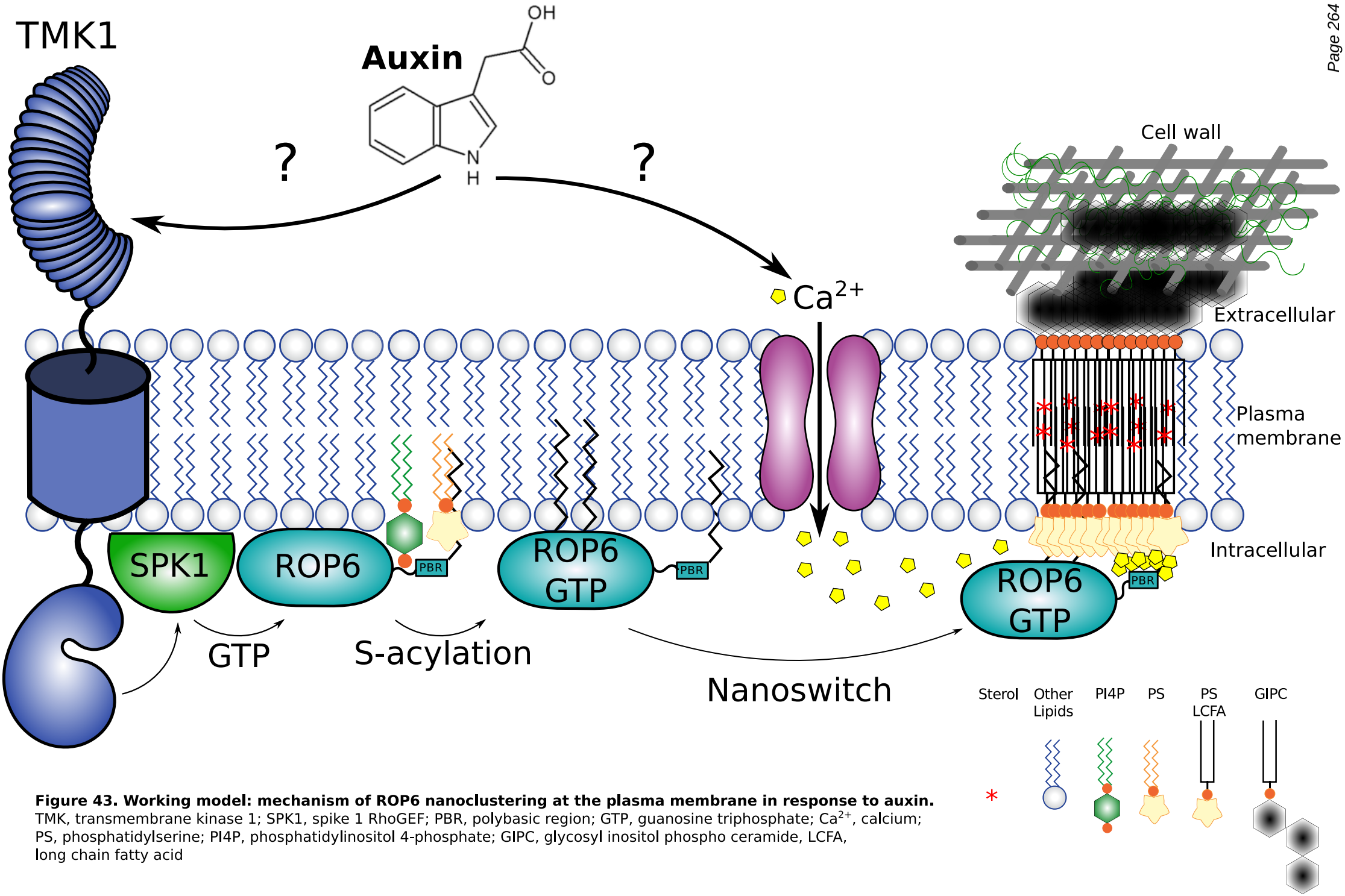

Figure 43. Working model: mechanism of ROP6 nanoclustering at the plasma membrane in response to auxin.
TMK, transmembrane kinase 1; SPK1, spike 1 RhoGEF; PBR, polybasic region; GTP, guanosine triphosphate; Ca^{2+}, calcium; PS, phosphatidylserine; PI4P, phosphatidylinositol 4-phosphate; GIPC, glycosyl inositol phospho ceramide, LCFA, long chain fatty acid

localized at the plasma membrane and expressed in the root meristematic zone and could be an appropriate candidate (Gomès et al., 2000; López-Marqués et al., 2012). Alternatively, as PI(4)P acts as a negative regulator of ROP6 nanoclustering contrarily to PS, ORP/Osh protein would be an interesting candidate. Auxin could promote ORP/Osh proteins activation, depleting PM-associated PI(4)P and enriching PM-PS at the same time.

Upon activation, ROP6 is transiently S-acylated on two cysteine residues, which are required for its function and for its targeting to detergent resistant membranes (DRM) (Sorek et al., 2010). This is in accordance with our data showing that ROP6 is getting immobilized when activated. It is also compatible with the interdigitation hypothesis, since acylation could favor highly ordered phase such as transbilayer interactions. Modeling suggest that both acylated cysteines (C21 and C156) are located in the GTPase domain and are expected to be buried when ROP6 is not activated (Sorek et al., 2010). However, Sorek et al., proposed that upon activation, the large conformational changes induced by GTP binding may expose the two cysteines to protein S-acyl transferases (PATs), which in turn would modify ROP6 acylation status and likely its localization into nanoclusters. To directly test the importance of S-acylation, I produced mutant versions of ROP6 in which I mutated C21 and C156 into alanine. Our preliminary experiments suggest that these two cysteines are indeed required for ROP6 nanoclustering (Martinière personal communication). Recently, a PAT protein has been found to acylate ROP2, which is required for ROP2 activity (Wan et al., 2017). It could be interesting to observe whether ROP6 still localizes in nanoclusters in the presence of auxin in this mutant background (or in related PAT mutants).

Calcium signaling is interconnected with ROP polarization since calcium concentration gradient correlates with ROP activity in polar tip growth (Himschoot et al., 2015). Moreover, phosphatidylserine has a particular affinity with calcium (Martin-Molina et al., 2015) and in turn could increase interaction between PS and ROP6. This suggests that calcium could trigger ROP6 clustering into PS immobile fraction. Such hypothesis would be consistent with the fact that ROP6 clustering is a rapid « non-genomic » event. In addition, it was recently shown that auxin treatment induces a transient cytoplasmic calcium increase, approximately 5 minutes following auxin treatment (Waadt et al., 2017). To tackle this hypothesis, it would first be important to test in vitro if calcium has any impact on ROP6 lipid interaction (notably with PS).

In vivo, we could apply a concomitant treatment of auxin and lanthanum, which is an inhibitor of calcium channel, and evaluate by super resolution microscopy ROP6 clustering. The reverse experiment could be done applying mastoparan, which promotes calcium channel activation.

From the three hypotheses highlighted above, the more documented so far is the role of S-acylation on ROP6 clustering. It is therefore likely that this lipid modification participates in switching the behavior of activated ROP6 from fast-diffusible single molecules to immobile nanoclusters. However, these hypotheses are not mutually exclusive and could act in combination to reinforce the switch-like behavior of ROP6 localization dynamics. I envisioned the following model for ROP6 localization in activated and inactivated situation. This model is of course highly speculative at the moment and should be tested experimentally (notably using some of the experiments that I suggested in this discussion).
ROP6 is recruited to membrane by its geranylgeranyl lipid modification and electrostatics interactions between anionic lipids and ROP6 PBR confine ROP6 localization at the plasma membrane. PI(4)P plays a major role in this process and we hypothesize that the bulk of PM PI(4)P are highly mobile, therefore recruiting ROP6 in a fast-diffusible state. Auxin is perceived outside the cell, somehow activates receptor kinases (such as TMKs, see introduction part 3/II/c), which likely in turn activate ROP-GEF (such as SPIKE) and thereby promotes ROP6 activation. ROP6 activation allows its S-acylation. Acylation increase the affinity of ROP6 for specific PM domains, which are prepatterned and enriched in PS and perhaps depend on specific sterol composition. Interactions between PS and ROP6 stabilize ROP6 localization in nanoclusters. A concomitant increase in cytosolic calcium may consolidate/promote PS-ROP6 interaction. Likewise, auxin itself may increase the presence of PS into nanoclusters to promote ROP6 immobilization (Figure 43).

c. Why are nanoclusters required for signaling?

Although it is important to discuss the mechanistic aspects of PS immobilization and ROP6 nanocluster formation upon auxin treatment, perhaps the most important question is: what is (are) the function(s) of ROP6 nanopartitioning?

In broad terms, the partitioning of proteins in PM domains is viewed as their localization into "signaling platforms". What is behind the concept of "signaling platform" is often vague, but the general idea is that these domains will locally concentrate protein partners or complexes, thereby contributing to signaling. In cases of ROP6 partitioning, it is relatively easy to understand how such concept could be involved in auxin signaling. Indeed, ROP6 nanopatterning follows a switch-like behavior (out of the cluster in resting condition, inside the cluster in activated condition). Therefore, ROP6 could meet its effectors only when present in nanodomains. As such, ROP6 activation (ROP6-GTP) would not be sufficient for signaling, since its subsequent recruitment into PM nanodomain is equally important. Such scenario would explain why ROP6-CA is inactive in the *pss1* mutant (i.e. present as ROP6-GTP but unable to interact with downstream effectors because it is not recruited in PM nanoclusters). To test such scenario, it would be interesting to address whether (some) ROP6 effectors are indeed localized into PM nanoclusters, either in a prepatterned way (present before ROP6 activation, like PS) or whether they are recruited to such domains following auxin treatment. Such question could be addressed by TIRFM and sptPALM imaging of effector molecules and/or imaging of ROP6/effector interaction by FRET/FLIM. In addition, ROP6 accumulation into PM nanodomains also includes the notion of "clustering". In the case of K-Ras, nanoclusters contain ~6-7 Ras proteins per nanocluster (Janosi et al., 2012). This is important because Ras dimerization is a prerequisite for signaling. Similarly, it could be possible that ROP6 dimerization or higher order complex could be important for signaling.

Emerging concepts developed by the Hancock lab propose that K-Ras nanocluster formation and disassembly act as a high-fidelity signal transmission system (Tian et al., 2007). To clarify this concept, I used an analogy explained in figure 44 based on waterwheel. Tian et al., established a model where extracellular signal from growth factor (GF) corresponds to an analog signal, since GF-dependent signaling pathway (RAF-MEK-ERK) occurs in a GF dose-dependent manner (Tian et al., 2007). RAF-MEK-ERK signaling cascade is controlled upstream by K-Ras. The presence of GF triggers the K-Ras nanoswitch from mobile to immobile fraction/nanoclusters. Activated K-Ras is assembled into transient nanoclusters on the plasma membrane for K-Ras signal transmission (Zhou and Hancock, 2015). They consider that unactivated K-Ras does not signal therefore the signal output is null. By contrast, one K-Ras nanocluster is able to trigger signaling and is considered as one. In this sense, K-Ras nanoclustering is considered as a digital signaling component. To sum up, the GF analog signal

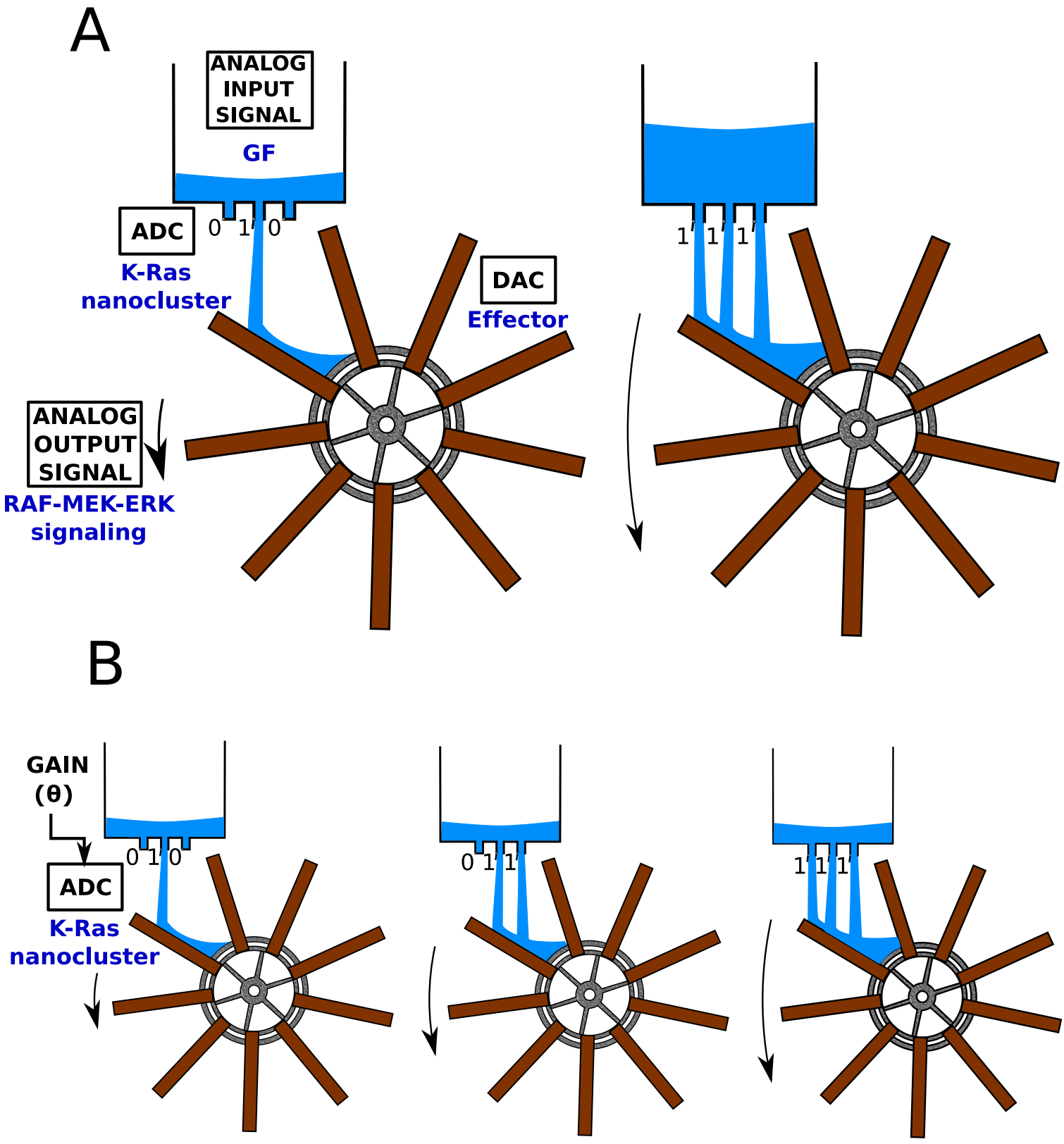

Figure 44. Schematic representation of analog-to-digital and digital-to-analog conversion and gain concepts. The tank filled up with water corresponds to the analog signal input. The three sluice gates correspond to the analog to digital converter (ADC) since closed sluice gate is equal to zero and opened sluice gate is equal to one. The wheelwater corresponds to digital to analog converter (DAC). The rotation speed of the wheelwater encodes the analog signal output. **A**, Schematic representation of the ADC to DAC encoding high fidelity signal transmission. The analog signal input (water) is encoded by the digital platform (opening/closing sluice gates) which is converted by a DAC (wheelwater) to trigger analog signal output (wheelwater rotation speed). The wheelwater speed rotation (analog output signal) is encoded with high fidelity according to the water volume (analog signal input) thanks to the number of opened/closed sluice gates (digital signal) through the action of ADC and DAC. **B,** Schematic representation of the gain concept. The gain allows to play with the sensibility of the system; i.e.: with the same amount of analog input signal the digitizer on its own directly modulates the analog output signal (opening/closing sluice gates).

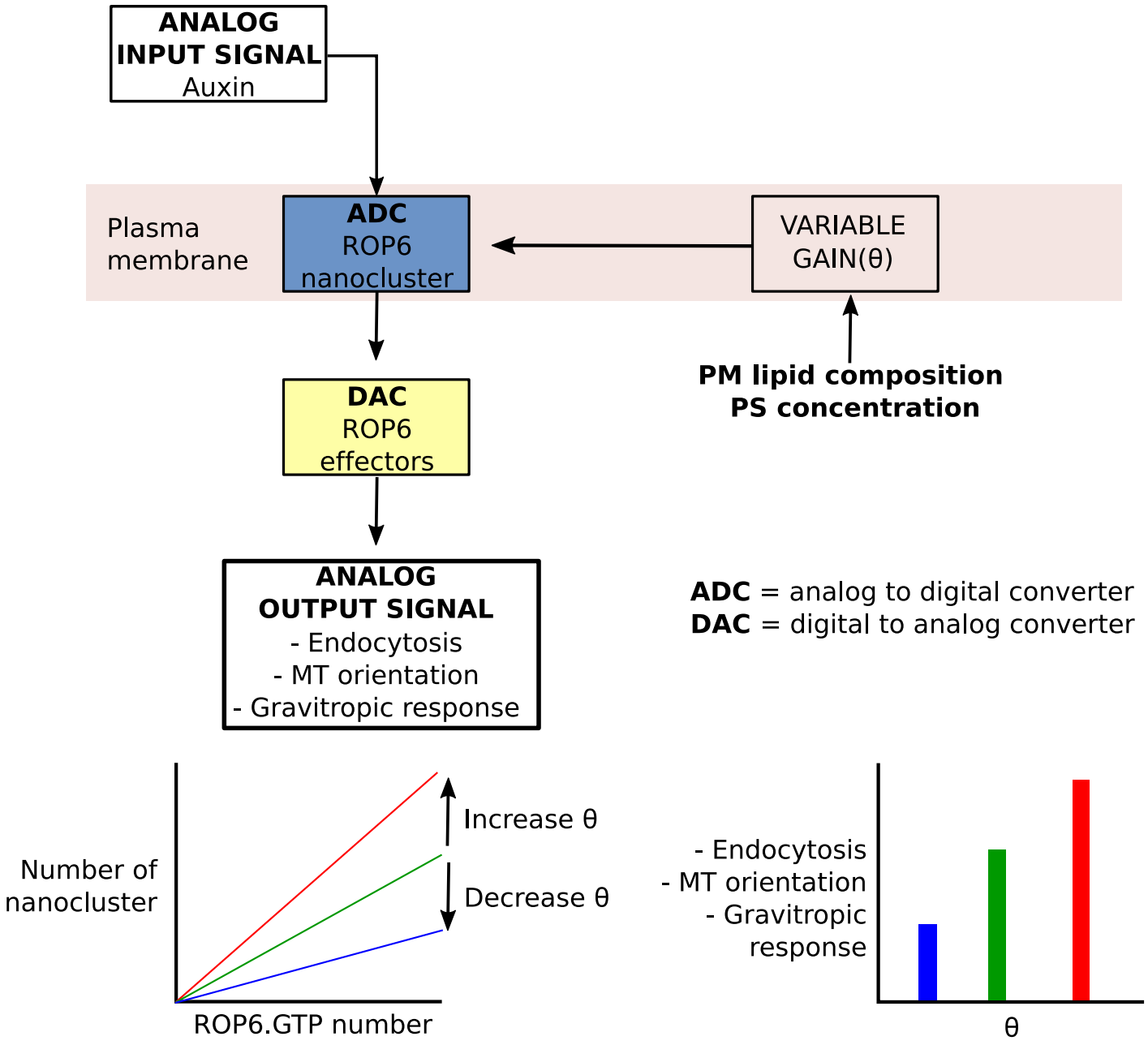

Figure 45. Hypothetic model defining that ROP6 nanoclusters are analog-digital convertors that digitize signal input. A fixed clustered fraction is set for ROP6 on the plasma membrane, which yields a linear correlation between the number of nanoclusters and the ROP6GTP level (left graph). Thus, a change in clustered fraction corresponds to a direct change in endocytosis, MT orientation and gravitropic response signal output (right graph). ROP6 clustered fraction is highly dynamic and is a function of auxin level and intrinsic cell plasma membrane properties, which can be manipulated physiologically by modulating PS concentration. PM, plasma membrane; PS, phosphatidylserine.

is perceived extracellularly and integrated at the plasma membrane by K-Ras, which in turn convert analog signal into digital signal. This process is considered as an analog-to-digital conversion (ADC; Figure 44A). Finally, digital signal is therefore transduced to RAF-MEK-ERK signaling cascade, which is an analog signal. This step is considered as a digital-to-analog conversion (DAC; Figure 44A). As aforementioned, GF-dependent signaling pathway (RAF-MEK-ERK) occurs in a dose-dependent manner, which implicates that digital signal must integrate signal modulation (Tian et al., 2007). A way to tune this parameter is by increasing the number of K-Ras nanoclusters, which in turn increase downstream signaling. The interesting question is now, how is the number of nanoclusters regulated? They found that specific lipids, notably PS, play critical roles in mediating the formation, stability and dynamics of K-Ras nanoclusters (Zhou and Hancock, 2015). They propose that PS could be considered as a way to increase the digital signal gain according to analog GF signal (Figure 44B). Altogether, this system is able to integrate strength of an extracellular analog signal and to transduce it into an analogous intracellular signal with the same strength through signal digitalization according to the number of nanoclusters. This system is then particularly powerful to ensure high-fidelity signal transmission between the extracellular and intracellular matrix but is tunable depending on the PM PS-concentration (i.e. digital gain).

A parallel could be made between K-Ras and ROP6 since they are both small GTPases carrying a PBR and a lipid anchor. Moreover, ROP6 is transiently associated with nanoclusters when activated by auxin and modulation of PS level impact directly ROP6 signaling in a dose-dependent manner, suggesting that PS could be involved in ROP6 nanocluster stability. Considering that PS is able to stabilize nanocluster formation, we could hypothesize that such system could exist to ensure auxin high fidelity transmission. In this case, analog signal emerging from extracellular auxin could be integrated and modulated into a digital signal by PS-dependent ROP6 clustering. The digital signal is transduced into analog signal by ROP6-effectors to trigger analog signal output such as inhibition of endocytosis and microtubule orientation promoting root gravitropism response (Figure 45). To verify this assumption, we should determine the number of ROP6 nanoclusters depending on auxin concentration and ROP6 nanocluster formation in plants containing different PS level using super resolution microscopy. If such system exists in plants and tunes the gravitropic response, this could demonstrate a physiological role of the high-fidelity signal transmission proposed for K-Ras. Because the level of PS at the PM is developmentally controlled, such hypothesis would suggest that plant cells, depending on their differentiation status may integrate ROP6 signaling with

different “gain”. This model would therefore suggest differences in auxin sensitivity and responses depending on the developmental context of the cells. This idea is fully compatible with the notion that auxin act in a context-specific manner. In addition, auxin itself seems to feedback on PS-PM concentration and as such could act on the sensitivity of its own response. Such complicated and intricate mechanisms is often the rule rather than the exception in biology, and clearly modeling approaches would be required to fully understand the biological meaning of such system. The digital-to-analog processing system for K-Ras was proposed based on computational modeling (Tian et al., 2007) and it would be interesting in the future to test whether such model could also be extended to ROP6/auxin signaling.

The plasma membrane nanoclustering could be easily coupled with the hypothesis of PM-partitioning into several platforms depending on electrostatics and lipid composition in order to trigger different signaling pathways (Figure 46). However, if such platforms could exist, how does protein know where to go? Recently, Zhou et al., 2017, highlights that the polybasic region of K-Ras does not rely only on electrostatic interaction and encodes lipid specificity (see intro VI/b, Figure 25) (Zhou et al., 2016). Briefly, K-Ras C-terminal membrane anchor is also called the hyper-variable region (HVR) because other RAS proteins contain different lipid modifications (e.g. prenylation) and other amino acids sequence in their PBR tail. The combinatorial lipid sorting code defined by the prenyl anchor and PBR sequence encode lipid specificity which directly influences its nanodomain organization, which in turn tunes K-Ras signal output. Mutation of one single PBR-associated lysine (K177 or K178) into glutamine does not have the same effect on membrane association and differentially affect signaling. Again, such concept may be extended from K-Ras to ROP signaling. Indeed, all ROPs have a C-terminal PBR, but they show some variation in sequences and net charges (Figure 46). Therefore, each PBR may have different lipid specificities, which could impact the signaling output of each ROP. In other words, depending on their PBR, each ROP could be addressed at different plasma membrane regions, interacting with different effectors. This hypothesis could explain how only 11 ROPs are involved in lots of different biological signaling pathways. To test this hypothesis, it would be important to study the localization of other ROP proteins, and check whether they are localized in nanodomains upon activation, and whether these nanodomains are the same or different from ROP6-containing clusters. My preliminary data suggest that ROP2 localization, like ROP6 localization, depends on PS (i.e. mislocalization of ROP2 in pss1 mutant) and its PBR (i.e. ROP2-7Q is largely located in intracellular compartment, data not shown).

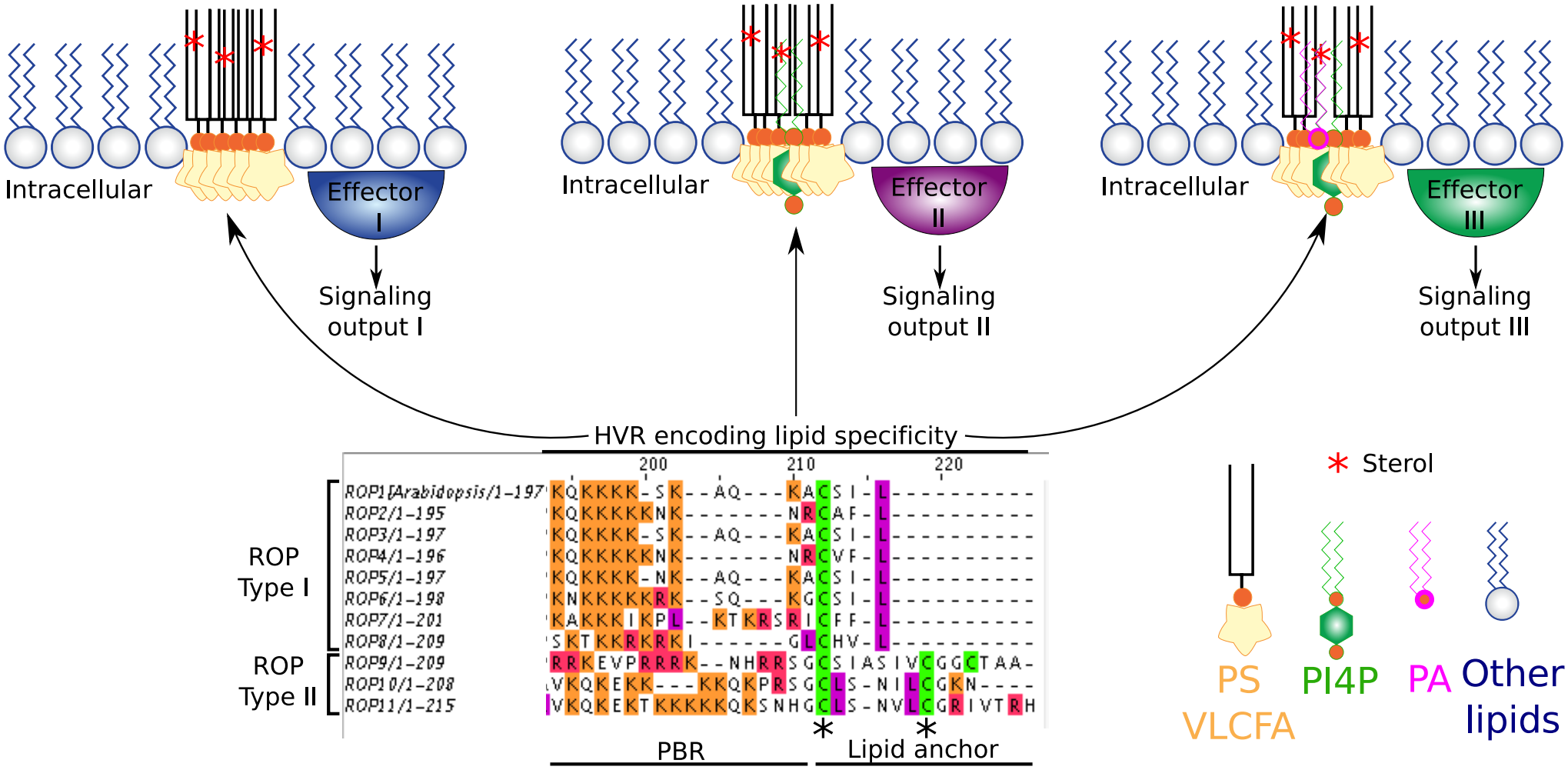

Figure 46. Schematic representation of ROP6-PBR encoding lipid specificity in order to trigger different PM-associated nanocluster and signal outputs. Sequence alignment of ROP-PBRs. Depending on lipid combinaison, concentration and surface charge different platforms could recruit different ROPGTPases since their PBRs encode different lipid specificity. PI4P, phosphatidylinositol 4-phosphate; PS, phosphatidylserine; PA, phosphatidic acid; LCFA, long chain fatty acid; PBR, polybasic region; HVR, hyper-variable region. Lysine (K) is highlighted in orange, arginine (R) in red, cystein (C) in green and leucine (L) in purple. Stars indicate cysteines targeted by lipid anchor modifying protein.

In addition, Zhou et al., 2017, showed that enrichment of the PBR in arginine (R) increase PS affinity in vivo. My preliminary results suggest that ROP6-7R (in which I mutated all the lysine residues into arginine in ROP6-PBR) is more active than ROP6 wild type (as quantified by pavement cell circularity and endocytosis inhibition (data not shown)). We now need to perform gravitropism experiments with ROP6-7R (should respond faster to gravity) and we should also analyze its organization into nanoclusters by sptPALM (should be more prone to localize to PS-enriched nanocluster than WT ROP6). In addition, to demonstrate that different ROPs have different lipid specificity in vivo, we could perform exogenous treatment with lipids such as PS, PI(4)P, PA and PI(4,5)P_2, and test the effect of these treatments on ROP nanoclustering. Finally, all-atom molecular dynamic (MD) simulations could be performed on different ROP-PBR to test whether they could have different anionic lipid preferences in silico.

To conclude, ROP nanoclustering may have several critical functions for signaling, including signal transmission via an analogue-digital-analog conversion relay but also signal compartmentalization between different ROPs (which have otherwise very similar sequences and bind similar effectors in vitro, but not in vivo). ROP nanocluster formation could therefore be a tool to generate both high fidelity and exquisite specificity during signal transduction. Using a combination of high resolution in planta imaging developed during my PhD, with modeling and simulation approaches, it will be possible in the future to test these different concepts and interrogate their importance in plant development and physiology.

Andersen, J.P., Vestergaard, A.L., Mikkelsen, S.A., Mogensen, L.S., Chalat, M., and Molday, R.S. (2016). P4-ATPases as Phospholipid Flippases—Structure, Function, and Enigmas. Front. Physiol. *7*.

Arisz, S.A., van Wijk, R., Roels, W., Zhu, J.-K., Haring, M.A., and Munnik, T. (2013). Rapid phosphatidic acid accumulation in response to low temperature stress in Arabidopsis is generated through diacylglycerol kinase. Front. Plant Sci. *4*.

Azouaoui, H., Montigny, C., Dieudonné, T., Champeil, P., Jacquot, A., Vázquez-Ibar, J.L., Le Maréchal, P., Ulstrup, J., Ash, M.-R., Lyons, J.A., et al. (2017). A High and Phosphatidylinositol-4-phosphate (PI4P)-dependent ATPase Activity for the Drs2p/Cdc50p Flippase after Removal of its N- and C-terminal Extensions. J. Biol. Chem. jbc.M116.751487.

Baldridge, R.D., and Graham, T.R. (2012). Identification of residues defining phospholipid flippase substrate specificity of type IV P-type ATPases. Proc. Natl. Acad. Sci. *109*, E290–E298.

Baldridge, R.D., and Graham, T.R. (2013). Two-gate mechanism for phospholipid selection and transport by type IV P-type ATPases. Proc. Natl. Acad. Sci. *110*, E358–E367.

Bohdanowicz, M., Schlam, D., Hermansson, M., Rizzuti, D., Fairn, G.D., Ueyama, T., Somerharju, P., Du, G., and Grinstein, S. (2013). Phosphatidic acid is required for the constitutive ruffling and macropinocytosis of phagocytes. Mol. Biol. Cell *24*, 1700–1712.

Botella, C., Sautron, E., Boudiere, L., Michaud, M., Dubots, E., Yamaryo-Botté, Y., Albrieux, C., Marechal, E., Block, M.A., and Jouhet, J. (2016). ALA10, a Phospholipid Flippase, Controls FAD2/FAD3 Desaturation of Phosphatidylcholine in the ER and Affects Chloroplast Lipid Composition in Arabidopsis thaliana. Plant Physiol. *170*, 1300–1314.

Bücherl, C.A., Jarsch, I.K., Schudoma, C., Segonzac, C., Mbengue, M., Robatzek, S., MacLean, D., Ott, T., and Zipfel, C. (2017). Plant immune and growth receptors share common signalling components but localise to distinct plasma membrane nanodomains. eLife *6*, e25114.

Chung, J., Torta, F., Masai, K., Lucast, L., Czapla, H., Tanner, L.B., Narayanaswamy, P., Wenk, M.R., Nakatsu, F., and Camilli, P.D. (2015). PI4P/phosphatidylserine countertransport at ORP5- and ORP8-mediated ER–plasma membrane contacts. Science *349*, 428–432.

Coleman, J.A., Vestergaard, A.L., Molday, R.S., Vilsen, B., and Andersen, J.P. (2012). Critical role of a transmembrane lysine in aminophospholipid transport by mammalian photoreceptor P4-ATPase ATP8A2. Proc. Natl. Acad. Sci. *109*, 1449–1454.

Costa, S.R., Marek, M., Axelsen, K.B., Theorin, L., Pomorski, T.G., and López-Marqués, R.L. (2016). Role of post-translational modifications at the β-subunit ectodomain in complex association with a promiscuous plant P4-ATPase. Biochem. J. *473*, 1605–1615.

Filseck, J.M. von, Čopič, A., Delfosse, V., Vanni, S., Jackson, C.L., Bourguet, W., and Drin, G. (2015). Phosphatidylserine transport by ORP/Osh proteins is driven by phosphatidylinositol 4-phosphate. Science *349*, 432–436.

Gomès, E., Jakobsen, M.K., Axelsen, K.B., Geisler, M., and Palmgren, M.G. (2000). Chilling tolerance in Arabidopsis involves ALA1, a member of a new family of putative aminophospholipid translocases. Plant Cell *12*, 2441–2453.

Gómez-Merino, F.C., Brearley, C.A., Ornatowska, M., Abdel-Haliem, M.E.F., Zanor, M.-I., and Mueller-Roeber, B. (2004). AtDGK2, a Novel Diacylglycerol Kinase from Arabidopsis thaliana, Phosphorylates 1-Stearoyl-2-arachidonoyl-sn-glycerol and 1,2-Dioleoyl-sn-glycerol and Exhibits Cold-inducible Gene Expression. J. Biol. Chem. *279*, 8230–8241.

Gómez-Merino, F.C., Arana-Ceballos, F.A., Trejo-Téllez, L.I., Skirycz, A., Brearley, C.A., Dörmann, P., and Mueller-Roeber, B. (2005). Arabidopsis AtDGK7, the Smallest Member of Plant Diacylglycerol Kinases (DGKs), Displays Unique Biochemical Features and Saturates at Low Substrate Concentration THE DGK INHIBITOR R59022 DIFFERENTIALLY AFFECTS AtDGK2 AND AtDGK7 ACTIVITY IN VITRO AND ALTERS PLANT GROWTH AND DEVELOPMENT. J. Biol. Chem. *280*, 34888–34899.

Gronnier, J., Crowet, J.-M., Habenstein, B., Nasir, M.N., Bayle, V., Hosy, E., Platre, M.P., Gouguet, P., Raffaele, S., Martinez, D., et al. (2017). Structural basis for plant plasma membrane protein dynamics and organization into functional nanodomains. eLife *6*, e26404.

Hammond, G.R.V., Machner, M.P., and Balla, T. (2014). A novel probe for phosphatidylinositol 4-phosphate reveals multiple pools beyond the Golgi. J. Cell Biol. *205*, 113–126.

Himschoot, E., Beeckman, T., Friml, J., and Vanneste, S. (2015). Calcium is an organizer of cell polarity in plants. Biochim. Biophys. Acta BBA - Mol. Cell Res. *1853*, 2168–2172.

Hong, Y., Zhang, W., and Wang, X. (2010). Phospholipase D and phosphatidic acid signalling in plant response to drought and salinity. Plant Cell Environ. *33*, 627–635.

Inoue, H., Baba, T., Sato, S., Ohtsuki, R., Takemori, A., Watanabe, T., Tagaya, M., and Tani, K. (2012). Roles of SAM and DDHD domains in mammalian intracellular phospholipase A1 KIAA0725p. Biochim. Biophys. Acta BBA - Mol. Cell Res. *1823*, 930–939.

Janosi, L., Li, Z., Hancock, J.F., and Gorfe, A.A. (2012). Organization, dynamics, and segregation of Ras nanoclusters in membrane domains. Proc. Natl. Acad. Sci. *109*, 8097–8102.

Kang, B.-H., Nielsen, E., Preuss, M.L., Mastronarde, D., and Staehelin, L.A. (2011). Electron Tomography of RabA4b- and PI-4Kβ1-Labeled Trans Golgi Network Compartments in Arabidopsis. Traffic *12*, 313–329.

Kato, T., Morita, M.T., Fukaki, H., Yamauchi, Y., Uehara, M., Niihama, M., and Tasaka, M. (2002). SGR2, a Phospholipase-Like Protein, and ZIG/SGR4, a SNARE, Are Involved in the Shoot Gravitropism of Arabidopsis. Plant Cell *14*, 33–46.

Kim, Y.J., Guzman-Hernandez, M.-L., Wisniewski, E., and Balla, T. (2015). Phosphatidylinositol-Phosphatidic Acid Exchange by Nir2 at ER-PM Contact Sites Maintains Phosphoinositide Signaling Competence. Dev. Cell *33*, 549–561.

Leventis, P.A., and Grinstein, S. (2010). The Distribution and Function of Phosphatidylserine in Cellular Membranes. Annu. Rev. Biophys. *39*, 407–427.

Li, M., Hong, Y., and Wang, X. (2009). Phospholipase D- and phosphatidic acid-mediated signaling in plants. Biochim. Biophys. Acta BBA - Mol. Cell Biol. Lipids *1791*, 927–935.

López-Marqués, R.L., Poulsen, L.R., Hanisch, S., Meffert, K., Buch-Pedersen, M.J., Jakobsen, M.K., Pomorski, T.G., and Palmgren, M.G. (2010). Intracellular Targeting Signals and Lipid Specificity Determinants of the ALA/ALIS P4-ATPase Complex Reside in the Catalytic ALA α-Subunit. Mol. Biol. Cell *21*, 791–801.

López-Marqués, R.L., Poulsen, L.R., and Palmgren, M.G. (2012). A Putative Plant Aminophospholipid Flippase, the Arabidopsis P4 ATPase ALA1, Localizes to the Plasma Membrane following Association with a β-Subunit. PLoS ONE *7*, e33042.

Lynch, D.V., and Steponkus, P.L. (1987). Plasma Membrane Lipid Alterations Associated with Cold Acclimation of Winter Rye Seedlings (Secale cereale L. cv Puma). Plant Physiol. *83*, 761–767.

Martinière, A., Lavagi, I., Nageswaran, G., Rolfe, D.J., Maneta-Peyret, L., Luu, D.-T., Botchway, S.W., Webb, S.E.D., Mongrand, S., Maurel, C., et al. (2012). Cell wall constrains lateral diffusion of plant plasma-membrane proteins. Proc. Natl. Acad. Sci. *109*, 12805–12810.

Martiniere, A., Bassil, E., Jublanc, E., Alcon, C., Reguera, M., Sentenac, H., Blumwald, E., and Paris, N. (2013). In Vivo Intracellular pH Measurements in Tobacco and Arabidopsis Reveal an Unexpected pH Gradient in the Endomembrane System. Plant Cell *25*, 4028–4043.

Matteis, A.D., Venditti, R., Masone, M.C., Rega, L., Polishchuk, E., Santoro, M., Tullio, G.D., and Montagna, R.L. (2017). Regulation and role of ER-Golgi contact sites. FASEB J. *31*, 104.2-104.2.

McDowell, S.C., López-Marqués, R.L., Poulsen, L.R., Palmgren, M.G., and Harper, J.F. (2013). Loss of the Arabidopsis thaliana P4-ATPase ALA3 Reduces Adaptability to Temperature Stresses and Impairs Vegetative, Pollen, and Ovule Development. PLOS ONE *8*, e62577.

McDowell, S.C., LÃ³pez-MarquÃ©s, R.L., Cohen, T., Brown, E., Rosenberg, A., Palmgren, M.G., and Harper, J.F. (2015). Loss of the Arabidopsis thaliana P4-ATPases ALA6 and ALA7 impairs pollen fitness and alters the pollen tube plasma membrane. Front. Plant Sci. *6*.

Mishkind, M., Vermeer, J.E.M., Darwish, E., and Munnik, T. (2009). Heat stress activates phospholipase D and triggers PIP $_2$ accumulation at the plasma membrane and nucleus. Plant J. *60*, 10–21.

Okazaki, K., Miyagishima, S., and Wada, H. (2015). Phosphatidylinositol 4-Phosphate Negatively Regulates Chloroplast Division in Arabidopsis. Plant Cell Online *27*, 663–674.

Poulsen, L.R., López-Marqués, R.L., Pedas, P.R., McDowell, S.C., Brown, E., Kunze, R., Harper, J.F., Pomorski, T.G., and Palmgren, M. (2015). A phospholipid uptake system in the model plant *Arabidopsis thaliana*. Nat. Commun. *6*, ncomms8649.

Preuss, M.L., Schmitz, A.J., Thole, J.M., Bonner, H.K.S., Otegui, M.S., and Nielsen, E. (2006). A role for the RabA4b effector protein PI-4Kβ1 in polarized expansion of root hair cells in Arabidopsis thaliana. J Cell Biol *172*, 991–998.

Qin, C., and Wang, X. (2002). The Arabidopsis Phospholipase D Family. Characterization of a Calcium-Independent and Phosphatidylcholine-Selective PLDζ1 with Distinct Regulatory Domains. Plant Physiol. *128*, 1057–1068.

Raghupathy, R., Anilkumar, A.A., Polley, A., Singh, P.P., Yadav, M., Johnson, C., Suryawanshi, S., Saikam, V., Sawant, S.D., Panda, A., et al. (2015). Transbilayer Lipid Interactions Mediate Nanoclustering of Lipid-Anchored Proteins. Cell *161*, 581–594.

Ruelland, E. (2002). Activation of Phospholipases C and D Is an Early Response to a Cold Exposure in Arabidopsis Suspension Cells. PLANT Physiol. *130*, 999–1007.

Sebastian, T.T., Baldridge, R.D., Xu, P., and Graham, T.R. (2012). Phospholipid flippases: Building asymmetric membranes and transport vesicles. Biochim. Biophys. Acta BBA - Mol. Cell Biol. Lipids *1821*, 1068–1077.

Simon, M.L.A., Platre, M.P., Assil, S., van Wijk, R., Chen, W.Y., Chory, J., Dreux, M., Munnik, T., and Jaillais, Y. (2014). A multi-colour/multi-affinity marker set to visualize phosphoinositide dynamics in Arabidopsis. Plant J. Cell Mol. Biol. *77*, 322–337.

Skirpan, A.L., Dowd, P.E., Sijacic, P., Jaworski, C.J., Gilroy, S., and Kao, T. (2006). Identification and characterization of PiORP1, a Petunia oxysterol-binding-protein related protein involved in receptor-kinase mediated signaling in pollen, and analysis of the ORP gene family in Arabidopsis. Plant Mol. Biol. *61*, 553–565.

Sohn, M., Ivanova, P., Brown, H.A., Toth, D.J., Varnai, P., Kim, Y.J., and Balla, T. (2016). Lenz-Majewski mutations in PTDSS1 affect phosphatidylinositol 4-phosphate metabolism at ER-PM and ER-Golgi junctions. Proc. Natl. Acad. Sci. *113*, 4314–4319.

Sorek, N., Segev, O., Gutman, O., Bar, E., Richter, S., Poraty, L., Hirsch, J.A., Henis, Y.I., Lewinsohn, E., Jürgens, G., et al. (2010). An S-Acylation Switch of Conserved G Domain Cysteines Is Required for Polarity Signaling by ROP GTPases. Curr. Biol. *20*, 914–920.

Stanislas, T., Hüser, A., Barbosa, I.C.R., Kiefer, C.S., Brackmann, K., Pietra, S., Gustavsson, A., Zourelidou, M., Schwechheimer, C., and Grebe, M. (2015). *Arabidopsis* D6PK is a lipid domain-dependent mediator of root epidermal planar polarity. Nat. Plants *1*, nplants2015162.

Testerink, C., and Munnik, T. (2005). Phosphatidic acid: a multifunctional stress signaling lipid in plants. Trends Plant Sci. *10*, 368–375.

Testerink, C., and Munnik, T. (2011). Molecular, cellular, and physiological responses to phosphatidic acid formation in plants. J. Exp. Bot. *62*, 2349–2361.

Thole, J.M., Vermeer, J.E.M., Zhang, Y., Gadella, T.W.J., and Nielsen, E. (2008). ROOT HAIR DEFECTIVE4 Encodes a Phosphatidylinositol-4-Phosphate Phosphatase Required for Proper Root Hair Development in Arabidopsis thaliana. Plant Cell Online *20*, 381–395.

Tian, T., Harding, A., Inder, K., Plowman, S., Parton, R.G., and Hancock, J.F. (2007). Plasma membrane nanoswitches generate high-fidelity Ras signal transduction. Nat. Cell Biol. *9*, 905–914.

Waadt, R., Krebs, M., Kudla, J., and Schumacher, K. (2017). Multiparameter imaging of calcium and abscisic acid and high-resolution quantitative calcium measurements using R-GECO1-mTurquoise in Arabidopsis. New Phytol. *216*, 303–320.

Wan, Z.-Y., Chai, S., Ge, F.-R., Feng, Q.-N., Zhang, Y., and Li, S. (2017). Arabidopsis PROTEIN S-ACYL TRANSFERASE4 mediates root hair growth. Plant J. *90*, 249–260.

Wattelet-Boyer, V., Brocard, L., Jonsson, K., Esnay, N., Joubès, J., Domergue, F., Mongrand, S., Raikhel, N., Bhalerao, R.P., Moreau, P., et al. (2016). Enrichment of hydroxylated C24- and C26-acyl-chain sphingolipids mediates PIN2 apical sorting at trans-Golgi network subdomains. Nat. Commun. *7*, 12788.

Xu, P., Baldridge, R.D., Chi, R.J., Burd, C.G., and Graham, T.R. (2013). Phosphatidylserine flipping enhances membrane curvature and negative charge required for vesicular transport. J Cell Biol *202*, 875–886.

Yeung, T., Terebiznik, M., Yu, L., Silvius, J., Abidi, W.M., Philips, M., Levine, T., Kapus, A., and Grinstein, S. (2006). Receptor Activation Alters Inner Surface Potential During Phagocytosis. Science *313*, 347–351.

Zhang, Y., and Du, G. (2009). Phosphatidic acid signaling regulation of Ras superfamily of small guanosine triphosphatases. Biochim. Biophys. Acta BBA - Mol. Cell Biol. Lipids *1791*, 850–855.

Zhou, Y., and Hancock, J.F. (2015). Ras nanoclusters: Versatile lipid-based signaling platforms. Biochim. Biophys. Acta BBA - Mol. Cell Res. *1853*, 841–849.

Zhou, Y., Wong, C.-O., Cho, K., Hoeven, D. van der, Liang, H., Thakur, D.P., Luo, J., Babic, M., Zinsmaier, K.E., Zhu, M.X., et al. (2015). Membrane potential modulates plasma membrane phospholipid dynamics and K-Ras signaling. Science *349*, 873–876.

Zhou, Y., Prakash, P., Liang, H., Cho, K.-J., Gorfe, A.A., and Hancock, J.F. (2016). Lipid-Sorting Specificity Encoded in K-Ras Membrane Anchor Regulates Signal Output. Cell.

Dans cette partie « annnexe », j'ai choisi de vous présenter trois articles dont je suis premier auteur parmi lesquels figurent un article de recherche et deux articles de revue.

Je suis également co-auteur sur trois articles de recherche :

Bayle, V., **Platre, M.P**., and Jaillais, Y. (2017). Automatic Quantification of the Number of Intracellular Compartments in Arabidopsis thaliana Root Cells. Bio-Protoc. *7*.

Gronnier, J., Crowet, J.-M., Habenstein, B., Nasir, M.N., Bayle, V., Hosy, E., **Platre, M.P**., Gouguet, P., Raffaele, S., Martinez, D., et al. (2017). Structural basis for plant plasma membrane protein dynamics and organization into functional nanodomains. eLife *6*, e26404.

Marquès-Bueno, M.M., Morao, A.K., Cayrel, A., **Platre, M.P**., Barberon, M., Caillieux, E., Colot, V., Jaillais, Y., Roudier, F., and Vert, G. (2016). A versatile Multisite Gateway-compatible promoter and transgenic line collection for cell type-specific functional genomics in Arabidopsis. Plant J. *85*, 320–333.

ANNEXE I : A multi-colour/multi-affinity marker set to visualize phosphoinositide dynamics in Arabidopsis

Published in final edited form as:
Plant J. 2014 January ; 77(2): 322–337. doi:10.1111/tpj.12358.

A multi-colour/multi-affinity marker set to visualize phosphoinositide dynamics in Arabidopsis

Mathilde Laetitia Audrey Simon[1,♪], **Matthieu Pierre Platre**[1,♪], **Sonia Assil**[2], **Ringo van Wijk**[3], **William Yawei Chen**[4], **Joanne Chory**[4,5], **Marlène Dreux**[2], **Teun Munnik**[3], and **Yvon Jaillais**[1,*]

[1]CNRS, INRA, ENS Lyon, UCBL, Université de Lyon, Laboratoire de Reproduction et Développement des Plantes, 46 Allée d'Italie, 69364 Lyon Cedex 07, France [2]CIRI, International Center for Infectiology Research; Université de Lyon; Inserm, U1111; Ecole Normale Supérieure de Lyon; CNRS, UMR5308; LabEx Ecofect, Lyon, F-69007, France [3]University of Amsterdam, Swammerdam Institute for Life Sciences, Section Plant Physiology, Postbus 94215, 1090 GE Amsterdam, The Netherlands [4]Plant Biology Laboratory, Salk Institute for Biological Studies, La Jolla, CA 92037, USA [5]The Howard Hughes Medical Institute, Salk Institute for Biological Studies, La Jolla, CA 92037, USA

Summary

Phosphatidylinositolphosphates (PIPs) are phospholipids that contain a phosphorylated inositol head group. PIPs represent a minor fraction of the total phospholipids, yet they are involved in many regulatory processes such as cell signalling and intracellular trafficking. Membrane compartments are enriched or depleted in specific PIPs, which constitute a signature for these compartments and contribute to their identity. The precise subcellular localisation and dynamics of most PIP species is not fully understood in plants. Here, we designed genetically encoded biosensors with distinct relative affinities and expressed them stably in *Arabidopsis thaliana*. Analysis of this multi-affinity "PIPline" marker set revealed previously unrecognized localisation for various PIPs in root epidermis. Notably, we found that PI(4,5)P_2 is able to drive PIP_2-interacting protein domains to the plasma membrane in non-stressed root epidermal cells. Our analysis further revealed that there is a gradient of PI4P, with the highest concentration at the plasma membrane, intermediate concentration in post-Golgi/endosomal compartments and lowest concentration in the Golgi. Finally, we also uncovered that there is a similar gradient of PI3P from high in late endosomes to low in the tonoplast. All together our library extends the palette of available PIP biosensors and should promote rapid progress in our understanding of PIP dynamics in plants.

Keywords

sensor; phosphoinositide; lipid binding domain; Arabidopsis thaliana; quantitative co-localisation; membrane trafficking; object-based analysis; lipid signalling; fluorescent protein; endosome

Introduction

Phosphatidylinositolphosphates (PIPs) are minor phospholipids, accounting less than a percent of total membrane lipids, yet they are of disproportionate importance for many membrane-associated signalling events: i) PIPs can be precursors of various second

*For correspondence (Phone +33 4 72 72 86 09; fax +33 4 72 72 86 00; yvon.jaillais@ens-lyon.fr).
♪These authors contributed equally to this work

messengers (e.g. inositol 1,4,5-trisphosphate, diacylglycerol), ii) they can activate many ion channels and enzymes, iii) they can be involved in virtually all membrane trafficking events including endocytosis and exocytosis and, iv) they can recruit proteins to the plasma membrane (PM) or intracellular compartments through several structured interaction domains (e.g. Pleckstrin Homology domain (PH), Phox homology domain (PX), Fab1/YOTB/Vac1/EEA1 domain (FYVE)) (De Matteis and Godi, 2004; McLaughlin and Murray, 2005; Lemmon, 2008; Balla *et al.*, 2009). PIPs can be phosphorylated at different positions of the inositol head group, which can generate up to seven different PIP species that include three phosphatidylinositol monophosphates [PI3P, PI4P and PI5P], three phosphatidylinositol biphosphate [$PI(3,4)P_2$, $PI(3,5)P_2$ and $PI(4,5)P_2$] and one phosphatidylinositol triphosphate [$PI(3,4,5)P_3$]. PIP kinases and phosphatases modify the phosphorylation state of the inositol head group, and phospholipases hydrolyse PIPs to release the soluble head group into the cytosol (Lemmon, 2008). The combined action of these enzymes produces the PIP signature of a cell, where certain membrane compartments are enriched or depleted of specific PIPs, contributing to their membrane identity (De Matteis and Godi, 2004; Lemmon, 2008; Balla *et al.*, 2009; Balla, 2013).

The localisation of the various PIP species has been an intense area of research (De Matteis and Godi, 2004; Hammond *et al.*, 2009a; Balla, 2013). Functional studies, together with biochemical and live-cell imaging, have built a relatively clear picture of the precise location of each PIP in cultured mammalian cell lines and in yeast. In animal cells, PI3P mainly resides in early endosomes, where it controls endosome maturation, cargo protein degradation/recycling and cell signalling notably through its interplay with Rab5 GTPases (Simonsen *et al.*, 1998; Christoforidis *et al.*, 1999; Jean and Kiger, 2012). PI4P is located in two different pools in the cell, one at the Golgi apparatus and the other one at the PM (Várnai and Balla, 2006; Hammond *et al.*, 2009a). Each pool of PI4P has separate and diverse functions. The main function of PI4P at the Golgi is to control membrane trafficking events, in particular, the sorting of proteins toward the PM or endosomes (Szentpetery *et al.*, 2010; Daboussi *et al.*, 2012; Jean and Kiger, 2012). PI4P, together with other PIPs, recruits strong cationic proteins to the PM (Hammond *et al.*, 2012). In yeast, the PM pool of PI4P also controls Endoplasmic Reticulum (ER)-to-PM tethering sites that regulate cell signalling and ER morphology (Stefan *et al.*, 2011; Manford *et al.*, 2012). Also, PM-localised PI4P is a source of $PI(4,5)P_2$ (Szentpetery *et al.*, 2010; Ling *et al.*, 2012). PI5P accumulates in the nucleus and at the PM under certain stimuli (Gozani *et al.*, 2003). $PI(3,5)P_2$ is thought to reside in late endosomes, where it regulates lysome/vacuole biogenesis in yeast (Friant *et al.*, 2003; Eugster *et al.*, 2004). $PI(4,5)P_2$ is localised at the PM where it has a large spectra of action such as anchoring signalling and membrane trafficking proteins (De Matteis and Godi, 2004; McLaughlin and Murray, 2005; Zoncu *et al.*, 2007; Hammond *et al.*, 2012; Balla *et al.*, 2009; Balla, 2013). $PI(4,5)P_2$ also controls ion channel activation and is a substrate of Phospholipase C, which triggers synthesis of the second messengers IP_3 and DAG (McLaughlin and Murray, 2005; Suh *et al.*, 2006). $PI(4,5)P_2$ is the source of $PI(3,4,5)P_3$, which together with $PI(3,4)P_2$, accumulate at the PM but only when specific signalling pathways are activated (e.g. growth factor signalling) (McLaughlin and Murray, 2005; Balla, 2013). $PI(3,4)P_2$ also controls late-stage clathrin-coated pit formation, independent of $PI(3,4,5)P_3$ (Posor *et al.*, 2013).

Much less is known about the function and localisation of PIPs in plants (Munnik and Vermeer, 2010; Munnik and Nielsen, 2011). The function of PIPs have been clearly established during polarized cell growth (e.g. tip growth of root hairs and pollen tubes), during membrane trafficking and response to stresses (Thole and Nielsen, 2008; Ischebeck *et al.*, 2010; Munnik and Nielsen, 2011). Most of the enzymes involved in PIP metabolism are encoded in plant genomes, with the notable exception of type I- and type II- PI3-kinases (PI3Ks) (Munnik and Nielsen, 2011). These PI3Ks are able to phosphorylate PI4P and

$PI(4,5)P_2$ to produce $PI(3,4)P_2$ and $PI(3,4,5)P_3$ and their absence suggest that these two PIPs are not produced in plants. Congruent with these observations, they have never been found in plant extracts (Meijer and Munnik, 2003; Munnik and Nielsen, 2011). The localisations of PI3P, PI4P and $PI(4,5)P_2$ have been studied using genetically encoded biosensors in various plant cell types including transgenic Arabidopsis (Vincent *et al.*, 2005; Vermeer *et al.*, 2006; van Leeuwen *et al.*, 2007; Ischebeck *et al.*, 2008; Thole *et al.*, 2008; Mishkind *et al.*, 2009; Vermeer *et al.*, 2009; Ischebeck *et al.*, 2011; Munnik and Nielsen, 2011). However, when data are available, only one marker per PIP species has been analysed. Here, we built a collection of transgenic Arabidopsis lines expressing various biosensors for each PIP species. This “PIPline” marker set allowed us to quantitatively analyse the localisation of various PIPs with respect to known compartment markers. Our collection provides a new toolbox to study PIP localisation and dynamics in the model plant Arabidopsis. We focused our analysis on the root epidermis but the PIPline collection should provide a new resource for the community to study PIPs in various cell types, developmental contexts or stress conditions.

Results

Generation of a set of transgenic marker lines that highlight PIPs associated with membrane compartments in Arabidopsis

Genetically encoded biosensors have been extensively used to indirectly reveal the localisation and dynamics of PIPs in intact living cells (Várnai and Balla, 2006; Balla, 2013). These markers consist of lipid-binding domains (LBD) that interact specifically with known PIP species in vitro. These domains localise in the compartments of the cell that accumulate the targeted PIPs and can be easily traced when fused with a fluorescent protein. We built a collection of biosensors that include, when available, several independent domains for each of the seven PIPs. By using LBDs from different proteins and from different species, we hope to limit the effects of endogenous cellular proteins on the localisation of the marker. Furthermore, each domain is likely to have a different PIP binding affinity in vivo. For our set of marker lines, we chose only LBDs with extensive evidences of specific interactions with a given lipid in vitro (Table S1). Another potential pitfall of LBD over-expression is that it might titrate the targeted lipid and subsequently compromise the localisation and function of endogenous PIP effectors (Várnai and Balla, 2006; Balla *et al.*, 2009). In order to limit potential over-expression problem, we drove the expression of our markers under the control of the promoter of the *UBIQUITIN10* (*UBQ10prom*) gene (Figure 1). Compared to the strong *35S* promoter, *UBQ10prom* provides a mild uniform expression pattern and this endogenous intron-bearing promoter limits the problems of silencing and mosaic expression often observed with the viral *35S* promoter (Geldner *et al.*, 2009). In order to obtain high contrast fluorescence with biosensors expressed at relatively low level, we counterbalanced the use of the mild *UBQ10* promoter, by fusing the LBDs with CITRINE, a brighter and monomeric version of the Yellow Fluorescent Protein (YFP) (Heikal *et al.*, 2000; Jaillais *et al.*, 2011) (Figure 1).

Next, we transformed Arabidopsis (Columbia accession) with each of the created biosensor constructs (see Table S1 for a list of all the 17 LBDs used in this study). None of the selected transgenic lines harboured any visible developmental phenotypes, suggesting that the mild ubiquitous expression of each LBD is not deleterious for the plants and likely does not extensively compete with endogenous proteins. Figure S1 shows the localisation of each marker that was sufficiently stable for observation by confocal microscopy (13 LBDs out of 17). For all our subsequent analyses, we decided to keep only the LBDs that interacted with membranes, either the PM, intracellular compartments, or both (Figure S1), as a soluble localisation is a default localisation in the absence of any targeting.

With the exception of the PH domain of OSBP, each of these LBDs have been extensively studied for their PIP binding properties in vitro by at least 4 distinct techniques (Table 1). The PH domain of OSBP is the domain that has been less characterized in vitro, with only liposome-binding assay and Surface Plasmon Reasonance (SPR) experiments (Levine and Munro, 2002). Therefore, we verified independently the specificity of this PI4P probe by a protein-lipid overlay experiment. For this purpose, we developed an assay to directly test the PIP binding properties of our fluorescently tagged PH^{OSBP} produced in transgenic Arabidopsis. In this assay, we found that CITRINE-PH^{OSBP} is binding preferentially to PI4P as well as PI(3,4)P_2 (Figure S2). As discussed above, PI(3,4)P_2 has never been found in plants, which is very likely due to the lack of type I and type II PI3Ks (Meijer and Munnik, 2003; Munnik and Nielsen, 2011). Therefore, PH^{OSBP} should be a bona fide PI4P reporter in plants. Similarly, the C-terminal domain of the TUBBY protein (TUBBY-C) has been shown to bind to PI(4,5)P_2, PI(3,4)P_2 and PI(3,4,5)P_3 in vitro (Santagata *et al.*, 2001). Because PI(3,4)P_2 and PI(3,4,5)P_3 are not synthesized in plants, TUBBY-C, like PH^{PLC}, is a reporter for PI(4,5)P_2 in planta.

Although we systematically designed our LBD constructs based on previously published data, our sensors might differ by few amino acids at their N- and C-termini. Therefore, we decided to validate our fluorescently-labelled LBDs by expressing them in yeast and human cell lines, two systems in which the localisation of these domains have already been studied and/or the localisation of each PIP is extensively validated (Table 1). These experiments showed that our LBDs behave as previously described constructs both in *Saccharomyces cerevisiae* (Figure 2a) and the human hepatocarcinoma cell line, Huh-7 (Figure 2b). PI3P probes (1x$FYVE^{HRS}$ and 1x$p40^{PX}$) were localised to endosomes and vacuole in yeast (Burd and Emr, 1998) and to early endosomes in Huh-7 cells; except for 1x$FYVE^{HRS}$ which was mostly diffuse in the cytoplasm in human cells in agreement with previous report (Gillooly *et al.*, 2000). PI4P markers (1xPH^{FAPP1} and 1xPH^{OSBP}) were localised in the Golgi apparatus in both systems (Levine and Munro, 2002; A., Balla *et al.*, 2005) and PI(4,5)P_2 sensors (1xPH^{PLC} and 1xTUBBY-C) were localised at the PM in both system (Szentpetery *et al.*, 2009); except 1xPH^{PLC} which accumulated mostly in the cytoplasm in yeast (Levine and Munro, 2002; Yu *et al.*, 2004)(Figure 2).

In *A. thaliana* root, LBDs that bind to the same lipid did not always exhibit exactly overlapping localisation domains. For example, the PI3P sensor 1x$FYVE^{HRS}$ was mainly cytosolic and weakly associated with intracellular compartments (Figure 3a), while 1xPX^{p40} was localised in intracellular compartments as well as weakly in the tonoplast (Figure 3b). Furthermore, the PI4P biosensor 1xPH^{FAPP1} was localised at the PM and intracellular compartments (Figure 3c), while 1xPH^{OSBP} was more restricted to the PM (Figure 3d). Finally, both PI(4,5)P_2 sensors (1xPH^{PLC} and 1xTUBBY-C) were localised at the PM, although 1xPH^{PLC} was also localised in the cytosol and 1xTUBBY-C in the nucleus (Figure 3e and f). These slight differences in localisation of LBDs that bind the same lipid might be due to various parameters such as differences in binding affinities (Table 1), expression level, protein stability, local pH, local electrostatic potential of the membrane, the protein affinity for a given membrane curvature or the need to bind to other cellular co-factors. Overall, these results highlight the need to use multiple independent biosensors for each PIP in order to have a more complete and dynamic view of PIP cellular localisation.

Engineering of biosensors with different affinities for their cognate lipids

Most cellular proteins are not localised only by one membrane interacting domain (Lemmon, 2008). It is often the combination of several LBDs or the joint action of a LBD with a lipid anchor or transmembrane segment that drive the protein to its final location (Lemmon, 2008). It is well established that this bipartite lipid recognition is key in

generating membrane specificity and/or extended residence time at the target membrane (Schultz, 2010). Therefore, in order to create high avidity biosensors (avidity being the combined strength of multiple bond interactions), we fused in tandem dimers the LBDs previously identified as interacting with membranes (Figure 1 and 4a). This strategy has previously been used to increase the binding avidity of several lipid biosensors (Gillooly *et al.*, 2000; Roy and Levine, 2004; Godi *et al.*, 2004). Increasing the relative avidity of a lipid sensor might have two effects on its localisation: i) it increases the proportion of membrane-bound sensor and ii) it preferentially targets the high avidity sensors toward membranes that are the most enriched with their lipid partners, because it increases its residence time at that particular membrane (Lemmon, 2008; Schultz, 2010). Low avidity sensors are less efficient in discriminating between two membranes with two different concentrations of their targeted PIP and they might highlight several pools of this PIP within the cell. By contrast, high avidity sensors will have increased residence time at the membrane that is the most enriched in the targeted PIP and they might therefore reveal variation in PIP concentration within the cell. In other word, high avidity sensors work like Velcro: they will grab more strongly to a surface with more spikes (in this case the spikes being PIPs) (Figure 4a).

Using SPR experiments, Gillooly et al. reported that 1xFYVE showed dissociation kinetics characteristic of a 1:1 binding, while 2xFYVE showed complex association / dissociation kinetics that could be fit into a bivalent model (Gillooly *et al.*, 2000). Therefore, the ability of one 2xFYVE molecule to interact with two molecules of PI3P likely explain its superior PI3P binding compared with 1xFYVE. This observation was further verified in vivo in human cells as the 2xFYVE probe strongly localises to early endosomes while 1xFYVE localisation is mostly diffuse in the cytosol (Gillooly *et al.*, 2000). In Arabidopsis root, the low avidity sensor (1xFYVE) was largely cytosolic and only weakly associated with intracellular compartments (Figure 4b and c). By contrast, the high avidity sensor (2xFYVE) was more strongly associated with intracellular compartments (Figure 4b and c) and from time to time also localised to the tonoplast. This result was confirmed independently by the localisation of the PX^{p40} PI3P sensor that also localised in intracellular compartments (Figure 3b).

The comparison of 1x and $2xPH^{FAPP1}$ previously suggested that $2xPH^{FAPP1}$ has a stronger PI4P binding in vitro that $1xPH^{FAPP1}$ (Godi *et al.*, 2004). In Arabidopsis roots, we found that the high avidity PI4P sensor $2xPH^{FAPP1}$ was more strongly localised to the PM and less to endomembrane compartments than the low avidity sensor $1xPH^{FAPP1}$ (Figure 4d and e). As explained above and illustrated in Figure 4a, these results suggest that the concentration of PI4P is greater at the PM than in intracellular compartments. Together with the observation that $1xPH^{OSBP}$ localises almost exclusively to the PM (Figure 3d), our results establish that PI4P accumulates primarily at the PM and, to a lesser extent, to one or various intracellular compartments.

Next, we investigated the properties and localisation of the $PI(4,5)P_2$ probes 1x and $2xPH^{PLC}$. In both yeast and human cell lines, the $2xPH^{PLC}$ fusion protein is extensively targeted to the PM, while $1xPH^{PLC}$ is more cytosolic (Levine and Munro, 2002; Hammond *et al.*, 2009b). We could not find in the literature any in vitro characterisation that compared 1x and $2xPH^{PLC}$ binding to $PI(4,5)P_2$. Therefore, in order to validate our constructs, we first verified whether they behaved as expected when expressed in yeast (Table 1). In agreement with previous report (Levine and Munro, 2002), we found that $1xPH^{PLC}$ is mainly cytosolic, while $2xPH^{PLC}$ is specifically targeted to the PM when expressed in *S. cerevisiae* (Figure 5a). Next, we validated that both probes are exquisitely specific for $PI(4,5)P_2$ in protein-lipid overlay assay, as they do not interact with any other lipids (Figure 5b). Using a similar assay, we verified that the TUBBY-C domain interacted in vitro with $PI(4,5)P_2$, $PI(3,4)P_2$ and $PI(3,4,5)P_3$ as previously reported (Santagata *et al.*, 2001) (Figure 5b).

Furthermore, we found that when using protein extract containing comparable quantity of sensors, CITRINE-2xPH^{PLC} binds more tightly to PI(4,5)P_2 than CITRINE-1xPH^{PLC} in protein-lipid overlay assay (Figure 5c and d). Next, we compared the subcellular localisation of the low (1xPH^{PLC}) and high (2xPH^{PLC}) avidity PI(4,5)P_2 sensors in Arabidopsis roots. Although 1xPH^{PLC} was mainly cytoplasmic, it also showed a clear PM localisation in non-dividing/non-stressed root epidermal cells (Figure 5e and f). In contrast, the 2xPH^{PLC} reporter was almost exclusively localised to the PM (Figure 5e and f). This observation was independently confirmed by the extensive PM localisation of the 1xTUBBY-C domain (Figure 3f). These results were surprising because in absence of stresses, PI(4,5)P_2 levels are known to be very low in plants (Munnik and Nielsen, 2011). This suggested either that i) PI(4,5)P_2 is able to drive proteins to the PM in non-stressed epidermal cells or ii) that expression of our biosensors up-regulated PI(4,5)P_2 metabolism to maintain the amount of free PI(4,5)P_2. Such feedback mechanism has been previously observed in tobacco BY-2 cells stably expressing YFP-2xFYVE (Vermeer *et al.*, 2006) and might explain why we did not observed any phenotypes in our transgenic lines. In order to discriminate between these two possibilities, we measured the quantities of the various phospholipid species in transgenic lines expressing CITRINE-1xPH^{PLC}, CITRINE-2xPH^{PLC}, CITRINE-TUBBY-C and a myristoylated CITRINE (myrCIT) as a non-PIP binding control (Jaillais *et al.*, 2011). As shown in Figure 5g and 5h, no significant differences between the four genotypes in term of lipid species quantity was found, nor in their response to salt or heat stress, which both trigger a rapid PIP_2 response (Figure 5g and h) (van Leeuwen *et al.*, 2007; Mishkind *et al.*, 2009). Altogether, our results suggest that the local concentration of PI(4,5)P_2 at the PM is sufficient to drive PIP_2-interacting proteins to this compartment in non-stressed root epidermal cells.

A multi-colour marker set for rapid co-localisation with other PIP biosensors and known membrane compartment markers

Next, all the LBDs that were associated with membranes (including both 1x and 2x versions, 9 LBDs in total, highlighted in red in Table S1) were further engineered as fusion proteins with additional fluorescent proteins, allowing their rapid combinatorial analysis in Arabidopsis. Cyan Wave lines used the CERULEAN fluorescent protein and had extremely weak fluorescence (Geldner *et al.*, 2009). We therefore decided to use a brighter cyan fluorescent protein, CyPet (Nguyen and Daugherty, 2005), fused in tandem dimer in order to further increase its brightness. Unfortunately, this strategy resulted in finding only four marker lines that exhibited sufficient level of fluorescence for confocal microscopy detection, although they were still very weak (Figure S3). In parallel, we fused the nine LBDs with a tandem dimer of the monomeric red fluorescent protein CHERRY (2xCHERRY) (Shaner *et al.*, 2004). Each CHERRY marker exhibited good fluorescence and had a similar cellular localisation to those of CITRINE lines (Figure S3). In reference to the name of the Wave line collection (Geldner *et al.*, 2009), we named our PIP biosensor set, the “PIPlines” (PnY for the CITRINE lines, PnR for the CHERRY lines and PnC for the CyPET lines, Figure 1 and Table S4). All DNA constructs and transgenic lines will be deposited in the stock centre for fast distribution of the PIPline collection.

As a proof of concept that our PIPlines are suitable for co-localisation analyses, we crossed yellow and red biosensors for PI3P (2xFYVE^{HRS}), PI4P (1xPH^{FAPP1}) and PI(4,5)P_2 (2xPH^{PLC}) (Figure 6). These crosses provide an additional resource to visualize the localisation of two different PIP species simultaneously in planta. As expected, we found extensive co-localisation when the same PIP was highlighted with both yellow and red biosensors (Figure 6a). Since the sequence and structure of CITRINE and CHERRY are distinct, these results rule out the potential non-specific targeting of the sensors by the fluorescent proteins. Moreover, we detected co-localisation at the PM between PI4P and

$PI(4,5)P_2$ biosensors (Figure 6b and c) and no co-localisation between PI3P and $PI(4,5)P_2$ biosensors, that localise in intracellular compartments and the PM respectively (Figure 4d). We also detected very limited co-localisation between PI3P and PI4P biosensors both of which are found in intracellular compartments (Figure 6e and f). These results suggest, similarly to tobacco BY2 cells (Vermeer *et al.*, 2009), that these PIP species largely accumulate in different compartments in Arabidopsis epidermal cells. These results are in accordance with the notion that the PIP composition of a given compartment represents a unique signature marking the identity for this organelle (De Matteis and Godi, 2004; Munro, 2004; Lemmon, 2008) and raise the question of the identity of these compartments in the Arabidopsis root epidermis.

PI3P localises to late endosomes/PVC in Arabidopsis root epidermis

In animal cells, PI3P mainly resides in early endosomes (Table 1, Figure 2b) (De Matteis and Godi, 2004; Lemmon, 2008). The subcellular localisation of PI3P has been previously analysed in tobacco BY2 cells using a 2xFYVE reporter (Vermeer *et al.*, 2006). In this system, PI3P was found to accumulate in late endosomes/PVC rather than Golgi bodies (Vermeer *et al.*, 2006). The fact that our PX^{p40} sensor localises to the tonoplast suggests that PI3P might also accumulate in a late endosomal compartment in Arabidopsis roots. To verify this hypothesis, we crossed the P18Y (CITRINE-$2xFYVE^{HRS}$) and P3Y (PX^{p40}-CITRINE) lines with transgenic lines expressing various red fluorescent organelle markers (Dettmer *et al.*, 2006; Jaillais *et al.*, 2006; Geldner *et al.*, 2009). In the F2 generation, we analysed the co-localisation between our PI3P biosensors and these compartment markers, qualitatively (Figure 7 and Figure S4) and quantitatively (Figure 8), using an object-based analysis. We determined that $2xFYVE^{HRS}$ co-localises extensively with markers of the late endosomes/PVC (Figure 7a and 8a). Similarly, $1xPX^{p40}$ also co-localises preferentially with late endosomal markers (Figure 8b and S4); although to a lesser extent, due to its additional localisation to the tonoplast (Figure S4). Altogether, our result showed that PI3P, like in tobacco BY-2 cells (Vermeer *et al.*, 2006), mainly accumulate in late endosomes/PVC and to a lesser degree at the tonoplast.

PI4P accumulates in endosomal compartments in Arabidopsis root epidermis

Next, we conducted a similar qualitative (Figure 9 and Fig S5) and quantitative (Figure 8) co-localisation analysis for our PI4P sensors in order to determine in which intracellular compartments they localise. Our quantitative analyses revealed that both $1xPH^{FAPP1}$ and $2xPH^{FAPP1}$ localised to early endosomes/TGN and recycling endosomes (collectively referred to as post-Golgi/endosomal compartments by Geldner et al., (2009), about 45% of co-localisation) as well as to the Golgi apparatus (Figure 8). In order to confirm that PI4P resides in a post-Golgi/endosomal compartment in Arabidopsis epidermal cells, we performed a co-localisation experiment with the endocytic tracer FM4-64 (Figure 9e and Figure 8c). FM4-64 is a vital dye that fluoresces in a lipophilic environment and cannot pass through membranes. It can therefore enter inside the cell only by endocytosis, where it labels endosomes. We found a good co-localisation between FM4-64 and the CITRINE-$1xPH^{FAPP1}$ marker (about 48% of co-localisation) (Figure 8), further confirming that PI4P accumulates significantly in a post-Golgi/endosomal compartment (Figure 9e). As a third approach, we also performed treatment with the fungal toxin Brefeldin A (BFA) (Figure 9f-j). BFA allows for a good discrimination between intracellular compartments of root epidermal cells, notably between Golgi and post-Golgi compartments that segregate around and inside the “BFA compartment”, respectively (Grebe *et al.*, 2003; Jaillais *et al.*, 2008; Geldner *et al.*, 2009). In accordance with our quantitative co-localisation analysis, a significant proportion of CITRINE-$1xPH^{FAPP1}$-labelled compartments were found to reside at the heart of the BFA compartment, together with FM4-64 as well as markers of early endosomes/TGN and recycling endosomes (Figure 9h-j). On the other hand, BFA largely

dissociated the PI4P sensor from the Golgi that was surrounding the CITRINE-1xPH^{FAPP1}-labelled BFA compartment (Figure 9g). Furthermore, we noticed that a significant proportion of CITRINE-1xPH^{FAPP1}-labelled compartments were resistant to BFA (Figure 9j). These BFA-insensitive PI4P-containing compartments mainly co-localised with early endosomes/TGN marker that is also partially insensitive to BFA (Figure 9h and (Geldner *et al.*, 2009)). Altogether, our results showed that in Arabidopsis root epidermis, PI4P localises at the PM and to one or possibly several post-Golgi/endosomal compartments (early endosomes/TGN and recycling endosomes) and to a lesser extent, the Golgi apparatus.

Discussion

The PIPline collection as a tool to dissect PIP function in Arabidopsis

Our set of PIP marker lines provides a comprehensive collection to study the localisation and dynamics of distinct PIP species in *Arabidopsis thaliana*. The PIPline marker set implements several new features over the already existing PIP reporters in Arabidopsis. First, we systematically engineered reporters with various avidities for each PIP species. The comparison of their respective localisation is indicative of the relative concentration of PIP in different cellular compartments. Second, our PIPline collection is multi-coloured, which allows for the co-labelling of several PIP species at the same time as well as their fast co-localisation with already established markers independent of their colour. Third, although we restricted our co-localisation analysis to root epidermal tissue, we used a broadly expressed promoter that will enable the study of plant PIPs in a variety of tissues and developmental contexts. Thus, it will be possible to analyse the impact of both abiotic and biotic stresses in the relevant tissue. Finally, we used several independent LBDs to report on the localisation of the same lipids, which revealed previously unrecognized localisation for various PIPs in root epidermis.

A map of PIP localisation in Arabidopsis root epidermis

Although genetically encoded PIP sensors have known limitations, our work, together with previous studies (Vermeer *et al.*, 2006; van Leeuwen *et al.*, 2007; Mishkind *et al.*, 2009; Vermeer *et al.*, 2009), suggests the model presented in Figure 10 for the localisation of PI3P, PI4P and PI(4,5)P_2 in non-stressed Arabidopsis root epidermis. Interestingly, we found that in this situation PI(4,5)P_2 is already present at the PM in sufficient quantity to localise PIP_2 binding proteins such as PH^{PLC} and 1xTUBBY-C. Previous analyses using the 1xPH^{PLC} sensor found that it is not localised to the PM in Arabidopsis root cell with the exception of the root hair tips and stressed cells (e.g. osmotic stress) (van Leeuwen *et al.*, 2007). In our growth conditions, we found a significant proportion of 1xPH^{PLC} at the PM of epidermal cells in the absence of any specific stresses. This might be due to differences of growth conditions (e.g. slightly different media). Another possible explanation is that we used the PH domain of PLCδ1 of *Rattus norvegicus* (Levine and Munro, 2002) while van Leeuwen et al., used the PH domain of human PLCδ1 (van Leeuwen *et al.*, 2007). It is possible the rat $PLC_{\delta1}$ has a slightly different (i.e. higher) affinity for PI(4,5)P_2 when expressed in Arabidopsis than its human counterpart, which could account for the differences observed in vivo. The differences of localisation might also be due to differences in the constructs design (e.g. linkers, promoters, fluorescent proteins, domain size). In any case, the YFP-1xPH^{HsPLC} previously described (van Leeuwen *et al.*, 2007) and our CITRINE-1xPH^{RnPLC} should be complementary tools, which together with the CITRINE-2xPH^{RnPLC} and CITRINE-1xTUBBY-C provide biosensors with four different apparent affinities for PI(4,5)P_2.

PI3P is localised in late endosomes/PVC and to a less extent to the tonoplast. The late endosomes/PVC localisation is consistent with previous reports in tobacco BY-2 cells

(Vermeer *et al.*, 2006) as well as the localisation of PI3P effectors in this compartment (Jaillais *et al.*, 2006; Pourcher *et al.*, 2010). In animals, PI3P accumulates in early endosomes rather than late endosomes (Balla, 2013; Lemmon, 2008; De Matteis and Godi, 2004). However it is not surprising since plant late endosomes share many similarities with animal early endosomes (Jaillais *et al.*, 2008), such as the presence of the small GTPases of the Rab5 family (Jaillais *et al.*, 2008; Geldner *et al.*, 2009). The coordinate action of Rab5 GTPases and PI3P at the surface of the plant late endosomes and animal early endosomes will attract their effector proteins (Jean and Kiger, 2012), many of which are conserved between the two kingdoms (e.g. SORTING NEXIN family (Jaillais *et al.*, 2006; Lemmon, 2008; Pourcher *et al.*, 2010; Cullen and Korswagen, 2012)).

PI4P was reported to accumulate in the Golgi apparatus in cowpea mesophyll protoplasts as well as in tobacco BY2 cells (Vermeer *et al.*, 2009), but its co-localisation with post-Golgi markers was not investigated. We accumulated several lines of evidence suggesting that our PI4P biosensors localise in a post-Golgi compartment in Arabidopsis epidermal cells, including i) co-localisation with markers of the early endosomes/TGN and the recycling endosomes, ii) co-localisation with the endocytic tracer FM4-64 and, iii) sensitivity to BFA. Our results are in accordance with the localisation of the Arabidopsis PI4-kinase β1 and β2 in post-Golgi compartments in Arabidopsis root (Kang *et al.*, 2011). Furthermore, loss of PI4-kinase β1 and β2 and of PI4-phosphatase (RHD4) activity induces TGN morphology defects in Arabidopsis roots (Preuss *et al.*, 2006; Thole *et al.*, 2008; Kang *et al.*, 2011). Because of the dual nature of the plant TGN as the early endosome, it is likely that PI4P will have major functions in both protein exocytosis and endocytosis. This key cellular position is highlighted by the function of PI4P in polarized cell expansion (Preuss *et al.*, 2006; Thole *et al.*, 2008; Thole and Nielsen, 2008; Vermeer *et al.*, 2009). However, it is clear that many more studies are required to understand how the various cellular pools of PI4P control specific cellular pathways. We believe that our PIPline marker set will catalyse future research on the various functions of PIPs in Arabidopsis on diverse topics including but not limited to membrane trafficking, cell signalling, cell morphogenesis, reproduction, development, response to abiotic and biotic stresses and adaptation to the environment.

Experimental procedures

Material and growth conditions

Plants were grown in soil with long daylight at 21°C and 70% humidity. For root analysis, seedlings were grown vertically on MS medium [(pH 5.7, 0.8% plant agar (Duchefa)] in the absence of sucrose, with continuous daylight condition for 6 to 9 days. Plants from the Columbia 0 accession and yeast from the BY4743 strain were used for transformation. The wave-lines, VHAa1/VHAa3 compartment markers and myrCIT lines were described before (Dettmer *et al.*, 2006; Geldner *et al.*, 2009; Jaillais *et al.*, 2011).

Imaging

All imaging were performed on an inverted Zeiss LSM710 confocal microscope using a 40x Plan-apochromatic objective (numerical aperture 1.2). Dual-colour images were acquired by sequential line switching, allowing the separation of channels by both excitation and emission. In the case of co-localisation, we also controlled for a complete absence of channel crosstalk. Hoechst was excited with a 405nm laser, CyPET was excited with a 445nm laser, GFP was excited with a 488nm laser, CITRINE was excited with a 515nm laser and mCHERRY/Alexa555 were excited with a 561nm laser. FM4-64 (Invitrogen) was applied at a concentration of 3 μM; BFA (Sigma-Aldrich) was applied at a concentration of 25 μM for 1 hour in liquid medium. Stock solutions were prepared in DMSO at 3 μM and 50 μM, respectively. Imaging was performed in the root epidermis in cells that are at the onset

of elongation. For quantitative imaging, pictures of epidermal root cells were taken with detector settings optimised for low background and at the limit of pixel saturation in order to obtain the best dynamic range possible.

Statistical analyses

Sample size was determined by variance analysis value ($p<0.05$) using Excel software (Microsoft). For the quantitative analysis of membrane localisation of low and high affinity biosensors, Student's *t*-tests were performed using Excel (Microsoft) ($p<0.05$). Quantitative co-localisation results were statistically compared using a bilateral test (Steel-Dwass-Critchlow-Fligner) using XLstat software (http://www.xlstat.com/). This non-parametric test is used to make all possible pairwise comparisons between groups with a probability of detecting localisation differences of 0.05%. Graphs were drawn using the Deltagraph5 software (http://www.rockware.com/).

See supplementary methods for: **cloning of the PIP-line constructs** (the protein IDs and primers used are presented in Table S2 and S3 and the sequences of all the constructs can be downloaded at http://www.ens-lyon.fr/RDP/SiCE/PIPline.html), **^{32}P-phospholipid labelling and lipid analysis, plant transformation and selection, quantitative image analysis, protein extraction and protein-lipid overlay assay and, Huh-7 transfection and immunofluorescence analysis.**

Supplementary Material

Refer to Web version on PubMed Central for supplementary material.

Acknowledgments

We thank all the members of the SiCE group for discussions, N. Geldner, K. Schumacher, J. Long, H. Stenmark, M. Yaffe, T. Levine, J.L. Farré, A. Marshall, S. Friant, L. Shapiro, C. Montell, W. Hahn, D. Root and R. Tsien for sharing material. This work was initially supported by grants from the U.S. National Institutes of Health (GM094428), and NSF (IOS-1045256) and The Howard Hughes Medical Institute (to J.C.), and then by grants from the Agence National pour la Recherche (ANR-12-JSV2-0002-01), and the Marie Curie Action (PCIG-GA-2011-303601) (to Y.J.) M.S. and S.A. are supported by a Ph.D. fellowship (MENRT) from the French ministry of higher education and research.

References

Ago T, Takeya R, Hiroaki H, Kuribayashi F, Ito T, Kohda D, Sumimoto H. The PX Domain as a Novel Phosphoinositide- Binding Module. Biochem Biophys Res Commun. 2001; 287:733–738. [PubMed: 11563857]

Balla A, Tuymetova G, Tsiomenko A, Várnai P, Balla T. A Plasma Membrane Pool of Phosphatidylinositol 4- Phosphate Is Generated by Phosphatidylinositol 4-Kinase Type-III Alpha: Studies with the PH Domains of the Oxysterol Binding Protein and FAPP1. Molecular biology of the cell. 2005; 16:1282–1295. [PubMed: 15635101]

Balla T. Phosphoinositides: tiny lipids with giant impact on cell regulation. Physiological Reviews. 2013; 93:1019–1137. [PubMed: 23899561]

Balla T, Szentpetery Z, Kim YJ. Phosphoinositide signaling: new tools and insights. Physiology (Bethesda). 2009; 24:231–244. [PubMed: 19675354]

Bravo J, Karathanassis D, Pacold CM, Pacold ME, Ellson CD, Anderson KE, Butler PJ, Lavenir I, Perisic O, Hawkins PT, Stephens L, Williams RL. The crystal structure of the PX domain from p40(phox) bound to phosphatidylinositol 3-phosphate. Mol Cell. 2001; 8:829–839. [PubMed: 11684018]

Burd CG, Emr SD. Phosphatidylinositol(3)-phosphate signaling mediated by specific binding to RING FYVE domains. Mol Cell. 1998; 2:157–162. [PubMed: 9702203]

Christoforidis S, Miaczynska M, Ashman K, Wilm M, Zhao L, Yip SC, Waterfield MD, Backer JM, Zerial M. Phosphatidylinositol-3-OH kinases are Rab5 effectors. Nat Cell Biol. 1999; 1:249–252. [PubMed: 10559924]

Cullen PJ, Korswagen HC. Sorting nexins provide diversity for retromer-dependent trafficking events. Nat Cell Biol. 2012; 14:29–37. [PubMed: 22193161]

Daboussi L, Costaguta G, Payne GS. Phosphoinositide-mediated clathrin adaptor progression at the trans-Golgi network. Nat Cell Biol. 2012; 14:239–250. [PubMed: 22344030]

De Matteis MA, Godi A. PI-loting membrane traffic. Nat Cell Biol. 2004; 6:487–492. [PubMed: 15170460]

Dettmer J, Hong-Hermesdorf A, Stierhof YD, Schumacher K. Vacuolar H+-ATPase activity is required for endocytic and secretory trafficking in Arabidopsis. Plant Cell. 2006; 18:715–730. [PubMed: 16461582]

Dowler S, Currie RA, Campbell DG, Deak M, Kular G, Downes CP, Alessi DR. Identification of pleckstrin-homology-domain-containing proteins with novel phosphoinositide-binding specificities. Biochem J. 2000; 351:19–31. [PubMed: 11001876]

Ellson CD, Gobert-Gosse S, Anderson KE, Davidson K, Erdjument-Bromage H, Tempst P, Thuring JW, Cooper MA, Lim ZY, Holmes AB, Gaffney PR, Coadwell J, Chilvers ER, Hawkins PT, Stephens LR. PtdIns(3)P regulates the neutrophil oxidase complex by binding to the PX domain of p40(phox). Nat Cell Biol. 2001; 3:679–682. [PubMed: 11433301]

Eugster A, Pécheur EI, Michel F, Winsor B, Letourneur F, Friant S. Ent5p is required with Ent3p and Vps27p for ubiquitin-dependent protein sorting into the multivesicular body. Molecular biology of the cell. 2004; 15:3031–3041. [PubMed: 15107463]

Farré JC, Vidal J, Subramani S. A cytoplasm to vacuole targeting pathway in P. pastoris. Autophagy. 2007; 3:230–234. [PubMed: 17329961]

Ferguson KM, Lemmon MA, Schlessinger J, Sigler PB. Structure of the high affinity complex of inositol trisphosphate with a phospholipase C pleckstrin homology domain. Cell. 1995; 83:1037–1046. [PubMed: 8521504]

Franke TF, Kaplan DR, Cantley LC, Toker A. Direct Regulation of the Akt Proto-Oncogene Product by Phosphatidylinositol-3,4-bisphosphate. Science. 1997; 275:665–668. [PubMed: 9005852]

Friant S, Pécheur EI, Eugster A, Michel F, Lefkir Y, Nourrisson D, Letourneur F. Ent3p Is a PtdIns(3,5)P2 effector required for protein sorting to the multivesicular body. Dev Cell. 2003; 5:499–511. [PubMed: 12967568]

Geldner N, Dénervaud-Tendon V, Hyman DL, Mayer U, Stierhof YD, Chory J. Rapid, combinatorial analysis of membrane compartments in intact plants with a multicolor marker set. Plant J. 2009; 59:169–178. [PubMed: 19309456]

Gillooly DJ, Morrow IC, Lindsay M, Gould R, Bryant NJ, Gaullier JM, Parton RG, Stenmark H. Localization of phosphatidylinositol 3-phosphate in yeast and mammalian cells. EMBO J. 2000; 19:4577–4588. [PubMed: 10970851]

Godi A, Campli AD, Konstantakopoulos A, Di Tullio G, Alessi DR, Kular GS, Daniele T, Marra P, Lucocq JM, De Matteis MA. FAPPs control Golgi-to-cell-surface membrane traffic by binding to ARF and PtdIns(4)P. Nat Cell Biol. 2004; 6:393–404. [PubMed: 15107860]

Gozani O, Karuman P, Jones DR, Ivanov D, Cha J, Lugovskoy AA, Baird CL, Zhu H, Field SJ, Lessnick SL, Villasenor J, Mehrotra B, Chen J, Rao VR, Brugge JS, Ferguson CG, Payrastre B, Myszka DG, Cantley LC, Wagner G, Divecha N, Prestwich GD, Yuan J. The PHD finger of the chromatin-associated protein ING2 functions as a nuclear phosphoinositide receptor. Cell. 2003; 114:99–111. [PubMed: 12859901]

Grebe M, Xu J, Möbius W, Ueda T, Nakano A, Geuze HJ, Rook MB, Scheres B. Arabidopsis Sterol Endocytosis Involves Actin-Mediated Trafficking via ARA6-Positive Early Endosomes. Curr Biol. 2003; 13:1378–1387. [PubMed: 12932321]

Hammond GRV, Fischer MJ, Anderson KE, Holdich J, Koteci A, Balla T, Irvine RF. PI4P and PI(4,5)P2 are essential but independent lipid determinants of membrane identity. Science. 2012; 337:727–730. [PubMed: 22722250]

Hammond GRV, Schiavo G, Irvine R. Immunocytochemical techniques reveal multiple, distinct cellular pools of PtdIns4P and PtdIns (4, 5) P2. Biochem J. 2009a; 422:23–35. [PubMed: 19508231]

Hammond GRV, Sim Y, Lagnado L, Irvine RF. Reversible binding and rapid diffusion of proteins in complex with inositol lipids serves to coordinate free movement with spatial information. J Cell Biol. 2009b; 184:297–308. [PubMed: 19153221]

He J, Scott JL, Heroux A, Roy S, Lenoir M, Overduin M, Stahelin RV, Kutateladze TG. Molecular basis of phosphatidylinositol 4-phosphate and ARF1 GTPase recognition by the FAPP1 pleckstrin homology (PH) domain. J Biol Chem. 2011; 286:18650–18657. [PubMed: 21454700]

He J, Vora M, Haney RM, Filonov GS, Musselman CA, Burd CG, Kutateladze AG, Verkhusha VV, Stahelin RV, Kutateladze TG. Membrane insertion of the FYVE domain is modulated by pH. Proteins. 2009; 76:852–860. [PubMed: 19296456]

Heikal AA, Hess ST, Baird GS, Tsien RY, Webb WW. Molecular spectroscopy and dynamics of intrinsically fluorescent proteins: coral red (dsRed) and yellow (Citrine). Proc Natl Acad Sci USA. 2000; 97:11996–12001. [PubMed: 11050231]

Ischebeck T, Seiler S, Heilmann I. At the poles across kingdoms: phosphoinositides and polar tip growth. Protoplasma. 2010; 240:13–31. [PubMed: 20091065]

Ischebeck T, Stenzel I, Heilmann I. Type B phosphatidylinositol-4-phosphate 5-kinases mediate Arabidopsis and Nicotiana tabacum pollen tube growth by regulating apical pectin secretion. Plant Cell. 2008; 20:3312–3330. [PubMed: 19060112]

Ischebeck T, Stenzel I, Hempel F, Jin X, Mosblech A, Heilmann I. Phosphatidylinositol-4,5-bisphosphate influences Nt-Rac5-mediated cell expansion in pollen tubes of Nicotiana tabacum. Plant J. 2011; 65:453–468. [PubMed: 21265898]

Jaillais Y, Fobis-Loisy I, Miège C, Gaude T. Evidence for a sorting endosome in Arabidopsis root cells. Plant J. 2008; 53:237–247. [PubMed: 17999644]

Jaillais Y, Fobis-Loisy I, Miège C, Rollin C, Gaude T. AtSNX1 defines an endosome for auxin-carrier trafficking in Arabidopsis. Nature. 2006; 443:106–109. [PubMed: 16936718]

Jaillais Y, Hothorn M, Belkhadir Y, Dabi T, Nimchuk ZL, Meyerowitz EM, Chory J. Tyrosine phosphorylation controls brassinosteroid receptor activation by triggering membrane release of its kinase inhibitor. Genes Dev. 2011; 25:232–237. [PubMed: 21289069]

Jean S, Kiger AA. Coordination between RAB GTPase and phosphoinositide regulation and functions. Nat Rev Mol Cell Biol. 2012; 13:463–470. [PubMed: 22722608]

Johannessen CM, Boehm JS, Kim SY, Thomas SR, Wardwell L, Johnson LA, Emery CM, Stransky N, Cogdill AP, Barretina J, Caponigro G, Hieronymus H, Murray RR, Salehi-Ashtiani K, Hill DE, Vidal M, Zhao JJ, Yang X, Alkan O, Kim S, Harris JL, Wilson CJ, Myer VE, Finan PM, Root DE, Roberts TM, Golub T, Flaherty KT, Dummer R, Weber BL, Sellers WR, Schlegel R, Wargo JA, Hahn WC, Garraway LA. COT drives resistance to RAF inhibition through MAP kinase pathway reactivation. Nature. 2010; 468:968–972. [PubMed: 21107320]

Kanai F, Liu H, Field SJ, Akbary H, Matsuo T, Brown GE, Cantley LC, Yaffe MB. The PX domains of p47phox and p40phox bind to lipid products of PI(3)K. Nat Cell Biol. 2001; 3:675–678. [PubMed: 11433300]

Kang BH, Nielsen E, Preuss ML, Mastronarde D, Staehelin LA. Electron Tomography of RabA4b- and PI-4Kβ1-Labeled Trans Golgi Network Compartments in Arabidopsis. Traffic. 2011; 12:313–329. [PubMed: 21134079]

Kwon Y, Hofmann T, Montell C. Integration of phosphoinositide- and calmodulin-mediated regulation of TRPC6. Mol Cell. 2007; 25:491–503. [PubMed: 17317623]

Lemmon MA. Membrane recognition by phospholipid-binding domains. Nat Rev Mol Cell Biol. 2008; 9:99–111. [PubMed: 18216767]

Lemmon MA, Ferguson KM, O'Brien R, Sigler PB, Schlessinger J. Specific and high-affinity binding of inositol phosphates to an isolated pleckstrin homology domain. Proc Natl Acad Sci USA. 1995; 92:10472–10476. [PubMed: 7479822]

Lenoir M, Coskun UN, Grzybek M, Cao X, Buschhorn SB, James J, Simons K, Overduin M. Structural basis of wedging the Golgi membrane by FAPP pleckstrin homology domains. EMBO report. 2010; 11:279–284.

Levine TP, Munro S. The pleckstrin homology domain of oxysterol-binding protein recognises a determinant specific to Golgi membranes. Current Biology. 1998; 8:729–739. [PubMed: 9651677]

Levine TP, Munro S. Targeting of Golgi-specific pleckstrin homology domains involves both PtdIns 4-kinase-dependent and -independent components. Current Biology. 2002; 12:695–704. [PubMed: 12007412]

Ling Y, Stefan CJ, MacGurn JA, Audhya A, Emr SD. The dual PH domain protein Opy1 functions as a sensor and modulator of PtdIns(4,5)P2 synthesis. EMBO J. 2012; 31:2882–2894. [PubMed: 22562153]

Málková Š, Stahelin RV, Pingali SV, Cho W, Schlossman ML. Orientation and Penetration Depth of Monolayer-Bound p40 phox-PX. Biochemistry. 2006; 45:13566–13575. [PubMed: 17087510]

Manford AG, Stefan CJ, Yuan HL, MacGurn JA, Emr SD. ER-to-Plasma Membrane Tethering Proteins Regulate Cell Signaling and ER Morphology. Dev Cell. 2012; 23:1129–1140. [PubMed: 23237950]

Marshall AJ, Krahn AK, Ma K, Duronio V, Hou S. TAPP1 and TAPP2 are targets of phosphatidylinositol 3-kinase signaling in B cells: sustained plasma membrane recruitment triggered by the B-cell antigen receptor. Mol Cell Biol. 2002; 22:5479–5491. [PubMed: 12101241]

McLaughlin S, Murray D. Plasma membrane phosphoinositide organization by protein electrostatics. Nature. 2005; 438:605–611. [PubMed: 16319880]

Meijer HJG, Munnik T. Phospholipid-based signaling in plants. Annu Rev Plant Biol. 2003; 54:265–306. [PubMed: 14502992]

Mishkind M, Vermeer JEM, Darwish E, Munnik T. Heat stress activates phospholipase D and triggers PIP2 accumulation at the plasma membrane and nucleus. Plant J. 2009; 60:10–21. [PubMed: 19500308]

Misra S, Hurley JH. Crystal structure of a phosphatidylinositol 3-phosphate-specific membrane-targeting motif, the FYVE domain of Vps27p. Cell. 1999; 97:657–666. [PubMed: 10367894]

Munnik T, Nielsen E. Green light for polyphosphoinositide signals in plants. Curr Opin Plant Biol. 2011; 14:489–497. [PubMed: 21775194]

Munnik T, Vermeer JEM. Osmotic stress-induced phosphoinositide and inositol phosphate signalling in plants. Plant Cell Environ. 2010; 33:655–669. [PubMed: 20429089]

Munro S. Organelle identity and the organization of membrane traffic. Nat Cell Biol. 2004; 6:469–472. [PubMed: 15170453]

Niu Y, Zhang C, Sun Z, Hong Z, Li K, Sun D, Yang Y, Tian C, Gong W, Liu JJ. PtdIns(4)P regulates retromer-motor interaction to facilitate dynein-cargo dissociation at the trans-Golgi network. Nat Cell Biol. 2013; 15:417–429. [PubMed: 23524952]

Nguyen AW, Daugherty PS. Evolutionary optimization of fluorescent proteins for intracellular FRET. Nat Biotechnol. 2005; 23:355–360. [PubMed: 15696158]

Posor Y, Eichhorn-Gruenig M, Puchkov D, Schöneberg J, Ullrich A, Lampe A, Müller R, Zarbakhsh S, Gulluni F, Hirsch E, Krauss M, Schultz C, Schmoranzer J, Noé F, Haucke V. Spatiotemporal control of endocytosis by phosphatidylinositol-3,4-bisphosphate. Nature. 2013; 499:233–237. [PubMed: 23823722]

Pourcher M, Santambrogio M, Thazar N, Thierry AM, Fobis-Loisy I, Miège C, Jaillais Y, Gaude T. Analyses of sorting nexins reveal distinct retromer-subcomplex functions in development and protein sorting in Arabidopsis thaliana. Plant Cell. 2010; 22:3980–3991. [PubMed: 21156856]

Preuss ML, Schmitz AJ, Thole JulieM, Bonner HKS, Otegui MS, Nielsen Erik. A role for the RabA4b effector protein PI-4K 1 in polarized expansion of root hair cells in Arabidopsis thaliana. J Cell Biol. 2006; 172:991–998. [PubMed: 16567499]

Quinn KV, Behe P, Tinker A. Monitoring changes in membrane phosphatidylinositol 4,5-bisphosphate in living cells using a domain from the transcription factor tubby. J Physiol (Lond). 2008; 586

Raiborg C, Bremnes B, Mehlum A, Gillooly DJ, D'Arrigo A, Stang E, Stenmark H. FYVE and coiled-coil domains determine the specific localisation of Hrs to early endosomes. Journal of Cell Science. 2001; 114:2255–2263. [PubMed: 11493665]

Rameh LE, Arvidsson AK, Carraway KL, Couvillon AD, Rathbun G, Crompton A, VanRenterghem B, Czech MP, Ravichandran KS, Burakoff SJ. A comparative analysis of the phosphoinositide

binding specificity of pleckstrin homology domains. J Biol Chem. 1997; 272:22059–22066. [PubMed: 9268346]

Roy A, Levine TP. Multiple Pools of Phosphatidylinositol 4-Phosphate Detected Using the Pleckstrin Homology Domain of Osh2p. J Biol Chem. 2004; 279:44683–44689. [PubMed: 15271978]

Salim K, Bottomley MJ, Querfurth E, Zvelebil MJ, Gout I, Scaife R, Margolis RL, Gigg R, Smith CI, Driscoll PC. Distinct specificity in the recognition of phosphoinositides by the pleckstrin homology domains of dynamin and Bruton's tyrosine kinase. EMBO J. 1996; 15:6241. [PubMed: 8947047]

Sankaran VG, Klein DE, Sachdeva MM, Lemmon MA. High-Affinity Binding of a FYVE Domain to Phosphatidylinositol 3-Phosphate Requires Intact Phospholipid but Not FYVE Domain Oligomerization. Biochemstry. 2001; 40:8581–8587.

Santagata S, Boggon TJ, Baird CL, Gomez CA, Zhao J, Shan WS, Myszka DG, Shapiro L. G-protein signaling through tubby proteins. Science. 2001; 292:2041–2050. [PubMed: 11375483]

Schultz C. Challenges in studying phospholipid signaling. Nat Chemical Biology. 2010; 6:473–475.

Shaner NC, Campbell RE, Steinbach PA, Giepmans BNG, Palmer AE, Tsien RY. Improved monomeric red, orange and yellow fluorescent proteins derived from Discosoma sp. red fluorescent protein. Nat Biotechnol. 2004; 22:1567–1572. [PubMed: 15558047]

Simonsen A, Lippé R, Christoforidis S, Gaullier JM, Brech A, Callaghank J, Tohk BH, Murphy C, Zerial M, Stenmark H. EEA1 links PI(3)K function to Rab5 regulation of endosome fusion. Nature. 1998; 394:494–498. [PubMed: 9697774]

Stahelin RV, Long F, Diraviyam K, Bruzik KS, Murray D, Cho W. Phosphatidylinositol 3-phosphate induces the membrane penetration of the FYVE domains of Vps27p and Hrs. J Biol Chem. 2002; 277:26379–26388. [PubMed: 12006563]

Stefan CJ, Manford AG, Baird D, Yamada-Hanff J, Mao Y, Emr SD. Osh Proteins Regulate Phosphoinositide Metabolism at ER-Plasma Membrane Contact Sites. Cell. 2011; 144:389–401. [PubMed: 21295699]

Suh BC, Inoue T, Meyer T, Hille B. Rapid chemically induced changes of PtdIns(4,5)P2 gate KCNQ ion channels. Science. 2006; 314:1454–1457. [PubMed: 16990515]

Szentpetery Z, Balla A, Kim YJ, Lemmon MA, Balla T. Live cell imaging with protein domains capable of recognizing phosphatidylinositol 4,5-bisphosphate; a comparative study. BMC Cell Biol. 2009; 10:67. [PubMed: 19769794]

Szentpetery Z, Várnai P, Balla T. Acute manipulation of Golgi phosphoinositides to assess their importance in cellular trafficking and signaling. Proc Natl Acad Sci USA. 2010; 107:8225–8230. [PubMed: 20404150]

Thole JM, Nielsen E. Phosphoinositides in plants: novel functions in membrane trafficking. Curr Opin Plant Biol. 2008; 11:620–631. [PubMed: 19028349]

Thole JM, Vermeer JEM, Zhang Y, Gadella TWJ, Nielsen E. ROOT HAIR DEFECTIVE4 Encodes a Phosphatidylinositol-4-Phosphate Phosphatase Required for Proper Root Hair Development in Arabidopsis thaliana. Plant Cell. 2008; 20:381–395. [PubMed: 18281508]

Tuzi S, Uekama N, Okada M, Yamaguchi S, Saitô H, Yagisawa H. Structure and dynamics of the phospholipase C-δ1 pleckstrin homology domain located at the lipid bilayer surface. J Biol Chem. 2003; 278:28019–28025. [PubMed: 12736268]

van Leeuwen W, Vermeer JEM, Gadella TWJ, Munnik T. Visualization of phosphatidylinositol 4,5-bisphosphate in the plasma membrane of suspension-cultured tobacco BY-2 cells and whole Arabidopsis seedlings. Plant J. 2007; 52:1014–1026. [PubMed: 17908156]

Várnai P, Balla T. Live cell imaging of phosphoinositide dynamics with fluorescent protein domains. Biochim Biophys Acta. 2006; 1761:957–967. [PubMed: 16702024]

Várnai P, Lin X, Lee SB, Tuymetova G, Bondeva T, Spät A, Rhee SG, Hajnóczky G, Balla T. Inositol lipid binding and membrane localization of isolated pleckstrin homology (PH) domains. Studies on the PH domains of phospholipase C delta 1 and p130. J Biol Chem. 2002; 277:27412–27422. [PubMed: 12019260]

Vermeer JEM, Thole JM, Goedhart J, Nielsen E, Munnik T, Gadella TWJ. Imaging phosphatidylinositol 4-phosphate dynamics in living plant cells. Plant J. 2009; 57:356–372. [PubMed: 18785997]

Vermeer JEM, van Leeuwen W, Tobeña-Santamaria R, Laxalt AM, Jones DR, Divecha N, Gadella TWJ, Munnik T. Visualization of PtdIns3P dynamics in living plant cells. Plant J. 2006; 47:687–700. [PubMed: 16856980]

Vincent P, Chua M, Nogue F, Fairbrother A, Mekeel H, Xu Y, Allen N, Bibikova TN, Gilroy S, Bankaitis VA. A Sec14p-nodulin domain phosphatidylinositol transfer protein polarizes membrane growth of Arabidopsis thaliana root hairs. J Cell Biol. 2005; 168:801–812. [PubMed: 15728190]

Yamashita SI, Oku M, Wasada Y, Ano Y, Sakai Y. PI4P-signaling pathway for the synthesis of a nascent membrane structure in selective autophagy. J Cell Biol. 2006; 173:709–717. [PubMed: 16754956]

Yu JW, Mendrola JM, Audhya A, Singh S, Keleti D, Dewald DB, Murray D, Emr SD, Lemmon MA. Genome-wide analysis of membrane targeting by S. cerevisiae pleckstrin homology domains. Mol Cell. 2004; 13:677–688. [PubMed: 15023338]

Zhan Y, Virbasius JV, Song X, Pomerleau DP, Zhou GW. The p40phox and p47phox PX domains of NADPH oxidase target cell membranes via direct and indirect recruitment by phosphoinositides. J Biol Chem. 2002; 277:4512–4518. [PubMed: 11729195]

Zoncu R, Perera RM, Sebastian R, Nakatsu F, Chen H, Balla T, Ayala G, Toomre D, De Camilli PV. Loss of endocytic clathrin-coated pits upon acute depletion of phosphatidylinositol 4,5-bisphosphate. Proc Natl Acad Sci USA. 2007; 104:3793–3798. [PubMed: 17360432]

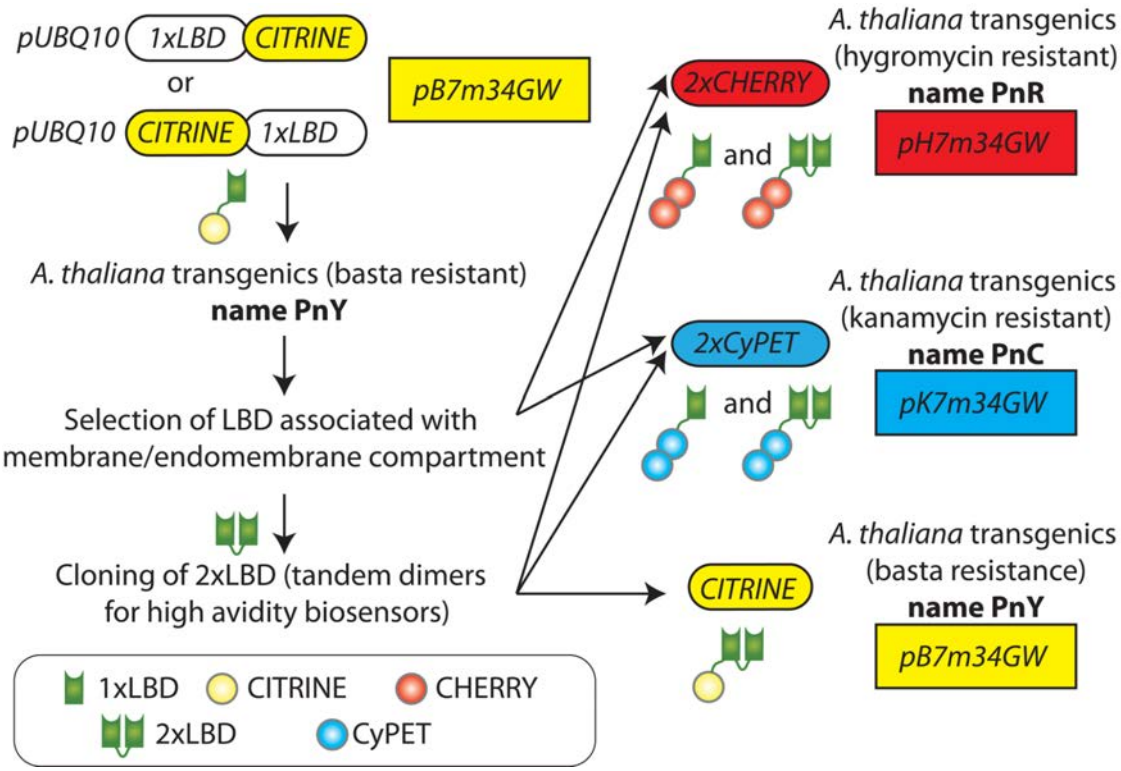

Figure 1. Strategy for the generation of the "PIPline" collection

All PIP biosensor constructs (hereafter referred to as "PIPline") were cloned into multisite gateway destination vectors (pB7m34GW, pH7m34GW and pK7m34GW). All the PIPlines are expressed under the control of the mild constitutive *UBQ10* promoter. Each PIPline has been ascribed a number (n). Yellow PIPlines are named PnY, red PIPline PnR, and cyan PIPline PnC. 1xLBD means that only one LDB is fused to the fluorescent protein; 2xLBD means that two identical LBDs are fused in tandem dimer with the fluorescent protein.

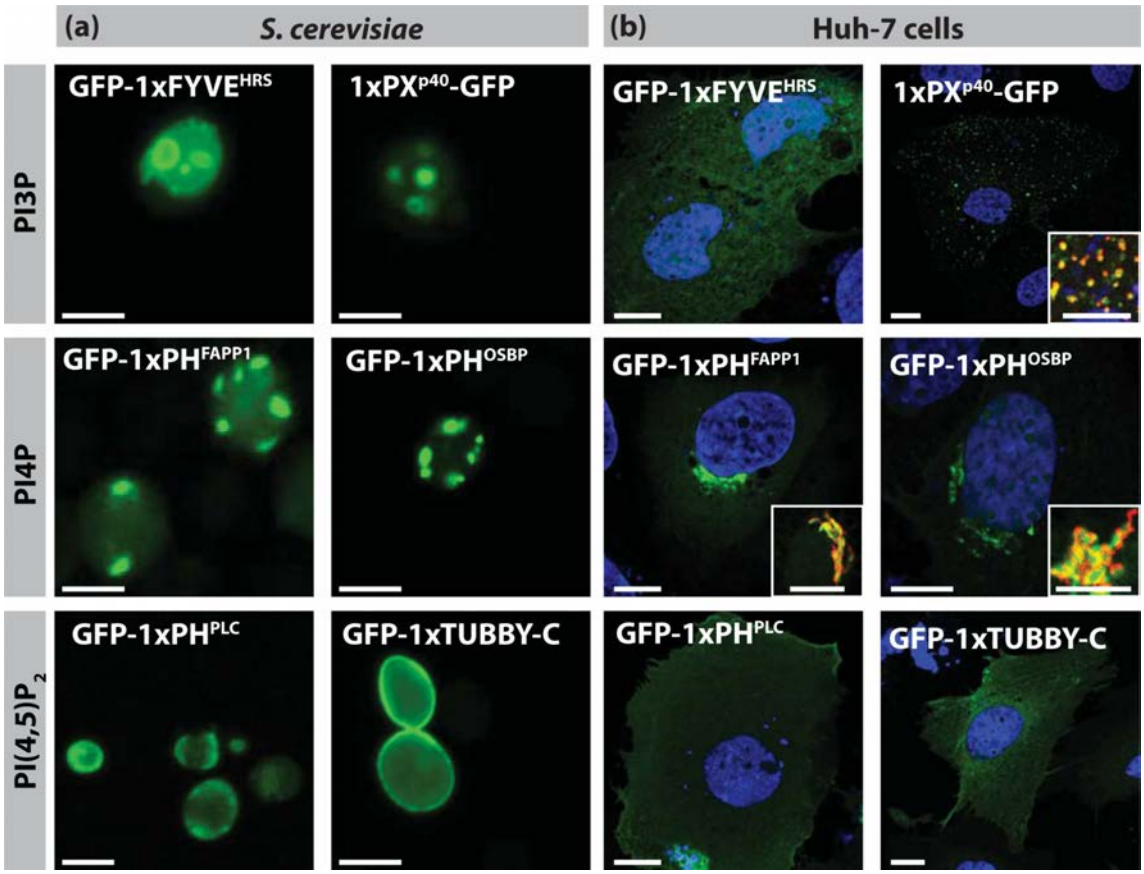

Figure 2. Localisation of the LBD used in this study in yeast and human cells

Confocal pictures of *S. cerevisiae* (a) and human hepatocarcinoma cell line Huh-7 (b) expressing GFP-tagged LBD. Inset in (b) are immuno-localisation showing that $1xPX^{p40}$ (green) co-localises with the early endosome marker EEA1 (red) and that $1xPH^{FAPP1}$/$1xPH^{OSBP}$ (green) co-localise with the Golgi marker GM130 (red). Blue: Hoechst-stained nuclei. Scale bars 5 μm.

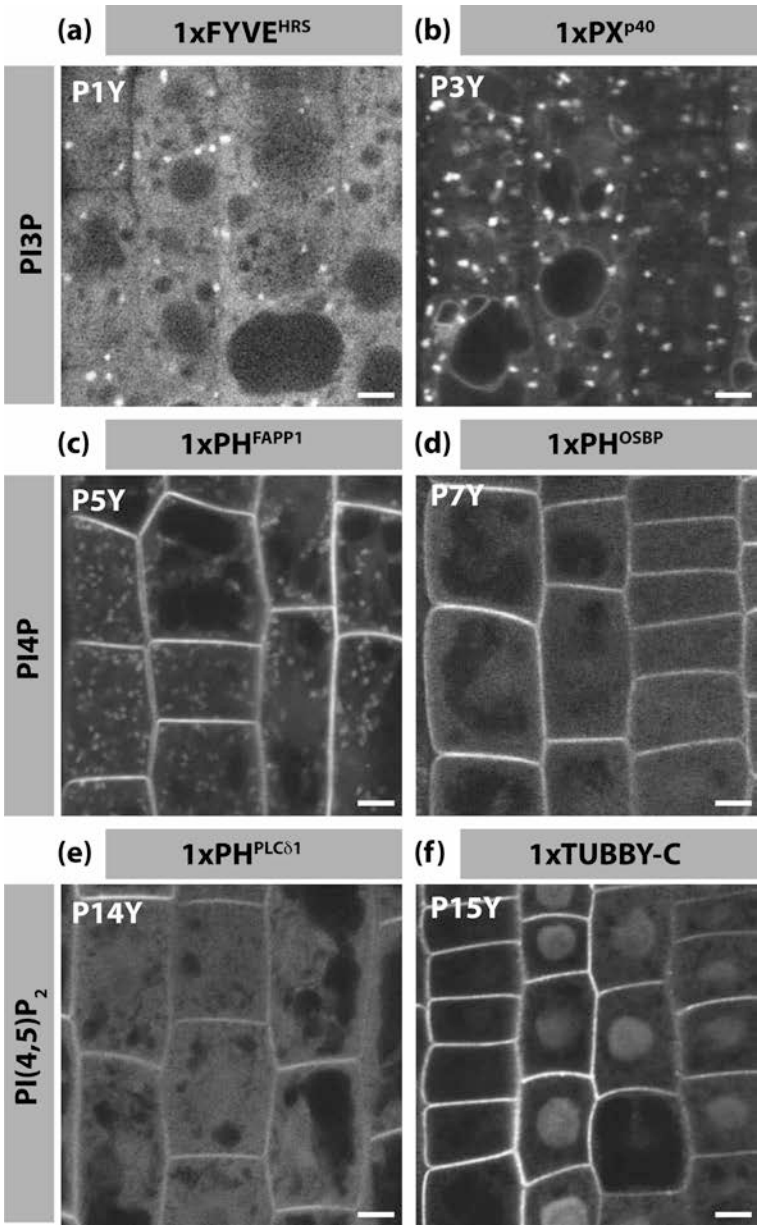

Figure 3. Localisation of PI3P, PI4P and PI(4,5)P_2 in Arabidopsis root epidermis

(a-f) Confocal pictures of Arabidopsis root epidermal cells expressing various CITRINE-tagged LBDs: (a) CITRINE-1xFYVE^{HRS}, (b) 1xPX^{p40}-CITRINE, (c) CITRINE-1xPH^{FAPP1}, (d) CITRINE-1xPH^{OSBP}, (e) CITRINE-1xPH^{PLC}, (f) CITRINE-1xTUBBY-C. The respective PIPline name is indicated in the top left corner. Scale bars 5 μm.

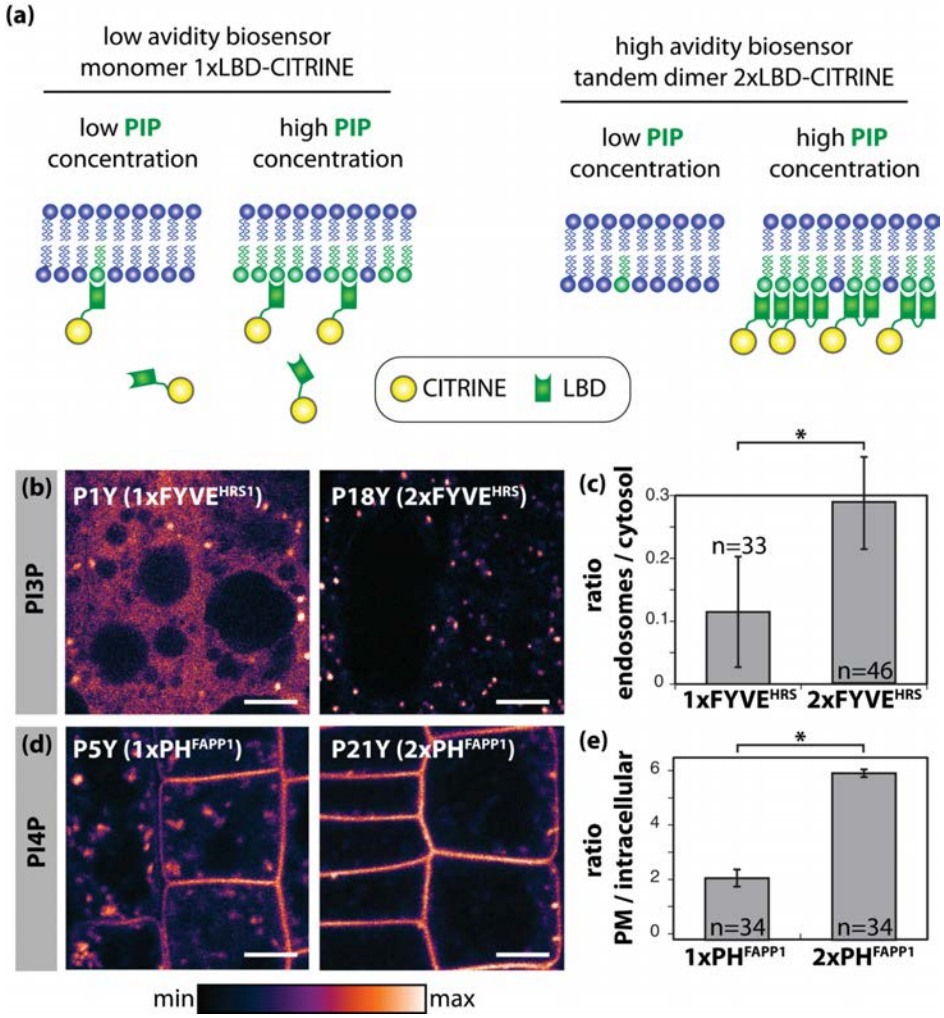

Figure 4. Engineering and analysis of low and high avidity PI3P and PI4P biosensors in Arabidopsis root epidermal cells

(a) Schematic representation of the strategy used to obtain low and high avidity PIP biosensors. (b) Confocal pictures of Arabidopsis root epidermal cells expressing CITRINE-tagged 1xFYVE^{HRS} and 2xFYVE^{HRS}. (c) Graph representation of the ratio of 1xFYVE^{HRS} (P1Y) and 2xFYVE^{HRS} (P18Y) endosomal signal relative to the levels of cytosolic signal. (d) Confocal pictures of Arabidopsis root epidermal cells expressing CITRINE-tagged 1xPH^{FAPP1} and 2xPH^{FAPP1}. (e) Graph representation of the ratio of 1xPH^{FAPP1} (P5Y) and 2xPH^{FAPP1} (P21Y) at the PM relative to the intracellular levels. Confocal pictures are colour-coded in pixel intensity following the LUT scale shown at the bottom. Scale bars 5 μm. Error bars represent standard deviation (s.d.). Asterisk mark: statistical difference ($p<0.05$) according to Student's *t*-test. n is the number of cells used in each quantitative analysis.

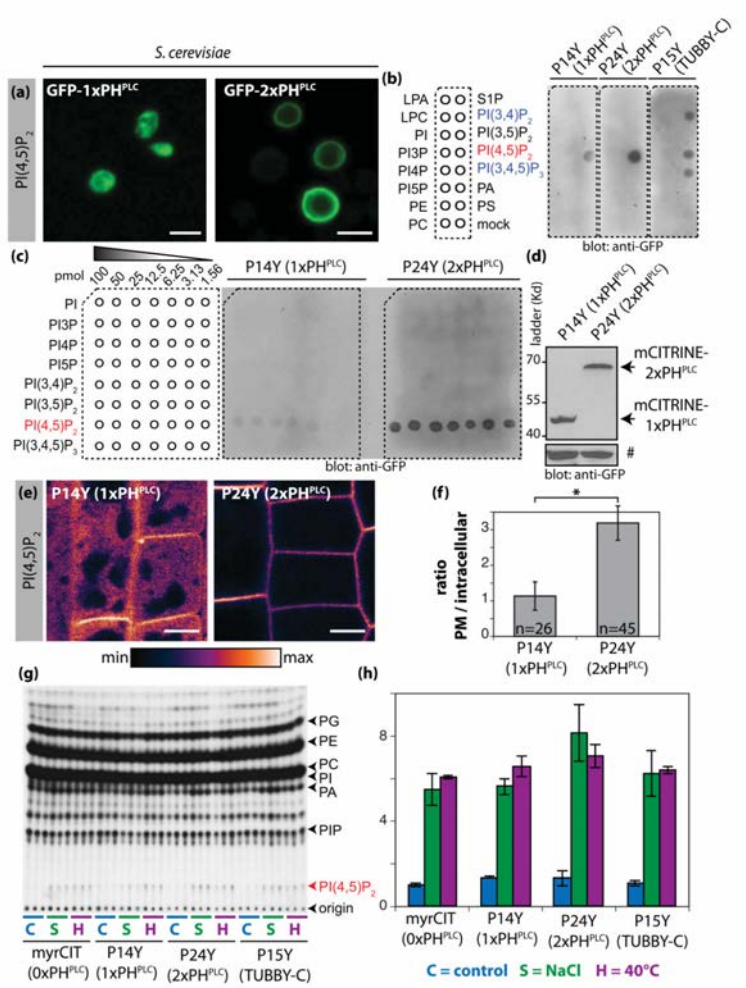

Figure 5. PI(4,5)P_2 is able to drive PIP_2-interacting domains to the PM in non-stressed root epidermal cells

(a) Confocal pictures of *S. cerevisiae* expressing GFP-1xPH^{PLC} (left) and GFP-2xPH^{PLC} (right). Scale bars 5 μm. (b) Protein-lipid overlay assay with CITRINE-1xPH^{PLC} (left), CITRINE-2xPH^{PLC} (middle) and CITRINE-TUBBY-C (right) proteins extracted from P14Y, P15Y and P24Y transgenic plants. The position of each lipid is indicated on the map on the left panel. (c) Protein-lipid overlay assay with the same quantities of CITRINE-1xPH^{PLC} (left), CITRINE-2xPH^{PLC} (right) extracted from P14Y and P24Y transgenic lines. The position and quantity of each lipid is indicated on the map on the left panel. (d) Western blot showing similar expression level of transgenic proteins. The non-specific band indicated by a sharp sign serves as a loading control. (e) Confocal pictures of Arabidopsis root epidermal cells expressing CITRINE-tagged 1xPH^{PLC} and 2xPH^{PLC}. Confocal pictures are colour-coded in pixel intensity following the LUT scale shown at the bottom. Scale bars 5 μm. (f) Graph representing the ratio of 1xPH^{PLC} (P14Y) and 2xPH^{PLC} (P24Y) at the PM relative to the intracellular signal. Error bars represent standard deviation (s.d.). Asterisk mark indicates statistical difference ($p<0.05$) according to Student's *t*-test. n is the number of cells used in each quantitative analysis. (g) Alkaline TLC profile of Arabidopsis seedlings labelled for 16H with $^{32}P_i$ and then incubated for 30 min at: 22°C in control buffer (C = control, blue), 22°C in control buffer supplemented with 250mM NaCl (S = Salt, green) or 40°C in control buffer (H = Heat, purple). Each lane is a pool of 3

seedlings and each condition was analysed in triplicate using the following genotypes: myristoylated 2xCITRINE (myrCIT) as a non-PIP_2 binding control ($0xPH^{PLC}$), P14Y (CITRINE-$1xPH^{PLC}$), P24Y (CITRINE-$2xPH^{PLC}$) and P15Y (CITRINE-TUBBY-C). An autoradiograph of a typical experiment is shown. (h) Quantification of PIP_2 levels by densitometry of the autoradiograph shown in (g). The fold change was calculated relative to levels of $PI(4,5)P_2$ present in myrCIT ($0xPH^{PLC}$) in the control condition from two independent experiments.

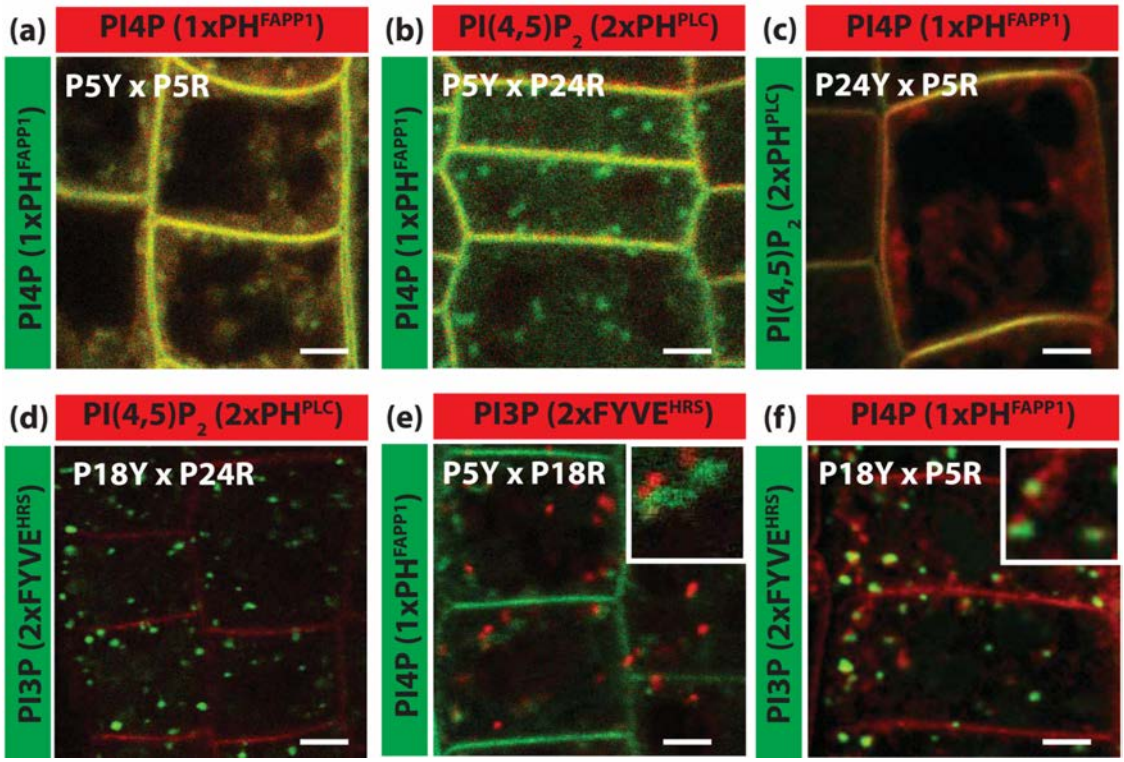

Figure 6. Simultaneous labelling of two PIP species in Arabidopsis root epidermis

(a-f) Confocal pictures of root epidermal cells co-expressing one CITRINE- and one CHERRY-tagged PIPline. Each image is an overlay of the green channel (CITRINE) and red channel (CHERRY), co-localisation being visualised by the yellow colour. (a) CITRINE-1xPH^{FAPP1} x 2xCHERRY-1xPH^{FAPP1}, (b) CITRINE-1xPH^{FAPP1} x 2xCHERRY-2xPH^{PLC}, (c) CITRINE-2xPH^{PLC} x 2xCHERRY-1xPH^{FAPP1}, (d) CITRINE-2xFYVE^{HRS} x 2xCHERRY-2xPH^{PLC}, (e) CITRINE-1xPH^{FAPP1} x 2xCHERRY-2xFYVE^{HRS}, (f) CITRINE-2xFYVE^{HRS} x 2xCHERRY-1xPH^{FAPP1}. The names of the PIPlines used in each cross are indicated at the top and left of each panel. Scale bars 5 μm.

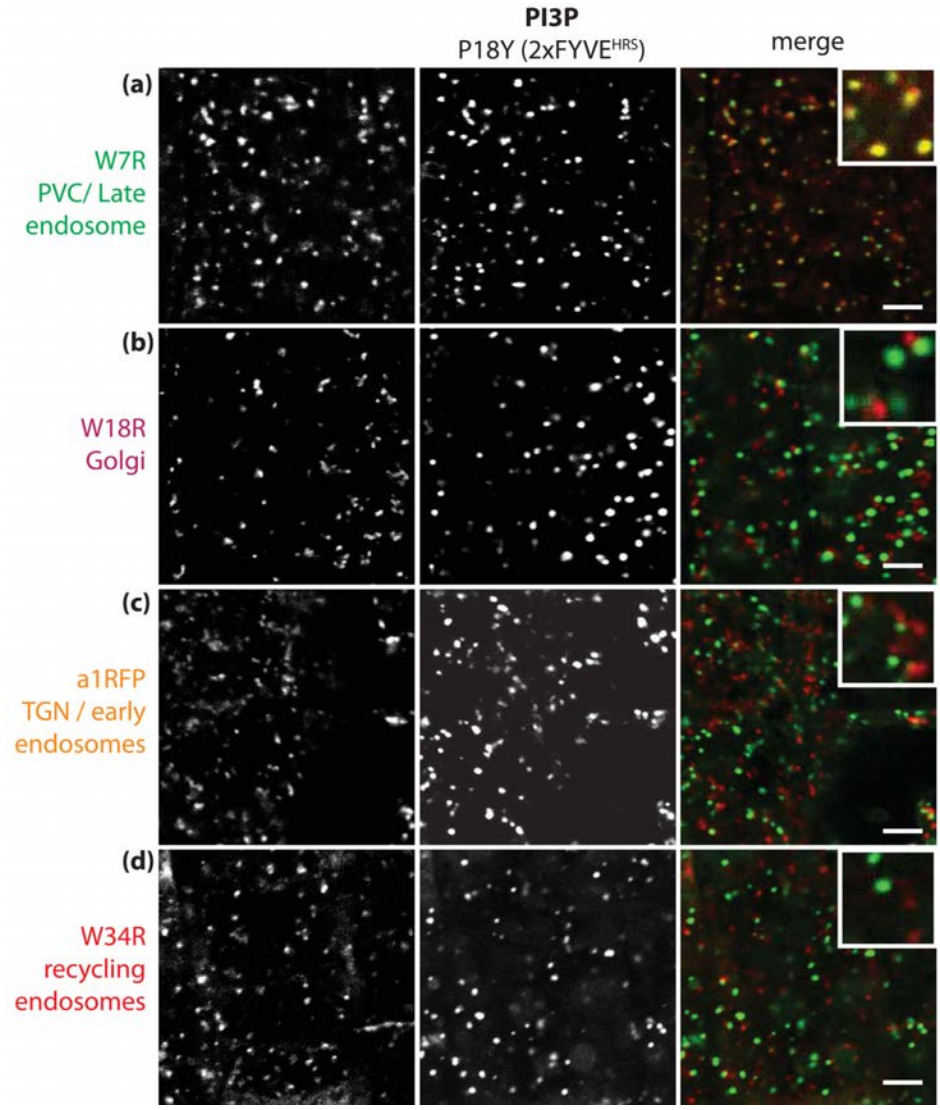

Figure 7. CITRINE-2xFYVE^{HRS} localises to late endosomes in Arabidopsis root epidermis

(a-d) Confocal pictures of root epidermal cells co-expressing CITRINE-2xFYVE^{HRS} with intracellular compartment markers fused with a red fluorescent protein: (a) W7R (late endosomes/PVC), (b) W18R (Golgi apparatus), (c) VHAa1-RFP (early endosomes/TGN) and (d) W34R (recycling endosomes). Left pictures correspond to the compartment markers, middle pictures correspond to CITRINE-2xFYVE^{HRS} (both depicted in grey scale for increased contrast), while the right pictures correspond to the overlay of both channels with the compartment markers in red and the 2xFYVE^{HRS} sensor in green. Scale bars 5 μm.

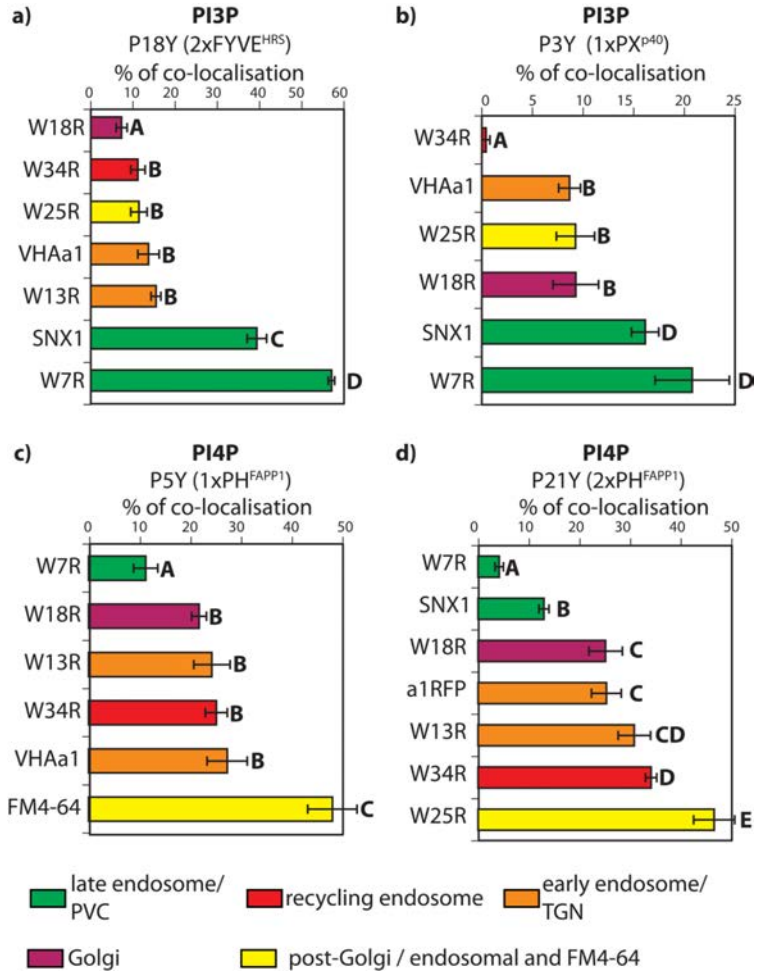

Figure 8. Quantitative analysis of intra-cellular co-localisations

Quantitative co-localisation data obtained by object-based analysis between various compartment markers and 2xFYVE^{HRS} (a), 1xPX^{p40} (b), 1xPH^{FAPP1} (c), 2xPH^{FAPP1} (d). Error bars represent standard deviation. Bold capital letters indicate statistical difference ($p<0.05$) according to Steel-Dwass-Critchlow-Fligner bilateral test. Co-localisations were quantified in 30 cells per conditions only on intra-cellular signals (i.e. excluding the PM).

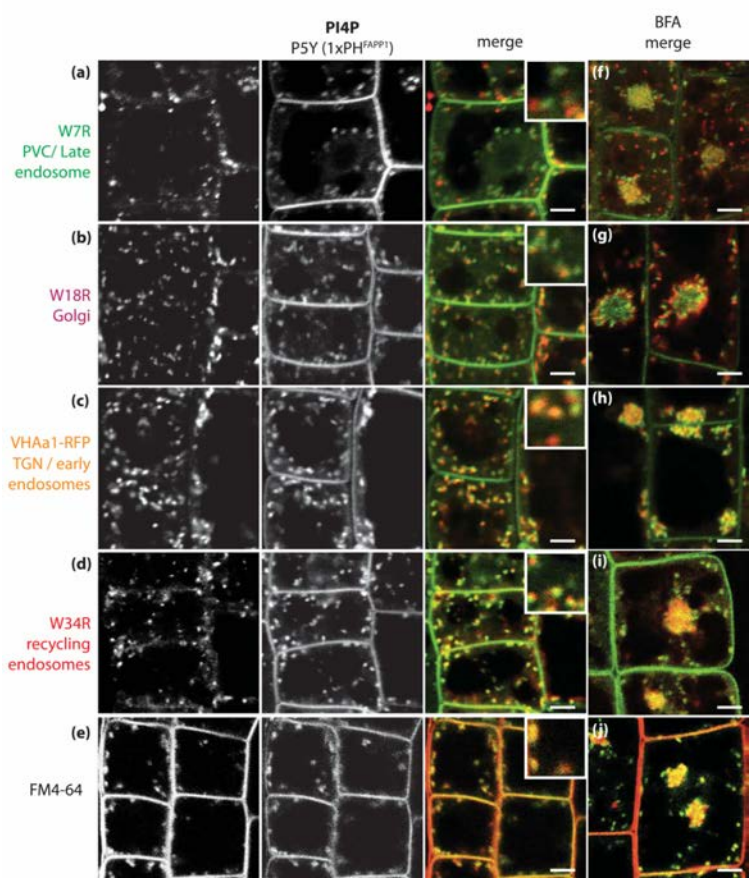

Figure 9. Intra-cellular CITRINE-1xPH^{FAPP1} localises to post-golgi/endosomal compartments in Arabidopsis root epidermis

(a-d) Confocal pictures of root epidermal cells co-expressing CITRINE-1xPH^{FAPP1} with intracellular compartment markers fused with a red fluorescent protein: (a) W7R (late endosomes/PVC), (b) W18R (Golgi apparatus), (c) VHAa1-RFP (early endosomes/TGN) and (d) W34R (recycling endosomes). (e) Co-localisation with red endocytic tracer FM4-64. Left pictures correspond to the compartment markers (a-d) or FM6-64 (e), middle picture correspond to CITRINE-1xPH^{FAPP1} (both depicted in grey scale for increased contrast), while the two right columns of pictures correspond to the overlay of both channels with the compartment markers in red and the 1xPH^{FAPP1} sensor in green. (f-j) Co-localisation between CITRINE-1xPH^{FAPP1} and the corresponding compartment markers in the presence of BFA at 25 μM for 1 hour. Scale bars 5 μm.

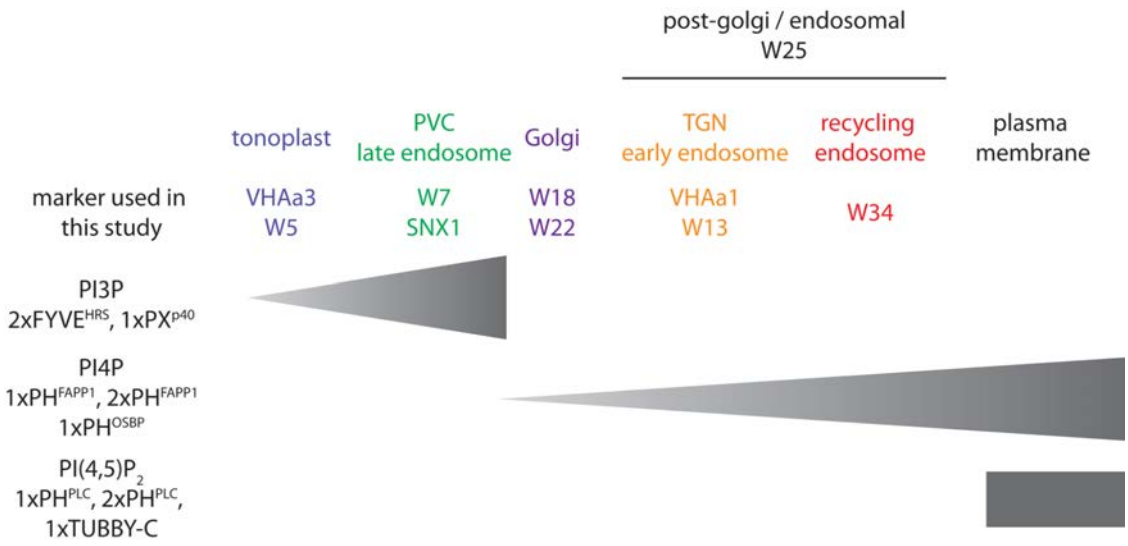

Figure 10. Summary of PI3P, PI4P and PI(4,5)P_2 localisation in Arabidopsis epidermal cells
The gradient of intensity of localisation in intracellular compartments is represented by the broadness of the triangle.

Table 1

In vitro and in vivo PIP binding specificities of LBDs used in the PIPline collection

Domain	In vitro interaction	In vitro techniques	Kd	In vivo localizatio : yeast	In vivo localization animal cells	Evidences for in vivo binding (yeast/animal)	References
1xFYVE^{HRS}	PI3P	liposomes, fat blot, SPR, crystalography, monolayer penetration analysis	≈0.5μM	endosome / vacuole	mostly cytosolic	Dependent on type III PI3K (VPS34), sensitive to PI3K inhibitor (e.g. Wm)	Burd *et al.*, 1998; Gillooly *et al.*, 2000; Misra and Hurley 2000; Sankaran *et al.*, 2001; Raiborg *et al.*, 2001; Stahelin *et al.*, 2002; He *et al.*, 2009
1xPX^{p40}	PI3P	liposomes, fat blot, SPR, ITC, crystalography, monolayer penetration analysis	≈5μM	endosome / vacuole	early endosome	Dependent on type III PI3K (VPS34), sensitive to PI3K inhibitor (e.g. Wm)	Ago *et al.*, 2001; Kanai *et al.*, 2001; Bravo *et al.*, 2001; Ellson *et al.*, 2001; Zhan *et al.*, 2002, Malkova *et al.* 2006
1xPH^{FAPP1}	PI4P	liposomes, fat blot, SPR, crystalography, monolayer penetration analysis, NMR spectroscopy	≈18.6 μM	golgi	golgi	Dependent on PI4K (Pik1 in yeast, PI4K-IIIa in human), in vivo protection of PI4P, expression mask binding of anti-PI4P antibody, sensitive to PI4K inhibitor (e.g. PAO), sensitive to PI4-pptases (e.g. SAC1, Inp54)	Dowler *et al.*, 2001; Levine *et al.*, 2002; Godi *et al.* 2004; Balla *et al.*, 2005; Hammond *et al.*, 2009a, Lenoir *et al.*, 2010; He *at al.*, 2011
1xPH^{OSBP}	PI4P	fat blot (this study), liposomes, SPR	≈3.5μM	golgi	golgi	Dependent on PI4K (Pik1 in yeast, PI4K-IIIa in human), sensitive to PI4K inhibitor (e.g. PAO), sensitive to PI4-pptases (e.g. SAC1, Inp54)	Levine *et al.*, 1998; Levine *et al.*, 2002; Balla *et al.*, 2005; Niu *et al.*, 2013
1xPH^{PLC}	PI(4,5)P2	fat blot (this study), liposomes, SPR, crystalography, NMR spectroscopy	≈1μM	mostly cytosolic	PM	localization sensitive to PLC inhibitor and activator sensitive to 5-pptases (e.g. INPP5B, OCRL), dependent on PI4P-5Kinase (e.g. mss4), expression mask binding to anti-PI(4,5)P2 antibody	Ferguson *et al.*, 1995; Lemmon *et al.*, 1995; Levine *et al.*, 2002; Varnai *et al.*, 2002; Tuzi *et al.*, 2003; Yu *et al.*, 2004; Szentpetery *et al.*, 2005; Zoncu *et al.*, 2007 Hammond *et al.*, 2009a; Hammond *et al.*, 2009b
1xTUBBY-C	PI(4,5)P2, PI(3,4)P2, PI(3,4,5)P3	fat blot (this study), liposomes, SPR, crystalography	nd	PM (*this study*)	PM	localization sensitive to PLC inhibitor and activator, sensitive to 5-pptases (e.g. INPP5B, OCRL)	Santagata *et al.*, 2001; Quinn *et al.*, 2008; Szentpetery *et al.*, 2009; Hammond *et al.*, 2012

Abbreviations: PI3K (PI3-kinase); PI4K (PI4-kinase); pptase (phosphatase); SPR (Surface Plasmon Resonance); ITC (Isothermal Titration Calorimetry), NMR (Nuclear Magnetic Resonance).

ANNEXE II : Anionic lipids and the maintenance of membrane electrostatics in eukaryotes

Published in final edited form as:
Methods Mol Biol. 2016 ; 1376: 175–194. doi:10.1007/978-1-4939-3170-5_15.

Guidelines for the use of protein domains in acidic phospholipid imaging

Matthieu Pierre Platre and **Yvon Jaillais***
CNRS, INRA, ENS Lyon, UCBL, Université de Lyon, Laboratoire de Reproduction et Développement des Plantes, 46 Allée d'Italie, 69364 Lyon Cedex 07, France.

Abstract

Acidic phospholipids are minor membrane lipids but critically important for signaling events. The main acidic phospholipids are phosphatidylinositol phosphates (PIPs also known as phosphoinositides), phosphatidylserine (PS) and phosphatidic acid (PA). Acidic phospholipids are precursors of second messengers of key signaling cascades or are second messengers themselves. They regulate the localization and activation of many proteins, and are involved in virtually all membrane trafficking events. As such, it is crucial to understand the subcellular localization and dynamics of each of these lipids within the cell. Over the years, several techniques have emerged in either fixed or live cells to analyze the subcellular localization and dynamics of acidic phospholipids. In this chapter, we review one of them: the use of genetically encoded biosensors that are based on the expression of specific lipid binding domains (LBDs) fused to fluorescent proteins. We discuss how to design such sensors, including the criteria for selecting the lipid binding domains of interest and to validate them. We also emphasize the care that must be taken during data analysis as well as the main limitations and advantages of this approach.

Keywords

Biosensor; phosphatidylinositol phosphate; phosphatidic acid; phosphatidylserine; genetically encoded probes; lipid binding domain; live imaging; PtdIns; lipid signaling; Phospholipase

Introduction

Anionic phospholipids have a negatively charged head group, which gives them specific properties, notably in terms of protein-lipid interactions. The main acidic phospholipids are phosphatidylserine (PS), phosphatidic acid (PA) and phosphatidylinositol (PI and PIPs). In erythrocytes, the PS/PA/PI proportions (by weight) are approximately 8.5%, 1.5% and 1.0%, respectively, but these may vary according to species or cell types [1].

Phosphatidylinositolphosphates (PIPs) are minor phospholipids, accounting less than one percent of total membrane lipids, yet they are of disproportionate importance for many membrane-associated signaling events: i) PIPs can be precursors of various second messengers (*e.g.* Inositol-3-Phosphate, Diacylglycerol), ii) they can activate many ion

*corresponding author: Yvon Jaillais, yvon.jaillais@ens-lyon.fr.

channels and enzymes, iii) they are involved in membrane trafficking and, iv) they can recruit proteins to the plasma membrane or intracellular compartments through several structured interaction domains (*e.g.* Pleckstrin Homology domain (PH), Phox homology domain (PX), Fab1/YOTB/Vac1/EEA1 domain (FYVE)) [1-4]. PIPs can be phosphorylated at different positions of the inositol head group, which can generate up to seven different PIP species that include three phosphatidylinositol monophosphates [PI3P, PI4P and PI5P], three phosphatidylinositol biphosphate [$PI(3,4)P_2$, $PI(3,5)P_2$ and $PI(4,5)P_2$] and one phosphatidylinositol triphosphate [$PI(3,4,5)P_3$]. PIP kinases and phosphatases modify the phosphorylation state of the inositol head group, and phospholipases hydrolyze PIPs to release the soluble head group into the cytosol [1,4]. The combined action of these enzymes produces the PIP signature of a cell, where certain membrane compartments are enriched or depleted of specific PIPs, contributing to their functional identity [1,3,4].

Phosphatidylserine (PS) is an important constituent of eukaryotic membranes and the most abundant acidic phospholipid (up to 10% of biological membrane) [1,5-7]. PS is involved in many signaling pathways, as it can recruit and/or activate proteins, notably through their stereospecific PS-binding domain and by regulating membrane surface charges [1,5,6,8]. One particularity of PS is its role as a lipid landmark in both extracellular and intracellular membranes leaflets. For instance, extracellular PS (exposed on the outer leaflet of the plasma membrane) serves as an “eat me” signal for the clearance of apoptotic cells [7,9]. Intracellular PS regulates a number of signaling pathways involving kinases, small GTPases and fusogenic proteins [5,8].

Phosphatidic acid (PA) is a precursor for the biosynthesis of many lipids [10,11]. Indeed, various enzymes add different chemical group on PA, such as Choline, Ethanolamine, Serine or Inositol to produce phosphatidylcholine (PC), phosphatidylethanolamine (PE), phosphatidylserine (PS) and phosphatidylinositol (PI). PA is also the substrate of Phospholipase D, which produces diacylglycerol, a second messenger involved in many signaling pathways [12]. Furthermore, the biophysical characteristics of PA influence membrane properties such as membrane curvature or membrane fusion [1,13,14]. In addition, PA itself recruits various proteins to membranes and PA-protein interaction activates many enzymes. As such, PA can be considered a *bona fide* lipid second messenger.

Subcellular localization of anionic phospholipids at a glance

The localization of the various acidic phospholipid species has been an intense area of research [4,15,16]. Functional studies, together with biochemical and live-cell imaging, have built a relatively clear picture of the precise location of most acidic phospholipids in yeast (Figure 1A), cultured mammalian cell lines (Figure 1B), and plants (Figure 1C).

In animal cells, PI3P mainly resides in early endosomes, where it controls endosome maturation, cargo protein degradation/recycling and cell signaling notably through its interplay with Rab5 GTPases [3] (Figure 1B). During autophagy induction in animal (*e.g.* triggered by amino acid starvation), PI3P is transiently produced at the Endoplasmic Reticulum (ER) membrane by the PI3-kinase VPS34 [17] (Figure 1B). PI3P production in the ER supports the formation of the omegasome a specialized ER domain at the origin of

the formation of the autophagophore (also known as the isolation membrane), that itself elongates to form the autophagosome (*i.e.*, double membrane vesicles) [17,18].

In yeast and animals, PI4P is located in at least two different pools in the cell, one at the Golgi apparatus and the other one at the plasma membrane [19-21] (Figure 1A and B). Each pool of PI4P has separate and diverse functions. The main function of PI4P at the Golgi is to control membrane trafficking events, in particular, the sorting of proteins toward the plasma membrane or endosomes [3,22-24]. PI4P, together with other PIPs, recruits strong cationic proteins to the plasma membrane [25]. In yeast, the plasma membrane pool of PI4P controls ER-to-plasma membrane tethering sites that regulate cell signaling and ER morphology [26-28] (Figure 1A). Furthermore, plasma membrane-localized PI4P is a source of $PI(4,5)P_2$ in animal cells [23,29]. A pool of PI4P has been recently described in late endosomes/lysosomes in animal cells but the function of PI4P in these compartments remains to be fully elucidated [20] (Figure 1B).

In mammals, the rare phosphoinositide, PI5P, accumulates in the nucleus and at the plasma membrane under certain stimuli, or during infection by certain pathogens such as the bacterium *Shigella flexneri* [30-34] (Figure 1B). Furthermore, it was recently showed that PI5P transiently accumulates at the ER during autophagy induction and can substitute PI3P at the omegasome [35] (Figure 1B).

In both animal and yeast, $PI(3,5)P_2$ is thought to reside in late endosomes, where it regulates lysosome/vacuole biogenesis [36-38] (Figure 1A and B). In every eukaryotes, $PI(4,5)P_2$ is localized at the plasma membrane where it has a large spectra of action such as anchoring signaling and membrane trafficking proteins [2,4,25,39-41] (Figure 1A-C). In addition, $PI(4,5)P_2$ controls ion channel activation and is a substrate of Phospholipase C, which triggers synthesis of the second messengers inositol 1,4,5-trisphosphate and diacylglycerol [2,4,42]. $PI(4,5)P_2$ is the source of $PI(3,4,5)P_3$, which together with $PI(3,4)P_2$, accumulate at the plasma membrane but only when specific signaling pathways are activated (e.g. growth factor signaling) [2,4](Figure 1B). $PI(3,4)P_2$ also controls late-stage clathrin-coated pit formation, independent of $PI(3,4,5)P_3$ [41,43].

PS is synthesized in the ER lumen and reaches the cytosolic leaflet through the action of P4-ATPases flipases [7,9]. Depending on the species, this translocation occurs either at the TGN and/or at the plasma membrane. This asymmetric PS distribution can be used as a signaling device by the regulated activation of scramblases, which rapidly exposes PS on the extracellular leaflet of the plasma membrane and plays important roles in blood clotting and apoptosis [7,16], as above-mentioned. On the cytosolic leaflet, PS mainly accumulates at the plasma membrane in yeast (Figure 1A), while it is present both at the plasma membrane and throughout the endosomal system in animal cells (Figure 1B) [5,8,44].

Like PS, PA is synthetized in the ER in all eukaryotic cells [10,11]. PA can also be synthesized *de novo* in other organelles such as for example mitochondria or chloroplasts [10]. However, the main pool of PA that is facing the cytosol is likely localized at the plasma membrane. This pool is locally produced by Phospholipase D and Diacylglycerol kinases [12].

Detection of acidic phospholipids by Lipid Binding Domains

Anionic lipids such as phosphoinositides are markers of organelle identity. Moreover, because they act as second messengers, their quantity varies rapidly (*i.e.* within minutes) upon stimulation of various signaling pathways. It is therefore key to be able to track the amount of these lipids in real time and at subcellular resolution. However, the investigation of lipid subcellular localization has proven to be difficult for various reasons. First, it is obviously not possible to label lipids by direct tagging with fluorescent proteins (FPs). Second, common methods of cell or tissue fixation do not fix lipids and are therefore not compatible with the study of lipid subcellular localization. Yet, many techniques have been used over the years to uncover the subcellular localization of acidic phospholipids and their respective dynamics upon various stimulations. These techniques were used either in fixed cells, such as for example immuno-labeling with anti-PIP antibodies [19] or live cells, such as for example direct labeling of lipid molecules or the use of genetically encoded biosensors [45]. The later method has been extensively used to indirectly reveal the localization and dynamics of PIPs in intact living cells and, currently, is probably the most widespread technique used to localize acidic phospholipid species [4,40,45]. Importantly, this method is directly amenable to live imaging techniques. Genetically encoded biosensors consist of lipid-binding domains (LBDs) that interact specifically with known lipid species *in vitro* (Figure 2A and B). These domains localize in the compartments of the cell that accumulate the targeted PIPs and can be easily traced when fused with a fluorescent protein (Figure 2A and B). LBDs are globular domains that mostly bind to acidic phospholipids such as PIPs and PS [1,46]. Broadly, they fall into two categories: non-specific LBDs and stereospecific LBDs. Non-specific LBDs recognize general membrane properties, such as curvature, lipid packing defects or charges [1,14]. Examples of non-specific LBDs include the BAR domain that recognizes membranes with a specific curvature or the KA1 domain that binds highly electronegative membrane [1,47]. Stereospecific LBDs bind particular acidic lipids with sometime exquisite specificity. PH, PX, FYVE and some C2 domains belong to this category [1,46]. To date most LBDs that have been used to report on lipid localization are stereospecific LBDs, yet in recent years non-specific LBDs have also been exploited to probe some basic properties of the cytosolic leaflet of membrane compartments. For example, the KA1 domain has been used as a reporter of membrane surface charges in human cells [25].

Design of genetically encoded acidic phospholipid probes

Construct strategy

To visualize a certain lipid species, the strategy is to fuse the LBD of interest with a fluorescent protein (FP) (Figure 2A). Most LBDs can be fused either to their N-terminal or C-terminal end without affecting their binding properties since they are derived from multi-domain proteins. To maximize the chances to obtain a stable and functional fusion protein, we usually place the LBD where it would be in its original protein context and separates it from the fluorescent protein by a short flexible linker (e.g. SAGGSAGG or GAGARS linkers). For example the PX domain of the $p40^{phox}$ protein is localized at its N-terminus. We therefore replaced the C-terminal part of this protein with fluorescent proteins, giving

PX^{p40}-FP constructs (Figure 2A). A fluorescent protein is usually sufficient to report each lipid, however methods based on Förster Resonance Energy Transfert (FRET) have also been used [48-51] (Figure 2C).

Most genetically encoded lipid sensors are soluble proteins and therefore are designed to report only the lipid species that are facing the cytosol. However, addition of a signal peptide to the probe has been generated to secrete the LBD and to follow the accumulation of its cognate lipid along the secretory pathway, such as for example its presence in the ER lumen [9]. However, because of the resolution limits of conventional light microscope, this approach requires Transmission Electron Microscopy (TEM) to distinguish between membrane-bound LBDs and soluble LBDs in the organelle's lumen.

Choosing the appropriate LBD, consideration on LBD specificity

The most critical aspect in the design a genetically encoded sensor for a given lipid is to take into account binding specificity and affinity of the LBDs. If one wants to report the localization of a given lipid, the ideal probe should be highly specific for this lipid. However, very few, if any, LBDs are completely specific for only one lipid. Most of the time, their affinity is greater for a lipid than for the others, yet this is enough to confer a specificity of recognition *in vivo*. Nonetheless, this should be verified, if possible by several *in vitro* lipid-binding assays. Such assays include qualitative methods (*e.g.* lipid-protein overlay assays) and more quantitative techniques such as liposome-binding assays, surface plasmon resonance or isothermal titration calorimetry. Finally, the structure of the LBD-lipid complex (*e.g.* by x-ray crystallography or NMR spectroscopy) might help to rationalize how the domain specifically recognizes a particular phospholipid headgroup [1].

Moreover, it is common that LBDs require the coincidence detection of a given lipid together with another molecule to promote membrane binding. The most widespread examples are LBDs that bind their target lipid in a calcium-dependent manner (*e.g.*, most C2 domain binds their lipids, mostly PS, only in the presence of Ca2+) [1]. Some LBDs also require the coincidence binding of another protein [1] (Figure 2B). For example, the PH domain of FAPP1 (and to a lesser extend the PH domain of OSBP) interacts with PI4P preferentially in the presence of the small GTPase ARF1 [21] (Figure 2B). This requirement for coincidence binding can lead to confounding results that are sometime difficult to evaluate. For example, the PH domain of FAPP1 is capable of binding PI4P alone, but *in vivo* membrane binding is enhanced by the presence of ARF1 [21]. Because ARF1 mainly localizes at the Golgi and TGN, two compartments that are enriched in PI4P, the PH domain of FAPP1 (and OSBP) preferentially localizes to these two compartments, although PI4P is also present at the plasma membrane [21] (Figure 1). This particular result led to the long-lasting belief that PI4P is mainly localized at the Golgi and TGN. Therefore, the PH domains of FAPP1 and OSBP are not optimum to report PI4P in all membranes. However, because PI4P association is required for membrane binding of these LBDs, they are suitable PI4P reporters in the Golgi and TGN and have been successfully used to this aim [52] (Figure 2B). When available, the use of probes that do not require coincidence binding with other molecules should be favored. Alternatively, if such LBD has not been characterized

yet, the use of LBD requiring coincidence binding should not be discarded entirely, but the results should be interpreted accordingly.

Choosing the appropriate LBD, consideration on LBD affinity

The second parameter that one should take into account is the relative binding affinity of the LBD for its target lipid. This is also an important parameter, since difference in relative affinity might result in different subcellular localization of the probe. The first obvious caveat is when the binding affinity is too weak, which leads to mostly or exclusively soluble localization of the probe (their localization by default, in the absence of binding, being soluble in the cytosol). For example, a single PI3P-binding FYVE domain is soluble when express in mammalian cells and only a tandem dimer construct (2xFYVE domain) is localized to early endosomes, where PI3P accumulates [53]. This leads to the second caveat, which is when binding affinities are too high and high-affinity LBDs might outcompete the lipid binding of endogenous proteins, leading to toxicity upon expression of the probe. However, because any given cell expresses hundreds of proteins harboring LBDs at the same time, it is unlikely that transgenic expression of LBDs will outcompete all the other lipid-binding proteins. It is however common that expression of acidic phospholipid probes affects some signaling pathways. It is therefore advisable to test the toxicity due to the expression of the probe and to favor cells or transgenic organisms with relatively weak expression of the probe (for example by using promoters that confer mild expression).

One should choose LBDs that have affinity ranging in between the two extreme scenarios discussed above. Because there is no way to predict *in silico* how a LBD will behave *in vivo* in a particular system, it is preferable to use, when available, several probes to report on the same lipid species. Because of slight changes in either binding affinity or specificity, we often observed that several reporters for the same lipid might harbor different, although overlapping, localization [40]. For example in Arabidopsis root, a 2xFYVE PI3P reporter is localized to late endosomes (where PI3P accumulates in plants, Figure 1C), while the PX domain of the $p40^{phox}$ protein, also a well characterized PI3P binding domain, localizes to both late endosomes and tonoplast (the membrane of the plant cell vacuole) [40] (Figure 1C). Although, it is not entirely understood how these differences in localization might be explained, these results are useful for several reasons. First, both probes localize to late endosomes, providing confirmation that PI3P is likely to accumulate in this compartment in plants. Second, because the PX domain also localizes to the tonoplast, this raised the possibility that PI3P might localized to this compartment. Although this conclusion should be taken with care, since it was confirmed with only one of the two LBD, it provided us with a new testable hypothesis. One way to explain the dissimilar localization of the FYVE and PX domains is to consider their difference in relative binding affinity. In fact, high affinity LBDs are expected to localize more specifically to the membrane compartment that accumulates the most its cognate lipid, while lower affinity LBDs are more likely to have a broader localization domain (Figure 3). Low affinity sensors are less efficient in discriminating between two membranes with two different concentrations of their targeted lipid species and as a result they might be targeted to both of these membranes (Figure 3A). By contrast, high affinity sensors will have increased dwell time at the membrane that is the most enriched in the targeted lipid and they will accumulate preferentially in this

compartment (Figure 3B). In other words, high affinity sensors work like a “Velcro fastener”: they will grab more strongly to a surface with more spikes (in this case the spikes being an acidic lipid) (Figure 3B). Therefore, it is possible that the high affinity 2xFYVE probe mainly localizes to late endosomes because this could be the cell compartment where PI3P accumulates the most, while the PX-based probe localizes also to the tonoplast because this compartment might also have PI3P but to a lesser extent than late endosomes. This is further exemplified when comparing the localization of single versus tandem dimer LBDs. For example in Arabidopsis, we found that the high affinity PI4P sensor $2xPH^{FAPP1}$ was more strongly localized to the plasma membrane and less to endomembrane compartments than the low affinity sensor $1xPH^{FAPP1}$ [40] (Figure 3C). When kept in mind, these variations in localization can actually be exploited to address the relative concentration of a given lipid in several membranes. For example, the results presented Figure 3C suggest that the concentration of PI4P is greater at the plasma membrane than in intracellular compartments in plants [40].

Validation of acidic phospholipid sensors

As mentioned in the previous section, it is important to test the *in vitro* binding specificity of a particular LBD. However, this apparent *in vitro* specificity does not necessarily reflect its localization *in vivo* or the localization of its cognate lipid in cells. In fact, a comprehensive study on all yeast PH domain suggest that *in vitro* binding specificity is not a good indicator of the localization of this domain *in vivo* and does not always predict whether the LBD will be a useful lipid probe or not [54]. Expression of each LBD has to be tested *in vivo* and if possible validated. A first screen will rapidly discard domains that do not properly accumulate, do not localizes to any membrane compartment or induce strong phenotypes [40]. It is then important to check whether the localization of the probe is in fact dependent on the presence of its cognate lipid. Among other approaches, this could be achieved by pharmacological or genetic inhibition of the lipid biosynthetic enzymes (e.g. phosphatidylinositol kinases, phosphatidylinositol phosphatases, phospholipases…). For example, a loss-of-function mutation in *mss4*, the yeast PI4P 5-kinase, leads to a soluble localization of a $2xPH^{PLC}$ probe that normally highlights $PI(4,5)P_2$ at the yeast plasma membrane [21]. An elegant approach is also the targeted recruitment of lipid kinases or phosphatases to a specific compartment using small molecules or light, because these approaches mediate rapid lipid modifications that are spatially restricted [20,25,39,42,55-59]. The localization of an ideal lipid reporter should be dependent on its cognate lipid in both loss- and gain-of-function experiment but not dependent on the production/loss of unrelated lipids. In other word, the probe should leave its endogenous membrane compartment upon loss of its cognate lipid at that membrane. Conversely, it should be recruited to a new membrane compartment upon production of its cognate lipid in this organelle. To date, very few probes have been tested extensively with such gain- and loss-of-function experiments. Besides, they are rarely so versatile, probably because of their requirement on coincidence binding to other molecules (see above the section on the design of genetically encoded acidic phospholipid probes). However, the recent characterization of the P4M PI4P reporter is a must read as an example on how to validate an acidic phospholipid sensor *in vivo* [20].

In order to validate the localization of a lipid sensor and therefore the cellular localization of a particular lipid, it is important to accumulate several lines of evidence to confirm this localization, such as for example the use of alternate techniques (immunolocalization, direct lipid labeling, …), the similar localization of independent LBDs known to bind the same lipid and/or the colocalization of the probe with endogenous lipid binding proteins.

Well-characterized acidic phospholipid sensors

Several LBDs have been used over the years in different systems and have been shown to behave robustly. In this section we will briefly describe these well characterized genetically encoded lipid sensors and, if applicable, point out their respective advantages and limitations. It is nonetheless important to consider the controls described above when using one of these reporters in a new biological context (*e.g.*, new species, new cell type).

Phosphoinositide sensors

PI3P

The most widely used probe for PI3P are derived from the PX domain of the $p40^{phox}$ protein and the tandem dimer of the FYVE domains (2xFYVE) from the HRS or EEA1 proteins [1,46,53,60,61]. These domains have been extensively used over the years and are well-accepted PI3P reporters. In animal cells, they mainly report the localization of PI3P in early endosomes [53], but plasma membrane localization has been observed in certain conditions (e.g. insulin treatment [62,63]). However, they do not highlight the pool of PI3P at the ER upon autophagy induction.

PI4P

As discussed above (see “choosing the appropriate LBD, consideration on LBD specificity” section), the PH domain of FAPP1 and OSBP report on the localization of PI4P at the Golgi/TGN but not in other membrane compartments due to their requirement for ARF1 binding [21]. The PH domain of the yeast OSBP-like protein OSH2 is not dependent on ARF1 binding [64]. It is localized both at the Golgi and plasma membrane in yeast but it is localized mainly at the plasma membrane and only weakly at the Golgi in mammalian cells [20,64]. Therefore, PH^{OSH2} seems to be a better reporter of plasma membrane PI4P than PH^{FAPP1} or PH^{OSBP}. The exact reasons for the plasma membrane preference of PH^{OSH2} are unknown, but might be due to residual $PI(4,5)P_2$ binding [20,64]. The newly described PI4P reporter, called P4M, seems to be able to report both Golgi and plasma membrane PI4P localization in animal cells and it detects as well a previously uncharacterized pool of PI4P in late endosomes [20]. This reporter seems to be superior to the PH domains of FAPP1, OSBP and OSH2 since it is very specific to PI4P and does not require coincidence binding with other proteins. However, because it has been described fairly recently, it is not yet clear whether this probe will behave similarly in a broad range of cellular contexts.

PI5P

Few PI5P-binding domains have been characterized, including the PH domains of Dok-1 and Dok-2 [34,32] and the PHD domain of ING2. A triple repeat of this domain

(3xPHD^{ING2}) has been used as a sensor of PI5P localization. It mainly localizes to the nucleus in animal cells [30,32]. However, immunolocalization and mass spectrometry methods suggest that PI5P localizes in membrane compartments such as the plasma membrane or endosomes [32,65]. 3xPHD^{ING2} was recently found to accumulate in omegasomes during autophagy induction by glucose starvation [35]. However, 3xPHD^{ING2} has not extensively been used over the years, perhaps because its expression inhibits PI5P-dependent processes [32]. Therefore, this reporter should be used with caution.

PI(4,5)P_2

The PH domain of PLCdelta1 (hereafter referred to as PLC) was one of the first LBD to be used as a lipid biosensor [4,45,66]. It has an exquisite selectivity for PI(4,5)P_2 and has been robustly expressed in many different cellular systems including yeast, mammalian and plant cells [4,21,32,40,66]. It allowed for example to monitor the reversible PI(4,5)P_2 hydrolysis triggered upon PLC activation; i.e. relocalization of membrane-bound PH^{PLC} into the cytosol upon PLC activation by agonists [66]. The C-terminal domain of the TUBBY protein has also been used as a PI(4,5)P_2 reporter [40,67-69], however this protein domain binds PI(3,4)P_2 *in vitro* in addition to PI(4,5)P_2 [69]. Both reporters are localized exclusively to the plasma membrane, while PI(4,5)P_2 has been found in Golgi and ER membrane. This point out to a possible limitation of these probes or simply to the fact that the concentration of PI(4,5)P_2 in these compartments is not sufficient to trigger membrane binding at these sites. It is also possible that the physico-chemical properties of these compartments (such as their packing or curvature) are not compatible with binding of these domains. Finally, we cannot exclude that both LBD actually rely on coincidence binding of PI(4,5)P_2 and a plasma membrane-resident protein. However, the fact that both reporters behave similarly in many different cellular contexts and species argues against this hypothesis. Altogether, PH^{PLCd1} and TUBBY-C are robust reporters of PI(4,5)P_2 dynamics at the plasma membrane but might not reflect the possible pool of this lipid in other membrane compartments.

PI(3,5)P_2

The ENTH domains of the yeast proteins Ent3p and Ent5p as well as the PROPPIN domains of Svp1p protein binds to PI(3,5)P_2 *in vitro* [36,37,70]. These proteins localize to the membrane of the yeast vacuole suggesting that PI(3,5)P_2 accumulates in this compartment [36,37,70], but expression of the isolated ENTH or PROPPIN domains does not give consistent results when express in heterologous systems such as animal cells or plants (personal communication). Recently, the cytoplasmic phosphoinositide-interacting domain (ML1N) of the transient receptor potential Mucolipin 1 (TRPML1) has been described to bind PI(3,5)P_2 *in vitro* in the nanomolecular range [38]. A 2xML1N construct was used successfully to report on the localization of PI(3,5)P_2 in late endosomes and lysosomes in animal cells [38]. Yet, this new tool remains to be tested in additional cellular contexts.

PI(3,4)P_2

Some PX and PH domains are binding PI(3,4)P_2 *in vitro* (e.g. the PX domain of p47 and the PH domains of TAPP1 and TAPP2) [60,71]. Mainly, PH^{TAPP1} has been used as a read-out

of $PI(3,4)P_2$ *in vivo* and revealed that this lipid mainly accumulates at the plasma membrane [43,72].

$PI(3,4,5)P_3$

The PH domain of AKT recognizes both $PI(3,4)P_2$ and $PI(3,4,5)P_3$ and has been extensively used as a read out of type I PI3-kinase activity [4,45]. Several PH domains have also been described to recognize specifically $PI(3,4,5)P_3$ but not $PI(3,4)P_2$, such as the PH domains from BTK, GRP1, ARNO or cytohesin1 [1,4,45,46]. $PI(3,4,5)P_3$ does not accumulate at the plasma membrane in the absence of specific stimulus but is synthetized upon stimulation by growth factor or insulin. For example, PH^{BTK} has been used to detect $PI(3,4,5)P_3$ generation at the plasma membrane upon stimulation of fibroblasts by EGF or PDGF [73].

PS

PS-binding C2 domains have been characterized early on, but in many cases, lipid binding occurs only in the presence of calcium [1]. This restricted the use of these domains to study PS localization *in vivo*. Nonetheless, the recombinant purified C2 domain of Annexin A5 has been used to detect the presence of PS on the plasma membrane outer leaflet, but this assay requires the presence of exogenous calcium and is not compatible with live imaging of intracellular events [8]. However, the C2 domain of Lactadherin Synthase 1 (LactC2) was shown to bind specifically PS in the absence of calcium and turned out to be an excellent PS reporter in many systems, including yeast and animal cells [8,9,15,74,75]. The PH domain of EVECTIN2, a protein localized to the recycling endosomes and involved in membrane traffic, was also shown to specifically bind PS *in vitro* and to report PS localization *in vivo* in human cells [44].

PA

To date, only PA-binding linear motifs but no PA-binding domains have been found and characterized [1]. These short stretches of sequences do not seem to have a particular globular structure and are often rich in basic amino acids. As such, these PA-binding motifs are relatively poorly stereospecific and are able to bind, although with various affinities, other acidic phospholipids [1,13]. Biosensors using these PA-binding motifs rather than LBDs have been used, such as the PA-binding sequence of the yeast SNARE protein, spo20p, or the yeast protein kinase, Raf1 [76]. Because of the questionable specificity of these motifs for PA, results obtained with these probes should be cautiously interpreted. Their use has nonetheless been instrumental to address some aspects of PA localization and dynamics [76-78].

Special care and caveat of the approach

We have highlighted some of the limitations and important controls that must be carried out while analyzing results deduced from genetically encoded lipid biosensors throughout this chapter. However, there are additional potential pitfalls of this approach that should also be considered. We have already covered potential problems due to toxicity. This toxicity might arise, in part, because of competition between endogenous protein and transgenically expressed LBDs for binding the same lipid. This situation is likely to occur when the

transgene is overexpressed by strong constitutive promoters and we advocate for the use of mild promoters and/or for the selection of cells or organisms that express weak-to-intermediate level of the reporters. Another strategy is to use inducible expression systems and to study the localization of the lipid sensor at the onset of expression following transgene induction. Furthermore, overexpression of LBDs might induce feedback regulation on the synthesis of the lipid, leading to over-accumulation of this lipid. Systems for mild expression, or better, inducible expression, will reduce these potential feedbacks. It is likely that this lipid over-accumulation is involved in some of the toxicity, which can be observed upon LBD overexpression, possibly by displacing endogenous proteins to new pool of lipids. In addition, it is important to keep in mind that in some cases, phosphoinositide binding LBDs are able to recognize both the membrane bound lipid and its soluble inositol phosphate counterpart, which could influence membrane association. Lastly, it is unlikely that all phosphoinositides are freely available for LBDs binding. Rather, some lipid species might be synthesized locally and readily engage interactions with endogenous lipid binding proteins as they are being synthesized. For example $PI(4,5)P_2$ is a very important lipid involved in clathrin mediated endocytosis (CME) and several proteins involved in this process are known to binds to this lipid, yet a PH^{PLC} reporter does not localize to clathrin coated pits (CCP) [79]. It is fully conceivable that $PI(4,5)P_2$ in CCPs are bound by the CME machinery and therefore not labeled by the PH^{PLC} probe.

Altogether, it is important to keep in mind that the absence of labeling by a lipid reporter is by no mean a proof of the absence of this lipid. However, the detection of a certain lipid pool by a LBD reporter, if controlled adequately (see section “validation of acidic phospholipid sensors”) is a useful tool, directly amenable to live imaging and dynamic studies.

Acknowledgement

We thank Mathilde Simon, Marie-Cécile Caillaud and Marlene Dreux for commenting the manuscript. Y.J. has received funding from the European Research Council - ERC Grant Agreement n. [3363360-APPL] and from the Marie Curie Action – CIG Grant Agreement n. [PCIG-GA-2011-303601] under the European Union's Seventh Framework Programme (FP/2007-2013).

References

1. Lemmon MA. Membrane recognition by phospholipid-binding domains. Nature reviews Molecular cell biology. 2008; 9(2):99–111. doi:10.1038/nrm2328. [PubMed: 18216767]
2. McLaughlin S, Murray D. Plasma membrane phosphoinositide organization by protein electrostatics. Nature. 2005; 438(7068):605–611. doi:10.1038/nature04398. [PubMed: 16319880]
3. Jean S, Kiger AA. Coordination between RAB GTPase and phosphoinositide regulation and functions. Nature reviews Molecular cell biology. 2012; 13(7):463–470. doi:10.1038/nrm3379. [PubMed: 22722608]
4. Balla T. Phosphoinositides: tiny lipids with giant impact on cell regulation. Physiological reviews. 2013; 93(3):1019–1137. doi:10.1152/physrev.00028.2012. [PubMed: 23899561]
5. Kay JG, Grinstein S. Phosphatidylserine-mediated cellular signaling. Advances in experimental medicine and biology. 2013; 991:177–193. doi:10.1007/978-94-007-6331-9_10. [PubMed: 23775696]
6. Kay JG, Koivusalo M, Ma X, Wohland T, Grinstein S. Phosphatidylserine dynamics in cellular membranes. Molecular biology of the cell. 2012; 23(11):2198–2212. doi:10.1091/mbc.E11-11-0936. [PubMed: 22496416]

7. Hankins HM, Baldridge RD, Xu P, Graham TR. Role of flippases, scramblases and transfer proteins in phosphatidylserine subcellular distribution. Traffic. 2015; 16(1):35–47. doi:10.1111/tra.12233. [PubMed: 25284293]
8. Yeung T, Gilbert GE, Shi J, Silvius J, Kapus A, Grinstein S. Membrane phosphatidylserine regulates surface charge and protein localization. Science. 2008; 319(5860):210–213. doi:10.1126/science.1152066. [PubMed: 18187657]
9. Fairn GD, Schieber NL, Ariotti N, Murphy S, Kuerschner L, Webb RI, Grinstein S, Parton RG. High-resolution mapping reveals topologically distinct cellular pools of phosphatidylserine. The Journal of cell biology. 2011; 194(2):257–275. doi:10.1083/jcb.201012028. [PubMed: 21788369]
10. van Meer G, Voelker DR, Feigenson GW. Membrane lipids: where they are and how they behave. Nature reviews Molecular cell biology. 2008; 9(2):112–124. doi:10.1038/nrm2330. [PubMed: 18216768]
11. Athenstaedt K, Daum G. Phosphatidic acid, a key intermediate in lipid metabolism. European journal of biochemistry / FEBS. 1999; 266(1):1–16. [PubMed: 10542045]
12. Cazzolli R, Shemon AN, Fang MQ, Hughes WE. Phospholipid signalling through phospholipase D and phosphatidic acid. IUBMB life. 2006; 58(8):457–461. doi:10.1080/15216540600871142. [PubMed: 16916782]
13. Horchani H, de Saint-Jean M, Barelli H, Antonny B. Interaction of the Spo20 membrane-sensor motif with phosphatidic acid and other anionic lipids, and influence of the membrane environment. PloS one. 2014; 9(11):e113484. doi:10.1371/journal.pone.0113484. [PubMed: 25426975]
14. Bigay J, Antonny B. Curvature, lipid packing, and electrostatics of membrane organelles: defining cellular territories in determining specificity. Developmental cell. 2012; 23(5):886–895. doi:10.1016/j.devcel.2012.10.009. [PubMed: 23153485]
15. Kay JG, Grinstein S. Sensing phosphatidylserine in cellular membranes. Sensors (Basel). 2011; 11(2):1744–1755. doi:10.3390/s110201744. [PubMed: 22319379]
16. Leventis PA, Grinstein S. The distribution and function of phosphatidylserine in cellular membranes. Annual review of biophysics. 2010; 39:407–427. doi:10.1146/annurev.biophys.093008.131234.
17. Dall'Armi C, Devereaux KA, Di Paolo G. The role of lipids in the control of autophagy. Current biology : CB. 2013; 23(1):R33–45. doi:10.1016/j.cub.2012.10.041. [PubMed: 23305670]
18. Axe EL, Walker SA, Manifava M, Chandra P, Roderick HL, Habermann A, Griffiths G, Ktistakis NT. Autophagosome formation from membrane compartments enriched in phosphatidylinositol 3-phosphate and dynamically connected to the endoplasmic reticulum. The Journal of cell biology. 2008; 182(4):685–701. doi:10.1083/jcb.200803137. [PubMed: 18725538]
19. Hammond GR, Schiavo G, Irvine RF. Immunocytochemical techniques reveal multiple, distinct cellular pools of PtdIns4P and PtdIns(4,5)P(2). The Biochemical journal. 2009; 422(1):23–35. doi:10.1042/BJ20090428. [PubMed: 19508231]
20. Hammond GR, Machner MP, Balla T. A novel probe for phosphatidylinositol 4-phosphate reveals multiple pools beyond the Golgi. The Journal of cell biology. 2014; 205(1):113–126. doi:10.1083/jcb.201312072. [PubMed: 24711504]
21. Levine TP, Munro S. Targeting of Golgi-specific pleckstrin homology domains involves both PtdIns 4-kinase-dependent and -independent components. Current biology : CB. 2002; 12(9):695–704. [PubMed: 12007412]
22. Cruz-Garcia D, Ortega-Bellido M, Scarpa M, Villeneuve J, Jovic M, Porzner M, Balla T, Seufferlein T, Malhotra V. Recruitment of arfaptins to the trans-Golgi network by PI(4)P and their involvement in cargo export. The EMBO journal. 2013; 32(12):1717–1729. doi:10.1038/emboj.2013.116. [PubMed: 23695357]
23. Szentpetery Z, Varnai P, Balla T. Acute manipulation of Golgi phosphoinositides to assess their importance in cellular trafficking and signaling. Proceedings of the National Academy of Sciences of the United States of America. 2010; 107(18):8225–8230. doi:10.1073/pnas.1000157107. [PubMed: 20404150]
24. Daboussi L, Costaguta G, Payne GS. Phosphoinositide-mediated clathrin adaptor progression at the trans-Golgi network. Nature cell biology. 2012; 14(3):239–248. doi:10.1038/ncb2427. [PubMed: 22344030]

25. Hammond GR, Fischer MJ, Anderson KE, Holdich J, Koteci A, Balla T, Irvine RF. PI4P and PI(4,5)P2 are essential but independent lipid determinants of membrane identity. Science. 2012; 337(6095):727–730. doi:10.1126/science.1222483. [PubMed: 22722250]
26. Stefan CJ, Manford AG, Emr SD. ER-PM connections: sites of information transfer and inter-organelle communication. Current opinion in cell biology. 2013; 25(4):434–442. doi:10.1016/j.ceb.2013.02.020. [PubMed: 23522446]
27. Manford AG, Stefan CJ, Yuan HL, Macgurn JA, Emr SD. ER-to-plasma membrane tethering proteins regulate cell signaling and ER morphology. Developmental cell. 2012; 23(6):1129–1140. doi:10.1016/j.devcel.2012.11.004. [PubMed: 23237950]
28. Stefan CJ, Manford AG, Baird D, Yamada-Hanff J, Mao Y, Emr SD. Osh proteins regulate phosphoinositide metabolism at ER-plasma membrane contact sites. Cell. 2011; 144(3):389–401. doi:10.1016/j.cell.2010.12.034. [PubMed: 21295699]
29. Ling Y, Stefan CJ, Macgurn JA, Audhya A, Emr SD. The dual PH domain protein Opy1 functions as a sensor and modulator of PtdIns(4,5)P(2) synthesis. The EMBO journal. 2012; 31(13):2882–2894. doi:10.1038/emboj.2012.127. [PubMed: 22562153]
30. Gozani O, Karuman P, Jones DR, Ivanov D, Cha J, Lugovskoy AA, Baird CL, Zhu H, Field SJ, Lessnick SL, Villasenor J, Mehrotra B, Chen J, Rao VR, Brugge JS, Ferguson CG, Payrastre B, Myszka DG, Cantley LC, Wagner G, Divecha N, Prestwich GD, Yuan J. The PHD finger of the chromatin-associated protein ING2 functions as a nuclear phosphoinositide receptor. Cell. 2003; 114(1):99–111. [PubMed: 12859901]
31. Viaud J, Lagarrigue F, Ramel D, Allart S, Chicanne G, Ceccato L, Courilleau D, Xuereb JM, Pertz O, Payrastre B, Gaits-Iacovoni F. Phosphatidylinositol 5-phosphate regulates invasion through binding and activation of Tiam1. Nature communications. 2014; 5:4080. doi:10.1038/ncomms5080.
32. Viaud J, Boal F, Tronchere H, Gaits-Iacovoni F, Payrastre B. Phosphatidylinositol 5-phosphate: a nuclear stress lipid and a tuner of membranes and cytoskeleton dynamics. BioEssays : news and reviews in molecular, cellular and developmental biology. 2014; 36(3):260–272. doi:10.1002/bies.201300132.
33. Ramel D, Lagarrigue F, Pons V, Mounier J, Dupuis-Coronas S, Chicanne G, Sansonetti PJ, Gaits-Iacovoni F, Tronchere H, Payrastre B. Shigella flexneri infection generates the lipid PI5P to alter endocytosis and prevent termination of EGFR signaling. Science signaling. 2011; 4(191):ra61. doi:10.1126/scisignal.2001619. [PubMed: 21934107]
34. Guittard G, Gerard A, Dupuis-Coronas S, Tronchere H, Mortier E, Favre C, Olive D, Zimmermann P, Payrastre B, Nunes JA. Cutting edge: Dok-1 and Dok-2 adaptor molecules are regulated by phosphatidylinositol 5-phosphate production in T cells. J Immunol. 2009; 182(7):3974–3978. doi:10.4049/jimmunol.0804172. [PubMed: 19299694]
35. Vicinanza M, Korolchuk VI, Ashkenazi A, Puri C, Menzies FM, Clarke JH, Rubinsztein DC. PI(5)P Regulates Autophagosome Biogenesis. Molecular cell. 2015; 57(2):219–234. doi:10.1016/j.molcel.2014.12.007. [PubMed: 25578879]
36. Eugster A, Pecheur EI, Michel F, Winsor B, Letourneur F, Friant S. Ent5p is required with Ent3p and Vps27p for ubiquitin-dependent protein sorting into the multivesicular body. Molecular biology of the cell. 2004; 15(7):3031–3041. doi:10.1091/mbc.E03-11-0793. [PubMed: 15107463]
37. Friant S, Pecheur EI, Eugster A, Michel F, Lefkir Y, Nourrisson D, Letourneur F. Ent3p Is a PtdIns(3,5)P2 effector required for protein sorting to the multivesicular body. Developmental cell. 2003; 5(3):499–511. [PubMed: 12967568]
38. Li X, Wang X, Zhang X, Zhao M, Tsang WL, Zhang Y, Yau RG, Weisman LS, Xu H. Genetically encoded fluorescent probe to visualize intracellular phosphatidylinositol 3,5-bisphosphate localization and dynamics. Proceedings of the National Academy of Sciences of the United States of America. 2013; 110(52):21165–21170. doi:10.1073/pnas.1311864110. [PubMed: 24324172]
39. Zoncu R, Perera RM, Sebastian R, Nakatsu F, Chen H, Balla T, Ayala G, Toomre D, De Camilli PV. Loss of endocytic clathrin-coated pits upon acute depletion of phosphatidylinositol 4,5-bisphosphate. Proceedings of the National Academy of Sciences of the United States of America. 2007; 104(10):3793–3798. doi:10.1073/pnas.0611733104. [PubMed: 17360432]
40. Simon ML, Platre MP, Assil S, van Wijk R, Chen WY, Chory J, Dreux M, Munnik T, Jaillais Y. A multi-colour/multi-affinity marker set to visualize phosphoinositide dynamics in Arabidopsis. The

Plant journal : for cell and molecular biology. 2014; 77(2):322–337. doi:10.1111/tpj.12358. [PubMed: 24147788]

41. Schmid SL, Mettlen M. Cell biology: Lipid switches and traffic control. Nature. 2013; 499(7457): 161–162. doi:10.1038/nature12408. [PubMed: 23823719]
42. Suh BC, Inoue T, Meyer T, Hille B. Rapid chemically induced changes of PtdIns(4,5)P2 gate KCNQ ion channels. Science. 2006; 314(5804):1454–1457. doi:10.1126/science.1131163. [PubMed: 16990515]
43. Posor Y, Eichhorn-Gruenig M, Puchkov D, Schoneberg J, Ullrich A, Lampe A, Muller R, Zarbakhsh S, Gulluni F, Hirsch E, Krauss M, Schultz C, Schmoranzer J, Noe F, Haucke V. Spatiotemporal control of endocytosis by phosphatidylinositol-3,4-bisphosphate. Nature. 2013; 499(7457):233–237. doi:10.1038/nature12360. [PubMed: 23823722]
44. Uchida Y, Hasegawa J, Chinnapen D, Inoue T, Okazaki S, Kato R, Wakatsuki S, Misaki R, Koike M, Uchiyama Y, Iemura S, Natsume T, Kuwahara R, Nakagawa T, Nishikawa K, Mukai K, Miyoshi E, Taniguchi N, Sheff D, Lencer WI, Taguchi T, Arai H. Intracellular phosphatidylserine is essential for retrograde membrane traffic through endosomes. Proceedings of the National Academy of Sciences of the United States of America. 2011; 108(38):15846–15851. doi:10.1073/pnas.1109101108. [PubMed: 21911378]
45. Varnai P, Balla T. Live cell imaging of phosphoinositide dynamics with fluorescent protein domains. Biochimica et biophysica acta. 2006; 1761(8):957–967. doi:10.1016/j.bbalip.2006.03.019. [PubMed: 16702024]
46. Kutateladze TG. Translation of the phosphoinositide code by PI effectors. Nature chemical biology. 2010; 6(7):507–513. doi:10.1038/nchembio.390. [PubMed: 20559318]
47. Moravcevic K, Mendrola JM, Schmitz KR, Wang YH, Slochower D, Janmey PA, Lemmon MA. Kinase associated-1 domains drive MARK/PAR1 kinases to membrane targets by binding acidic phospholipids. Cell. 2010; 143(6):966–977. doi:10.1016/j.cell.2010.11.028. [PubMed: 21145462]
48. Nishioka T, Frohman MA, Matsuda M, Kiyokawa E. Heterogeneity of phosphatidic acid levels and distribution at the plasma membrane in living cells as visualized by a Foster resonance energy transfer (FRET) biosensor. The Journal of biological chemistry. 2010; 285(46):35979–35987. doi:10.1074/jbc.M110.153007. [PubMed: 20826779]
49. Cicchetti G, Biernacki M, Farquharson J, Allen PG. A ratiometric expressible FRET sensor for phosphoinositides displays a signal change in highly dynamic membrane structures in fibroblasts. Biochemistry. 2004; 43(7):1939–1949. doi:10.1021/bi035480w. [PubMed: 14967034]
50. van der Wal J, Habets R, Varnai P, Balla T, Jalink K. Monitoring agonist-induced phospholipase C activation in live cells by fluorescence resonance energy transfer. The Journal of biological chemistry. 2001; 276(18):15337–15344. doi:10.1074/jbc.M007194200. [PubMed: 11152673]
51. Sato M, Ueda Y, Takagi T, Umezawa Y. Production of PtdInsP3 at endomembranes is triggered by receptor endocytosis. Nature cell biology. 2003; 5(11):1016–1022. doi:10.1038/ncb1054. [PubMed: 14528311]
52. Niu Y, Zhang C, Sun Z, Hong Z, Li K, Sun D, Yang Y, Tian C, Gong W, Liu JJ. PtdIns(4)P regulates retromer-motor interaction to facilitate dynein-cargo dissociation at the trans-Golgi network. Nature cell biology. 2013; 15(4):417–429. doi:10.1038/ncb2710. [PubMed: 23524952]
53. Gillooly DJ, Morrow IC, Lindsay M, Gould R, Bryant NJ, Gaullier JM, Parton RG, Stenmark H. Localization of phosphatidylinositol 3-phosphate in yeast and mammalian cells. The EMBO journal. 2000; 19(17):4577–4588. doi:10.1093/emboj/19.17.4577. [PubMed: 10970851]
54. Yu JW, Mendrola JM, Audhya A, Singh S, Keleti D, DeWald DB, Murray D, Emr SD, Lemmon MA. Genome-wide analysis of membrane targeting by S. cerevisiae pleckstrin homology domains. Molecular cell. 2004; 13(5):677–688. [PubMed: 15023338]
55. Toth DJ, Toth JT, Gulyas G, Balla A, Balla T, Hunyady L, Varnai P. Acute depletion of plasma membrane phosphatidylinositol 4,5-bisphosphate impairs specific steps in endocytosis of the G-protein-coupled receptor. Journal of cell science. 2012; 125(Pt 9):2185–2197. doi:10.1242/jcs.097279. [PubMed: 22357943]
56. Heo WD, Inoue T, Park WS, Kim ML, Park BO, Wandless TJ, Meyer T. PI(3,4,5)P3 and PI(4,5)P2 lipids target proteins with polybasic clusters to the plasma membrane. Science. 2006; 314(5804): 1458–1461. doi:10.1126/science.1134389. [PubMed: 17095657]

57. Giordano F, Saheki Y, Idevall-Hagren O, Colombo SF, Pirruccello M, Milosevic I, Gracheva EO, Bagriantsev SN, Borgese N, De Camilli P. PI(4,5)P(2)-dependent and Ca(2+)-regulated ER-PM interactions mediated by the extended synaptotagmins. Cell. 2013; 153(7):1494–1509. doi: 10.1016/j.cell.2013.05.026. [PubMed: 23791178]

58. Idevall-Hagren O, Dickson EJ, Hille B, Toomre DK, De Camilli P. Optogenetic control of phosphoinositide metabolism. Proceedings of the National Academy of Sciences of the United States of America. 2012; 109(35):E2316–2323. doi:10.1073/pnas.1211305109. [PubMed: 22847441]

59. Hammond GR. Membrane biology: Making light work of lipids. Current biology : CB. 2012; 22(20):R869–871. doi:10.1016/j.cub.2012.09.005. [PubMed: 23098593]

60. Kanai F, Liu H, Field SJ, Akbary H, Matsuo T, Brown GE, Cantley LC, Yaffe MB. The PX domains of p47phox and p40phox bind to lipid products of PI(3)K. Nature cell biology. 2001; 3(7):675–678. doi:10.1038/35083070. [PubMed: 11433300]

61. Ellson CD, Gobert-Gosse S, Anderson KE, Davidson K, Erdjument-Bromage H, Tempst P, Thuring JW, Cooper MA, Lim ZY, Holmes AB, Gaffney PR, Coadwell J, Chilvers ER, Hawkins PT, Stephens LR. PtdIns(3)P regulates the neutrophil oxidase complex by binding to the PX domain of p40(phox). Nature cell biology. 2001; 3(7):679–682. doi:10.1038/35083076. [PubMed: 11433301]

62. Safi A, Vandromme M, Caussanel S, Valdacci L, Baas D, Vidal M, Brun G, Schaeffer L, Goillot E. Role for the pleckstrin homology domain-containing protein CKIP-1 in phosphatidylinositol 3-kinase-regulated muscle differentiation. Molecular and cellular biology. 2004; 24(3):1245–1255. [PubMed: 14729969]

63. Maffucci T, Brancaccio A, Piccolo E, Stein RC, Falasca M. Insulin induces phosphatidylinositol-3-phosphate formation through TC10 activation. The EMBO journal. 2003; 22(16):4178–4189. doi: 10.1093/emboj/cdg402. [PubMed: 12912916]

64. Roy A, Levine TP. Multiple pools of phosphatidylinositol 4-phosphate detected using the pleckstrin homology domain of Osh2p. The Journal of biological chemistry. 2004; 279(43): 44683–44689. doi:10.1074/jbc.M401583200. [PubMed: 15271978]

65. Sarkes D, Rameh LE. A novel HPLC-based approach makes possible the spatial characterization of cellular PtdIns5P and other phosphoinositides. The Biochemical journal. 2010; 428(3):375–384. doi:10.1042/BJ20100129. [PubMed: 20370717]

66. Varnai P, Balla T. Visualization of phosphoinositides that bind pleckstrin homology domains: calcium- and agonist-induced dynamic changes and relationship to myo-[3H]inositol-labeled phosphoinositide pools. The Journal of cell biology. 1998; 143(2):501–510. [PubMed: 9786958]

67. Ben El Kadhi K, Roubinet C, Solinet S, Emery G, Carreno S. The inositol 5-phosphatase dOCRL controls PI(4,5)P2 homeostasis and is necessary for cytokinesis. Current biology : CB. 2011; 21(12):1074–1079. doi:10.1016/j.cub.2011.05.030. [PubMed: 21658948]

68. Szentpetery Z, Balla A, Kim YJ, Lemmon MA, Balla T. Live cell imaging with protein domains capable of recognizing phosphatidylinositol 4,5-bisphosphate; a comparative study. BMC cell biology. 2009; 10:67. doi:10.1186/1471-2121-10-67. [PubMed: 19769794]

69. Santagata S, Boggon TJ, Baird CL, Gomez CA, Zhao J, Shan WS, Myszka DG, Shapiro L. G-protein signaling through tubby proteins. Science. 2001; 292(5524):2041–2050. doi:10.1126/science.1061233. [PubMed: 11375483]

70. Dove SK, Piper RC, McEwen RK, Yu JW, King MC, Hughes DC, Thuring J, Holmes AB, Cooke FT, Michell RH, Parker PJ, Lemmon MA. Svp1p defines a family of phosphatidylinositol 3,5-bisphosphate effectors. The EMBO journal. 2004; 23(9):1922–1933. doi:10.1038/sj.emboj.7600203. [PubMed: 15103325]

71. Dowler S, Currie RA, Campbell DG, Deak M, Kular G, Downes CP, Alessi DR. Identification of pleckstrin-homology-domain-containing proteins with novel phosphoinositide-binding specificities. The Biochemical journal. 2000; 351(Pt 1):19–31. [PubMed: 11001876]

72. Marshall AJ, Krahn AK, Ma K, Duronio V, Hou S. TAPP1 and TAPP2 are targets of phosphatidylinositol 3-kinase signaling in B cells: sustained plasma membrane recruitment triggered by the B-cell antigen receptor. Molecular and cellular biology. 2002; 22(15):5479–5491. [PubMed: 12101241]

73. Varnai P, Rother KI, Balla T. Phosphatidylinositol 3-kinase-dependent membrane association of the Bruton's tyrosine kinase pleckstrin homology domain visualized in single living cells. The Journal of biological chemistry. 1999; 274(16):10983–10989. [PubMed: 10196179]
74. Fairn GD, Hermansson M, Somerharju P, Grinstein S. Phosphatidylserine is polarized and required for proper Cdc42 localization and for development of cell polarity. Nature cell biology. 2011; 13(12):1424–1430. doi:10.1038/ncb2351. [PubMed: 21964439]
75. Yeung T, Heit B, Dubuisson JF, Fairn GD, Chiu B, Inman R, Kapus A, Swanson M, Grinstein S. Contribution of phosphatidylserine to membrane surface charge and protein targeting during phagosome maturation. The Journal of cell biology. 2009; 185(5):917–928. doi:10.1083/jcb.200903020. [PubMed: 19487458]
76. Kassas N, Tryoen-Toth P, Corrotte M, Thahouly T, Bader MF, Grant NJ, Vitale N. Genetically encoded probes for phosphatidic acid. Methods in cell biology. 2012; 108:445–459. doi:10.1016/B978-0-12-386487-1.00020-1. [PubMed: 22325614]
77. Zhang F, Wang Z, Lu M, Yonekubo Y, Liang X, Zhang Y, Wu P, Zhou Y, Grinstein S, Hancock JF, Du G. Temporal production of the signaling lipid phosphatidic acid by phospholipase D2 determines the output of extracellular signal-regulated kinase signaling in cancer cells. Molecular and cellular biology. 2014; 34(1):84–95. doi:10.1128/MCB.00987-13. [PubMed: 24164897]
78. Bohdanowicz M, Schlam D, Hermansson M, Rizzuti D, Fairn GD, Ueyama T, Somerharju P, Du G, Grinstein S. Phosphatidic acid is required for the constitutive ruffling and macropinocytosis of phagocytes. Molecular biology of the cell. 2013; 24(11):1700–1712. doi:10.1091/mbc.E12-11-0789. [PubMed: 23576545]
79. Antonescu CN, Aguet F, Danuser G, Schmid SL. Phosphatidylinositol-(4,5)-bisphosphate regulates clathrin-coated pit initiation, stabilization, and size. Molecular biology of the cell. 2011; 22(14):2588–2600. doi:10.1091/mbc.E11-04-0362. [PubMed: 21613550]

Europe PMC Funders Author Manuscripts

Europe PMC Funders Author Manuscripts

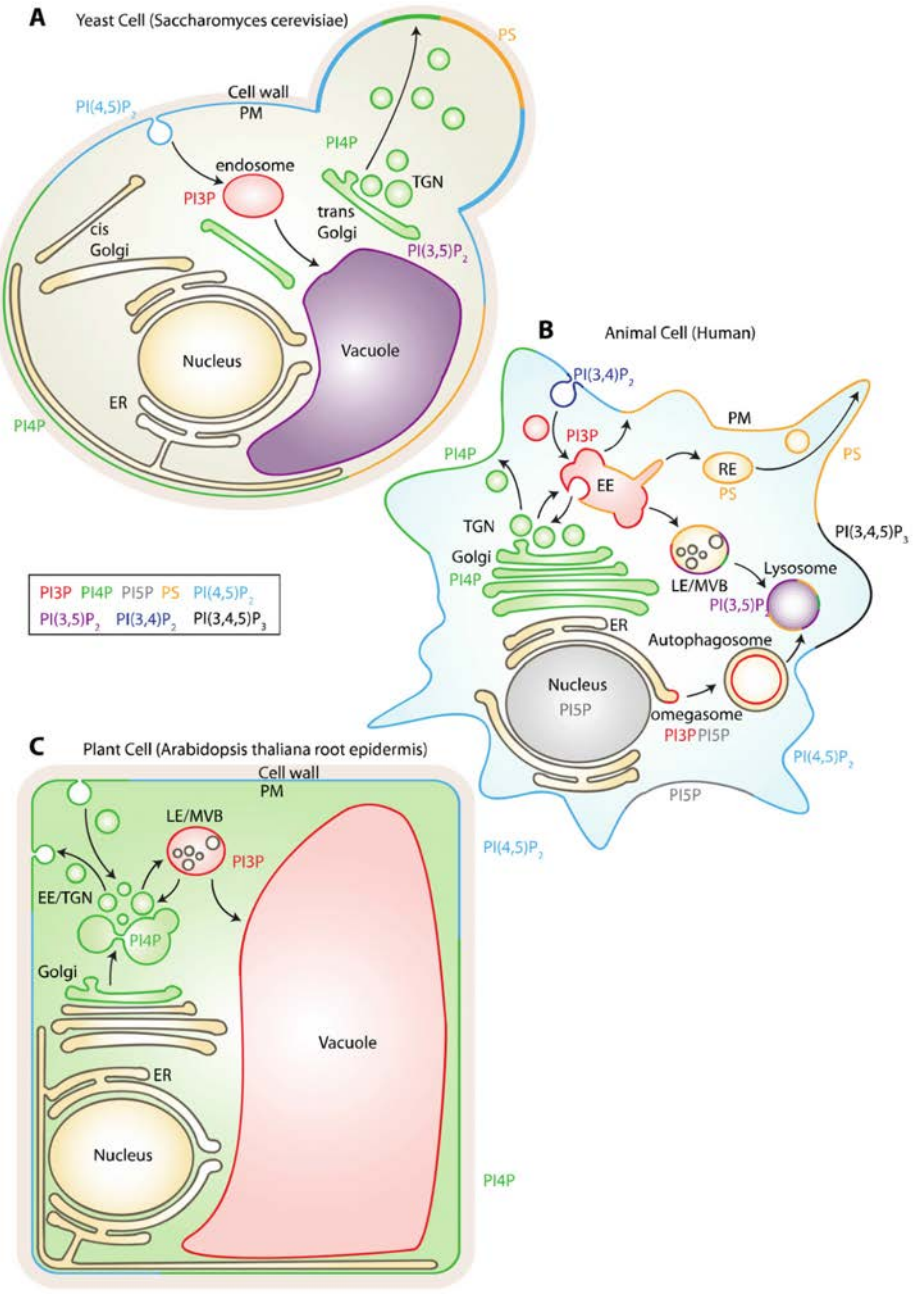

Figure 1. Summary of the subcellular localization of anionic phospholipids in yeast (A), animal (B) and plant (C) cells

Note that the reported localization are not exhaustive and might vary depending on cell types or signaling activities. The cartoon representing the cell in panel B is adapted from Jean and Kiger 2012.

Europe PMC Funders Author Manuscripts

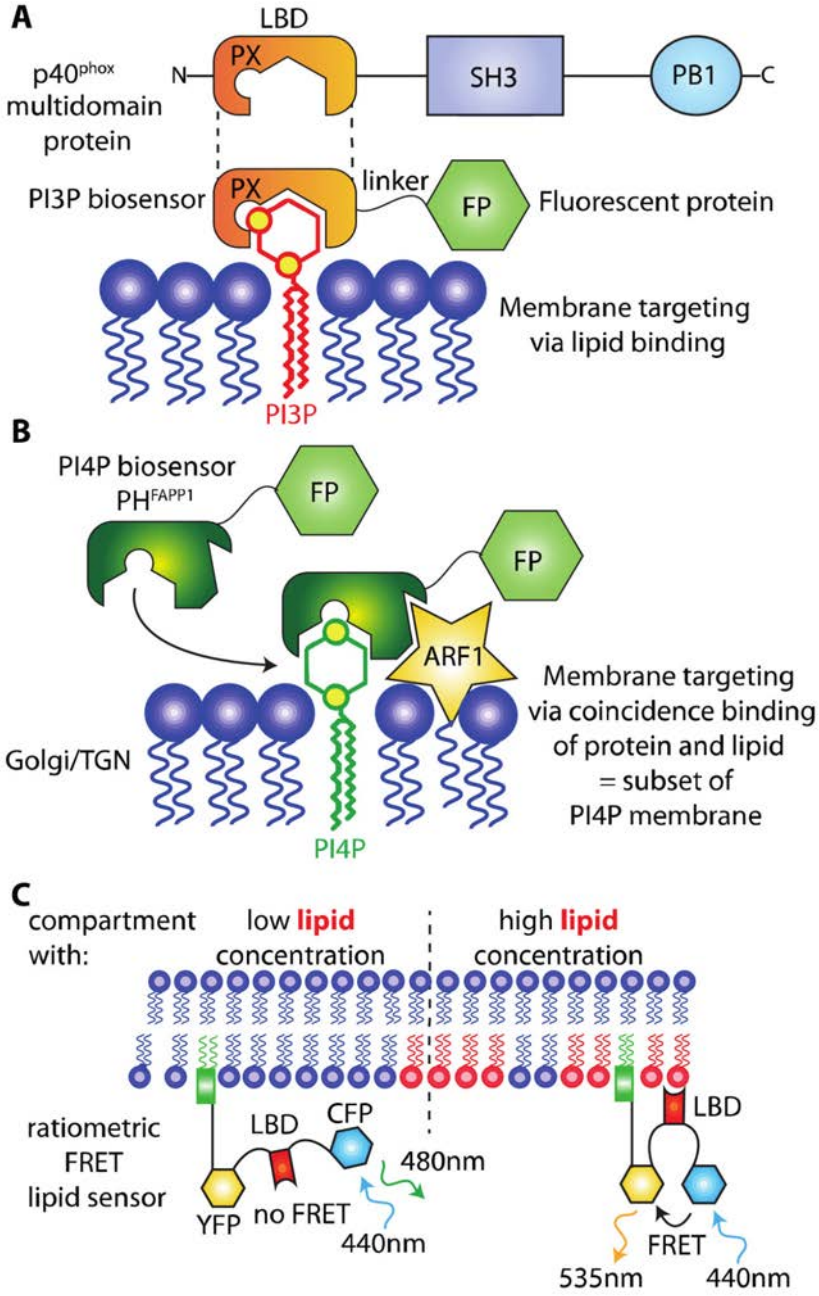

Figure 2. General principle of genetically encoded lipid biosensors

A) A lipid-binding domain (LBD) from a multidomain protein (p40^{phox} in this example) is fused with a fluorescent protein (FP). This protein fusion acts as a biosensor for PI3P. B) Some LBDs require binding to both a lipid and another molecules (*i.e.*, Ca2+, proteins). This coincidence binding specifies the localization of the corresponding biosensor to a subset of the lipid-enriched membrane, which also contains the target protein. In this example, the PH domain of FAPP1 binds PI4P and ARF1, hereby restricting its localization to the Golgi/TGN. C) Ratiometric FRET sensors are targeted to membranes independently of lipid

binding (*e.g.*, via a lipid anchor or a transmembrane segment) and report on the presence of the lipid based on the conformational changes induced in the sensor when the LBD binds its lipid (which increases or decreases the proximity between the two FPs and therefore their FRET ratio).

Europe PMC Funders Author Manuscripts

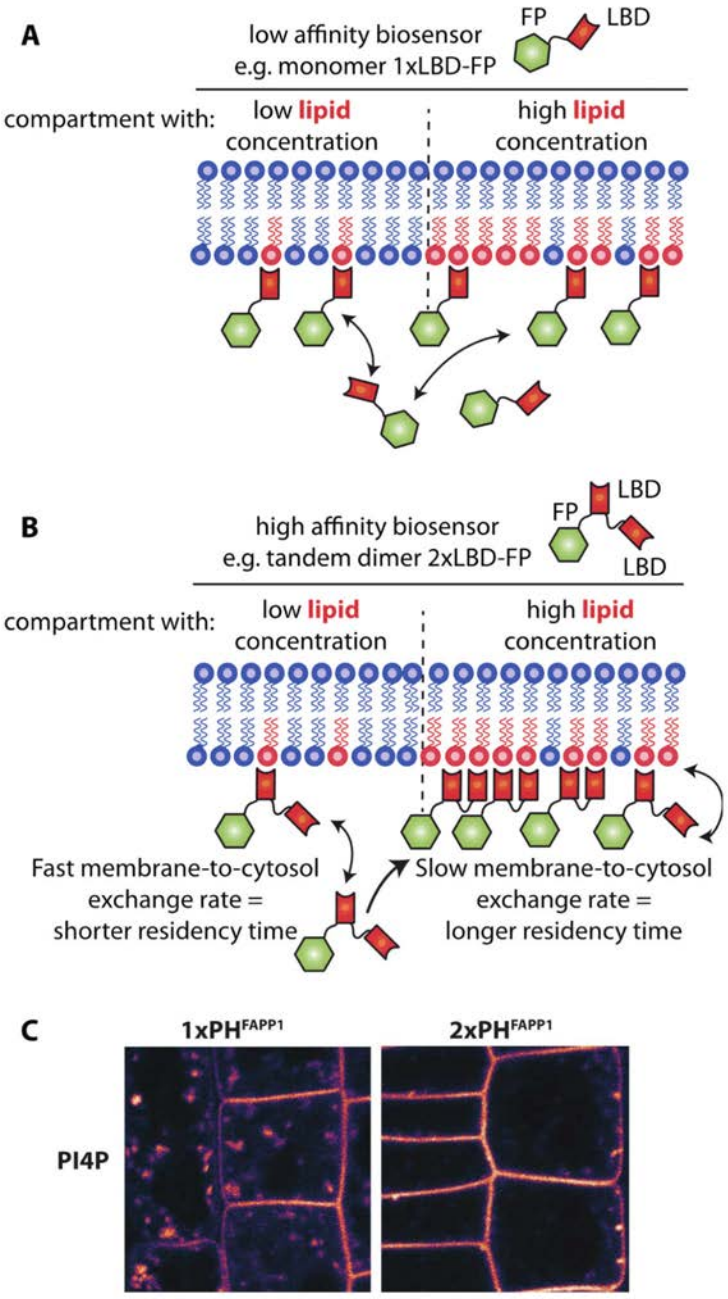

Figure 3. LBD affinities influence the subcellular localization of the sensors

When several pools of the same lipid exist within the cell, low or high affinity sensors will behave differently with respect to these pools. A) A low affinity sensor (e.g., 1xLBD) will localize to both membranes with slightly more sensor molecules at the compartment with the highest lipid concentration, while (B) a high affinity sensor (e.g., 2xLBD) will localize preferentially to the compartment with the highest lipid concentration. C) Example of low

(1xPH^{FAPP1}) and high (2xPH^{FAPP1}) affinity sensor localization in Arabidopsis root cell (image from Simon et al., 2014 Plant Journal).

Europe PMC Funders Author Manuscripts

ANNEXE III : Anionic lipids and the maintenance of membrane electrostatics in eukaryotes

PLANT SIGNALING & BEHAVIOR
2017, VOL. 12, NO. 2, e1282022 (5 pages)
http://dx.doi.org/10.1080/15592324.2017.1282022

Taylor & Francis
Taylor & Francis Group

MINI-REVIEW

OPEN ACCESS

Anionic lipids and the maintenance of membrane electrostatics in eukaryotes

Matthieu Pierre Platre and Yvon Jaillais

Laboratoire Reproduction et Développement des Plantes, Univ Lyon, ENS de Lyon, Université Claude Bernard Lyon 1, CNRS, INRA, Lyon, France

ABSTRACT

A wide range of signaling processes occurs at the cell surface through the reversible association of proteins from the cytosol to the plasma membrane. Some low abundant lipids are enriched at the membrane of specific compartments and thereby contribute to the identity of cell organelles by acting as biochemical landmarks. Lipids also influence membrane biophysical properties, which emerge as an important feature in specifying cellular territories. Such parameters are crucial for signal transduction and include lipid packing, membrane curvature and electrostatics. In particular, membrane electrostatics specifies the identity of the plasma membrane inner leaflet. Membrane surface charges are carried by anionic phospholipids, however the exact nature of the lipid(s) that powers the plasma membrane electrostatic field varies among eukaryotes and has been hotly debated during the last decade. Herein, we discuss the role of anionic lipids in setting up plasma membrane electrostatics and we compare similarities and differences that were found in different eukaryotic cells.

ARTICLE HISTORY
Received 15 December 2016
Revised 4 January 2017
Accepted 4 January 2017

KEYWORDS
Anionic lipid; arabidopsis; biosensor; endocytosis; membrane surface charge; membrane territory; phosphatidylserine; phosphoinositide; phospholipid; plasma membrane identity

The inner leaflet of the plasma membrane (PM) of animal cells is composed of about 20% of anionic lipids that provide negative charges (electric field estimated at 5V/cm) giving the potential to permanently or transiently attract cytosolic cationic molecules, including peripheral membrane proteins.[1] The concept of an electrostatic potential driven by membrane surface charges (MSC) was postulated long ago by biophysicists.[2] However tools to sense this predicted feature were only developed during the last decade via the generation of genetically encoded biosensors (Fig. 1).[3-7] These biosensors, which will be referred as MSC-probes thereafter, consist of cationic peptides or folded protein domains that transiently associate with anionic phospholipids based on their negative charges and irrespective of their head group (Fig. 1B).[3,4,7] When fused to a fluorescent protein, these MSC-probes label strictly the cytosolic face of the plasma membrane in all eukaryotic cell type analyzed including yeast, plant and mammalian cells[3,4,8-10] (Fig. 2C). This common feature highlights a unique signature of the plasma membrane as the most anionic membrane in cells. This particular plasma membrane property is paramount to localize signaling proteins, including for example small GTPases and kinases.[3-10] However, in each eukaryotic kingdom, different anionic lipids are used to power this high plasma membrane electrostatic field (Fig. 2B).

Phosphoinositides cooperativity powers membrane electrostatics in mammals

In mammals, phosphatidylserine [PS], phosphatidylinositol-4-phosphate PtdIns(4)P, phosphatidylinositol- 4,5-biphosphate [PI(4,5)P_2], and phosphatidylinositol-3,4,5-triphosphate [PtdIns(3,4,5)P_3] are localized at the cell surface (Fig. 2A).[11,12] These lipids are candidates to power the PM electrostatic field. Phosphoinositides are low abundant lipids but highly anionic, with PtdIns(4)P, PtdIns(4,5)P_2 and PtdIns(3,4,5)P_3 containing respectively 3, 5 and 7 net negative charges.[13] Since PtdIns(4,5)P_2 is a distinctive lipid of the plasma membrane and relatively abundant compared with other plasma membrane-localized phosphoinositides, it was a prime candidate to drive plasma membrane MSC. However, inducible PtdIns(4,5)P_2 depletion at the plasma membrane has no effect on the localization of MSC-probes, suggesting that this lipid does not specify the plasma membrane electrostatic field on its own.[4,9] Interestingly, inhibition of PtdIns(3,4,5)P_3 synthesis by type-I PI3-Kinase inhibitors together with inducible depletion of PM PtdIns(4,5)P_2 delocalized MSC-probes to intracellular compartments, showing that these lipids are redundantly required for PM MSC.[4] Later on, concomitant inducible depletion of plasma membrane-associated PtdIns(4)P and PtdIns(4,5)P_2 also demonstrated a role for PtdIns(4)P in plasma membrane surface charges together with PtdIns(4,5)P_2[9] (Fig. 2C). Altogether, PtdIns(4,5)P_2 seems to be critical in defining plasma membrane MSC in human cells but acts redundantly with PtdIns(3,4,5)P_3 and/or PtdIns(4)P (Fig. 2B).

PtdInsPs are highly anionic but represent only 1–2% of total phospholipids in living cells.[13] Other less anionic lipids might also contribute to MSC notably due to their higher abundance. In animals, PS represents about 10 to 20% of plasma membrane phospholipids but PS is less anionic than phosphoinositides (net charge −1).[1,14] Inhibition of ATP synthesis prevents phosphorylation of PtdInsPs by kinases while lipid phosphatases are still active, triggering the rapid

CONTACT Yvon Jaillais yvon.jaillais@ens-lyon.fr Laboratoire de Reproduction et Développement des Plantes, Univ Lyon, ENS Lyon, UCB Lyon 1, CNRS, INRA, 46 Allée d'Italie, Lyon, Rhône 69364, France.

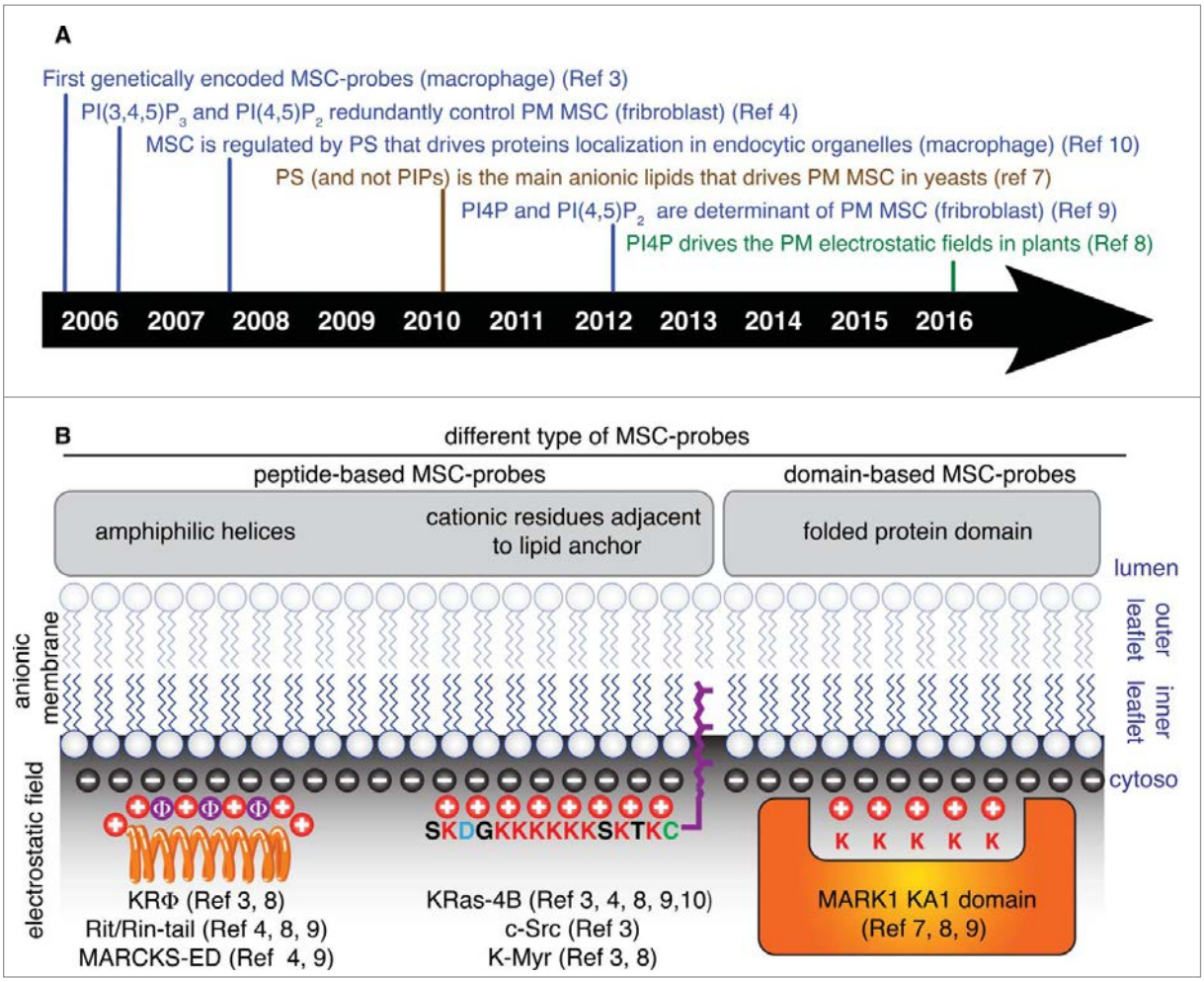

Figure 1. (A) Timeline showing landmark papers for the in vivo study of membrane surface charges (MSC) in various organisms. Color indicates the model system used in the study: blue, human cell lines; brown, *Saccharomyces cerevisiae*; Green, *Arabidopsis thaliana* and *Nicotiana benthamiana*. (B) Schematic representation of peptide-based MSC-probes (Left and middle panels) and domain-based MSC-probes (right panel). Black circles indicate negative membrane surface charges, red circles show cationic residues in MSC-probes that interact with MSC through electrostatic interactions, and purple circles indicate aromatic residues that provide hydrophobic interaction for membrane anchoring. The lipid anchor is represented in purple (for clarity only farnesylation is given as an example, but other lipid modifications have been used, such as the N-terminal myristoylation in c-Src or K-myr reporters, see ref 3). K-Ras4B MSC-probe corresponds to the C-terminal tail of K-Ras4B, c-Src probe corresponds to the N-terminal tail of c-Src, K-myr is a synthetic construct that has a N-terminal myristoylation adjacent to the K-Ras4B charged peptide. MSC, membrane surface charges, KA1 domain, Kinase Associated1 domain; MARK1, Microtubule Associated Regulated Kinase1; MARCKS-ED, Myristoylated Alanine-Rich C Kinase Substrate-Effector Domain.

depletion of phosphoinositides from cellular membranes.[10] However, this treatment does not affect the PS pool, since it is not constantly regulated by phosphorylation[10] In this condition and therefore in the absence of PtdInsPs, MSC-probes lose their specific plasma membrane localization and relocalize to all PS-bearing organelles, including the PM but also all plasma membrane-derived organelles along the endocytic pathways (Fig. 2A).[10] This result confirms the importance of phosphoinositides in driving the specific electrostatic signature of the cell surface.[10] However, in the absence of phosphoinositides, MSC-probes partially retain their plasma membrane localization, suggesting a role for PS in plasma membrane MSC.[10]

In addition, because in the absence of phosphoinositide, MSC-probes localize to all PS-containing compartments,[10] PS might be involved in driving the electrostatic properties of endocytic compartments. Bigay and Antonny proposed that PS defined an electrostatic territory in cells that corresponds to all PM-derived organelles.[5,6] However, this hypothesis is mainly based on coincidence between the presence of negative charges, as visualized by MSC-probes, and the presence of PS on these membranes.[10] To our knowledge, this theory has not been challenged by genetic and/or pharmacological perturbation(s) of the PS pool.

Overall, PtdInsPs are the main anionic lipids that regulate plasma membrane surface charge in mammals, while PS seems to have a broader role in controlling membrane electrostatics of all PM-derived organelles (Fig. 2B-C)[3-6,9,10]

Maintenance of plasma membrane electrostatics in yeast: It's all about PS

Based on findings in mammals, the potential involvement of PtdInsPs was analyzed in yeast. To address the relative role of PtdInsPs in plasma membrane electrostatic field, temperature-sensitive alleles that reduces both PtdIns(4)P and PtdIns(4,5)P_2 or PtdIns(4,5)P_2 alone were used. Surprisingly,

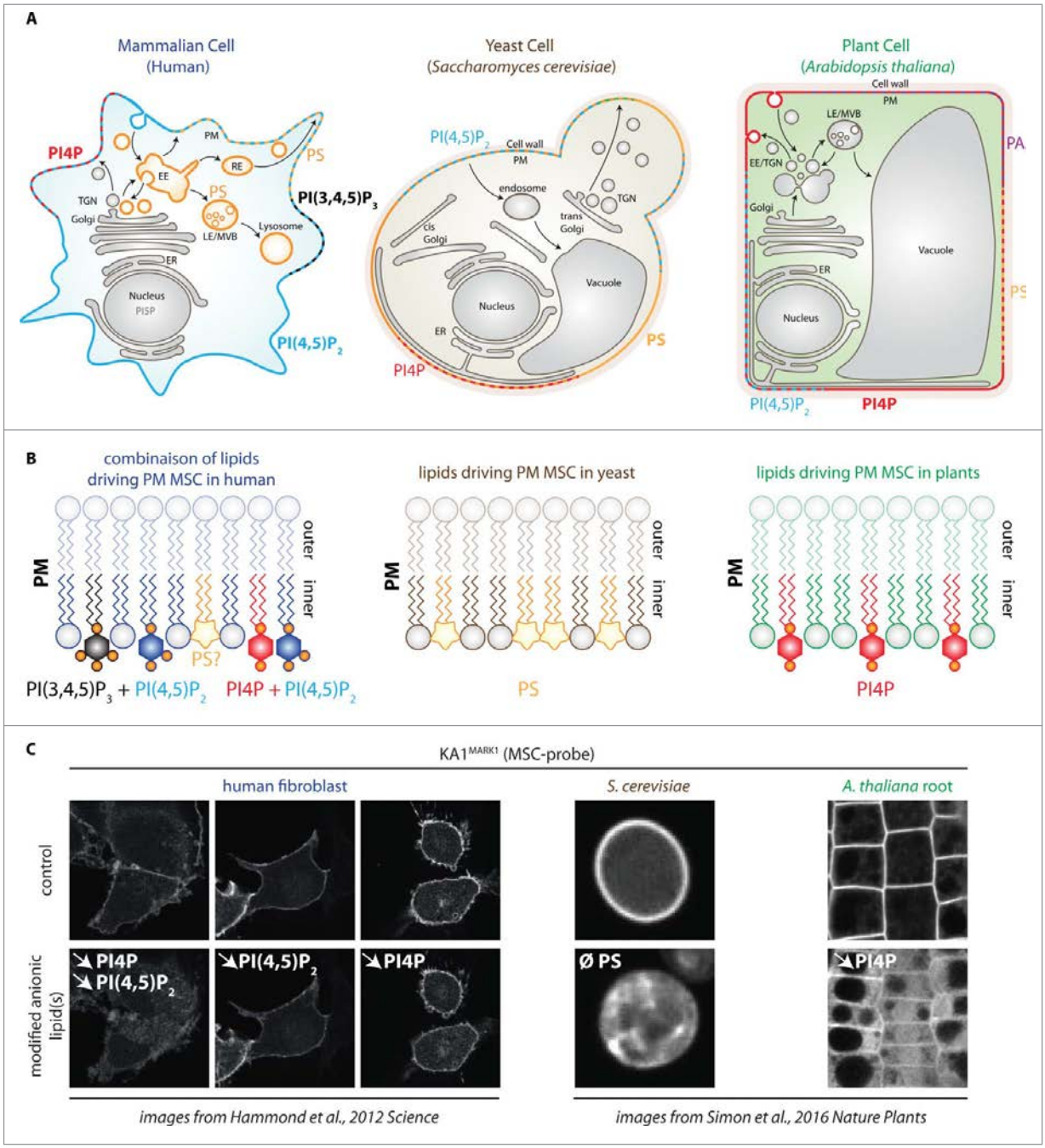

Figure 2. Contribution of different anionic phospholipids in plasma membrane surface charge. (A) schematic representation of human, yeast and plant cells. Anionic phospholipids that localize at the cell surface are indicated for each cell type. For clarity, PI3P, PI5P and PtdIns(3,4)P_2 have been omitted, although they have been shown to localize at the plasma membrane in animal cells at very low quantity and/or upon specific stimuli.[11] The localization of PS in plasma membrane-derived organelles is indicated by the orange color. Note that for practical purposes, dashes indicate the presence of several lipid species on the same membrane, however, this does not mean that they are necessarily organized in discrete domains. (B) schematic representation of the anionic lipids required for plasma membrane MSC in mammals (left), yeast (middle) and plants (right). Note that in human, PtdIns(4,5)P_2 acts redundantly with either PtdIns(4)P or PtdIns(3,4,5)P_3. (C) confocal pictures showing the localization of the KA1 domain of MARK1 in human fibroblast cells (left), *S. cerevisiae* (middle) and *A. thaliana* root epidermis (right). KA1 is a domain that interacts with all negatively charged lipids and therefore acts as a sensor of membrane electrostatics (so called MSC-probe). Top panels are control cells and bottom panels show conditions in which anionic phospholipids have been genetically or chemically perturbed. The targeted lipid(s) is indicated in white (downward pointing arrows indicate the reduction in the given lipid content and Ø total absence in the lipid in the Δ*cho1* yeast mutant). Note that $KA1^{MARK1}$ localizes at the cell surface in mammals, yeasts and plants, but that this strict plasma membrane localization relies on different anionic phospholipid in these cells. EE, early endosome; LE, late endosome; RE, recycling endosomes; TGN, *trans*-golgi network; ER, endoplasmic reticulum; MSC, membrane surface charge. Pictures of fibroblasts are from Hammond et al.[9] and pictures from yeast and plants are from Simon et al.[8] The cartoon representing the cell from the top left cornel is inspired from Jean and Kiger 2012 and adapted by permission from Macmillan Publisher Ltd: [NATURE REVIEW MOLECULAR CELL BIOLOGY], ref. 12 copyright (2012).

at restrictive temperature, KINASE ASSOCIATED1 (KA1) domains, which are domains that bind to all anionic phospholipids and therefore act as MSC-probes, remain strictly localized at the PM in all these yeast mutant strains.[7] These results suggest that unlike in animals, PtdInsPs do not play a major role in PM MSC.[7]

By contrast to mammals in which PS is spread all along the endocytic pathway,[10,14,15] PS is highly enriched at the PM in yeast (Fig. 2A).[7,10] Therefore, PS is a good candidate to specify plasma membrane electrostatics in yeast cells. Cho1p is the only PS synthase in yeast, and the *cho1* mutant does not produce any PS.[10,16] mislocalization of the KA1 MSC-probes in *cho1* shows a prominent contribution of PS in plasma membrane surface charge (Fig. 2C).[7,8] Altogether, these results suggest either no or minor roles of PtdInsPs in plasma membrane surface charge in yeast, while PS is the main anionic lipid regulating the plasma membrane electrostatic potential.[7]

PtdIns(4)P massively accumulates at the plasma membrane in plants and drives its electrostatic field

By contrast to yeast and animals, PtdIns(4)P massively accumulates at the plasma membrane in plants.[8,17] In Arabidopsis root cells, short-term (up to 30 min) pharmacological inhibition of PI4-Kinase (PI4K) rapidly depletes the cellular PtdIns(4)P pool but has no effect on PtdIns(4,5)P_2.[8] This results is surprising since PtdIns(4)P is the precursor of PtdIns(4,5)P_2. However, short-term depletion of PtdIns(4)P has also no effect on PtdIns(4,5)P_2 in human fibroblast cells, suggesting that in both kingdoms the metabolism of these two lipids are largely independent within this short time frame.[8,9] In addition, PtdIns(4)P is substantially more abundant than PtdIns(4,5)P_2 in plant tissues,[17,18] therefore the residual PtdIns(4)P molecules might be sufficient to sustain PtdIns(4,5)P_2 synthesis. The relative abundance of PtdIns(4)P over PtdIns(4,5)P_2 and its accumulation at the cell surface suggest that it might be involved in plasma membrane electrostatics. Indeed, inhibition of PI4K largely delocalized MSC-probes from the plasma membrane.[8] In addition, genetic depletion of PtdIns(4)P specifically at the plasma membrane induced the ectopic localization of MSC-probes in less anionic endomembrane compartments.[8] Together, these results indicate that PtdIns(4)P is important for plasma membrane electrostatics and that, by contrast to mammals, it does not act redundantly with PtdIns(4,5)P_2.

However, it is worth noting that MSC-probes retain a certain degree of plasma membrane localization upon PtdIns(4)P depletion (Fig. 2C), and that therefore other anionic lipids might contribute to the plant plasma membrane electrostatic field.[8] Candidate lipids include PtdIns(4,5)P_2, PS and/or phosphatidic acid (PA) that all localized at the plasma membrane at least in some plant cell types (Fig. 2A).[8,17,19] Pharmacological and/or genetic perturbation of PtdIns(4,5)P_2 and PA indeed suggest that these lipids are involved in the plasma membrane localization of proteins with cationic stretches.[20] Therefore, as seen for mammals, lipid cooperativity might also be important for membrane electrostatics in plants. Nevertheless, unlike in animals, depletion of PtdIns(4)P alone is sufficient to perturb PM electrostatics in plants (Fig. 2C), highlighting the unusual importance of PtdIns(4)P in specifying the identity of the plant plasma membrane.

Concluding remarks

To conclude, the plasma membrane is highly electronegative across eukaryotes, but differences exist concerning the lipids involved in the maintenance of plasma membrane electrostatics (Fig. 2B). The main difference comes from yeast where PS is the major anionic lipid that drives plasma membrane surface charge, while PtdInsPs are not required.[7] This striking contrast brings the question of the role of PS in membrane electrostatics in multicellular eukaryotes such as plants or mammals. Indeed, while PS has been postulated to control electrostatic properties of plasma membrane-derived organelles,[5,6] this has not been fully addressed experimentally. Future researches are therefore awaited to tackle this question. Similarly, it would be interesting to explore the contribution of PA in membrane electrostatics.

Disclosure of potential conflicts of interest

No potential conflicts of interest were disclosed.

Acknowledgment

We thank Laia Armengot, Isabelle Fobis-Loisy, Mehdi Bichir Doumane, Thierry Gaude, Vincent Bayle for critical comments on the manuscript, Julien Gronnier for the membrane template used in Fig. 1B and Fig. 2B, Gerald Hammond (University of Pittsburg, USA) for sharing the pictures of KA1(MARK1) in fibroblasts and Amy Kiger (UCSD, San Diego, USA) for the template of the animal cell in Fig. 2A. The orange spring in Fig. 1 was reproduced with permission from Vecteezy.com. Y.J. has received funding from the European Research Council—ERC Grant Agreement no. [3363360-APPL] under the European Union's Seventh Framework Program (FP/2007–2013).

ORCID

Yvon Jaillais http://orcid.org/0000-0003-4923-883X

References

1. Lemmon MA. Membrane recognition by phospholipid-binding domains. Nat Rev Mol Cell Biol 2008; 9:99-111; PMID:18216767; http://dx.doi.org/10.1038/nrm2328
2. McLaughlin S. The electrostatic properties of membranes. Annu Rev Biophys Biophys Chem 1989; 18:113-36; PMID:2660821; http://dx.doi.org/10.1146/annurev.bb.18.060189.000553
3. Yeung T, Terebiznik M, Yu L, Silvius J, Abidi WM, Philips M, Levine T, Kapus A, Grinstein S. Receptor activation alters inner surface potential during phagocytosis. Science 2006; 313:347-51; PMID:16857939; http://dx.doi.org/10.1126/science.1129551
4. Heo WD, Inoue T, Park WS, Kim ML, Park BO, Wandless TJ, Meyer T. PI(3,4,5)P3 and PtdIns(4,5)P2 lipids target proteins with polybasic clusters to the plasma membrane. Science 2006; 314:1458-61; PMID:17095657; http://dx.doi.org/10.1126/science.1134389
5. Bigay J, Antonny B. Curvature, lipid packing, and electrostatics of membrane organelles: defining cellular territories in determining specificity. Dev Cell 2012; 23:886-95; PMID:23153485; http://dx.doi.org/10.1016/j.devcel.2012.10.009
6. Jackson CL, Walch L, Verbavatz JM. Lipids and their trafficking: an integral part of cellular organization. Dev Cell 2016; 39:139-53; PMID:27780039; http://dx.doi.org/10.1016/j.devcel.2016.09.030
7. Moravcevic K, Mendrola JM, Schmitz KR, Wang YH, Slochower D, Janmey PA, Lemmon MA. Kinase associated-1 domains drive MARK/PAR1 kinases to membrane targets by binding acidic phospholipids. Cell 2010; 143:966-77; PMID:21145462; http://dx.doi.org/10.1016/j.cell.2010.11.028
8. Simon ML, Platre MP, Marquès-Bueno MM, Armengot L, Stanislas T, Bayle V, Caillaud MC, Jaillais Y. A PtdIns(4)P-driven electrostatic field controls cell membrane identity and signalling in plants. Nature

Plants 2016; 2:16089; PMID:27322096; http://dx.doi.org/10.1038/nplants.2016.89
9. Hammond GR, Fischer MJ, Anderson KE, Holdich J, Koteci A, Balla T, Irvine RF. PtdIns(4)P and PtdIns(4,5)P2 are essential but independent lipid determinants of membrane identity. Science 2012; 337:727-30; PMID:22722250; http://dx.doi.org/10.1126/science.1222483
10. Yeung T, Gilbert GE, Shi J, Silvius J, Kapus A, Grinstein S. Membrane phosphatidylserine regulates surface charge and protein localization. Science 2008; 319:210-13; PMID:18187657; http://dx.doi.org/10.1126/science.1152066
11. Platre MP, Jaillais Y. Guidelines for the use of protein domains in acidic phospholipid imaging. Methods Mol Biol 2016; 1376:175-94; PMID:26552684; http://dx.doi.org/10.1007/978-1-4939-3170-5_15
12. Jean S, Kiger AA. Coordination between RAB GTPase and phosphoinositide regulation and functions. Nat Rev Mol Cell Biol 2012; 13:463-70; PMID:22722608; http://dx.doi.org/10.1038/nrm3379
13. Balla T. Phosphoinositides: tiny lipids with giant impact on cell regulation. Physiol Rev 2013; 93:1019-37; PMID:23899561; http://dx.doi.org/10.1152/physrev.00028.2012
14. Leventis PA, Grinstein S. The distribution and function of phosphatidylserine in cellular membranes. Annu Rev Biophys 2010; 39:407-27; PMID:20192774; http://dx.doi.org/10.1146/annurev.biophys.093008.131234
15. Yeung T, Heit B, Dubuisson JF, Fairn GD, Chiu B, Inman R, Kapus A, Swanson M, Grinstein S. Contribution of phosphatidylserine to membrane surface charge and protein targeting during phagosome maturation. J Cell Biol 2009; 185:917-28; PMID:19487458; http://dx.doi.org/10.1083/jcb.200903020
16. Atkinson K, Fogel S, Henry SA. Yeast mutant defective in phosphatidylserine synthesis. J Biol Chem 1980; 255:6653-61; PMID:6771275
17. Simon ML, Platre MP, Assil S, van Wijk R, Chen WY, Chory J, Dreux M, Munnik T, Jaillais Y. A multi-colour/multi-affinity marker set to visualize phosphoinositide dynamics in Arabidopsis. Plant J 2014; 77:322-37; PMID:24147788; http://dx.doi.org/10.1111/tpj.12358
18. König S, Hoffmann M, Mosblech A, Heilmann I. Determination of content and fatty acid composition of unlabeled phosphoinositide species by thin-layer chromatography and gas chromatography. Anal Biochem 2008; 378:197-201; PMID:18466755; http://dx.doi.org/10.1016/j.ab.2008.03.052
19. Potocký M, Pleskot R, Pejchar P, Vitale N, Kost B, Zárský V. Live-cell imaging of phosphatidic acid dynamics in pollen tubes visualized by Spo20p-derived biosensor. New Phytol 2014; 203:483-94; PMID:24750036; http://dx.doi.org/10.1111/nph.12814
20. Barbosa ICR, Shikata H, Zourelidou M, Heilmann M, Heilmann I, Schwechheimer C. Phospholipid composition and a polybasic motif determine D6 PROTEIN KINASE polar association with the plasma membrane and tropic responses. Development 2016; 143(24):4687-700; PMID:27836964; http://dx.doi.org/10.1242/dev.137117